

1

AGARD-CP-354

AGARD-CP-354

AGARD

ADVISORY GROUP FOR AEROSPACE RESEARCH & DEVELOPMENT

7 RUE ANCELLE 92200 NEUILLY SUR SEINE FRANCE

AGARD CONFERENCE PROCEEDINGS No.354

Aeroelastic Considerations in the Preliminary Design of Aircraft

DISTRIBUTION STATEMENT A

Approved for public release;
Distribution Unlimited

DTIC
ELECTE
S OCT 25 1983 D
B

NORTH ATLANTIC TREATY ORGANIZATION

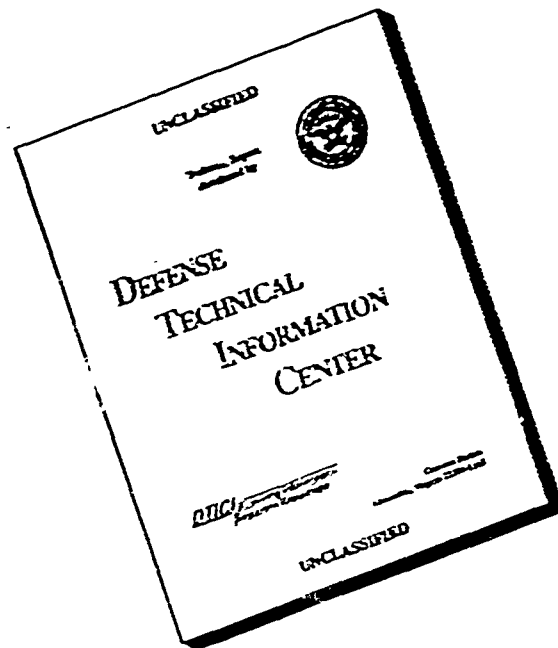


DISTRIBUTION AND AVAILABILITY
ON BACK COVER

AD-A233982

DTIC FILE COPY

DISCLAIMER NOTICE



THIS DOCUMENT IS BEST
QUALITY AVAILABLE. THE COPY
FURNISHED TO DTIC CONTAINED
A SIGNIFICANT NUMBER OF
PAGES WHICH DO NOT
REPRODUCE LEGIBLY.

NORTH ATLANTIC TREATY ORGANIZATION
ADVISORY GROUP FOR AEROSPACE RESEARCH AND DEVELOPMENT
(ORGANISATION DU TRAITE DE L'ATLANTIQUE NORD)

AGARD Conference Proceedings No.354
AEROELASTIC CONSIDERATIONS IN THE
PRELIMINARY DESIGN OF AIRCRAFT

REPRODUCED BY
NATIONAL TECHNICAL
INFORMATION SERVICE
U.S. DEPARTMENT OF COMMERCE
SPRINGFIELD, VA 22161

Papers presented at the 56th Meeting of the Structures and Materials Panel in London,
United Kingdom, on 11--12 April 1983.

THE MISSION OF AGARD

The mission of AGARD is to bring together the leading personalities of the NATO nations in the fields of science and technology relating to aerospace for the following purposes:

- Exchanging of scientific and technical information;

Continuously stimulating advances in the aerospace sciences relevant to strengthening the common defence posture;

- Improving the co-operation among member nations in aerospace research and development;

Providing scientific and technical advice and assistance to the North Atlantic Military Committee in the field of aerospace research and development;

Rendering scientific and technical assistance, as requested, to other NATO bodies and to member nations in connection with research and development problems in the aerospace field;

Providing assistance to member nations for the purpose of increasing their scientific and technical potential,

Recommending effective ways for the member nations to use their research and development capabilities for the common benefit of the NATO community.

The highest authority within AGARD is the National Delegates Board consisting of officially appointed senior representatives from each member nation. The mission of AGARD is carried out through the Panels which are composed of experts appointed by the National Delegates, the Consultant and Exchange Programme and the Aerospace Applications Studies Programme. The results of AGARD work are reported to the member nations and the NATO Authorities through the AGARD series of publications of which this is one.

Participation in AGARD activities is by invitation only and is normally limited to citizens of the NATO nations.

The content of this publication has been reproduced directly from material supplied by AGARD or the authors.

Published September 1983

Copyright © AGARD 1983
All Rights Reserved

ISBN 92-835-0338-4



Preceding page blank

Printed by Specialised Printing Services Limited
40 Chigwell Lane, Loughton, Essex IG10 3TZ

REPORT DOCUMENTATION PAGE			
1. Recipient's Reference	2. Originator's Reference	3. Further Reference	4. Security Classification of Document
	AGARD-CP-354	ISBN 92-835-0338-4	UNCLASSIFIED
5. Originator	Advisory Group for Aerospace Research and Development North Atlantic Treaty Organization 7 rue Ancelle, 92200 Neuilly sur Seine, France		
6. Title	AEROELASTIC CONSIDERATIONS IN THE PRELIMINARY DESIGN OF AIRCRAFT		
7. Presented at	presented at the 56th Meeting of the Structures and Materials Panel in London, United Kingdom, on 11-12 April 1983.		
8. Author(s)/Editor(s)	Various		9. Date September 1983
10. Author's/Editor's Address	Various		11. Pages 332
12. Distribution Statement	This document is distributed in accordance with AGARD policies and regulations, which are outlined on the Outside Back Covers of all AGARD publications.		
13. Keywords/Descriptors	<div style="display: flex; justify-content: space-between;"> <div style="width: 45%;"> Aircraft Airframes Design </div> <div style="width: 45%;"> Aeroelasticity Flutter Dynamic structural analysis </div> </div>		
14. Abstract	<p>This publication contains the papers presented at the SMP Spring 1983 Specialists Meeting on Aeroelastic Considerations in the Preliminary Design of Aircraft. Current aerospace design trends which involve the increasing application of composite structures have forced the use of large-scale structural analysis at an early design stage; at the same time structural optimization and aeroelastic tailoring are becoming practical tools for shaping the initial project. Whilst the potential for designing minimum weight structures which deform beneficially under load exists, the hazards of extracting energy from the airstream and generating unfavourable deformations and aeroelastic instabilities must also be recognized. These papers review trends in aeroelastic analysis, aeroelastic tailoring, structural optimization and flutter optimization.</p>		

PREFACE

Several trends are converging in the aerospace industry. Composite structures with directional stiffness and strength are gradually evolving from use in secondary to primary structures. The rapid pace of development in large-scale structural modeling and analysis is allowing the loads, stress and dynamics engineers to keep abreast of airframe design changes and to influence those changes early in the design cycle. Structural optimization and aeroelastic tailoring are becoming practical tools for the preliminary designer. As a result, designers are faced with the problem and opportunity of designing minimum-weight structures which deform in beneficial ways during cruise and under maneuver loads. As structures become more efficient devices for extracting energy from the airstream, then the potential also increases for unfavorable deformations and aeroelastic instabilities. The purpose of this Meeting was to review the latest trends in aeroelastic analysis, aeroelastic tailoring, structural-optimization and flutter-optimization and to increase the utility of those techniques in aircraft design offices.

James J. Olsen
Chairman, Sub-Committee on
Aeroelasticity

CONTENTS

	Page
PREFACE	iii
	Reference
<u>SESSION I – TRANSPORTS</u>	
PRELIMINARY AEROELASTIC DESIGN OF STRUCTURES (PADS) – METHODS DEVELOPMENT AND APPLICATION by N.A.Radovich	1
APPROCHE AEROSPATIALE DE L'ETUDE DU FLOTTEMENT AU NIVEAU DE L'AVANT-PROJET par M.Curbillon	2
AEROELASTIC TAILORING OF HIGH ASPECT-RATIO COMPOSITE WINGS IN THE TRANSONIC REGIME by C.J.Borland and D.W.Gimmestad	3
<u>SESSION II – TRANSPORTS</u>	
AEROELASTIC DESIGN OF CIVIL TRANSPORTS AT THE PROJECT STAGE by R.E.J.Brazier, A.E.Dudman and B.W.Payne	4
TRANSONIC FLUTTER CLEARANCE FOR A SUPERCRITICAL TRANSPORT AIRCRAFT IN THE PRELIMINARY DESIGN STAGE by N.Pronk, H.Walgemoed and R.J.Zwaan	5
INFLUENCE OF MAIN DESIGN PARAMETERS ON FLUTTER BEHAVIOUR FOR AIRCRAFT CONFIGURATIONS WITH HEAVY CONCENTRATED MASSES TAKING INTO ACCOUNT TRANSONIC EFFECTS by S.Vogel and H.Zimmermann	6
AEROELASTIC DESIGN CONSIDERATIONS FOR TURBO-PROP POWERPLANT INSTALLATIONS by J.J.Glaser	7
THE DEVELOPMENT OF FAST-FLOW (A PROGRAM FOR FLUTTER OPTIMIZATION TO SATISFY MULTIPLE FLUTTER REQUIREMENTS) by B.A.Rommel	8
THE INITIAL DESIGN OF ACTIVE CONTROL SYSTEMS FOR A FLEXIBLE AIRCRAFT by I.W.Kaynes and D.E.Fry	9
<u>SESSION III – HELICOPTERS</u>	
AEROELASTIC DESIGN CONSIDERATIONS IN THE DEVELOPMENT OF HELICOPTERS by H.Strehlow and B.Enenkl	10
THE INFLUENCE OF AEROELASTIC STABILITY REQUIREMENTS ON HELICOPTER DESIGN by S.P.King	11
AEROELASTIC CONSIDERATIONS IN THE DESIGN OF HIGH SPEED ROTORS by Wen-Liu Miao and R.H.Blackwell	12
ANALYSE PREVISIONNELLE DU COMPORTEMENT AEROELASTIQUE DES ROTORS ARRIERE par G.Genoux et G.Blachère	13

Reference

THE ROLE OF AEROELASTICITY IN THE PRELIMINARY DESIGN OF HELICOPTER ROTORS

by V.Giavotto, M.Borri, A.Russo and A.Ceriotti

14

SESSION IV – COMBAT AIRCRAFT

AEROELASTICITE ET OPTIMISATION EN AVANT-PROJET

par C.Petiau et D.Boutin

15

AEROELASTIC CONSIDERATIONS IN PRELIMINARY DESIGN OF A MILITARY COMBAT AIRCRAFT

by M.Ormerod and D.G.Gibson

16

PRELIMINARY DESIGN OF AIRCRAFT USING STRUCTURAL OPTIMIZATION METHODS

by H.Gödel, G.Schneider and H.Hörnlein

17

A FLUTTER OPTIMIZATION PROGRAM FOR COMPLETE AIRCRAFT STRUCTURAL DESIGN

by S.Siegel

18

FAST FLUTTER CLEARANCE BY PARAMETER VARIATION

by V.Giavotto, P.Mantegazza, T.Merlini, L. De Otto, M.Lucchesini and R.Mantelli

19

Preliminary Aeroelastic Design of Structures [P A D S]
Methods Development and Application

1-1

N. A. Radovcich, Ph.D.
Group Engineer
Advanced Flutter & Dynamics Methods
Lockheed-California Company
P.O. Box 551, Burbank, CA 91520 USA

SUMMARY

Preliminary design for an optimal aircraft configuration may require the integration of aeroelastic considerations into the configuration selection process.

Preliminary Aeroelastic Design of Structures (PADS) is a highly computerized design system for generating structural weight data which include aeroelastic effects for advanced aircraft configurations. These data can then be used to update the statistical and semianalytical weight data base during configuration trade-off studies.

In this paper, three aspects of PADS are discussed: 1) the formulation of computer operating system technology and data management techniques which will permit the definition and execution of engineering processes in a user friendly environment, 2) a definition of engineering processes for preliminary aeroelastic design of structures which may be used to design an aircraft for strength and stiffness in the elapsed time normally available for a conceptual design phase, and 3) the presentation of results from the PADS validation effort, computer software as well as engineering processes, using a known airplane design data base.

LIST OF ACRONYMS & DEFINITIONS

ACS- active control system
ASSET- Advanced Systems Synthesis and Evaluation Technique
CADAM*- Lockheed's computer aided design system
CBUS- Continuous Batch User Specification
CPP- command processor program in CBUS
DBM- data base management
DMS- data base management system
DOF- degree of freedom
FAMAS- Lockheed's matrix data based computing system for aeroelastic analysis
FINDEX- Lockheed's DMS for matrices and NASTRAN tables
FSD- fully stressed design algorithm
Lockheed- Lockheed-California Company
MLC- maneuver load control
NASA- National Aeronautics and Space Administration
NASTRAN- structural finite element program developed by NASA
PADS- Preliminary Aeroelastic Design of Structures
PSASA- panel sizing and stress allowables
RAP- resource allocator program in CBUS
RDMS- run data management system
SIC- structural influence coefficients
SMG- structural model generator, a finite element model generator which represents a family of aircraft designs.

INTRODUCTION

Preliminary design for an optimal aircraft configuration may require the integration of aerelastic considerations into the configuration selection and design process. Aeroelastic design incorporates the effects of aircraft flexibility on static and dynamic loads, control effectiveness, and aeroelastic stability into the sizing of the structure. Configurations of aircraft in the early design stage are usually based on statistical and analytical weight methods computed from approximate loads and stress analyses. This often leads to the freezing of external geometry before strength and flutter analyses are sufficiently advanced, thereby decoupling the powerful, but time-consuming, process of structural design-to-minimum-weight from the configuration optimization process. If the elapsed time to perform more accurate loads, structural design, and flutter optimization analyses is shortened, then structural optimization can proceed in concert with the overall configuration optimization, and more efficient advanced types of aircraft can be designed.

In the past, the level of effort required for an accurate aeroelastic design was not justifiable relative to the answers provided by statistical methods which were supported by historical data bases. Today, however, there are many combinations of advanced technologies and configurations, such as supercritical airfoils, high aspect ratio wings, forward swept wings, active controls, aeroelastic tailoring, and new materials, that have no historical data base from which to derive the statistical or parametric weight equations.

* Registered trademark of CADAM, Inc.

1-2 Airplane design involves complex interactions between the conceptual designer, the customer with design specifications, and the engineers with final design and manufacturing requirements. Since many facets of the engineering process defy quantification, the computer methodology used to improve the flow of design information must be: 1) flexible, and 2) highly modular. Flexibility will permit inputs into the design process from many sources, and modularity will deter obsolescence when new engineering design processes become available.

The goal of Preliminary Aeroelastic Design of Structures (PADS) is to develop computer operating system architecture and design methodology to be used to generate an accurate aeroelastic design within the conceptual and early preliminary design phases. This aeroelastic design data base will permit more accurate weights to be established during the configuration trade-off studies. The long term goal is to define an accurate aeroelastic design within an elapsed time which is measured in weeks and to perform a design perturbation within elapsed time which is measured in days. Design perturbations include changes to any variable which does not require significant data preparation. For the wing, these variables will include sweep, planform definition, taper, airfoil sections, t/c , and aspect ratio.

The work to achieve these goals is in progress. PADS capabilities currently include a structural finite element model generator, weight distribution, grid transformations, steady maneuver loads for symmetric conditions, flutter analysis, and structural sizing. This paper will address three areas:

- The formulation of computer operating system technology and data management techniques which will permit the definition and execution of engineering processes in a continuous, user-friendly computing environment.
- The definition of engineering processes for preliminary aeroelastic design of structures which may be used to derive an accurate structural weight for a wing in the elapsed time normally available for a conceptual design phase.
- The presentation of results from the PADS validation effort, computer software as well as engineering processes, using a known airplane design data base.

PROBLEM DEFINITION

Aeroelastic analysis of an aircraft structure is a substantial undertaking involving many disciplines and complex data paths. A short time ago, preliminary aeroelastic analysis was reserved for projects on the verge of achieving go-ahead status while preliminary aeroelastic design was not even attempted.

There are two options available for acquiring a rapid aeroelastic analysis and design capability: generate or acquire special programs tailored to rapid analysis procedures; or adapt existing engineering methodology and the associated computer tools to requirements of rapid analyses. Software maintenance is a major part of any proposed computer-aided design system. Lockheed-California Company (Lockheed) has an extensive library of computer programs which support airplane design through final and production design phases. It would be convenient to extend the application of that software into the preliminary design phase instead of creating specialized software.

Computer programs used to perform final aeroelastic analyses are well established in any major aircraft design company. At Lockheed, the list of computer programs generically include:

- A user-friendly matrix algebra based computing system
- Grid transformation programs
- A finite element based structural analysis program
- Steady and unsteady aerodynamic programs
- Weight estimation and distribution programs
- Steady maneuver aeroelastic load programs
- Transient maneuver aeroelastic load programs
- Ground handling load programs
- Dynamic loads (gust, taxi, landing) programs
- Flutter analysis programs
- Structural resizing program with stiffness (flutter) and deflection constraints
- Structural sizing programs for stress and fatigue
- Feedback control functions synthesis programs for load relief and flutter suppression

- Data base management (DBM) programs for card image data, matrices, and tables 1-3
- Structural finite element model generator program
- Plotting programs
- General utility programs known as pre- and postprocessors

When PADS development was initiated in 1976, computer programs and computing systems were generally available at Lockheed for preliminary aeroelastic design, but certain computer access and job preparation problems prevented these programs from being used on quick design studies. In particular:

- The overwhelming number of details associated with computer job definition made the most trivial computer job setup a challenge. Misplacing a single comma or being off one space in the input format field caused the job to fail.
- The computing tasks were serially related to each other. Job "A" had to run successfully before Job "B" could be submitted. Many computer jobs required one day turnaround and, with setup difficulties, one week could pass before the results were available.
- Analytical modeling requirements for each discipline were different.
- Data flow between disciplines involved paper flow and manual transcription.
- The trail on "How was it done last time?" was not always protected from unfavorable personnel transfers.
- Many preparations for computer job submittals required transcribing of input data by hand.
- When the process required hundreds of computer submittals and hundreds of individual input deck setups, it was impractical to mobilize engineering personnel just to feed the computer for a quick project.

Against the background of existing data management systems, existing computing systems of great sophistication, and high-level languages oriented to the user-friendly atmosphere, the company decided to use the production design computing tools and to attack directly their known deficiencies with respect to preliminary design applications. A computing system was postulated which would act as a bare tree from which existing computer programs could be hung as needed in a user-friendly and highly modular environment.

APPROACH

Lockheed's Advanced Systems Synthesis and Evaluation Technique (ASSET) computer program provides a rapid and cost-effective solution to configuration selection for any aircraft mission, but only within the limitation that the structural weight must be based on semianalytical and statistical data. An ASSET study usually requires that a baseline aircraft model be created and exercised in ASSET to represent an actual known aircraft data base. This model then is modified through adjustments to parametric coefficients to simulate changes to baseline aircraft systems, structural arrangement, material usage, design parameters, and mission requirements. Once complete, the model is passed into the ASSET design cycle for sizing, configuration trade-off analysis, and performance evaluation.

The PADS goal is to update the weight data base during configuration trade-off studies as well as to perform general aeroelastic analysis and design in a highly computerized environment. Figure 1 shows the possible interaction between PADS and ASSET during a typical configuration trade-off study. Aeroelastic inputs to ASSET will lead to significant improvements in the configuration selection process, especially when advanced designs combine advanced structural materials, such as composites, with unusual geometry.

PADS development consists of two distinct efforts:

- The development of the computer operating system which will permit continuous computing capability in a user-friendly and engineering-defined environment.
- The definition and mechanization of basic engineering processes for use in aeroelastic design and analysis.

The computer operating system will have applications outside of PADS whenever a requirement exists to integrate diverse computing programs under one operating system.

The Concept of a Software Bus

The design specifications of the operating system for PADS mirror the specifications of a computer hardware bus. The specifications of the computer hardware bus define an interfacing system for use in interconnecting data processing, data storage, and peripheral data control devices in a closely coupled configuration. Two objectives of a hardware bus are 1) to provide communication between two devices on the bus without

1-4

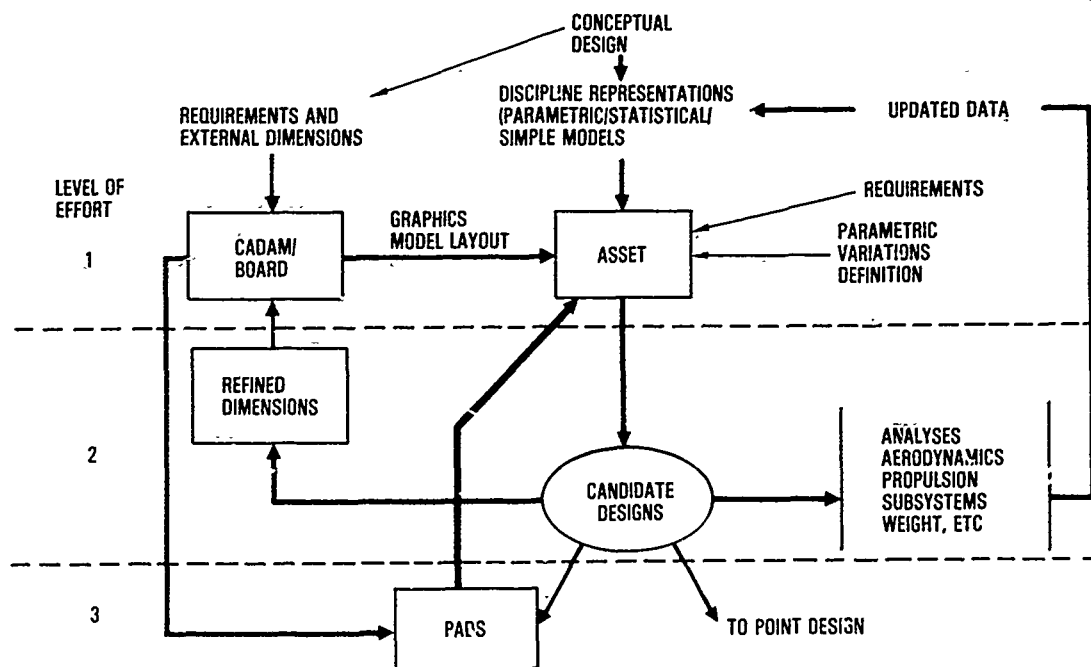


FIGURE 1. PADS AND ASSET INTERFACE

disturbing the internal activities of the other devices interfaced to the bus, 2) to specify protocols that precisely define the interaction between the bus and devices interfaced to it.

If the word "devices" is replaced by "load modules/programs", the above specifications for a hardware bus come close to defining the specifications for a computer operating system in terms of a software bus. One of the reasons the operating system was named Continuous Batch User Specification was to carry over the bus concept into the operating system acronym, namely CBUS.

Modeling criteria

Each engineering discipline will define the modeling requirements according to its functions and responsibilities. There will be no outside constraints except where more than one discipline will be affected. For the modeling tasks which affect many disciplines, such as structural finite element modeling, unsteady aerodynamics, and weight distributions, one discipline will be designated as "prime", usually by tradition. This discipline will then integrate the requirements of the other cognizant disciplines into the modeling definition.

The structural modeling effort is by far the most time consuming of any aeroelastic modeling task. There are practical limits to reducing the elapsed time required to generate and checkout a 3-D finite element model. Experience gained with the use of user coded programs which generate, correct, and manipulate computer files led to the engineering development and coding of computer programs for rapid generation of principal parts of the finite element model using relatively few input variables.

A finite element model generator will be assembled from this technology. Data for the model generator will be defined to represent a specific family of aircraft designs which may be generated using relatively simple inputs. The collection of model generator programs and the input data required to represent a particular family of aircraft designs will be referred to as a structural model generator (SMG).

Wing geometric data for input to the finite element model generator will consist of certain key variables that define the wing planform together with a 3-D parametric representation of the wing section shapes. The section shape representation is available from the aerodynamics department and serves as the input data base for the aerodynamic performance programs which are used to generate aerodynamic data for ASSET. This arrangement will permit variations in aspect ratio, t/c, planform, taper, sweep, and dihedral with relatively simple inputs. Other details of the finite element model such as wing location relative to the fuselage, fuselage length, and empennage characteristics may also be included as part of the simple input variables. The concept of a finite element model generator for a family of aircraft designs is critical to satisfying the preliminary design schedule constraints.

Data flow continuity

Since existing computer programs will be used in the PADS system, the conditioning of data from various sources will be accomplished by the aggressive use of pre- and postprocessors. If the flow of data is interrupted in an existing engineering process with a large number of subjective interpretations, and the engineering process is not

1-6 Command processor/resource allocator/target

The command processor provides the architecture within which the user can organize data flow and computing tasks into engineering functional blocks. This architecture in the ideal form, therefore, lacks any engineering intelligence or functionality. The CBUS operating system permits the user to address the engineering requirements with the full benefits of an integrated computing environment but without the usual constraints of entry protocol, imposed computing module formats, and fixed data paths and/or data types. With functionality definitions and data management tasks outside of the command processor control, the user has the flexibility to mechanize within CBUS most processes that can be described on an IBM 370 computer operating system.

After the command processor generates a data stream that can be interpreted by the resource allocator program (RAP), the command processor releases control to the monitor. The monitor then calls the resource allocator to interpret the input data stream generated by the command processor. When the resource allocator interprets enough of the file to execute a process, the resource allocator modifies the computer resources according to the file's instructions and returns control back to the monitor. The monitor then executes the target named in that process.

When the target task is completed, the monitor goes back to the resource allocator to interpret more of the data stream provided by the command processor. The resource allocator reallocates the resources; it then returns control to the monitor, which calls the next target program. This process is repeated until the data stream is expended. When the process is complete, the monitor then returns control back to the command processor to get another stream of data which the resource allocator may interpret and the monitor may execute.

The target can be any data management system (DMS) program, any analysis program, or any load module of any type. The sequencing of these target programs performs in a typical process the following:

- Moves data into files required by the next target
- Operates on the input files to produce output files
- Moves output data into storage

The monitor sees every program as a target whether it is the command processor, the resource allocator, or any other load module. The labels given the command processor, resource allocator, and target are only an aid to describe the relationship each has with the monitor and the CBUS operating system.

Additional details of the system's operational characteristics may be found in Appendix A.

Run data management system

The run data management system (RDMS) is one of the target programs. The RDMS manages computer files which are used during the CBUS execution to store and retrieve data blocks which have been generated by target programs. RDMS also manages the data blocks known as "macros" and "commands" which are accessed by the command processor. Figure 3 illustrates the typical files that the RDMS accesses in the role of a target program.

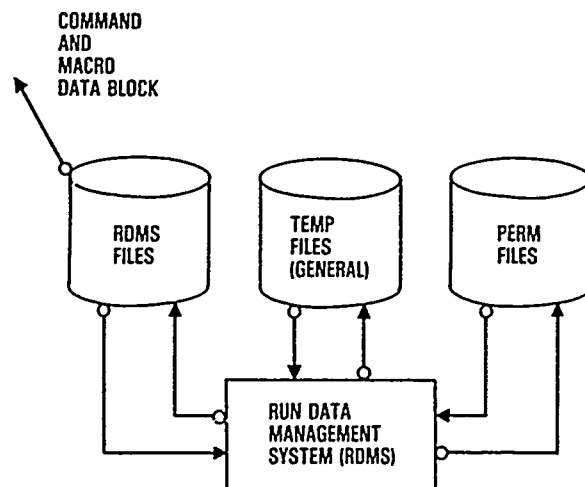


FIGURE 3. RDMS FILE INTERFACES

CBUS portability

CBUS is currently running on an IBM 370 operating system. The monitor (assembly language) and the resource allocator (FORTRAN) make references unique to the IBM 370

operating system. Recoding of these programs would be required before installation on a different computer could be attempted. 1 - 7

Batch and Interactive processing

CBUS is a direct descendant of an operating system used to drive interactive analysis programs on refreshable graphics terminals. All aspects of CBUS are totally compatible with the interactive processing mode. In the UNIX terminology [Ref.1], the command processor would become the shell which would interpret the user requests, call programs from memory or files, and execute them one at a time or in a series called "pipe". The system prompt for UNIX usually is "\$". For CBUS the prompt is "e". While the conversion to an interactive mode would be trivial, the resources required to execute some of the processes would be significant, especially in light of user priority formally associated with the interactive computing mode.

USER INTERFACE

The user interfaces with the CBUS operating system through commands, and through the command processor language. A command specifies a process in a language which is interpretable by the CBUS command processor at the user input level. A process is a particular method of doing something, generally involving a number of computer programs and/or operations. A command contains all the defaults necessary for executing a process. The command processor recognizes four levels of macro configured data structures; namely, macro, subcommand, command, and supercommand. The different levels of macros, as illustrated in Figure 4, make possible definition of primitive processes which can be used as building blocks for any number of higher level processes. The macro and subcommand are building blocks for commands while commands are building blocks for supercommands.

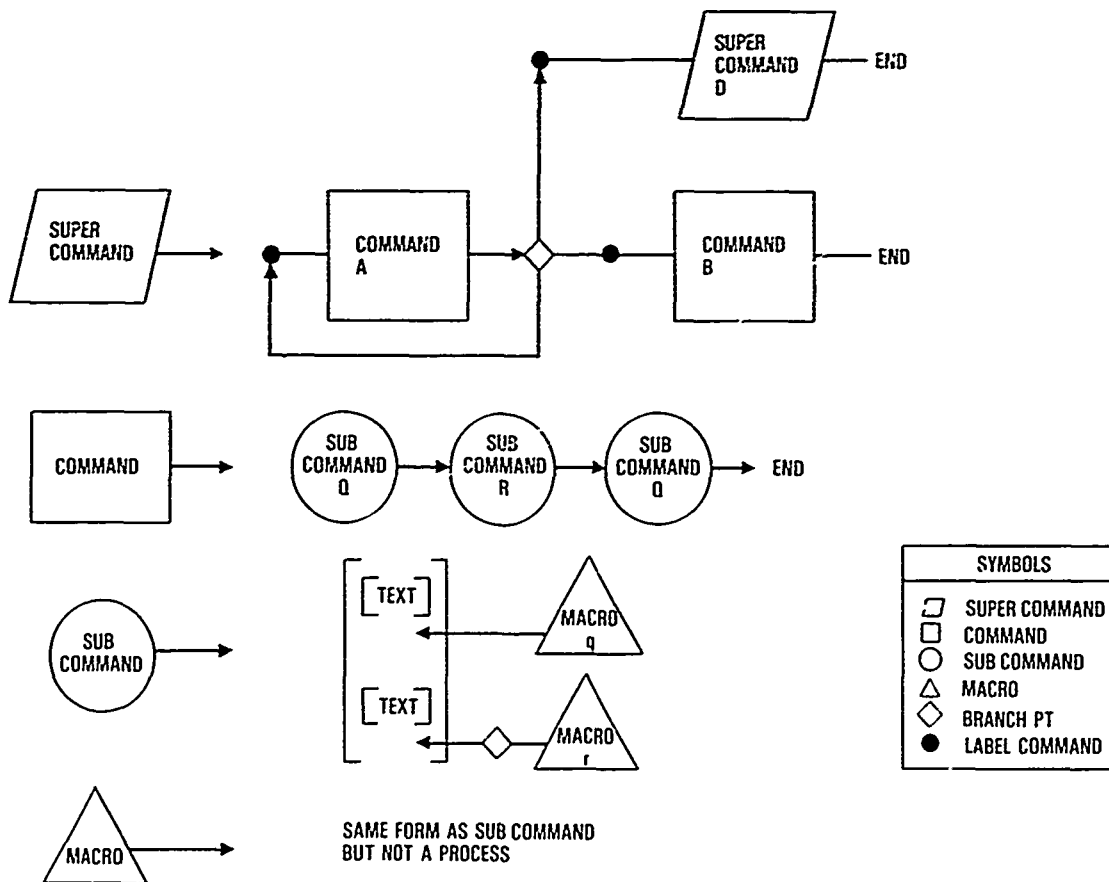


FIGURE 4. MACRO STRUCTURE EXAMPLES

Macro

The term macro as used in the CBUS operating system defines any collection of data, whether function-related or data base-related, which is accessible by specifying a prescribed eight character alphanumeric name. The macro as defined in Ref. 2 is: "a way of packaging routines for future use ... a macro facility is made possible by a special processor that can be embedded within an assembler or exist as a separate piece of software; if separate, it will be given as input a source program consisting of a mixture of macros and AL statements, transform the macros in AL, and pass the resulting program to a simple assembler." AL refers to assembly language. The macro in CBUS has the above function except that AL now refers to any language or data statements.

Subcommand

A subcommand is a self-contained instruction set which defines a process to be performed and is accessible in the CBUS operating system by the same naming convention as is available for a macro. A subcommand is not directly available to the user but must reside in a command. Subcommands, however, access macros and have "defaults" for "attributes" (see below) which the user or commands can alter. Subcommands cannot access a command or supercommand. Subcommands are components of commands which may be modified by the calling command through specification of the subcommand attributes. A subcommand can reference another subcommand. A subcommand is likely to contain a number of references to program load modules. However, the sequence in which the program load modules are executed is fixed in a subcommand.

Command

A command contains, in a fixed sequence, a collection of references to subcommands as well as all defaults for attributes associated with subcommands and macros. This collection is required to define the command's process. The command is the primary unit which is accessible by the user and has the same naming convention as the macros and subcommands. Commands do not contain logical branching functions for referencing subcommands.

Supercommand

A supercommand contains references to commands and supercommands, and includes all defaults necessary to perform its function. Supercommands, therefore, permit recursive operations because a supercommand can reference itself. The primary characteristic of a supercommand is its access to the CBUS command language which, therefore, permits logical branching and inline alter capability for the defaults. To the user, a supercommand appears to be another command. To the CBUS command processor, however, the supercommand is processed until a command is defined which can be passed to the monitor/resource allocator for execution.

Attribute and Default

Attribute as used here is any item required for execution of the process which can be altered, deleted, or assigned by names and keywords. They include any data quantities, program names, data names, keywords for CBUS commands, FORTRAN statements, etc. The term default refers to the naming of the attributes within any of the macro structures being discussed in this section.

User-friendly

Technically, the term user has two connotations: 1) the user operating through the command processor language, 2) the user who is the CBUS programmer of commands and macros. The user operating through the command processor language will find the system user-friendly because of the following characteristics:

- The user requests processes to be executed by names which were generated by the CBUS programmer.
- The user input format is free form.
- A process contains all defaults for execution.
- The user deck defines what is to be done and not how it is being done.

The generation of commands and macros, however, requires the use of a lower level language. There are more rules associated with coding commands and macros than with executing processes through the CBUS command processor language. The language for building commands, therefore, is less user-friendly.

COMMAND PROCESSOR LANGUAGE

The user command language is a high level language which permits the typical user to define complex computing functions through commands and branch capabilities. Some of the essential features will be demonstrated by example.

Initializing PADS

A typical setup to initialize the CBUS operating system is:

```
@ START
@ PADS
```

The command, START, enables the CBUS operating system to execute system bootstrap operation (see Appendix A for details). START loads primitive system commands and prepares the CBUS for interpreting the next command line. In this case, the next line requests the system to execute the command, PADS, which loads all commands/macros associated with the functionality of preliminary aeroelastic design of structures. Sometimes the commands and other data are stored on permanent data sets when many re-entries into PADS are expected.

The command, RESTART, replaces the START and the PADS commands. The setup would then appear as: 1-9

```
@ RESTART
PERMPIF = RF1000.PIF
PERMPMF = RF1000.PMF
```

where the two entries after RESTART are altercards (to be defined later) which identify the names of the permanent data sets that contain the PADS system commands and data entries. PERMPIF keyword points to the data set containing the index data and the PERMPMF keyword points to the data set containing the data records.

Input data assembly

The next set of commands pulls in data from external storage systems. Certain of these are encoded so that a preprocessor scanning the user input cards builds the data stream that will automatically assemble the data blocks requested by the user. A typical setup for this operation is:

```
@ BUILD
JOB (5555,500); (ID for output data sets)
*
ID(JOB=5555,SECT=400)
IN/1000,THRU,2000/5123/6000,THRU,7000/
*
* read into PADS DMS
*
@ READTAPE
```

where, under command BUILD, matrices 1000 thru 2000, etc from job number 5555 and section number 400 are located in Lockheed's DBM system called FINDEX and stored on a temporary disc data set for the command, READTAPE, to read into the RDMS. Cards with "*" in the first column are comment cards.

Branching Capability

Also available to the user is a set of commands that allow branching within the command processor input deck. These include the following commands:

```
@GOTO _____ , @ _____ : ,
@CALL _____ , @RETURN ,
@IF (expressions) THEN GOTO _____ ,
```

where _____ is an alphanumeric character label up to eight characters in length.

The first of these commands is an unconditional GOTO to a label. The label command is distinguished from a normal command by a ":" as shown in the second item of the list. The next branch function is the command CALL which is analogous to the FORTRAN subroutine CALL without arguments. The command RETURN provides the branch back to the point of the call. Another function is a conditional statement based on a logical IF, which provides alphanumeric identification with the functionality of less than, greater than, or equal to evaluations, similar to syntax in FORTRAN IV.

The variables specified in the conditional "IF" option may come from two sources: from the in-line definition of the variable in the user deck, and from the application programs that are requested in the commands. As the variables are entered into a scalar library file, the intermediate products are saved and existing variables are updated. Consequently, implied DO loops are available to the user.

Altercards

While a command contains all the attribute defaults necessary to execute the process, there are certain attributes that must be named at the time the process is invoked. This is required because the process directly operates on the named attribute. There are other attributes that are named at the time the process is invoked that have to do with data management control. These requirements to name attributes within the command or macro are satisfied using a facility in the CBUS system called altercard.

Altercards are statements within the user deck that follow a command line. A command line first character is "@". All statements up to the next command line are considered by CBUS to be altercards for the command being invoked. A typical example follows:

```
@ VIBRATION ; this is a command to perform a
*          vibration analysis
*   MASS=3000 ; this is an altercard to define
*            the mass matrix
*   STIFF=4000 ; this is an altercard to define
*            the stiffness matrix
*   MODES=20 ; this is an altercard to define the number of
*            vibration modes to be computed
@ FLUTTER ; the next command; terminates the altercard
*          list for the command VIBRATION
```

The command, VIBRATION, could have been coded to accept the following form for the altercard:

```
@ VIBRATION
  VIBCARD = 3000 4000 20
@ FLUTTER
```

or with the attributes already imbedded within the command;

```
@ VIBRATION
@ FLUTTER
```

Additional information on altercard and CBUS alter capability, together with data block naming convention, may be found in Appendix A.

Error handling procedures

Since the CBUS operating system accesses many major systems in one computer run, care is exercised so as not to continue the computation process if there is either (1) an abnormal ending (ABEND) out of one of the target programs, or (2) a condition code generated by the last target program which tells the user that continuing is not worth-while.

Recovery procedure

A user-directed recovery procedure permits the user to save data generated up to the ABEND or condition code failure. An ONERROR command label is placed in the user deck to designate the point to which CBUS will branch when either an ABEND or condition code is detected. The process that may be performed on an ONERROR branch may include data management clean up and save routines, printouts of execution logs, and tables that refer to the tracking of the program data flow. The commands under the label of ONERROR must be thoroughly tested to avoid a double ABEND or error. RAP accepts only one branch to an ONERROR. If an error occurs after the CBUS system branches to ONERROR, RAP will instruct the monitor to terminate the job immediately.

THE DESIGN PROCESS

In practice, a design process is a good roadmap which identifies the path to a rational design. However, as in any travels, the successful designer must be ready to follow other routes if the design data justifies the excursion. Therefore, a plan showing probable paths and sequences of operations is at best a general guide rather than a definitive route through the design process. Within the context of these reservations, a design process will be outlined in terms of the engineering processes described in Appendix B.

The first step in the design process is to define the objectives of the task and the necessary level of design detail required to satisfy those objectives. The design team must then review the requirements, cost out the project, and define a schedule. This is an iterative process between the customer and the design team as with any project with a specific amount of available resources. This phase is labelled "DESIGN OBJECTIVES" in Figure 5.

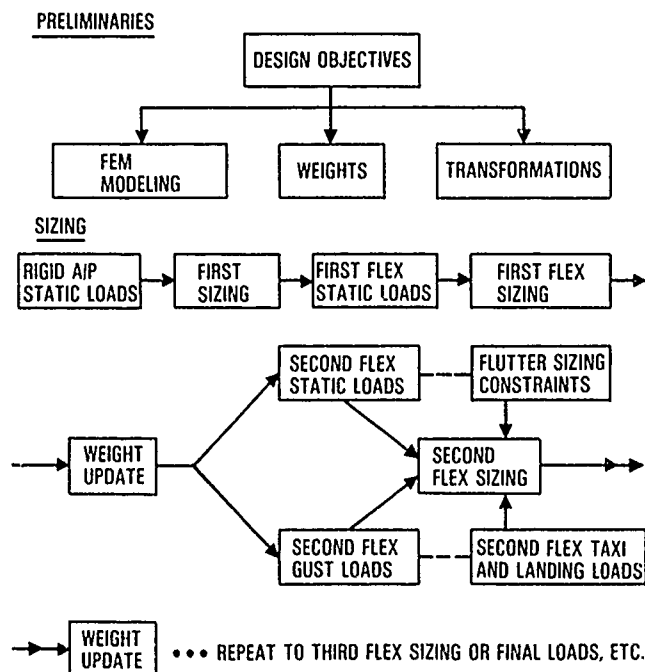


FIGURE 5 DESIGN PROCESS OVERVIEW

1-11

The next step is the generation of the structural finite element model, initial weight distributions, and initial entries into the various modules to generate geometry tables for each grid system to be used in the design. This provides the necessary data base for the computations of all transformation matrices between the various grid systems. The completion of the transformation task marks a major milestone in the design.

The initial internal loads intensities are generated from static loads for a rigid airplane and uniform properties for those structural finite elements to be sized. A panel sizing and stress allowable (PSASA) process then generates from the load intensities the initial sizing and the associated stress allowables for the specified margins of safety. There may be multiple entries into the internal loads generator and panel sizing procedures before a converged sizing is produced using rigid airplane static loads.

The computations for static loads and internal loads intensities are repeated using the sizing derived from rigid airplane loads. The term "first flex sizing" refers to the use of the design's first flexibility matrix in the computation of the static aeroelastic loads to derive the sizing.

The first flex sizing data provides a basis for updating the weight data and for generating dynamic loads input (gust, taxi, landing) along with the flutter minimum sizing constraints. The second flex sizing should be close to the sizing which satisfies strength and stiffness requirements. If the loads and stiffness interactions are highly coupled, the process may require another iteration through the third flex sizing. At the conclusion, there should be a final pass through the analysis modules in order to quantify the design relative to the design constraints.

VALIDATION EFFORT

There are two phases to the process by which PADS is being evaluated: 1) the validation of CBUS operating system and the analysis programs, and 2) the validation of the design process for the objectives of preliminary design. Both phases require an existing production airplane design which has an extensive data base for weight, design loads, sizing, etc., for comparisons. These quantities are not only required for reasonableness checks, but also to quantify the areas of design that may not be properly represented in the design process.

Reference airplane

The airplane selected as a reference design is the L-1011-500 ACS. The airplane 3-view is shown in Figure 6. This configuration has a maximum gross weight of 504,000 pounds and a payload of 40,000 pounds at a range of 5200 nautical miles. The cruise Mach number is 0.83 and the cruise altitude is 37,000 feet. This version is a long-range derivative of the L-1011-1. Active control technology was used to minimize structural wing changes when the -500 wing span was extended to improve fuel economy. The maximum design zero fuel weight is 338,000 pounds. The typical operating empty weight is 252,000 pounds.

Computer Program Validation

All major computing programs (FAMAS, NASTRAN, etc.), except the weight distribution program, the panel sizing and allowable program, the fully stressed design sizing program, and the program for structural resizing for flutter, were used in the production design of the basic L-1011 and its derivatives.

The validation process reduces to the following tasks: 1) to verify that the existing computer programs and systems operate properly in the CBUS environment, 2) to verify that the many pre- and postprocessor modules do what they were designed to do, 3) to verify that the CBUS data management systems properly function in their storing and retrieving modes, 4) to generate comparative data for programs not extensively used.

The initial validation of the CBUS operating system occurred in 1976-77 time period. Many tests were conducted to ensure that the role of the monitor along with the resource allocator were equivalent to the batch entry mode for any target program. Check cases were generated in the standard batch and compared with comparable CBUS computer runs.

The pre- and postprocessor outputs were compared to known data files. The postprocessors which processed the results and displayed the output in a graphical form were valuable in making questionable data inputs and other problem areas visible.

Checks for the run data management system (RDMS) were performed by comparing CBUS generated files with known data files. Many indirect checks were made by comparing the outputs of programs using RDMS with results generated in normal batch.

The panel sizing and stress allowable procedure was checked against known allowable and sizing data for certain internal load conditions. As an additional check, the fully stressed design procedure was compared to the panel sizing procedure for compatibility. The weight distribution program has internal checks for mass and moments of inertia quantities. The results of the program were favorably compared to known mass distributions. The structural resizing for flutter programs also will contain internal checks in terms of reconciling the modules and sizing changes with the flutter results using the resized structural properties.

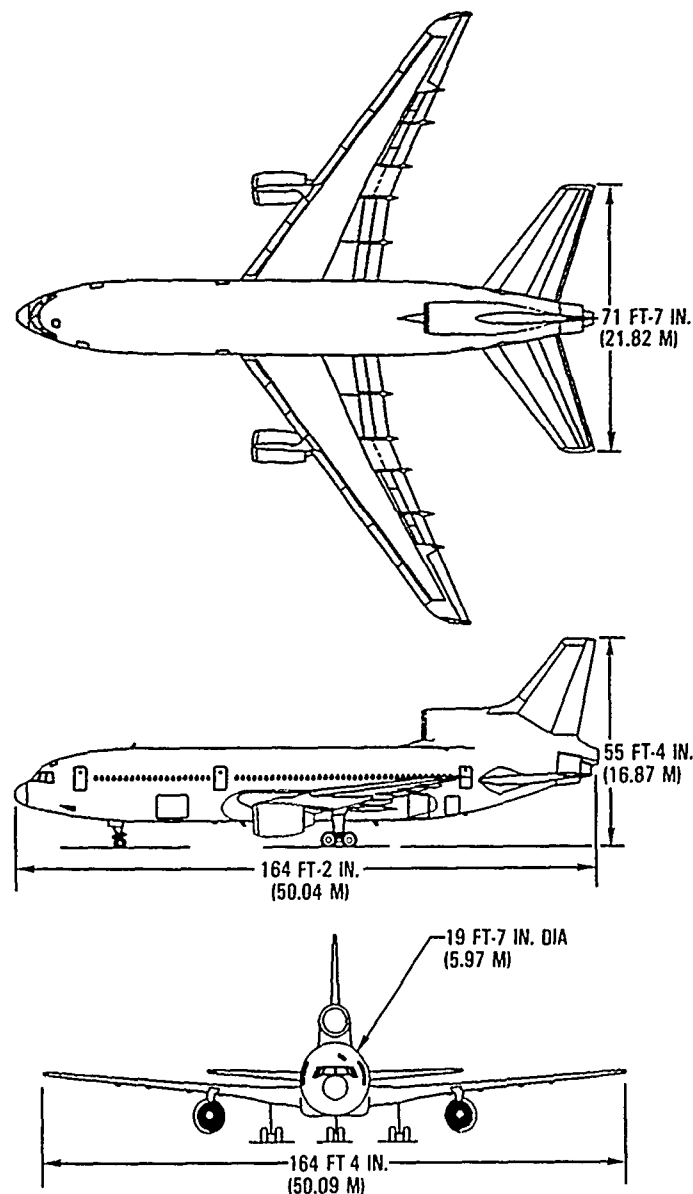


FIGURE 6. L-1011-500 ACS THREE VIEW

Design process validation

The final step in the design process validation is to generate airplane design characteristics of a known design from data and criteria normally available at the preliminary design level. The problem of validation, however, is compounded if some of the elements of the design process (i.e., how the final design was established) are ill-defined or not known. For this reason, the design process validation is currently limited to wing panel design.

The processors associated with the design process are described in Appendix B. Engineering Processes. There are two assumptions which govern the current implementation of these processors:

- Symmetric conditions only
- A limited number of flight conditions.

In addition, transient maneuver and static discrete gust loading conditions were deleted from the static loads processes. Part of the validation process is to review the assumptions and deleted tasks against the design results.

Two processes were identified to require additional definition: 1) model design factors, Figure B-4; 2) model weight to hardware weight factors, Figure B-1.

Two studies are being conducted. The first study is a weight comparison which compares subsets of model-weights from the finite element model with the reference airplane production model sizing. Production model sizing is derived from production hardware components for use in production stress analyses. Lower and upper panel hardware weights were computed over the same regions of the wing for which the subsets of model

weights were determined. Ratios of hardware weights to model weights are computed along the span. 1-13

The second study generates PADS sizing for zero margins of safety and for reference airplane production margins of safety. The difference between the reference airplane production model sizing and the PADS sizing may help establish the model design factor methodology, if no other significant unknowns appear during the design comparisons. Since static loads are the design critical loads on the reference airplane, gust loads generation was not included in the study. Flutter requirements on the basic L-1011 design were specified in terms of a minimum torsional stiffness requirement. The possible role of flutter requirements on the reference airplane will be assessed after strength design is completed. These studies are in progress; results to date are discussed in the next section. While flutter and gust loads were not used in the PADS sizing study, both processes were exercised using the production model sizing in order to validate the results of each discipline with known analyses.

NUMERICAL WORK IN PROGRESS

There are many design details which can not practically be included in a preliminary design effort. However, if these details add significantly to weight and strength, then some accountability must be made in the design process. One objective of this numerical exercise is to quantify some of the detail design effects in terms of two approximate processes. The first process, model design factors, will account for model sizing increases required to accommodate design details which currently do not have any design criteria. Two PADS sizings will be presented in the study of the model design factors: 1) structure sized to zero margins of safety, 2) structure sized to production margins of safety. The second process, model to hardware weight adjustments, will account for the differences between model weight derived from a finite element model representation of structural components and hardware weight derived from actual weighing of structural components.

Another objective of the design exercise is the evaluation of FSD in conjunction with the panel sizing (PSASA) program, which also produces stress allowables. Finally, the results of each engineering process will be checked for accuracy using the data base available for the reference airplane, namely the L-1011-500 ACS which is described in the validation section. The reference airplane has an active control system for maneuver load control (MLC). As part of exercising the PADS system, a wing panel sizing will be performed on the reference airplane with and without MLC for zero margins of safety. The results of the numerical study are summarized in Table 1.

TABLE 1. SUMMARY OF NUMERICAL RESULTS

I Weight Factors: Hardware Weight/Production Model Weight = 1.2						
II PADS Sizings: Normalized Surface Weights						
Zero Margins				Production Min. Margins		
	Upper Surface	Lower Surface	Both Surfaces	Upper Surface	Lower Surface	Both Surfaces
Reference Airplane				1	1	1
PSASA Sizing w/ MLC	.83	.764	.792	.89	.88	.89
FSD Sizing w/MLC	.845	.781	.808	--	--	--
PSASA Sizing w/o MLC	.89	.85	.868	--	--	--

Structural finite element model definition

The finite element model consists of three parts: 1) the wing, which is a full 3-D model, Figure 7, with a medium degree of detail, including control surfaces, flaps, gears, and leading and trailing edge structure; 2) the fuselage over the wing box, which is a full 3-D barrel section; and 3) the forward fuselage, aft fuselage, and the empennage, which are modeled with beam elements. There are 3,741 degrees of freedom in the NASTRAN F-set, 228 degrees of freedom for the definition of the structural influence coefficients, and 161 for the A-set stiffness matrix. The wing contour data base was obtained from the aerodynamics representation used in drag and lift studies. The ribs were modeled one model rib to two airplane ribs. The finite element layout for panels (upper) is shown in Figure 8. The panels were modeled using a Lockheed/NASTRAN quadrilateral membrane element which includes separate input of the stringer characteristics.

Weight

Weight was distributed over 501 panel points. An ASSET Group Weight Statement

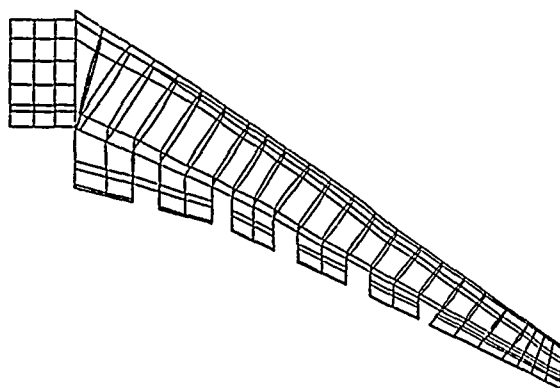


FIGURE 7. WING SECTION 3-D STRUCTURAL FINITE ELEMENT MODEL

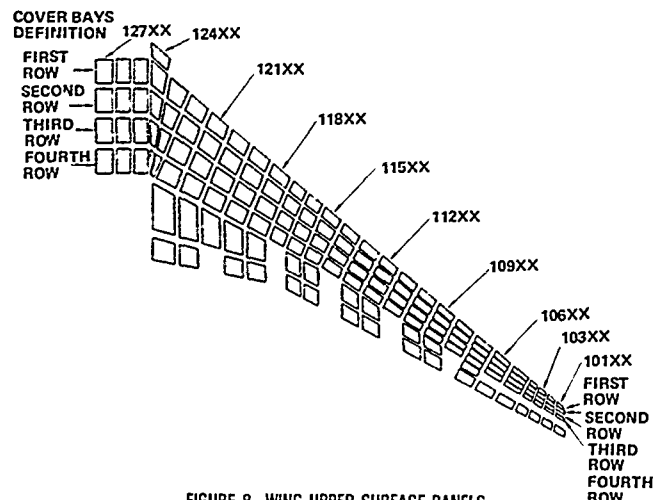


FIGURE 8. WING UPPER SURFACE PANELS

provided the component weights which correspond to the actual hardware weights. Standard normalized curves were used for span and chordwise distributions. Fuel volume was computed from 3-D computer drawings.

Static loads

Flight conditions were selected on the basis of a subset of the critical loads for the production airplane wing box. Both active controls on and active controls off conditions were used for symmetric maneuvers. Ground handling (brake roll, etc.), and a pseudo taxi condition were also included. The airplane was trimmed for each flight condition, thereby producing net balanced airplane loads. The 25 load conditions are listed in Table 2.

TABLE 2. STATIC LOADS CONDITIONS

LOAD COND.	A	B	C	D	E	F	G	H
Flight Cond. No.	1101	1102	1103	1104	1105	LANDING	TAXI	BRAKE ROLL
Weight — 1000 lb	350.3	504.0	504.0	504.0	504.0	368.0	506.0	506.0
C.G. — % MAC	12.5	17.13	17.13	17.13	17.13	26.9	14.1	26.9
Flight Cond.	Mid-Cruise	Va	Vc	Vd	Flap Ext.	—	—	—
Mach No.	0.8	0.48	0.82	0.88	0.33	0.28	—	—
Ve — KEAS	360.0	316.0	356.0	418.0	220.0	182.0	—	—
Altitude — 1000 ft	20.0	0.0	21.3	17.3	0.0	0.0	—	—
MANEUVER CONDITION			ACTIVE CONTROL (MLC)			LOAD CONDITION		
1G Level Flight — (Basic)			ON			A		
Positive Steady Maneuver — (PSM)			ON			A thru E		
Negative Steady Maneuver — (NSM)			ON			A thru E		
Positive Steady Maneuver — (PSM)			OFF			A thru E		
Negative Steady Maneuver — (NSM)			OFF			A thru E		
Landing			ON			F		
Landing			OFF			F		
Taxi			—			G		
Brake Roll			—			H		
<hr/> 25 Loads								

Stress

A panel sizing and stress allowable (PSASA) process uses internal load intensities from the finite element model to select the sizing necessary to satisfy strength, fatigue, and many other design criteria. This inhouse procedure is used to compute margins of safety for production designs. The process also makes use of a special data base to reduce the computer run times, an important factor in an iterative procedure. The data base is keyed to two configurations, namely Z-stringers for the upper surface and J-stringers for the lower surface. Materials for both configurations were 7075-T7651 plate for the skin and 7075-T6511 extrusion for the stringers.

The reference airplane production minimum margins of safety were taken from the stress reports. The grid in the stress report did not coincide with the panel layout shown in Figure 8. A linear interpolation was performed on the production margins of safety without regard to loading condition compatibility. The margins of safety for the wing box, however, did not exist. The wing box margins of safety were therefore set to zero.

Flutter

A flutter analysis on the reference airplane using production model sizing generated

stability V-f-g plots for variable density solution of the flutter equation. A Doublet Lattice unsteady aerodynamics program generated the aerodynamics for nine reduced frequencies at Mach 0.88. The flutter analysis used 20 natural vibration modes. Vibration modal displacements and V-f-g plots were produced.

Vertical Gust

A vertical gust analysis was also performed on the reference airplane using the production model sizing and aerodynamics generated in the flutter analyses. The pre- and postprocessors and the primary gust modules were only exercised up through panel and integrated loads. This includes frequency response functions, power spectral densities, root-mean-square (rms) values for unit (1 ft/sec rms) gust, frequency of peak values and selected correlation coefficients. A separate weight condition and vibration analysis were produced. Neither the vertical gust nor the flutter analyses were performed on the structures generated by the PADS's sizing process.

Baseline analyses and results

Internal loads and deflections were computed using production model sizing and the results were compared for reasonableness to known quantities. The analyses were continued through flutter and gust. The unsteady aerodynamics were compared with production kernel function aerodynamics. Checks were made on the weight matrix and the stiffness matrix. The overall results were good to excellent. The gust results are currently being evaluated.

A major effort was made to establish empirical weight factors between the production model and hardware weights. NASTRAN was used to compute model weights for seven chordwise bays for each wing structural component. Hardware weights were then determined for the same bays and structural component definitions. The overall hardware/model weight factor for the panels was 1.2. The hardware to model weight factor distribution with span is shown in Figure 9. The spanwise variations of the factors were greater than expected.

The PADS design process for zero margins

The design process followed the path outlined in Figure 5. First, a bones drawing defined the critical coordinates for the structural finite element model generator. A structural (finite element) model generator was available on a computer file and most of the dependent displacement equations were directly applicable. With the structures geometry table and initial processor runs for weight, static loads, and flutter completed, the PADS command for grid transformations generated the transformation matrices for the rigid airplane static loads computations. All finite element sizing except for the upper and lower panels was taken from the production data base. The upper and lower panels included stringer definitions as well as skin thicknesses. The region to be sized included both the wing center box and the outer wing sections. The maneuver load control (MLC) reflected the production configuration. Theoretical aerodynamics were used.

The first sizing run, which included the generation of internal loads based on the static loads for a rigid airplane, uniform panel sizing, and one pass through the PSASA process, produced reasonable results. The structure was sized for zero margins of safety. The process continued with the computations for the flexibility matrix, static loads for the flexible airplane and another pass through the PSASA process. The second sizing reflected the load relief provided by the airplane flexibility. The process continued with another pass through the PSASA program to produce a third sizing. Then using the second flexible loads, the FSD produced another sizing.

Results for PADS design with zero margins

As shown in Figure 8, the panels for the wing box are arranged in four strips or bays, each bay going from wing tip to fuselage center line. The first three digits of the panel ID designate the panel element location within the bay. Figures 10 through 17 show upper and lower panel unit weights versus the panel ID for reference airplane production sizing, rigid airplane loads sizing, first and second flexible loads sizing.

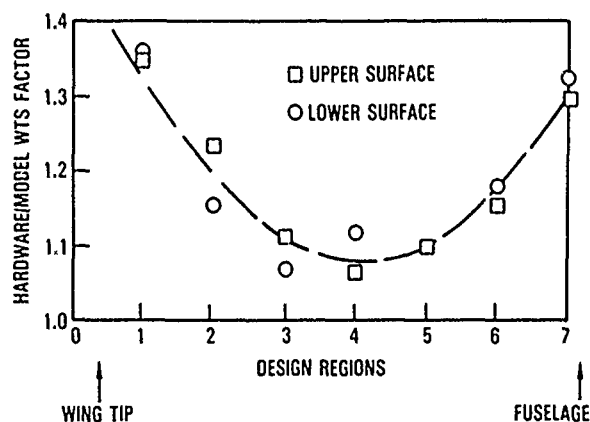


FIGURE 9. MODEL WEIGHTS TO HARDWARE WEIGHTS FOR COVER PANELS

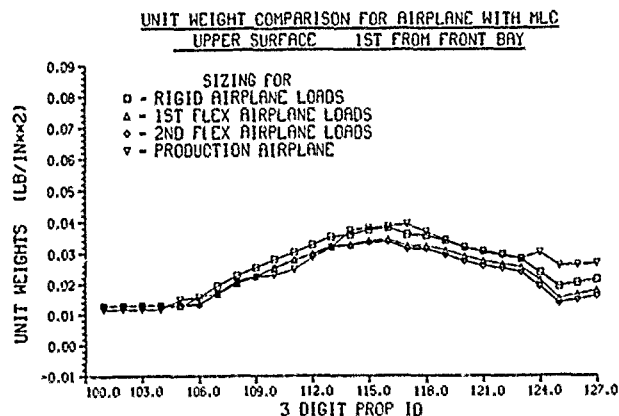


FIGURE 10. UPPER SURFACE FIRST UNIT BAY WEIGHT WING DISTRIBUTIONS FOR ZERO STRUCTURAL MARGINS OF SAFETY

1-16

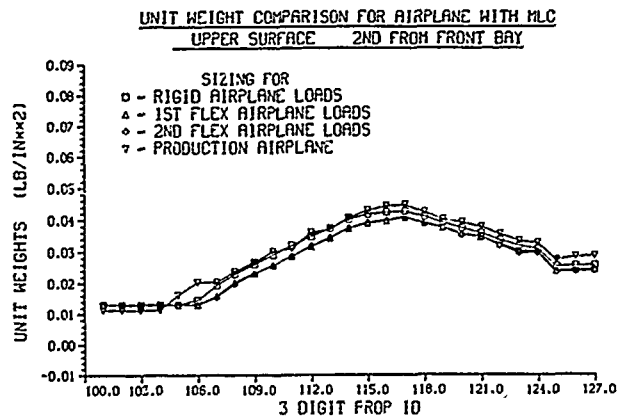


FIGURE 11. UPPER SURFACE SECOND UNIT BAY WEIGHT WING DISTRIBUTIONS FOR ZERO STRUCTURAL MARGINS OF SAFETY

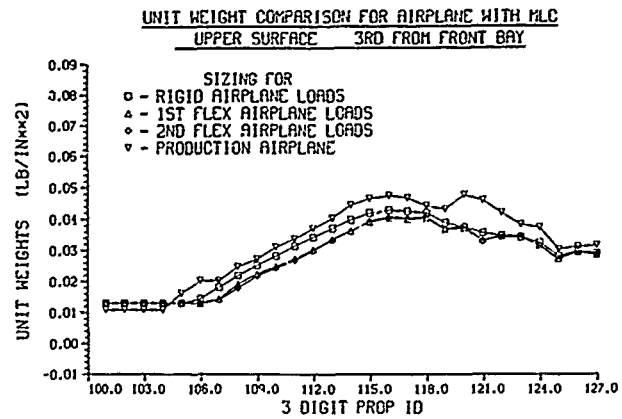


FIGURE 12. UPPER SURFACE THIRD UNIT BAY WEIGHT WING DISTRIBUTIONS FOR ZERO STRUCTURAL MARGINS OF SAFETY

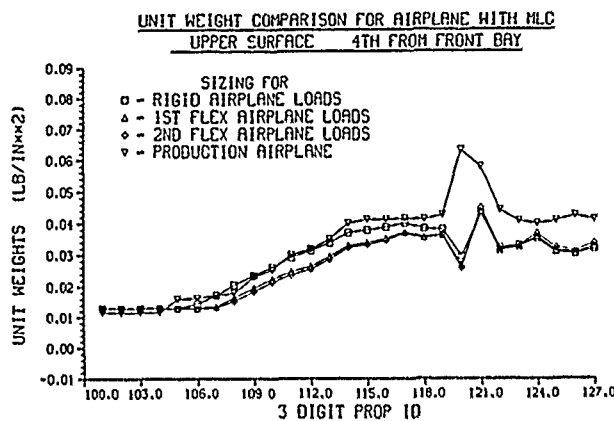


FIGURE 13. UPPER SURFACE FOURTH UNIT BAY WEIGHT WING DISTRIBUTIONS FOR ZERO STRUCTURAL MARGINS OF SAFETY

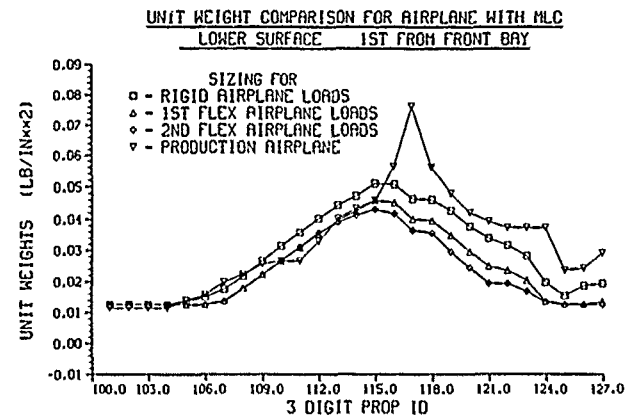


FIGURE 14. LOWER SURFACE FIRST BAY UNIT WEIGHT WING DISTRIBUTIONS FOR ZERO STRUCTURAL MARGINS OF SAFETY

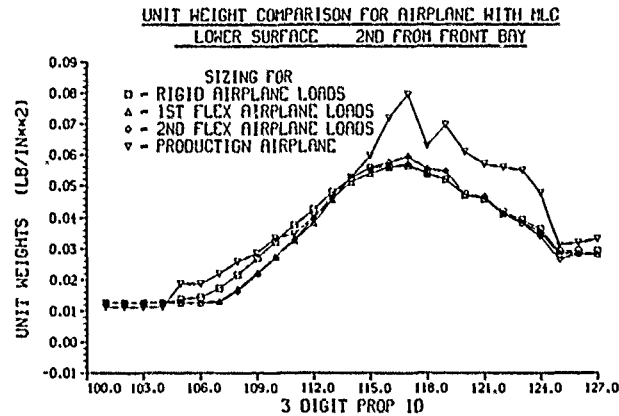


FIGURE 15. LOWER SURFACE SECOND UNIT BAY WEIGHT WING DISTRIBUTIONS FOR ZERO STRUCTURAL MARGINS OF SAFETY

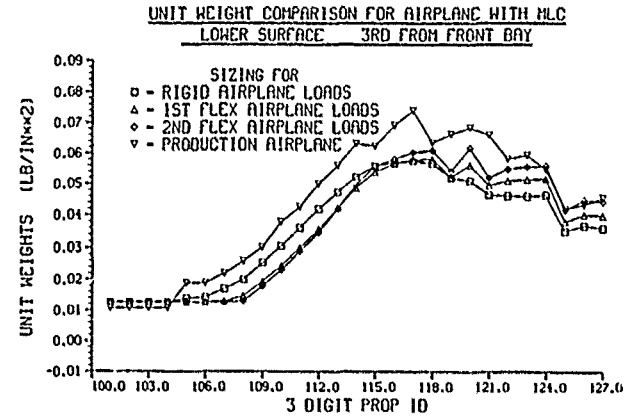


FIGURE 16. LOWER SURFACE THIRD BAY UNIT WEIGHT WING DISTRIBUTIONS FOR ZERO STRUCTURAL MARGINS OF SAFETY

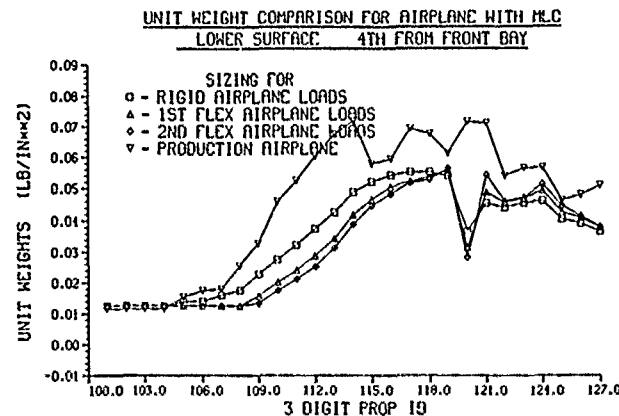


FIGURE 17. LOWER SURFACE FOURTH UNIT BAY WEIGHT WING DISTRIBUTIONS FOR ZERO STRUCTURAL MARGINS OF SAFETY

The plots show significant differences between reference airplane production model sizing and the PADS sizing results. The PADS sizing was 21 percent lighter than the production model sizing. Figures 18 and 19 show the unit weight differences between production sizing and the PADS sizing in an isometric view of wing planform. The differences in skin thicknesses exceed 0.25 inches (0.64 cm) in some areas of the wing. These results are currently under review.

1-17

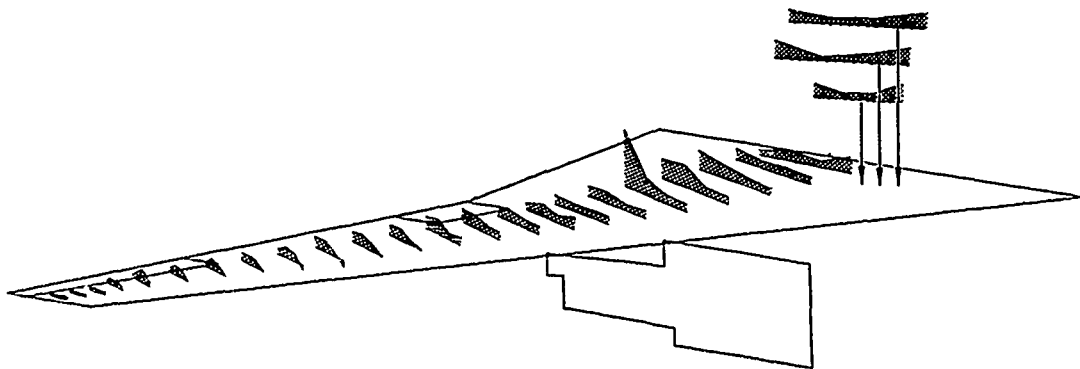


FIGURE 18. UPPER SURFACE PRODUCTION MINUS PADS SIZING UNIT WEIGHTS FOR ZERO STRUCTURAL MARGINS OF SAFETY

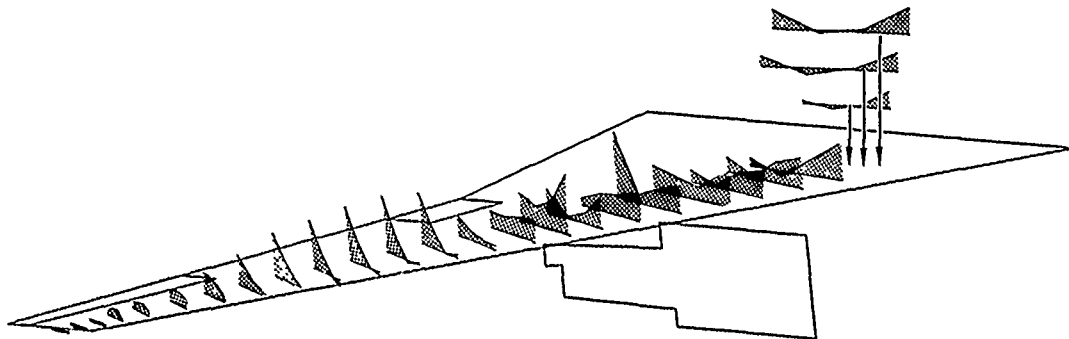


FIGURE 19. LOWER SURFACE PRODUCTION MINUS PADS SIZING UNIT WEIGHTS FOR ZERO STRUCTURAL MARGINS OF SAFETY

The FSD sizing showed reasonable agreement with the PSASA sizing for some regions of the wing and more than expected variations in other areas. The difference in total panel weight was 1.6 percent with the FSD solution being the heavier of the two. These results will require more study and experimentation. The formulation of the stress interaction curves in the FSD program will probably be the first area to be reviewed.

Results of PADS design using production margins of safety

Two passes were made through the PSASA procedures using the reference aircraft interpolated production margins of safety. The comparison with production model sizing shows a significant improvement over the PADS results for zero margins. The PADS sizing was 11 percent lighter than the production model sizing. Figures 20 and 21 show the unit weight differences between production sizing and the PADS sizing for production margins in an isometric view of wing planform.

Sizing without MLC for zero margins

Using the second flexible static loads sizing with MLC and zero margins of safety as the starting point, airplane wing panel sizings were generated for an airplane without MLC. The first pass used the second flexible loads with MLC. The loads for MLC-on were removed from the stacking matrix and the remaining loads, MLC-off, which had been defined at lower load factors to reflect the low exposure, were factored to represent loads for an airplane without MLC. NASTRAN then was used to compute internal loads for input to the PSASA process. Using the sizing output of the panel sizing effort, NASTRAN was used to compute the flexibility matrix and the static loads were updated. New internal loads and sizings were generated. The internal loads and sizing procedures were then repeated while holding the external loads constant.

Results for airplane without MLC for zero margins

The objectives of these sequences of calculations were twofold: 1) to determine the weight increment in the panels for an airplane without MLC (w/o MLC), 2) to determine the convergence of the PSASA process while holding the external loads constant.

The panel's model weight w/o MLC was 6.8 percent over the PADS design with MLC (w/MLC). Figures 22 and 23 show the convergence of the panel sizing program for the third-from-front bay. This bay showed the largest variations in the unit weights.

1-18

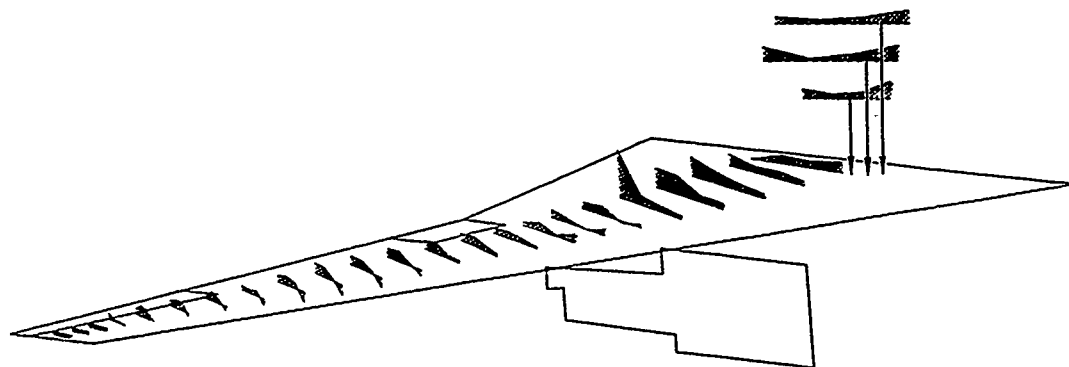


FIGURE 20. UPPER SURFACE PRODUCTION MINUS SIZING UNIT WEIGHTS FOR PRODUCTION STRUCTURAL MARGINS OF SAFETY

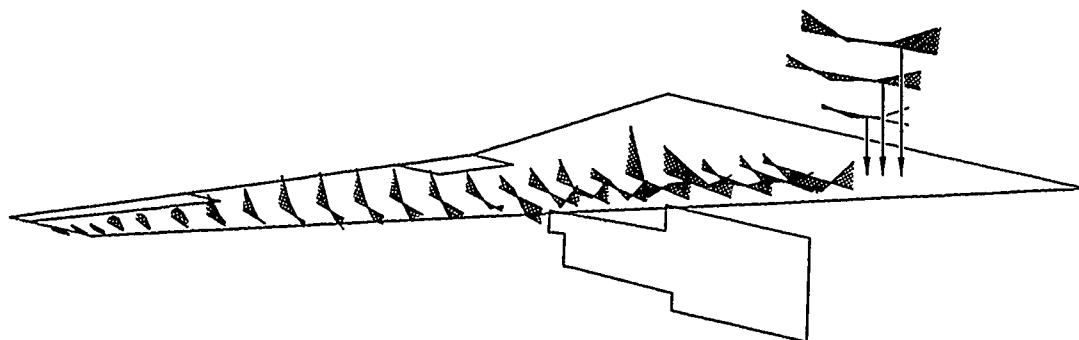


FIGURE 21. LOWER SURFACE MINUS PADS SIZING UNIT WEIGHTS FOR PRODUCTION STRUCTURAL MARGINS OF SAFETY

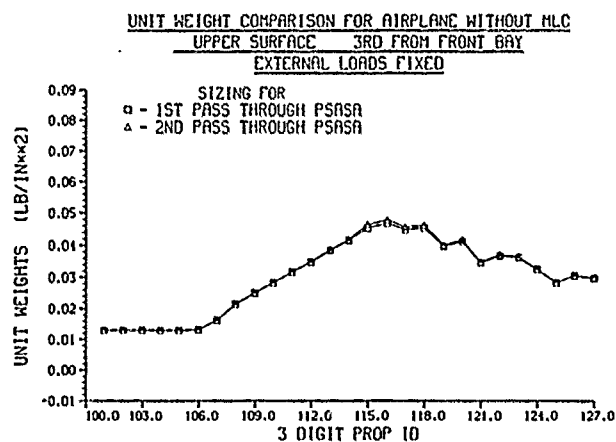


FIGURE 22. PSASA SIZING CONVERGENCE FOR THIRD BAY UPPER COVERS

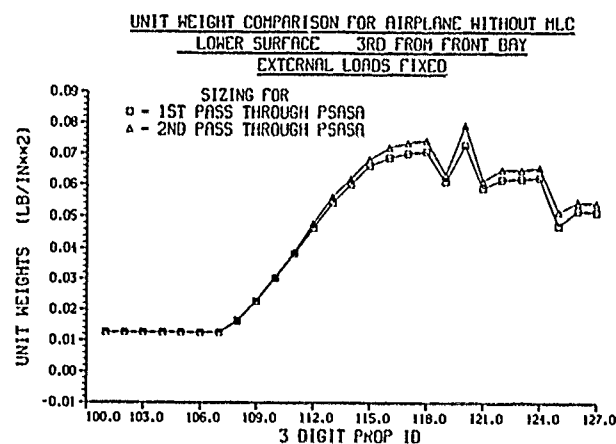


FIGURE 23. PSASA SIZING CONVERGENCE FOR THIRD BAY LOWER COVERS

Computer run statistics

The following PADS computer run statistics were compiled for the computer job submittals that generated the results published in this paper. The statistics exclude computer runs required to generate the structural finite element model.

There were 15 PADS job submittals under CBUS. They were equivalent to 167 non-CBUS job setups. There were 358 entries into RDMS and other data base management systems for matrices, card image data, and tables. NASTRAN was accessed 11 times; FORTRAN programs were accessed 72 times; FAMAS system was accessed 55 times; PL/I programs were accessed 19 times. The computer runs generated 850 output matrices, 30 card image data sets, and 325 plots.

Elapsed time statistics

The following elapsed time statistics include computer job setup times for the task. It does not include the time required to generate the basic input data sets for the various disciplines. It does include modifications to the input data sets. Normally, the computer jobs are prepared for submittal during the normal work shift and the computer jobs are processed overnight. The level of effort is effectively one person.

- One day..... one pass through static loads, internal loads, sizing, stiffness and flexibility matrices, and flutter
- Three days.. grid transformation, weight, ... , first flex loads
- Seven days.. wing configuration change up to first flex loads.

1-19

PADS DEVELOPMENT STATUS

Engineering processes

The status of PADS development is summarized in Table 3. The first column lists the eleven engineering functions discussed in Appendix B. Column two gives the percentage completion of basic technology module, development of which is not under the PADS charter but which is needed in order to generate the corresponding PADS process. Column 3 gives the percentage completion of the command. Column 4 is the percentage completion of automating the preparation of basic input data from generalized scalar libraries and other data sources. This is probably a never-ending effort. Column 5 lists the operational status of each engineering process. A yes indicates the process was used in a PADS design exercise. The percentage of completions quoted in the table serves to provide a rough measurement of progress to achieving the PADS goals which were stated in the INTRODUCTION. The perception of work to be done will change as more of the capabilities become operational.

TABLE 3. PADS DEVELOPMENT STATUS

Col 1 Engineering Process	2 Tech % Completion	3 Commands % Completion	4 Auto Input % Completion	5 Production Status
Weight	80	80	30	yes*
Grid Transformations	95	95	75	yes
Finite Element Modeling	80	50	50	yes**
Stress				
Panel Sizing and Stress Allowable	95	95	50	yes
FSD	100	95	50	yes
Adjusted Sizing	0	0	0	NO
Static Loads	95	95	30	yes
Steady Symmetric Maneuver				
Landing	95	95	30	yes
Brake Roll				
Pseudo Taxi				
Flutter	100	100	75	yes
Resize for Flutter	70	50	30	NO
Gust Loads	80	50	50	yes*
Taxi Loads	80	30	30	NO
Landing Loads	80	0	0	NO
Active Controls Synthesis	50	0	0	NO
* = 50% completed ** = not a PADS command				

Since PADS development is based on the integration of existing computing systems by extensive use of pre- and postprocessors, all of the programs developed to automate the data flow are available outside of the PADS/CBUS system through normal batch access.

There are currently 400 CBUS system commands and macros for the PADS effort. The user typically codes the input deck with references to no more than 50 individual commands and supercommands.

CBUS operating system

The CBUS operating system development is 90 percent complete. Although a scalar library is in the system's architecture and has been coded, testing of the capability of scalar libraries, and, more important, the development of ground rules for their naming and control have not been completed.

Documentation

Documentation is currently the pacing item to making the PADS/CBUS system a full production tool. The immediate need is the formulation of comprehensive user and system manuals. The user manual will be an interactive query program along the lines of a computer HELP program. This program would permit the uninitiated user to pick commands

1-20 from a menu and to ask for guidance in the application of the particular command. The help feature will also output a PADS user deck at the user option. The user will also have the option to produce a hard copy of the user manual.

Future work

The first order of business is the completion of the design of the reference airplane and the resolution of the engineering processes which are required for preliminary design. The PADS capability will then be applied to the study of the effect of wing aspect ratio and wing thickness/chord ratio on fuel efficiencies.

This Lockheed inhouse work is being coordinated with NASA's Langley Research Center multilevel design research activity under a cooperative effort to design an aircraft wing for fuel efficiency. The primary objective of this effort is to study and evaluate the multilevel and the PADS/ASSET approaches to aircraft wing design. Lockheed is providing a common design data base for this effort to NASA under the contract NAS1-16794. The contract technical monitor is Dr. J. Sobieski. The first phase of this study is projected for completion November 1984.

CONCLUSIONS

- A rapid aeroelastic analysis and design capability has been acquired by adapting existing engineering methodology and the associated computer tools to the requirements of preliminary design.
- The PADS goal of developing a computer operating system and design methodology to generate an accurate aeroelastic design within the conceptual and early preliminary design phases has been substantially demonstrated.
- The CBUS operating system satisfied the requirements for flexibility and modularity and achieved all objectives stated in the operating system specifications.
- The CBUS operating system and the run data base management system satisfied all requirements for validation.
- The validation and testing of the design and engineering processes is not complete.
- A PADS type of operation requires a high degree of coordination among the disciplines. Adequate design visibility and control must be addressed.

The following observations are provided as a summary review in support of the above conclusions:

CBUS Operating System

- An operating system has been defined and coded which provides the user with a continuous computing operation without interfering with the standalone function of any participating program or system.
- The concept of a command has been developed as a driver for the data flow control and program execution requirements of an engineering process.
- The concept of altercards provides data paths into the command to change default attributes and/or to invoke other options.
- A command processor language has been developed which provides logical branching capabilities but leaves the naming of the commands/macros to the user.
- The concept of a supercommand provides the grouping of commands and other supercommands and includes all the command processor language capabilities.

Data Management System

- All existing data management systems are available to provide retrieval and storage of permanent data blocks and communication with these systems is achieved by means of commands and subcommands.
- An internal data management system has been defined which supports the retrieval and storage of data by simple qualifiers so as to retain the simple functionality of a command.

Design and Engineering Processes

- An aeroelastic design process has been defined in terms of production design computing tools and without violating the conceptual and early preliminary design phase elapsed time constraints.
- The design process has been modularized into specific engineering processes that closely followed the production design definitions.
- The concept of a finite element model generator for a family of aircraft structures has been formulated to satisfy the elapsed time constraints.

Validation Using a Known Design Data Base

- The model to hardware weight ratios showed greater than expected variations with 1-21 span.
- The engineering processes defined as the panel sizing and stress allowable generator, fully stressed design, weight, static loads, gust loads, and flutter were exercised and checked using a known aircraft design data base.
- The PADS wing panel sizing of a reference airplane design produced panel model weights that were 21 percent below the reference airplane values for zero structural margins of safety. The difference was reduced to 11 percent when production structural margins were used in sizing the panels.

APPENDIX A - CBUS OPERATIONAL CHARACTERISTICS

Initialization procedure

To begin, the computer operating system (OS) executes the CBUS monitor program, and the CBUS operating system prepares to run the initial entry procedure. The software recognizes as shown in Figure 2 by means of the first time flag that this is the first entry into the monitor and that it has no data to pass on to the resource allocator; so control via the monitor passes to the command processor for instructions on proceeding.

The command processor in turn knows from the monitor that it is making the initial entry and looks to the user-supplied data stream to find out what it is to do. At this time the command processor does not have access to commands or macros with which to interpret the user input data. Therefore, as part of the initialization phase, a data set is supplied to the CBUS operating system which contains the commands necessary to interpret the first command requested by the user. The command processor reads the START data set which includes commands such as START and RESTART and uses these commands as the initial library of commands with which to interpret the user commands. The CBUS operating system initialization procedure then is completely controlled by the user. The initialization procedure is outside the operating system and is entirely encoded by commands in the same manner that commands are written for any other function. The initialization phase of the CBUS operating system is completed when the command processor interprets the user's first command and returns control back to the monitor.

Run Data Management System

RDMS is a standalone program that provides the CBUS operation with a facility to store and retrieve certain data blocks to be used during the computer run. The RDMS is exclusive in one area: commands/macros to be used by the command processor are assumed to be stored in this system. The data blocks which the system will accept are 1) fixed length 80 column records, 2) two-dimensional arrays known as matrices, 3) NASTRAN tables using variable length records. As the need arises, other data block formats may be included in the system.

RDMS uses one file to store the physical data blocks and another file to catalog the data qualifiers and the pointer data for random access to the stored data blocks. This random access system is known as "NOTE/POINT". The system uses IBM Basic Sequential Access Method (BSAM) which provides both sequential and direct access. Direct access is provided through the OS/VS data management macros NOTE and POINT. NOTE returns the relative track address of the stored data block and POINT uses that address to position the physical device for reading the data block. Hence, the necessity of providing a catalog of data qualifiers and pointer data (track addresses).

Data qualifiers include the five digit matrix number, job number, section number, date, time of day, number of rows/number of records, number of columns, real/complex/general flag, and an eight character variable name. Data retrieval is possible by specifying qualifiers either on an individual or group basis.

RDMS is accessible by either a command or subcommand. It either loads data into files which will be needed by the next target for execution, or it stores data generated by the target for future reference. With this architecture, the data management system is uncoupled from the target data requirements. If another data management system is required, the only change would be to the data store and retrieval commands and subcommands.

Data blocks naming conventions

The concept of commands would be significantly impaired if all data blocks required by a command would have to be named along with the command. The PADS approach was modeled on the experience of cataloging data blocks in Lockheed's FINDEX system. The FINDEX system catalogues data blocks with the following primary qualifiers: reference file number, the run section number, and the matrix number. Additional qualifiers of date and time are used to resolve ambiguities in the data request if there are multiple entries in FINDEX with the same first three qualifiers.

In PADS, a matrix number is assigned to each data block used in the design process. The number is registered in the PADS data log book and is not changed between designs. The reference file number is reserved for a project type identification. The section

number is a five digit number which is subdivided into class number (one digit), design number (two digits), and user number (two digits). The class digit is currently not used. The user number returns to the batch users the equivalent of the whole section number. The design number is the identifier of the design cycle in the design process. All data references in a command are resolved except for the reference file number and the five digit section number.

This process is further simplified by buffering computing commands with data retrieval and data store commands. The run data management system (RDMS) has the capability to select data blocks by range of matrix numbers and by sub-groups. One specifies a set of data blocks for retrieval by the RDMS by specifying values of reference file number, input design number, and output design number and optionally one or more of the following: class number, user number, matrix number, and the eight character name. The RDMS returns to the system just those data blocks which carry sets of these identifiers with values matching ALL of the SPECIFIED values.

So instead of passing to the commands matrix numbers, section numbers, etc for input and output, only the input design number and the output design number need be specified along with the reference file number.

Alter Capability

A command includes all instructions and attribute default assignments necessary for execution. The functionality concept requires that the user be able to alter the command's default attributes. Attributes which could be candidates for change are names of data sets to be incorporated into the process, constants to be used in the computations, and naming of output data sets associated with the process. The alter capability also permits the complete definition of the function with all defaults, while retaining the flexibility to generate a radically new version of the function without creating and storing a new version of an existing command/macro code.

An alter capability is available at every level of the command/macro tier by providing an alter command card after the data line which is to be altered. The alter command line executes the prescribed alter function when the user supplies an altercard with the identical keyword which is also imbedded in the alter command line. The function capability of an alter command card is as follows: insert, integer, floating point, alpha, copy, put, delete, blank, else, and or. The insert function is one of the more powerful commands because it permits the insertion of other macros in the data stream. The most used functions are an integer, alpha, floating point, or exponential formats which override the designated fields on the preceding line. The user enters a keyword, followed by an equal sign, and lists the parameters to be used when the alter command line is executed. The input format for both the command line and the altercard is free form, a delimiter being either a blank or a comma. An example of alter capability follows:

```
THIS IS THE LINE TO BE ALTERED ; appears in the macro
@@@ keyword 13 4 ALPHA          ; is the alter command card
                                ; with the ALPHA function
```

If the user supplied the following altercard

```
keyword=CARD,
```

then the above line would read as

```
THIS IS THE CARD TO BE ALTERED.
```

With subcommands within commands within other commands, one subcommand is very likely to be referenced more than once within a command. The method used to migrate the proper user keyword to the intended subcommand is based on attaching another qualifier to the calling function invoking the subcommand. This additional qualifier may then be used as part of the extended keyword name. The extended keyword name would then consist of the keyword, followed by an underscore, followed by the additional qualifier. The same logic is used for duplicate commands within a supercommand. The extended keyword is additionally qualified by a double underscore followed by the qualifier attached to the command calling function.

The number of altercards often exceed a reasonable number and the cards have a tendency to clutter up the functional layout of the user deck. The user has the option to store altercards in an altermacro, which in turn is named as a single unit while invoking the command. Since altercards enter the system in a number of ways, a hierarchical stacking of altercards is necessary.

The altercards can be grouped into four categories: global, command user-supplied, subcommand default, and altermacro. Global altercards are those that the user can specify to apply to the entire run. Altercards supplied by the user under the command definition have the highest priority, and will override the global altercards. The altermacro, altercards imbedded in a macro, is placed below the global altercards and above the default cards supplied in the subcommand.

The subdivision of the aeroelastic design process into specific engineering functions is somewhat presumptuous, especially since the basic premise governing this approach is to retain, under each discipline's charter, the definition of what constitutes a design process as well as what is the methodology to be used. The naming of eleven major engineering functions, therefore, is only an attempt at quantifying the process while being fully aware of the need for flexibility and adaptability. For now, the eleven major engineering functions under consideration are: grid transformations, weight, finite element modeling, stress, static loads, flutter, structural resizing for flutter, gust loads, active controls synthesis, taxi loads, and landing loads.

Within each function, there are many processes involving input data preparation, computing, and evaluation of results. The ideal goal is to assemble one or two supercommands for each of the major engineering functions so that the complete design process could be defined by less than fifty user command cards. Some commands will define computing sequences while other commands will define data preparation and postprocessing of results. The automation of data preparation through the use of preprocessors, a library of common scalar values, and better operational functions involving tables is a never-ending task. In fact, the automation of data preparation and the presentation of results is the core of the PADS development.

Grid Transformations

The underlying premise to the development of PADS capability is the use of production tools and proven procedures to formulate the necessary analytical processes to be used in weight, flutter, loads, etc. This approach results in a general proliferation of grid/coordinate systems. A method was devised to generate systematically the transformations between the many grid systems without sacrificing flexibility.

The grid transformation process requires location and type-of-displacement labeling of the degrees of freedom (DOF) for the two grids involved in the transformation. However, certain sections of the airplane have special requirements concerning the transformation process; for example, aileron control surface mass elements should be beamed to flexibility degrees of freedom on the aileron and not to the degrees of freedom on the outer wing. So in addition to location and DOF information, the geometry table as shown in Table B-1 includes group identifications, such as inner wing, outer wing, aileron, pylon, fuselage, etc. The transformation between grids therefore is limited to boundaries defined by the airplane groups. The responsibility of generating geometry tables resides with the discipline which defines the grid.

TABLE B-1. GEOMETRY TABLE FORMAT

INFORMATION IN THE COLUMNS OF A GEOMETRY TABLE SIZE - N x 6						DESCRIPTION OF VALUE INSERTED IN COLUMN 2	
1	2	3	4	5	6	VALUE	DESCRIPTION
TYPE MATRIX	AIRPLANE GROUP	DEGREE OF FREEDOM	LOCATION IN SPACE			10.0101	WING BOX
			FS	BL	WL	10.0201	WING FIN
						:	:
						:	:

DESCRIPTION OF VALUE INSERTED IN COLUMN 1					DESCRIPTION OF VALUE INSERTED IN COLUMN 3	
	WEIGHT	STRUCTURE	AERODYNAMIC		DEGREE OF FREEDOM	VALUE
			LOAD	DOWN- WASH		
STATIC LOADS ANALYSES	1.0	2.0	5.0	5.0	X	1.
DYNAMIC LOADS ANALYSES	1.0	3.0	7.0	8.0	Y	2.
FLUTTER ANALYSES	1.0	4.0	9.0	10.0	Z	3.
					ϕ	4.
					θ	5.
					ψ	6.

Table B-2 summarizes the various grids used in the PADS aeroelastic analyses. The naming convention used in the table is based on Lockheed's conventions and not on any industry standard.

Weight

The weight process defines the mass, mass distribution, and mass moment of inertia for use in loads and flutter analyses. ASSET generates a Group Weight Statement, vehicle geometry description, mission profile summary, vehicle performance data, and production and operating cost estimates. Once output reasonableness has been established, this Group Weight Statement is utilized as the first mass estimate.

TABLE B-2. GRID DEFINITION SUMMARY

Grid No.	Type	Description	Trans to Other Grids	Responsible Discipline
1.	Weight	Where weight data is distributed for lumped and concentrated masses	2,3,4, 7.	Weight
2.	Structural Model	Where the full set of SICs is defined	10.	Flutter, Loads
3.	SIC	A reduced set of item 2., normally equal to item 2.		Dyn, Static Loads, Taxi, Landing
4.	Stiffness	A subset of item 2., where the stiffness is defined	7.	Flutter
5.	Unsteady Aero Force	Where the unsteady aerodynamic forces are defined	2,4.	Flutter, Dyn. Loads
6.	Unsteady Aero Downwash	Where the unsteady aerodynamic downwash is defined	2,4.	Flutter, Dyn. Loads
7.	Basic Loads	Where inertial and aero loads are combined; where dynamic loads are placed before stacking	2.	Static Loads
8.	Steady Aero Force	Where steady aerodynamic forces are defined	7.	Static Loads
9.	Steady Aero Downwash	Where steady aerodynamic downwash terms are defined	7.	Static Loads
10.	Finite Element Model	Where the finite element model DOF are defined	2.	Struct. Modeling Stress

Mass distribution is achieved through the use of similar aircraft component distribution data base. A suitable candidate distribution is chosen and modified to reflect anticipated changes in distribution. The total component weight is distributed with these normalized curves.

Fuel weight and distribution will be determined utilizing tank volumes calculated from the wing geometry data contained in the finite element model. Appropriate volume correction factors will be applied. Currently, fuel mass properties are determined through the CADAM fuel tank and mass distribution modules.

After the generation of the initial weight distributions, the next weight task is to provide a weight update process to incorporate derived sizing data. The weight update process starts with the adjusted model sizing (see Stress section) as shown in Figure B-1. With the computation of the model weights in the finite element grid, the next task is to map those weights into the weight grid. The model weights are then multiplied by empirical factors to reflect the differences between the ideal model weights defined analytically and the final hardware design weights. The output of the weight update process is an improved weight program input deck for the next sizing pass.

Finite Element Modeling

There are two forms of finite element modeling: 1) that which is required for stress considerations, and 2) that which is required for structural flexibility/stiffness considerations. The task here is to generate a finite element structural model computer data deck which will serve the objectives of both. Figure B-2 illustrates the various steps leading to a NASTRAN model deck. Critical to the quick design concept is a structural model generator (SMG) which would generate a family of finite element models using relatively simple inputs. These inputs would primarily be a function of the airplane external geometry and generally not a function of model configuration arrangements.

The 3-D modeling of the structure begins with a "bones" drawing of critical geometric control points to be used in the programs which generate and assemble finite element program input decks. The 3-D description for the wing is derived from a data base which Aerodynamics generates as part of their aerodynamic configurations studies. Control surfaces, flaps, and the associated actuation systems are modeled as necessary. Leading and trailing edge surfaces are modeled for load carrying requirements and not stress sizing.

Stress

The stress process generates sizing for those components of the structure which are not being sized for aeroelastic effects, and provides stress allowables for sizing structural elements based on strength and fatigue considerations. The model design

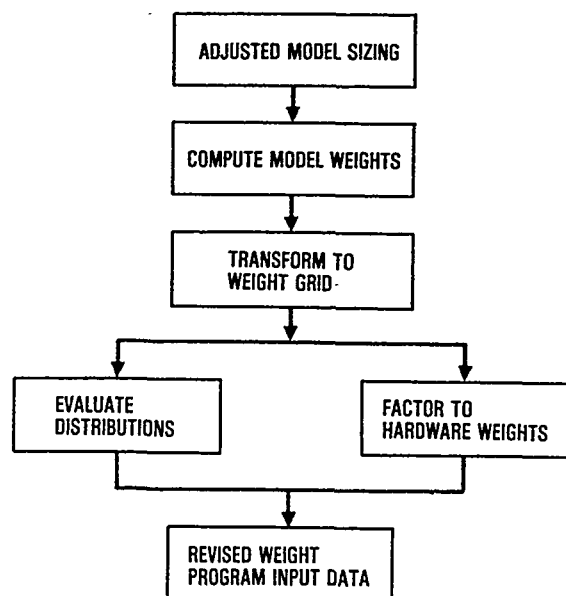


FIGURE B-1. WEIGHT UPDATE FUNCTION

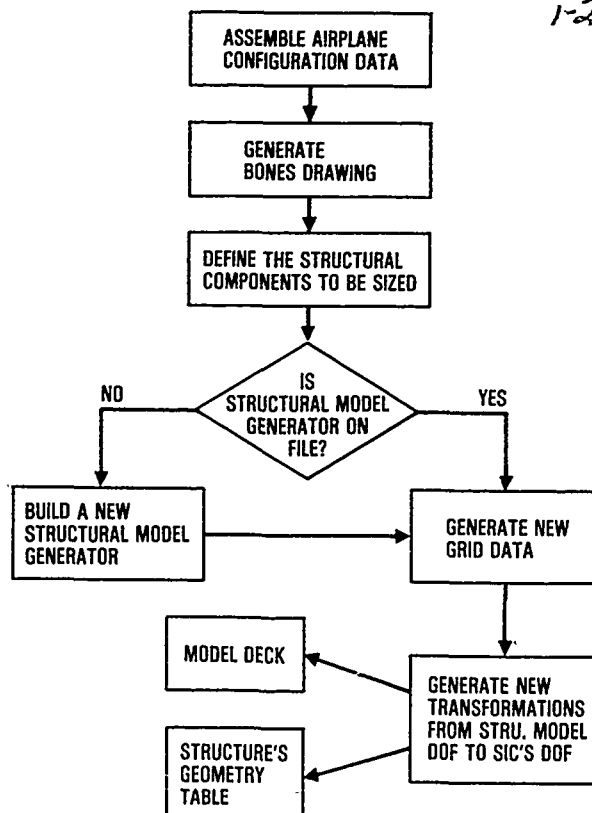


FIGURE B-2. STRUCTURE MODELING FUNCTION

factors methodology for conditions not covered by external loads, stiffness, and/or deflection requirements will also be required.

Two tools are available at Lockheed to size structural elements based on strength criteria, the fully stressed design (FSD) and the panel sizing and stress allowable (PSASA) program. Figure B-3 shows the possible paths to structural sizing, 1) PSASA for stress allowables and FSD for sizing, 2) PSASA for sizing.

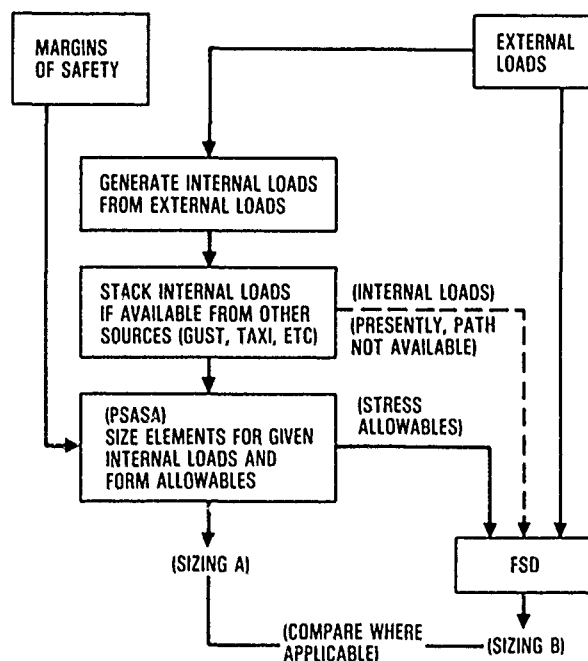


FIGURE B-3. STRESS SIZING FUNCTION

PSASA generates the stress allowables and new sizings for use in the fully stressed design (FSD) program. PSASA is a complex array of programs which permit production level computations of stress interactions for a variety of conditions including panel buckling and several local buckling modes. If the design involves only panels, then sizing is possible using PSASA. PSASA is currently limited to combined uniaxial and shear loadings. However, PSASA does accept as input margins of safety for each element being sized.

FSD requires a stress allowable for each element to be sized. The stress allowables

1-26 remain constant within NASTRAN as the elements are sized to the internal loads. The internal loads are computed from the updated sizings and the external loads. Three to four iterations are necessary for the process to converge.

The design factors that are not covered by available criteria and stiffness/deflection requirements include the local effects of access covers and other cutouts, landing gear chordwise loads, landing gear loads redistribution, stringer runouts, pylon attachment, and inner wing to center box attachment. As shown in Figure B-4, there are currently two approaches under consideration to accommodate design factors not covered by available criteria:

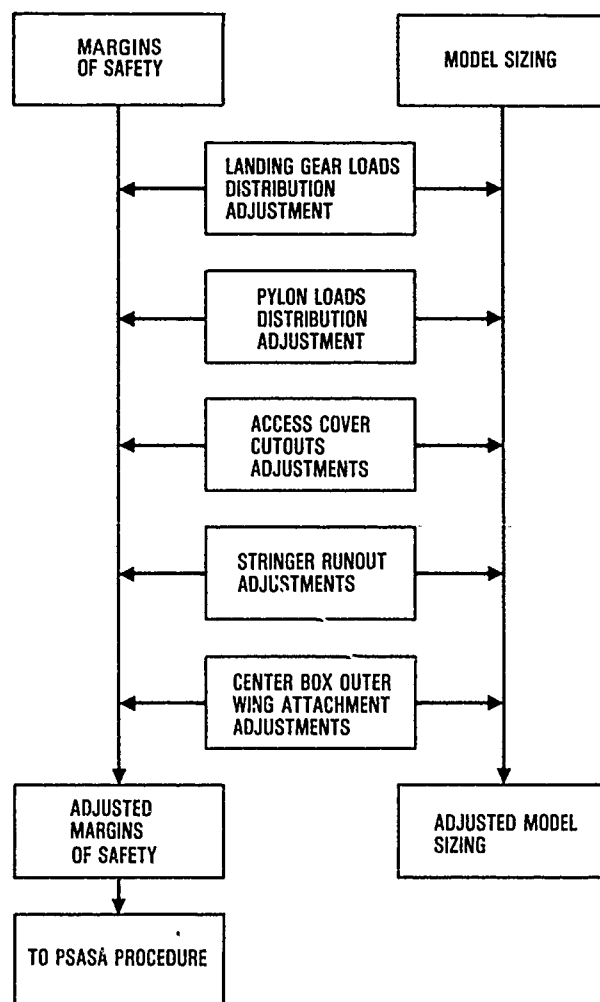


FIGURE B-4. MODEL DESIGN FACTORS

- Direct method - increase the strength sizing values
- Indirect method - modify the structural margins of safety

A methodology for generating model design factors is currently under study. Once the procedure becomes available, the adjusted model sizing will then be used, first to define the structure's stiffness and flexibility characteristics for use in flutter and dynamic loads analyses, and second to update the weight distributions.

Static Loads

The static loads process provides external net loads distributions for the complete airplane. Steady maneuver loads, as shown in Figure B-5, are derived for a trimmed aircraft with and without active control load alleviation for both rigid and flexible structures. The vortex lattice steady aerodynamics method is used to generate the aerodynamic influence coefficients (AIC). The methodology permits the use of aerodynamics data from other sources. The flexible airload distributions are generated using the AIC's from the theoretical vortex lattice procedure. Static loads can also generate transient maneuver and static discrete gust loading conditions.

Flight conditions from the flight envelope are selected when the criteria have been defined. The inertial loads and airloads are combined in the basic loads grid. Integrated section values of bending moments and shears, if needed, are also computed on this grid. The panel loads are then transformed to and stacked in the structural model grid for use in establishing model sizing.

Flutter

This process evaluates a design for structural/aerodynamic stability deficiencies. Flutter analysis consists of generating unsteady aerodynamics in the form of AIC matrices, forming a vibration analysis, and then assembling the elements into an eigenvalue problem. The process, as shown in Figure B-6, has been highly mechanized. A complete flutter analysis is possible after 4 to 8 hours of input data preparation. 1-27

The procedure, while highly mechanized, is also modular and therefore very flexible. Patches for nacelle aerodynamics, and adjustments to pylon flexibility have been implemented. The whole spectrum of active control functions from autopilot to flutter suppression may also be accommodated. The solution of the flutter determinant produces

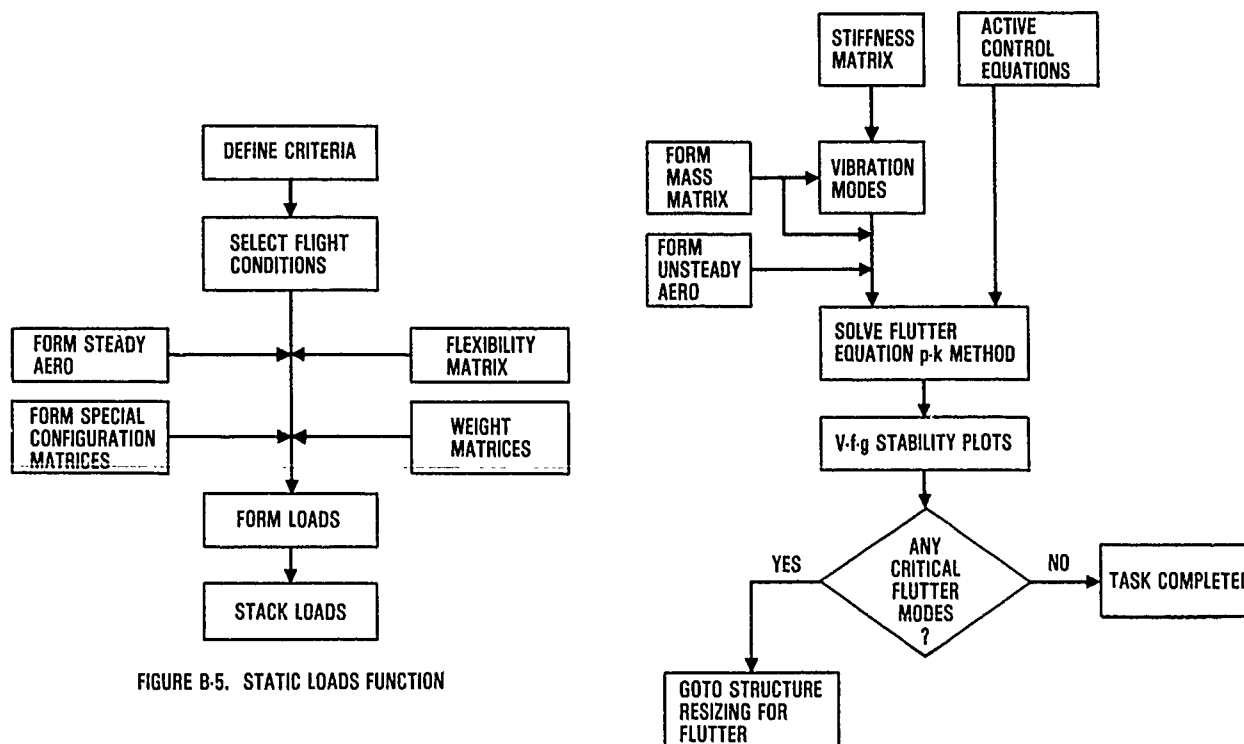


FIGURE B-5. STATIC LOADS FUNCTION

FIGURE B-6. FLUTTER ANALYSIS FUNCTION

plots of modal damping and frequency vs. airspeed. The method of solution is the p-k procedure.

Structural resizing for flutter

The structural resizing for flutter resolves flutter deficiencies by modifying the stiffness and weight distributions of the design as shown in Figure B-7. The first task defines the mechanism associated with the flutter deficiencies and establishes the areas of the structure which would be most effective in resolving those deficiencies. The second task is to define design parameters for specific areas of the structure and then to compute from the finite element model the mass and stiffness incremental matrices for a unit change in each parameter. Each design parameter will usually represent a collection of finite elements such as skin thickness in a specific area of the structure, which are slaved to the value of the design parameter.

The third task, known as initial resizing, computes flutter speed/damping derivatives and defines increments in design parameters necessary to resolve the flutter deficiencies.

The final task reduces the structural weight while holding the flutter characteristics fixed. This process is usually termed structural optimization for flutter.

Gust loads

The gust loads function provides either external loads or internal loads distributions for an airplane subjected to continuous atmospheric turbulence. Figure B-8 shows the general flow of analyses for the gust loads function. For most situations, a design envelope form of criterion will be selected over a mission analysis criterion, simply because a mission analysis approach is far too cumbersome to incorporate into the PADS system. At Lockheed, however, design to mission analysis dynamic gust loads is always a requirement. It is important, therefore, that design gust velocities for use in PADS be selected so that the resulting loads will match as closely as possible the mission analysis loads to be obtained later. A side study may be necessary for this purpose.

1-28

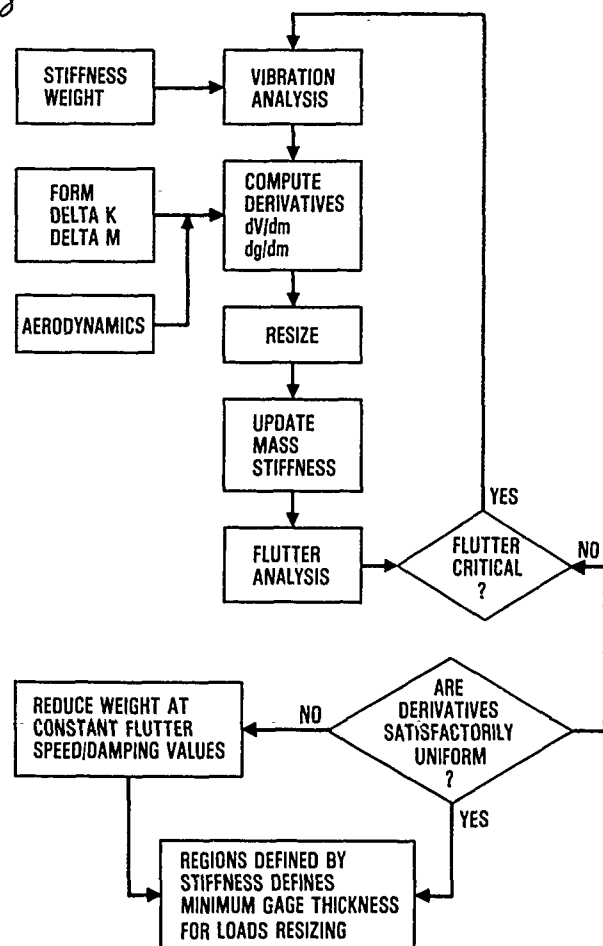


FIGURE B-7. STRUCTURAL RESIZING FOR FLUTTER

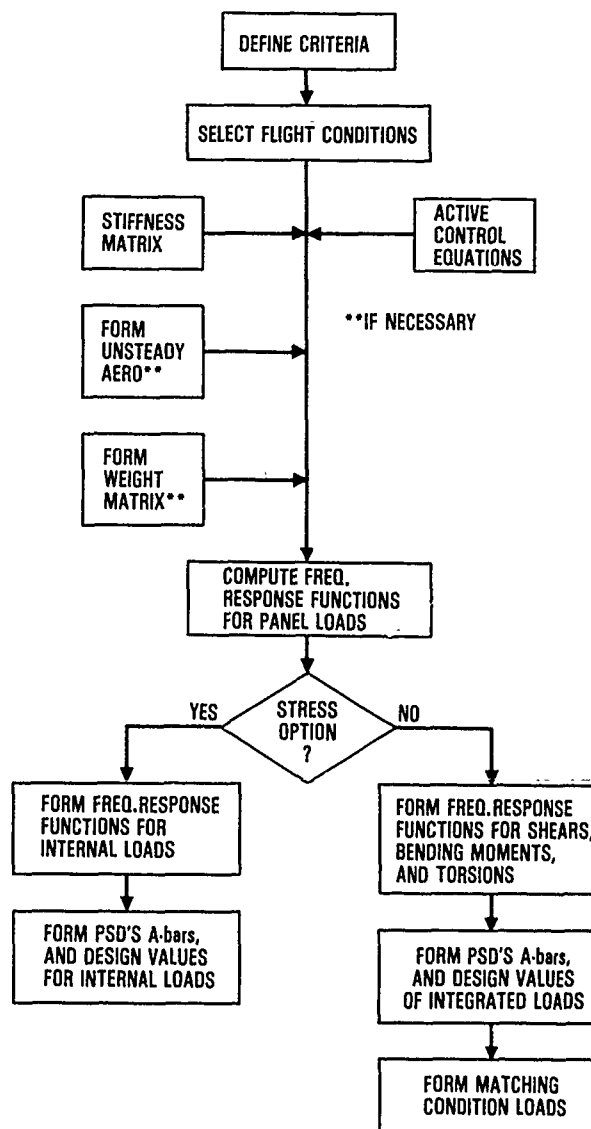


FIGURE B-8. GUST LOADS FUNCTION

There are three specific tasks to generate a gust input to the design.

As before, the first task is to select flight conditions which are anticipated to be critical for gust. The conditions may be selected on the basis of experience or as a result of side studies.

The second phase is to assemble the gust input data and to compute the airplane frequency response characteristics in terms of displacement response and the associated panel loads.

The third phase involves a choice between an external loads or internal loads approach. The external loads approach takes the panel loads in frequency response form and forms shears, bending moments, and torsions at specific sections in the structure. This is more suited to high aspect ratio wings than to delta configurations. The shear, bending moment, and torsion loads are then converted to power spectral density (PSD) quantities by using the gust power spectral density as represented by the Von Karman equation. Load quantities are then derived by integrating the PSD over the frequency to produce A-bar values (ratios of root mean square load to root mean square gust velocity). Multiplication by the design gust velocity, U_{σ} , then gives design loads. Since this process removes phase from the load quantities, a process known as matching condition generation attempts the best fit of all the A-bar load quantities to form distributed load conditions. Computed correlation coefficients are utilized in this process. The matched condition loads are then stacked with the external loads from static loads. The matching condition process, however, is highly interactive and does not lend itself to automation.

The internal loads distribution task is an attempt not only to overcome the automation difficulties of the external loads option but also to make the procedure more general in application to other planforms, such as the delta configuration. This approach takes the panel loads from task two (in the frequency response form) and converts to internal loads, using the finite element program. The internal load PSD's and A-bar's are then determined, and the A-bars are multiplied by U_{σ} to give design values. For each panel computed correlation coefficients (between say axial load and shear flow) are

1-29

utilized to establish appropriate internal-load combinations for design. These quantities are then used directly in the stress sizing function which designs the finite elements to satisfy internal loads requirements. Gust internal loads would then be another internal loads condition to complement the static loads internal loads.

Active controls

The active control function derives feedback control functions for load alleviation, flutter suppression, ride quality, gust loads alleviation, and handling qualities. This issue can either dominate the design process or help the traditional disciplines to achieve the objectives of the design without the full complement of structural weight which would be required for a design without active control systems.

The task for active controls then is to establish a basis for going to feedback control technology in exchange for structural weight and or drag. This evaluation is possible without deriving the control function in Laplace terms or digital filter terms. The methodology for accomplishing this is called the method of constraints.

The first phase in the method of constraints [Ref. 3] is to establish quantitative goals for flutter margin enhancement, gust loads reduction, etc. Then a sensitivity study is conducted to determine the suitability of existing control surfaces and the placement of sensors to achieve these targets. If the existing control surfaces are not suitable, then a simple trade-off should decide if another surface should be added to the design.

The next phase is to compute the feedback gains and phases required to achieve the derived values. The results are then displayed on a generalized Bode plot (one that includes both the frequency and damping of the motion) to establish the reasonableness of the combined set of gains and phases to achieve the desired results. This eyeballing of the gain and phase requirements into a curve is not a particularly difficult task and can be mechanized. When phase requirements for the same frequency are separated by more than 90 degrees, as is the common case where modes are closely spaced, the trade-offs on phase are made at the expense of increased gain values. The trade-offs are limited to producing acceptable gain and phase margin requirements.

The final step is the demonstration by means of appropriate analyses that the candidate generalized Bode plots (one for each control surface and sensor combination) indeed result in achieving the goals for flutter, gust, etc.

Taxi loads

The taxi loads process has as its output the identical two possibilities that the gust process presented, namely external loads and internal loads. While the gust process is a frequency domain problem, the taxi process involves a time domain analysis. The gear dynamics and the runway and taxiway surface models the airplane must taxi over are critical to the loads determination.

Landing loads

The landing loads function generates dynamic loads distributions for landing conditions. The approach is similar to the taxi and gust analyses but with more definitive design conditions. The principal loadings are down bending on the wing and fuselage loads.

REFERENCES

1. Thomas, R., A User Guide to the UNIX System, Berkeley, California, OSBORNE/McGraw-Hill, 1982.
2. Ralston, A., Ralston Encyclopedia of Computers Science and Engineering, second edition, Van Nostrand Reinhold Company, New York, New York, 1983, Page 892.
3. Radovcich, N. A., and Richman, R., "Active Control Synthesis by Method of Constraints Using Large Dynamic Models", AIAA paper NO. 81.0642-CP, AIAA Dynamics Specialist Conference-Atlanta, Georgia.

ACKNOWLEDGEMENTS

The author wishes to acknowledge his appreciation to the many colleagues who contributed to his education in the field of aeroelastic design, computer systems, and computer operating systems. He also wishes to express his thanks to the many who have assisted him with this paper, especially to Gernot Haggenmacher (Structural Methods), Herman Hassig (Flutter), Fred Hoblit (Dynamic Gust Loads), Dave O'Keefe (Static Loads), and Margaret White (Data Base Management Systems). He owes a particular debt to Dave Dreim (PADS system manager), without whose help and dedication the numerical results in this work could not have been produced. He is grateful to the ad hoc PADS development and design team for work spanning many years, especially, in addition to those mentioned above, to Burt Clanton (PADS programmer, RDMS), Roberto Contini (Structures, PSASA), Ruben Gloria (Flutter), Ron Jensen (Static Loads), Richard Levin (Stress), Larry Linner (Weight), Sanjeev Pathak (Structural Methods), Robert Peterson (grid transformation), Jan Sweers (Dynamic Gust), and Diane Slattery whose expert advice made the full use of FAMAS/FINDEX job entry and data management capabilities a painless operation. He is grateful also to Jim McIntosh (now with CADAM, Inc) who in 1976 responded to the need of a continuous computing capability and developed the software known today as the Monitor and the Resource Allocator, to Tom Dacon for assistance in the original development, and to Vic Davis for adding the ABEND features to the Monitor. Finally the author recognizes the work of Robert Richman for the initial development of the PADS commands and for the first PADS design exercise.

APPROCHE AEROSPATIALE DE L'ETUDE DU FLOTTEMENT
AU NIVEAU DE L'AVANT-PROJET

Michel CURBILLON
AEROSPATIALE - Division Avions
Direction des Etudes Toulouse
316, Route de Bayonne BP 3153
31053 TOULOUSE CEDEX

0. RESUME :

Par son importance du point de vue sécurité et certification, le comportement en flottement d'un avion est un élément à apprécier le plus tôt possible dans l'étude d'un projet.

En effet, la géométrie, la conception structurale et le dimensionnement peuvent être fortement influencés par ce phénomène.

Après avoir rappelé brièvement la formulation du problème pour en présenter les éléments essentiels, cette communication précise les objectifs d'une étude du comportement en flottement dans le cadre de l'avant-projet. Elle aborde ensuite le problème de la modélisation de l'avion pour le calcul des modes propres et les calculs de flottement proprement dits. Elle se termine par quelques exemples extraits d'études récentes de l'AEROSPATIALE.

SUMMARY :

By its importance from the safety and certification point of view, the flutter behaviour of a plane is a subject to be estimated as soon as possible in the study of a new project.

Indeed, geometry, structural conception and sizing could be strongly influenced by this phenomena.

After a short recall concerning the equations in order to present the most important factors, this paper defines the objectives of the flutter study at the design stage. Afterwards, the approach of the simplified mathematical model, normal modes and flutter calculations are exposed. The end of the paper gives examples from Aérospatiale studies.

NOTATIONS

n	: Nombre de points matériels de la structure
T	: Energie cinétique
U	: Energie potentielle
D	: Energie dissipée
Q	: Forces extérieures appliquées à l'avion.
[M]	: Matrice de masses
[D]	: Matrice de dissipations
[K]	: Matrice de raideurs
[FA]	: Forces aérodynamiques extérieures
ω	: Pulsation de mouvement harmonique
N	: Fréquences propres du système conservatif associé
[P]	: Matrice modale du système conservatif associé
[M]	: Matrice diagonale des masses généralisées
[A]	: Matrice diagonale des viscosités généralisées
[K]	: Matrice diagonale des raideurs généralisées
[a]	: Matrice colonne des forces aérodynamiques généralisées
ρ	: Densité de l'air à l'altitude z de vol
V	: Vitesse avion
[A(m,k)]	: Matrice de coefficients d'influence aérodynamique instationnaires
Wc	: Vitesse de perturbation locale, normale au profil.
M	: Nombre de Mach
k	: $= \frac{\omega}{V}$: pulsation réduite
M _c	: Moment de charnière
B	: Coefficient d'amortissement de la servocommande
$\dot{\theta}$: Vitesse de braquage de la gouverne
B _l	: Coefficient d'amortissement linéarisé
θ_0	: Amplitude du mouvement gouverne
C _{st}	: Impédance structurale d'ancrage de la servocommande
C _a	: Impédance de la servocommande montée sur avion
C _{sc}	: Impédance de la servocommande seule

2-2

1. INTRODUCTION - GENERALITES

Au niveau de la justification d'une structure d'avion, les phénomènes aéroélastiques, tant statiques que dynamiques, jouent un rôle très important. Aussi, afin d'assurer une conception et un prédimensionnement corrects de la structure et de certains systèmes, il apparaît nécessaire de les prendre en compte le plus tôt possible dans l'étude d'un projet.

Le flottement est un de ces phénomènes. De par sa nature et des paramètres qui le gouvernent, il est fonction de la conception générale du projet et du dimensionnement de sa structure. Mais, compte tenu de son impact sur la sécurité et la certification de l'avion, il peut imposer en retour des modifications de géométrie, de dimensionnement, de conception structurale, d'implantation de réservoirs de carburant et de spécifications de certains systèmes tels que les servocommandes, circuit carburant (séquences d'épuisement des réservoirs).

De ce fait, il apparaît essentiel d'apprécier très rapidement le comportement en flottement d'un nouveau projet d'avion.

Cette publication a pour objet de présenter, après un bref rappel de la formulation du problème, l'approche suivie par AEROSPATIALE pour l'étude de ce comportement, au stade de l'avant-projet avancé, ainsi que quelques exemples illustrant cette approche.

2. FORMULATION DU PROBLEME DE FLOTTEMENT2.1. Equation générale du mouvement

Un avion peut être considéré comme un système mécanique approximativement linéaire que l'on peut discrétiser sous forme de n points matériels. Sous l'action des forces aérodynamiques, la structure se déforme et chacun des points occupe dans l'espace une position qui peut être déterminée à tout instant par la résolution des équations de Lagrange :

$$\textcircled{1} \quad \frac{d}{dt} \left(\frac{\partial T}{\partial \dot{z}} \right)^T - \frac{\partial T}{\partial z} + \frac{\partial W}{\partial z} + \frac{\partial D}{\partial z} = Q$$

Cette équation représente, en notation matricielle, un système de n équations différentielles correspondant aux n points matériels choisis. Les coefficients du premier membre ne dépendent que des caractéristiques mécaniques du système et sont obtenus après calcul des énergies potentielle, cinétique et de dissipation. En ce qui concerne le second membre, il dépend des forces aérodynamiques qui s'appliquent sur l'avion et est obtenu par le calcul des travaux virtuels des forces appliquées.

$$\delta W = \Delta z^T \cdot Q$$

Nous obtenons alors l'équation classique

$$\textcircled{2} \quad [M] \{\ddot{z}\} + [D] \{\dot{z}\} + [K] \{z\} = \{F_A\}$$

2.2. Equation du mouvement dans la base modale :

En considérant uniquement le système libre conservatif associé, l'équation (2) devient :

$$\textcircled{3} \quad [M] \{\ddot{z}\} + [K] \{z\} = 0$$

Cette équation différentielle admet des solutions de la forme : $\{z\} = \{z_0\} e^{j\omega t}$

$$\text{d'où } \textcircled{4} \quad \left[\omega^2 [M] - [K] \right] \{z\} = 0$$

où ω^2 apparaît comme valeurs propres de la matrice $[M]^{-1}[K]$ et $\{z\}$ comme vecteurs propres associés. D'où les fréquences propres N et les modes propres $[\phi]$ du système.

En se plaçant dans la base formée par les modes propres $[\phi]$, nous pouvons représenter le mouvement des points avion par la superposition linéaire suivante en séparant les variables d'espace et de temps :

$$\textcircled{5} \quad \{z_{xyz,t}\} = [\phi_{xyz}] \{q_t\}$$

Compte tenu des propriétés du système (orthogonalité des modes propres) et en appliquant l'hypothèse de Basile nous obtenons alors l'équation sous sa forme classique.

2-3

$$⑥ \quad [\mu] \{\ddot{q}\} + [\rho] \{\dot{q}\} + [\gamma] \{q\} = \{Q_A\} \quad \text{avec} \quad ⑦ \quad \{Q_A\} = [\phi_A]^T \{F_A\}$$

où $\{F_A\}$ représente, dans le cadre de l'étude du flottement, les forces aérodynamiques induites par les mouvements de l'avion lui-même.

2.4. Paramètres

De ce rappel sur l'équation classique régissant le comportement en flottement d'un avion, il ressort que les paramètres de base pour un calcul de flottement sont :

- la matrice de masses $[M]$
- la matrice de raideurs $[K]$

d'où le calcul des modes propres du système conservatif associé $[\phi]$

- les forces aérodynamiques généralisées de mouvements $\{Q_A\}$

d'où le calcul du comportement en flottement.

3. OBJECTIF DES CALCULS DE FLOTTEMENT AU NIVEAU DE L'AVANT-PROJET AVANCE :

L'examen des paramètres précédents montre assez clairement que la mise en oeuvre d'un calcul de flottement demande un certain nombre d'informations qui ne peuvent être fournies que par un avant-projet ayant déjà atteint une certaine maturité.

Ce type d'étude s'insère donc à un niveau tel qu'il est possible, de par les informations disponibles, d'estimer des distributions de masses et des efforts généraux pour un tout premier prédimensionnement. Ceci signifie que la conception structurale générale avion, bien que susceptible de varier, a déjà été étudiée.

Les objectifs principaux d'un calcul de flottement au stade de l'avant-projet dit "avancé" nous paraissent être dans ces conditions les suivants :

- I - Connaître le comportement en flottement le plus tôt possible pour :
 - . savoir si il est critique ou non
 - . savoir si il y a un risque de problème potentiel
 - . dans le cas où la réponse aux deux questions précédentes est positive :
 - identifier le phénomène et les configurations les plus critiques
 - proposer des solutions améliorant le comportement et permettant de définir la ou les modifications globalement les moins pénalisantes.
- II - Suivre l'évolution du comportement en flottement de l'avion en fonction de l'avancement du projet par prise en compte :
 - . des modifications diverses non dictées par le flottement lui-même
 - . de l'affinement des données de base.

En ce qui concerne les solutions à étudier pour améliorer le comportement, toute possibilité doit être envisagée à ce stade de développement du projet :

- modifications géométriques
- modifications de structure :
 - . principes constructifs
 - . choix technologique
 - . dimensionnement.
- modifications massiques
- modifications de système :
 - . implantation des réservoirs
 - . circuit carburant (séquence d'épuisement)
 - . servocommande
 - . système de contrôle automatique généralisé (C.A.G.)

Pour répondre à ces objectifs, le modèle mathématique à utiliser doit donc être :

- simple et rustique, mais aussi représentatif que possible
- souple d'emploi
- susceptible d'être modifié rapidement
- efficace par son temps de réponse.

2-4 4. APPROCHE AEROSPATIALE

4.1. Généralités :

De ce qui suit dans cette publication, nous traitons d'avions "classiques" équipés de surfaces portantes de grand allongement.

D'une manière générale l'approche que nous avons retenue dans nos études récentes pour ce type d'avion n'a pas fait l'objet de développements informatiques spécifiques.

Nous avons utilisé des moyens de calcul existants en essayant d'améliorer leurs intégrations respectives, ceci par souci d'efficacité. D'où une approche informatique modulaire ayant l'avantage de fournir des résultats intermédiaires permettant de juger de la validité et de la qualité du modèle proposé ainsi que de permettre une meilleure interprétation des résultats. Les principales étapes de notre approche sont :

- calcul des modes propres
- calcul des forces aérodynamiques généralisées de mouvements
- résolution de l'équation de flottement et visualisation des résultats.

Les théories aérodynamiques et les méthodes de résolution que nous nous proposons d'utiliser étant éprouvées, la validité des calculs de flottement va dépendre directement de la qualité des modes propres calculés. Pour ce faire, nous essayons d'utiliser au mieux les "maigres" informations disponibles à ce stade du projet pour construire une schématisation dans l'esprit élasticité, sans négliger les aspects mécaniques propres aux structures d'avion.

4.2. Modes propres du système conservatif associé :

En ce qui concerne le calcul des modes propres du système conservatif associé, nous nous sommes orientés vers le calcul direct des modes propres de l'avion complet.

Ce calcul est effectué à partir de matrices de masses $[M]$ et de raideurs $[K]$ relatives à l'avion complet incluant le fuselage, la voilure, les empennages, les bords d'attaque, etc. ... Dans la mesure où l'avion présente un plan de symétrie, ce qui est généralement le cas, nous utilisons systématiquement les propriétés qui en découlent, et nous travaillons sur un demi-avion en comportement symétrique ou antisymétrique.

Pour la construction de ce modèle dynamique aboutissant au calcul des modes propres, nous procédons suivant l'ordre ci-dessous :

- I - discrétisation massique : définition géométrique des points matériels et répartitions massiques sur ces points $[M]$
- II - modélisation structurale : schématisation structure et calcul de la matrice de raideurs $[K]$ sur les degrés de liberté associés aux points massiques.
- III - calcul des modes propres. $[\phi]$

4.2.1. Discrétisation massique du système

La discrétisation massique de l'avion a pour objet de définir un nombre fini de points matériels permettant de représenter correctement la distribution des masses avion : structure, système, propulsion, carburant, charge payante. Le premier travail consiste donc à définir la géométrie ou "grille" des points matériels et les matrices de répartition de masses sur ces points $[M]$ pour différentes configurations massiques avion.

Le principe de discrétisation que nous avons retenu est caractérisé par une représentation à l'aide de masses concentrées ponctuelles respectant :

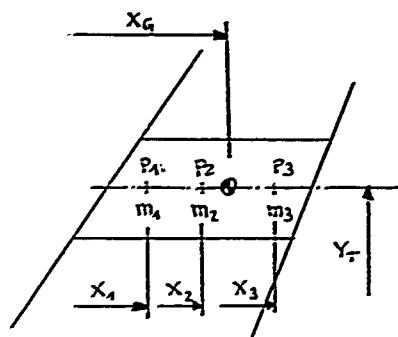
- pour les surfaces portantes : masse, centrage et inertie de tangage (voilure, empennage horizontal) ou de lacet (dérive) par tranche.
- pour le fuselage : la masse par tranche de fuselage considéré.
- pour les grosses masses concentrées (moteurs, charges externes) masses et inerties ramenées au centre de gravité de la masse considérée.

Cette discrétisation est mise en oeuvre à partir d'une répartition de masses par tranches, incluant un nombre suffisant de tranches et provenant d'une estimation massique de type avant-projet.

Cette présentation conduit à des matrices de masses diagonales $[m_i]$

Le calcul des masses ponctuelles est effectué suivant le schéma suivant :

Pour une tranche de surface portante, voilure par exemple, caractérisée par sa position en envergure Y_r , sa masse m , la position en profondeur de son centre de gravité X_G et son inertie de tangage I_y autour du centre de gravité, nous définissons 3 masses m_1 , m_2 et m_3 situées en 3 points P_1 , P_2 , P_3 , alignés tels que :



$$\begin{aligned} (8) \quad & m_1 + m_2 + m_3 = m \\ & m_1 X_1 + m_2 X_2 + m_3 X_3 = m X_G \\ & m_1 (X_G - X_1)^2 + m_2 (X_G - X_2)^2 + m_3 (X_G - X_3)^2 = I_y \end{aligned}$$

La résolution du système d'équations (8) définit les 3 masses m_1 , m_2 , m_3 pour une géométrie donnée. Le choix de la géométrie est basé sur des critères simples visant à ce que la résolution de (8) ne conduise pas à des masses négatives.

En appliquant cette méthode à toutes les tranches, nous représentons correctement, pour une voilure par exemple, sa masse, son centrage et son inertie de tangage. Les inerties de lacet et de roulis ne sont pas strictement respectées, mais restent suffisamment représentatives.

Pour le fuselage, nous utilisons uniquement les masses concentrées au centre de gravité des tranches massiques, en négligeant les inerties propres de chacune des tranches. Ceci est tout à fait acceptable dans la mesure où le nombre de tranches fuselage est suffisant.

La définition de la grille massique est effectuée en respectant l'ordre suivant :

a - discrétisation de la masse à vide en ordre d'exploitation (MVOE) où sont choisis :

- . les points de fuselage sur l'axe fuselage
- . les points surfaces portantes : 3 points par tranche, alignés sur les longerons avant et arrière et une ligne en arrière du longeron arrière.
- . les points pour les grosses masses concentrées.

b - discrétisation du carburant en cherchant à le répartir sur les points déjà utilisés pour la MVOE.

Malheureusement, ceci n'est pas toujours possible et nous sommes amenés à enrichir la grille MVOE par une nouvelle ligne de points. Ceci est souvent nécessaire dans le cas de réservoirs à l'intérieur du caisson. Nous répartissons alors le carburant sur les lignes longerons avant et arrière et sur la nouvelle ligne que nous choisissons entre les longerons avant et arrière.

c - discrétisation de la charge payante par répartition isostatique sur les points fixés pour la MVOE.

La planche 1 illustre le principe de la discrétisation massique retenue pour un avion du type A.300B.

Nous disposons alors d'une grille massique unique sur laquelle nous pouvons disposer des répartitions :

- . de XVOE $[m]_{HVOE}$
- . de différents cas de remplissage des réservoirs.
 $[m]_{C1}, [m]_{C2}, \dots$
- . de différentes configurations de charges payantes.
 $[m]_{CP1}, [m]_{CP2}, \dots$

Par additions et combinaisons nous pouvons obtenir toute répartition de masse associée à toute configuration de vol sur une grille unique.

4.2.2. Calcul de la matrice de raideurs :

Après cette première opération de définition de la grille massique, nous calculons la matrice de raideurs $[K]$ traduisant les liaisons mécaniques entre ces points massiques, tout en respectant leurs degrés de liberté propres.

Cette matrice de raideur est obtenue à partir d'un modèle structural basé sur les hypothèses suivantes :

- chaque élément majeur est considéré comme une poutre équivalente de rigidités variables travaillant en flexion-torsion et dont la fibre neutre est confondue avec l'axe élastique de l'élément étudié.

La planche 2 illustre ceci pour un fuselage et une voilure d'avion de type A.300B.

- les surfaces portantes sont considérées comme infiniment rigides en profondeur, ainsi que les grosses masses concentrées ramenées à leur centre de gravité (moteurs par exemple).

Les caractéristiques mécaniques (rigidités) des différents éléments sont calculées à partir d'efforts de prédimensionnement, issus eux-mêmes de calculs d'efforts généraux de type avant-projet. L'axe élastique d'une surface portante est positionné au centre du caisson, sauf si celui-ci présente une grande dissymétrie sur l'un des deux longerons. C'est le cas de l'exemple donné planche 3 dans la partie interne de voilure où le longeron arrière est renforcé pour supporter les efforts en provenance de l'atterrisseur principal. Dans ce cas, l'axe élastique est légèrement rapproché en direction du longeron arrière.

Le calcul de la matrice de raideurs $[K]$ est effectué en utilisant le code de calcul par éléments finis ASELF développé entièrement à l'AEROSPATIALE Toulouse.

Pour notre calcul et fonction des hypothèses précédentes, nous utilisons ASELF en n'employant que 3 types d'éléments parmi ceux disponibles dans sa bibliothèque, à savoir :

- . barre en effort normal
- . poutre en flexion avec cisaillement
- . poutre en torsion

Ceci nous conduit à une schématisation du type de celle présentée planche 3 avec surfaces portantes en "arêtes de poisson", fuselage et mât moteur en poutres simples.

A l'aide de ce type de schématisation et des caractéristiques mécaniques des éléments, nous calculons la matrice de raideurs libre dans l'espace. Si l'on travaille sur un demi-avion, elle est associée à des conditions limites de type symétrique ou antisymétrique conduisant à des modes propres symétriques ou antisymétriques. La matrice de raideurs $[K]$ est ramenée sur les seuls degrés de liberté associés aux points massiques par une condensation statique du type Guyan.

Il peut paraître inopportun d'utiliser un outil aussi puissant et sophistiqué à ce niveau de calcul. Cependant, après étude comparative, cette voie nous est apparue très vite comme la plus efficace. En effet, le code ASELF est extrêmement simple et très souple d'emploi. Sa puissance de calcul conduit à des temps de réponse et des coûts extrêmement faibles, très bien adaptés à notre problème. Par ailleurs, ce code par ses possibilités, permet un grand nombre d'évolutions. Par exemple, considérons un nouveau projet reprenant un sous-ensemble existant sur un autre avion, un mât moteur par exemple. Ce mât moteur a déjà donc fait l'objet d'une justification basée sur un modèle structural sophistiqué. En utilisant la procédure de sous-structuration, ce modèle est très facilement intégrable à notre modèle simplifié à la place de la schématisation par poutres et barres.

4.2.3. Calcul des modes propres :

Le calcul des modes propres se fait par résolution de l'équation (4) et se ramène à la recherche des valeurs et vecteurs propres de la matrice dynamique.

Le calcul des valeurs propres est effectué après tridiagonalisation de la matrice dynamique (méthode Givens Householder) et utilisation des propriétés de la suite de Sturm au niveau des polynômes caractéristiques des sous-matrices de la matrice tridiagonalisée.

Après calcul et normalisation, les modes propres sont visualisés sur machine à dessiner automatique.

4.3. Forces aérodynamiques généralisées de mouvements :

Les forces aérodynamiques généralisées de mouvements sont calculées à partir de coefficients aérodynamiques instationnaires bi ou tridimensionnels, obtenus par application de la théorie de la surface portante en régime instationnaire pseudocompressible.

Les calculs effectués en bidimensionnel sont sans interaction, les calculs tridimensionnels peuvent prendre en compte des interactions entre surfaces portantes.

Dans la majorité des cas, nous utilisons une aérodynamique tridimensionnelle mise en oeuvre par une méthode de collocation (Ref. 1) ou de doublets (Ref. 2). Nous obtenons alors une matrice de coefficients d'influence aérodynamiques instationnaires permettant le calcul de forces aérodynamiques locales liées à des incidences locales.

$$\{F_A\} = \frac{1}{2} \rho V^2 [A_{(M,k)}] \left\{ \frac{w_c}{V} \right\}$$

La matrice $[A]$ est calculée pour des valeurs discrètes du nombre de Mach M et de la pulsation réduite $k = \frac{\omega}{V}$.

En passant dans la base modale l'incidence locale s'écrit en sachant que :

$$\{q\} = \{q_0\} e^{j\omega t} \quad \text{et} \quad k = \frac{\omega}{V}$$

$$\left\{ \frac{w_c}{V} \right\} = \left[\left[\frac{\partial [\phi_c]}{\partial x} \right] + jk [\phi_c] \right] \{q\}$$

d'où l'expression des forces généralisées de mouvements :

$$\{Q_{A(M,k)}\} = \frac{1}{2} \rho V^2 [\phi_A]^T [A_{(M,k)}] \left[\left[\frac{\partial [\phi_c]}{\partial x} \right] + jk [\phi_c] \right] \{q\}$$

$$= \frac{1}{2} \rho V^2 [Q] \{q\}$$

$$[Q] = [\phi_A]^T [A] \left[\left[\frac{\partial [\phi_c]}{\partial x} \right] + jk [\phi_c] \right] \{q\}$$

Les matrices des déformées sur les points aérodynamiques $[\phi_A]$, $[\phi_c]$

et $\left[\frac{\partial [\phi_c]}{\partial x} \right]$ sont calculées par interpolation à partir de $[\phi]$ à l'aide d'un spline du 3ème ordre (Ref. 3).

4.4. Résolution de l'équation de flottement :

La résolution de l'équation de flottement

$$\left[-[\gamma_k] \Omega^2 + j \Omega [\rho_k] + [\gamma_k] - \frac{1}{2} \rho V^2 [Q(n, k)] \right] \{q\} = 0$$

est conditionnée par le fait que les forces aérodynamiques généralisées de mouvements ne sont connues que pour des valeurs discrètes du nombre de Mach M et de la pulsation réduite k . Deux méthodes de résolution sont disponibles :

- par balayage en k (Ref. 4)
Méthode très rapide mais mal adaptée à une présentation automatique et demandant des matrices $[A(n, k)]$ pour un certain nombre de valeurs de la pulsation réduite
- par double balayage (méthode $p-k$)
 . mode par mode avec suivi (Ref. 5)
 . vitesse par vitesse (Ref. 6)

Méthodes moins rapides mais adaptées à un traitement automatique par machine à dessiner et demandant des matrices $[A]$ pour un nombre réduit de k . Elles permettent par ailleurs la prise en compte de l'impédance de servocommandes et de systèmes de contrôle automatiques généralisés (Ref. 7), ce qui n'est pas le cas de la méthode " k ".

Le choix de la méthode de résolution est fonction du problème à résoudre.

La présentation des résultats est effectuée généralement sous la forme de courbes donnant l'évolution des fréquences et des amortissements aérodynamiques en fonction de la vitesse pour un nombre de Mach constant. Il est possible également d'obtenir les mêmes courbes d'évolution à altitude constante.

Nous avons retenu ces méthodes de résolutions et de présentation car il nous paraît essentiel de connaître non seulement la valeur de la (ou des) vitesses critiques, si il y en a, mais surtout :

- l'évolution des fréquences et des amortissements en fonction de la vitesse avion
- la nature des couplages pouvant apparaître.

5. EXEMPLES D'APPLICATION DE L'APPROCHE AEROSPATIALE

Après avoir précisé les grandes lignes de l'approche AEROSPATIALE en ce qui concerne les calculs de flottement au niveau de l'avant-projet, voici quelques exemples d'application.

5.1. Exemples de modélisation :

Deux exemples de modélisation conduisant au calcul de modes propres sont donnés planches 1 à 8. L'un concerne un gros avion de transport civil de type A.300B, l'autre un petit avion de tourisme quadriplace le TB 20, construit par la SOCATA, filiale de l'AEROSPATIALE.

5.1.1. Gros avions de transport civil - A.300B :

Pour une étude en symétrie, la grille massique retenue pour l'A.300B est donnée planche 1. Nous retrouvons ici :

- la ligne de points massique fuselage recevant les masses MVOE et la charge payante.
- les tranches voilures contenant chacune 4 points.

La masse MVOE est répartie sur les lignes longeron avant, longeron arrière et la ligne extrême arrière. Le carburant est réparti sur les lignes longeron avant, ligne milieu caisson et longeron arrière.

- les tranches empennage horizontal avec 3 points par tranche
- le centre de gravité de l'ensemble moteur + nacelle

La matrice de raideurs, liant les différents points massiques est obtenue à partir d'une schématisation par poutres équivalentes, dont les caractéristiques mécaniques sont visualisées planche 2. D'où un modèle avec voilure et empennage en "arêtes de poisson", fuselage et mât moteur, poutre, dessiné planche 3. En ce qui concerne le mât moteur, il est représenté par des poutres dont les rigidités sont équivalentes à celles fournies comme base pour son dimensionnement.

Si pour le fuselage et les surfaces portantes ce modèle apparaît comme représentatif, il peut être critiquable quant à la schématisation de la liaison voilure-fuselage (voir planche 4, figure 4.1). En conséquence, nous avons essayé d'améliorer la représentativité de cette liaison en la simulant par un système de poutres, baptisé "trapèze", visualisé planche 4, figure 4.2. Ce système permet de représenter, dans son principe, le passage des efforts voilure-fuselage :

- Moment de torsion M_y et effort tranchant T_z par l'intermédiaire de la nervure 1 (poutre 2) et des cadres forts au niveau des longerons AV et AR (poutres 3 et 4).
- Moment de flexion M_x par l'intermédiaire du caisson traversant (poutre 1). L'équilibre est assuré par raison de symétrie, la poutre 2 étant articulée sur les poutres 3 et 4.

Les rigidités des poutres 1, 2 et 3 permettent de caractériser la rigidité de la liaison voilure-fuselage au point J. Au niveau de l'avant-projet ces valeurs sont fonction de l'expérience. Par exemple, il est possible de considérer la rigidité de flexion du caisson traversant (poutre 1) comme légèrement supérieure à celle de la voilure à son emplanture et la rigidité de torsion au niveau du point J comme très supérieure à la rigidité de torsion de la voilure à son emplanture.

Ceci conduit à la structure figure 4.3 planche 4.

Les principaux modes propres obtenus avec ce modèle mathématique sont donnés planche 5, figure 5.1. A titre de comparaison et pour situer le niveau de qualité de ce type de modèle, nous donnons figure 5.2 les modes propres relevés au cours d'un essai de vibrations au sol, effectué dans la même configuration massique. Nous constatons, pour ces modes propres fondamentaux, une très bonne concordance calcul-essai tant en ce qui concerne les fréquences que les modes propres.

5.1.2. Avion léger de tourisme quadriplace TB 20 :

Pour ce petit avion à commandes de vol manuelles, nous avons défini une grille massique en respectant les gouvernes et leurs commandes. (Voir planche 6). Signalons que cet appareil est équipé d'un empennage horizontal monobloc avec antitab, assurant la commande de profondeur. Ce monobloc est équilibré massiquement par une masse installée en extrémité d'une perche rentrant à l'intérieur du fuselage arrière.

Compte tenu des problèmes posés par les commandes de vol manuelles, nous avons également schématisé ces dernières dans notre modèle structure (figure 7.1, planche 7), à savoir :

- gouvernes (aileron - monobloc + antitab - direction)
- timoneries
- commande (manche et palonnier)

La figure 7.2 de la planche 7 illustre la schématisation retenue pour la commande de profondeur.

Ce type de schématisation, tant massique que structural, permet de juger de l'influence de nombreux paramètres :

- raideur de timonerie (en jouant sur k_T)
- rapports de timonerie (en jouant sur la géométrie)
- équilibrage gouverne (en jouant sur les masses d'équilibrage).

La planche 8 donne, à titre d'exemple, les modes propres symétriques caractéristiques de l'empennage monobloc obtenus par calcul avec le modèle précédent et par un essai de vibrations au sol. Précisons que, dans le calcul présenté, les raideurs de timonerie ont été ajustées sur des mesures effectuées au cours d'un essai statique.

Nous constatons également une assez bonne corrélation calcul-essai.

Ces deux exemples montrent que le type d'approche proposé conduit à des modes propres très représentatifs. Ceci correspond donc à un impératif important auquel doit satisfaire notre modèle mathématique.

5.2. Exemples d'études paramétriques :

Afin de souligner la diversité des problèmes à aborder nous proposons les trois exemples ci-après :

5.2.1. Etude d'un avant-projet d'avion de transport :

Nous avons été amenés à travailler sur un avant-projet d'avion de transport à fuselage étroit court-courrier, équipé de deux réacteurs montés en pod sous voilure (voir figure 9.1, planche 9).

L'aspect flottement en régime symétrique de cet avion est traité en utilisant l'approche décrite précédemment :

- discrétisation massique
- schématisation structurale (voir Fig. 9.2, planche 9)
- calcul des modes propres
- calcul des forces aérodynamiques généralisées de mouvements
- étude du comportement en flottement.

L'examen des calculs de flottement conduit à la situation résumée planche 10, à savoir :

- présence d'un couplage de type flexion-torsion entre le mode de flexion 2 noeuds voilure (mode 1) et le mode de mouvement vertical du moteur entraînant la voilure en torsion (mode 3).
- ce couplage par rapprochement de fréquences conduit à une instabilité à l'intérieur du domaine à justifier.

Pour essayer d'améliorer ce comportement, nous avons envisagé les modifications suivantes :

- déplacements du moteur tant en latéral qu'en longitudinal. (Voir planche 11). Un recul du moteur (R_2), si il ne change pas fondamentalement la vitesse critique, diminue sensiblement la force du couplage.
- combinaisons de paramètres (voir planche 2)
 - . recul du moteur + renforcement voilure (C1)
 - . recul du moteur + renforcement voilure + perche massique en extrémité de voilure (C2).

La solution C2 conduit à une augmentation de la vitesse critique et à une diminution sensible du couplage sans cependant le repousser au-delà du domaine à justifier.

- modification de rigidités du mât moteur (voir planche 13) en latéral (figure 13.1) et en vertical (figure 13.2).

La figure 13.3 résume cette étude. Les solutions les plus efficaces consistent à augmenter ou à diminuer sensiblement la raideur verticale, la zone acceptable obtenue en agissant sur la raideur latérale étant trop réduite et trop "pointue".

De cette étude, il ressort que les éléments suivants son favorables :

- recul du moteur
- renforcement de la rigidité de torsion de la voilure interne
- renforcement de la raideur du mât moteur ou, au contraire, assouplissement très important.

5.2.2. Etude de servocommandes à amortisseur intégré :

Dans le cadre du projet décrit précédemment, nous avons été amenés à étudier la commande de la gouverne de profondeur par l'utilisation de deux servocommandes.

L'utilisation de servocommandes classiques conduit aux comportements donnés planche 14.

- Fig. 14.1 : sans panne hydraulique
- Fig. 14.2 : avec double panne hydraulique

Dans ce dernier cas, la gouverne est libre en rotation. De ce fait, sous l'action des raideurs aérodynamiques, sa fréquence augmente avec la vitesse, "croise" les autres modes propres et provoque des instabilités à cause du comportement sous équilibré de la gouverne en l'absence d'équilibrage de cette dernière (exemple mode 7 - Flexion 2 noeuds empennage horizontal).

Un tel comportement peut être évité par l'utilisation de servocommandes à amortisseur intégré. Par rapport à des servocommandes classiques, elles comportent un "by pass" permettant de mettre les deux chambres en communication par l'intermédiaire d'un orifice turbulent.

En fonctionnement normal le "by pass" est fermé et la servo se comporte comme une servocommande classique. Si par la suite d'une panne, l'alimentation hydraulique de la servocommande n'est plus assurée, celle-ci reste alors pleine de liquide hydraulique et le "by pass" s'ouvre automatiquement, mettant les deux chambres en communication (voir fig. 15.1, planche 15). La servo fonctionne alors comme un amortisseur et la circulation du liquide hydraulique entre les deux chambres à travers un gicleur turbulent conduit à la caractéristique non linéaire :

$$M_c^t = B \dot{\theta}^2$$

Afin d'introduire cette caractéristique directement dans les équations de flottement, en utilisant la notion d'impédance de servocommande, nous linéariserons cette forme quadratique pour obtenir un moment résistant linéarisé

$$M_{CL}^t = B_L \dot{\theta}$$

La méthode du travail équivalent, basée sur l'égalité des énergies dissipées par cycle par la forme quadratique et la forme linéaire donne une relation entre B et B_L

$$B_L = \frac{\theta \omega}{3\pi} \cdot B \cdot \theta_0$$

pour un mouvement harmonique $\theta = \theta_0 e^{j\omega t}$

L'amplitude θ_0 devient alors un paramètre supplémentaire.

Dans ces conditions, l'impédance de la servocommande installée sur avion s'écrit :

$$\frac{1}{C_a} = \frac{1}{C_{st}} + \frac{1}{C_{sc}} = \frac{1}{C_{st}} + \frac{1}{j\omega B_L}$$

d'où $C_a = RC_a + jLC_a$ (voir Fig. 15.1, Pl. 15)

Les calculs de flottement sont effectués pour différentes valeurs du produit $B\theta_0$ intervenant dans l'impédance de la servocommande auxquels vont correspondre des couples de valeurs B et θ_0 .

La figure 15.2, planche 15 donne l'évolution du domaine d'instabilité en fonction du produit $B\theta_0$.

L'instabilité disparaît du domaine à justifier si :

$$B\theta_0 > 0.09 \frac{mN}{\%}$$

Ceci signifie que l'avion équipé de deux servocommandes à amortisseur intégré, réglées tel que $B\theta_0 = 0.09$ volant à $Z = 50.000$ ft - $M = 0.88$ avec une double panne hydraulique sera en situation stable si on l'écarte de sa position d'équilibre, mais avec un mouvement de rotation gouverne de 2.3 degré pour des servos ayant un coefficient d'amortissement $B = 0.3 \frac{mN}{(\%)^2}$

Cette étude nous conduit à définir un coefficient $B\theta_0$ minimum permettant d'avoir un système stable.

Ceci fournira un élément important au niveau des spécifications des servocommandes.

5.2.3. Etude d'un tab à ressort :

Dans le cadre du projet d'avion d'entraînement "Epsilon", nous avons été amenés à étudier le montage d'un tab à ressort sur les ailerons.

L'Epsilon est un avion biplace en tandem, équipé d'un moteur à pistons de 300 CV et de commandes de vol manuelles (voir fig. 16.1, Pl. 16).

Le principe du tab à ressort est donné planche 16, Fig. 16.2 et les performances d'un tel système en fonction du taux d'automacité du tab (k_3) et de la raideur du ressort (K_2) sont tracées Fig. 16.3, planche 16.

En fonction de cette étude de performances de type QDV, le problème était de connaître l'influence de ces 2 paramètres sur le comportement en flottement de l'avion.

L'approche générale pour cet avion est tout à fait comparable à celle décrite précédemment pour le TB 20. L'ensemble aileron, tab à ressort et commande a fait l'objet d'une attention particulière.

Du point de vue discrétisation massique, nous avons séparé la voilure, l'aileron, le tab à ressort et la commande (manche en gauchissement). Pour l'aspect structure la planche 17 visualise la schématisation adoptée :

- la géométrie des points P2 et P3 définit le taux d'automacité du tab k_3
- la raideur des barres de torsion T simule la raideur du ressort de commande k_2

L'étude du comportement en flottement dans la première configuration étudiée

$$k_2 = 0.6 \text{ mdaN/}^\circ$$

$$k_3 = 3.$$

montre un couplage entre les modes Harmonique rotation aileron et flexion 3 noeuds voilure. (Voir planche 18, Fig. 18.1 courbe (1)) conduisant à une instabilité. Il provient d'un comportement sous équilibré de l'aileron dans le mode flexion 3 noeuds voilure. Ce comportement est facilement amélioré en jouant sur l'équilibrage dynamique de l'aileron (courbes 2 et 3, Fig. 18.1, planche 18).

L'influence des paramètres k_2 et k_3 est donnée planche 18, Fig. 18.2.

De cette étude, il ressort que :

- un taux d'automacité $k_3 = 3$ associé à une raideur du ressort $k_2 = 0,6 \text{ mn daN/}^\circ$ présente un bon compromis.
- il est nécessaire de modifier l'équilibrage de l'aileron. La solution équilibrage amélioré 2 (courbe (3)) étant la solution recommandée.

Signalons que l'avion a volé avec les réglages et l'équilibrage proposés ci-dessus à la satisfaction générale et ce dans tout le domaine de vol à justifier.

6. CONCLUSIONS :

L'approche AEROSPATIALE de l'étude du flottement au niveau de l'avant-projet repose en premier lieu sur le calcul de modes propres à partir d'un modèle structural simplifié.

Ce modèle est caractérisé par une schématisation structurale sous forme de poutres équivalentes s'appuyant sur une grille de masses ponctuelles, les données massiques et mécaniques étant issues d'études de type avant-projet.

Les calculs de flottement proprement dits utilisent des forces aérodynamiques généralisées instantanées, liées aux mouvements ou issues de méthodes classiques et de méthodes de résolution adaptées au problème posé.

Les moyens de calculs, quant à eux, n'ont pas fait l'objet de développement particulier, si ce n'est une intégration visant à améliorer leur efficacité.

Malgré sa relative simplicité, nous avons montré que cette approche conduit à des résultats très représentatifs. Par ailleurs, sa souplesse et sa polyvalence permettent de répondre à des problèmes de type très différents.

La suite logique d'une telle approche est l'introduction de méthodes d'optimisation dynamique en liaison avec des moyens de conception assistée par ordinateur et d'une modélisation structure nouvelle, intermédiaire entre la schématisation par poutre décrite ici et une schématisation par éléments finis sophistiquée telle que celles utilisées actuellement pour la justification structurale.

R E F E R E N C E S

- 1 - L. DAROVSKY et R. DAT
Détermination des forces aérodynamiques instationnaires tridimensionnelles.

AGARD Report 512 - Juin 1965

- 2 - W.P. RODDEN, J.P. GIESING and T.P. KALMANN
New Developments and Applications of the subsonic Doublet - Lattice Method for non planar Configurations.

AGARD - CP-80/71

- 3 - P. DIRINGER
Interpolation, dérivation et intégration à l'aide de fonctions spline.

LA RECHERCHE AEROSPATIALE

- 4 - R. DAT - J.L. MEURZEC
Sur les calculs de flottement par la méthode du balayage en fréquence réduite.

LA RECHERCHE AEROSPATIALE

- 5 - H.J. HASSIG
An approximate true damping solution of the flutter equations by determinant iterations.

JOURNAL of AIRCRAFT - Vol. 8 - N° 11 - November 71.

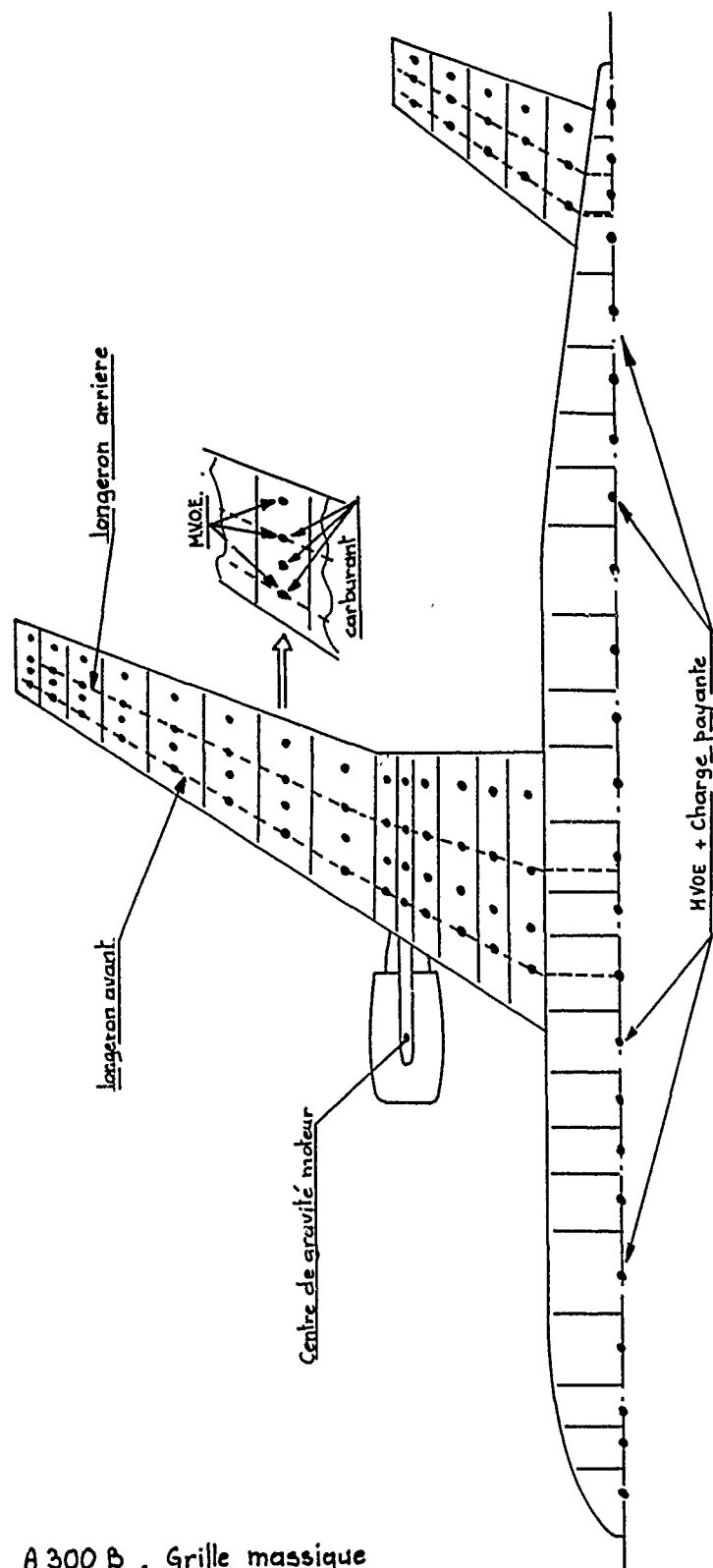
- 6 - W.P. RODDEN - R.L. HARDER - E.D. BELLINGER
Aeroelastic addition to NASTRAN

NASA - CR 3094

- 7 - A. LOTZE - O. SENSBURY - H. KUHN

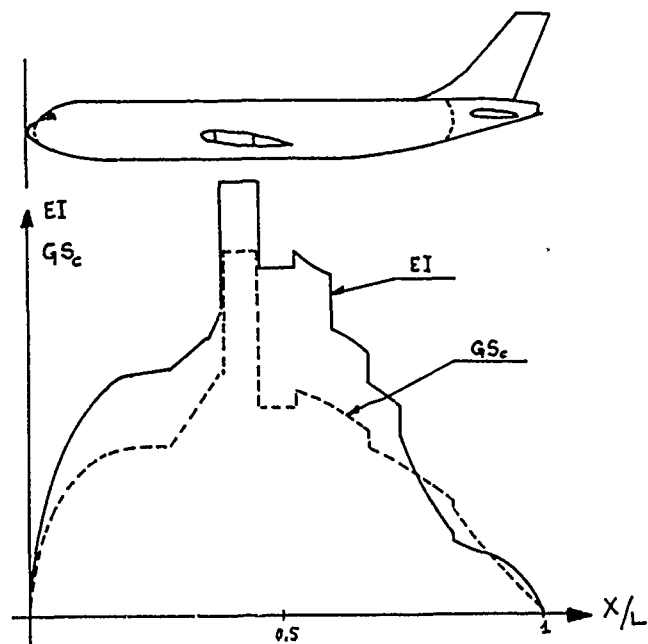
Flutter Investigations of a combat aircraft with a command and stability augmentation system.

Presented at the AIAA - Aircraft systems and technology meeting - LOS ANGELES - 4.6. 1975.



A300B . Grille massique

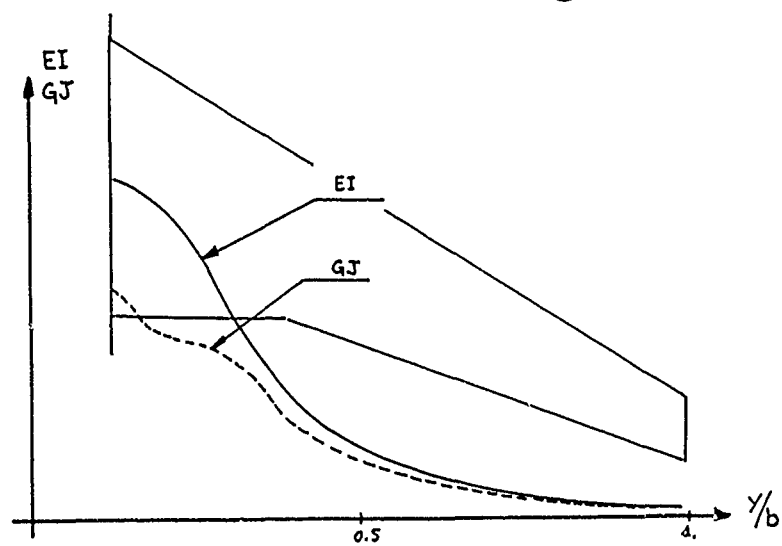
Pl- 1



A 300 B

Rigidités fuselage

fig 2.1



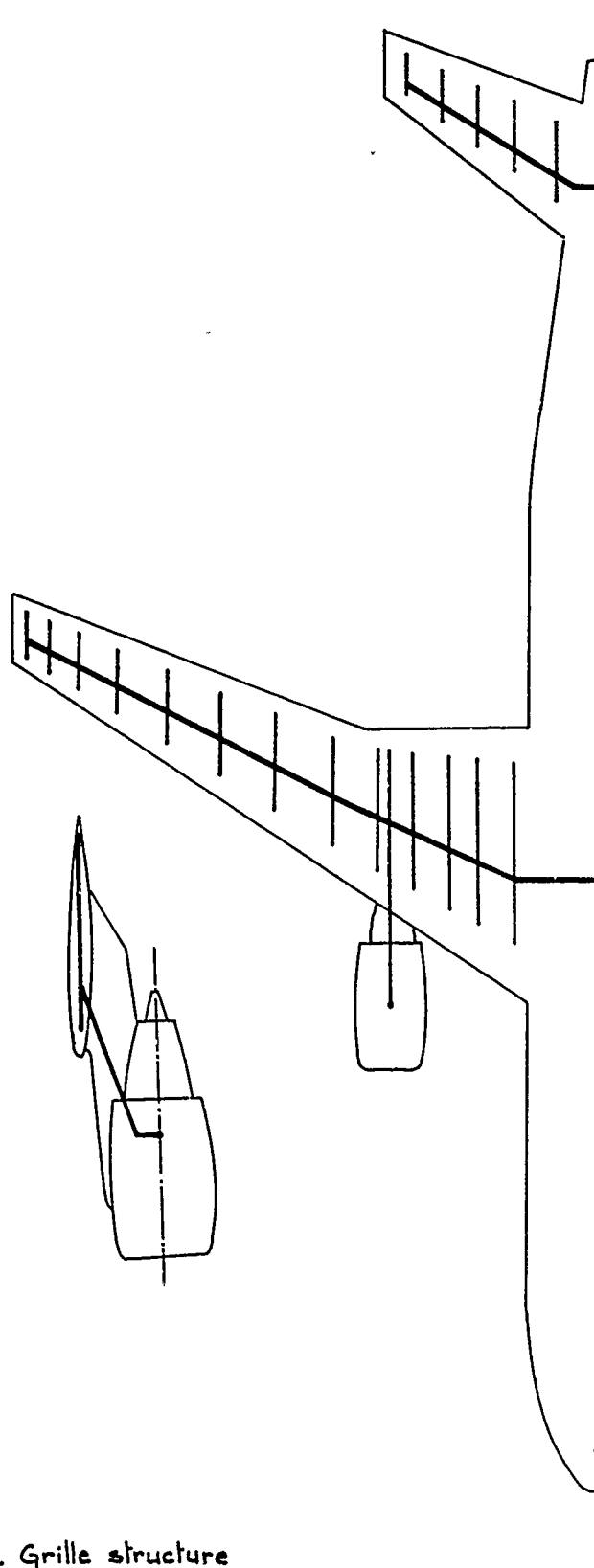
A 300 B

Rigidités voilure

fig 2.2

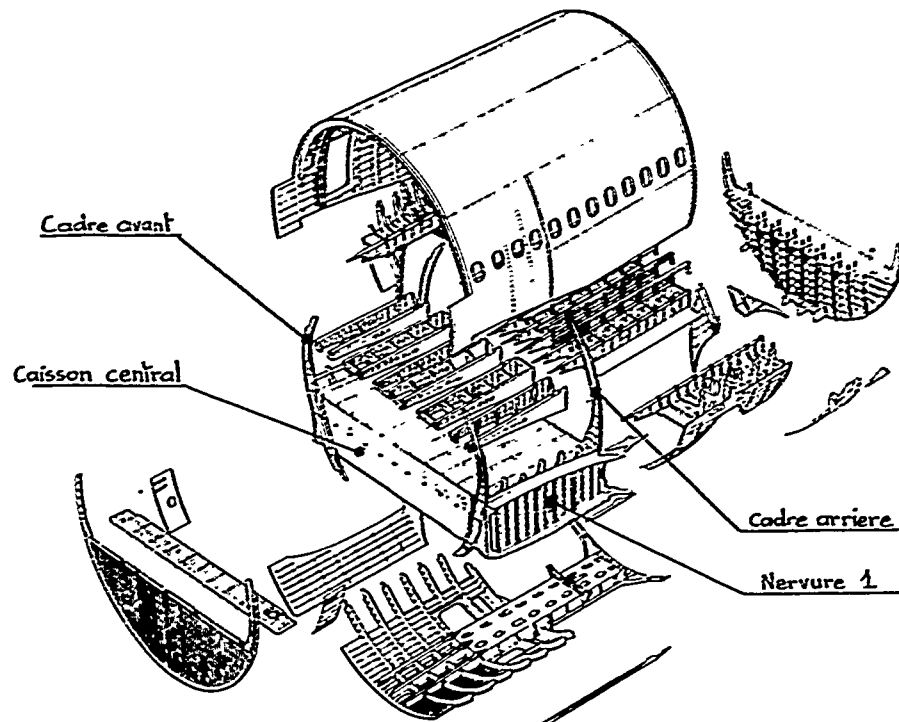
A 300 B - Rigidités fuselage et voilure

Pl . 2



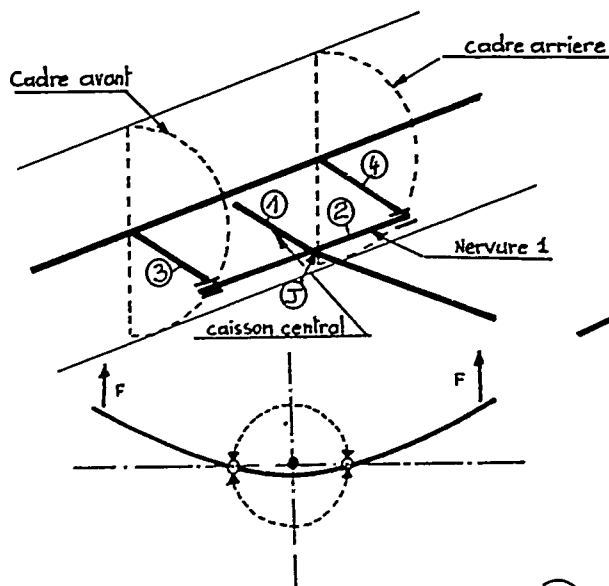
A300 B - Grille structure

Pl. 3



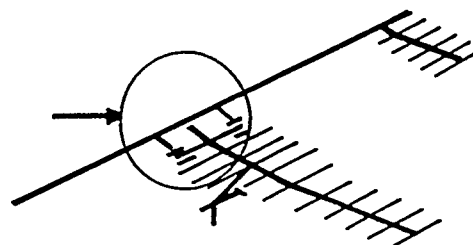
A 300 B. Tronçon fuselage central

Fig 4.1



A 300 B. Schématisation fuselage central

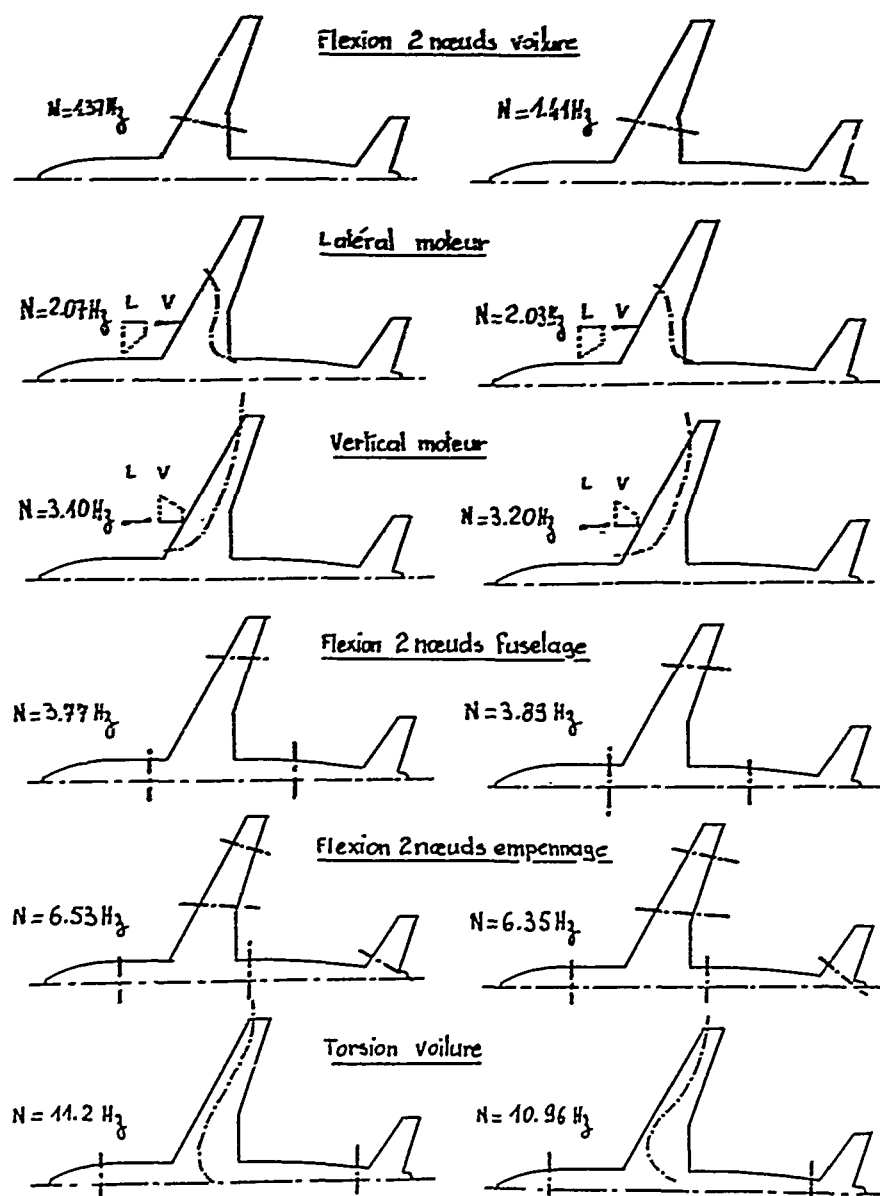
Fig 4.2



A 300 B. Structure

Fig 4.3

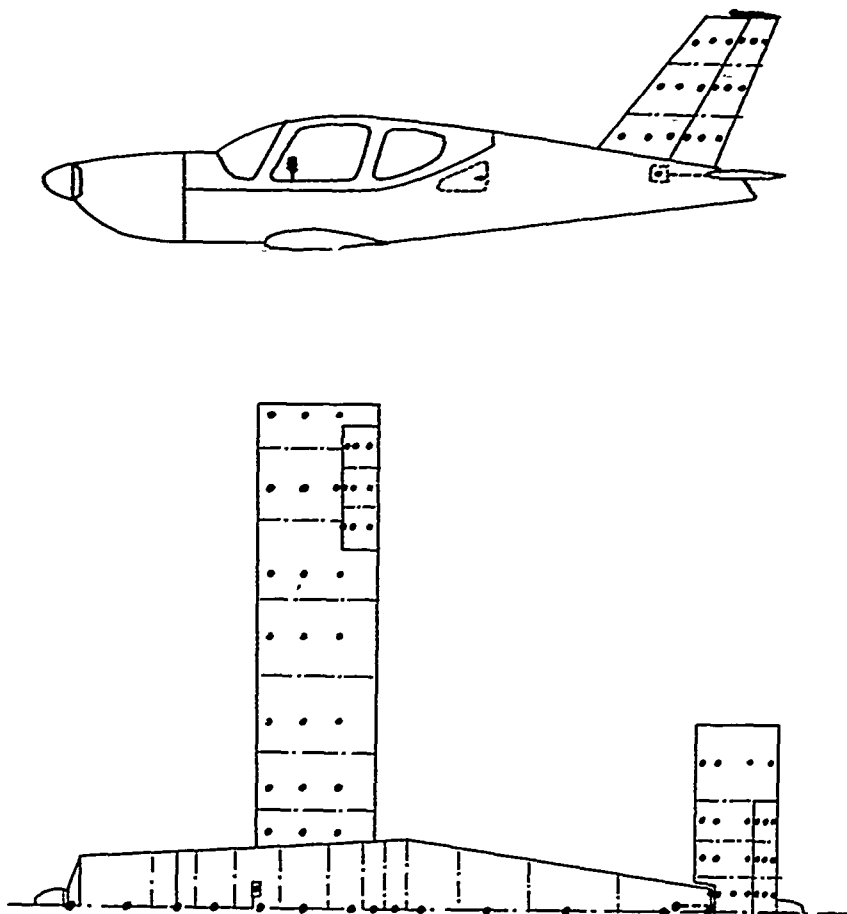
A 300 B - Liaison voilure-fuselage



Calcul
fig 5.1

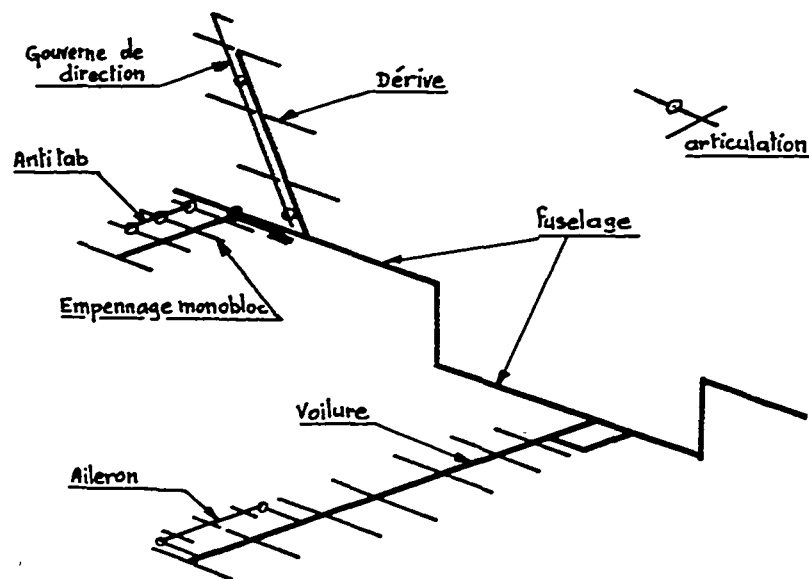
Essai
fig 5.2

A 300B - Modes propres symétriques

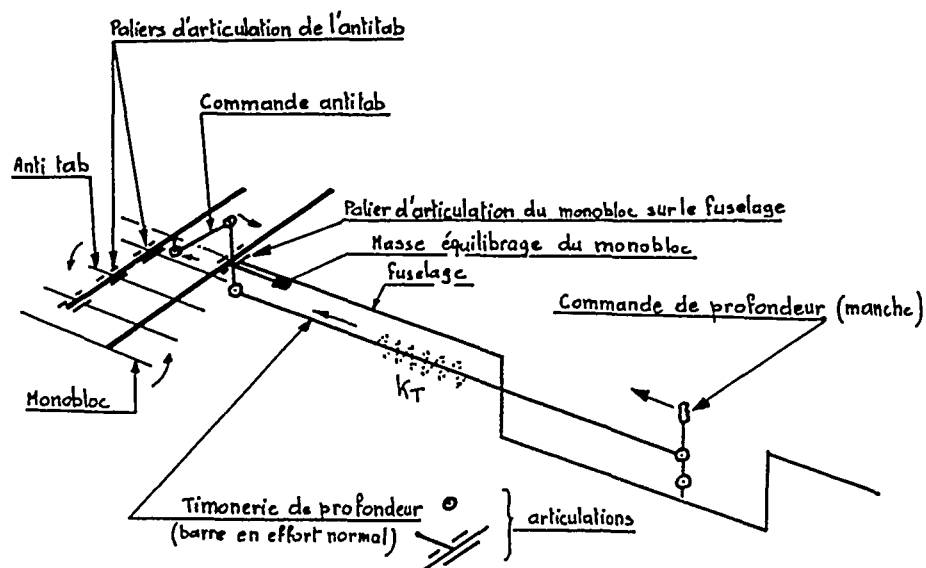


TB 20 - Grille massique

Pl. 6



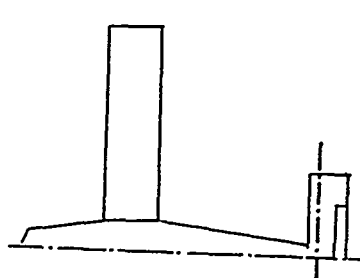
TB 20 - Schématisation structure principale fig 7.1



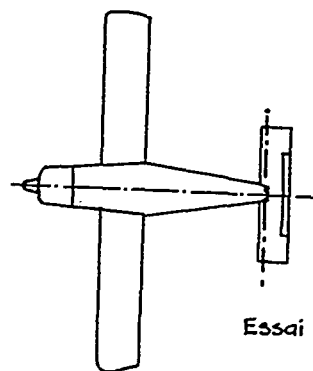
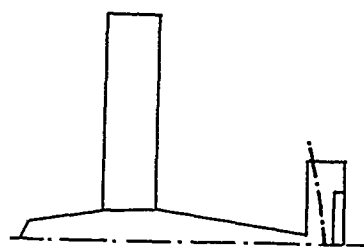
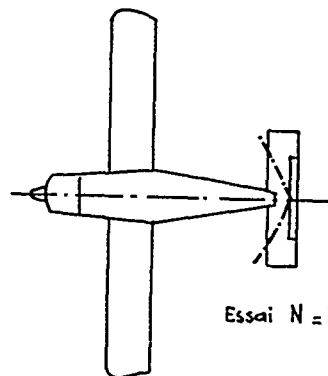
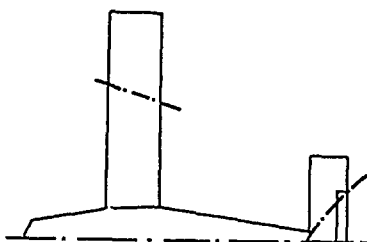
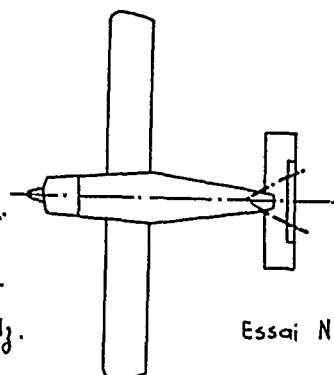
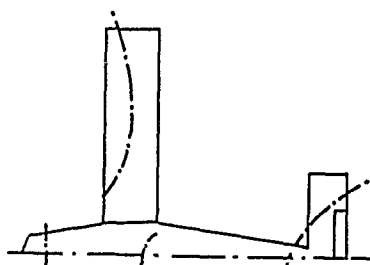
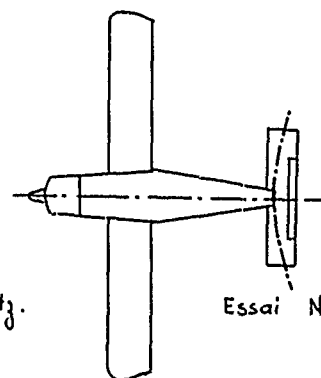
TB 20. Schématisation commande de profondeur. fig. 7.2

Rotation Monobloc

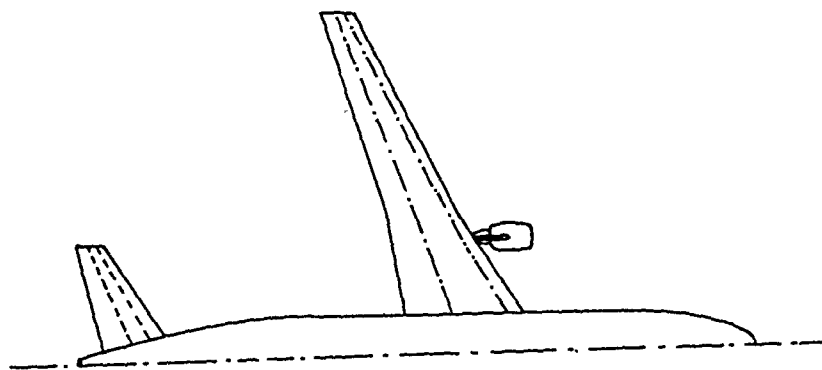
Calcul



Essai

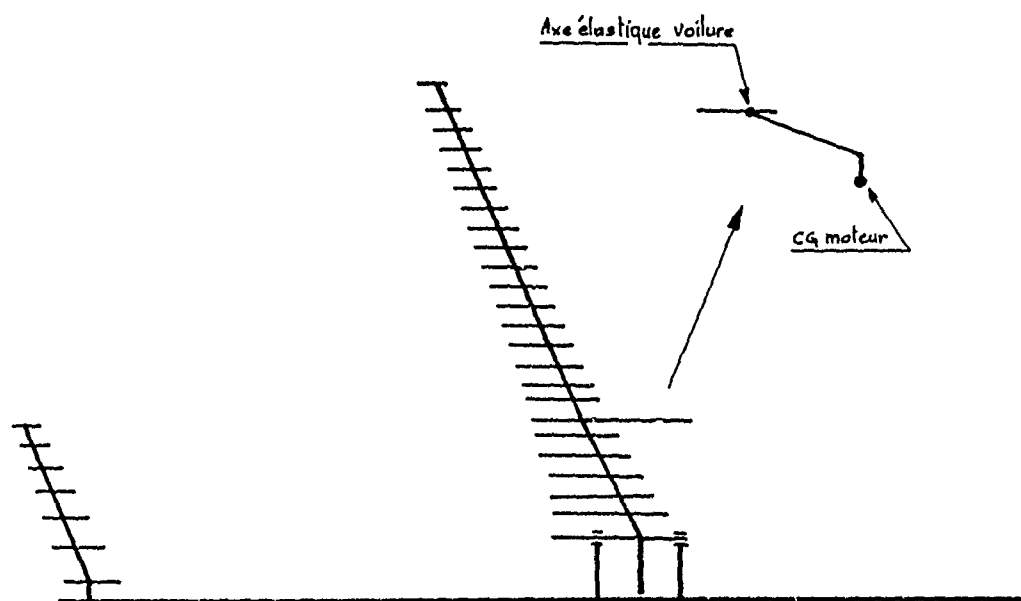
Flexion support masse équilibrage monoblocCalcul $N = 21.3 H_z$ Essai $N = 21.5$ Flexion 2 nœuds monoblocCalcul $N = 26.2 H_z$ Essai $N = 25.06 H_z$ Harmonique rotation monoblocCalcul $N = 42.8 H_z$ Essai $N = 41.8 H_z$ TB 20 . Modes propres symétriques . Calcul - essai.

Pl .8



Implantation générale

Fig. 9.1

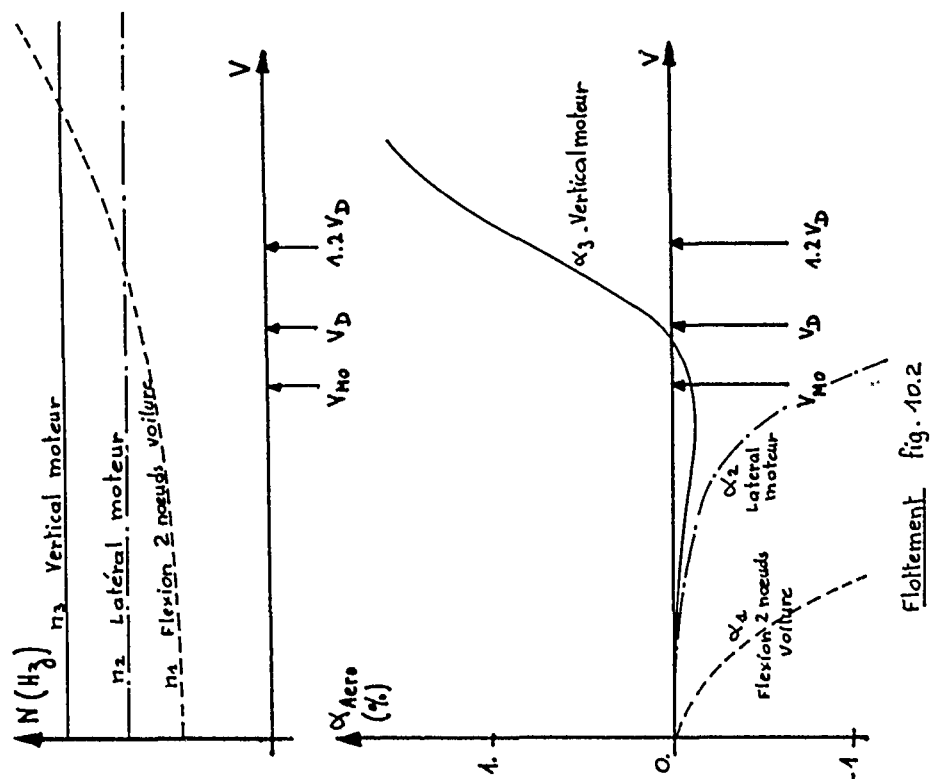


Schémalisation structurale

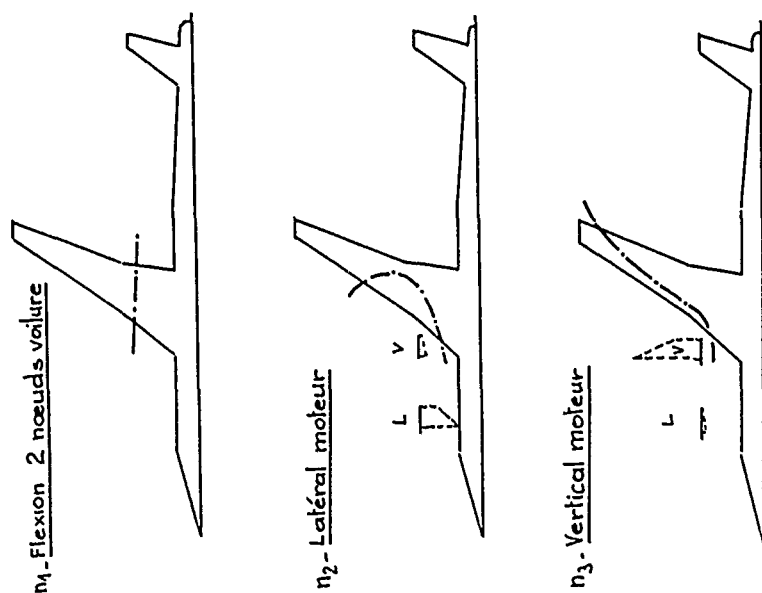
Fig. 9.2

Avion de transport à fuselage étroit

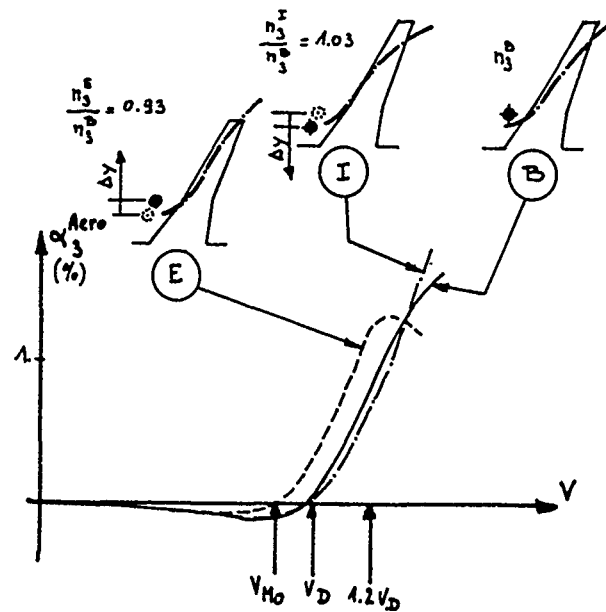
Pl. 9



Flottement fig. 10.2

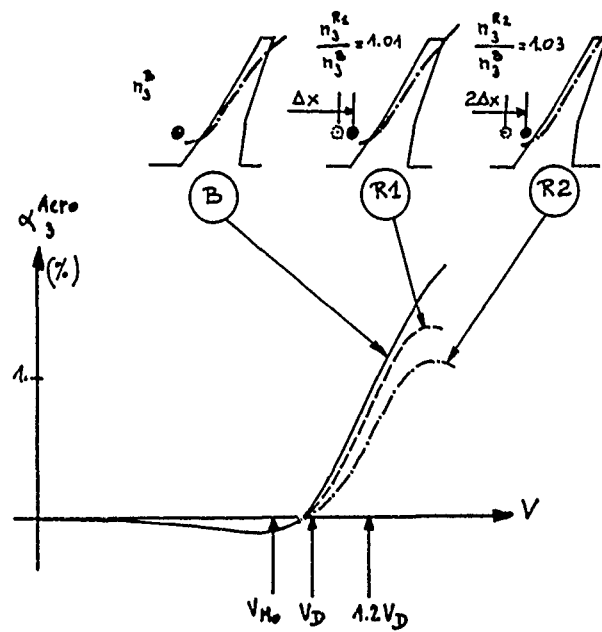


Modes propres fig 10.1



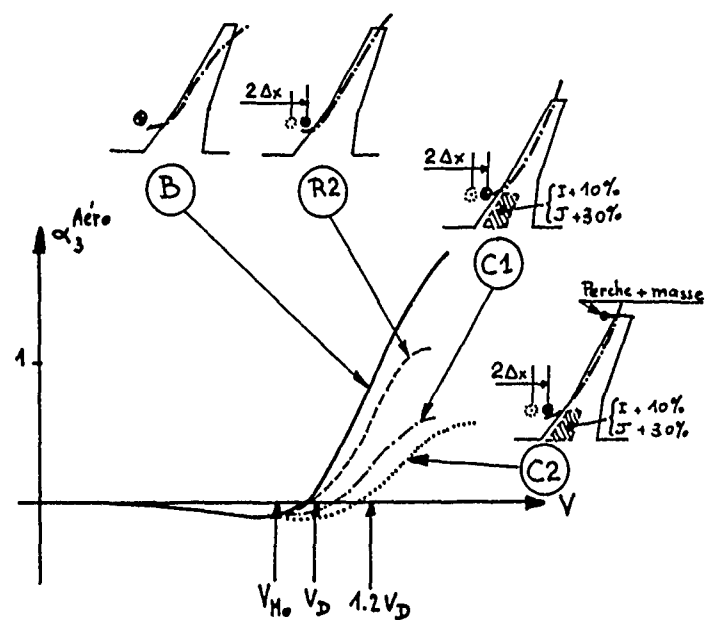
Déplacements latéraux

Fig 11.4

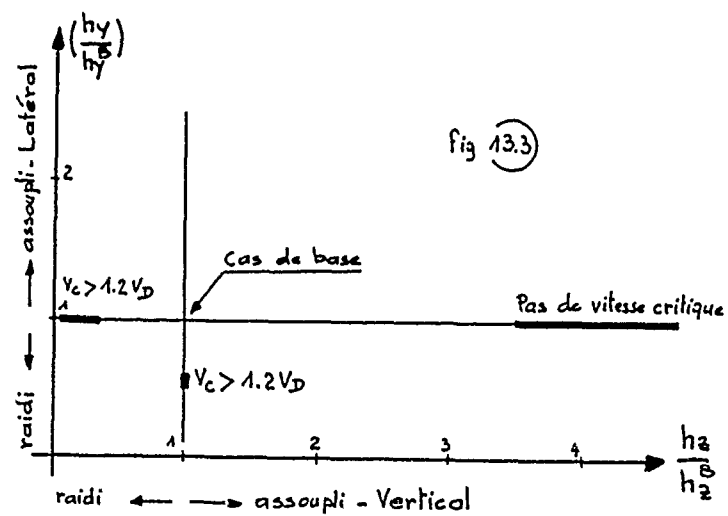
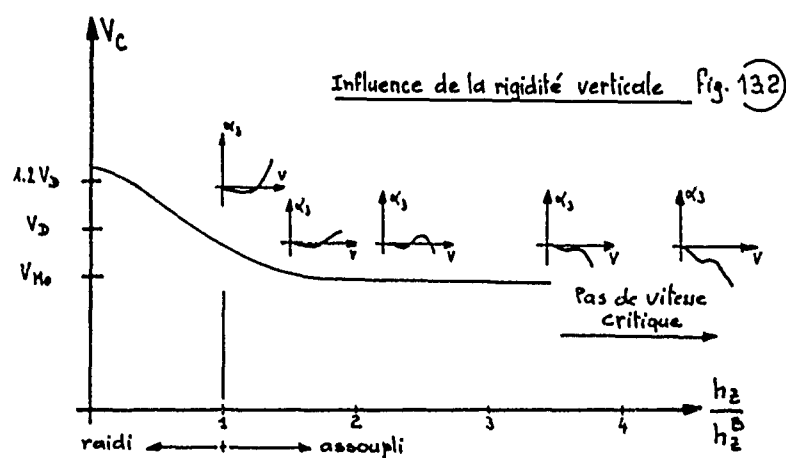
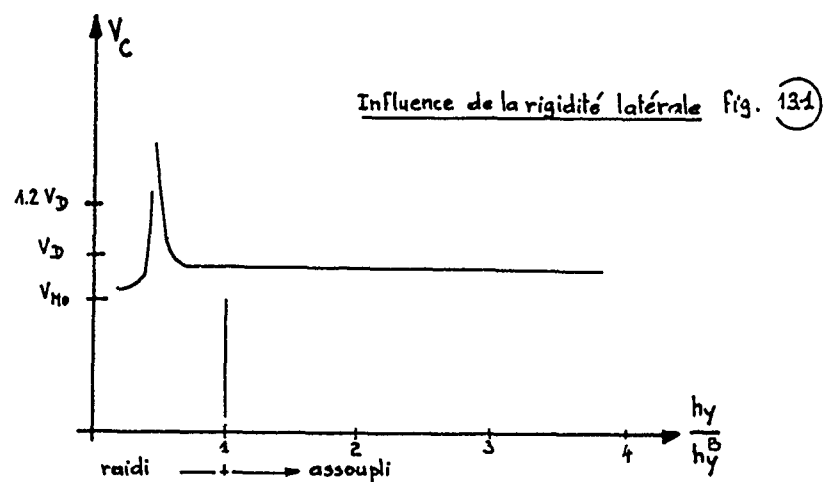


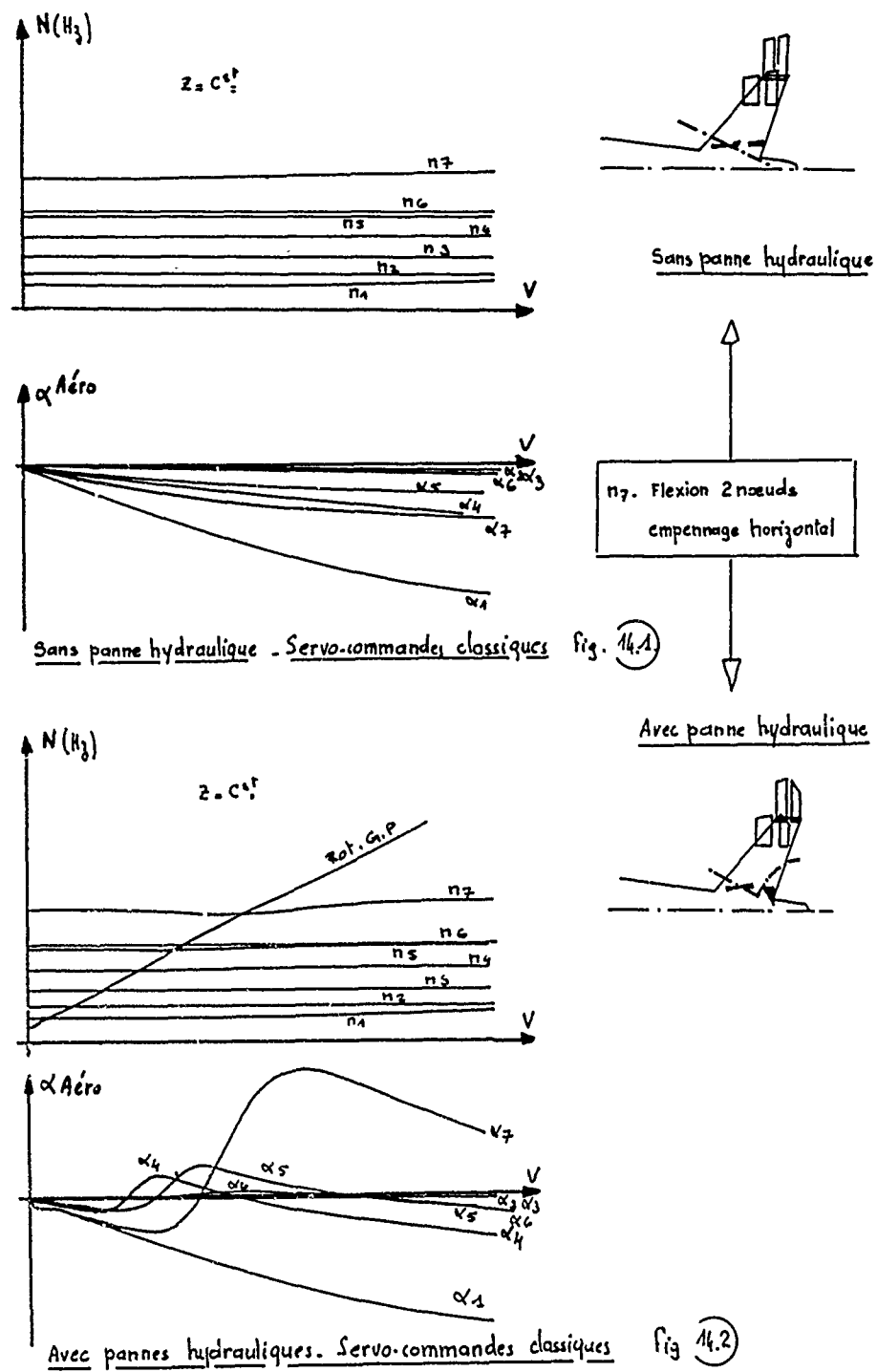
Déplacements longitudinaux

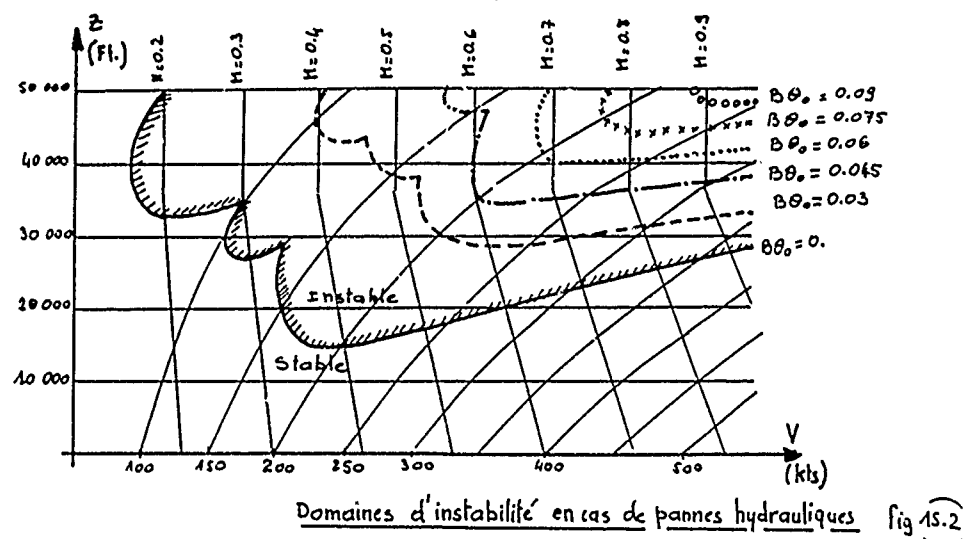
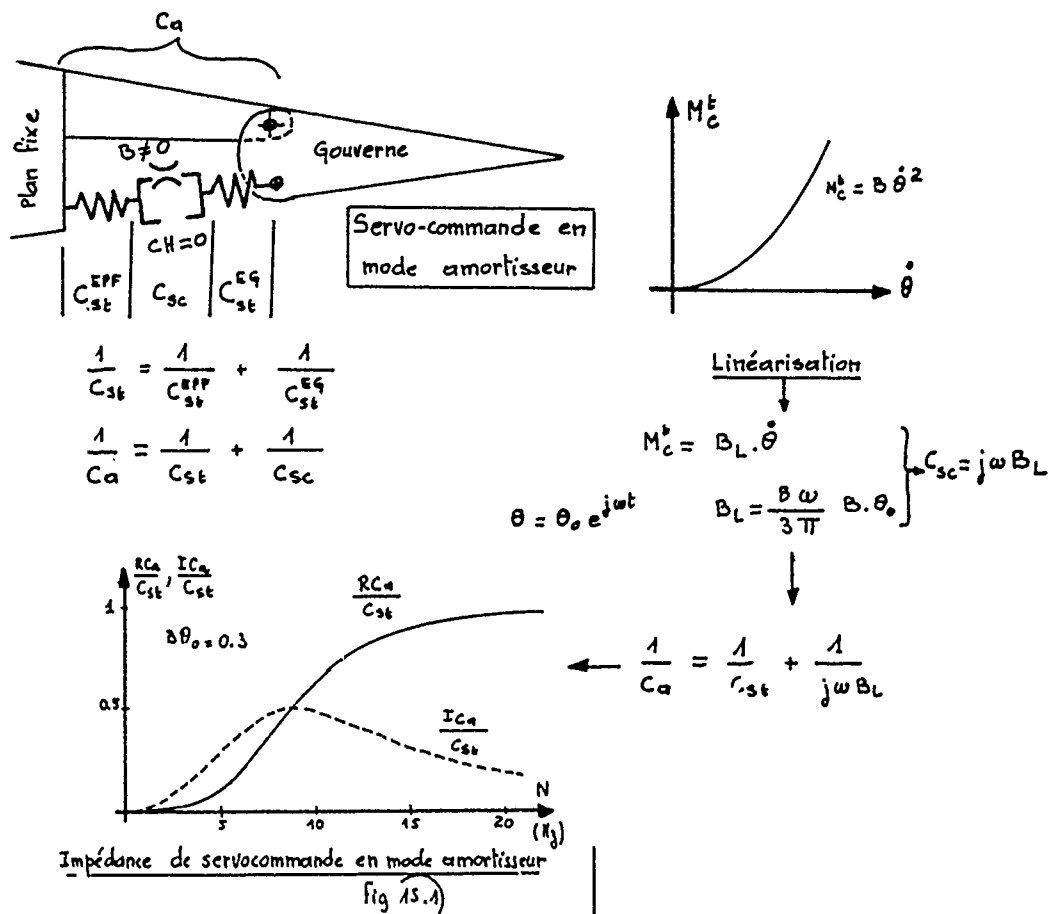
Fig 11.2



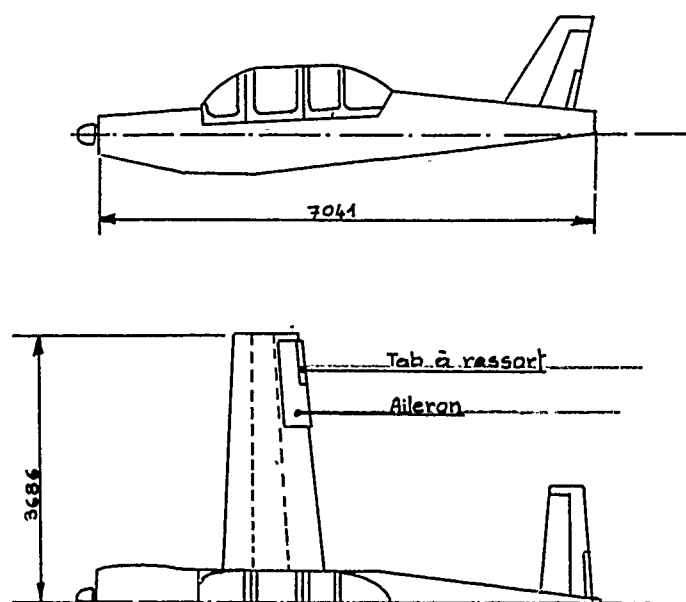
Avion de transport à fuselage étroit - Combinaison de paramètres Pl. 12



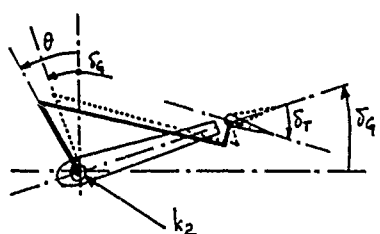




Avion de transport à fuselage étroit. Etude servo-commandes G.P. Pl.15



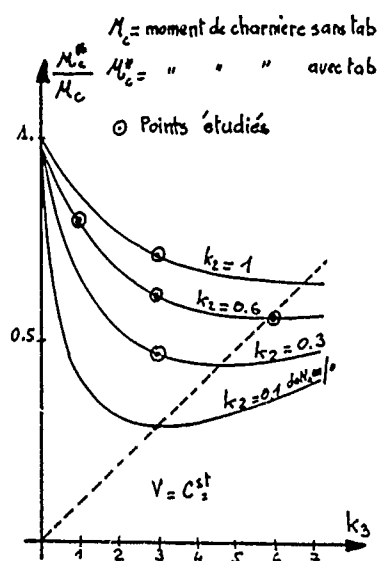
Epsilon - Implantation générale fig 16.1



δ_A = braquage de la gouverne
 δ_T = braquage du tab à ressort
 θ = rotation du guignol de la gouverne
 k_2 = raideur du ressort de tab
 $\delta_T = -k_3 (\theta - \delta_A)$
 k_3 = taux d'automatisme du tab à ressort
 braquage à moment de charnière nul
 $M_c^t = 0, V = 0 \quad \theta = \delta_A$
 $\delta_T = 0.$

— $M_c^t \neq 0 \quad \theta \neq \delta_A$
 $\delta_T = -k_3 (\theta - \delta_A)$

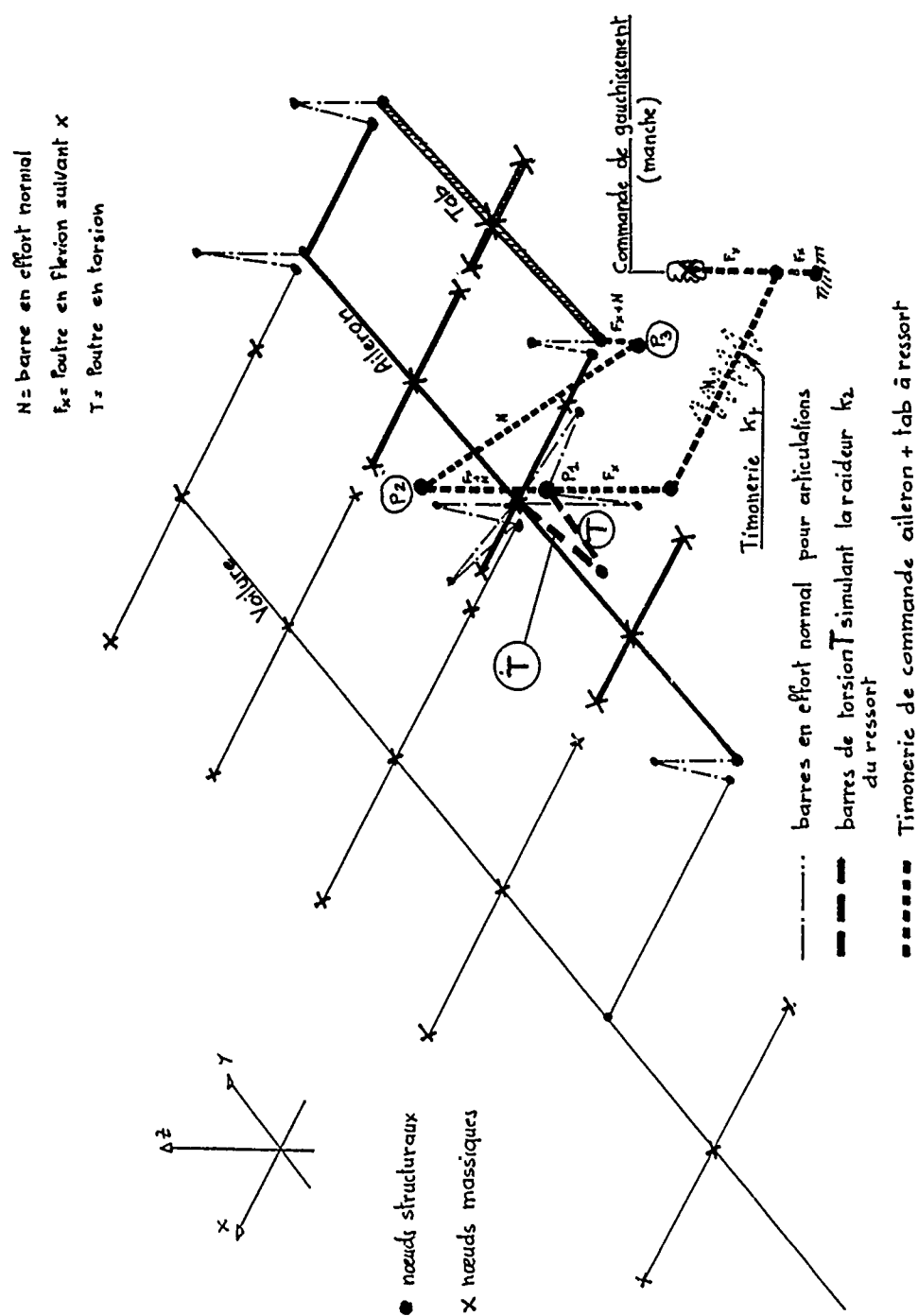
Tab à ressort - principe fig 16.2



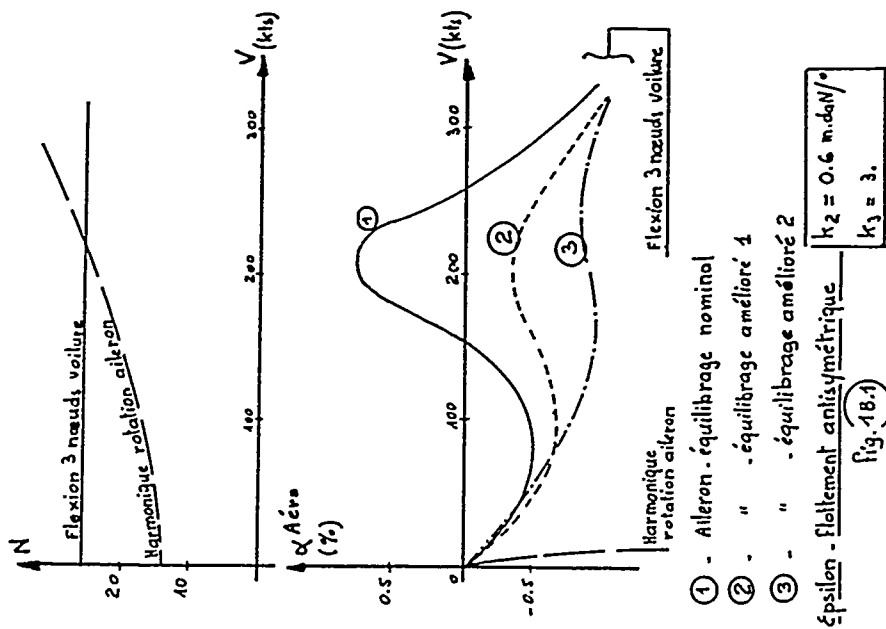
Tab à ressort - performances fig 16.3

Epsilon - Etude aileron avec tab à ressort

Pl.16

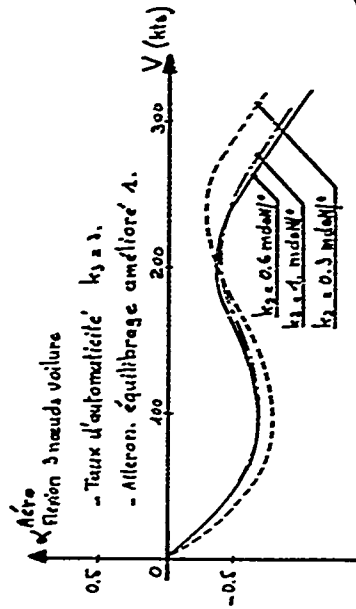


Epsilon - Schématisation de l'aileron avec tab à ressort Pl.17

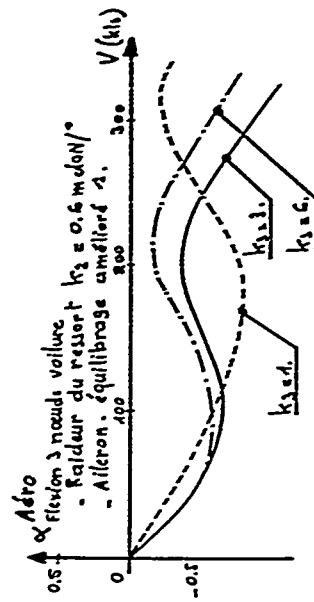


Épsilon - Etude aileron avec tab à ressort

Pl. 18



Influence de la raideur du ressort Fig. 18.2



Influence du taux d'automatie' du tab Fig. 18.3

3-1

AEROELASTIC TAILORING OF HIGH-ASPECT-RATIO
COMPOSITE WINGS IN THE TRANSONIC REGIME

by

C. J. Borland and D. W. Gimmestad
Boeing Military Airplane Company
Seattle, Washington 98124

SUMMARY

Currently available aeroelastic tailoring methods for composite aircraft structure employ linearized analysis of aeroelastic loads in the optimization cycle. For aircraft whose primary structural design conditions lie in the transonic regime, however, these loads may be considerably in error and may therefore lead to an other than optimum design. For aircraft with advanced technology or supercritical airfoil sections, the aerodynamic loading is extremely sensitive to changes in shock position and strength, which are affected in turn by small changes in geometry due to aeroelastic loading. In this paper, a procedure for coupling a rapid, accurate transonic aeroelastic analysis method, based on nonlinear small-disturbance theory, with a simple design optimization method for high-aspect-ratio composite box-beam-type structures is described. A sample aeroelastically tailored preliminary design employing nonlinear transonic aerodynamics is presented.

INTRODUCTION

Aeronautical technology has advanced very rapidly in recent years in a number of areas. The use of advanced composite and metallic materials, the development of efficient aerodynamic designs through new methods of computational fluid dynamics, and the use of active control technology, structural design optimization, and more efficient propulsion systems are a few of the areas that hold the promise of providing significantly improved performance and cost-effectiveness in coming generations of both civil and military aircraft. However, the fulfillment of this promise can only reach its highest potential if the related technologies can be applied in an integrated and interdisciplinary fashion.

A critical problem in the transport aircraft industry, that of designing an efficient high-aspect-ratio wing employing composite materials in the primary structure for operation in the transonic speed regime, is a prime example of a complex situation requiring an integrated approach. Aerodynamic performance, stability and control, structural analysis and design, and aeroelasticity must be considered simultaneously. In this paper, three distinct but related technologies – computational methods for aeroelastic analysis of transonic aircraft, structural design optimization methods, and structural analysis of composite materials – have been coupled to form a procedure for preliminary design of high-aspect-ratio wings using composite materials in the primary structural box. The resulting method is not intended to be a fully developed design tool nor to include at this time all the required aspects of the preliminary design task. In the present work, for example, the effect of aeroelasticity on static loads is incorporated in the automated design of the wing, but other aeroelastic considerations such as flutter and control effectiveness are not. These and other considerations would be required in a comprehensive preliminary design method. This work is intended, rather, to provide an example of how various interrelated technologies might be coupled in a simple but effective method for preliminary design.

BACKGROUND

Since the work described in this paper employs several different technological approaches, the backgrounds of the component parts of the preliminary design method will be described separately.

Transonic Aeroelastic Analysis and the Impact of Computational Fluid Dynamics

Since the first appearances of transonic flow phenomena on aircraft near the beginning of the Second World War, researchers have sought for practical methods for analysis of transonic flow and its effects upon aircraft design and

performance. Until 1970, this search was essentially fruitless, due to the fundamental nonlinear nature of the equations governing transonic flow. In that year Murman and Cole¹ published the landmark paper describing a mixed-flow finite differencing scheme for solving the two-dimensional steady nonlinear transonic small-disturbance equation. (Although a previous scheme for analyzing transonic flow by numerical solution of the Euler equations was previously described by Magnus and Yoshihara² the computation time required was prohibitive.) The remarkable feature of the Murman and Cole method was the simplicity of the scheme that was required to get incredibly good answers for transonic flow with embedded shocks. The scheme was quickly extended to three dimensions for moderately swept wings by Bailey and Ballhaus.³ This method was further extended by Mason et al.⁴ to account for wing-fuselage interference and to nearly complete aircraft configurations (fuselage, wing, nacelles, winglets) by Boppe.⁵ The two-dimensional method for airfoils was extended to low-frequency unsteady flow by Ballhaus and Goorjian⁶ and to high frequency unsteady flow by Rizzetta and Chin.⁷ A three-dimensional method for steady and unsteady flow over wings was developed by Borland, Rizzetta, and Yoshihara.⁸ This method was coupled with an aeroelastic solution procedure for steady (i.e., static aeroelastic loads) and unsteady (i.e., dynamic loads and flutter) analysis.⁹ The two-dimensional unsteady code was extended to include viscous effects by Rizzetta,¹⁰ and the three-dimensional code was similarly extended by Rizzetta and Borland.¹¹ Some interesting aeroelastic studies employing the two-dimensional unsteady,^{12,13} three-dimensional steady¹⁴ and three-dimensional unsteady^{9,15} methods have also been performed, although these are clearly still in their infancy.

All of the foregoing methods have employed one version or other of transonic small-disturbance theory. Methods employing the more complete full-potential equation have been developed by Jameson and Caughey¹⁶ and Holst¹⁷ for three-dimensional steady flow, by Goorjian¹⁸ for two-dimensional unsteady flow, and by Shankar, et al.¹⁹ and, most recently, Bridgeman et al.²⁰ for three-dimensional unsteady flow. Full-potential methods generally require more expenditure of computational resources than small-disturbance methods and may not give significantly better answers for typical transport wing configurations. Although many of these methods, and the associated computer codes, are still in the nature of research tools, there have been several instances of aircraft redesign^{21,22} based on these analysis capabilities. Most modern aircraft design organizations now employ computational fluid dynamics methods in some fashion, and many rely on them quite heavily. This is a far cry from the practice of 10 years ago, when the aerodynamic design of aircraft was based almost exclusively on wind tunnel and flight test experience.

The situation in aeroelastic design and analysis is far less advanced. Aeroelasticity, by its very definition, implies a coupling between aerodynamic and structural considerations. During the development of the B-52, at the very beginning of the period which lead to the design of the modern jet transport fleet, Gray and Schenk²³ discovered the benefits of incorporating aeroelasticity in the loads analysis of high-aspect-ratio swept wings. A 10% reduction in design loads was achieved, leading to a considerably more efficient structure. The longevity of the B-52 (intended as an interim airplane later to be replaced by the supersonic B-58) and its adaptability to situations and flight operations outside of the original concept are a testament to good design practice. The TN3030 method of Gray and Schenk still forms the backbone of aeroelastic design of subsonic high-aspect-ratio transport aircraft.

More sophisticated methods of aeroelastic design, employing lifting surface theories (such as doublet-lattice²⁴ for subsonic flow and mach box²⁵ for supersonic flow) and finite element structural analysis methods,²⁶ came into routine use with the coming of the computer as an everyday tool in the sixties and seventies. The transonic regime, where aeroelastic problems are often the most critical, remained elusive. Highly sophisticated and expensive wind tunnel test procedures were employed to ensure that no surprises would be discovered once a new aircraft entered flight test. Unfortunately, that was not always the case.²⁷

It appears there are now practical tools based on the newly available methods discussed above for many previously unsolved problems in aircraft aeroelasticity.⁹ A thorough exploration of the validity and applicability of these methods and their incorporation into routine design practice, together with the development of needed improvements and additional capabilities (such as analysis of separated flow), are still required.

Structural Optimization

The use of formal mathematical methods for optimizing structural design has, similarly, only come to fruition with the availability of the computers starting in the late sixties and seventies. There is a wealth of literature in this field, and Ashley's summary²⁸ is an excellent one. Few methods, however, have been incorporated into the aeroelastic design process. Among those that have are the TSO,²⁹ FASTOP,³⁰ SWEEP,³¹ COMBO,³² and ORACLE³³ programs. Inherent in each of these methods are some basic limitations to keep the required computational and manpower resources within

reason. In some methods, such as TSO, "mathematical programming" optimization methods are used. These evaluate many candidate designs by systematic variations of design variables and evaluations of "objective functions" and "constraints" and their gradients. Other methods employ "optimality criteria," modifying the design in a less formalized systematic method to achieve a desired goal. In the ORACLE program, for example, an isotropic box-beam wing structure is designed for aeroelastic loads by cycling a wing with an initially chosen stiffness distribution through a loads computation module, sizing the structural box to these loads using a fully stressed design algorithm, and repeating the process until a converged design is achieved; i.e., the stiffnesses resulting from the design are the same as those used in the loads computation. Because fully stressed design does not yield minimum weight except under a highly restrictive set of circumstances (nonredundant structure, single load case, fixed loads not a function of the design, linear relations of stress and weight), there is no guarantee that such a process will yield the most efficient (minimum weight) structure.

Structural Analysis of Composite Materials

The use of composite materials opens several new possibilities in the structural design process. Although a primary benefit of composite materials (such as graphite-epoxy) is a reduction in weight for constant strength, the unique directional stiffness and strength properties of the materials can be used to advantage. The process by which the characteristics of a structure are varied to achieve a desired goal (such as reduced weight) under specified constraints (such as flutter and strength requirements) by inducing favorable load-deflection coupling effects has become known as "aeroelastic tailoring." Whereas in metal structure only the thickness can be varied to provide variations in strength and stiffness for a given structural arrangement (ribs, spars, skins, stringers, etc.), with composite material the total thickness, the thicknesses of individual layers of the laminate, and the fiber directions all can be varied. It is possible also to modify the structural arrangement (stringer locations, number of spars, etc.) as part of optimization but this would be a more involved process than is considered here. An extension of the ORACLE method, known as CORK,³⁴ uses the same aeroelastic cycle described earlier but sizes composite structure for minimum weight per unit span subject to material strain constraints through the use of mathematical programming optimization. A computer code known as SAND³⁵ is employed for design of each of multiple cross-sections of a box beam representing the structure of a high-aspect-ratio transport-type wing. In the current version of CORK, only the total material thickness is varied internally in the optimization process, but variations in the thickness of the individual lamina and fiber direction can be specified in parametric studies by the user. CORK is capable of handling anisotropic composite structure, where the lamina in differing directions (such as ± 45 deg) are not present in equal proportions or where nonstandard directions are used in the layup.

AEROELASTIC TAILORING IN THE TRANSONIC REGIME

All of the aeroelastic tailoring and optimization methods described above, in addition to inherent limitations on structural modeling, have a common assumption: that the aeroelastic loads on the resized structure are determined by use of linear subsonic (or in some cases supersonic) aerodynamic theories. For aircraft such as military or commercial transports whose primary structural design conditions lie in the transonic regime, in a mach number range of 0.75 to about 0.95, these aeroelastic loads may be considerably in error and may therefore lead to other than optimum preliminary designs. For aircraft with advanced technology or supercritical airfoils, the problems will be magnified. Although these airfoils are designed for optimum aerodynamic performance at a specific flight condition, their aerodynamic characteristics at off-design flight conditions (where structural design conditions usually occur) tend to be much more sensitive to small changes than conventional airfoil sections. Small changes in geometry due to aerodynamic loading may lead to relatively large changes in shock position and strength, which therefore directly affects the loading. Furthermore, advanced or supercritical airfoils tend to be highly aft-loaded, which may induce a stronger effect of elastic load relief on swept-back wings than is observed for conventional airfoils. Aeroelastic methods employing linear aerodynamic theory, unless wind tunnel corrections are used, tend to underestimate these effects. It seemed necessary therefore, to develop an aeroelastic tailoring system for preliminary design that would take advantage of more accurate methods for computing transonic flow on aeroelastic configurations. A description of the system developed and some demonstration of its use in achieving improved designs is the subject of the remainder of this paper.

A schematic flow chart of the system developed is shown in figure 1. Briefly, given an aerodynamic configuration (planform, section geometries, and twist), structural configuration (estimated mass and inertia properties, spar geometry, and elastic axis location), and flight condition (mach number, gross weight, dynamic pressure, and normal design limit load

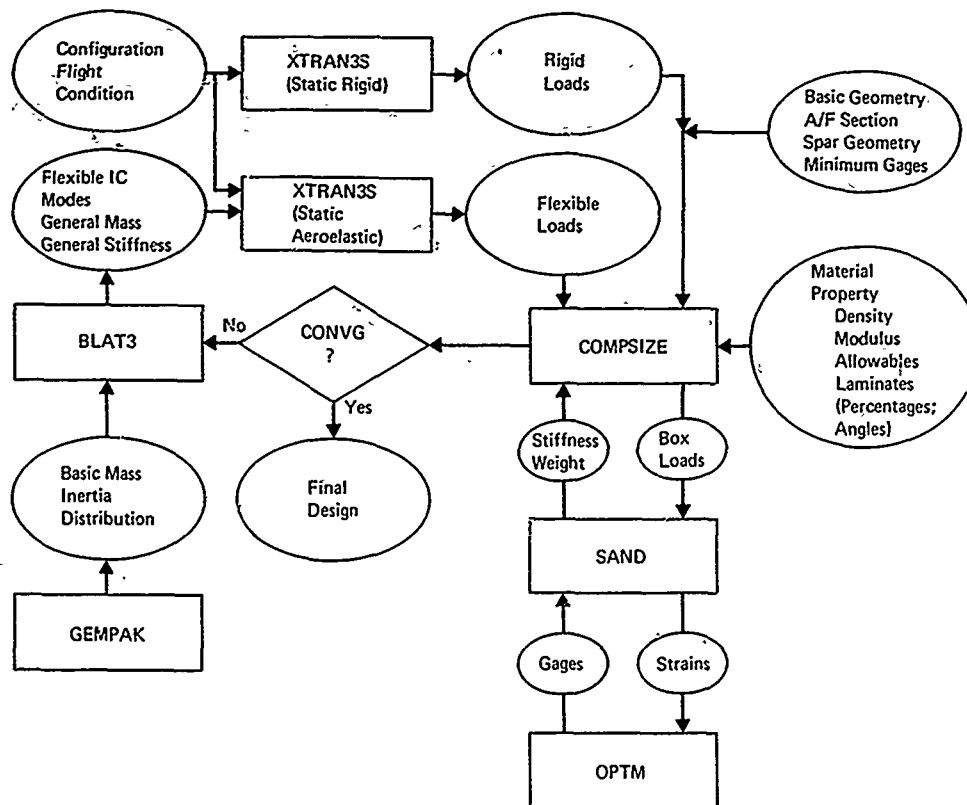


FIGURE 1. TRANSONIC AEROELASTIC OPTIMIZATION SYSTEM

factor), a set of "static rigid" loads is calculated using the pilot code version of the XTRAN3S three-dimensional transonic aerodynamics method.³⁶⁻³⁸ (The pilot code version has been employed because of recent efficiency improvements).

Because of the nonlinear nature of the method, an iterative solution is required to arrive at the correct angle of attack, where the developed total lift matches the product of gross weight and design limit-load factor. Similarly, an iterative solution for jig twist corresponding to a specified lg spanwise lift distribution is required. The distributed external loads, in the form of integrated shear, moment, and torsion along the elastic axis, are then input to a composite box-beam structural sizing method known as COMPSIZE. This method has been adapted from the CORK program to interface with the transonic loads program rather than the original linear aeroelastic analysis method. COMPSIZE ratios the applied limit loads to ultimate load design conditions and sets up an input file for the repetitive execution of SAND. The SAND program provides a minimum weight per unit span design of the upper and lower cover thicknesses and the required gages for the front and rear spars. (SAND also has options for design of multiple-cell boxes, spar caps, stringers, and other features, but these were not exercised in the current study.) The stresses, strains, and margins of safety are calculated, and a specified maximum strain, together with minimum gage requirements, is used to constrain the design. A mathematical programming optimizer, OPTM, based on the steepest descent sidestep method, is used to minimize the constrained objective function of weight per unit span. After an optimized design is achieved, the bending and torsional stiffness are calculated for each section. SAND is executed once for each of up to 15 representative sections of the wing.

Given the calculated stiffness distribution and mass-inertia properties estimated by GEMPAK (a part of the ORACLE system), a preliminary weights estimation program, the vibration frequencies and natural vibration mode shapes of the resized wing are calculated by a beam-type wing structural dynamics analysis program known as BLAT3.³⁹ BLAT3 also provides the generalized mass and stiffness matrices. The modes and structural matrices are then input to the XTRAN3S pilot code, operating in a static aeroelastic solution mode. The natural mode shapes are used as superposed generalized coordinates in providing a set of modified (i.e., structurally deflected) boundary conditions used in the transonic flow analysis. The output of the code is the deformed elastic shape and corresponding transonic pressure distribution of the flexible wing. These are internally consistent because the static structural equations are solved at each iterative step of the transonic numerical solution. Again, iterative procedures are used to obtain the angle of attack and jig twist necessary to match the required spanwise lift distribution and total static load. A revised set of integrated shear, bending, and torsional loads, now representing the actual design limit-load distribution on a flexible wing, is then input to the COMPSIZE program, and a new wing structural design is generated. The process can then be repeated until a converged design solution is achieved, as measured by the reduction of structural weight changes between design cycles to below some predetermined level. It may be observed that the system described here employs a combination of mathematical programming and

optimality criteria approaches, in that the design is cycled through aeroelastic and structural design calculations until the "criteria," a converged solution, is satisfied.

DESIGN OF A TRANSPORT COMPOSITE WING

The system described above has been exercised by developing an optimized design for a hypothetical transport wing. Figure 2 shows the aerodynamic planform and structural parameters; figure 3 shows the section characteristics. The planform and sections were chosen to match those of the "Lockheed Wing-A" configuration for which a large body of rigid model transonic wind tunnel data is available.⁴⁰ A maximum zero fuel weight of approximately 427,000 lb (193,739 kg) was chosen. This corresponds to a wing loading of 100 lb/ft² (438.3 kg/m²) and a root chord of 400 in (1016 cm), typical of modern widebody transports with zero fuel. A zero fuel condition was chosen to simplify the example, although other fuel loadings may be more critical for a practical design case. Spar locations of 13% and 61% were chosen as typical of current design practice. The upper and lower composite cover panels were specified as graphite-epoxy in a 0/+45/-45/90 deg layup referenced to the elastic axis with the layers distributed in a 30/30/30/10 percent ratio. The resulting material is orthotropic, with none of the bend-twist coupling characteristics typical of aeroelastically tailored anisotropic composite structure. (Although percentage distributions in the laminate and fiber orientation angles are not currently included as design variables in the optimization process, this could be accomplished and would help assess the benefits of aeroelastic tailoring with anisotropic materials at an early stage in the design process.) The front and rear spars are specified as

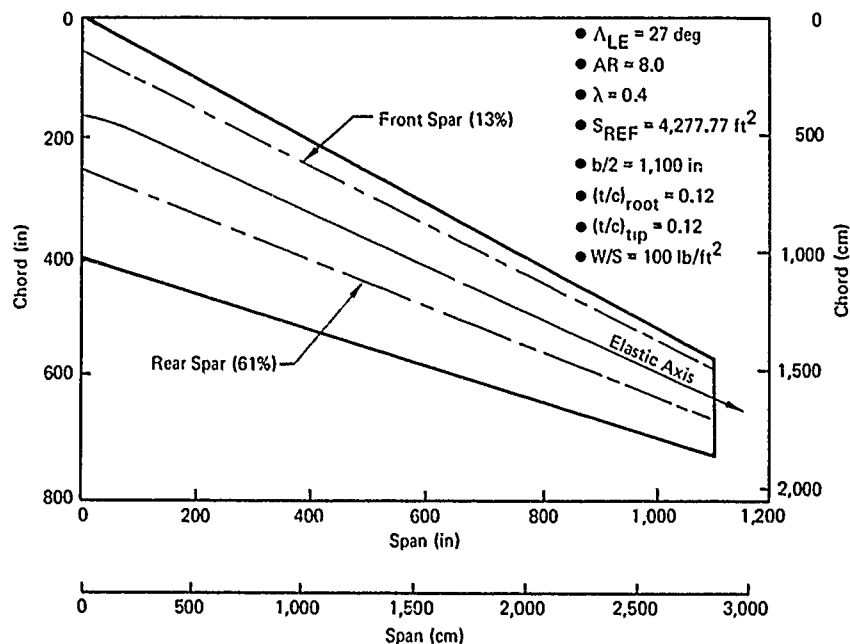


FIGURE 2. COMPOSITE WING TEST CASE—PLANFORM AND STRUCTURAL PARAMETERS

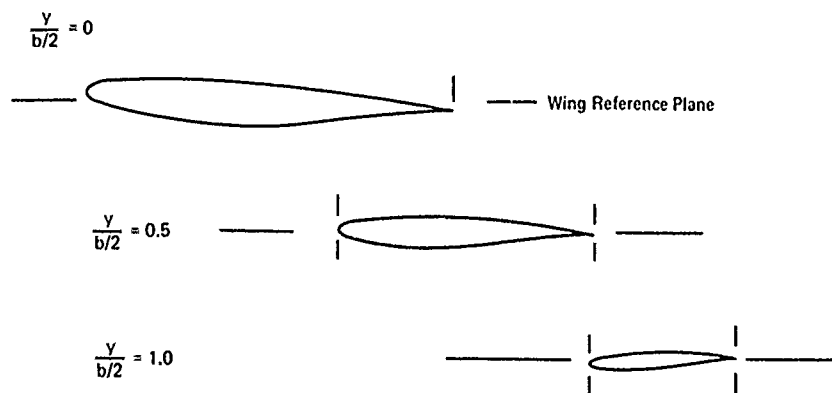


FIGURE 3. COMPOSITE WING TEST CASE—AIRFOIL SECTION CHARACTERISTICS

3-6

aluminum alloy. The airfoil section, specified at the tip and root and lofted linearly in between, is a state-of-the-art supercritical airfoil, obtained by an inverse design procedure from a specified pressure distribution.⁴⁰ The single limit-load condition chosen for the design exercise is a 2.5g symmetric pullup at a typical design dive speed (V_D) of 420 kn (216 m/sec) CAS, which for a mach number of 0.82 at an altitude of approximately 15,000 ft (4,572 m), corresponds to a dynamic pressure of 4.0 lb/in² (27.6 kPa). In a practical design case, an "envelope" design considering many conditions, including low-speed high angle of attack conditions that cannot be treated by the present method, would be developed. The original wind tunnel model had a nose-up twist at the root of 2.76 deg and a nose-down twist at the tip of 2.04 deg. This shape was modified for the initial rigid loads and for each cycle of the redesign by a process known as "jig twisting," i.e., modifying the unloaded shape to ensure that a specified 1g load distribution would be maintained as closely as possible. The specified 1g load distribution is usually a compromise between aerodynamic performance and structural design requirements. A typical "target" load distribution is shown in figure 4, along with the load distribution achieved by jig twisting the rigid wing. For the present example, jig twisting involves interpolation of two-dimensional section lift characteristics obtained from the XTRAN3S nonlinear transonic code at different angles of attack, since an iterative solution for a specified load is not currently included. It may be seen that this simple process cannot identically achieve the target loads, but it is felt to be adequate for the current example. The 1g loads are calculated at a typical maximum operating speed (V_{MO}) of 360 kn (1895 m/sec) CAS at a dynamic pressure of 2.79 lb/in² (19.2kPa), corresponding to 23,000 (7,010 m) ft at a mach number of 0.82.

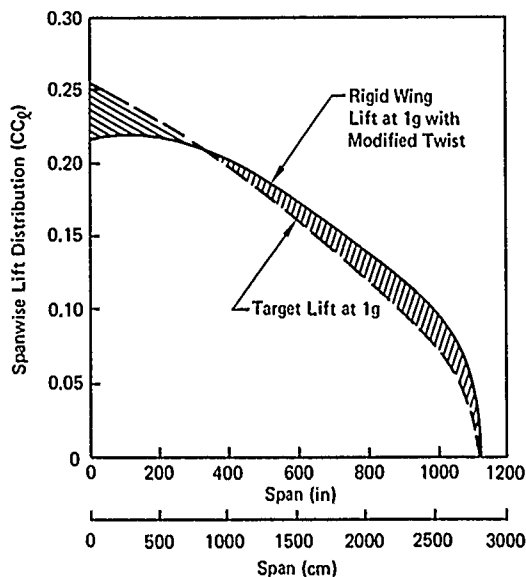


FIGURE 4. SPANWISE LIFT DISTRIBUTION AT 1g FOR THE RIGID WING

Figure 5 shows the 1g load distribution on the flexible wing after one, two, and three design cycles, including the effects of jig twisting at each step. Although there is some variation from the target loads, the jig-twist procedure permits a relatively constant 1g load distribution to be maintained. The original twist distribution, the rigid loads jig twist and the resulting twist for three aeroelastic design cycles are shown in figure 6. The fairly rapid variation near the tip is typical of current generation transport aircraft.

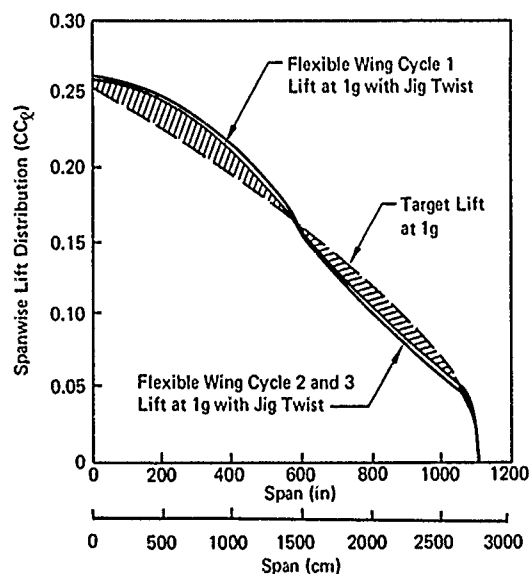


FIGURE 5. SPANWISE LIFT DISTRIBUTIONS AT 1g FOR THE FLEXIBLE WING

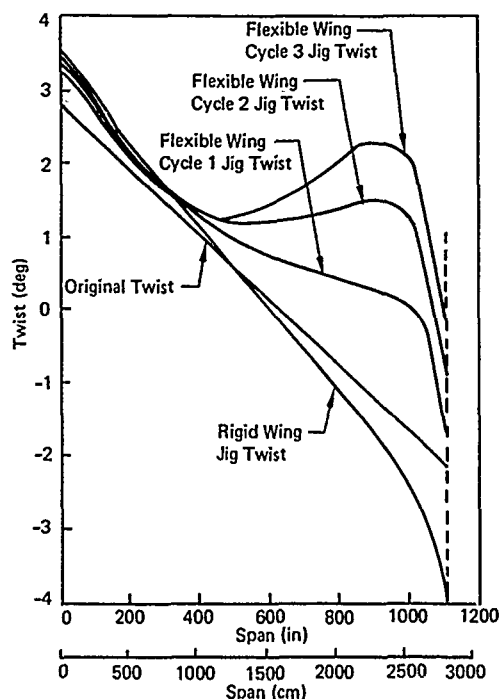
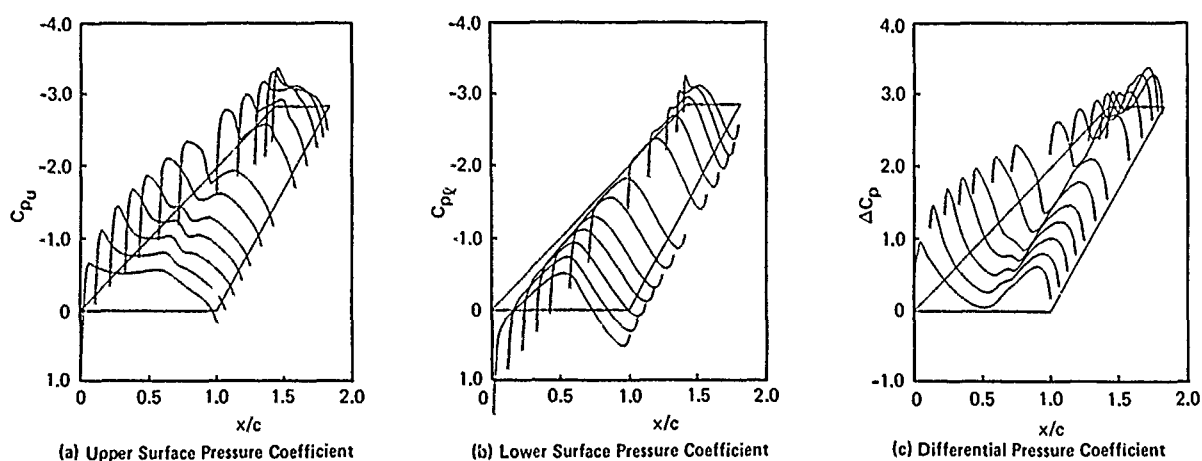


FIGURE 6. JIG TWIST DISTRIBUTIONS FOR THE RIGID AND FLEXIBLE WINGS

Figure 7 shows the pressure distribution on the jig-twisted rigid wing at the design limit-load factor of 2.5 as predicted by the transonic code. Figures 7a and 7b show the upper and lower surface pressure distributions, respectively, while figure 7c shows the differential, or lifting, pressure that contributes to integrated structural load. The angle of attack is 0.604 deg. It can be seen that there are two weak shocks on the upper wing surface on the inboard position of the wing. These coalesce to a single shock near the center, but then another weak shock forms on the aft part of the wing on the outboard portion. The presence of the second shock causes higher differential loads near the tip. On the lower surface, the pressure distributions are strongly influenced by the curvature in the "cove" region of the supercritical airfoil. The net effect, as shown in figure 7c, is that the wing is highly aft-loaded over the entire span. This leads to nose-down torsional moments in the structure, which reinforce the effects of decreased streamwise slope due to vertical bending of the elastic axis of the swept wing (also known as "washout").

FIGURE 7. TRANSONIC NONLINEAR PRESSURE DISTRIBUTIONS ON THE RIGID WING
AT $M_{\infty} = 0.82$, $\alpha = 0.604$ deg

The spanwise lift distributions (section lift coefficient multiplied by local chord), and local section centers of pressure are shown in figure 8a and 8b. The integrated shear, moment, and torsion loads, calculated about the elastic axis but plotted versus the span, are shown in figures 9a through 9c. Also shown are aerodynamic characteristics, rigid loads, and loads on the flexible configuration after one, two, and three design cycles through COMPSIZE. The aftward shift of center of pressure for the flexible cases indicates the effect of nose-down twist, with a resultant loss of lift, near the wing tip. The inboard shift of the spanwise lift distribution and aft shift of the center of pressure yield reductions in the integrated structural design loads when the coupled aeroelastic solution is performed. This permits the optimizer to reduce the upper

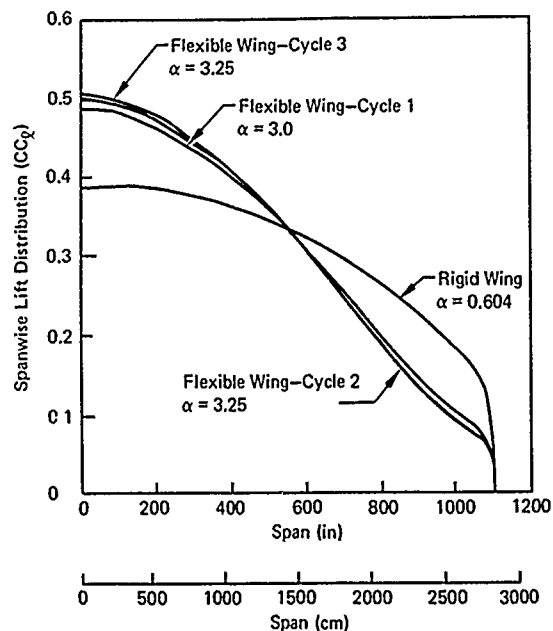


FIGURE 8a. SPANWISE LIFT DISTRIBUTIONS AT 2.5g FOR THE RIGID AND FLEXIBLE WINGS

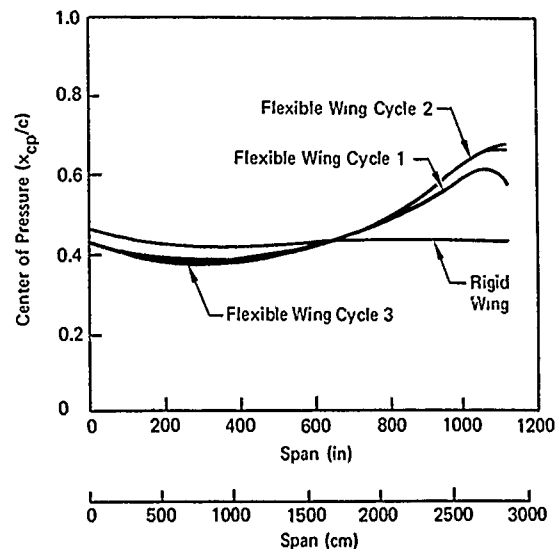


FIGURE 8b. SPANWISE DISTRIBUTION OF CENTER-OF-PRESSURE LOCATION FOR THE RIGID AND FLEXIBLE WINGS

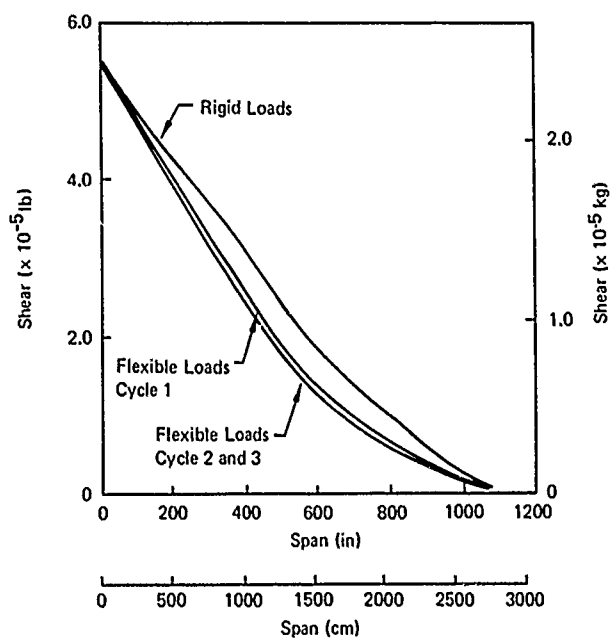


FIGURE 9a. INTEGRATED SHEAR DISTRIBUTIONS FOR THE RIGID AND FLEXIBLE LOAD CASES

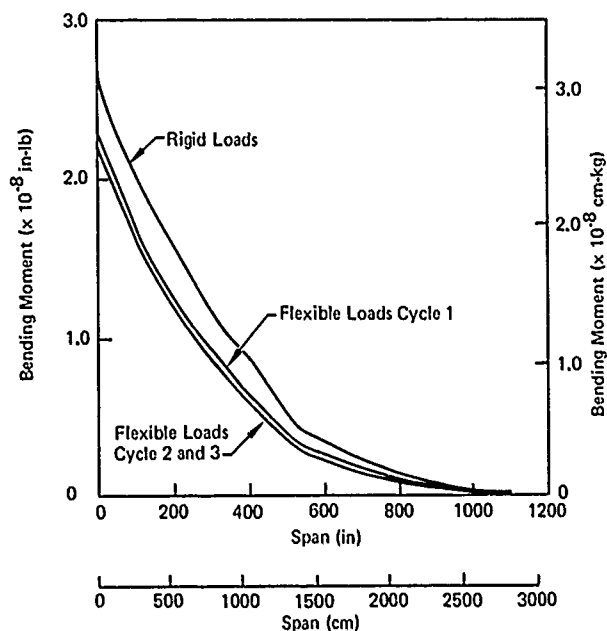


Figure 9b. INTEGRATED BENDING MOMENT DISTRIBUTION FOR THE RIGID AND FLEXIBLE LOAD CASES

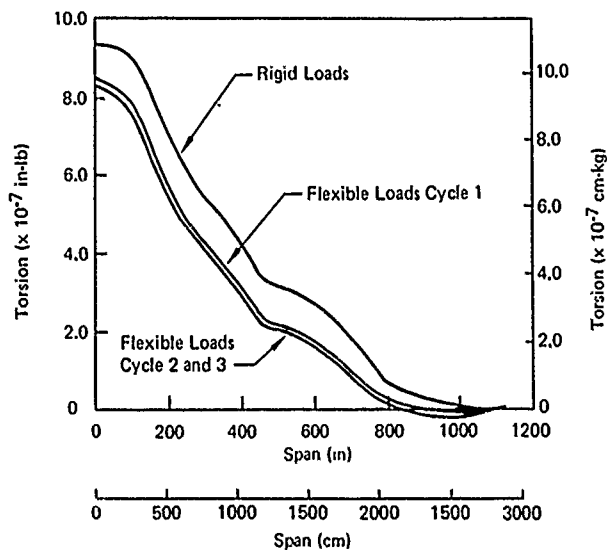


FIGURE 9.c INTEGRATED TORSION DISTRIBUTIONS FOR THE RIGID AND FLEXIBLE LOAD CASES

and lower cover gages, and hence structural weight, for all sections that are above minimum gage. Figure 10 shows the total wing weight (spars plus composite covers) for four COMPSIZE design cycles, using the rigid loads and the flexible loads after the first three cycles as input. The total structural weight was reduced less than 0.1% as a result of the last design cycle, indicating that the design loads were essentially unchanged. The process was thus terminated after three full aeroelastic cycles.

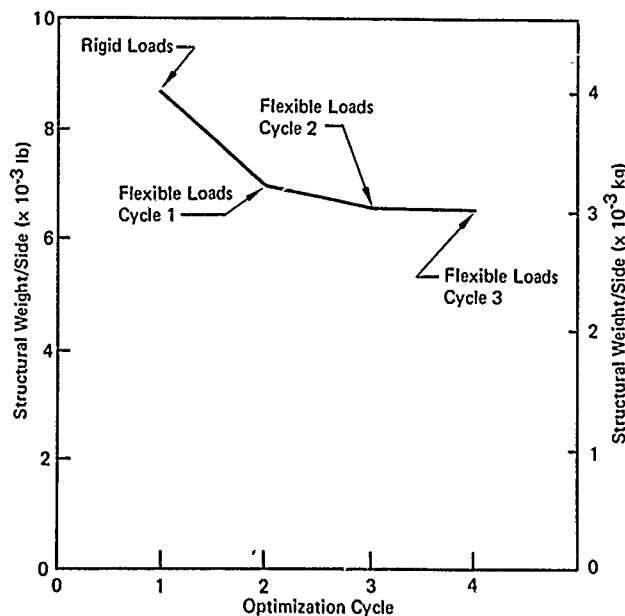


FIGURE 10. TOTAL STRUCTURAL WEIGHT ACHIEVED BY THE OPTIMIZATION PROCESS

The resulting upper, lower, and differential pressure distributions on the flexible wing are shown in figures 11a, 11b, and 11c. A loading pattern similar to that on the rigid wing exists on the root and midsections, except for a stronger inboard shock due to the higher angle of attack necessary to maintain a constant load factor — 3.25 deg versus 0.604 deg on the rigid wing — but the upper surface loading near the tip has been altered. On the lower surface, a strong negative pressure peak, terminated by a local shock, exists near the leading edge at the tip, as a result of the nose-down deflection of approximately 10.6 deg at the outboard edge of the wing. Figure 12 shows the deflected shape of the wing from the rigid position. Actual deflection of the trailing edge tip is approximately 177 in (4.49 m), or 14.5% of the structural span at this load condition. The upper and lower skin gages and the resulting bending and torsional stiffness distributions obtained for four design cycles are shown in figures 13 through 15.

It may be noted that much of the outboard portion of the wing reaches minimum gage as a result of the optimization process. In a practical design case this may not be realizable due to other loading conditions not considered here.

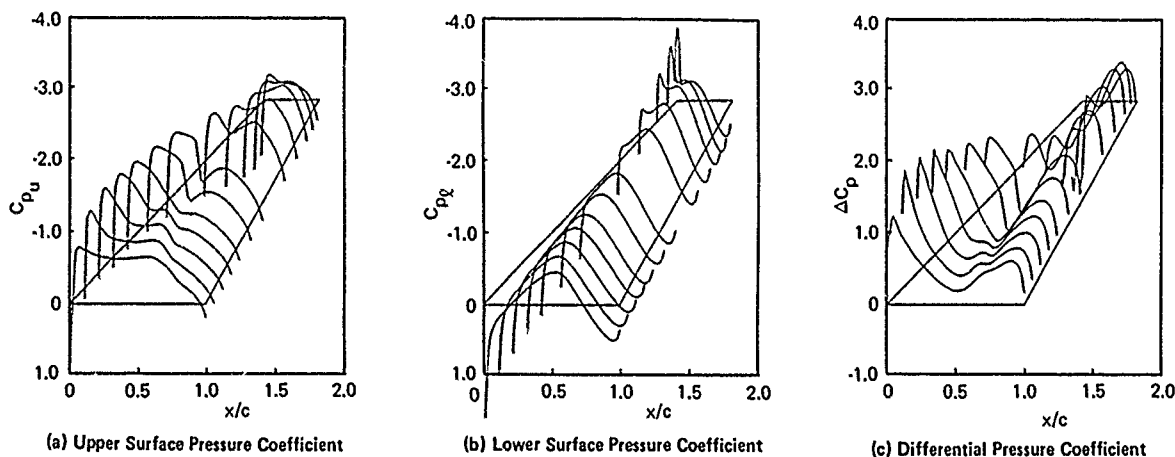


FIGURE 11. TRANSONIC NONLINEAR PRESSURE DISTRIBUTIONS ON THE FLEXIBLE WING (THIRD DESIGN CYCLE) AT $M_{\infty} = 0.82$, $\alpha = 3.25$ deg

3-10

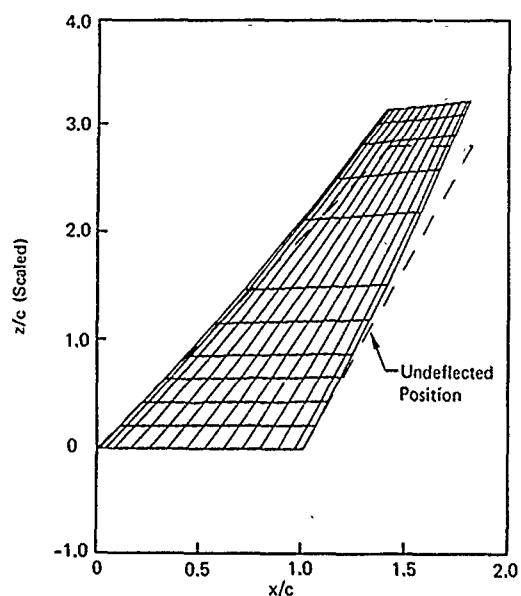


FIGURE 12. DEFLECTED SHAPE OF THE FLEXIBLE WING

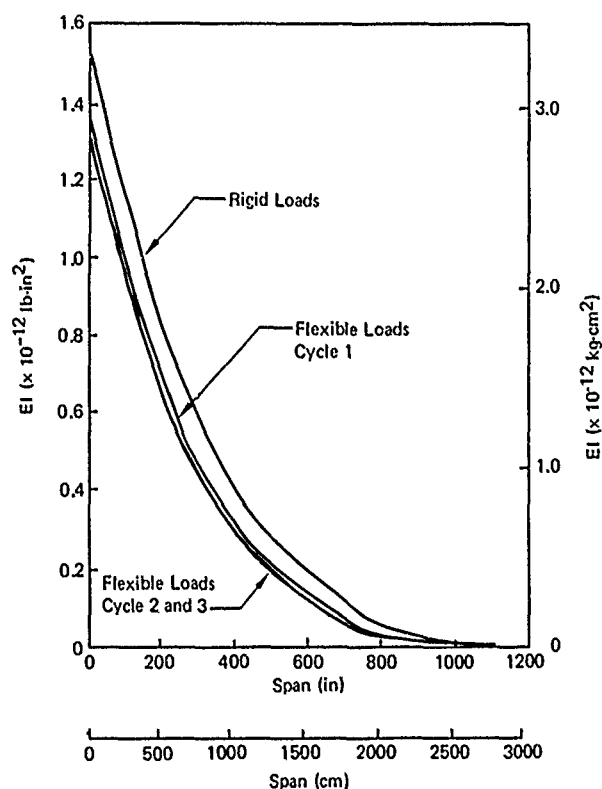


FIGURE 14. BENDING STIFFNESS DISTRIBUTIONS FOR RIGID AND FLEXIBLE LOAD CASES

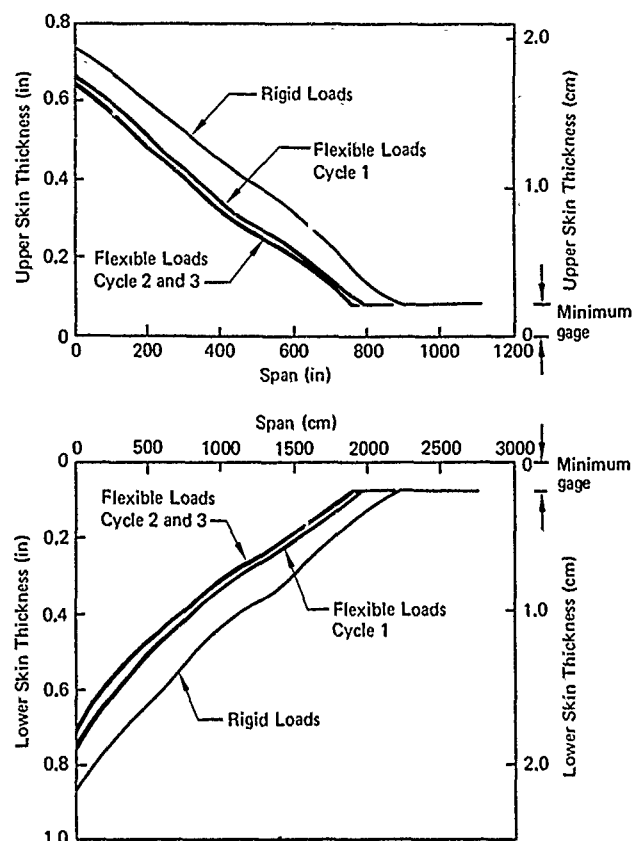


FIGURE 13. UPPER AND LOWER COVER THICKNESS FOR THE RIGID AND FLEXIBLE LOAD CASES

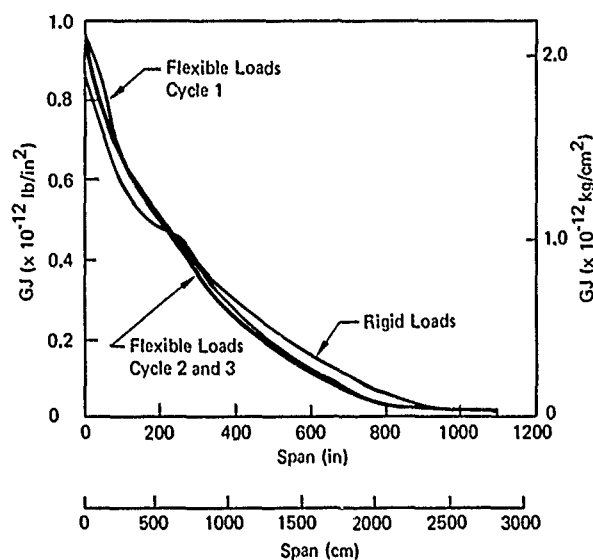


FIGURE 15. TORSIONAL STIFFNESS DISTRIBUTIONS FOR RIGID AND FLEXIBLE LOAD CASES

In the foregoing analysis, no empirical corrections based on wind tunnel data have been applied. In actual design practice, experimental load distributions and center-of-pressure locations, if available, would be used to develop initial design loads. It is worth noting, however, that the only wind tunnel data usually available early in the aircraft design process are either two-dimensional section data or three-dimensional data from the testing of rigid models representing the expected 1g cruise configuration. Use of these data in an aeroelastically cycled design would be adequate unless changes in the flow-field phenomena due to aeroelastic deflection were present (such as those seen by comparing figures 7 and 11). In this case, wind tunnel data on each deflected geometry (requiring either an aeroelastically scaled model or separate rigid models) would be necessary to replace the cycled nonlinear aeroelastic calculation in achieving optimized designs.

Modifications should be made to the existing system to make it a more comprehensive design tool. Chief among these would be incorporation of multiple load cases, a more accurate and efficient jig-twist solution for a specified lg cruise load distribution, incorporation of inertia loads due to structural weight changes, exercise of the viscous boundary layer effects present in the pilot code, provision for a flutter optimization procedure, and incorporation of composite material layer thickness distribution and fiber orientation variation in the optimization process.

Finally, the computer resources required by the method described herein should be discussed. The method has been implemented on the CRAY-1S computer as three distinct job steps: nonlinear aeroelastic analysis (including jig-twist solution), structural optimization, and modal analysis. The aeroelastic analysis step is the most expensive, requiring 3 to 5 min of computation time for a single converged aeroelastic analysis with a one million word core requirement. (Since each step requires an iterative solution to get both the correct total load and the correct jig-twist distribution, four or more additional runs may be required for each cycle. This requirement can be reduced as the design converges.) The structural design program COMPSIZE requires 10 to 12 sec of computation time for each complete wing design cycle. The modal analysis requires an additional 2 sec. In summary, 15 to 20 min computation time is required for each complete design cycle, or about 1 hr for a complete flexible wing design at a given point design condition.

CONCLUSIONS

A system has been developed for preliminary design of high-aspect-ratio wings, operating in the transonic speed regime, that may employ composite materials in the primary structural box. The system uses a rapid, accurate nonlinear transonic finite-difference code to generate static aeroelastic load solutions and a mixed optimality criteria mathematical programming optimization method to achieve minimum weight per unit span at the given point design condition. A hypothetical transport wing, using an advanced supercritical airfoil section, has been optimized through the system.

ACKNOWLEDGEMENT

The authors wish to acknowledge the many helpful comments and suggestions made by their colleagues in The Boeing Company during the preparation of this paper, especially those of K. G. Bhatia, B. F. Dotson, M. T. McIntosh, and J. W. Nisbet. This work was supported by the Independent Research and Development Program of the Boeing Military Airplane Company.

REFERENCES

1. Murman, E. M., and Cole, J. D., "Calculation of Plane Steady Transonic Flows," AIAA Journal, Vol. 9, January 1971, pp. 114-121.
2. Magnus, R. J., and Yoshihara, H., "Inviscid Transonic Flow Over Airfoils," AIAA Paper 70-47, January 1970.
3. Ballhaus, W. F., and Bailey, F. R., "Numerical Calculation of Transonic Flow About Swept Wings," AIAA Paper 72-677, June 1972.
4. Mason, W., Mackenzie, D. A., Stern, M. A., and Johnson, J. D., "A Numerical Three-Dimensional Viscous Transonic Wing-Body Analysis and Design Tool," AIAA Paper 78-10, January 1978.
5. Boppe, C. W., and Stern, M. A., "Simulated Transonic Flows for Aircraft with Nacelles, Pylons, and Winglets," AIAA Paper 80-104, January 1980.
6. Ballhaus, W. H., and Goorjian, P. M., "Implicit Finite-Difference Computations of Unsteady Transonic Flows About Airfoils," AIAA Journal, Vol. 15, December 1977, pp. 1728-1735.
7. Rizzetta, D. P., and Chin, W. C., "Effect of Frequency in Unsteady Transonic Flow," AIAA Journal, Vol. 17, July 1979, pp. 779-781.
8. Borland, C. J., Rizzetta, D. P., and Yoshihara, H., "Numerical Solution of Three-Dimensional Unsteady Transonic Flow Over Swept Wings," AIAA Journal, Vol. 20, March 1982, pp. 340-347.
9. Borland, C. J., and Rizzetta, D. P., "Nonlinear Transonic Flutter Analysis," AIAA Journal, Vol. 20, November 1982, pp. 1606-1615.
10. Rizzetta, D. P., "Procedures for the Computation of Unsteady Transonic Flows Including Viscous Effects," NASA CR-166249, August 1981.
11. Rizzetta, D. P., and Borland, C. J., "Numerical Solution of Three-Dimensional Unsteady Transonic Flow Over Wings Including Inviscid/Viscous Interaction," AIAA Paper 82-0352, January 1982.

- 3-12 12. Yang, T. Y., Guruswamy, P., and Striz, A. G., "Aeroelastic Response Analysis of Two Dimensional, Single and Two Degree of Freedom Airfoils in Low-Frequency, Small Disturbance Unsteady Transonic Flow," AFFDL-TR-79-3077, June 1979.
13. Rizzetta, D. P., "Time Dependent Response of a Two-Dimensional Airfoil in Transonic Flow," AIAA Journal, Vol. 17, January 1979, pp. 26-32.
14. Chipman, R., Waters, C., and MacKenzie, D., "Numerical Computation of Aeroelastically Corrected Transonic Loads," AIAA Paper 79-0766, April 1979.
15. Guruswamy, P., and Goorjian, P. M., "Comparisons Between Computations and Experimental Data in Unsteady Three-Dimensional Transonic Aerodynamics, Including Aeroelastic Applications," AIAA Paper 82-0690, May 1982.
16. Jameson, A. and Caughey, D. A., "A Finite Volume Method for Transonic Potential Flow Calculations," AIAA Paper 77-635, June 1977.
17. Holst, T. L., "A Fast, Conservative Algorithm for Solving the Transonic Full-Potential Equation," AIAA Paper 79-1456, July 1979.
18. Goorjian, P. M., "Implicit Computations of Unsteady Transonic Flow Governed by the Full Potential Equation in Conservation Form," AIAA Paper 80-150, January 1980.
19. Sankar, N. L., Malone, J. B., and Tassa, Y., "An Implicit Conservative Algorithm for Steady and Unsteady Three-Dimensional Transonic Potential Flows," AIAA Paper 81-1016, Palo Alto, California, June 1981.
20. Bridgeman, J. O., Steger, J. L., and Caradonna, F. X., "A Conservative Finite Difference Algorithm for the Unsteady Transonic Potential Equation in Generalized Coordinates," AIAA Paper 82-1388, August 1982.
21. Gingrich, P. B., Child, R. D., and Panageas, G. M., "Aerodynamic Configuration Development of the Highly Maneuvering Aircraft Technology Remotely Piloted Research Vehicle," NASA CR-143841, 1977.
22. Timmons, L. M., "Improving Business Jet Performance: The Mark Five Sabreliner," SAE Paper 790532, April 1979.
23. Gray, W. L., and Schenk, K. M., "A Method for Calculating the Subsonic Steady-State Loading on an Airplane With a Wing of Arbitrary Plan Form and Stiffness," NACA TN3030, December 1953.
24. Albano, E. D., and Rodden, W. P., "A Doublet-Lattice Method for Calculating Lift Distribution on Oscillating Surfaces in Subsonic Flows," AIAA Journal, Vol. 7, February 1969, pp. 279-285.
25. Zartarian, G., and Hsu, P. T., "Theoretical Studies on the Prediction of Unsteady Supersonic Airloads on Elastic Wings," WADC Technical Report 56-97, December 1955.
26. Turner, M. J., Clough, R. W., Martin, H. C., and Topp, L. J., "Stiffness and Deflection Analysis of Complex Structures," Journal of the Aeronautical Sciences, Vol. 23, September 1956, p. 805ff.
27. Ashley, H., "Role of Shocks in the Sub-Transonic Flutter Phenomenon," Journal of Aircraft, Vol. 17, March 1980, pp. 187-197.
28. Ashley, H., "On Making Things The Best - Aeronautical Uses of Optimization," Wright Bros. Lecture, AIAA Aircraft Systems and Technology Meeting, Dayton, Ohio, August 1981.
29. Lynch, R. W., et al., "Aeroelastic Tailoring of Advanced Composite Structures for Military Aircraft," AFFDL-TR-76-100, February 1978.
30. Markowitz, Joel, et al., "FASTOP-3: A Strength Deflection and Flutter Optimization Program for Metallic and Composite Structures," AFFDL-TR-78-50, May 1978.
31. Asceni, L., et al., "A Structural Weight Estimation Program (SWEEP) for Aircraft," ASD/XR 74-10, June 1974.
32. Austin, F., "Aeroelastic Tailoring of Advanced Composite Lifting Surfaces in Preliminary Design," AIAA 17th Structures, Structural Dynamics and Materials Conference, 1976.
33. Manning, K. J. R., et al., "ORACLE-A Program for Preliminary Structural Design of High Aspect Ratio Wings," Boeing Document D6-41475, April 1974.
34. Gimmestad, D. W., "An Aeroelastic Optimization Procedure for Composite High Aspect Ratio Wings," AIAA Paper 79-0726, April 1979.
35. Dobyns, A. L., "Sandwich Wing Box Analysis Program (SAND II)," Boeing Document D180-17893-1, February 1974.
36. Borland, C. J., and Rizzetta, D. P., "Transonic Unsteady Aerodynamics for Aeroelastic Applications - Vol. I: Technical Development Summary," AFWAL-TR-80-3107, Vol. I, June 1982.
37. Borland, C. J., Thorne, R. G., and Yeagley, L. R., "Transonic Unsteady Aerodynamics for Aeroelastic Applications - Vol. II: User's Manual," AFWAL-TR-80-3107, Vol. II, June 1982.
38. Thorne, R. G., and Yeagley, L. R., "Transonic Unsteady Aerodynamics for Aeroelastic Applications - Vol. III: Programmer's Manual," AFWAL-TR-80-3107, Vol. III, June 1982.
39. Gimmestad, D. W., "A Simplified Flutter Analysis Formulation with Bent Beam Capability," Boeing Document D6-23417 TN, August 1968.
40. Hinson, B. L., and Burdges, K. P., "Acquisition and Application of Transonic Wing and Far-Field Test Data for Three-Dimensional Computational Method Evaluation--Volume I," AFSOR-TR-80-0421, March 1980.

AEROELASTIC DESIGN OF CIVIL TRANSPORTS AT THE PROJECT STAGE

by

R.E.J. Brazier, A.E. Dudman, B.W. Payne
British Aerospace, Plc
Weybridge-Bristol Division
Brooklands Road
Weybridge, Surrey KT13 0SF
UK

SUMMARY

The design of a competitive civil transport aircraft must take account of aeroelastic effects and aeroelastic requirements at the project stage. The overall design will be decided by other considerations but the final 'tuning' of the design, leading to structural/performance optimisation has to include aeroelastic data on static distortion, dynamic loading and flutter requirements. In order to be able to produce these data at the project stage, where geometry and configuration changes need to be assessed rapidly, a system has been developed by which quick and reliable predictions can be made.

1.0 INTRODUCTION

The role of aeroelasticity has always had a part to play in the design of civil transport aircraft but in the middle fifties, when computers were in their infancy, it was not possible to carry out complex aeroelastic calculations quickly enough for the effects to be incorporated into the design at the project stage. As a result the project design was always based on strength considerations with a notional view of the airworthiness stiffness criteria, reference figure 1. As the evolution of transport aircraft progressed, leading to closer design tolerances, the stiffness demands from aeroelastic considerations had to be included with the strength demands. Thus it became necessary to include aeroelasticity at earlier stages of the design process making more and more use of the increasing power of computers. However, in that period the availability of basic structural and aerodynamic data did not allow a full understanding of the aeroelastic effects prior to the main project design decisions regarding the first sizing of structural components.

Today with the advent of the dedicated departmental computers, which are as powerful as mainframe machines of a decade ago, it has become possible to include aeroelasticity in the aircraft project design process by way of static aeroelastic distortion, flutter, gust and landing response in interactive analysis loops, in order to obtain optimum design, reference Figure 2.

Aeroelastic calculations proceed together with work in related disciplines, namely aerodynamics, structures, weights and systems. At the beginning of a new project, adequate data are generally limited to basic geometry, major aircraft performance characteristics plus general aerodynamics and weight data with a minimum of structural data, all of which is insufficient for aeroelastic calculations. The major components affected by aeroelasticity are the lifting surfaces, i.e. wing, tailplane and fin and of these the wing is the largest, heaviest and most complex. Consequently in the early stages the major effort of the aeroelastic engineers needs to be expended upon the wing, although the choice of the tailplane, if it is a T-Tail, and the engine position can sometimes dominate the early project analysis as well. In order that the overall design process on the wing, or other surfaces may proceed without delay, it is essential that the relevant data is available from the related design disciplines.

In the definitive design loops, the aeroelastic engineers obtain the data from the related design disciplines for a given standard of aircraft design, and then carry out the aeroelastic predictions. However, this becomes too time consuming for the initial project review of the design and therefore we, the aeroelastic engineers at Weybridge, have developed a suite of computer programs on our own dedicated computers which produces basic aerodynamic, structural and weight data. These data are then integrated into standard aeroelastic prediction programs, covering static aeroelastics, flutter, gust response and landing response analyses. Once the design iteration process has been initiated, the aerodynamic stiffness and weight data are updated as they become available from the related design disciplines.

A major feature of our technique is that the various aeroelastic tasks, although using a common data base, are kept separate so that optimisation of design is achieved under specialist control. The idea of a single large optimisation computer program being in control of the design has been avoided since it has always been considered that the inherent assumptions may not apply to the current task and checking the results would take as long as carrying out the task in our normal way.

In order to complete a number of design loops, at the project stage, it is necessary to have good interactive computers producing results quickly and explicitly. Mainframe computers tend to be centralised with remote outlets and use time sharing and batch processing so that the above requirements are not generally met. However, a dedicated departmental computer can meet these requirements and over the past eight years we have obtained our own machines and found them to be ideal for project analyses.

This report outlines the concepts of aeroelastic design of civil transports at the project stage, describes the formulation of the data and computing requirements and relates the aeroelastic predictions to the project design.

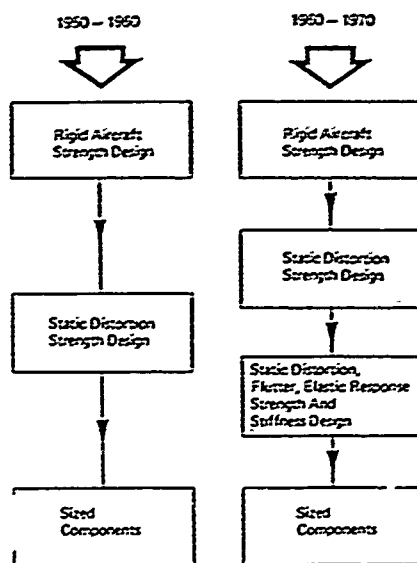


Fig. 1 Early Project Design

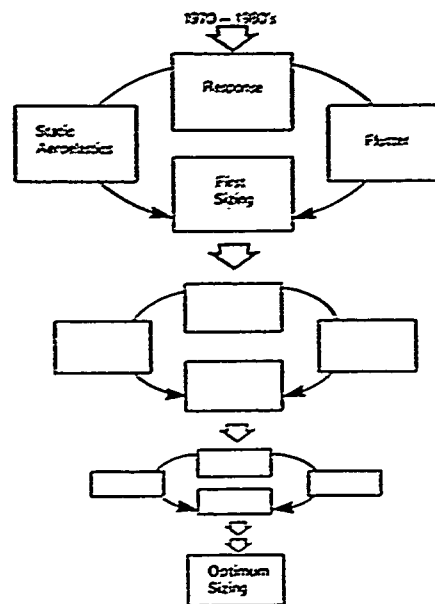


Fig. 2 Current Project Design

2.0 DEFINITION OF THE AEROELASTIC PROBLEM

The term aeroelasticity has been applied by aeronautical design engineers to a class of problem which studies the interaction of aerodynamic and elastic forces and basically is a result of flexible structures inducing additional aerodynamic forces. However, the term aeroelasticity is not completely descriptive, since many important phenomena involve inertial forces as well as aerodynamic and elastic forces, so we will define aeroelastic phenomena as those problems that involve interactions between inertial, aerodynamic and elastic forces, either in part or all together. A.R. Collar, classified problems in aeroelasticity by means of a triangle of forces. Figure 3 shows a summary of this aeroelastic triangle of forces reduced into only three basic aeroelastic phenomena:-

- o Static aeroelasticity : relating aerodynamic with elastic forces
- o Response : relating inertial, aerodynamic and elastic forces
- o Flutter : relating inertial, aerodynamic and elastic forces

all of which have a profound effect upon the design of structural components in modern, flexible, aircraft. To a lesser extent, but none the less important, aeroelastic phenomena affect the mass distribution, lifting surface planforms and control system design. With the need for aircraft with better performance and lighter structures, active control technology is expected to be used more often in modern aircraft design. This will result in control system design being dominated by aeroelastic requirements.

Within the three basic aeroelastic phenomena, static aeroelasticity, response and flutter, all the fundamental problems for project analyses can be aligned, as shown in figure 3. Static aeroelasticity involves load and control efficiency where the influence of elastic deformations of the structure affects the aerodynamics and controllability of the aircraft respectively. Response concerns both the transient and the continuous response of aircraft structural components to rapidly applied loads, whereas flutter concerns the dynamic stability of the structure due to the effects of inertia, elastic and aerodynamic forces, both of which can be considered in a passive and active form. Aeroelastic effects on the rigid-body aerodynamic stability are also considered.

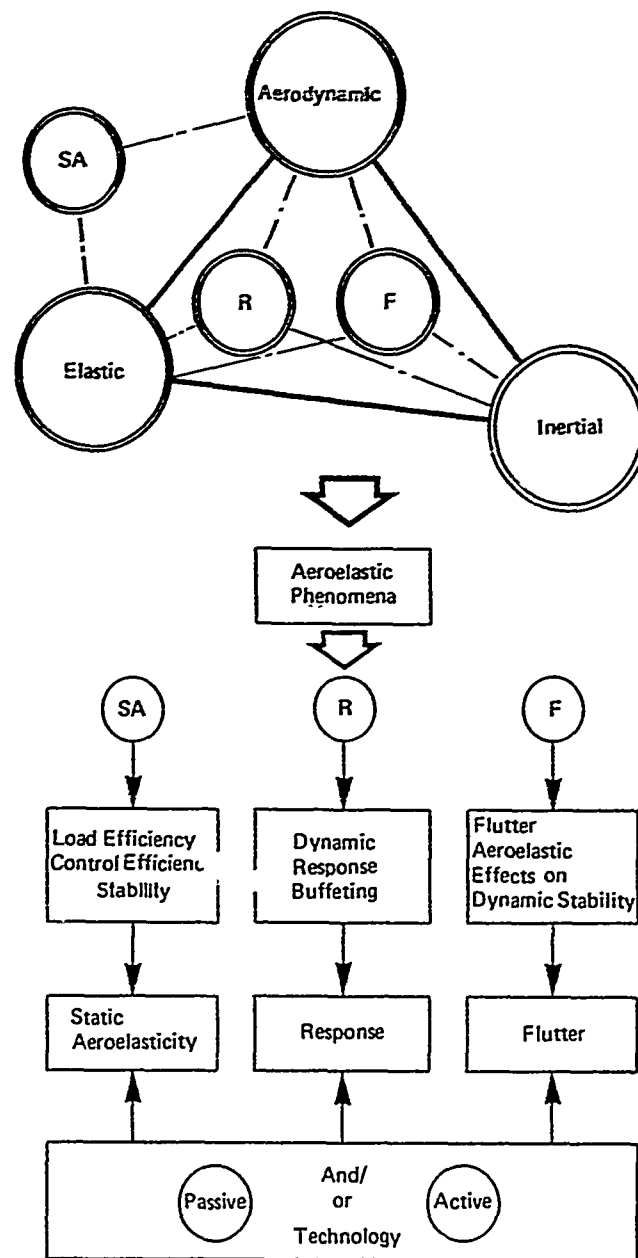


Fig. 3 Aeroelastic Triangle of Forces

3.0 AEROELASTIC DESIGN PHILOSOPHY

Our philosophy for project aeroelastic design work is based strongly on our past experience with previous projects of a similar type, together with any relevant research. Therefore there is a need to maintain consistency between predictions and obtain confidence in the results, which can only be done by allowing the design office specialists in the related areas of structures, aerodynamics, weights and systems to have a working knowledge of each other's disciplines. This allows data to be questioned by recipients and ensures that past experience and current requirements are taken into account.

It is important that the dominant tasks are isolated and that the optimum results are obtained quickly for the related design specialists by using simple mathematical models relating to each separate aeroelastic phenomenon. These models, generally in branch mode form are assembled using dedicated computing facilities and a consistent data base. The use of branch mode analysis enables sensitivity studies to be carried out with the important design parameters, so that rates of exchange can also be evaluated. This leads to the necessary confidence in the results and allows for several iterative loops of the design data to be achieved by the specialists before obtaining the best optimum project design.

4.0 FORMULATION OF THE DATA

4.1 General

It is desirable to have definitive data before carrying out any sort of calculations but at the beginning of a project the basic data required for aeroelastic calculations are scarce because the related specialists need to analyse, evaluate, review and then issue their data. As has already been stated, aeroelastic work requires data not only on geometry but also on stiffness, aerodynamics and mass distributions. Initially, however, the only data available generally consist of basic geometry, overall aircraft performance requirements, basic aerodynamics plus, perhaps, general undercarriage characteristics. At the project stage, the major aeroelastic problems concern the lifting surfaces of the aircraft. For civil transports these are generally of moderately high aspect ratio and are constructed in the classic form of a structural box to which are attached leading and trailing edges largely dedicated to slats, flaps, airbrakes and other control surfaces. With this raw knowledge the aeroelastic engineer can begin his contribution to the structural design process.

With the knowledge of the dominant tasks, the mathematical models relating to the various aeroelastic phenomena can be defined. In order that the structural design process may begin, initial estimates of the stiffness and mass distributions are made using a structural data program. This section of the report describes the formulation of the data necessary for providing the initial structural estimates, together with the structural and aerodynamic models.

4.2 Structural Data Program

Originally a program was written to predict a project weight estimate of a lifting surface designed by an envelope of manoeuvre and gust response cases. The basic concept of the program was formulated to enable overall changes in weight due to changes in configuration to be calculated on a consistent rather than an accurate basis. With development over many years, the program has become more accurate, with an end result of predicting the distribution of mass and stiffness of a lifting surface. This program has become a valuable tool for the initial stages of project design. These data are used to construct the initial mathematical model of the aircraft structure.

This program requires only basic geometry of the lifting surfaces and fuselage, together with the aircraft performance data in terms of overall aircraft structure and fuel weight, centre of gravity, flight envelope details and general aerodynamic derivatives. With a knowledge of the above data the rigid loads and accelerations can be produced. Then assuming a guessed wing weight, the distributed bending moments and shear for each manoeuvre and gust flight case can be produced. Given the type of structure required, the weight of the main load carrying structure is found, and together with an estimate of the extra items, such as flaps, controls, etc., the total wing weight can be estimated together with the stiffness distributions. Using these data the inertia relief and the distortion of the structure is evaluated using an iterative process to a given tolerance, reference Figure 4.

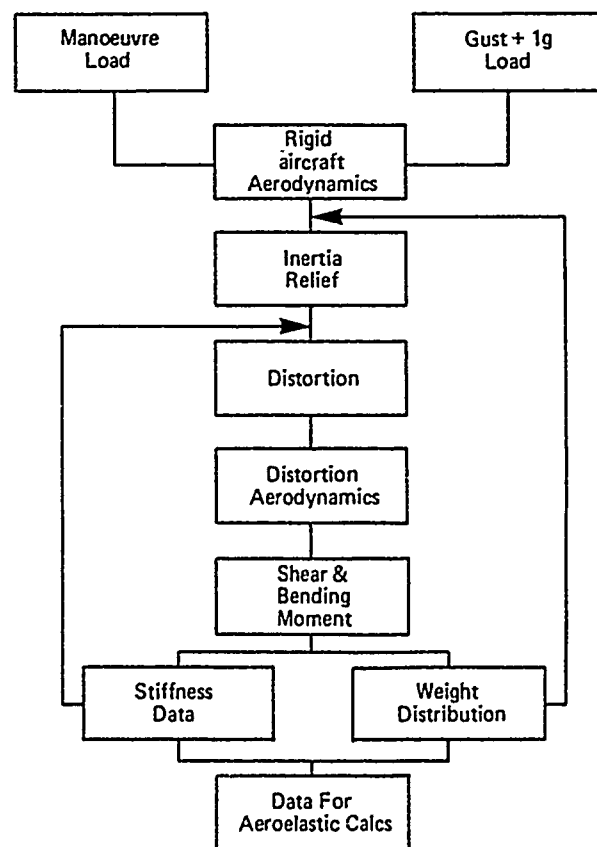


Fig. 4 Structural Data Program

4.3 Structural Models

A mathematical model to predict the static and dynamic characteristics of the structure can be produced by using distributions of inertia and stiffness either obtained from the structural data program or the related design specialists.

Static aeroelastic calculations are carried out by using the flexibility matrices describing the structure concerned, whereas the model for describing the dynamic characteristics for response and flutter can be represented quite adequately by a series of "branches" based on the lumped mass and flexural axis concept together with the Engineer's Beam Theory, reference Figure 5. Options are available to use either flexibility or stiffness matrix analyses in the evaluation of the branch modes.

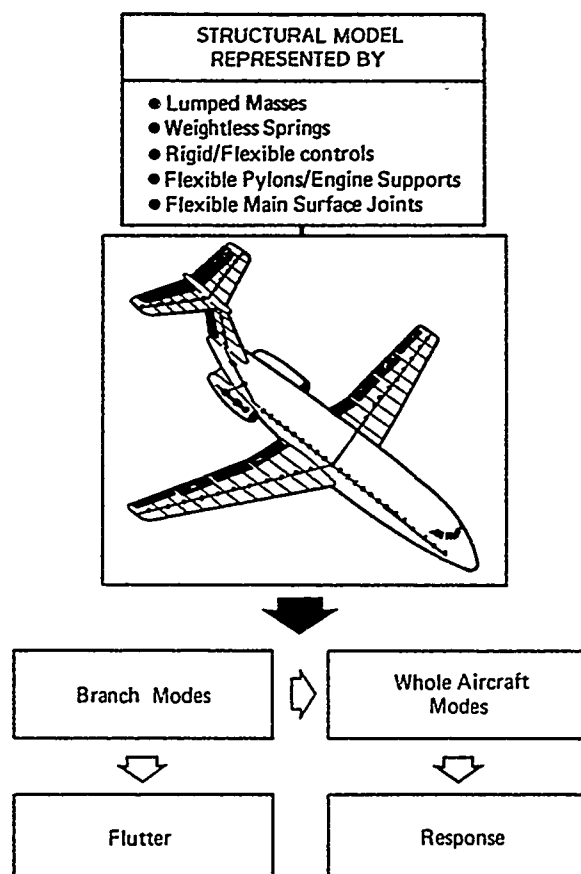


Fig. 5 Structural Model

Control surfaces and flexibly mounted engines may be added with joint flexibilities and the free-free whole aircraft represented using a few normal modes for each branch plus the required rigid aircraft modes. For gust work it is generally sufficient to take lifting surface branch modes up to and including the fundamental torsion mode in order to adequately model the statically distorted surfaces, so that, for example, a symmetric aircraft is represented by, typically, fifteen to twenty free-free normal modes.

Sensitivity studies in flutter analysis can involve structural stiffness, aerodynamic derivatives and mass distribution and it is beneficial to work using the branch mode model of the aircraft. If the sensitivity of the solution to certain data is to be studied, steps can be taken to select the branch modes accordingly, for instance one might use tailplane pitch as a branch mode so as to be able to study the effects of tailplane pitch stiffness.

4.4 Aerodynamic Models

For aeroelastic analysis, the aerodynamic models depend basically upon past experience, wind-tunnel data and the correlated theory, as shown in Figure 6. The major contributions to static aeroelastic deformation prediction for the level flight case arise generally from the zero incidence and rigid incidence aerodynamic forces and these, therefore, need to be known with confidence and fortunately such data are usually obtained from steady three-dimensional (3-D) aerodynamic theory, plus information from wind tunnel data. The aerodynamic forces due to deformation are of secondary importance and can be predicted adequately using a three-dimensional theory for a flat plate.

Aerodynamic loads due to steady control deflections are evaluated using "equivalent slopes" together with three dimensional theory.

In the case of outboard ailerons where rolling moment efficiency often reduces to a minimum, it is generally necessary to carry out sensitivity studies on the local aerodynamic centre position since at high Mach numbers the linear theory is inadequate to model this effect with any confidence, although the spanwise loadgradings are modelled adequately. Corrections may be made for rigid incidence lift curve slope and local aerodynamic centre but these generally have effects only within the tolerance of other data being used.

For the response and flutter analyses unsteady aerodynamic forces may be estimated using quasi-steady two-dimensional (2-D) strip theory for fuselages and particularly controls. Aerodynamics for lifting surfaces are usually calculated using quasi-steady strip theory for gust load prediction, since it is quick and easy to match issued data for rigid incidence, but for flutter both strip theory and three-dimensional theory are used. Generally the strip theory gives a clearer warning of possible problems and is simpler to use in sensitivity studies and the three-dimensional theory is used to obtain a more accurate solution for the datum case.

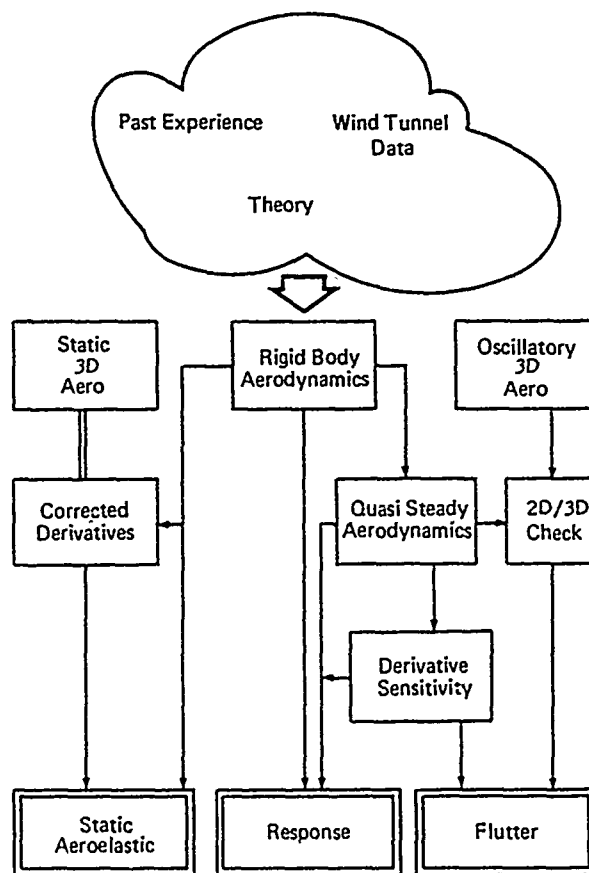


Fig. 6 Aerodynamic Model

5.0 COMPUTING

The modern mainframe computer has become larger over the years mainly due to 'data processing' demands and also more generalised in its use, thus making it more centralised and remote from the user. It employs time sharing systems with local terminals, but basically expects users to concentrate on using the 'batch' processing system. This has led to a tendency for program complexity to expand to use the computing limits of the machine and to underdevelop the on-line computing facilities. Although these features are acceptable and adequate for the later stages of the design where advantage can be taken of the great core size and processing speed available it is not acceptable for the project design work.

At the project stage, the demand is for small, simple programs, user interaction, fast turn round, good plotting/graphics facilities plus the ability to do work at any time of the day. These features are basically only available on a dedicated computer and over the past decade Weybridge has developed a suite of programs which have concentrated on optimising programme size and efficiency thus offsetting the limitations inherent in a mini-computer based system. These computers, although relatively small, are adequate for the tasks involved and, with excellent editing and plotting facilities, are used to produce graphs and diagrams of a standard suitable for direct inclusion in reports and presentations. The "instant" turnaround allows quick correction of any changes in the data as results are printed or plotted locally. The plotting facilities give the opportunity of adding extra data to areas of interest. Because the machines are departmental, access is organised internally and they can be used at any time as opposed to the mainframe which has limited hours of availability, and priority work is organised external to the departments. A summary of the comparison between mainframe and dedicated computers is shown in Figure 7.

One last benefit which may not be obvious from the aforesaid is the greatly improved motivation of the staff, when using an inter-active departmental computer, and a willingness to get jobs done and well presented through the close involvement.

	MAIN FRAME	DEPARTMENTAL
Availability	Limited	Unlimited
Priority Work	No Control	Controlled Internally
Turn Round	Slow	Fast
Plotting	Fixed/Delayed	Infinitely Variable/Instant
Interaction	Limited	Unlimited
Speed	Variable	Adequate
Program Size	Large	Adequate For Project Work
Cost Effectiveness	Variable	Optimal

Fig. 7 Comparison Between Computers

6.0 PROJECT PREDICTIONS

6.1 General Design Problems

As stated in section 2.0, all the main predictions work and requirements for project analyses can be aligned within the three basic sections as follows:-

- o Static aeroelasticity which affects steady load evaluation (for ultimate and fatigue cases), built in anti-distortion twist, stiffness requirements for control efficiency and distorted aircraft stability.
- o Response analyses which lead to strength and fatigue requirements for gust and landing requirements, undercarriage, dynamic characteristics and environmental conditions for equipment.
- o Flutter which relates to lifting surface stiffness, control impedance requirements and mass requirements.

In the project analyses, these sections are treated separately for optimisation. However, within the aeroelastic area the sensitivity studies produce rates of exchange for selected parameters which are then considered by the related disciplines in the other design areas for overall optimisation of the design.

A summary of the aeroelastic phenomena analysed at the project stage is given in the following paragraphs.

6.2 Static Aeroelasticity

Static aeroelasticity concerns load and control efficiency, where the distortion of the structure tends to redistribute the airloads. Dependent upon the geometry and structural stiffness, the additional forces due to the deformation can either decrease or increase the assumed rigid airloads and in extreme circumstances can lead to static divergence and control reversal respectively. For civil transports of today, divergence is seldom a problem, whereas the prediction of the steady load distributions and control efficiency are of paramount importance especially with the introduction of active control technology.

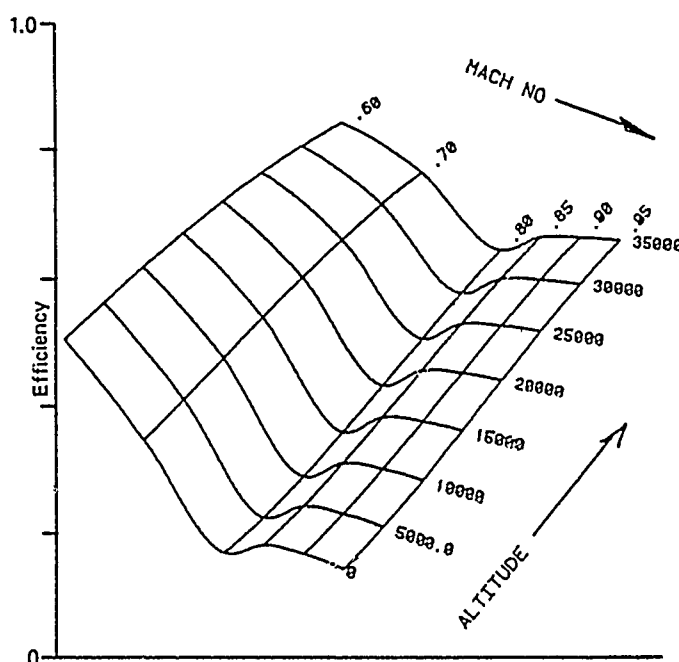


Fig. 8 Aileron Efficiency

In the static aeroelastic analysis the applied loads are considered as separate inputs to the elastic component of interest which is cantilevered at some convenient point. The applied loads are either aerodynamic e.g. rigid incidence, rigid control rotation, or inertial, e.g. wing structure weight in level flight. These loads and the elastic forces are then balanced by the aerodynamic forces due to distortion, the latter being calculated using a three-dimensional theory (plus corrections). There is a choice of solving either for a range of dynamic pressures or for a range of altitudes for the given Mach Number. The component results may then be summed for any flight condition to evaluate distortion and net load data. A typical carpet of results for aileron efficiency is plotted against Mach Number and altitude in Figure 8.

6.3 Response

Dynamic response loads have a primary influence on the structural design and are the result of rapidly applied inputs due to gusts, landing or other dynamic conditions. Essentially the transient response manifests itself into increased bending and torsional stresses in the structure and the design has to be capable of taking these into account by increasing the structural material. The two most important dynamic response problems are gust and landing.

6.3.1 Gust Response

Incremental loads due to gust response are calculated using a free-free mathematical model of the flexible aircraft with the aerodynamic forces calculated using quasi-steady strip theory. The aircraft is modelled as a number of aerodynamic surfaces, e.g. front fuselage, inner wing, etc., so that the effect of the gust passing over the aircraft is represented. Appropriate aerodynamic lag functions due to the gust (Kussner) and due to the response (Wagner) are included for each of these surfaces.

Gust response calculations have to cover both the discrete gust and continuous turbulence, the latter requiring the evaluation of the frequency response at "all" frequencies, in practice, up to a frequency sufficiently high to achieve convergence on the statistical data. The response to the discrete gust is obtained by multiplying the frequency response by the Fourier Transform of the discrete gust and then performing an Inverse Transform on the product. The discrete gusts considered are of the form '1-cosine' for a range of gust gradient, the distance travelled to reach the maximum gust velocity. In practice the discrete gust calculations range from $2.5c$ to $50c$ (c = wing mean chord) gust gradient distances to ensure that tuning effects of aircraft flexible and rigid modes are covered. Peak values are interpolated for each "interesting" quantity e.g. load, stress or acceleration, reference Figure 9.

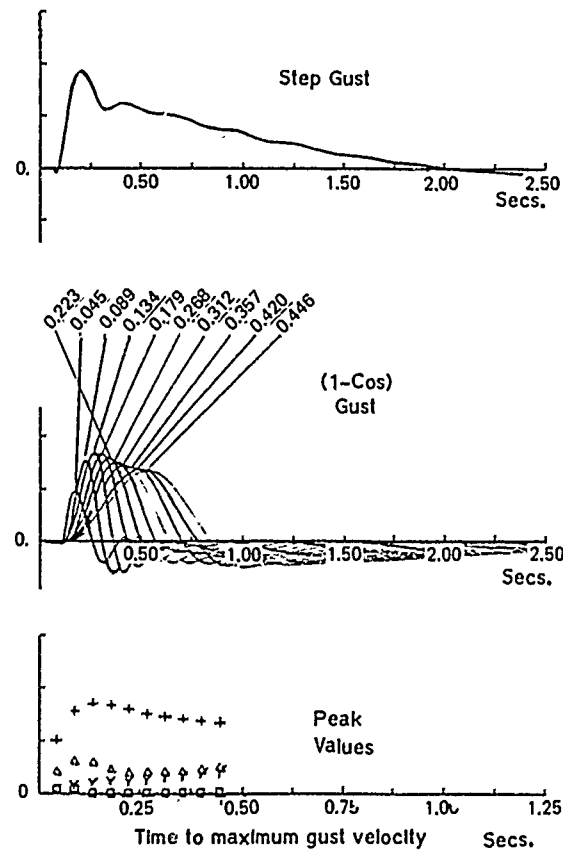


Fig. 9 Response to Discrete (1-Cos) Gust

Overswing Factors

These calculations, however, are time consuming and it is not sensible to try to cover all the design flight cases using this method in a short time-scale. A simple fast method of predicting the required interesting quantities for all the design flight cases is to use the Pratt formula technique. The Pratt formula was originally formulated to predict rigid aircraft c.g. peak acceleration due to a discrete gust but, with modification, has been shown to give a first order prediction of loads all over the aircraft. Thus it is possible to highlight critical flight cases quickly and then, using the results of the full calculations, predict more accurate data for these cases. If the ratio of the full calculation result to the Pratt formula result is referred to as the overswing factor then loads for other flight cases not too distant can be approximated by factoring the Pratt formula value by the overswing values for that point.

In practice overswing factors are calculated for each interesting quantity for:

- o 12.5 c
- o tuned gust
- o continuous turbulence (design envelope)

Typical results and overswing factors are shown in Figure 10.

345.2 KT EAS 21,785 FT AUV 132,664 LB 5,512 LB FUEL										
M=0.88		345.2 KTS EAS	21785 FT	UDE= 68.526		USIG= 85.888		RHO=0.0011918		V=823.57
IO	LOAD	SOV*UDE	12.5 CHORD DOV*UDE	TUNED DOV*UDE	GUST LENGTH	ABAR*USIG	NB	12.5DOV SOV	DOV SOV	ABAR*USIG SOV*UDE
55	V SF WING ROOT	82429.85	82474.69	86383.25	7.5	68637.81	1.495	1.881	1.847	0.833
56	V SF STN 11.349	74683.91	72958.81	77619.37	7.5	60817.16	1.587	0.977	1.839	0.804
57	V SF STN 12.427	72626.78	70616.86	75447.88	7.5	57959.48	1.649	0.972	1.839	0.798
58	V SF STN 16.882	64443.69	61896.58	68913.12	7.5	58364.20	1.949	0.968	1.869	0.782
59	V SF STN 16.513	63178.59	60662.95	67957.12	7.5	49241.64	2.884	0.968	1.876	0.780
60	V SF STN 17.823	61988.43	59438.58	67884.37	7.5	48133.68	2.861	0.968	1.882	0.778
61	V SF STN 22.698	67722.17	59598.82	61951.79	18.8	58497.32	1.483	0.888	0.915	0.746
62	V SF STN 26.848	58119.44	58537.63	52832.59	7.5	42404.85	1.374	0.878	0.989	0.731
63	V SF STN 28.372	54664.82	47378.52	49757.19	7.5	39731.86	1.413	0.867	0.918	0.727
64	V SF STN 31.289	48754.49	41585.89	43216.48	7.5	34956.82	1.493	0.853	0.886	0.717
65	V SF STN 34.846	42712.89	36261.95	37768.45	18.8	38442.32	1.631	0.849	0.884	0.713
66	V SF STN 39.721	38793.33	25986.21	26955.22	18.8	21696.37	1.695	0.841	0.875	0.705
67	V SF STN 45.395	18938.59	15456.84	15795.57	18.8	13182.22	1.368	0.816	0.834	0.696
68	V SF STN 47.898	15339.23	12676.35	13119.78	18.8	10752.55	1.449	0.826	0.855	0.701
69	V SF STN 51.878	7611.27	6685.69	7587.21	7.5	5516.89	2.686	0.878	0.997	0.725
70	V BH WING ROOT	29.68	27.14	28.26	7.5	22.48	1.369	0.914	0.952	0.757
71	V BH STN 11.349	24.34	21.93	22.76	7.5	10.14	1.365	0.981	0.935	0.75
72	V BH STN 12.427	23.33	20.94	21.78	7.5	17.34	1.357	0.898	0.938	0.743
73	V BH STN 16.882	28.21	17.93	18.43	18.8	14.98	1.315	0.887	0.912	0.737
74	V BH STN 16.513	19.88	17.52	18.81	18.8	14.58	1.387	0.885	0.910	0.736
75	V BH STN 17.823	19.39	17.14	17.59	18.8	14.27	1.299	0.884	0.907	0.736
76	V BH STN 22.698	13.58	11.64	12.25	7.5	9.73	1.434	0.863	0.988	0.721
77	V BH STN 26.848	18.19	8.74	9.28	7.5	7.38	1.496	0.657	0.911	0.716
78	V BH STN 28.372	9.18	7.88	8.29	7.5	6.58	1.612	0.657	0.912	0.715
79	V BH STN 31.289	7.24	6.28	6.68	7.5	5.16	1.522	0.656	0.911	0.713
80	V BH STN 34.846	5.68	4.88	5.11	7.5	3.98	1.514	0.857	0.914	0.712
81	V BH STN 39.721	2.96	2.53	2.69	7.5	2.11	1.511	0.855	0.907	0.711
82	V BH STN 45.395	1.19	1.83	1.13	7.5	8.85	2.115	0.867	0.955	0.728
83	V BH STN 47.898	0.82	0.72	0.82	7.5	8.68	2.528	0.882	0.999	0.729
84	V BH STN 51.878	8.26	0.24	0.29	5.8	8.19	3.657	0.923	1.144	0.761

Fig. 10 Typical Set of Gust Response Results

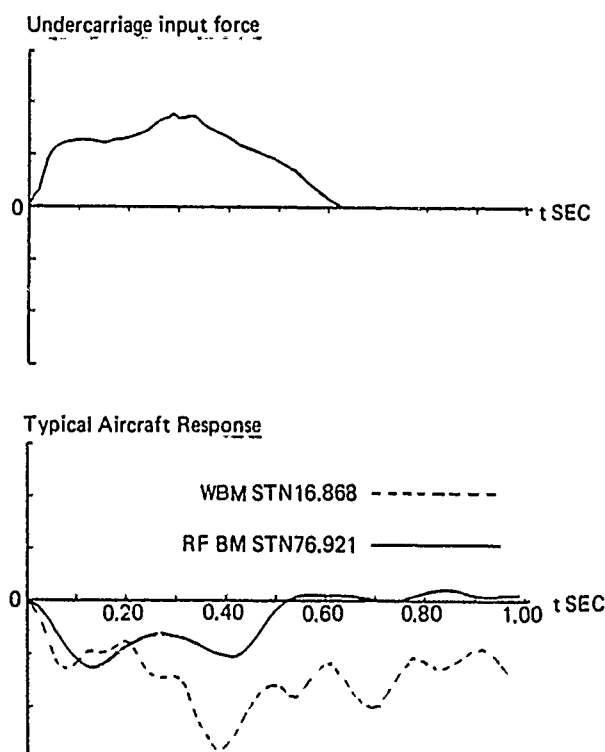


Fig. 11 Project Landing Response

4-10

6.3.2 Landing Response

The mathematical model used for landing response calculations is similar to that used for gust calculations except that the flaps are out and the undercarriage is down. Initially the only landing gear input data normally available is generally an estimate of the time history of the vertical force at the top of the main undercarriage leg. This will have been obtained by scaling from previous similar aircraft or from a very simple mathematical model of the oleo representing a gas compression curve and hydraulic damping, and probably some friction, plus tyre compression data. Spin up/spring back effects are ignored at the first stage unless they are expected to have a significant influence on the structure.

At the later stages, a load against stroke curve for the oleo and tyre characteristics will be more firmly established and the force time histories in the vertical and fore-and-aft directions at the top of the leg calculated for a rigid aircraft at a given descent rate, reference Figure 11. Spin-up forces are also included at this stage either by applying the rigid leg drag forces to the fore-and-aft flexibility or by including this flexibility in the calculation. Given the input force time histories the interesting quantities are calculated by integration, reference Figure 11, and the peak values extracted.

6.4 Flutter

Modern aircraft are subject to all kinds of flutter behaviour which can have the most far-reaching effects of all aeroelastic phenomena on the project design. Preventive measures usually involve either increased stiffness or decreased coupling by adjustment in mass distribution or a combination of both. Heavy mass items such as engines are often located partly by considerations of optimum conditions for flutter prevention. The aircraft must be shown to be stable in both the unfaild and the 'fail-safe' conditions for all payload and fuel configurations within the flight envelope.

Project flutter calculations may be put into two main categories viz:-

- o main surfaces
- o controls

Stability is examined using damping versus speed plots, reference Figure 12, and the ability to interact with the computer in this task is most valuable. In order to highlight flutter instabilities calculations are generally carried out for constant Mach Number and altitude, varying only the equivalent airspeed although matching altitude and speed for a given Mach number is also used.

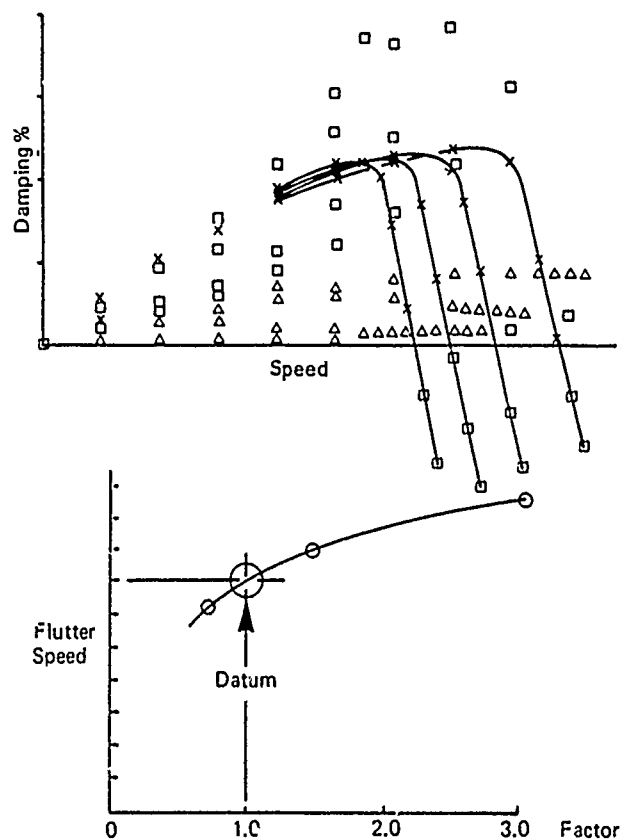


Fig. 12 Main Surface Flutter:
Example of Sensitivity Study

6.4.1 Main Surface Flutter

The aim is to predict any likely flutter problems and to carry out sensitivity studies to try to find acceptable means of achieving adequate flutter margins and highlighting areas for more detailed investigations. Close liaison with the weights and structures specialists is kept and studies on changes in mass configuration and stiffness carried out to find the best solution to the problem. The branch mode model is ideal for such studies, especially if the problems have been foreseen and the branch modes formed with the express aim of sensitivity studies. In order to understand the flutter mechanism, the problems are reduced to a minimum number of degrees of freedom. Figure 12 shows how a sensitivity study on a reduced problem reveals the essential flutter characteristics and gives an insight into how adequate margins can be obtained with confidence.

6.4.2 Control Flutter

Control flutter is generally sensitive to mass, stiffness and aerodynamic data and here again sensitivity studies are carried out. Strip theory aerodynamics are preferred because of the ease of introducing measured data and of varying the flutter derivatives. Power control unit impedance requirements can be specified with some confidence at an early stage.

7.0 INTERACTION WITH RELATED SPECIALISTS

The aeroelastics engineer carrying out project work needs to maintain close contact with all other related specialists who are involved in the design, including the areas of structures, aerodynamics, the drawing office, weights and systems. This results in the constant flow of data from one area to another and optimisation of the design is carried out as a result of this interaction. With the specialists of each area knowing the general requirements of all the other areas the necessary optimisation process can be achieved so that the final design is reached by a rational process. This continuous dialogue between specialists ensures that every decision is understood and agreed to by those who have experience and responsibility for that part of the design. It would be a formidable task indeed to try to absorb all the skills of this process into a computer program for use in the project environment. Further, an enormous amount of checking would be required in order to assess the results and ensure that there were no errors nor that any assumptions were being exceeded. Therefore we believe that the correct approach for project design is to maintain close interaction of related specialists who assess their own optimum requirements.

8.0 CONCLUDING REMARKS

The development of transport aircraft has made it necessary to include aeroelastic data and requirements at the project design stage. It is also very desirable to carry out an iterative process involving the related specialists in order to arrive at an optimum design. Our experience in project design has convinced us that the essential requirements are:-

- o to optimise for each requirement separately but then to compromise by
- c maintenance of close interactive dialogue with specialists in related design areas.
- o To be able to produce aeroelastic data quickly and with confidence using simple models and dedicated computers.

TRANSONIC FLUTTER CLEARANCE FOR A SUPERCRITICAL TRANSPORT AIRCRAFT IN THE PRELIMINARY DESIGN STAGE

by

N.Pronk, H.Walgemoed, Fokker B.V.,
P.O. Box 7600
1117 2J Schiphol

and

R.J.Zwaan, National Aerospace Laboratory (NLR)
P.O. Box 90502
1006 B.M. Amsterdam
The Netherlands

SUMMARY

Recently, design studies for a short-haul transport with a supercritical wing were made by Fokker with assistance of NLR.

One of the aeroelastic questions to be answered already in the preliminary design phase of these wings was the question of flutter-freedom in the foreseen flight envelope.

In the presentation a survey is given of the steps taken in the flutter clearance, especially those which were prompted by the transonic aspects. Aerodynamic investigations are discussed involving transonic wind-tunnel tests on oscillating supercritical airfoils, transonic flutter tests on a supercritical wing model and the development of calculation methods. A flutter analysis method for these transonic conditions is verified on the wind-tunnel model results and applied to the full-scale design, showing the influence of the transonic aerodynamics.

1. INTRODUCTION

This paper highlights some aspects of the flutter clearance activities of Fokker and NLR during the preliminary design stage of an advanced short-haul transport aircraft. The activities were terminated in 1982. A sketch of the aircraft design is given in figure 1. This design was characterized by a high aspect ratio supercritical wing, high bypass ratio turbofan wing mounted engines and a T-tail. All these design features had their own aeroelastic aspects, which deserved careful attention from the very beginning of the preliminary design stage.

This paper focuses primarily on the flutter clearance of the supercritical wing. Due to the transonic environment in which this wing should operate, the influence of the so-called transonic flutter dip had to be studied. To achieve this goal, an intensive research program was carried out by Fokker and NLR, in which NLR provided the theoretical and experimental expertise on unsteady transonic flow and created a data base of transonic unsteady aerodynamic data.

Furthermore NLR verified the concept of using these data on a three-dimensional wing in a wind-tunnel flutter model test. Fokker, on its part, created the structural dynamic model of the full-scale design and introduced the transonic data into the flutter analysis. The investigations were administered by the Netherlands Agency for Aerospace Programs (NIVR).

2. DYNAMIC CHARACTERISTICS OF THE AIRCRAFT DESIGN

2.1. General remarks

The purpose of the present study was not to predict the flutter speed of the subject aircraft design as accurately as possible in a multitude of flight conditions, but merely to investigate the influence upon the wing flutter characteristics of some methods to calculate the unsteady aerodynamic forces. Consequently, no aerodynamic forces on fuselage and tail surfaces were applied in any of the calculations to be discussed.

All mass and stiffness data were determined analytically. Only symmetrical motions will be discussed here for one loading condition, viz. completely filled wing fuel tanks and empty fuselage, this being approximately the condition with the lowest flutter speed. With the exception of the engine pylon, all component vibration modes were calculated using elastic beam models. Although the use of a finite element model would have had certain advantages, especially when dealing with more complicated structures, such as the wing-body junction, the engine pylon or the vertical fin-rear fuselage attachment, in this parametric study the simpler beam models were considered adequate.

2.2. Center wing

Flexibility of the center wing section, which is the part of the wing torsion box inside the fuselage, was taken into account by means of a bending degree of freedom. The center wing was simply supported at the wing root.

2.3. Outer wing

The outer wing was attached to the center section and was clamped at the wing root. Five outer wing vibration modes were taken into account as branch modes, three of them containing mainly bending and the other two mainly torsion. No in-plane bending was taken into account, since these modes appeared to have only a negligible influence upon the flutter behavior.

5-2 2.4. Engine

A 6x6 matrix of flexibility influence coefficients was derived from a finite element model of the engine pylon design, attached to a rigid wing structure. Using this matrix and the relevant inertia data, six engine branch modes were calculated, three of which were used in the flutter calculations. The latter modes can be considered as yawing, pitching and rolling of the engine.

2.5. Fuselage and tail

Both forward and rear fuselage were clamped at the wing-body junction. For each of them, only one bending mode was taken into account in the flutter calculations. The tail surfaces were assumed rigid.

2.6. Coupled modes

The aforementioned branch modes, in addition to the symmetric rigid body modes, were used to determine the normal modes of the aircraft design. The frequencies and mode shapes of the six most important normal modes are shown in figure 2.

In order to save computer time, the flutter calculations were carried out on the basis of as few degrees of freedom as permissible. For one set of generalized aerodynamic forces, the flutter characteristics of the present model were compared with those of a dynamic model which comprised significantly more branch modes, such as additional wing modes (including in-plane bending modes), engine modes, fuselage and tail modes. Qualitatively, there appeared to be virtually no differences in flutter behavior between both models, and the quantitative differences were only small. This was not very surprising, since the critical flutter frequencies were relatively low, so that the flutter characteristics were hardly influenced by high-frequency degrees of freedom. The wing in-plane bending modes had only a negligible influence, because the aerodynamic forces associated with them were almost zero.

A final remark concerns the fuselage bending modes, since their inclusion in the dynamic model is not obvious a priori. However, these modes significantly affected the shape of the inner wing torsion/-engine pitching mode, as they caused the nodal line position of this mode near the wing tip to shift forward with respect to the case of a rigid fuselage. This nodal line position greatly influenced the interaction between this mode and the fundamental wing bending mode and hence the flutter characteristics which correspond to classical wing bending/torsion flutter. Because a forward nodal line position was beneficial, neglecting the fuselage bending modes would lead to unrealistically low flutter speeds.

3. INVESTIGATION OF TRANSONIC EFFECTS IN UNSTEADY AIRLOADS AND FLUTTER CHARACTERISTICS

3.1. General

The investigations discussed in this section were carried out by NLR. They were of theoretical and experimental nature, and had the following objectives:

- a. generation of unsteady transonic aerodynamic data
- b. exploration of transonic effects on flutter characteristics.

Almost all work was done under contract with the NIVR. The results formed direct input for Fokker's flutter analysis for the full-scale design and, more generally, provided knowledge to guide further steps in the flutter clearance investigations.

When the investigations were started, NLR could rely on the results of many years of research on unsteady transonic flow. This research, of which the greater part was also performed under contract with the NIVR, involved various wind-tunnel tests with the conventional airfoil NACA 64A006 and the supercritical airfoil NLR 7301, which have become well-known meanwhile (ref. 1). The tests provided physical understanding of the effects of nonuniformity of the mean flow field, and of the moving shock wave on the unsteady airloads. The analysis of these results culminated into the doctoral thesis of Tjeldeman (ref. 2). A typical example is shown in figure 3 with detailed pressure distributions on the upper side of the pitching NLR 7301 airfoil ($t/c = 0.165$, $x_0/c = 0.40$). On the left the effect of a moving shock wave is presented, on the right a shock free case. These distributions, mutually differing completely and also different in comparison with thin-airfoil theory, make plausible that flutter calculations based on conventional lifting surface theory, would involve unacceptable risks.

The investigations at NLR are presented schematically in figure 4, more or less chronologically from left to right. At the beginning a calculation method for 2-D unsteady transonic airloads was available. Although the wing geometric design was not yet completely frozen, it was clear that the wing would have a large aspect ratio. This circumstance led to the opinion that a 2-D transonic calculation method in combination with a 3-D subsonic method should be adequate to determine so-called quasi-three-dimensional (Q-3-D) airloads. The underlying idea can be easily noticed in figure 4.

To check the Q-3-D method experimentally, two ways were open: a wing pressure model test and a wing flutter model test. A choice had to be made as doing both tests would have too great demands on budget and manpower. Although a pressure model test would enable the most direct verification, a flutter model test was preferred because then also transonic flutter characteristics of the wing could be studied, in particular the occurrence of transonic dips in the flutter boundaries.

When the development of the full-scale aircraft was terminated, a calculation method for 3-D unsteady transonic airloads was nearly completed. The method is being evaluated. Finally, a full-scale flutter model was planned to be tested at the end of the scheduled full-scale design phase, but with the realization hardly any start was made.

In the remaining of this section the major steps in the NLR investigations and the most significant results will be discussed.

3.2. Determination of 2-D unsteady airloads

5-3

3.2.1. Calculation methods

The methods which were used to calculate 2-D unsteady transonic airloads are indicated in figure 5.

The first method is LTRAN2-NLR, based on the original LTRAN2 code of Ballhaus c.s. and extended by NLR for application to moderate reduced frequencies ($k < 0.4$) (ref. 3). The code is based on the transonic small perturbation equation for the velocity potential which is solved with a time-marching procedure. For the unsteady case generally two cycles are sufficient.

To reduce the computing time required to obtain unsteady airloads, a second computer code, FTRAN2, was developed (ref. 4). It is a time-linearized method, proceeding from the same mean steady flow field calculated with LTRAN2-NLR. The method has no frequency restriction.

A third computer code is LTRANV, which combines LTRAN2-NLR with Green's lag entrainment method for steady turbulent boundary layers (ref. 5). The code was developed for application to weak interactions between outer flow and boundary layer.

3.2.2. Wind-tunnel experiments

Two wind-tunnel tests were carried out, each test with a different model. The airfoil geometry, being the same in both cases, was representative for sections in the outer wing part of the full-scale design.

It had a thickness of 12% and experimental design values of $M = 0.75$ and $C_L = 0.44$ ($\alpha = 0.75^\circ$). In the first test the model was fitted with a control surface with a hinge axis at 80% of the chord. A part of the test program was repeated after installing an aerodynamic balance.

In the second test the model could be driven in a pitching motion about one of the selectable axis positions and, less usually, also in a heaving motion (ref. 6). The principle of the driving mechanism is shown in figure 6. By changing the position of the driving rods a new airfoil motion could be selected. This excitation set-up provided a check on the admissibility of superposing airfoil motions in transonic flow.

In both tests detailed unsteady pressure distributions were measured on both upper and lower side. A computer-controlled data acquisition and reduction system, PHAROS, was used, which is essentially a transfer function analyzer with 48 simultaneously operating channels (ref. 6). Lift, moment and hinge moment coefficients were obtained by numerical integration.

3.2.3. Results

Calculated and measured unsteady pressure distributions and aerodynamic coefficients were obtained for a wide range of Mach numbers, reduced frequencies, mean airfoil positions and amplitude variations. A survey is given in figure 7. Altogether over 2400 pressure distributions were measured and analyzed carefully. A typical example of amplitude variations is presented in figure 8, showing that adequate accuracy could be maintained down to extremely small amplitudes. Another example is given in figure 9 for the unsteady lift and moment coefficients in separated flow, corresponding to a pitching and heaving motion. They show remarkably alternating values which are related to rapid phase shifts.

An example of comparing calculated and measured data is presented in figure 10, showing the lift coefficients due to pitching about 45% chord (left) and due to control surface rotation (right). Both results correspond to a flow with a strong, moving shock wave. A few remarks can be made immediately:

- Transonic effects are recognized easily by the larger magnitude and phase lag at small reduced frequencies.
- Transonic theory overpredicts the experimental values. The differences are mainly due to the absence of boundary layer effects in the calculations and they are greatest for the control surface rotation.
- LTRAN2-NLR and FTRAN2 produce almost identical unsteady results.
- For the pitching motion an irregularity in the measured magnitude and phase is shown at very low frequency, which is caused by wind-tunnel wall interference.

3.3. Calculation of 3-D unsteady airloads

3.3.1. Quasi-three-dimensional method

The aim of this calculation method is to approximate the transonic unsteady airloads on an oscillating 3-D wing of large aspect ratio. An outline of the method in the form of a diagram is presented in figure 11 (ref. 7). The main assumption is that the 3-D spanwise load distribution is independent of the 2-D transonic properties of the wing sections and depend only on wing planform, Mach number, vibration mode and reduced frequency like in subsonic flow.

Accordingly the wing planform is subdivided into streamwise strips. The transonic airloads on each strip are approximated by combining a 2-D transonic method with a 2-D and a 3-D Doublet-Lattice method. The latter methods are used to determine AIC's, involving effects due to sweep angle, finite span and taper.

The Q-3-D method was developed along similar lines as the method being used by Fokker in the flutter calculations for the full-scale design.

3.3.2. Three-dimensional method

When LTRAN2-NLR was put into use, it was realized that an extension to 3-D flow would imply a rather time-consuming code. A useful alternative was found in a time-linearized approach which led to the development of FTRAN2 and at the termination of the full-scale development, to FTRAN3. The latter code is based on a hybrid method combining the advantages of finite difference and integral methods. The method is still in its evaluation phase and is being used in flutter calculations for the flutter model discussed in section 3.4.

3.4. Wind-tunnel flutter tests

Two wind-tunnel flutter tests were performed on a semi-span model of a supercritical wing in subsonic and transonic flow. The aim was to generate a data base for the verification of the calculation methods for unsteady transonic airloads and to explore the transonic flutter boundaries at different wing incidences.

The flutter model was attached through an instrumented torsional spring to a turn-table in the wind-tunnel side wall (figure 12). The two degrees-of-freedom were wing bending (mode 1) and wing rotation about the spring axis (mode 2). Model response was measured by strain-gage bridges on the spring and by accelerometers in the model. Also the mean pressure distribution on the wing upper side could be measured in one section. A flutter damper allowed attaining to the flutter boundaries and even exceeding them without risks.

The results of the first flutter test were discussed already in ref. 8. The envelope of test points of the second flutter test is shown in figure 13.

It includes the design point of the wing and many off-design conditions, also exceeding the buffet onset boundary. A survey of the results is presented in figure 14, showing at the top flutter boundaries for three wing incidences. In each boundary a transonic dip is easily recognized. Comparison with the flutter frequency curves (middle) learns that mode 1 is unstable. The transonic dip shifts to lower Mach numbers with increasing wing incidence. At the highest wing incidence even two dips occur. Comparison with the trailing edge pressure (bottom) shows that the dip at the lowest Mach number range corresponds to mainly attached flow, although the right-hand side of the dip is influenced already by flow separation. The dip at the highest Mach number range corresponds completely to separated flow, while now mode 2 is unstable.

A comparison of calculated and measured flutter boundaries for the lowest model incidence is presented in figure 15. It shows that flutter calculations in which the Doublet-Lattice method is used, cannot predict a transonic dip, as could be expected. The Q-3-D method employing the 2-D airloads calculated with LTRAN2-NLR predicts indeed the descent of the flutter boundary with increasing Mach number, but a clear transonic dip was not found. The results are slightly conservative, which could be expected on the basis of experience from flutter model tests in transonic flow (e.g. ref. 9). Also results calculated with the Q-3-D method employing 2-D experimental data are shown. Now the location of the transonic dip is predicted correctly, although the flutter boundary has a non-conservative margin, mainly because of tunnel wall interference effects in the experimental data.

The comparison for the highest model incidence in figure 16 is interesting in two respects. First, the flutter boundary calculated with the Q-3-D method is less steep than the measured curve, so that the prediction becomes even nonconservative.

Possibly, the Q-3-D method - which is based on the transonic small perturbation concept - becomes questionable at this model incidence. Secondly, as the Q-3-D method is unable to predict airloads in separated flow, the newly introduced Extended Quasi-Steady (EQS) method was applied. This engineering-type method, which is still being evaluated at NLR, combines experimental data from 2-D unsteady and 3-D steady wind-tunnel tests on the basis of modified strip theory.

For zero frequency the correct spanwise distributions of C_l and C_m are obtained, while for non-zero frequencies the airloads show the anomalous features as was illustrated already in figure 9. The flutter results in figure 16 show a qualitatively correct and quantitatively acceptable agreement.

The results of both Q-3-D method and EQS method were considered encouraging enough to apply them also for the full-scale design.

4. PREDICTIONS OF FLUTTER CHARACTERISTICS OF THE AIRCRAFT DESIGN

4.1. Generalized aerodynamic forces

For the Doublet-Lattice calculations, the wing was divided into 17 streamwise strips of 7 panels each, whereas for the pylon and the engine pod a total of 48 panels was used. Calculations were made for three Mach numbers: 0.7, 0.75 and 0.8. The transonic aerodynamic forces calculated with the Q-3-D method (as discussed in section 3), employed different sets of 2-D unsteady coefficients. It was assumed that the influence of the engine pod upon the generalized aerodynamic forces depended on Mach number only and not on the way in which a transonic correction, if any, was applied.

The 2-D coefficients could be divided into classes, viz:

- those calculated with LTRAN2-NLR
- experimental data obtained from NLR wind-tunnel tests, see section 3.2.2.

These coefficients were measured for only a limited range of frequencies, but the data were extended with calculated coefficients to reduced frequencies up to $k = 0.5$, in order to make them suitable for the calculation process.

Calculated 2-D coefficients were available for $M = 0.7$ and $M = 0.75$ for five and two steady lift coefficients, respectively. For $M = 0.8$, LTRAN2 did not produce reliable results. Measured 2-D unsteady coefficients were available for four steady lift coefficients for each of the three Mach numbers considered.

The original intention was to start from estimated steady spanwise lift distributions and interpolate between 2-D unsteady coefficients for each local lift coefficient. However, the results obtained through this process were not always reliable, because the number of available steady lift coefficients was too small and the dependence of the unsteady coefficients on the steady lift coefficient was not smooth enough. The interpolation was therefore circumvented by assuming a constant C_l along the wing span. Although such a constant C_l distribution was unrealistic, this assumption was not too bad over a considerable part of the wing span. Moreover, it was expected that the influence of increasing the angle of attack on the flutter characteristics could be predicted quite well.

4.2. Influence of Mach number in subsonic flow

Using Doublet-Lattice aerodynamics on wing, pylon and engine pod, flutter calculations were performed for $M = 0.7$, 0.75 and 0.8 . Plots of airspeed vs. frequency and damping for the fundamental wing bending mode and inner wing torsion/engine pitching mode (see fig. 2) are presented in figure 17. These and other calculations were made with the p-k method, assuming an altitude of 15,000 ft above sea level. This altitude was chosen because it was approximately the altitude where V_D of the subject aircraft corresponded with $M = 0.75$. Since the transonic dip was expected at or near $M = 0.75$, being the Mach number where the wing lift curve slope reached its maximum value, this altitude was considered critical with respect to transonic wing flutter. Zero structural damping was assumed. Figure 17 shows that the flutter speed increases slightly with increasing airspeed, which is contradictory to initial expectations. This trend is due to the presence of aerodynamic forces on pylon and pod, since similar calculations with aerodynamics on wing only showed the opposite trend, although for considerably higher flutter speeds.

The inner wing torsion/engine pitching mode is the critical flutter mode, because of the intersection of its frequency curve with the curve of the fundamental wing bending mode. This flutter mode is a so-called hump mode as it becomes stable again at a higher speed.

4.3. Influence of engine pylon stiffness

The pylon used in the present calculations was designed for both strength and stiffness requirements. The engine pylon pitching stiffness was a major parameter which controlled the frequency of the inner wing torsion/engine pitching mode, and hence influenced the wing flutter characteristics. To get insight into the criticality of the pylon pitching stiffness, some flutter calculations were repeated for varying uncoupled engine pitching frequencies, all other branch modes remaining unaffected.

In figure 18, the relation between flutter speed and uncoupled engine pitching frequency is shown for Doublet-Lattice aerodynamics at $M = 0.75$. Obviously, there appeared to be two ways to prevent flutter within the required flutter boundary. Firstly, by ensuring that the engine pitching stiffness would be sufficiently high to result in an adequate frequency separation between the fundamental wing bending mode and the inner wing torsion/engine pitching mode. Secondly, by making the pylon so flexible in pitching that the inner wing torsion frequency would become lower than the wing bending frequency. However, the latter approach was not feasible for the type of wing/engine combination considered here, because of pylon strength requirements.

The local peak in figure 18 is due to coincidence of the engine yawing and pitching frequencies. This situation was not completely realistic, however, since a decrease in pitching stiffness necessarily would involve some decrease in yawing stiffness.

A potential problem could have existed with respect to fail-safe flutter since a structural failure of the pylon would lead to a reduced pylon pitching stiffness and hence to a significant reduction of the flutter speed.

4.4. Application of the Q-3-D method

4.4.1. Application of calculated 2-D unsteady coefficients

4.4.1.1. $M = 0.7$

The influence of applying 2-D unsteady coefficients calculated with LTRAN2-NLR in the Q-3-D method is shown in figure 19 for $M = 0.7$ and $C_l = 0.384$, 0.490 , 0.608 and 0.660 . A similar calculation was performed for $C_l = 0.237$, but the results were virtually the same as for $C_l = 0.384$. All flutter branches of figure 19 become unstable at a lower speed than for Doublet-Lattice aerodynamics, with $C_l = 0.608$ leading to a 7.4% flutter speed reduction. The critical model is still the same hump mode as in figure 17.

4.4.1.2. $M = 0.75$

For $M = 0.75$, only two sets of calculated 2-D unsteady coefficients were available, viz. for $C_l = 0.289$ and $C_l = 0.499$, which resulted in flutter speeds of 0.94 and 1.24 times the corresponding Doublet-Lattice flutter speed, respectively. The higher flutter speed at $C_l = 0.499$ is caused by a change in the flutter mechanism; the fundamental bending mode has become critical instead of the hump mode of inner wing torsion/engine pitching.

4.4.2. Application of measured 2-D unsteady coefficients

4.4.2.1. $M = 0.7$

For this condition four flutter calculations were made, viz. for $C_l = 0.30, 0.39, 0.47$ and 0.70 . The predicted flutter speeds were 1.02, 1.01, 1.07 and 1.02 times time speed calculated with Doublet-Lattice aerodynamics, respectively. These and other results obtained with measured 2-D coefficients should be treated with some caution, since the coefficients were measured at Reynolds numbers of approximately 2.10^6 , whereas the actual aircraft would operate at $Re = 10^7$ and higher. This effect has to be investigated further. Also, the measured coefficients were subject to wind-tunnel wall interference effects for which corrections could be made only at $k = 0$.

4.4.2.2. $M = 0.75$

Curves of airspeed vs. frequency and damping pertaining to quasi-three-dimensional airloads employing measured 2-D coefficients for $M = 0.75$ and $C_l = 0.31, 0.40, 0.51$ and 0.61 are shown in figure 20. The calculated flutter speeds are 1.10, 0.93, 1.14 and 1.01 times the corresponding flutter speed for Doublet-Lattice aerodynamics, respectively.

Probably, the transonic dip (if considered as a function of C_l or angle of attack at constant Mach number instead of a function of Mach number at constant angle of attack, which is usual) is located in the vicinity of $C_l = 0.4$.

As can be seen immediately in figure 20, the flutter behavior at $C_l = 0.61$ is completely different from all other cases considered. Here, it is not the coupling with the fundamental wing bending mode which causes the inner wing torsion/engine pitching mode to become unstable, but rather a one-degree-of-freedom flutter case involving only the first wing bending mode. The relatively low flutter speed at $C_l = 0.61$ might be related to the "second transonic dip" which was discussed in section 3.4 in connection with the wind-tunnel flutter tests. This second dip was shown there to correspond to separated flow and indeed, steady pressure model tests for similar flow conditions revealed that flow separation took place over the entire wing span. This flutter case will be discussed further in section 4.5.

4.4.2.3. $M = 0.8$

For this Mach number, 2-D unsteady coefficients were available for $C_l = 0.28, 0.33, 0.36$ and 0.42 , i.e. for approximately the same angles of attack for which coefficients were measured at $M = 0.7$ and $M = 0.75$. The resulting flutter plots are presented in figure 21. At $C_l = 0.28$ the lowest flutter speed was predicted, which was 0.94 times the comparable flutter speed for Doublet-Lattice aerodynamics. No indication of a second transonic dip was found, although the flow was separated over a major part of the wing at the three highest lift coefficients considered.

4.5. Application of the "Extended Quasi-Steady" method

As was pointed out in section 3.4., the validity of the Q-3-D method was questioned for conditions where flow separation occurs over a significant part of the wing. For this reason the alternative EQS method was introduced at NLR.

Thereupon the EQS method was also applied to the full-scale design for three conditions which have been discussed already in section 4.4., viz. $M = 0.75$, $C_l = 0.61$ and $M = 0.8$, $C_l = 0.36$ and 0.42 . The results of these calculations are shown in figure 22. Comparison with figures 20 and 21 show that the flutter behavior is qualitatively the same as for the Q-3-D method. For the $M = 0.8$ cases, even a good quantitative agreement is observed.

At $M = 0.75$, $C_l = 0.61$, however, the flutter speed reduces from 1.01 for the Q-3-D method to 0.65 times the corresponding Doublet-Lattice value.

This one-degree-of-freedom flutter phenomenon can be attributed largely to the imaginary part of the unsteady lift coefficient due to heaving, k_a'' , becoming slightly negative for small values of the reduced frequency (fig. 9b), whereas this coefficient is positive for attached flow.

4.6. Influence of steady lift coefficient

Results of sections 4.4.1. and 4.4.2. have been collected in figure 23 to show conveniently the influence of the lift coefficient on the flutter boundaries. The total lift coefficients C_L were made to correspond to the local lift coefficients C_l for which the flutter boundaries were calculated, using the data of steady pressure model tests.

With due account of the approximative nature of the unsteady airload calculations and of the interfering influences of tunnel walls and too low Reynolds numbers, the results in figure 23 are considered reliable enough to demonstrate an undeniable influence of C_L (or of the load factor n). This means, more in general, that the calculation of transonic flutter boundaries should not be restricted to e.g. level flight conditions, but a search should have to be made for those conditions within the flight envelope for which the flutter boundaries are most critical. If the design phase of the present full-scale design could have been continued, this search would certainly have been given further attention.

5. CONCLUSIONS

Aeroelastic configurations for a supercritical wing transport in the preliminary design phase were discussed. Much emphasis was put on investigating the influence of transonic flow effects on the flutter characteristics of the supercritical wing. Subjects were: unsteady airloads calculations, unsteady pressure model tests, flutter model tests and flutter calculations for the full-scale design.

Although the design phase was not finished, the steps taken in the flutter clearance were already sufficient to yield considerable knowledge of the transonic flutter characteristics as well as many data which would have contributed as well substantially to a successful completion of the design phase. More specifically:

1. The pressure model tests provided excellent data bases for the evaluation of computer codes for unsteady airloads and for the analysis of flutter model test results.
2. The flutter model tests resulted in an adequate understanding of the transonic dips in the flutter boundaries, both in attached and in separated flow.
3. An engineering-type calculation method (Q-3-D method) for the determination of unsteady transonic airloads was developed, which was verified by the flutter model tests. Satisfactory agreement was found at small wing incidences. An alternative method (EQS method) for higher wing incidences where flow separation occurred, appeared to lead to reasonable agreement with the flutter test results.
4. Unsteady airloads data from wind-tunnel tests and calculations in combination with the Q-3-D and EQS methods were used in flutter calculations for the full-scale design. The results showed a distinct influence of the steady lift coefficient or load factor. A search for the critical load factor within the flight envelope corresponding to the lowest flutter boundary would have been a necessary next step.

6. ACKNOWLEDGEMENT

The authors acknowledge the assistance of Mr. A. Steiginga, NLR.

7. REFERENCES

1. N.C. Lambourne
c.s. Compendium of unsteady aerodynamic measurements.
AGARD Report No. 702, 1982.
2. H. Tijdeman
NLR TR 77090 U, 1977. Investigations of the transonic flow around oscillating airfoils.
3. R. Houwink
J. van der Vooren Improved version of LTRAN2 for unsteady transonic flow computations.
AIAA Journal, Vol. 18, No. 8, August 1980,
pp. 1008-1010.
4. M.H.L. Hounjet A field panel method for the calculation of inviscid transonic flow about
thin oscillating airfoils with shocks.
Int. Symp. on Aeroelasticity, Nuremberg, Germany,
Oct. 5-7, 1981.
5. R. Houwink Unsteady viscous transonic flow computations using the LTRAN2-NLR code
coupled with Green's lag-entrainment method.
2nd Symp. on Num. and Phys. Aspects of Aerodynamic Flows,
Calif. State Univ., Long Beach, Jan. 17-20, 1983.
6. J.J. Horsten Recent developments in unsteady pressure measurement techniques at NLR.
Int. Symp. on Aeroelasticity, Nuremberg, Germany,
Oct. 5-7, 1981.
7. A. Steiginga
J.J. Meijer A revised quasi-3-dimensional concept to determine unsteady airloads on
oscillating high-aspect ratio wings in transonic flow.
NLR TR 82062 L, 1982.
8. R. Houwink
A.N. Kraan
R.J. Zwaan A wind-tunnel study of the flutter characteristics of a supercritical wing.
J. Aircraft, Vol. 19, No. 5, May 1982,
pp. 400-405.
9. R. Destuynder
H. Tijdeman An investigation of different techniques for unsteady pressure measurements
in compressible flow and comparison with lifting surface theory.
AGARD-R-617, 1974.

5-8

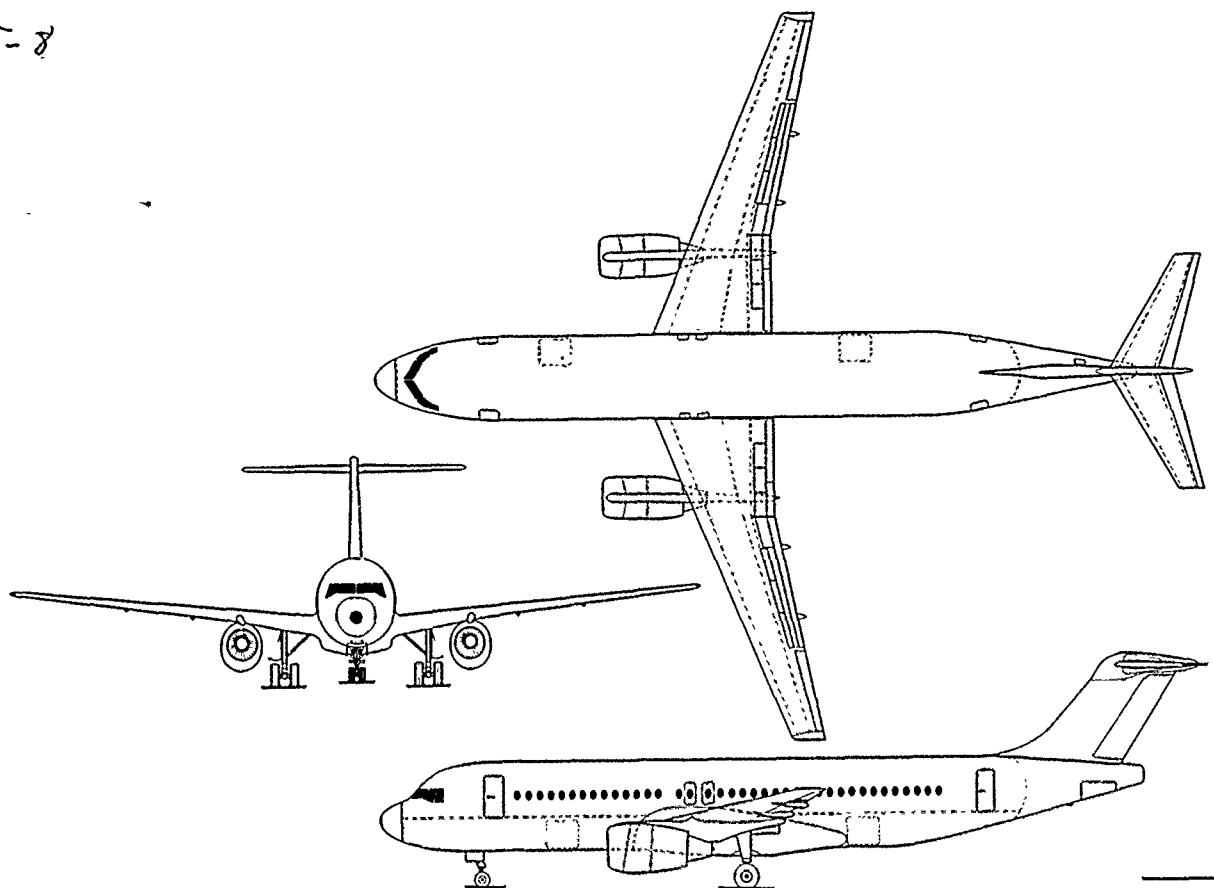


Fig. 1 Views of full-scale design

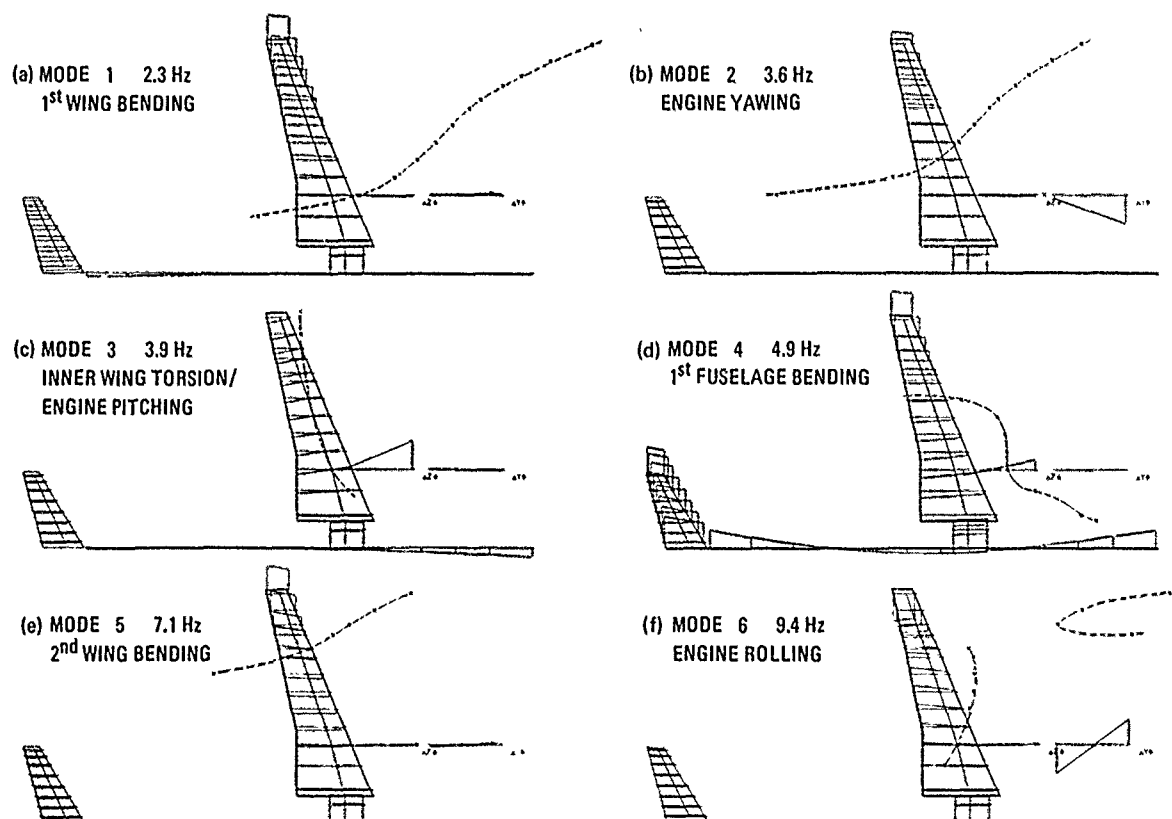


Fig. 2 Coupled modes of the full-scale design

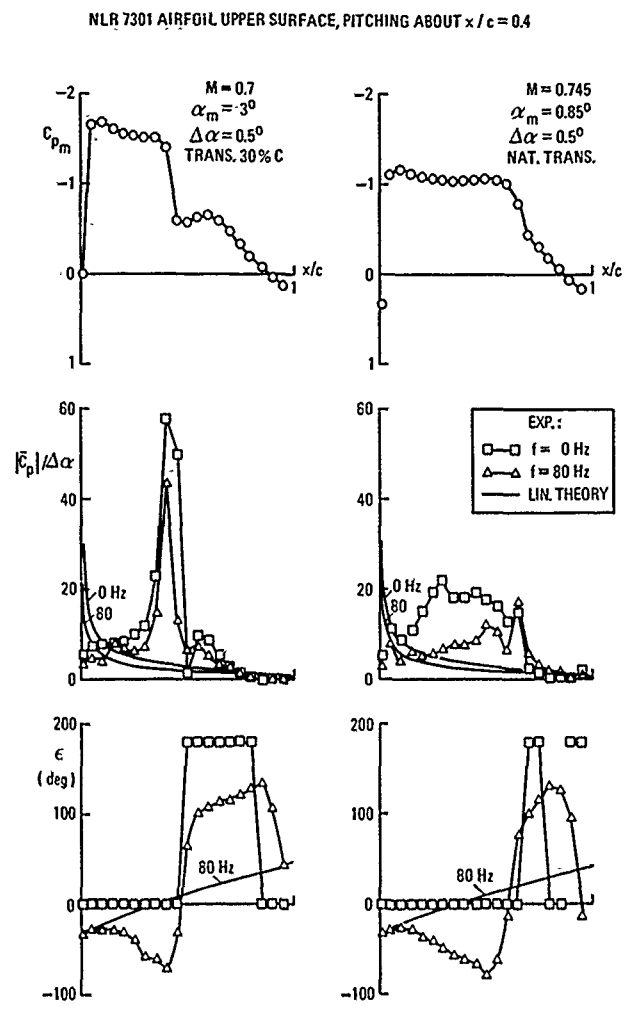


Fig. 3 Experimental results of previous wind-tunnel measurements with NLR 7301 airfoil oscillating in pitch

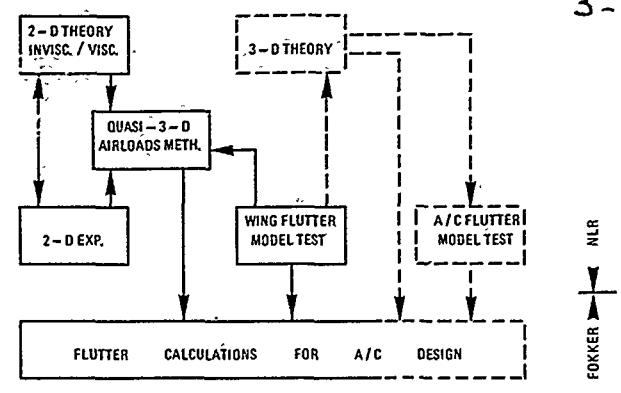


Fig. 4 Investigations of modelling unsteady transonic airloads and transonic flutter characteristics, carried out or planned by NLR during the aircraft design stage

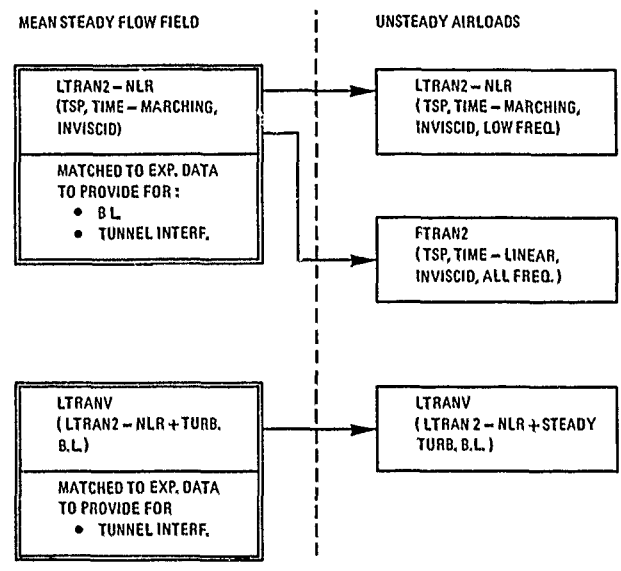


Fig. 5 Calculation methods at NLR for 2-D unsteady transonic airloads

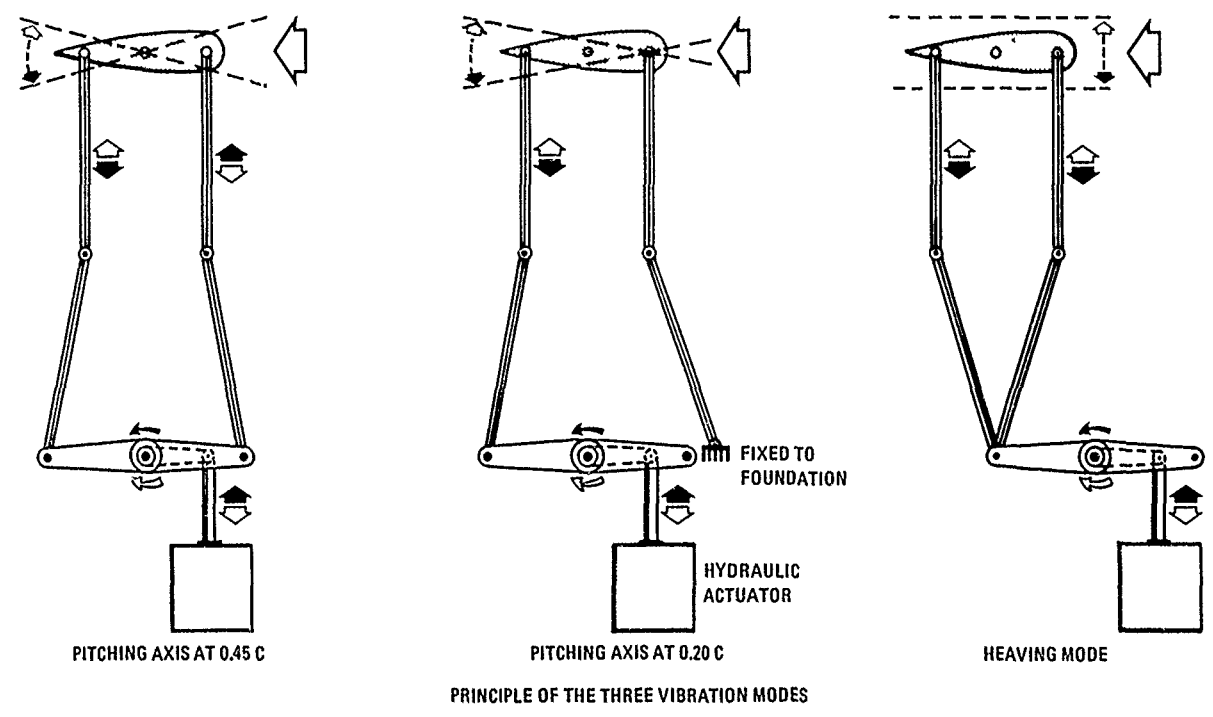
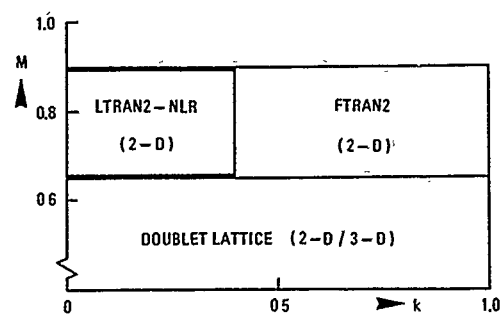
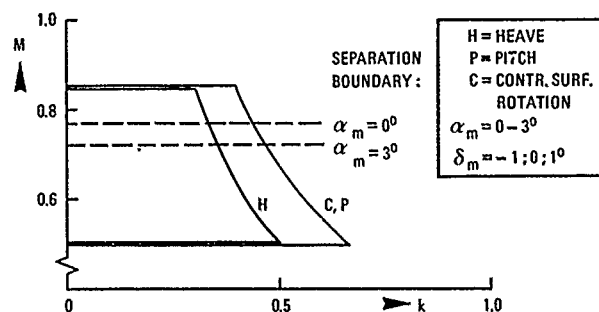


Fig. 6 Principle of the three vibration modes (Ref. 6)



(A) AVAILABLE CALCULATED RESULTS, $0 \leq \alpha_m \leq 3^\circ$



(B) AVAILABLE EXPERIMENTAL RESULTS

Fig. 7 Survey of available 2-D calculated and experimental unsteady airloads data for supercritical airfoil

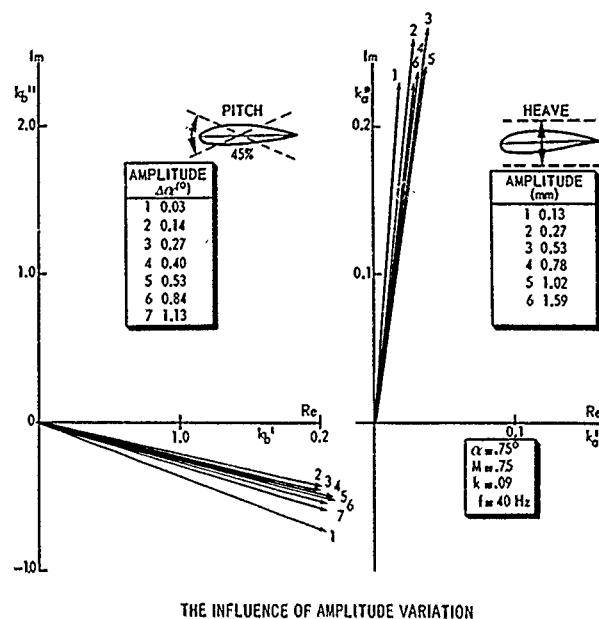


Fig. 8 The influence of amplitude variation (Ref. 6)

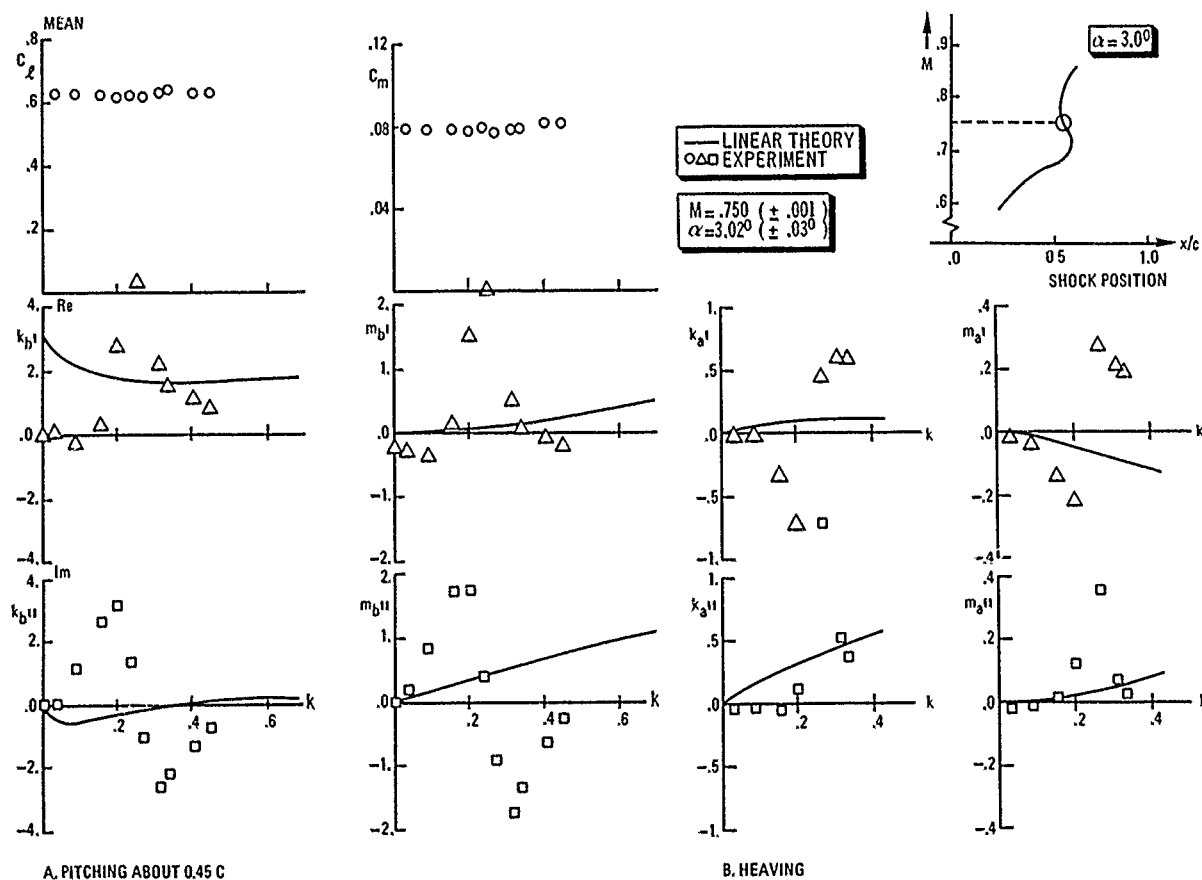


Fig. 9 Aerodynamic coefficients in separated flow

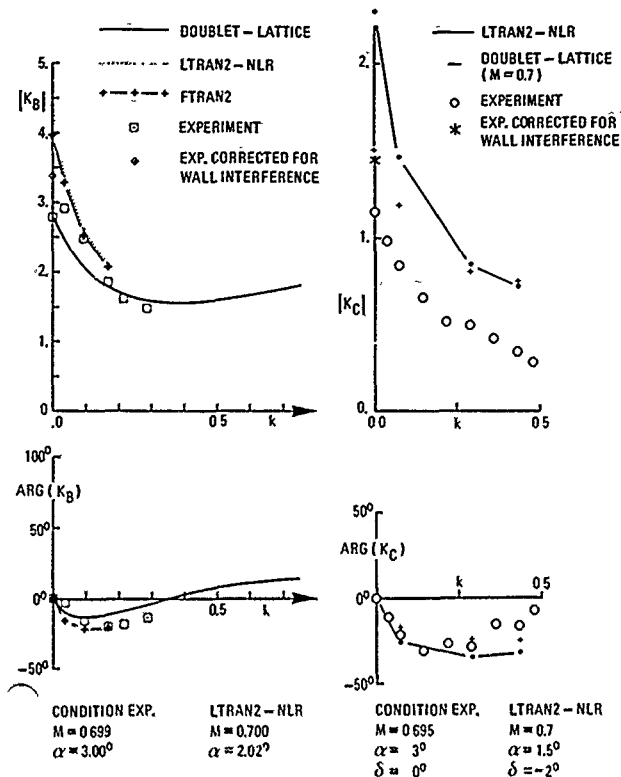


Fig. 10 Comparison of calculated and experimental lift coefficients for a 12 % thick supercritical airfoil oscillating in pitch about $x/c = 0.45$ (left) and with oscillating control surface with axis at $x/c = 0.80$ (right)

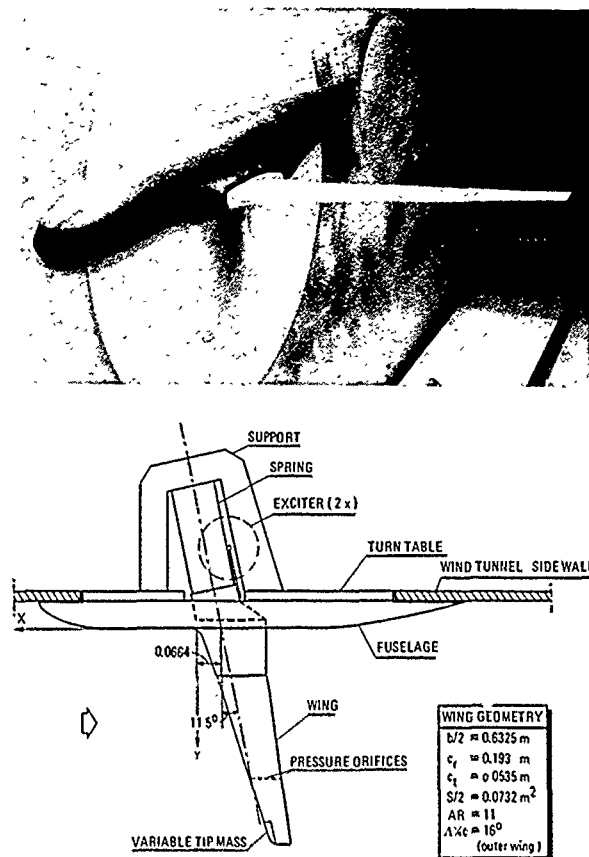


Fig. 12 Global view of flutter model and support

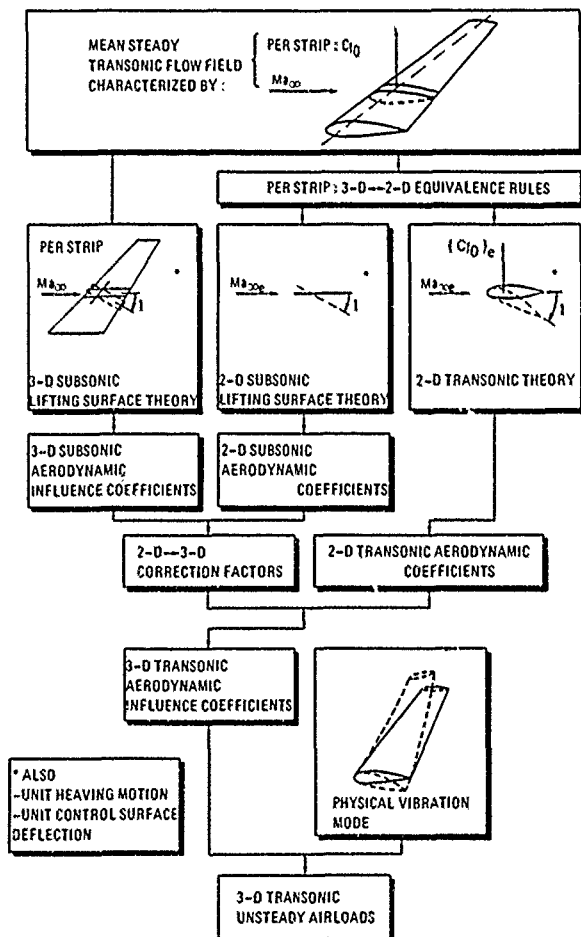


Fig. 11 Engineering method to calculate unsteady airloads on a high aspect ratio wing oscillating in transonic flow (Ref. 7)

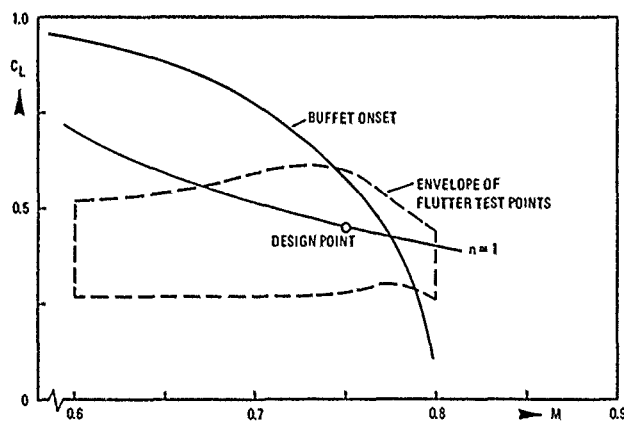


Fig. 13 Envelope of test points in 2nd wind-tunnel flutter test

5-12

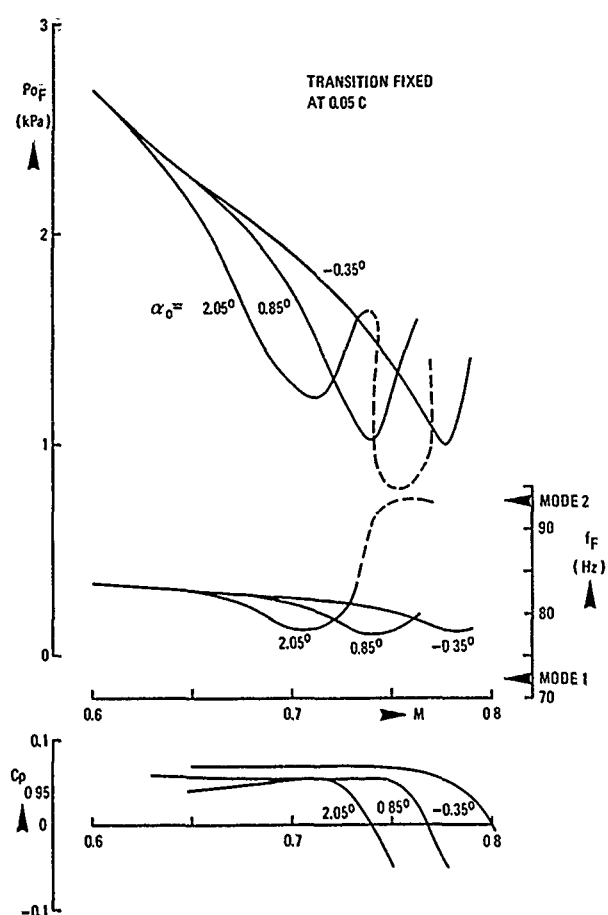


Fig. 14 Results of wind-tunnel flutter test

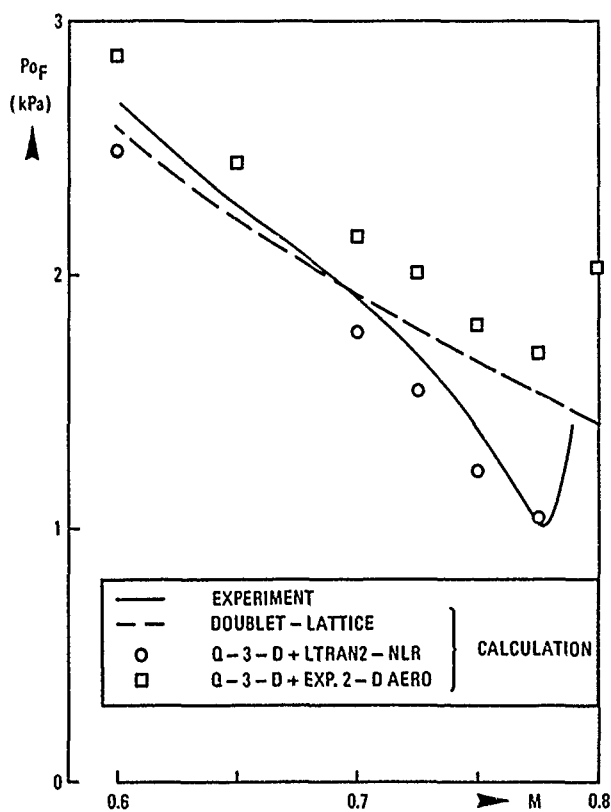
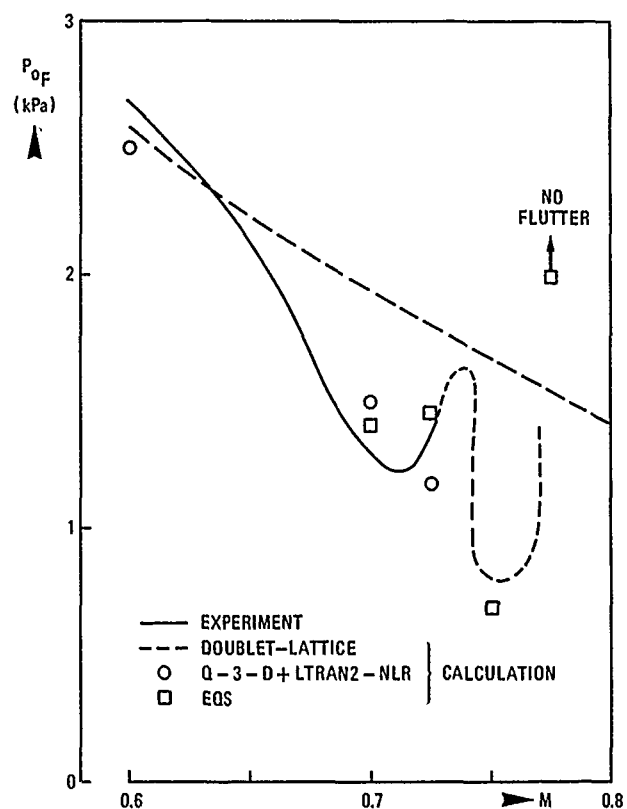
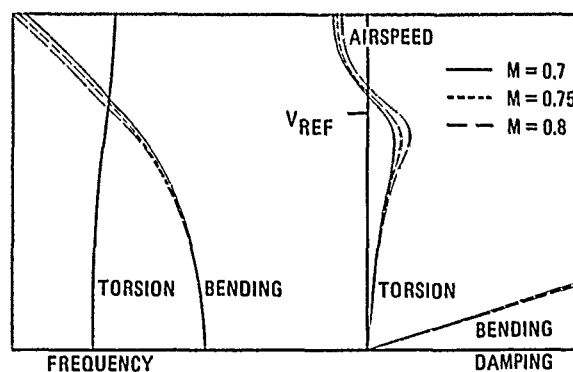
Fig. 15 Comparison of calculated and measured flutter boundaries of wind-tunnel flutter test ($\alpha = -0.35$ deg)Fig. 16 Comparison of calculated and measured flutter boundaries of wind-tunnel flutter test ($\alpha = 2.05$ deg)

Fig. 17 Flutter characteristics of aircraft design for Doublet-Lattice aerodynamics

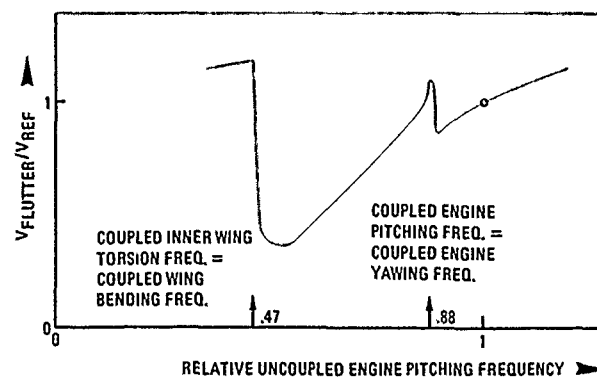


Fig. 18 Flutter speed as function of uncoupled engine pylon pitching frequency

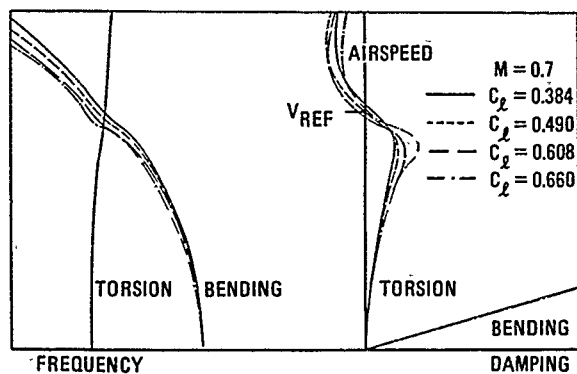


Fig. 19 Flutter characteristics of aircraft design for application of calculated aerodynamics

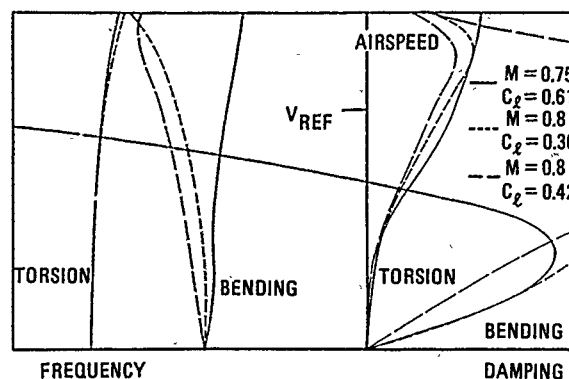


Fig. 22 Flutter characteristics of aircraft design for EQS aerodynamics

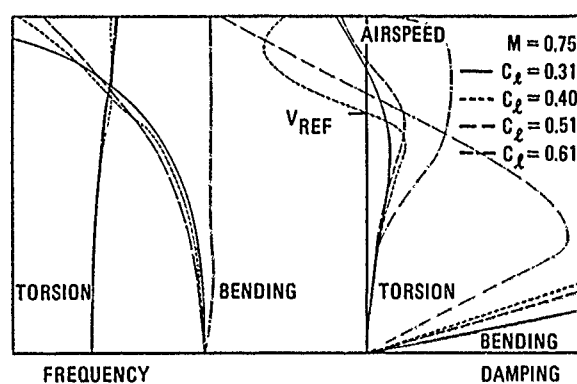
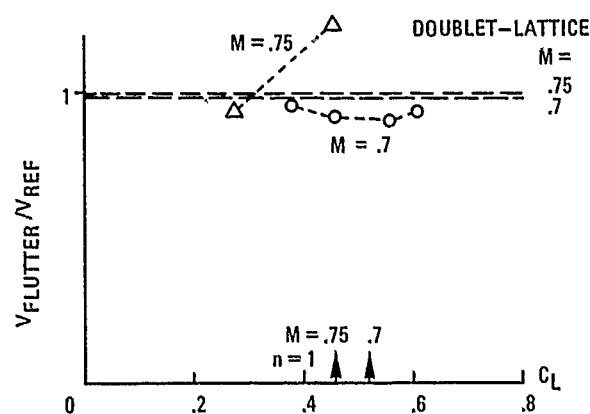


Fig. 20 Flutter characteristics of aircraft design for application of measured aerodynamics



A. Q-3-D METHOD WITH 2-D THEORETICAL AIRLOADS

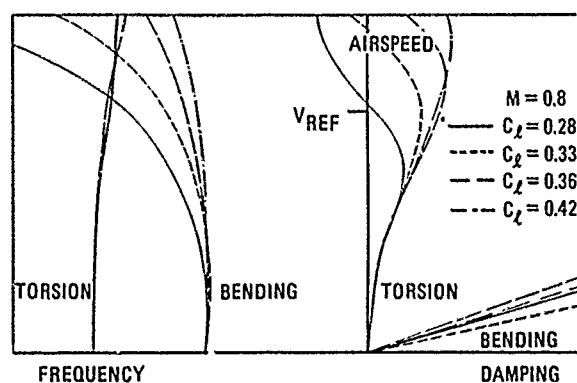
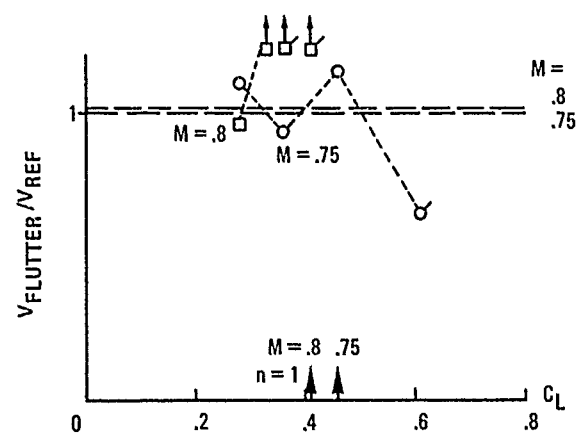


Fig. 21 Flutter characteristics of aircraft design for application of measured aerodynamics



B. Q-3-D METHOD AND EQS METHOD (FLAGGED) WITH 2-D EXPERIMENTAL AIRLOADS

Fig. 23 Influence of steady lift coefficients on the flutter boundaries

6-1

INFLUENCE OF MAIN DESIGN PARAMETERS ON FLUTTER BEHAVIOUR
FOR AIRCRAFT CONFIGURATIONS WITH HEAVY CONCENTRATED MASSES
by

Helmut Zimmermann and Siegfried Vogel
MBB/Vereinigte Flugtechnische Werke GmbH, D-2800 Bremen,
Germany

SUMMARY

Heavy concentrated masses fitted elastically to the wing can induce flutter in an aircraft. This flutter case is well known for fighter aircraft with certain store configurations. For transport aircraft this flutter case becomes more and more important especially for wing-engined aircraft with heavy engines, and modern transonic profiles. The structural and aerodynamic influence parameters for this flutter case are described for a particular project. A flutter speed inside the flight envelope caused by this type of flutter can only be prevented by taking account of aeroelastic criteria and their influence on the early design of the aircraft. For a frozen design this flutter case can only be prevented by penalizing the weight and drag properties of the aircraft. Because transonic aerodynamics also decreases the flutter speed (known as the transonic dip) for aircraft with modern transonic profiles this flutter case deserves special consideration.

1. INTRODUCTION

Although fighter and transport aircraft generally differ widely in their flutter behaviour, a fighter aircraft with external stores can exhibit the same type of flutter as a wing-engined transport aircraft. This type of flutter may be symmetrical and/or antisymmetrical, and may be caused by modes of the following shape:

- fundamental wing bending
- engine pitch (inner wing torsion) with a quasi-rigid pitching of the outer wing.

The flutter speed in this case is influenced by the sideward bending or yawing motion of the external store (or engine) and the torsion of the outer wing. For a fighter aircraft this type of flutter is bound to occur eventually within the flight envelope, since new and unexpected requirements for stores configurations may arise during the life of a fighter aircraft type, long after the design has been fixed. This may occasionally lead to flight envelope limitations for certain store configurations.

For transport aircraft a limitation of the flight envelope must be prevented by appropriate design changes. Because the weight and pitching inertia of the engine, as well as the distance between the wing elastic axis and the engine c.g., strongly influence the flutter behaviour, this type of flutter must be considered carefully during the early design stages of a transport aircraft. The severity of the problem increases with increasing engine power, because the attendant increase in fan shroud diameter makes it necessary to shift the engine further upstream to avoid any detrimental aerodynamic interference with the wing with enough ground clearance for a short main undercarriage. This up-stream shift of the engine lowers the flutter speed. This effect may be even more critical if the wing is designed to fly in the transonic range, where unsteady aerodynamic effects already tend to reduce the flutter speed. If the replacement of the engine by more powerful types, for instance, leads to such a kind of flutter problem similar to the problem for fighters, where new store configurations become necessary, then a redesign of the pylon or the addition of masses on the wing become necessary. Because of the severity of the problem it seems useful to elucidate the flutter behaviour of aircraft with big concentrated masses from different points of view.

The design of a new aircraft above all of a transport aircraft is determined by various design aspects and constraints. The design aspects imply an optimum aerodynamic design, and a low-weight stress design leading to low cost per passenger-mile. The constraints are long inspection intervals resulting in low maintenance costs, and low production costs for the manufacturer. The latter means simplifications in the production or, for example, using the same aircraft parts for different projects. From a management point of view it is self-evident that an aircraft should be free of flutter without penalizing the above mentioned optimization process. Therefore a flutter case within the flight envelope of an aircraft, found after the preliminary design or, even worse, after fixing the design places the aeroelastician in a difficult position, because to eliminate this flutter case the aeroelastician requires changes which upset the optimization design procedure.

Therefore the design of an aircraft must be shown to be free of flutter at a very early stage of the project. Because the design constraints imposed by aerodynamics, weight, loads, and stresses by themselves rarely, if ever, tend to contribute to a good aeroelastic design, this means that the aeroelastic department must be involved in the optimization procedure right from the beginning. If this is done, and the aeroelastic constraints are balanced against all other constraints at every iteration of the design, the weight and drag penalties will be kept to a minimum.

2. GENERAL DESIGN PROCEDURE

The design of an aircraft usually proceeds in the following fashion: First of all the basic geometrical configuration of the aircraft is arrived at by an iterative process between the design, aerodynamics, and other departments. Secondly, after the design loads have been estimated for the various substructures, the structure is designed by fixing the position, number, and shapes of ribs, frames, stringers, as well as skin thicknesses, on the basis of previous experience, and the stress values are calculated for the resulting structure.

The design loads for the wing of a transport aircraft are determined by gust loads for a lightly loaded wing, and by manoeuvre loads for heavily loaded wings. These load cases determine the wing bending moments and thus the thicknesses of skins, spars, stringers and so on, in conjunction with manufacturing constraints. The ratio between skin thickness and stringer areas is determined by buckling and fatigue criteria, and previous experience. Sometimes flaps and slats also influence skin and spar thicknesses. The pylon and its wing-attachment is designed for crash loads, as well as the undercarriage attachment with its back-up structure. The design of the fuselage is normally governed by crash loads and interior pressure.

If we accept the foregoing as a representative description of the design procedure, where the geometry is largely determined by aerodynamics and the particular requirements of the project, and the stiffness mainly by load criteria, it becomes apparent that no design criterion can be found among them which helps to prevent the flutter case under consideration. From this it is clear that the aeroelastician must influence the design and must be involved in the iteration of the design steps from the beginning.

3. DESCRIPTION OF THE FLUTTER CASE AND ITS CAUSES

As mentioned above, the flutter case is dominated by two modes:

- fundamental wing bending
- engine pitching, especially for wing-mounted twin-engine aircraft.

For transport aircraft the fundamental wing-bending frequency usually depends on the fuel content; the more fuel, the lower the frequency. The frequency of the engine pitching mode is nearly independent of the fuel content of the wing. In flight the two mode frequencies are changed by the airloads on the wing and the nacelle such that, in general, the bending mode frequency increases with dynamic pressure, and the engine pitch mode decreases (Fig. 1). Where these two frequencies cross, flutter is likely to occur, as will be shown later. One way of circumventing this undesirable state of affairs would be to eliminate the crossing entirely by lowering the engine pitch frequency below or slightly above that of the fundamental mode. There are, however, two factors that make this seemingly simple option impractical. Firstly, because the fundamental frequency depends to a large extent on the fuel load, the engine pitch frequency would have to be lowered sufficiently to take care of all fuel load conditions. In this case the pitching motion of the engine would have to be decoupled from the wing. Because of the large weight and size of modern turbo-fan engines this option may be safely ruled out.

A second and more realistic alternative is therefore to accept the existence of the frequency crossing, and then to try to improve the flutter behaviour by the position of the nodal line of the engine-pitch mode, which has a marked influence on damping. If the nodal line crosses the leading edge near the tip, no flutter is going to occur as a rule. If, however, the nodal line crosses the trailing edge near the tip, the damping of the inner wing torsion decreases in the speed range near the frequency crossing (Fig. 2) of the two modes being considered, and flutter is most likely to occur. This behaviour can be explained by the marked difference between the aerodynamic coupling terms for the two nodal line positions, i.e.

$$\int \varphi_i p_j dF \quad \text{and} \quad \int \varphi_j p_i dF,$$

where p_i is the unsteady pressure difference distribution over the wing caused by the motion of the mode with mode shape φ_i . The sign of the coupling term $\int \varphi_i p_j dF$, with φ_i as the engine pitch mode shape, is given by the relative position of the nodal line to the aerodynamic centre.

Therefore it becomes important to examine factors that influence the position of nodal line of this mode. These factors are listed below without regard to their relative importance:

1. Fuselage stiffness
2. Pylon stiffness
3. Engine c.g. position
4. Attachment stiffness between pylon and wing and pylon and engine
5. Ratio of bending and torsion stiffness of the wing near the pylon station
6. Shear flexibility of the wing
7. Sweep of the wing
8. Attachment fuselage-wing
9. Masses at the tip of the wing

Although the influence parameters for shifting the nodal line of this mode are quite clear it is not possible to give universal design criteria. The reasons are that:

1. Although the tendency of the changes in the influence parameter on the flutter behaviour are clear, the required size of such changes are different for different projects.
2. The design loads lead to different structural proportions for skin thicknesses, stringer areas and so on for differing geometries of the wing, the wing box, and others. Therefore any changes proposed by the aeroelastician may, after redesign, lead to no appreciable flutter improvement, or even to negative aeroelastic effects in particular cases.
3. If one of the parameters is poorly designed from an aeroelastic point of view, changes of the other parameters will influence the flutter behaviour only insignificantly.

In trying to avoid this situation, the aeroelastician is faced by the following problems:

1. Most of the parameters listed above are not well known at the beginning of the design project
2. The relevant parameters with a significant influence on flutter behaviour must be found out.

The only practical solution to this problem for the aeroelastician is to vary the parameters extensively in his calculations to detect and pinpoint the sensitive parameters at the beginning of the design project. All this amounts to an optimization process.

4. SENSITIVITY TO THE STRUCTURAL PARAMETERS

To show the influence of the aeroelastic parameters on flutter, vibration and flutter calculations were made for a particular aircraft. Fuselage and wing were represented by beams. The wing-fuselage attachment stiffness was obtained by Finite-Element methods. Engine pylon flexibility matrices were also based on FEM, the pylon-wing attachment stiffness was estimated, and the tail was sometimes represented by a mass, sometimes by beams of known stiffness. The vibration model is shown in Fig. 3. The unsteady airforces were calculated with the doublet-lattice theory for $M = 0.84$. The calculations were done with and without pod-airforces. For pod-airforces airforces of a circular annular cylinder were used. The geometry of the cylinder corresponds to that of the fan shroud. The flutter calculation method is an improved p-k method [1]. The calculation was made for matched altitude for the selected M-number.

First of all the difference in the flutter behaviour between the dry and the wet wing will be shown, wet meaning nearly full of fuel, dry meaning nearly empty. Fig. 4 shows the nodal lines of the engine pitch mode, and the eigen frequencies of the first three symmetrical modes for the two fuel cases. Note the large difference in the fundamental mode frequencies, whereas the engine pitch frequencies are hardly affected by the fuel load. The nodal line for the wet wing lies upstream of that for the dry wing.

At the bottom of Fig. 4 the results of the corresponding flutter calculations are shown, in the form of frequencies and damping vs. flight speed. The frequency plot shows the increase of the fundamental bending mode due to increasing dynamic pressure for the different fuel cases. The difference between the fundamental bending frequencies for the dry and wet wing are nearly constant when plotted versus speed. The variation of damping with speed is shown only for the engine pitch mode. The plot shows that the dry wing with a higher frequency of the fundamental bending and with the upstream nodal line at the wing tip has a lower flutter speed.

Next the influence of changing the pylon flexibility within a reasonable range is shown in Fig. 5. The nodal line moves upstream at the wing tip with decreasing flexibility and the flutter speed increases. If the pylon is assumed to be rigid the engine pitch mode changes its character and couples with a fuselage mode resulting in a qualitatively different damping behaviour which is difficult to compare with the other cases.

In the following parameter studies the pylon flexibility is held constant at 0.322×10^{-6} m/N. The influence of the engine c.g. position on flutter is shown in Fig. 6 as frequency and damping plots. The nodal line moves upstream at the wing tip with downstream shift of engine c.g. as shown at the top of Fig. 6, and the flutter speed increases or disappears entirely.

One of the parameters which has a significant influence on flutter for this aircraft is the torsion attachment stiffness between wing and fuselage. The top of Fig. 7 shows the engine pitch nodal line for three different attachment stiffnesses, together with the values of the corresponding attachment stiffnesses and mode frequencies. The damping curves at the bottom of the Fig. 7 show that when the torsion stiffness is increased beyond a certain value no influence on the nodal line and the flutter speed can be noticed. It should be pointed out here that this attachment stiffness is fixed by the design of the center fuselage and the wing root, depending largely on the fuselage shape. This makes it one of the parameters that cannot be altered later on to accommodate flutter.

Another parameter relevant to flutter behaviour is the shear flexibility between wing root and pylon (for this variation a higher pylon stiffness was used). On the top of Fig. 8 the nodal lines of the engine pitch modes are shown for several shear flexibilities. The corresponding damping curves below show that the smallest flutter speed is obtained if the shear flexibility is neglected entirely. Increasing the shear flexibility also increases the flutter speed until it disappears. In principle a larger shear flexibility can be obtained by a smaller profile thickness decrease near the wing root, but this is usually impossible for a frozen design.

Another influence parameter is the fuselage bending stiffness. The nodal line for the engine pitch mode is shifted upstream at the wing tip for decreasing fuselage stiffness. The damping with flight speed for the engine pitch mode shows flutter at low flight speeds for the stiffer fuselage. The corresponding curve for the more flexible fuselage shows no flutter. Fig. 9.

To illustrate the effect of wing bending and torsional stiffness on flutter, several calculations were made for a hypothetical wing, in which the stiffnesses of the inner wing were increased. The increase of stiffness was achieved by successively extending the region of reinforcement from the wing root up to and a little beyond the pylon station. For one set of calculations both bending and torsional stiffnesses were raised by a common factor, for the remaining calculations the torsional stiffness was raised more than the bending stiffness (Fig. 10). In general it can be said that the more the torsional stiffness was increased in relation to the bending stiffness, the more the flutter speed increased, but increasing both stiffnesses by the same factor also resulted in an improvement of the flutter speed.

The calculations revealed two general trends:

1. Increasing the torsional stiffness by a larger factor than the bending stiffness was more effective in raising the flutter speed, than raising both stiffnesses by the same factor.
2. Stiffening the region near the pylon was more effective than stiffening the wing near the root.

The disproportional change of torsional stiffness and bending stiffness may in principle be achieved in two ways:

1. By increasing the depth of the wing box. This would lead to a thinner skin to keep the stresses at the same level. Because of buckling considerations, however, the stringer areas would then have to be increased, leading to a higher bending stiffness, which would cancel the increase in torsion-to-bending ratio. This approach would therefore not lead to the desired aeroelastic improvement.
2. By increasing the skin thickness. This would indeed increase the torsion-to-bending stiffness, but would lead to a skin thickness larger than required by load considerations with an attendant weight penalty.

The following conclusion may be drawn from this study of an hypothetical wing, with shear flexibility included. To achieve an optimum design for the wing between wing root and engine pylon a flutter optimization calculation must be performed which must include the load and stress design criteria for various dimensions of the wing box.

5. SENSITIVITY TO AERODYNAMIC PARAMETERS

In Fig. 11 one can see the panelling of the different aircraft parts - for the doublet lattice calculation of the wing and the horizontal tail, and for the slender body elements of the fuselage. In this figure the relative dimension of the hollow cylinder used for the calculation of the pod airforces is also shown.

Fig. 12 shows the influence of unsteady pod airforces for the present flutter case. The pod airforces have three important effects which act partly against each other. One of them is an increasing damping for modes with engine movements, which is a positive influence. The second effect is a negative stiffness contribution, which leads to a decrease in the frequencies for modes containing angular engine movements with increasing dynamic pressure. In the demonstrated case the engine pitch frequency is reduced and the frequency crossing occurs at lower speed values. An additional negative effect arises from the increasing aerodynamic coupling terms, which increase the flutter intensity. Therefore, the flutter speed can be increased or decreased by the pod airforces depending on the configurations.

Fig. 13 shows the influence of the elastic tailplane with and without unsteady aerodynamics. The elasticity and the unsteady aerodynamics of the horizontal tail has practically no influence on the behaviour of this flutter case.

The amplitudes of the front fuselage for the engine pitch mode are of considerable magnitude because they balance the engine pitch amplitudes. The corresponding fuselage airforces increase the damping, but also the coupling. This is evident from Fig. 14.

Although the presented flutter case can be described by a two degree of freedom system, where one of them is the fundamental bending and the second the inner wing torsion (engine pitch) mode, the other modes also influence the flutter speed, in a negative way. The introduction of the outer wing torsion leads to an increase of the bending mode frequency with dynamic pressure, and thus decreases the flutter speed. The additional coupling leads to a stronger flutter case generally. See Fig. 15.

The preceding cases were calculated with subsonic unsteady airforces using doublet lattice theory. For the connection of the structural with the aerodynamic reference points an interpolation is necessary, and different interpolation procedures may lead to some differences in the frequency and damping behaviour. Fig. 16 shows a comparison between different airforce calculation methods, the doublet lattice method, and the kernel function method according to Laschka. The aerodynamic reference points differ considerably between the two methods and the interpolation was also made in a different manner. Due to the sensitivity of the presented flutter case small changes in numerical methods give here noticeable changes especially in the damping curves. This comparison is given because we want to show some transonic effects which we tried to include by applying various corrections to Laschka's method.

The methods for the calculation of unsteady airforces by transonic theories are at the moment generally not in such a state that they can be used for economic flutter calculations, especially in an early development stage. But one has to be able to assess the transonic effects already in the development stage, and take them into account in flutter calculations, especially for advanced wings with so-called supercritical profiles.

Fig. 17 shows the differences in the steady spanwise lift slope distribution, and the spanwise aerodynamic-centre location between theoretical and wind tunnel results for a modern wing. The Mach number is $M = 0.78$ and the measured values are for two incidences, corresponding to overall lift coefficients of ca. 0.3 and ca. 0.5, which is the design point. The measured lift curve slope is considerably larger, and the measured aerodynamic center lies upstream of the calculated one for the same case. The measured bulges near the pylon station are due to interference, whereas in these theoretical investigations the pylon effect was omitted.

Fig. 18 shows for the same configuration, but for a different model and different wind tunnel, the unsteady spanwise lift and moment derivatives for a pitching oscillation about the elastic axis with ca. 40 Hz. The scale of the model was 1:20. In the neighbourhood of the pylon station the measured pressure distribution and thus the C_L and C_m values may be incorrect, but the important outer wing values show that the measured lift and moment derivatives exceed the theoretical ones by a considerable amount. The magnitude is bigger and the phase lag smaller than predicted by subsonic theory.

If one defines an unsteady aerodynamic centre by division of the complex values of C_m and C_L , one can find that the forward shift from the one quarter line is up to 50 % larger in magnitude, whereas the measured phase lag is only 1/3 of the theoretical one for this investigated pitching mode. This justifies the possibility of using quasisteady corrections in the transonic domain. An example of the influence of a spanwise quasisteady correction on the presented flutter case is given in Fig. 19. Here one can find the frequency and damping behaviour versus speed

1. for pure theoretical subsonic airforces
2. for increased spanwise C_L without correction of a.c. and
3. for an additional forward shift of the aerodynamic centre

It is evident that both transonic effects lead to lower flutter speeds and the forward shift of the a.c. also increases the flutter intensity. This tendency - known as transonic dip - exists normally for advanced wings for a wide range of Mach numbers, and we have observed that the influence on full-scale aircraft may be more evident than on wind-tunnel models. As long as no essential change in the flow pattern occurs, this tendency increases with increasing incidence or lift coefficient.

Only when the flight Mach number exceeds a particular transonic value (which depends on the wing design) where the flow pattern changes qualitatively (above the maximum of C_L versus Mach number) the subsonic theory may give conservative values for the flutter behaviour of modern transport aircraft.

Flutter calculation made for an aircraft with unsteady aerodynamics estimated with the above mentioned method and matched to flight vibration test results show a decrease of the critical speed for the critical transonic M-number by approximately 9 % in comparison to flutter calculation results with doublet-lattice theory.

Conclusion:

The flutter behaviour for the reported flutter case for an aircraft with heavy concentrated masses elastically fitted to the wing is influenced by a series of structural parameters. Most of these parameters are fixed by the load and stress requirements. The engine forward position is a parameter which strongly influences the flutter behaviour but it also influences the drag on the aircraft. The box size of the inner wing can be adjusted within the scope of aerodynamic possibilities. The skin and spar thicknesses and the stringer areas are determined, dependent on the box size, by the load and stress design. But the box size and its lay-out can be obtained under the named constraints by a flutter optimization procedure. These above mentioned parameters must be influenced by the aeroelastician before design freezing in order to obtain a design optimally balanced with regard to aerodynamics, weight and aeroelasticity.

References:

- [1] Ein Beitrag zur Lösung der Flattergleichung unter Berücksichtigung von Servosteuerung und Flugregler
S. Vogel, ZFW 1. 1977, Heft 2

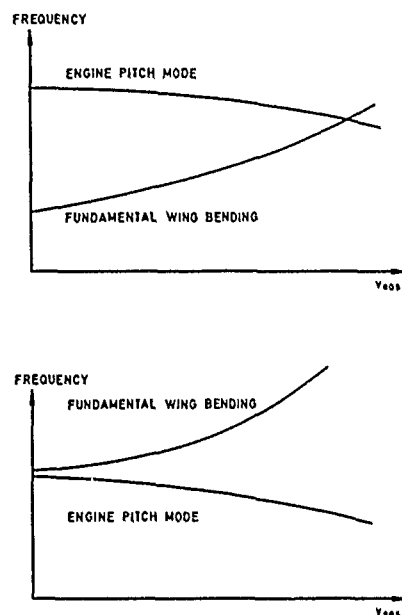


FIG. 1 TWO DIFFERENT WING BENDING AND ENGINE-PITCH FREQUENCY VARIATIONS WITH FLIGHT SPEED

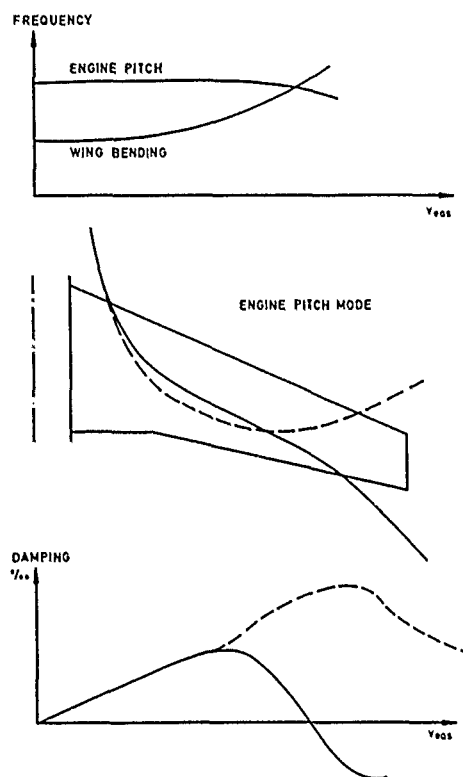


FIG. 2 FLUTTER BEHAVIOUR FOR DIFFERENT NODAL LINES OF THE ENGINE-PITCH MODE

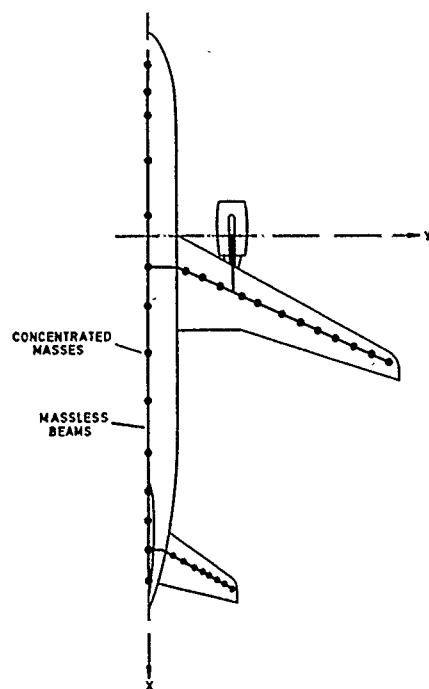


FIG. 3 DYNAMIC BEAM MODEL OF THE AIRCRAFT

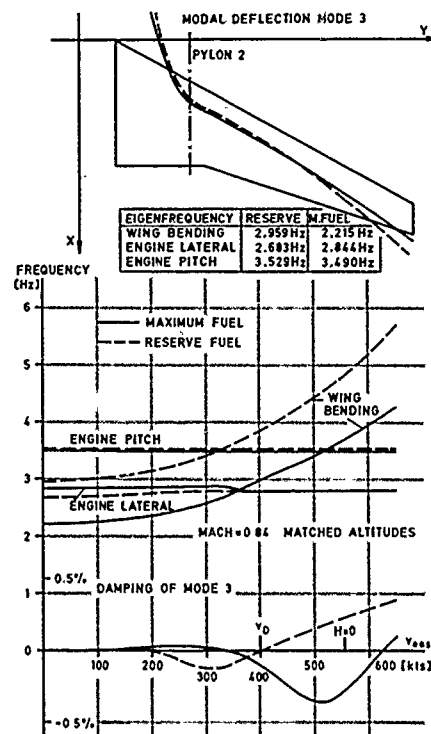


FIG. 4 EFFECT OF WING FUEL CONTENT

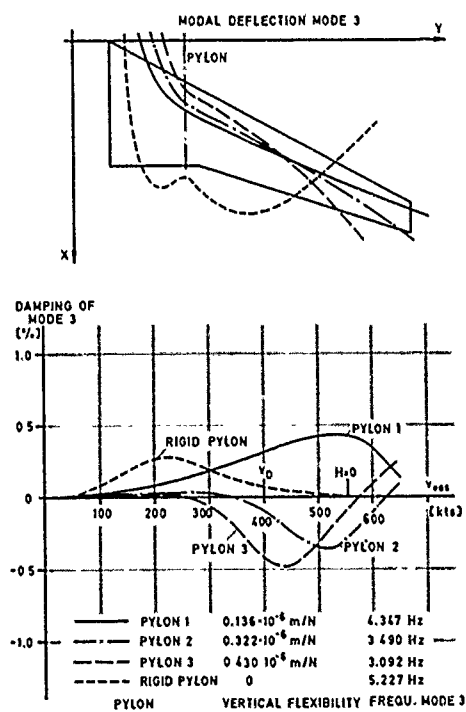


FIG. 5 EFFECT OF VERTICAL PYLON STIFFNESS

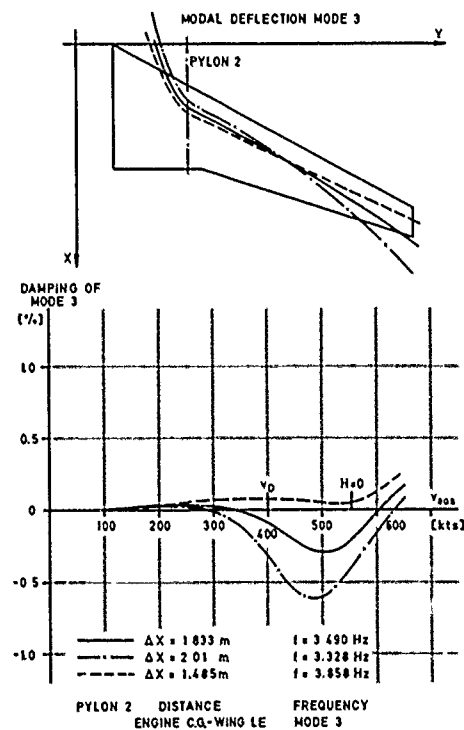


FIG. 6 EFFECT OF DISTANCE ENGINE C.G.-WING L.E.

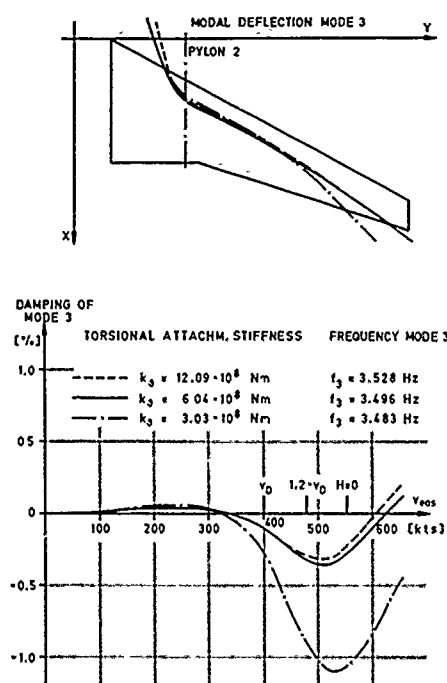


FIG. 7 EFFECT OF TORSIONAL STIFFNESS OF THE WING-FUSELAGE JUNCTION

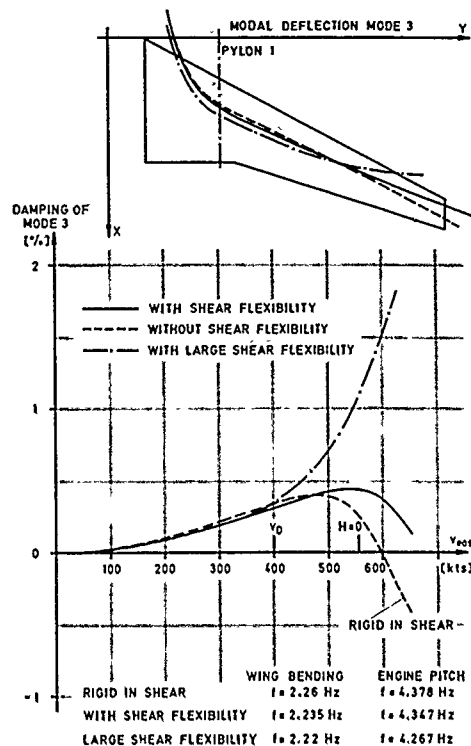


FIG. 8 EFFECT OF INNER WING SHEAR FLEXIBILITY

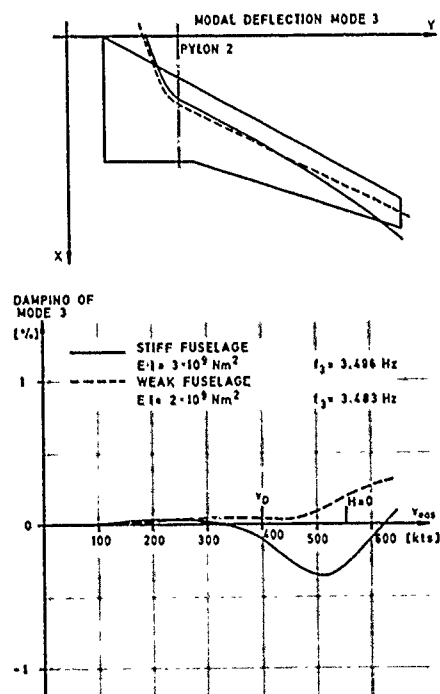


FIG. 9 EFFECT OF FUSELAGE BENDING STIFFNESS

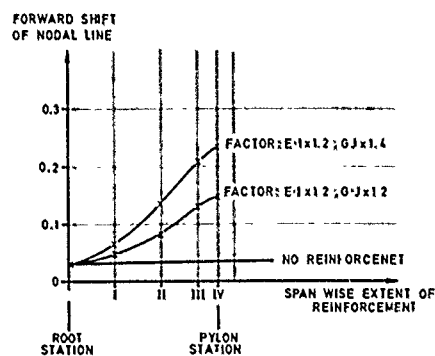


FIG. 10 SHIFT OF MODE 3 NODAL LINE DUE TO INNER WING REINFORCEMENT

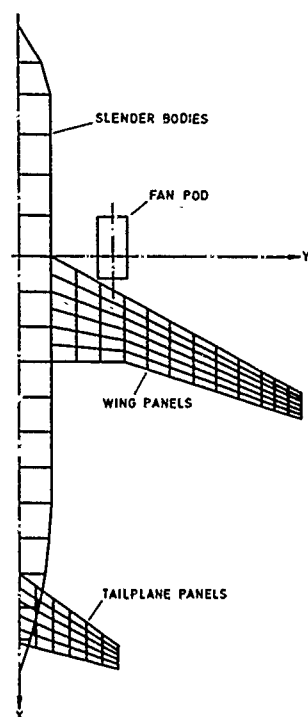


FIG. 11 AERODYNAMIC MODEL OF THE AIRCRAFT

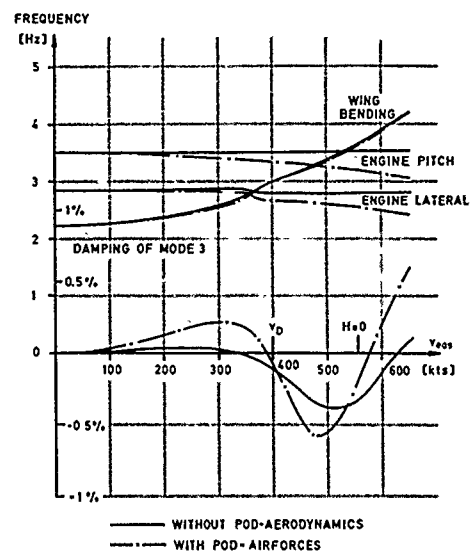


FIG. 12 EFFECT OF FAN POD AERODYNAMICS

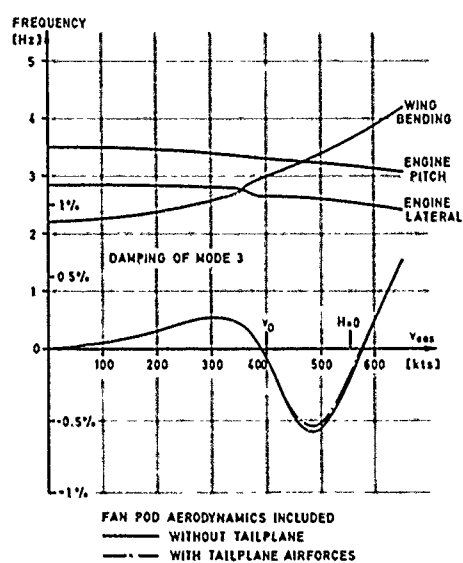


FIG. 13 EFFECT OF TAILPLANE AERODYNAMICS

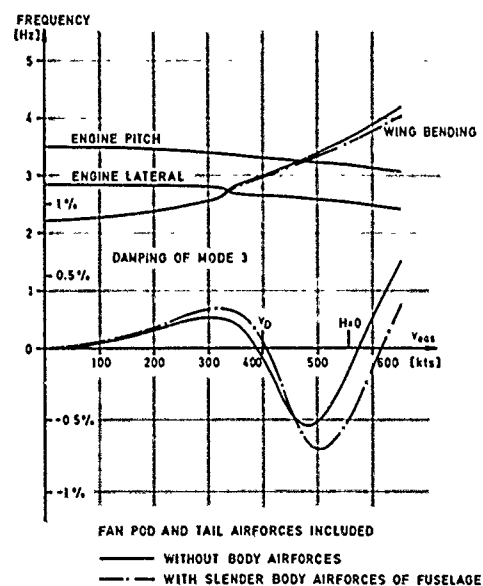


FIG. 14 EFFECT OF FUSELAGE AERODYNAMICS

6-10

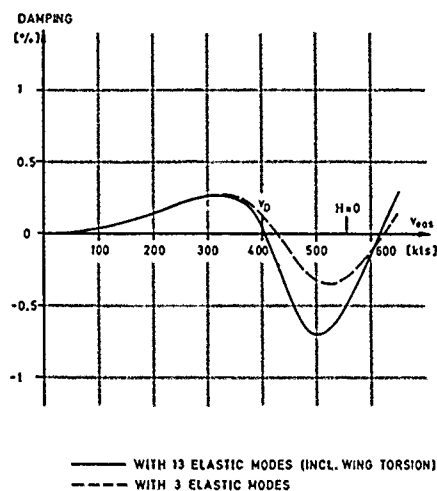


FIG. 15 EFFECT OF INCLUDED EIGENMODES ON THE DAMPING OF MODE 3

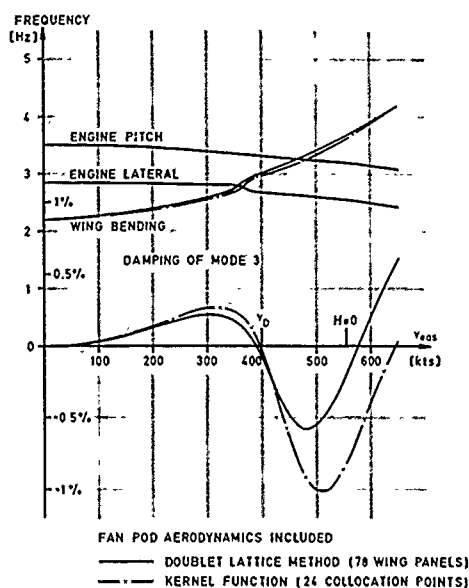


FIG. 16 COMPARISON OF DIFFERENT CALCULATION METHODS FOR UNSTEADY AIRLOADS

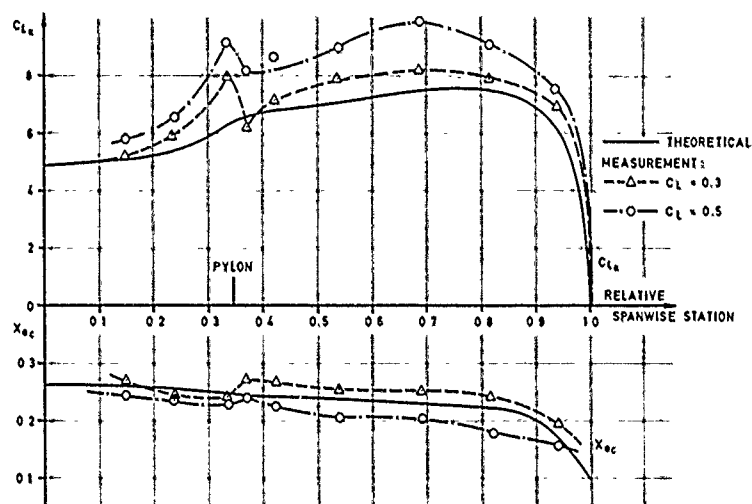
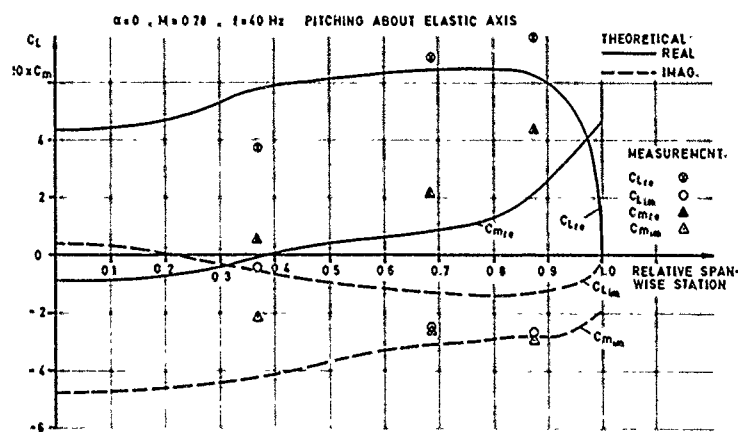
FIG. 17 STEADY SPANWISE LIFT SLOPE $C_{L\alpha}$ AND AERODYNAMIC CENTRE X_{ac} LOCATION $M=0.78$ 

FIG. 18 UNSTEADY SPANWISE LIFT AND MOMENT DISTRIBUTION

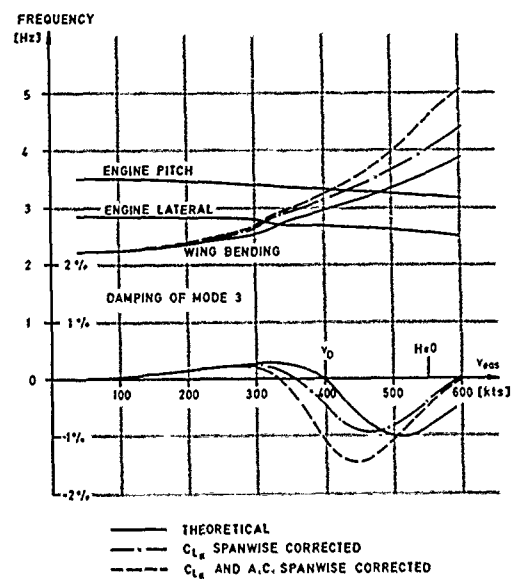


FIG. 19 EFFECT OF STEADY TRANSONIC CORRECTION

Aeroelastic Design Considerations for Turboprop Powerplant Installations

by

John J. Glaser

Chief of Aeroelastics
The De Havilland Aircraft of Canada, Limited
Downsview, Ontario, Canada

ABSTRACT

Presented is the experience gained by de Havilland Canada in designing turboprop powerplant suspension systems to minimize vibrations resulting from propeller unbalance. An overview is first given of turboprop suspension considerations including whirl flutter, vibration isolation and landing loads. This is followed by an outline of the design evolution of the DHC-7 suspension system proven successful in service. The design features of the DHC-8 system, currently under development, are also presented. The paper concludes by giving recommendations pertinent to preliminary design and development.

INTRODUCTION

It would appear that turboprops are here to stay. Consuming less fuel than turbojets (Figure 1) they are more economical to operate on short stage lengths. As the price of fuel increases, the stage length over which turboprops maintain their advantage increases as shown in Figure 2. This advantage is expected to broaden in the future as a result of NASA's STAT (Small Transport Aircraft Technology) program. For example, three advanced technology transport designs proposed by industry (Figure 3, Reference 1) are estimated to provide fuel savings of 26-to-40% and DOC savings of 16-to-24% for a 100 nautical mile trip. Prop-fan development is also being conducted as part of the STAT program. Although there are a number of technical problems, the prop-fan offers better installed propulsion efficiencies than current high bypass turbofans for Mach numbers up to .8.

An important trend that has developed over the last few years is the increased demand for passenger and crew comfort. Although noise and vibration on aircraft were once considered to be unavoidable, expectations have changed due to the standards set by the modern jets. Today's passengers demand equivalent comfort levels in propeller driven aircraft and expect it can be achieved with current technology.

This paper is concerned with one aspect of the comfort problem - the vibrations induced by propeller unbalance. Its objective is to show, by example, that the sensitivity to propeller unbalance can be minimized through good powerplant suspension design. While it is recognized in the case of a poor design that vibrations can be reduced by strict quality control and dynamic balance procedures, these procedures are costly and time consuming. Even then, the vibration sensitivity to wear and repair will be high and flight in icing conditions can be disturbing. All things considered, it can only be concluded that the powerplant suspension system must be designed to give good vibration isolation.

TURBOPROP INSTALLATIONS AT DE HAVILLAND CANADA

To date de Havilland Canada has designed 4 transport category turboprop installations (Table 1 and Figure 4). The first installation employed a Caribou aircraft as a test bed for GE's YT64 engine. At the time, the concern for whirl flutter was very high because the Caribou program was undertaken shortly after the Electra accidents. This program was necessarily supported by a whirl flutter model (Figure 5) to assist in the development of our analytical methods and to provide an independent check on the flutter boundary.

The Caribou program ultimately led to the Buffalo. Although propeller induced vibrations were of concern, those concerns were still overshadowed by our preoccupation with whirl flutter. As a result, the Buffalo's sensitivity to propeller unbalance turned out to be a little higher than desired and a few vibration desensitization modifications were introduced. For example, lower spring rate isolators were used to support the pilot's instrument panel and aileron mass balance was redistributed to attenuate aileron control wheel vibrations.

To prevent history from repeating itself, the Aeroelastics at de Havilland were asked to participate in the preliminary design of the DHC-7 suspension system. This particularly significant decision was made because the DHC-7 was aimed at the burgeoning commuter market where higher standards of comfort would be required. Now that more than 300,000 flight hours have been accumulated in service it can be claimed with confidence that the DHC-7 turboprop aircraft provides a new standard in passenger and crew comfort. This has been achieved in no small part by the aircraft's rather unique powerplant suspension design.

The DHC-8 aircraft is currently under development. Although the experience gained from the DHC-7 has provided a good basis, a number of factors have made the DHC-8 design more challenging.

7-2 OVERVIEW OF TURBOPROP SUSPENSION CONSIDERATIONS

(a) Static Loads

The primary purpose of the suspension system is to support the weight of the powerplant and to react the thrust and torque loads. If isolators are used, the associated loads must be carried without bottoming, otherwise their intended purpose will have been defeated. In one case, that of a small twin turboprop aircraft, maximum isolator deflections for normal flight conditions were specified so that dynamic excursions would not cause fouling between engine and cowl. The deflection limits specified were

- Max translation under $lg = .25$ cm (.1 inch)
- Max pitch under thrust and $lg = +1$ degree
- Max roll under torque = 1 degree

Although not a problem in this particular case, the specification of displacement criteria imposes lower limits on suspension frequencies which may conflict with the desire to achieve good vibration isolation.

(b) Propeller Whirl Flutter and Divergence

The simplified equations given in Figure 6 can be used to shed light on the mechanisms of propeller whirl flutter and divergence. These equations correspond to Pines' equations for a two-dimensional wing section with freedoms in pitch and plunge (Reference 2). If the inertia and stiffness terms are considered alone, two natural modes of vibration are obtained, one in pitch and one in yaw. The gyroscopic terms couple the pitch and yaw freedoms to produce forward and backward whirl modes; these are precession motions with directions measured relative to propeller rotation. The frequencies of these modes vary with propeller rotational speed as illustrated in the insert in Figure 6. Damping causes these precession motions to decay in a spiral.

The propeller also generates aerodynamic forces associated with arbitrary motions. If the propeller axis is displaced in pitch, a down-going blade will see a larger angle of attack than an up-going blade. This results in a net upward or outward acting force and a yawing moment which acts in the backward whirl direction. Similar forces are produced at any angular position of the propeller shaft. The outward acting forces work against the restoring springs and if the flight speed is sufficiently large these forces will cause divergence in the lower stiffness direction. The moments assist motion in the backward whirl mode and at a sufficiently large flight speed the whirling motion will grow in magnitude - the condition called whirl flutter.

The equations given in Figure 6 are too simple for realistic flutter speed estimates and must be extended to include all nacelle and wing modes and a more complete aerodynamic theory. At de Havilland, the quasi-steady aerodynamics of Houbolt and Reed (Reference 3) are used, but modified to include Ribner's spinner factor (Reference 4) and the aerodynamic lag terms of Reed and Bland (Reference 5). We find this formulation provides conservative results as illustrated by the comparison with Caribou model data (Figure 7).

Some factors influencing whirl flutter are summarized in Figure 8. The influence of stiffness is best expressed by the diagram showing typical boundaries for divergence and whirl flutter. This diagram expresses in a different way what is already known from wing flutter; namely, that the flutter speed tends to decrease as the frequency ratio approaches unity. Expressed differently, the whirl flutter speed for a system with unequal spring rates, can be increased by increasing the higher spring rate and/or by reducing the lower spring rate. The influence of pivot point location on whirl flutter is shown in the second diagram in Figure 8. A rearward shift in pivot point (keeping frequencies constant) is indicated to have a stabilizing effect depending on the level of structural damping. Here, increased stability is attributed to the increase in aerodynamic damping associated with the translational velocity of the propeller plane. A decrease in propeller inertia, or propeller RPM, is also stabilizing because each reduces the magnitude of gyroscopic coupling between the pitch and yaw degrees of freedom. Wing flexibility influences nacelle frequencies and rotation point locations and also introduces wing damping; the combined effect on whirl flutter can only be determined by analysis.

(c) Vibration Isolation

In addressing the question of vibration isolation, consideration must be given to its three components; the excitation, the system transmissibility and the criteria for evaluating responses.

(i) Excitation

Excitation at the propeller rotation speed is referred to as 1P excitation and results from propeller unbalance. Upon investigation it is found that propeller unbalance can be subdivided into four categories; inertia force, inertia moment, aerodynamic force and aerodynamic moment. Some of the contributing factors to each type of unbalance are indicated in Table 2. It should be emphasized that static unbalance constitutes only one type of unbalance and therefore static balance alone may not be sufficient to correct a rough propeller. A second aspect which should be noted is that inertia and aerodynamic unbalance forces may vary relative to each other throughout the propeller operating range. This is because inertia forces vary with RPM squared while aerodynamic forces vary with propeller thrust. Finally, the various types of unbalance are not completely independent. For example, differing blade thrust loadings will result in unequal out-of-plane deflections and contribute to inertia moment unbalance.

Figure 9 from Reference 6 gives quantitative data for the various types of unbalance plotted against takeoff power. Total and expected values are also plotted. Although this data is based on

pre-1945 propellers, it is still used today in the absence of better information.

The relative importance of force and moment unbalance for a particular installation depends on the powerplant's frequency response characteristics. Figure 10 considers a hypothetical installation in which the node of the thrust axis travels from a point behind the propeller at low RPM to a point approaching infinity at high RPM. The associated table indicates that force unbalance will have no effect if the node is located at the propeller and that moment unbalance will have no effect if the node is located at infinity. The table also indicates that neither force nor moment unbalance can be corrected if the node is located at the balance plane. This problem can be overcome in practice by making two separate balance planes available.

In summary, the foregoing considerations reinforce the need for good vibration isolation because it is generally impossible to have a perfectly balanced propeller for all operating conditions.

(ii) Vibration Transmissibility

The concepts of vibration transmissibility are most clearly expressed in the results of a single degree-of-freedom system subjected to sinusoidal force excitation (Figure 11). The ratio of transmitted force magnitude F_t to excitation force F_0 is of interest and is termed the transmissibility. The transmissibility curves of Figure 11 are different from those usually given because they have been plotted with respect to the frequency ratio f_n/f_{ex} in order to give prominence to the natural frequency f_n . The message conveyed, however is the same. Vibration isolation is achieved when the natural frequency is less than .707 times the excitation frequency and increases with decreasing natural frequency. The maximum isolation that can be achieved is limited by other constraints such as the maximum displacement under static load.

If for some reason it is impractical to take advantage of the isolation range, the low amplification range should be used, in which case, the natural frequency must be greater than 1.5 times the excitation frequency. If the natural frequency has a value close to the excitation frequency, Figure 11 clearly shows that a large degree of damping is required to limit response force amplitudes.

Figure 12 considers a dynamic model more representative of powerplant installations, that of a 2 degree of freedom system with freedoms in pitch and plunge. Although vertical plane coordinates have been chosen, the results are quite general. As Figure 12 indicates the system's frequencies depend on the so-called cg overhang \bar{x} , which separates the frequencies as \bar{x} gets larger and on the values of the uncoupled frequencies when \bar{x} equals zero. Applying what has been learned from the single degree of freedom case, the following design options, in order of preference, can be identified.

- Place both system frequencies in the isolation frequency range. This is best achieved by having a small cg overhang and nearly equal uncoupled frequencies.
- Place one system frequency in the isolation frequency range and the second frequency in the low amplification range. This is best achieved with well separated uncoupled frequencies and with a large cg overhang.
- Place both system frequencies in the low amplification range. This is best achieved by having a small overhang and nearly equal uncoupled frequencies.

(iii) Vibration Response Criteria

To evaluate a specific suspension design, vibration responses due to propeller unbalance should be calculated and compared with accepted standards. This generally requires a complete dynamic model of the aircraft with consideration given to the complete ranges of aircraft speed, altitude, fuel and cargo. Powerplant and accessory responses can then be evaluated by comparison with manufacturer's specifications or MIL Standards, while passenger and crew comfort assessments can be made using ISO 2631 standards. If any of the comparisons are unsatisfactory, the suspension design should be re-examined to determine if improvements are possible.

(d) Landing Loads

During landing impact each main gear experiences a vertical ground reaction and a wheel spin up force. Typical force-time histories for the DHC-7 aircraft are given in Figure 13. These forces cause powerplant accelerations which can be quite large for wing mounted nacelle and landing gear configurations. For these configurations, a reasonable estimate for the maximum normal acceleration at the powerplant cg can be obtained with the aid of Figure 14 which plots measured and calculated accelerations against an acceleration factor. The measured and calculated accelerations are generally larger because the factor does not consider dynamic effects nor the contribution from the vertical reaction force. Figure 15 shows that the maximum normal acceleration is mildly dependent on the elastic centre location and is at a maximum when the elastic centre lies on the cg. In all probability, the maximum pitch acceleration can be estimated using a formula similar to that for normal acceleration. As can be seen, it has a greater dependency on elastic centre location and is at a minimum when the elastic centre is located a short distance behind the cg. Large pitch accelerations should be avoided because they imply large normal accelerations at the extremities of the powerplant and large engine bending moments.

(e) Summary of Powerplant Suspension Requirements

In summary, the powerplant suspension system must perform the following tasks:

- Carry the powerplant's weight, thrust and torque; a requirement imposing lower limits on stiffness to prevent excessive displacements under static load.

- Provide adequate whirl flutter margins taking into account structural failures and isolator disconnects. This too imposes lower limits on stiffness.
- Provide good vibration isolation. This imposes upper limits on stiffness and generally conflicts with static displacement and flutter requirements.
- Minimize powerplant responses (which can be particularly large for wing mounted nacelle and landing gear configurations). This introduces a requirement on the elastic centre location for large powerplant motions.

DESIGN EVOLUTION OF THE DHC-7 POWERPLANT SUSPENSION SYSTEM

This section outlines the design evolution of the DHC-7 powerplant suspension system. Although presented in an orderly fashion, the actual design process was anything but orderly and at times, the prospects of achieving the intended goals appeared bleak. Through perseverance a satisfactory design was ultimately identified and developed.

(a) Single-Plane Suspension

(i) Rigid Wing Studies

Initial studies were conducted using six identical isolators uniformly distributed on a ring positioned at the mount plane location provided by the manufacturer. The stiffnesses of these isolators act in combination with the nacelle structure which was represented by an estimated 6 x 6 flexibility matrix. Isolator stiffness directions were defined relative to the thrust axis and were labelled axial, radial and tangential (Figure 16). The axial stiffness was adjusted to give pitch and yaw frequencies required for whirl flutter stability, while the tangential spring rate was chosen to limit the roll deflection under torque to 1°. Since radial and tangential isolator spring rates were assumed equal, all system frequencies were determined by the flutter and torque deflection requirements.

The first set of results obtained were decidedly unacceptable because two modes, heave and sway, had frequencies within the propeller 1P range. To obtain some perspective on the problem, the analysis was extended to determine the influence of shifts in mount plane location, whether achievable or not, relative to the original position 44.5 cm (17.5 inches) behind the powerplant cg. The structural stiffness was assumed invariant in this study and the isolator axial stiffnesses were adjusted to obtain a flutter speed of 1.2 V_g. Figure 16 summarized these results and indicated the following possible solutions.

- Increase the isolator and/or structural stiffnesses so that the suspension frequencies straddle the 1P range.
- Relax the requirement on isolator tangential stiffness in order to lower the translation frequencies below the 1P range. In this case torque deflections would become excessive but could be restrained by a torque tube or swaybar type device.

A third option, that of shifting the elastic centre to the powerplant cg by focusing (i.e. tilting) the isolators was attempted, but without success, as a means to get all four frequencies below the 1P range. Although a large enough shift could be obtained from the isolators alone, the maximum shift obtained from combined isolators and structure was inadequate being only approximately 18 cm (7 inches).

(ii) Flexible Aircraft Studies

Flexible aircraft analyses were conducted to evaluate the two possible solutions identified in the rigid wing study. The first approach, that of straddling the 1P range was easily achieved for the lateral modes, however wing flexibility in the vertical plane would have imposed demanding stiffness increases on both the isolators and the nacelle structure. This design option was not considered further. The second approach, that of reducing the translation frequencies appeared more promising even though the lowering of the nacelle heave mode forced a wing torsion mode into the 1P range. However, further investigation was ultimately discontinued in the light of very high landing load predictions.

A relatively simple comparative study was undertaken to establish landing load trends. In this study the time history response for a representative dynamic model was calculated and applied to three different suspension configurations:

- | | |
|-------------------|--|
| Configuration I | A single-plane suspension located 44.5 cm (17.5 inches) behind the powerplant cg - the initial configuration. |
| Configuration II | A single-plane suspension located at the gearbox approximately 25.4 cm (10 inches) ahead of the powerplant cg. |
| Configuration III | A two-plane suspension with isolators located at the gearbox and a steadier isolator located 94 cm (37 inches) behind the powerplant cg. |

The bending moment envelopes obtained for these three configurations are plotted in Figure 17. The highest bending moments were obtained for Configuration I and are simply the consequence of the large cg overhang. The bending moments for Configuration II, although lower, were still demanding over the exhaust case. The lowest bending moments were obtained for Configuration III which stimulated investigation of the two plane mount arrangement.

(b) Two-Plane Suspension

(i) Rigid Wing Results

An attractive advantage of the two-plane suspension scheme is the ability to position vertical and lateral elastic centres virtually anywhere between the two mount planes by the choice of translation spring rates. The first two-plane configuration examined was Configuration III with both elastic centres positioned at the cg. However, the results for this case, summarized in Table 3, were not felt to be optimum because the pitch and yaw frequencies fell within the amplification range. Further work led to the so-called bed mount arrangement which eliminated the ring of mounts in the front plane.

The analysis model for the bed mount concept simply assumed vertical and lateral springs connected to the thrust axis at stations 43 cm (17 inches) ahead of and 104.1 cm (41 inches) behind the powerplant cg (Table 3). The plan was to determine the spring rates needed to satisfy flutter, vibration and landing load requirements; the locations of isolators, means of carrying thrust and torque, and the division between structure and isolator stiffnesses were questions to be resolved afterwards.

A final design configuration was ultimately identified and called Configuration IV; its design properties are compared with those of Configuration III in Table 3. In the new design the pitch and plunge frequencies are approximately equal and their value, 7 Hz, is as low as static deflections will allow. The loss in flutter speed accompanying the reduction in pitch frequency from 12 to 7 Hz between Configurations III and IV was amply regained by the combination of a 9.7 Hz yaw frequency and the 66 cm (26 inch) rearward shift in lateral elastic centre.

(ii) Flexible Aircraft Results

Fuselage vibration responses due to propeller unbalance were greatly improved by the bed mount arrangement. In fact, vibration isolation was considered to have been minimized on the basis that the pitch, plunge and lower yaw frequencies of Configuration IV could not be lowered further because of static displacement and whirl flutter requirements.

The bed mount arrangement also brought further reductions in engine bending moments. As indicated in Table 3, the bending moment at the critical station on the engine was reduced approximately 50% from the Configuration III value.

(c) Design Implementation

Configuration IV became the design target (Table 3). It is characterized by having low stiffness in the vertical plane with the elastic centre near the cg and high stiffness laterally particularly at the rear. The requirement for high lateral stiffness at the back of the engine suggested that thrust and torque be carried there also.

The division between structure and isolator stiffnesses was initially based on the assumption that the isolators should be lower in stiffness than the structure. This approach resulted in challenging structural stiffness targets and when it was realized that a significant weight penalty would result, the idea of designing the nacelle for stiffness was abandoned. The approach ultimately taken was to design the structure to meet strength requirements and to make up for any discrepancies in stiffness by modifications to the isolators and, if necessary, to the structure. In the end, modifications to the structure were not needed. Nevertheless, the emphasis placed on stiffness is believed to have had a beneficial influence on design.

The final isolator arrangement is shown in Figure 18. It consists of 4 elastomeric isolators, 3 at the back of the engine and one, a ring mount, at the front. Isolator spring rates were chosen to permit interchangeability between inboard and outboard nacelles. The ring mount is relatively soft vertically but has high stiffness laterally. In the fore-aft sense it is free to accommodate differential temperature expansion because of its hinged attachment. The two lower isolators at the rear have a low vertical stiffness, while fore-aft and lateral stiffnesses are very high for carrying thrust and torque loads. Torque is carried in conjunction with the rear upper isolator which also has a high lateral stiffness. The upper isolator was designed to provide little restraint in the fore-aft sense in order to prohibit contributions to engine bending moments during landings. Also, no vertical restraint is provided by the upper mount because the supporting V-frame is hinged at the firewall.

To minimize engine pitch accelerations during landing, the rear isolators which are supported by fairly substantial structure, were provided with two stages of vertical stiffness; low for normal flight and high for the larger excursions experienced during landing. The displacement range of the first stage and the stiffness of the second stage were chosen so that the effective elastic centre for large engine motions would lie just behind the powerplant cg.

(d) Installation Development

Table 4 presents data on how well design targets were met. The ratio of measured to estimated structural stiffnesses given in the first two columns show that vertical plane values have exceeded target by as much as 24%. Since these structural springs act in series with relatively low stiffness isolators, the maximum combined increase does not exceed 4%. These results were considered quite acceptable. The same cannot be said for the lateral stiffnesses where, because of poorly estimated shear contributions, the deficiencies range from 20 to 40%. It was imperative to compensate for the shortfall in front lateral stiffness for flutter stability purposes. This was accomplished by a very large increase in isolator stiffness as indicated in the third column of Table 4.

The isolator stiffness ratios given in the third column of Table 4 reflect the values used in establishing conservative flutter stability boundaries. These ratios are based on the lowest values

measured in the flutter frequency range, and generally apply for conditions of high ambient temperature, high static load and high vibration amplitude. These values were reduced a further 10% to allow for manufacturing variation. For vibration isolation purposes, it was considered appropriate to use the largest dynamic stiffness values measured at 1P frequencies. These ratios are given in the fourth column of Table 4. A comparison of values between columns three and four indicates the broad range in dynamic stiffnesses possible for elastomeric isolators. In this circumstance, since flutter stability cannot be compromised, vibration isolation must suffer. Isolator static stiffness ratios are given in the fifth column of Table 4. In all cases, target values are exceeded. This is not an unacceptable situation because it implies less displacement under static load.

Inertia comparisons are also given in Table 4 and are generally higher than those used in the design. Relative to the actual cg location, the vertical plane elastic centre is well positioned being only 5 to 7 cm (2 to 3 inches) ahead of the cg for either nacelle.

The frequency comparisons given in Table 4 for flutter computations generally reflect the higher inertias and the lower stiffnesses that were achieved. No specific targets were set for the roll and fore-aft modes because they do not affect whirl flutter and are not responsive to propeller unbalance forces being essentially pure modes. Although the indicated reductions in the pitch and yaw frequencies result in lower flutter speeds, satisfactory flutter margins were maintained. In the case of a rigid wing the outboard nacelle has the lower whirl flutter speed because of its lower structural stiffness. However, wing flexibility increases its stability and decreases the stability of the inboard nacelle leaving the inboard nacelle with the lower flutter speed.

Fuselage vertical vibrations based on the highest measured isolator stiffnesses are presented in Figures 19 and 20. The magnitudes of propeller unbalance used, derive from Figure 9 and were treated as pure inertia unbalance; that is, the total forces and moments were varied with RPM squared. The results apply for the DHC-7 at relatively high weight with wing tanks full, flying at 235 kt eas. Vibration responses are compared with ISO 2361-1978 reduced comfort boundaries. These comparisons are to some degree qualified because arbitrary values have been selected for propeller unbalance and airframe structural damping (taken to be .02 for all modes).

Figure 19 presents vertical vibration responses at the aircraft cg as a function of propeller RPM. Results are given for a single inboard and a single outboard propeller as well as for all four propellers phased to give the maximum total response. Lateral unbalance forces were determined to be just as important as vertical, making it impossible for all maximums to occur simultaneously. This aspect was considered in calculating the total response shown in Figure 19. Lateral vibration responses, although equal in magnitude to vertical, have not been presented because they are much less annoying on the basis of the ISO standard.

Within the 1P range maximum fuselage response values are associated with the wing third bending mode at 17.5 Hz. This applies for all fuselage stations except for the cockpit which is a maximum at 16.5 Hz. Figure 20 gives the distribution of fuselage responses and shows that the inboard nacelles contribute approximately 60% to the total. Maximum response amplitudes are indicated to occur in the rear half of the cabin and in the cockpit, where they achieve levels corresponding to the 6 hour ISO reduced comfort boundary. Although comparison with the ISO standard has been qualified, this result is nevertheless reassuring when it is recognized that current DHC-7 average and maximum block times in scheduled service are approximately 40 and 80 minutes respectively.

The response peak just below the 1P range in Figure 19(a) is associated with the fuselage bending mode. When the cabin is empty the frequency of this mode is 14.5 Hz and this causes higher vibration responses in the lower RPM range. Considering the influence of fuel and cargo, it is highly unlikely that an excitation frequency range as large as that for the DHC-7 would be completely free of modes; in fact between 13 and 22 Hz the DHC-7 has 9, two influencing comfort significantly. Since the aero-elastician has little control over airframe frequencies or the propeller RPM range, his only recourse as indicated earlier is to minimize vibration transmissibility by having low powerplant suspension frequencies.

In summary, the suspension design target for the DHC-7 was reasonably well achieved and calculations based on measured properties confirm acceptable flutter boundaries and dynamic landing loads. The sensitivity to propeller unbalance has not been determined quantitatively but the many qualitative assessments now available confirm that excellent vibration isolation has been achieved.

DHC-8 POWERPLANT SUSPENSION

The design objectives for the DHC-8 are the same as for the DHC-7. The extent to which these objectives have been achieved cannot be given in full because the DHC-8 suspension system is still under development. At the time of writing, measured structural and isolator stiffnesses are not yet available and first flight is still a few months away. Nevertheless, the suspension design concept can be given, the major differences with the DHC-7 can be identified and some problems experienced to date can be described.

(a) Powerplant Characteristics

Figure 21 shows DHC-8 and DHC-7 (inboard) nacelle profiles and presents some comparative data. Compared to the DHC-7, the DHC-8 has a heavier powerplant and its propeller has a larger diameter and a higher polar moment of inertia. The propeller speed range is essentially the same for both aircraft and corresponds to the frequency range of 15 to 20 Hz. Unlike the integral design of the PT6-50 engine, the PW-120 has a separate gearbox and engine. These two components are connected by a relatively flexible intake duct also called the interconnect structure.

(b) Design Concept

Based on DHC-7 experience, a two-plane mount arrangement was adopted from the start. Although the engine manufacturer had provided mount pads on both the gearbox and engine, the engine mount pads could not be used because there was no suitable structure nearby to provide support; instead, the rear flange of the turbine casing was used.

Initially an attempt was made to satisfy the flutter requirements by placing the yaw frequency above the pitch frequency as for the DHC-7. Unlike the DHC-7, the required lateral stiffnesses could not be achieved in the structure without a significant weight penalty; consequently, this approach was abandoned in favour of one with a pitch frequency higher than yaw. The design point chosen for the DHC-8 is plotted in Figure 22 in relation to the various constraint boundaries. Also shown is the achieved point for the DHC-7 inboard nacelle. The DHC-8's design has the advantage that it can accommodate a shortfall in front lateral stiffness, found to be large in the case of the DHC-7, because a reduction in yaw frequency will increase the flutter stability margin.

The disadvantage of the DHC-8 design point is that vibration isolation, although positive, is not expected to be as good as for the DHC-7. This is indicated in the results of Figure 23 for a flight condition corresponding to the DHC-7 case of Figure 19; i.e. maximum weight, maximum wing fuel and typical cruise flight. Propeller unbalance levels were obtained from Figure 9 and are approximately two times larger than the DHC-7's. The maximum response occurs in the wing second torsion mode at a frequency of 15.8 Hz with the maximum amplitude achieved corresponding to the ISO, 8 hour reduced comfort boundary. Although the comfort level is the same as for the DHC-7, the maximum response occurs at a lower frequency where the ISO standard has a higher value and where propeller forces are lower, being proportional to RPM squared. The combined effect implies a response amplitude 40% higher than that of the DHC-7.

The separate, flexibly connected gearbox of the PW 120 engine dictated that thrust and torque be carried by the front mounts. This in turn meant that a torque tube or swaybar device would be required so that low translation stiffness isolators could be used. It was initially assumed that two isolators would be adequate in each mount plane. After preliminary studies however, the requirement for a third front isolator was identified to meet isolator disconnect flutter requirements.

The final engine mount arrangement is shown in Figure 24. The three front plane isolators and torque tube are attached to a horse collar supported by a combination of semi-monocoque structure and trusses. The isolators in the rear mount plane are positioned on the cool side of the firewall and support the engine through 4 short links.

(c) Design Complications

Although the DHC-8 powerplant has a two-plane arrangement like the DHC-7 there are some very significant differences which make the DHC-8 suspension design more complex (Figure 25). For example, the DHC-7 powerplant can be treated as a rigid body because its integral engine-gearbox design provides a bending frequency of 76 Hz. In contrast, the vertical bending frequency for the DHC-8 powerplant is only 30 Hz due to interconnect structure flexibility. This flexibility results in a forward shift in elastic centre with an attendant loss in whirl flutter speed; suspension frequencies must therefore be higher in the DHC-8 to achieve adequate flutter margins.

A second significant difference is that the DHC-8's mode shapes are more highly coupled due to the torque tube, engine flexibility and the skewed principal axis of inertia of the powerplant. As a result, all suspension modes must be kept out of the LP range with appropriate margins. For the DHC-8, this has been accomplished for all modes except the 21.9 Hz fore-aft mode (Table 5) which is responsive to propeller moment unbalance due to heavy coupling with the engine vertical bending mode (Figure 26). The frequency of this mode rises to about 24 Hz when wing flexibility is included and response amplitudes reduce accordingly at maximum RPM. Nevertheless, the powerplant fore-aft mode will receive a watchful eye as the program develops.

A third difference from the DHC-7 is that the DHC-8 suspension is redundant for damage tolerance reasons explained previously. That is, pitching moments are carried by the isolators in the front mount plane as well as by the isolators across the two planes. This leads to higher engine loads during landing.

CONCLUDING REMARKS

Much can be done to reduce the sensitivity to propeller unbalance in the design of a turboprop powerplant suspension system as has been demonstrated in the case of the DHC-7. The basic design concept must be established in the preliminary design stage with continual monitoring and readjustment, as required, during development to ensure that overall objectives are achieved. The following comments and recommendations are based on the experience of four de Havilland Canada transport category turboprop designs.

- Aeroelasticians should participate in the design of the powerplant suspension system from its inception.
- The objectives of a powerplant suspension system are best achieved by a two-plane mount arrangement.
- The engine design should permit some flexibility in the choice of mount plane locations.
- Excessive engine flexibility can increase the difficulty in achieving the suspension design requirements. Weight saving in the engine may become a weight penalty in the nacelle structure.

- There is a need to achieve higher stiffness-to-weight ratio nacelle structures.
- The designer should expect inaccuracies in estimated data. Contingency plans should be in place for critical parameters if design targets are not achieved.
- The degree to which design objectives have been achieved should be established by test. The information obtained will be of benefit to future designs.


ACKNOWLEDGEMENTS

The author would like to thank de Havilland Canada for the opportunity to present the material in this paper. Appreciation is also extended to the Department of National Defence and to the National Research Council, Ottawa, Canada for partial funding and support.

REFERENCES

1. Williams, Louis J.
Galloway, Thomas "Design for Supercommuters"
Astronautics and Aeronautics, pages 20-30
February 1981
2. Pines, S. "An Elementary Explanation of the Flutter Mechanism" Proc.
National Specialists Meeting on Dynamics and Aeroelasticity,
Institute of the Aeronautical Sciences, Forth Worth, Texas
November 1958
3. Houbolt, John C.
Reed, Wilmer H. III "Propeller-Nacelle Whirl Flutter"
Journal of Aerospace Sciences
March 1962
4. Ribner, H.S. "Propeller in Yaw"
NACA Rep 820, 1945
5. Reed, W.H. III "An Analytical Treatment of Aircraft Propeller
Bland, S.R. Precession Instability"
NASA TN D-659, January 1961
6. Best, Stanley G. "Propeller Balancing Problems"
SAE Journal (Transactions), Vol. 53, No. 11
November 1945

DHC TURBOPROP AIRCRAFT - TRANSPORT CATEGORY



AIRCRAFT	FIRST FLIGHT	ENGINE	TAKEOFF POWER kW	PROPELLER FLIGHT RPM RANGE	V _D KT EAS SEA LEVEL
DHC 4 CARIBOU T64 TEST BED	22 SEPT 1961	YT64 GE-4	2 X 2089	850 - 1160	243
DHC-5 BUFFALO	9 APRIL 1964	GE T-64	2 X 2337	850 - 1160	291
DHC-7 DASH 7	27 MAR 1975	PWC PT-6A 50	4 X 836	900 - 1200	294
DHC 8 DASH 8	JUNE 1983 *	PWC PW 120	2 X 1343	900 - 1200	310

* SCHEDULED DATE

TABLE 1



CLASSIFICATION OF PROPELLER UNBALANCE

UNBALANCE TYPE	TYPICAL UNITS	SOME CONTRIBUTING FACTORS
INERTIA FORCE	gram cm	<ul style="list-style-type: none"> ● PROPELLER NOT IN STATIC BALANCE ● PROPELLER AXIS NOT CONCENTRIC WITH SHAFT
INERTIA MOMENT	gram cm ²	<ul style="list-style-type: none"> ● UNEQUAL BLADE CHORDWISE MASS DISTRIBUTIONS ● OUT-OF-PLANE BLADES ● PROPELLER AXIS SKEWED TO SHAFT AXIS
AERODYNAMIC FORCE	gram cm	<ul style="list-style-type: none"> ● UNEQUAL BLADE LOADING IN TORQUE
AERODYNAMIC MOMENT	gram cm ²	<ul style="list-style-type: none"> ● UNEQUAL BLADE LOADING IN THRUST

$$\text{UNBALANCE FORCE OR MOMENT} = \frac{\text{kg m or kg m}^2}{g} \times \left(\frac{2\pi \times \text{PROP RPM}}{60} \right)^2 \text{ N or Nm}$$

TABLE 2

COMPARISON OF CONFIGURATION III & IV DESIGNS

	CONFIGURATION	
	III	IV DESIGN TARGET
FREQUENCY Hz.		
PITCH	12	7
YAW	12	9.7
PLUNGE	7	7
SWAY	7	40
ELASTIC CENTRE AFT OF CG		
VERTICAL PLANE	0	0
LATERAL PLANE	0	44 cm (26")
FLUTTER SPEED	1.2 V _D	1.33 V _D
DYNAMIC LANDING MAX BENDING MOMENT AT CENTRE OF EXHAUST CASE (LIMIT)	(75 000 LB IN) 8474 Nm	(40 000 LB IN) 4519 Nm

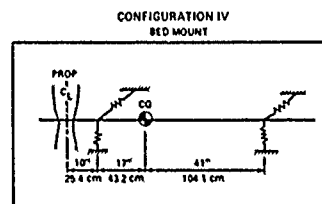
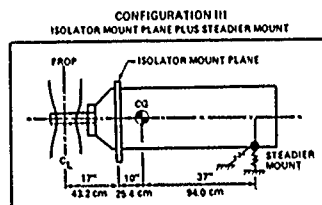


TABLE 3

DHC-7 POWERPLANT SUSPENSION COMPARISON OF TARGET AND ACHIEVED VALUES

STRUCTURAL STIFFNESS

STIFFNESS DIRECTION		MEASURED ESTIMATED	
		INNER NACELLE	OUTER NACELLE
VERTICAL	FRONT	1.24	1.06
	REAR	1.17	1.03
LATERAL	FRONT	70	59
	UPPER REAR	76	79
	LOWER REAR	61	58

ISOLATOR DYNAMIC STIFFNESS

MEASURED TARGET	
FLUTTER	TRANS- MISSIBILITY
1.06	2.1
1.01	1.6
1.60	3.3
1.25	1.3
86	1.3

ISOLATOR STATIC STIFFNESS

MEASURED TARGET
1.84
1.60
4.43
1.25
1.01

WEIGHTS

	ACTUAL DESIGN
WEIGHT	1.09
PITCH	1.18
YAW	1.15

FREQUENCIES (FLUTTER ANALYSIS)


MODE	ACHIEVED TARGET	
	I/B NACELLE	O/B NACELLE
PITCH	91	.91
YAW	87	.81
HEAVE	1.06	1.01
SWAY	91	.96

FREQUENCIES (TRANSMISS CALCS)

MODE	ACHIEVED TARGET	
	I/B NACELLE	O/B NACELLE
PITCH	1.16	1.16
YAW	.96	.87
HEAVE	1.47	1.27
SWAY	.95	1.03

TABLE 4

COMPARISON OF DHC-8 & DHC-7 SUSPENSION FREQUENCIES



		DHC-8 Hz	ACHIEVED DHC-7 (INBOARD NACELLE) Hz
SUSPENSION MODES - TARGET			
PITCH	Θ	8.4	6.4
YAW	Ψ	7.2	9.4
HEAVE	z	9.1	7.4
SWAY	y	30.5	36.5
FORE-AFT	x	21.9	21.3
ROLL	ϕ	13	17.3
POWERPLANT MODES - ESTIMATED			
VERTICAL BENDING	z	30	76
LATERAL BENDING	y	40	~76

TABLE 5

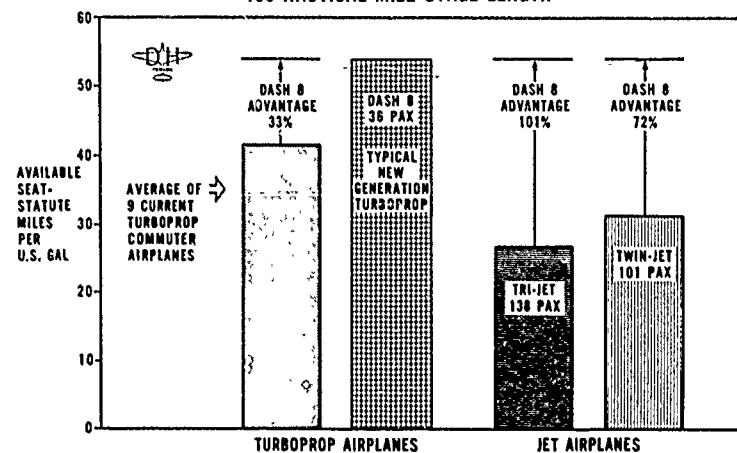
TURBOPROPS - MORE SEAT-MILES PER GALLON
150 NAUTICAL MILE STAGE LENGTH

FIGURE 1

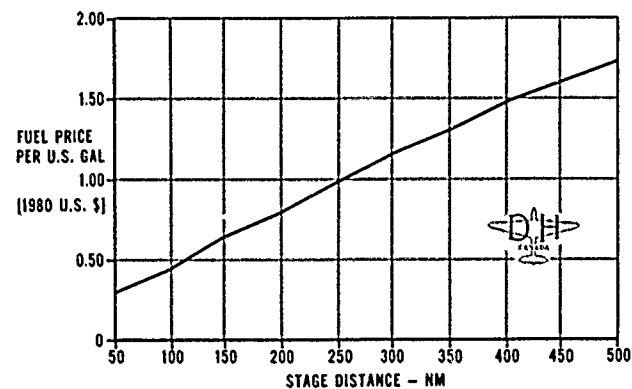
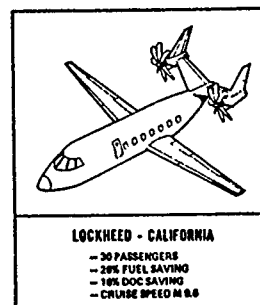
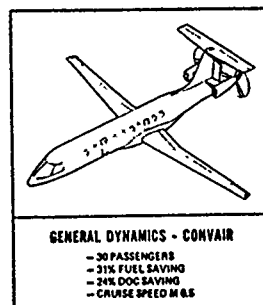
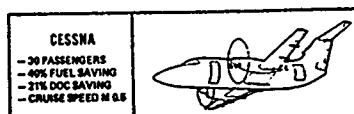
FUEL PRICE
AT WHICH DASH 7 DIRECT OPERATING COSTS
PER ASNM BECOME LESS THAN THOSE OF DC-9-30

FIGURE 2

ADVANCED TECHNOLOGY TRANSPORT DESIGNS

NASA'S SMALL TRANSPORT AIRCRAFT TECHNOLOGY (STAT) PROGRAM

NOTE: INFORMATION FROM
"ASTRONAUTICS & AERONAUTICS" (FEB 1981)



SAVINGS ARE WITH RESPECT TO BASELINE AIRCRAFT PERFORMANCE FOR 100 NM STAGE
- ASSUMING A FUEL PRICE OF \$1/U.S. GAL.

FIGURE 3

TURBOPROP INSTALLATIONS AT DE HAVILLAND CANADA TRANSPORT CATEGORY AIRCRAFT



DHC-4 CARIBOU (TEST BED)
FIRST FLIGHT SEPT 22 1981



DHC-5 BUFFALO
FIRST FLIGHT APRIL 9 1966



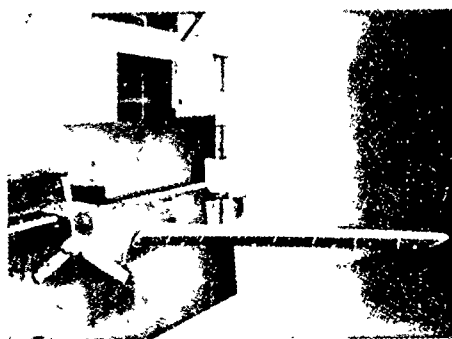
DHC-7
FIRST FLIGHT MAR 27 1975



DHC-8
FIRST FLIGHT SCHEDULED JUNE 1983

FIGURE 4

WHIRL FLUTTER MODEL DHC-4 CARIBOU TEST BED WITH G.E. YT-64 ENGINES



UNIVERSITY OF WICHITA WIND TUNNEL

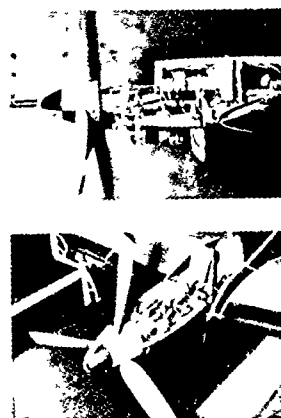


FIGURE 5

EQUATIONS OF MOTION - SIMPLIFIED WHIRL FLUTTER MODEL

$$I\ddot{\phi} + K_{\phi}\phi + I_p\Omega\dot{\psi} = \frac{1}{2}\rho V^2 S' (-eC_{3\phi}\phi + 2RC_{m\psi}\psi)$$

$$I\ddot{\psi} + K_{\psi}\psi - I_p\Omega\dot{\phi} = \frac{1}{2}\rho V^2 S' (eC_{3\psi}\psi + 2RC_{n\phi}\phi)$$

INERTIA - STIFFNESS GYROSCOPIC

AERODYNAMIC TERMS

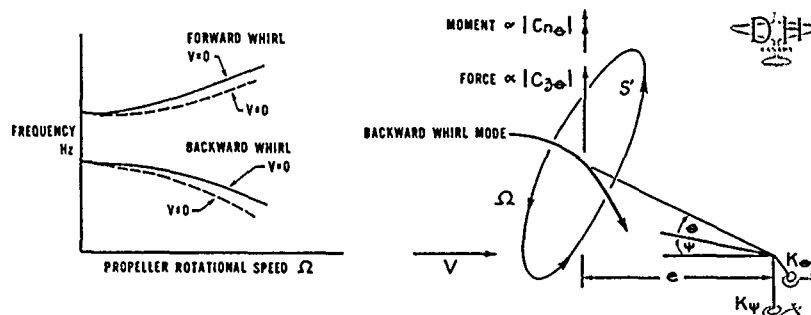


FIGURE 6

CARIBOU T64 TEST BED WHIRL FLUTTER MODEL

COMPARISON OF WHIRL FLUTTER RESULTS

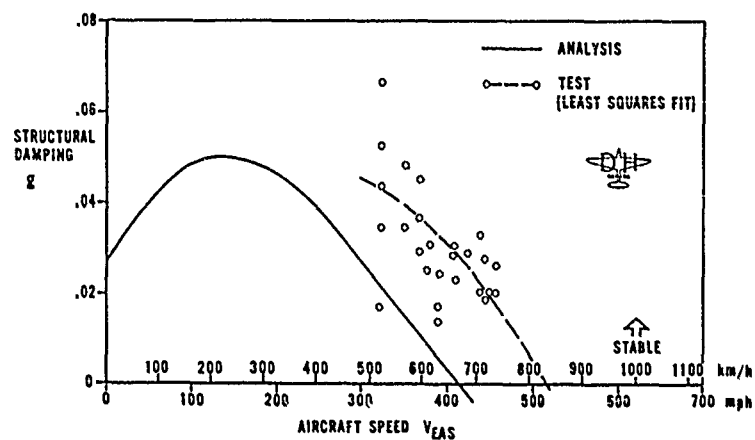


FIGURE 7

SOME FACTORS INFLUENCING WHIRL FLUTTER

- PITCH & YAW STIFFNESS
- PIVOT POINT LOCATION

- MECHANICAL DAMPING
- WING FLEXIBILITY

- PROPELLER POLAR INERTIA & RPM

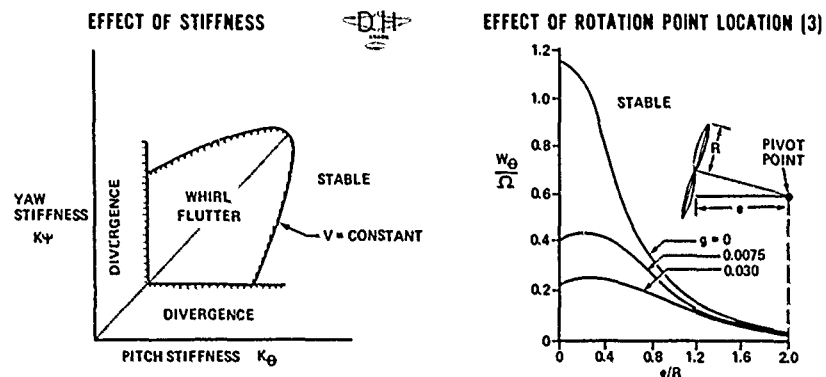


FIGURE 8

COMPONENTS OF PROPELLER UNBALANCE

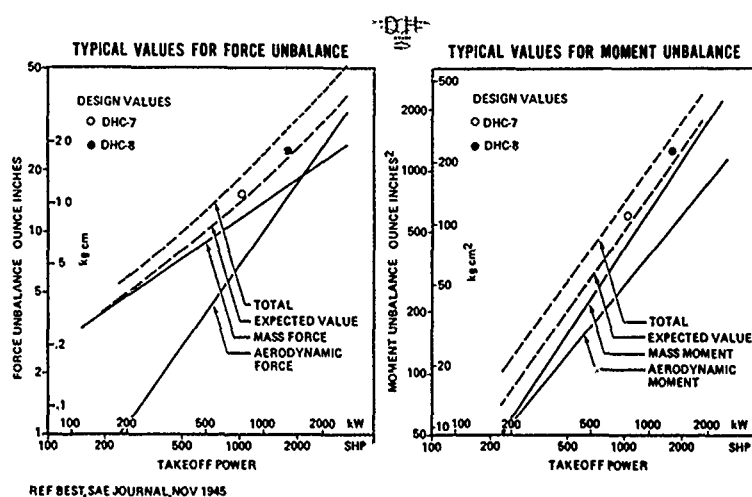


FIGURE 9

PROPELLER UNBALANCE SENSITIVITY

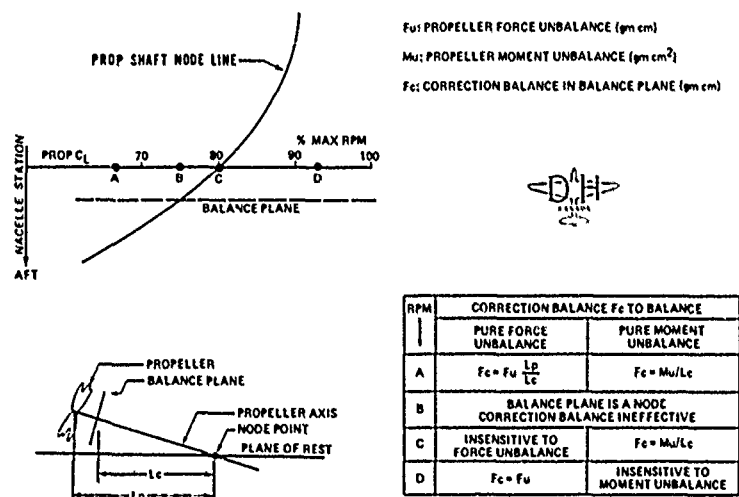


FIGURE 10

VIBRATION TRANSMISSIBILITY FOR A SINGLE DEGREE OF FREEDOM SYSTEM

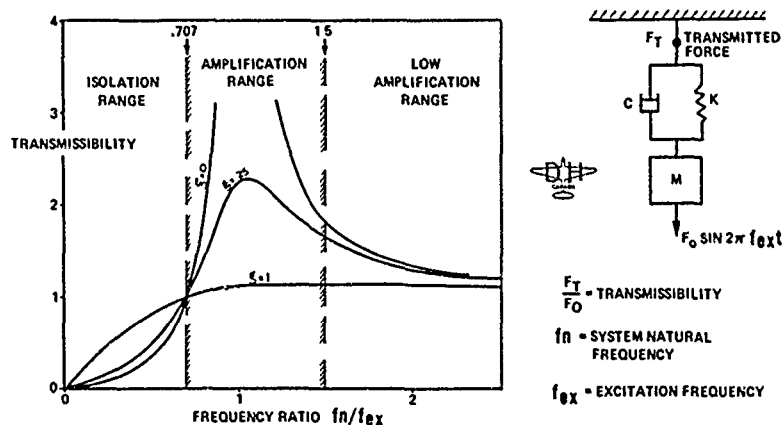
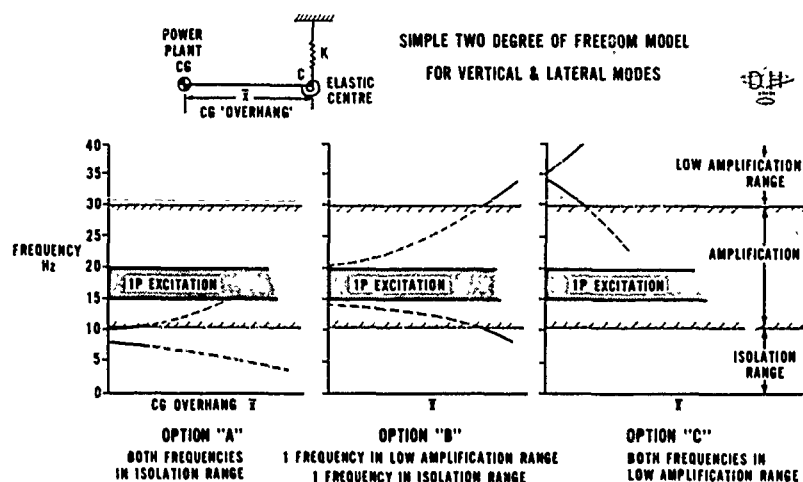
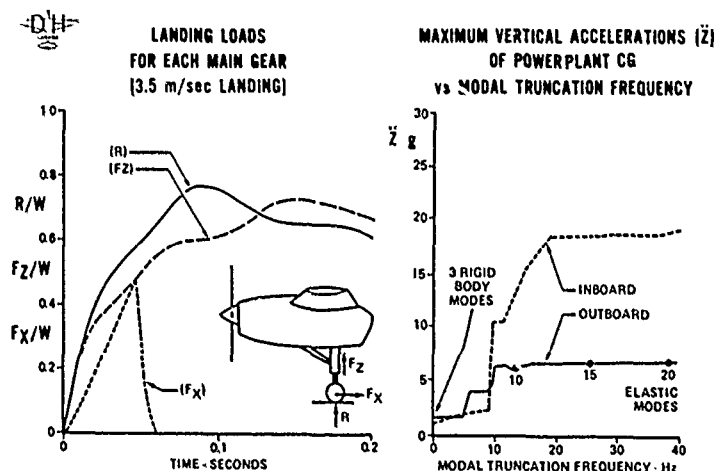


FIGURE 11

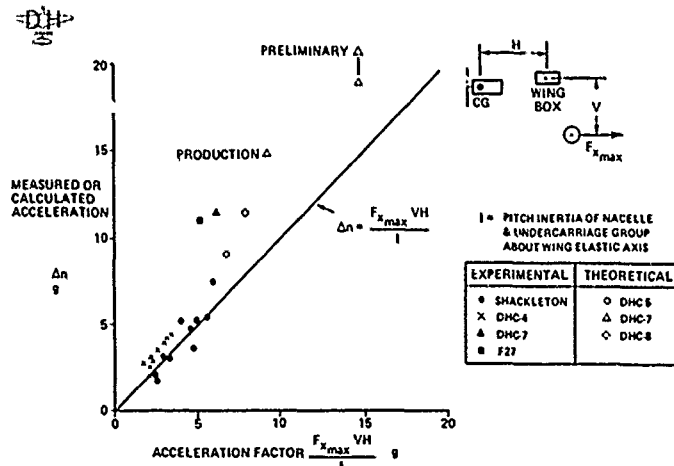
POWERPLANT SUSPENSION DESIGN OPTIONS



DHC-7 LANDING LOADS AND RESPONSES



FACTORS INFLUENCING POWERPLANT CG ACCELERATIONS FOR WING MOUNTED ENGINE & LANDING GEAR



POWERPLANT ACCELERATION RESPONSES — HARD LANDING ANALYSES

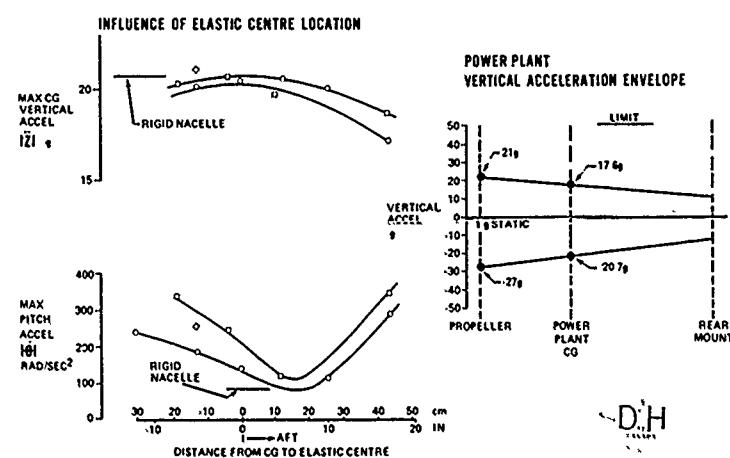


FIGURE 15

DHC-7 POWERPLANT SUSPENSION SINGLE PLANE STUDIES WITH RIGID WING

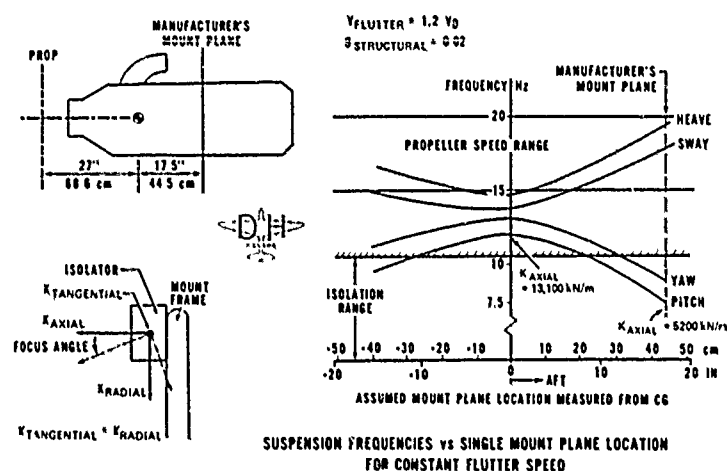


FIGURE 16

DHC-7 PRELIMINARY DYNAMIC LANDING STUDY MAXIMUM VERTICAL BENDING MOMENTS FOR VARIOUS MOUNT ARRANGEMENTS

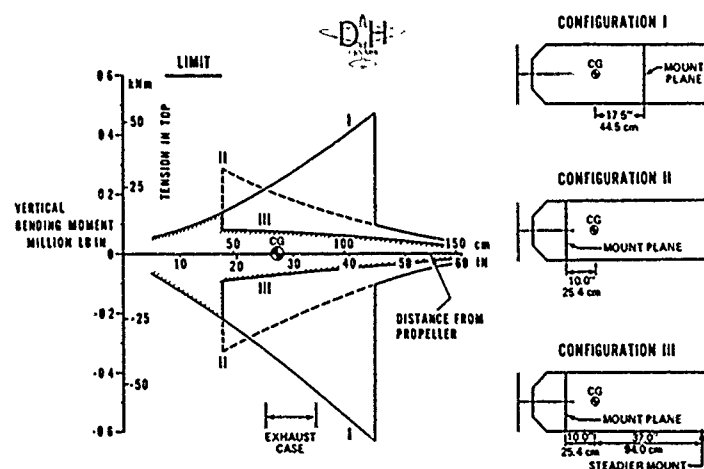


FIGURE 17

DHC-7 ENGINE MOUNT ARRANGEMENT

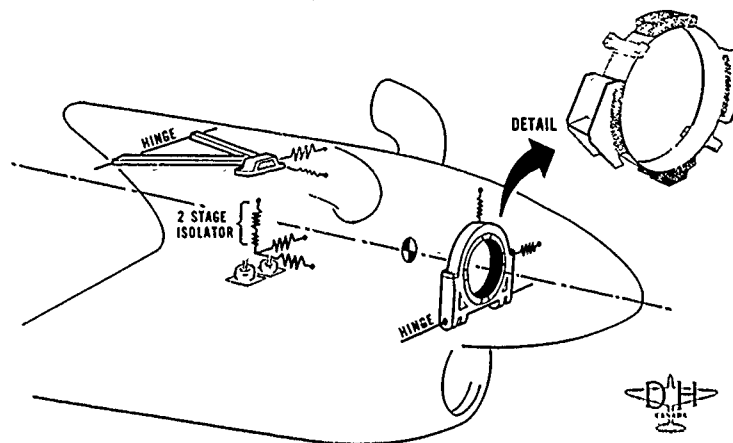


FIGURE 18

DHC-7 VERTICAL VIBRATION RESPONSE AT AIRCRAFT CG

DUE TO
PROPELLER UNBALANCE



- A/C WEIGHT: 19 504 kg (43 000 LB)
- MAX WING FUEL
- A/C SPEED: 235 KT EAS
- ALTITUDE: 7500 FT

TYPICAL UNBALANCE
PHASED FOR MAX RESPONSE:
1.1 kg cm FORCE UNBALANCE EACH
110 kg cm² MOMENT UNBALANCE EACH

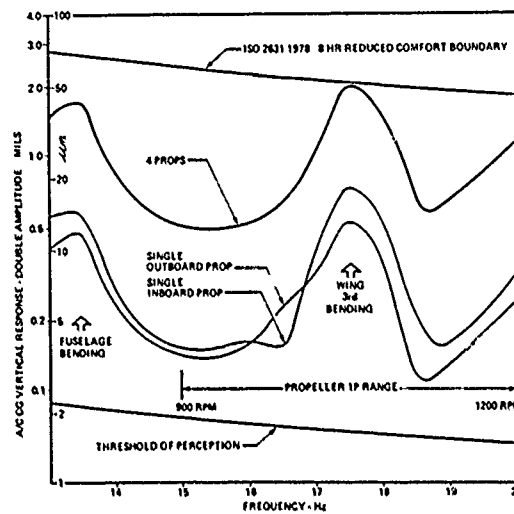


FIGURE 19

DHC-7 MAXIMUM FUSELAGE VERTICAL VIBRATIONS DUE TO PROPELLER UNBALANCE

(ALL DATA APPLIES FOR 17.5 Hz EXCEPT AT PILOT'S STATION WHICH IS A MAX AT 16.5 Hz)

A/C SPEED: 235 KT EAS

ALTITUDE: 7500 FT

TYPICAL UNBALANCE PHASED FOR MAX RESPONSE:

1.1 kg cm FORCE UNBALANCE EACH

110 kg cm² MOMENT UNBALANCE EACH

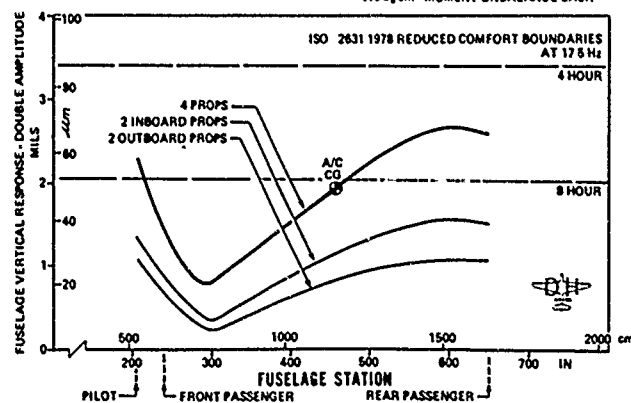


FIGURE 20

COMPARISON OF DHC-7 (INBOARD) & DHC-8 NACELLES

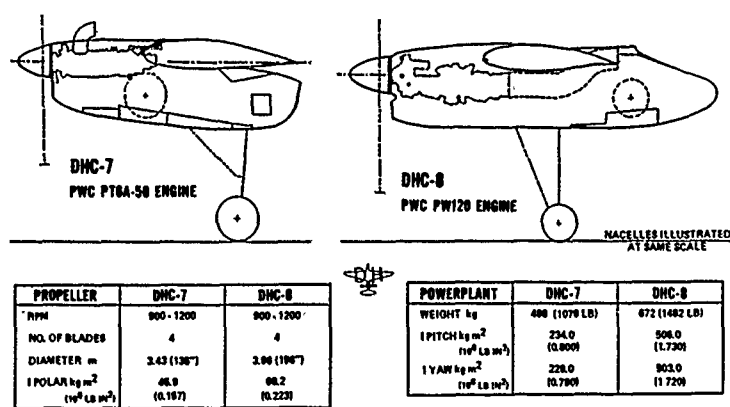


FIGURE 21

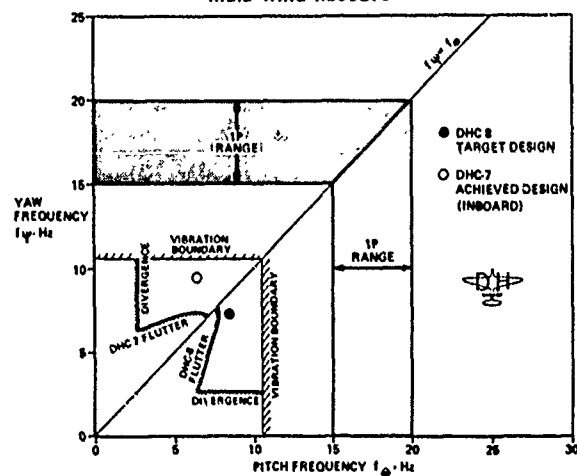
DHC-8 & DHC-7 ENGINE SUSPENSION DESIGN POINTS
RIGID WING RESULTS

FIGURE 22

DHC-8 ENGINE MOUNT ARRANGEMENT

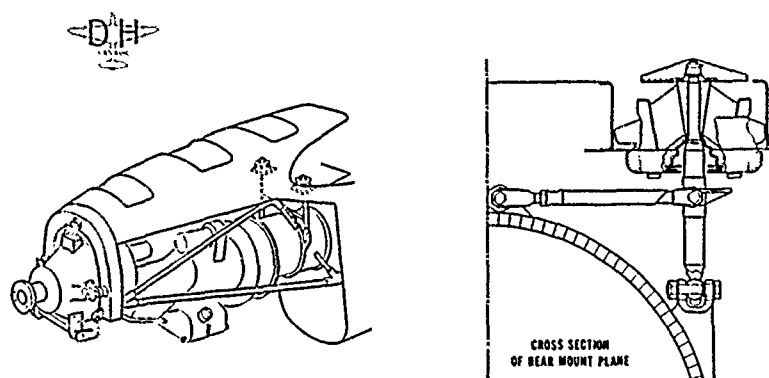
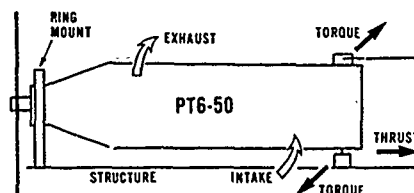


FIGURE 23

COMPARISON OF POWERPLANT SUSPENSIONS

DHC-7

- RIGID ENGINE
- DETERMINATE SUSPENSION



DHC-8

- FLEXIBLE ENGINE
- REDUNDANT SUSPENSION
- TORQUE COMPENSATOR
- AWKWARD MASS

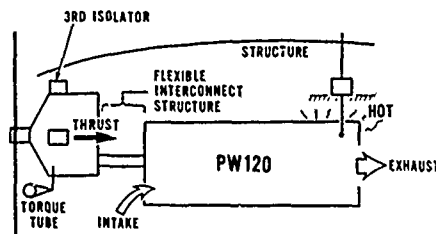


FIGURE 24

DHC-8
VERTICAL VIBRATION
RESPONSE
AT AIRCRAFT CGDUE TO
PROPELLER UNBALANCE

DH

- A/C WEIGHT 12,825 kg (28,500 LB)
- MAX WING FUEL
- A/C SPEED 245 KT EAS
- ALTITUDE 12,500 FT

TYPICAL UNBALANCE
PHASED FOR MAX RESPONSE
1.8 kg cm FORCE UNBALANCE EACH
230 kg cm² MOMENT UNBALANCE EACH

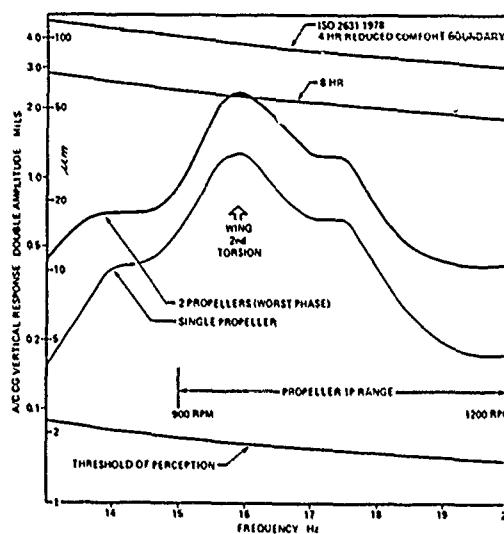


FIGURE 25

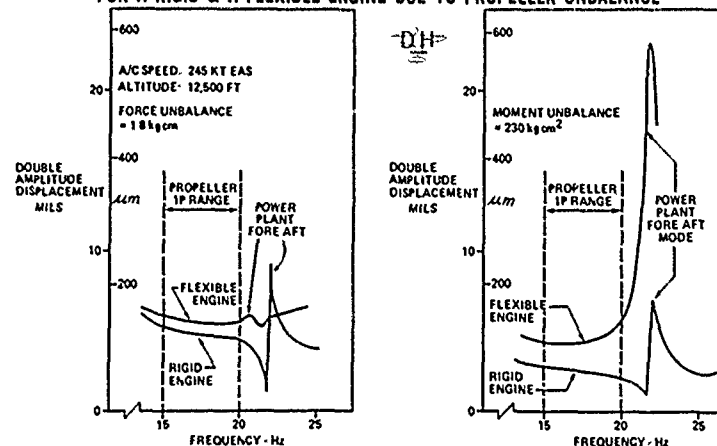
DHC-8 AIRCRAFT
VERTICAL DISPLACEMENT RESPONSE AT FRONT MOUNT PLANE
FOR A RIGID & A FLEXIBLE ENGINE DUE TO PROPELLER UNBALANCE

FIGURE 26

**THE DEVELOPMENT OF FAST-FLOW
(A PROGRAM FOR FLUTTER OPTIMIZATION TO SATISFY MULTIPLE FLUTTER REQUIREMENTS)**

by

Bruce A. Rommel

Senior Engineer

Douglas Aircraft Company

McDonnell Douglas Corporation

3855 Lakewood Blvd.,

Long Beach, California, U.S.A. 90846

SUMMARY

FAST-FLOW is being developed as a production program for finite-element flutter optimization. This program is the third step in an automated sequential structural design process that begins with an optimization for buckling and static strength. FAST-FLOW features a user-selected design optimization procedure such as the feasible-direction design search in CONMIN or a criteria optimizer to provide the structural resizing. Multiple flutter requirements resulting from variations in payload, fuel state, speed, and altitude are simultaneously satisfied. FAST-FLOW tracks both flutter speed and hump mode damping factors in design space. Second-order Taylor approximations of the flutter speeds and hump mode damping factors may be updated periodically during a fully automated design cycle. During an update, the model is reassembled in modal form, modes are updated, and the location of the flutter speeds and hump modes is reestablished. Then, the gradient and Hessian matrices used in the Taylor approximations for each requirement are updated. These design sensitivities are then used in a fast redesign cycle with the optimizer until the design converges or a new update is required. Program architectural considerations are presented and contrasted with standard structural analysis programs. The impact of finite-element dynamics on standard production flutter analysis procedures is also discussed.

SYMBOLS

- [A] = matrix of constraint gradients. This matrix is augmented by the push-off factors. If the design is feasible, it is further augmented by the gradient of the objective function
- α = the design step size. α^* is the optimum step size
- b = The reference semichord
- [B] = the coefficient matrix in the special LP in the direction-finding algorithm of CONMIN

$$[B] = -[A] [A]^T$$
- {C} = the coefficients of the linear objective function in the special LP direction-finding algorithm of CONMIN. For infeasible designs, this vector contains the gradients of the objective function and the design push-off factor
- {D} = the design vector. In CONMIN, the design vector is given by the vector {X}
- D_i = an element in the design vector
- $\{D_i - D_o\}$ = the change in the design vector from the reference point $\{D_o\}$
- [D] = the diagonal decomposition of the stiffness matrix in subspace iteration
- ∂ = denotes partial differentiation
- ∇ = the gradient
- F = the weight objective function described by Equation (13.1)
- g = the structural damping factor
- g_N = the structural damping factor in the N_{TH} mode
- g_H = the structural damping factor at the top of the hump mode
- g_R = the reference structural damping factor
- G_j = the J_{TH} constraint
- $[H_{VFO}]$ = the Hessian matrix

8-2

I, J, K	=	dummy indices or subscripts
$[K]$	=	the stiffness matrix
K	=	the reduced frequency
K_F	=	the reduced frequency for flutter
$[\bar{K}]$	=	the complex generalized stiffness
$[K_E]$	=	the element stiffness matrix
$[\bar{K}_I]$	=	the complex generalized stiffness for the I_{TH} finite element
$[K_q]$	=	the generalized stiffness matrix
K_N	=	the reduced frequency for the N_{TH} mode
k_I	=	the stiffness function for the I_{TH} finite element
$[L]$	=	the lower triangular decomposition of the stiffness matrix in subspace iteration
L	=	an equation number extracted from the element directory vector $\{LM\}$
$\{LM\}$	=	the finite-element directory vector
λ	=	an eigenvalue
λ_N	=	the N_{TH} mode eigenvalue
λ_F	=	the flutter eigenvalue
λ_{IN}	=	the imaginary part of the complex eigenvalue
λ_{RN}	=	the real part of the complex eigenvalue
$[M]$	=	the mass matrix
$[M_E]$	=	the element mass matrix
$[M_I]$	=	the generalized mass matrix for the I_{TH} finite element
m_I	=	the mass function for the I_{TH} finite element
$[M_q]$	=	the generalized mass matrix
N	=	denotes the N_{TH} mode when used as a subscript
NAC	=	the number of active or violated constraints
$NCON$	=	the number of constraints
NDV	=	the number of free design variables
NFC	=	the number of flutter constraints
NHC	=	the number of hump mode constraints
$NUMEL$	=	the number of finite elements in the model
ν	=	the reduced velocity ($\nu = 1/K$)
ν_o	=	the initial value of reduced velocity
ν_F	=	the value of reduced velocity at flutter
$\{\varphi_{GLOBAL}\}$	=	the global modes from subspace iteration
$\{\varphi_E\}$	=	the real normal modes for an element
$\{\varphi_U\}$	=	the real normal modes updated by the modal assembler solver

$\{\Phi\}$	= a complex eigenvector
$\{\bar{\Phi}_{UN}\}$	= the complex right eigenvector for the N_{TH} mode. The bar denotes that the vector is normalized to a unit value of the complex generalized stiffness
$[\bar{\Phi}_{VN}]$	= the complex left eigenvector for the N_{TH} mode. The bar denotes that the vector is normalized to a unit value of the complex generalized stiffness
$[Q]$	= the reduced generalized matrix of aerodynamic influence coefficients (AICs)
$[Q_{J+1}]$	= temporary eigenvectors in subspace iteration
R	= denotes the real part when used in a subscript
S	= the total energy density due to the mass, damping, and stiffness of the structure
T	= the total energy density due to the aerodynamics
U,V	= Lagrange multipliers in the direction-finding algorithm of CONMIN
ω	= the circular frequency
V	= the velocity
V_F	= the flutter velocity
$\{X\}$	= the design vector in CONMIN
$[X_S]$	= Ritz vectors in subspace iteration

ARRAY SYMBOLS:

$\left\{ \right\}$	= a column vector
$\left[\right]$	= a row vector
$\left[\right]$	= a matrix
$\left[\right]^T$	= a matrix transpose
$\left[\right]^{-1}$	= a matrix inverse

INTRODUCTION

FAST-FLOW will be used in production as a program for finite-element structural optimization to satisfy flutter requirements resulting from variations in payload and fuel weight. Aircraft flutter speeds are highly dependent on the aircraft geometry and on its distribution of weight and stiffness. Transport aircraft must fly with a number of payload configurations as well as significant changes in fuel weight. These weight changes seriously alter the aircraft structural modes and consequently the flutter speeds.

Flutter optimization is required in two distinct areas of aircraft design. The new aircraft design process must select an optimum configuration from a number of different aircraft geometries. The derivative aircraft design process involves least-weight modifications to an existing design. In both of these areas of design, multiple flutter and strength requirements are imposed by variations in payload and fuel residuals. Figure 1 shows some of the parameters which must be investigated in the design of a commercial transport. The derivative aircraft design process will alter some of these parameters, and flutter margins may be reduced. If the flutter margin is negative for any fuel weight or payload configuration, structural redesign is required to raise the flutter speed. In addition to these variations, an aircraft at any given configuration may exhibit multiple modes of flutter.

Structural modifications to raise the flutter speed of one mode may result in lowering the flutter speed of another mode. Transport aircraft often possess stable incipient hump modes. These modes are very sensitive to changes in structural properties. Thus, the flutter optimization process is constrained by multiple modes of flutter and by the hump modes.

Flutter optimization research was initiated at Douglas Aircraft Company in the late 1960s and early 1970s by Warren and McGrew (References 1 through 3). Warren resized the structure of an all-movable horizontal stabilizer. McGrew's research was directed toward flutter optimization of complete aircraft configurations using "stick-models" like that shown in Figure 2.

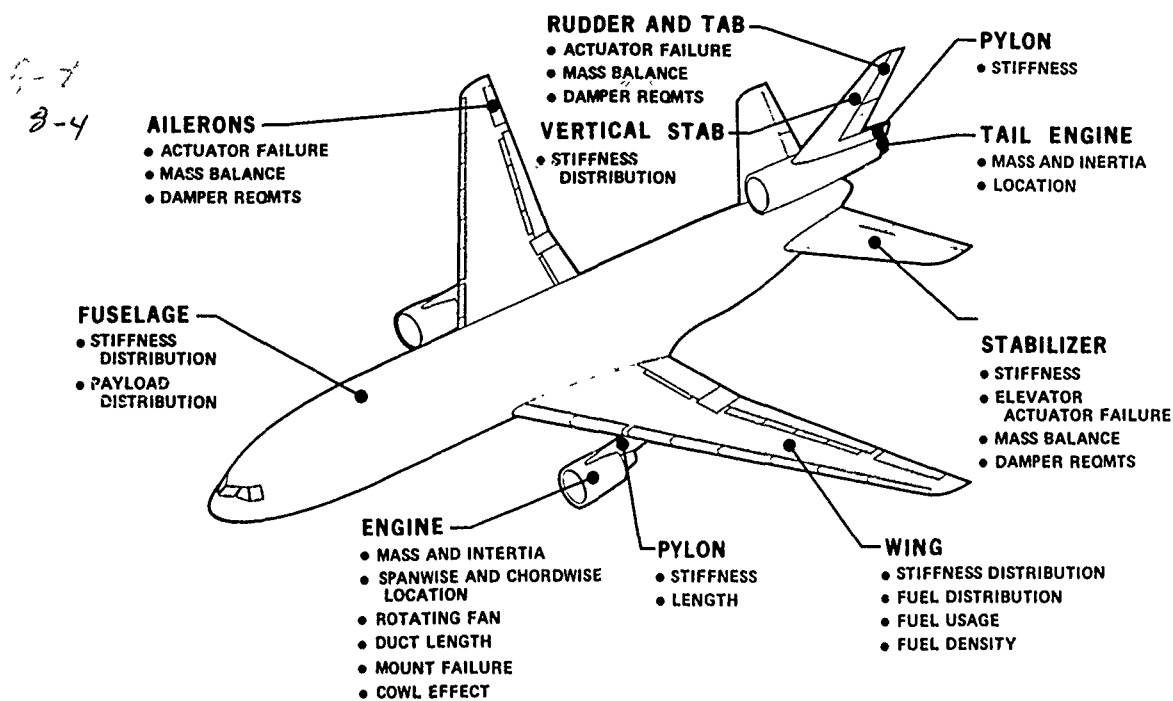


FIGURE 1. PARAMETERS ANALYTICALLY INVESTIGATED FOR FLUTTER

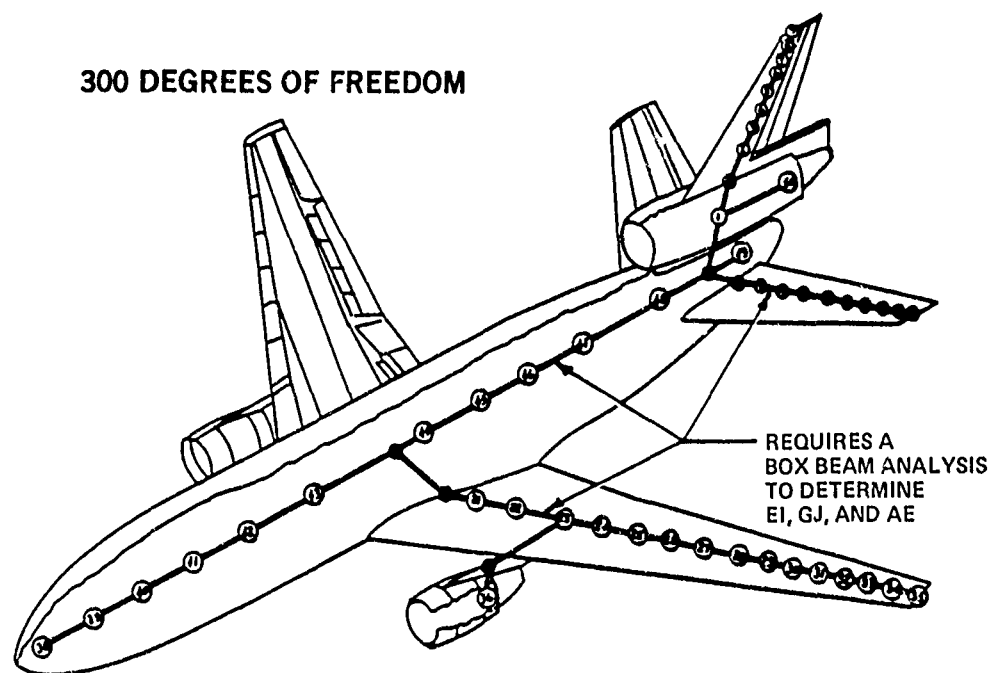


FIGURE 2. BEAM-STICK MODELS USED FOR FLUTTER OPTIMIZATION IN THE EARLY 1970s

In the late 1960s, Dodd and Tate began work on static strength optimization at Douglas Aircraft (References 4 through 7). Tate's system, described in Reference 7, was called the "Computer Aided Structural Design," or CASD program, and represented an all-new development. Dodd's system was called the "Automatic Reanalysis and Redesign for Optimum Weight," or ARROW program. ARROW was an improvement on the FORTRAN Matrix Abstraction Technique or FORMAT program (Reference 8). ARROW added a structural design optimization capability to the FORMAT system. Both ARROW and CASD employed forms of the Fully Stressed Design, or FSD, algorithm for structural resizing.

In the early 1970s, CASD was mated with the Computer Graphics for Structural Analysis, or CGSA, system. CGSA is a finite-element modeling extension to the Computer Aided Design and Drafting, or CADD, system. Together, CGSA and CASD were used in the design development of the F-15 and F-18 aircraft.

Another structural optimization project of the early 1970s was the development of a buckling optimization capability by Dietz (Reference 9). Dietz's SEARCH program optimizes stringer size and stringer spacing of compression panels. This program is used to provide compression allowables for the CASD and ARROW static strength optimizations.

Late in 1978, the author took over the flutter optimization research from McGrew. At this time, several realities concerning flutter optimization were apparent. Both the CASD and ARROW optimizers were complete and operational. Dodd was performing static strength optimization of complete aircraft models like that shown in Figure 3 with his ARROW program. Flutter optimization had left the experimental stage and was in production in such programs as FASTOP, SOAR, WIDOWAC, TSO, and PARs (see References 10 through 19). The existing flutter optimization program used a search technique similar to that employed in 1970 by Rudisill and Bhatia (Reference 20) and was now obsolete. The flutter optimizer utilized a completely different structural representation from that being used for static strength. This required converting the finite-element representation back into a beam model. Arrow wing bodies such as the SST shown in Figure 3 do not lend themselves to stick-model representations. Technical developments in the early 1970s such as subspace iteration made it possible to perform modal analysis of finite-element models with 5,000 or more degrees-of-freedom (Reference 21). A rapid expansion of computer power (speed and size) in the 1980s was forecasted.

A flutter optimization capability was required which would be compatible with CGSA, and the CASD and ARROW models. FASTOP had been tried on an experimental basis and was found to be very expensive to operate. Maintenance and improvements to increase efficiency would probably cost as much as a new development. Other externally developed programs were likewise discarded in favor of a new independent development. In 1979, work was initiated on this new system. This paper describes the main features of this new system. No optimization results will be presented due to the preliminary state of development of FAST-FLOW.

1,280	JOINTS
644	LOAD VECTORS
2,834	BARS
2,149	PANELS (1,328 TRIANGULAR MEMBRANES AND 821 SHEAR WEBS)
7,817	STRESSES
10,473	ELEMENT FORCES
5,803	DEGREES OF FREEDOM
6	APPLIED LOAD CONDITIONS (UPDATED FOR WIND TUNNEL)
3	FULLY STRESSED DESIGN ITERATIONS

THE CHALLENGE OF THE FUTURE (5,803 DEGREES OF FREEDOM)

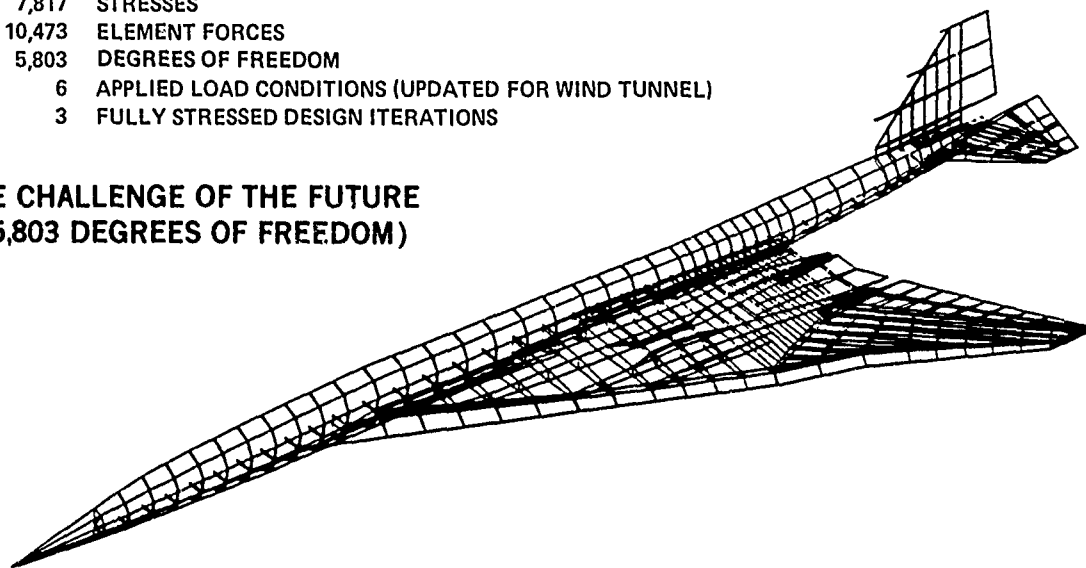


FIGURE 3. TYPICAL ADVANCED DESIGN FINITE-ELEMENT MODEL FOR STATIC STRENGTH IN THE LATE 1970s

THEORETICAL DEVELOPMENTS IN THE FIRST YEAR

Previous experience with optimization programs had shown that the program architecture and analytics were strongly influenced by the optimizer algorithm. The first step in the investigation was to conduct a literature search. The paper by Stroud in 1974 nicely summarized the state of the art of flutter optimization at that time (Reference 22). Numerous other reports indicated that Vanderplaats' CONMIN (Reference 23) and Miura's NEWSUMT (Reference 24) were the best of the currently available numerical search optimizers. CONMIN employed an improved version of the feasible directions search algorithm (see Reference 25). NEWSUMT employed an improved version of the sequential unconstructed minimization technique. A copy of each program and its users' manual was received from Vanderplaats and Miura.

A unified approach to optimality criteria resizing had been presented by Kiusalaas (Reference 18), but a modular "off-the-shelf" criteria resizer was not found. It was a goal of the FAST-FLOW project to establish a program capable of performing flutter optimization with both numerical search and criteria optimization. However, previous work on optimization at Douglas had shown that considerable effort would be required to bring an optimizer algorithm up from scratch. Therefore, an early project decision was required to establish one of the two numerical search programs as the main optimizer. When the system was operational, other optimizers could be developed and added to the system. A modular program which would allow plug-in and out functions was planned even at the conceptual stage of the development.

The prospect of multiple optimizers and the demands of each were considered to be too much to deal with at this early stage of the development. Previous investigators had shown that either CONMIN or NEWSUMT could be used for flutter optimization (References 10 through 12, 14 through 17, and 26). A decision was made to focus the early development on the CONMIN optimizer.

The next step was to convert CONMIN to functional operation on the IBM 370. A test program was written, and a flowchart was prepared of the CONMIN optimizer, as shown in Figure 4. This flowchart and the simple check problems revealed several features of

8-6

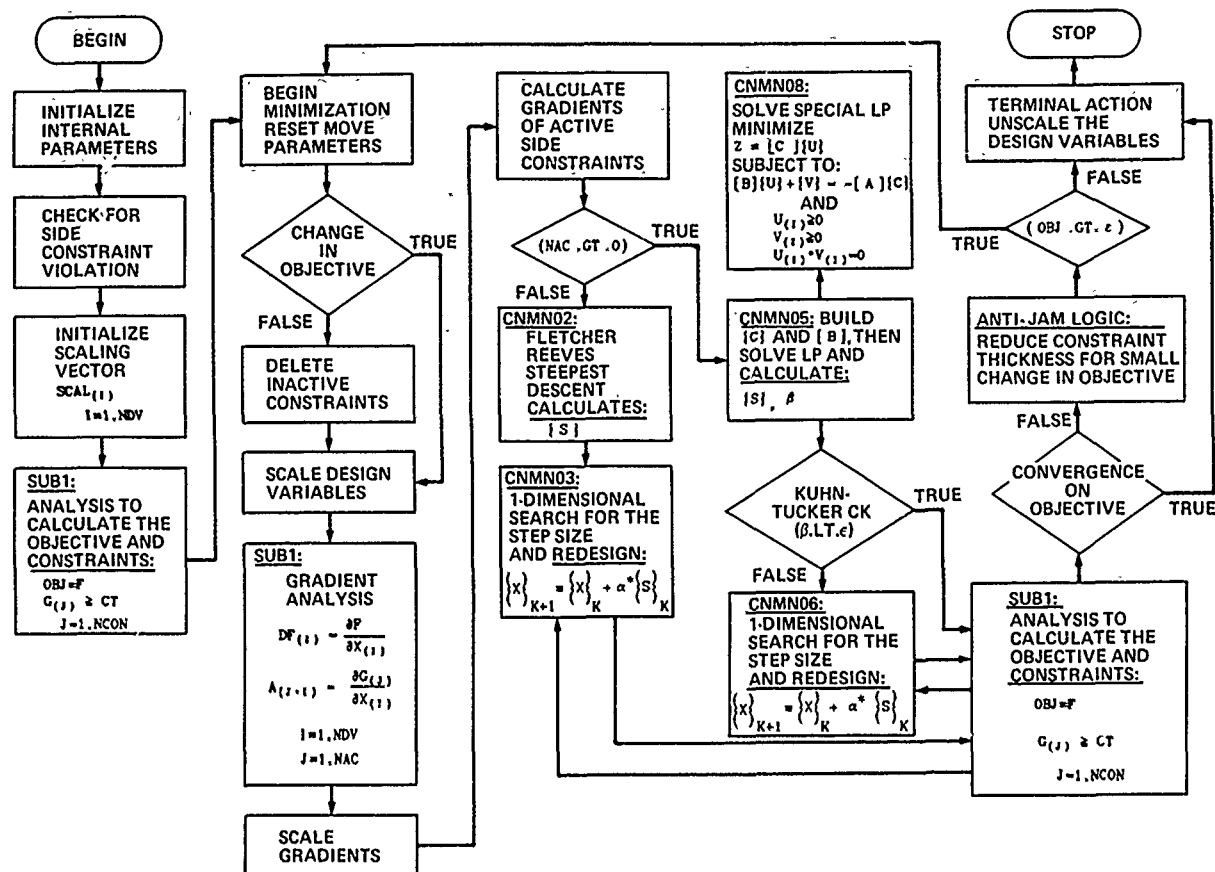


FIGURE 4. THE CONMIN OPTIMIZER

CONMIN which were significant to flutter optimization. The first of these was that the optimum design could be approached from either the feasible or infeasible domains. This is significant since the strength-optimized design must be presumed to be flutter-deficient or flutter optimization is not required. Also, design moves may be taken which may result in slightly infeasible designs. Design moves are also permitted which do not result in any active or violated constraints. When constraints are active or violated (NAC.GT.O), CONMIN finds the feasible direction by solving a special linear program (LP) problem on the approximate order of the number of active constraints (NAC). The size of the design vector (NDV) is of almost no consequence in this direction-finding algorithm. For comparison, the feasible direction finding algorithm in the SOAR flutter optimizer solved a linear programming problem on the order of (2NDV+NAC+1). For large-scale structural synthesis, this linear programming problem becomes impractical.

The size of the linear program is determined by the bounding condition on the direction vector. Zoutendijk, in Reference 27, proposed to bound the direction vector $\{S\}$ by either bounding the elements in $\{S\}$ between -1 and +1 or by bounding the norm of $\{S\}$ to be less than 1. Zoutendijk preferred to bound the norm and that is the condition used by Vanderplaats in CONMIN (see Reference 25). This results in a quadratic programming problem similar to Wolfe's algorithm. In a similar manner, it reduces to an excluded basis linear programming problem. Thus, the special LP in CONMIN may be regarded as an excluded basis simplex algorithm.

The flowchart of Figure 4 and the test problems also revealed a serious difficulty in using CONMIN for flutter optimization. The one-dimensional search to find the optimum step size was accomplished at the expense of multiple constraint evaluations. To understand how this requirement impacts flutter optimization, one must consider how the flutter constraints may be formulated.

Figure 5 shows the character of the structural modes on the V-g plane. In these figures the American Standard Convention for flutter damping is assumed so that negative damping corresponds to a flutter stable airplane. Each structural mode will behave like one of the four modes of Figure 5(a). These modes are stable modes, violent flutter modes, hump flutter modes, or stable incipient flutter modes. Acceptable flutter performance is achieved when all flutter modes become unstable above some critical velocity (V_R) which is outside the flight envelope. Figure 5(b) shows a typical design situation with two unstable flutter modes. The objective of flutter optimization is to move the flutter speeds up so that they cross the axis into the feasible domain. It may be argued that the character of the structural modes on the V-g plane describes the method of search rather than the flutter characteristic. The American K-method and P-K methods give different modal characteristic curves on the V-g plane. The British method gives still another set of modal characteristic curves on the V-g plane. However, at the neutral stability point, all the methods agree on the flutter speed (V_F). It is this flutter characteristic (V_F) which is to be controlled by the flutter optimizer. This may be accomplished by constraining the flutter velocity (V_F) to be greater than the required speed (V_R).

Conventional flutter analysis is accomplished by recursive eigenvalue evaluation of the flutter determinate. If this type of analysis must be performed several times for each step size calculation, then the cost of analysis will be prohibitive. Clearly, a simple relation between changes in the design variables and the flutter speeds is required. This equation is found in the form of a second-order Taylor series in design space.

$$V_F = V_F^0 + \left[\frac{\partial V_F^0}{\partial D_1} \right] \{ D - D_0 \} + \frac{1}{2} \left[D - D_0 \right] \left[\frac{\partial^2 V_F^0}{\partial D_1 \partial D_1} \right] \{ D - D_0 \} \quad (1)$$

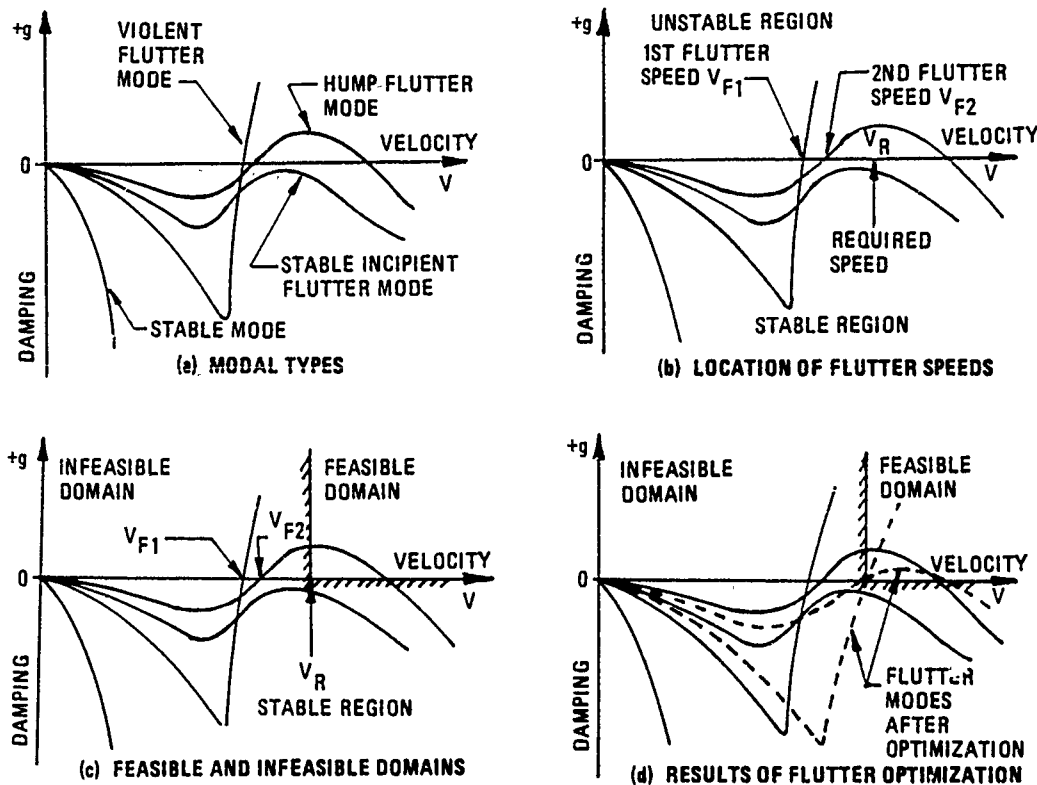


FIGURE 5. CHARACTER OF THE STRUCTURAL MODES

In two separate papers Rudisill and Bhatia gave the first and second flutter derivatives of the flutter determinate (References 20 and 28). In the symbolism of this paper these equations were:

$$\frac{\partial V_F}{\partial D_1} = - \frac{V_F}{K_F} \frac{\partial K_F}{\partial D_1} - \frac{V_F}{2\lambda_F} \frac{\partial \lambda_F}{\partial D_1} \quad (2)$$

and

$$\begin{aligned} \frac{\partial^2 V_F}{\partial D_1 \partial D_j} = & \left(\frac{V_F}{K_F \lambda_F} \right) \left[\frac{2\lambda_F}{K_F} \frac{\partial K_F}{\partial D_1} \frac{\partial K_F}{\partial D_j} + \frac{1}{2} \left(\frac{\partial K_F}{\partial D_1} \frac{\partial \lambda_F}{\partial D_j} + \frac{\partial \lambda_F}{\partial D_1} \frac{\partial K_F}{\partial D_j} \right) + \frac{3K_F}{4\lambda_F} \frac{\partial \lambda_F}{\partial D_1} \frac{\partial \lambda_F}{\partial D_j} \right] \\ & - \left(\frac{V_F}{K_F \lambda_F} \right) \left[\lambda_F \frac{\partial^2 K_F}{\partial D_1 \partial D_j} + \frac{K_F}{2} \frac{\partial^2 \lambda_F}{\partial D_1 \partial D_j} \right] \end{aligned} \quad (3)$$

Equations (2) and (3) are the equations for the elements in the gradient vector and Hessian matrix required in the Taylor series of Equation (1). In this form, these derivatives clearly show that each flutter mode may be characterized in design space by the behavior of two independent parameters. These are the flutter frequency and the reduced frequency for flutter. The flutter frequency is determined by the flutter eigenvalue (λ_F). Each flutter mode may thus be conceived to be a hypersphere passing through design space, as shown in Figure 6. The Taylor expansion will give good approximations in a region about the design point where the derivatives have been found. If the design move is large, however, the derivatives must be updated to be valid. The derivatives of Equations (2) and (3) are deceptively difficult to evaluate. To obtain these derivatives, the mass and stiffness derivatives for each finite element under design must be calculated. In addition, the derivatives of the generalized aerodynamic influence coefficients (AICs) must also be calculated. This may be accomplished indirectly by first computing the derivatives of the AICs with respect to the reduced frequency (K). The design derivatives of the AICs may then be found as:

$$\left[\frac{\partial Q}{\partial D_i} \right] = \left(\frac{\partial K_F}{\partial D_i} \right) \left[\frac{\partial Q}{\partial K} \right] \quad (4)$$

and

$$\left[\frac{\partial^2 Q}{\partial D_i \partial D_j} \right] = \left(\frac{\partial K_F}{\partial D_i} \right) \left(\frac{\partial K_F}{\partial D_j} \right) \left[\frac{\partial^2 Q}{\partial K^2} \right] + \frac{\partial^2 K_F}{\partial D_i \partial D_j} \left[\frac{\partial Q}{\partial K} \right] \quad (5)$$

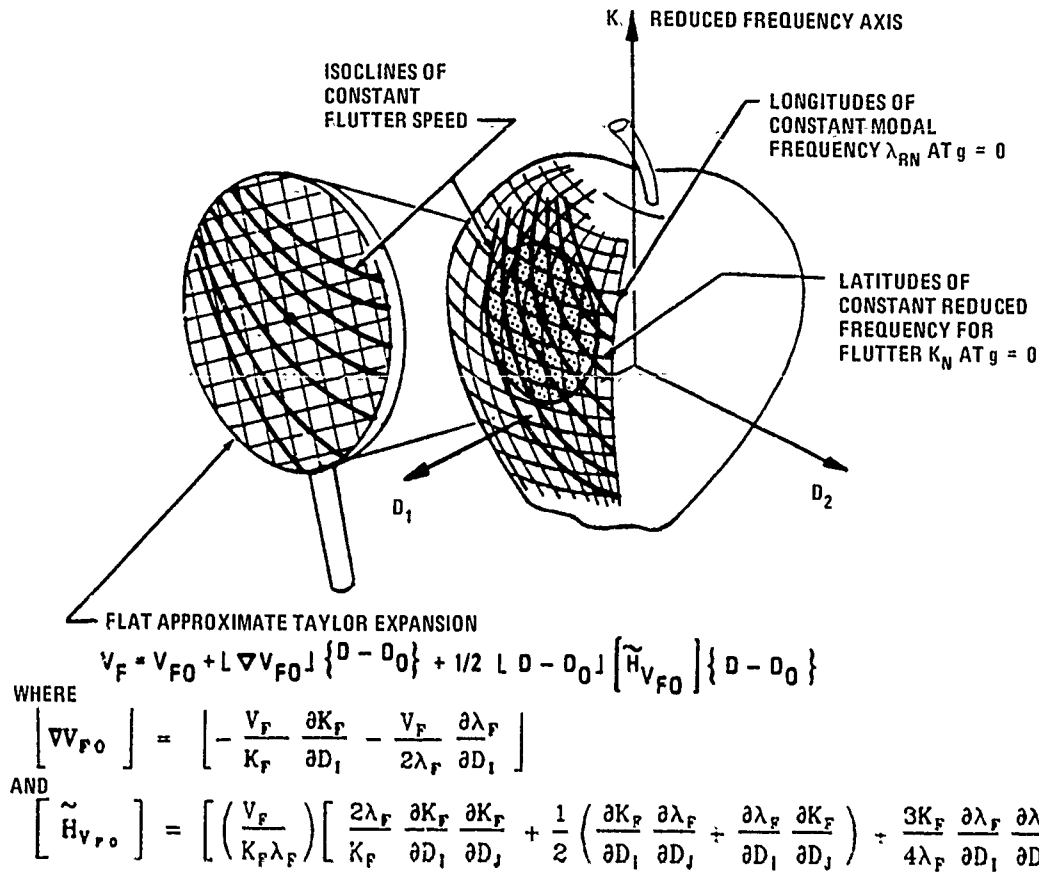


FIGURE 6. A FLUTTER MODE PERCEIVED AS A HYPERSPHERE PASSING THROUGH DESIGN SPACE

Thus, both the first and second derivatives of the generalized AICs must be found to compute the Hessian matrix in Equation (1). Unfortunately, most programs which compute the unsteady AICs do not compute these derivatives. This is a strong incentive to look for an optimization technique which does not require these derivatives. However, these derivatives determine where the flutter velocity is going. Consider how Rudisill and Bhatia first computed the flutter derivative. They started with the K-method flutter equation given by:

$$\left[\bar{K} \right]^{-1} \left[\left[\bar{M} \right] + \left[\bar{Q} \right] \right] \{ \Phi \} = \lambda \{ \Phi \} \quad (6)$$

Rudisill and Bhatia then calculated the first derivative of the flutter eigenvalue as:

$$\frac{\partial \lambda_N}{\partial D_1} = \left[\bar{\Phi}_{VN} \right] \left[\frac{\partial m_1}{\partial D_1} \left[\bar{M}_1 \right] - \lambda_N \frac{\partial k_1}{\partial D_1} \left[\bar{K}_1 \right] \right] \{ \bar{\Phi}_{UN} \} + \frac{\partial K_N}{\partial D_1} \left[\bar{\Phi}_{VN} \right] \left[\frac{\partial Q}{\partial K} \right] \{ \bar{\Phi}_{UN} \} \quad (7)$$

This equation is of the form:

$$\frac{\partial \lambda_N}{\partial D_1} = S_{RN} + iS_{IN} + \frac{\partial K_N}{\partial D_1} \left(T_{RN} + iT_{IN} \right) \quad (8)$$

where $S_N = (S_{RN} + iS_{IN})$ represents an energy density due to the structural mass damping and stiffness terms.

$$S_N = \left[\bar{\Phi}_{VN} \right] \left[\frac{\partial m_1}{\partial D_1} \left[\bar{M}_1 \right] - \lambda_N \frac{\partial k_1}{\partial D_1} \left[\bar{K}_1 \right] \right] \{ \bar{\Phi}_{UN} \} \quad (9)$$

and $T_N = (T_{RN} + iT_{IN})$ represents an energy density due to the aerodynamics.

$$T_N = \left[\bar{\Phi}_{VN} \right] \left[\frac{\partial Q}{\partial K} \right] \{ \bar{\Phi}_{UN} \} \quad (10)$$

The condition for flutter is that the structural damping factor vanishes:

$$s_N = \frac{\lambda_{IN}}{\lambda_{RN}} = 0 \quad (11)$$

that is, the surface of the hypersphere of Figure 6 is a surface for which:

$$\lambda_{IN} = 0 \quad (11.1)$$

To stay on this surface, the imaginary part of the derivative of the flutter eigenvalue must vanish as well. So, we have the requirement.

$$\frac{\partial \lambda_{IN}}{\partial D_I} = 0, \quad J=1, NDV \quad (11.2)$$

Applying this condition to Equation (8), the flutter derivatives of the metrical parameters are found as:

$$\frac{\partial K_F}{\partial D_J} = - \frac{S_{IN}}{T_{IN}}, \quad J=1, NDV \quad (12.1)$$

and

$$\frac{\partial \lambda_F}{\partial D_J} = S_{RN} - S_{IN} \left(\frac{T_{RN}}{T_{IN}} \right), \quad J=1, NDV \quad (12.2)$$

The point of the above review is that the AIC derivatives are required to compute the flutter derivatives. These flutter derivatives ($\partial V_F / \partial D_I$) are required by any flutter optimization algorithm including criteria optimization.

It should be noted that the complex eigenvalue derivative of Equation (7) has separated into the two real derivatives in Equation (12). These are the derivatives of the metrical parameters (K_F and λ_F) which locate the flutter mode in design space. Now, let us return to the derivatives of the flutter velocity as given by Equations (2) and (3). It can be seen that the first design derivative and a good approximation of the second design derivatives can be found with only the first derivatives of the metrical parameters. If the metrical curvature terms in Equation (3) are ignored, 90 percent of the computer time and 98 percent of the computer storage can be saved.

Now, a means of computing the gradients of the AICs had to be found. The AICs are complex functions of the reduced frequency (K), where ($K = b\omega/v$).

Some sample AICs were generated and were found to be fairly smooth functions of (K). A new spline routine was then developed which would return good function values and derivatives through the third derivative. Subsequent tests with strip theory have continued to show good results with this spline.

With this technology in place, it was now realized that a technique was at hand for automating the flutter search. This is a search, at a fixed design point, to locate all of the flutter modes. Even noncritical flutter modes must be found to ensure that the optimizer does not raise one flutter speed while lowering another. Of particular interest is the location and sensitivity of the hump modes.

The search for the hump modes is just like the search for the flutter modes except we are looking for the velocity and frequency for which the damping gradient ($\partial g / \partial v$) vanishes. These searches are difficult to automate because of the behavior of the structural modes on the V-g and V-f planes. As shown in Figure 7(a), these modal characteristic curves may be double-valued. Indeed, cases have been exhibited with complete loops in the modal curves on the V-g plane. Worse yet, it takes several reduced frequencies to determine a complete modal curve. Since the AICs are complex functions of the reduced frequency, the solution of the complex eigenvalues of Equation (6) is required at each of several reduced frequencies.

As shown in Figure 7(b), the eigenvalues tend to switch their position in the eigenvalue spectrum. Thus, each value of reduced frequency represents a point solution. The eigenvalues at one value of reduced frequency cannot be ordered with those at another value of reduced frequency. This is known as the mode tracking problem. Bhatia, Rudisill, and Cooper proposed two different approaches to solving this problem (see References 29 through 31). On the surface, these approaches appear to be quite different. On close analysis, however, they are found to be quite similar. Both approaches substitute derivative data for ordering data so that a point solution can be used to predict a crossing value. Bhatia's approach was based on a Laguerre iteration procedure.

A novel aspect of the Bhatia-Laguerre iteration is that it is carried out on the damping-reduced velocity ($g-v$) plane. This straightens out the modal characteristic curves and forces them to be single-valued. Rudisill and Cooper fitted a spline to the function value and its derivatives. They carried out their search on the ($\psi-v$) plane, where (ψ) is the damping (g) weighted by the square of the circular frequency (ω^2). This has the additional benefit of smoothing out the modal characteristics. After some study of these two methods, a new procedure was developed which may be described as a Taylor search on the ($g-v$) plane. All three procedures utilize the higher eigenvalue derivatives which may be calculated from the complex eigenvalues and vectors and the AIC derivatives. Convergence is cubic and closure may be achieved with as few as one or two iterations. The convergence is more rapid if the initial values of reduced velocity (v_o) are near the final converged values (v_F).

Damping derivatives are used to discriminate the various modal types. Hump modes can be identified from violent flutter modes on the basis of the damping derivatives. The iteration then determines the flutter match points and the tops of the hump modes. At the initial design point the starting values are a comb of reduced frequency points. Subsequent design points use the Taylor series of Equation (1) to locate the starting values of reduced velocity. Thus, the Taylor series approximation of Equation (1) serves as a "feedback con-

8-10

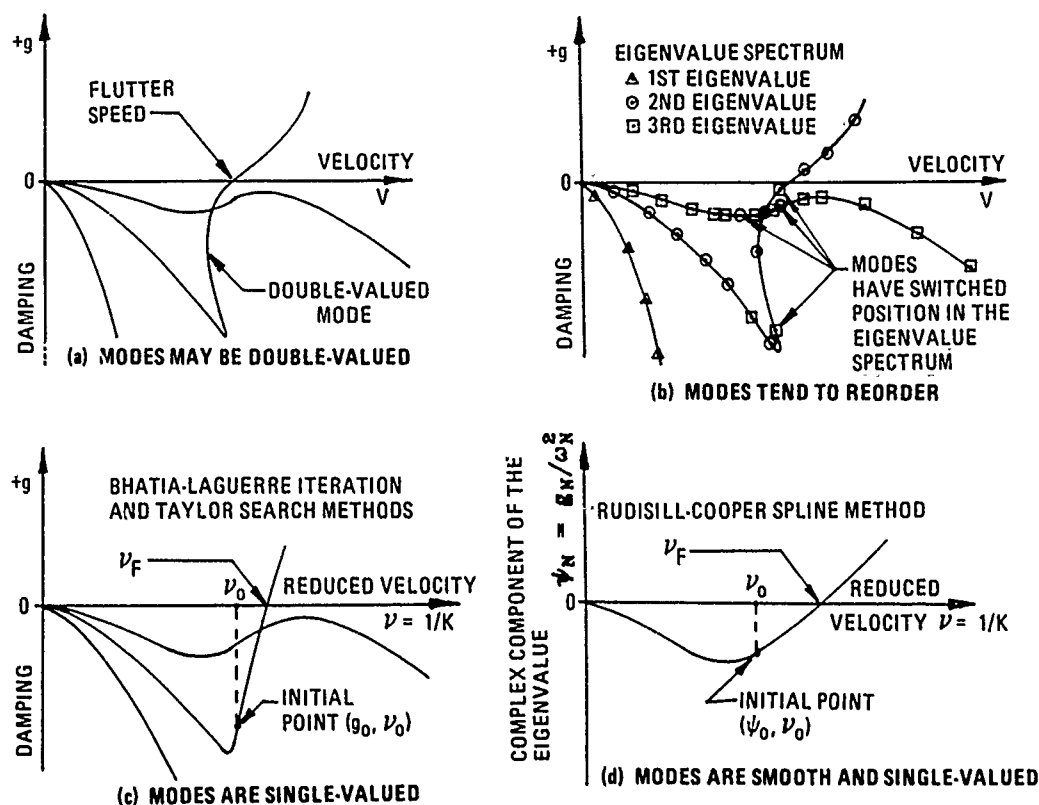


FIGURE 7. THE SEARCH FOR FLUTTER SPEEDS

troller" to track the flutter speeds in design space. When the flutter roots converge, the gradient and Hessian matrixes in Equation (1) may be updated. This provides for dynamic tracking of the flutter modes in design space.

With this last development, a strategy for the development of the Flutter Load cases Optimized Weight (FLOW) program began to evolve. The basic bulk data file would be read and stored in a structured data base for rapid reassembly. A set of global modes could then be computed by subspace iteration, as shown in Figure 8. The power of subspace iteration comes from the fact that, regardless of the size of the problem in physical coordinates, the eigenvalue problem solved is only on the order of the number of Ritz vectors used in the iteration. For flutter, a large number of Ritz vectors would be 50 to 80. The essential features of this iteration are a large-order decomposition followed by several solutions, transformations, and eigenvalue solutions.

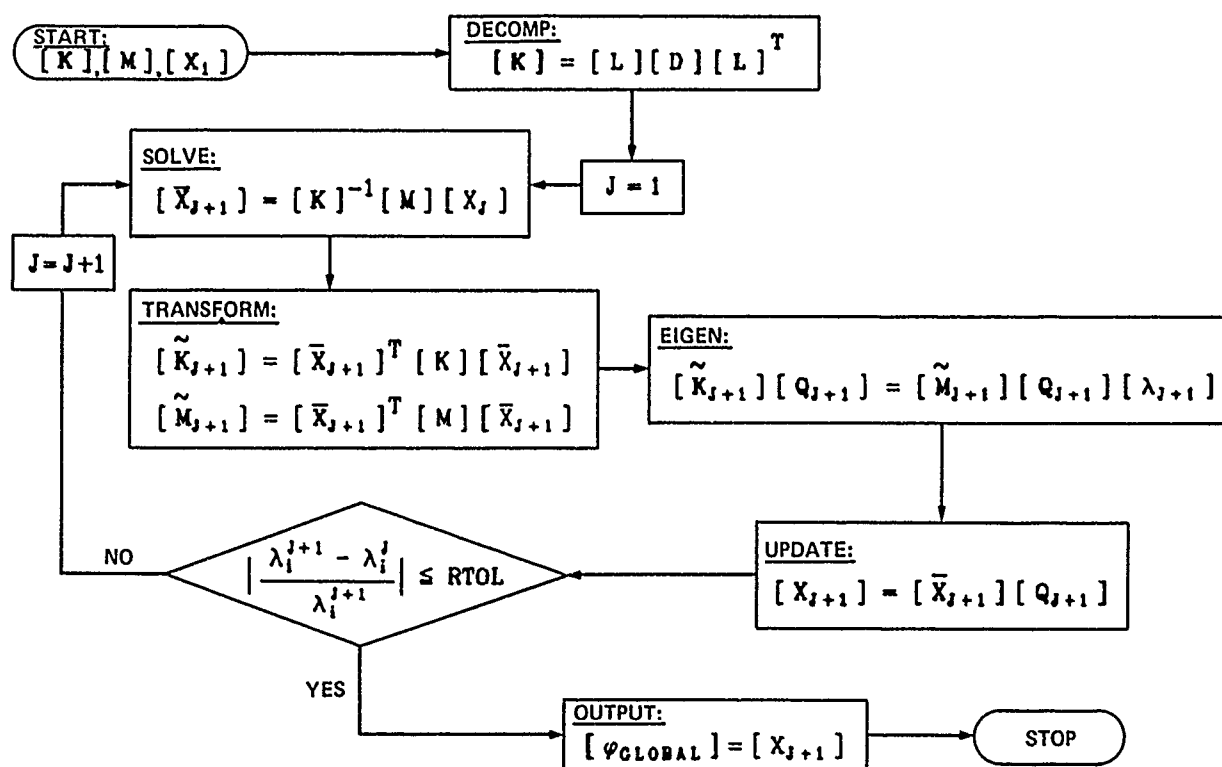


FIGURE 8. SUBSPACE ITERATION

This technique becomes attractive only when the decomposition, solutions, and transformations can exploit sparse matrix storage schemes. When this is possible, these operations can be performed efficiently in compressed storage. All sparse matrix schemes employ a directory of some type. To be efficient, this directory must be built up during the assembly of the global mass and stiffness matrix. Thus, the model assembly process is mated to the solution process. This large-order global modal solution is accomplished with the Global Assembler Solver. A simple, effective method for this assembler solver is the variable-bandwidth skyline technique developed by Bathe, Wilson, and Peterson and described in Reference 21. The advantage of this scheme is that it requires a minimum of directory space.

An integer vector containing the locations of the diagonal elements in vector store is all that is needed in this directory. The difference between any two successive entries in this vector is the number of elements in the skyline. For an out-of-core solution, both the directory and the stiffness matrix in vector store are divided into blocks of equations.

The next step was to select a library of finite elements for structural dynamics and flutter optimization. This library is shown in Figure 9. Nominally, this is the same library as is used by CASD and ARROW. In addition to the usual library of stringer, beam or frame members, shear panel, membrane, and thin shell elements, this library includes intranodal springs, nodal and eccentric lumped mass elements, and torque tubes as well as the general element.

The springs and general elements are required for modeling devices and are not generally resizable during optimization. Commercial aircraft often contain skins that are thick enough in places to require the inclusion of the bending stiffness of the shell. This is true even when the bending stresses may be ignored in the static analysis. Up to 60 percent of the weight of a commercial aircraft may be due to nonstructural mass items. The structural dynamics model must account for this nonstructural mass to bring the model up to weight and balance. This may be accomplished in three ways. In addition to the usual structural mass density, nearly all elements in the library have an associated surface mass density as well. During structural optimization, the portion of the element weight controlled by the material mass density is all that varies. Thus, it is necessary to distinguish between these two physical properties in the element. Nonstructural mass may also be lumped at the structural nodes. Heavy mass items may be located at or eccentrically to the structural nodes. To avoid structural short-circuits and the effect of unrealistic inertial moments, eccentric lumped mass elements are also required. These lumped mass elements compute space-averaged accelerations and return space-averaged inertia forces to the nearby structural nodes. Two or three structural nodes may be referenced by these eccentric lumped mass elements. Eccentric lumped masses may also be used for balance masses and are therefore resizable during structural optimization.

After several design steps have been taken using the approximate analysis of Equation (1), the derivative data in the Taylor series may have to be updated. This requires a model reassembly and modal update. It was realized that this model update could be performed in the modal coordinates of the global model, as shown in Figure 10. The structural data base, containing the bulk data from the modeler, is read by the assembler. These data are then sent to the subroutines which will generate the element mass and stiffness matrices and the element directory vector. The directory contains the global equation numbers spanned by the element equations. It is then used to extract the element modes from the global modes. The element modes, in turn, are used to transform the element mass and stiffness matrices to modal coordinates. The result is the contribution to the modal mass and stiffness matrix from each of the finite elements. A

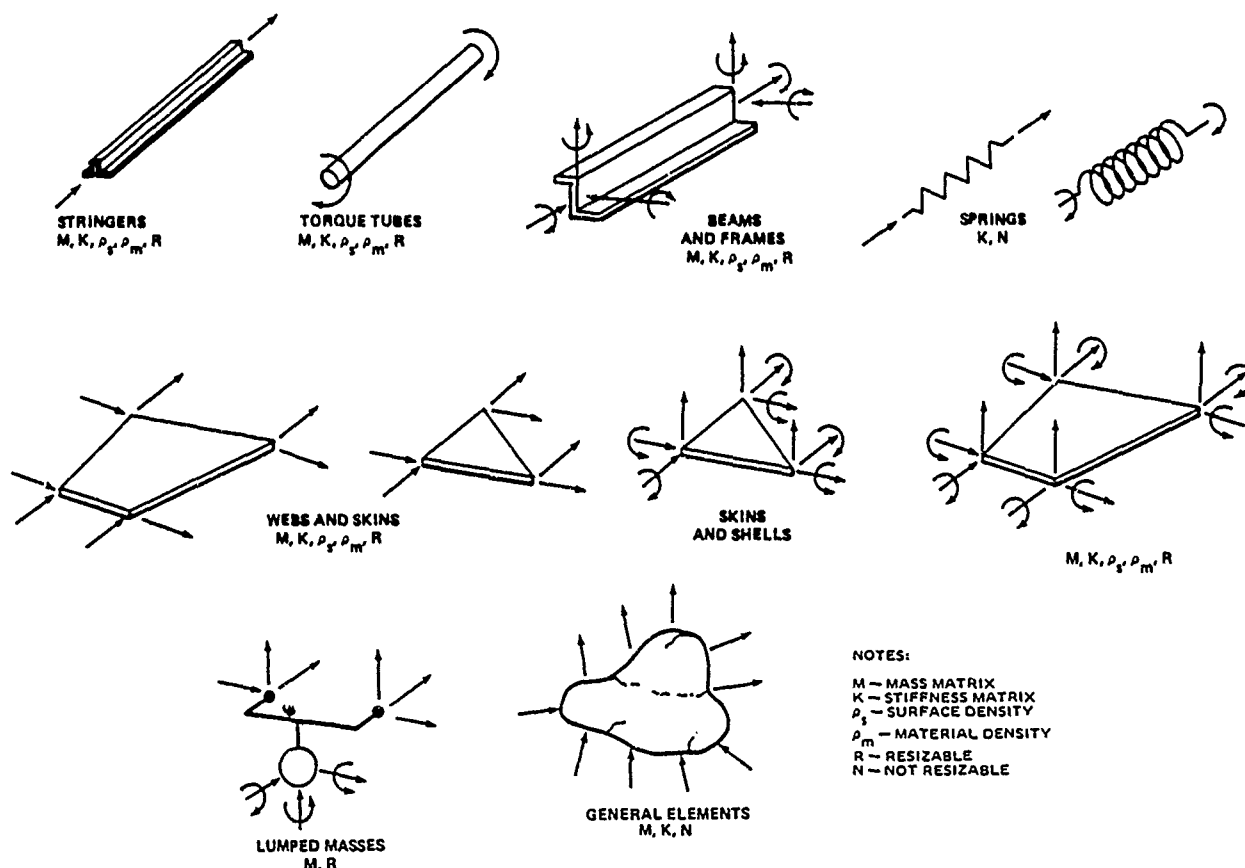


FIGURE 9. STRUCTURAL DYNAMICS LIBRARY OF REQUIRED FINITE ELEMENTS

8-12

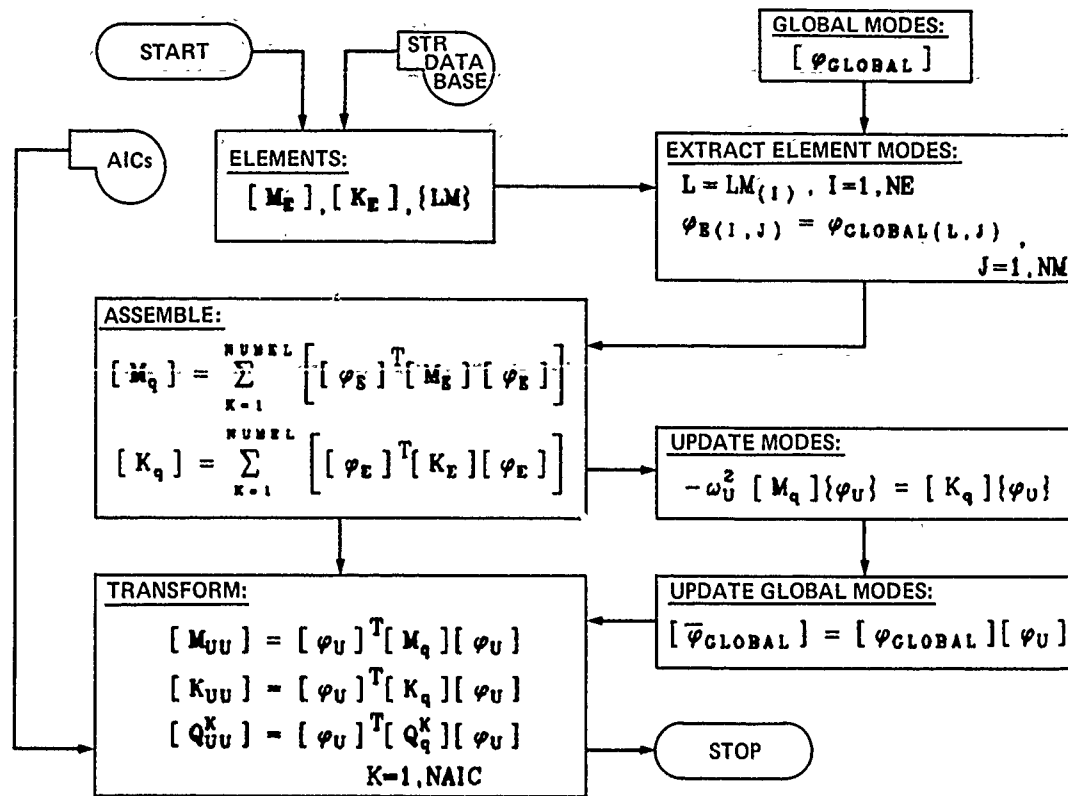


FIGURE 10. MODAL ASSEMBLER SOLVER

similar procedure is used to compute the element design derivatives in modal coordinates. The element modal mass and stiffness matrices are then summed to form the modal mass and stiffness matrices of the global assembly.

Since the design point has moved, these global modal mass and stiffness matrices will not be diagonal. Thus, following the assembly process, a modal analysis is performed to update the global modes. Following the modal update, the modal mass and stiffness matrices are reorthogonalized in the transform block. At the same time, the AICs are reduced to generalized coordinates and are updated by these new modes. Thus, the global modes serve as "Ritz vectors" to reduce the number of dynamic degrees-of-freedom. In this sense, the global modes serve the same function as the beam model representation of Figure 2. The modal update of Figure 10 is equivalent to one cycle of subspace iteration. Using this update procedure, the global modes will track one update step behind the optimizer in the design cycle.

For each flutter load case, a unique set of global modes is required since changes in the model may result in new or additional degrees of freedom. These changes may be due to fuel weights, cargo or passenger distributions, flap settings, or wing stores. To account for such variations, it was realized that some efficiencies in the assembler could be achieved. In every model there will be some basic elements which do not change and which are not resized by the optimizer. The elements under design form another class of elements. Finally, in each load case there will be a set of case-dependent elements. The summation in the model assembly block of Figure 10 may be separated into these three categories of elements. Then, as each new load case is encountered, only the case-dependent elements have to be generated and assembled.

When the model is assembled, the flutter and hump modes are located and the design sensitivities of the flutter velocities and damping factors are computed for each case.

Using these design sensitivities, the flutter velocities and hump-mode damping factors can be rapidly computed from a second order Taylor expansion like that in Equation (1). The objective function for the FLOW program is the structural weight. Structural weight is chosen as the merit function to be minimized since this parameter can be readily calculated from the finite element structural model. Other factors such as producibility and maintainability which affect the life-cycle costs cannot be readily computed from a structural model. The actual structural resizing occurs in a high-speed design loop which solves the nonlinear programming problem given by Equation (13).

Minimize:

$$F(D_1) = W_0 + \sum_{i=1}^{NDV} \frac{\partial W_1^0}{\partial D_i} (D_i - D_0) \quad (13.1)$$

subject to

$$G_J(D_1) = 1.0 - \frac{V_{FJ}}{V_R} \leq 0, \quad J=1, N_{FC} \quad (13.2)$$

and

$$G_J(D_1) = \frac{g_{HJ} - g_R}{g_{HMAX} - g_R} \leq 0, \quad J=1, NHC \quad (13.3)$$

And subject to the side constraints imposed to satisfy static strength and geometric requirements.

$$DLB_1 \leq D_1 \leq DUB_1, \quad I=1, NDV \quad (13.4)$$

The flutter optimization in the FLOW program is the third step in a sequential design process. Therefore, the lower bounds on the design variables are the initial design values set by the preceding static strength optimization.

As the first year ended, the functional block diagram of Figure 11 was drawn up. This diagram shows the features of the optimizer main processor or the FLOW phase of the FAST-FLOW program. The main analysis features including the structuring of the structural data base and computation of the global modes are in the front-end processor. The front-end processor is called the Flutter Analysis and Structural Transformation, or FAST, phase of the FAST-FLOW program.

The first year's work was completed with a report containing, in detail, the theoretical development of all equations and methods to be used in the FAST-FLOW program (Reference 32).

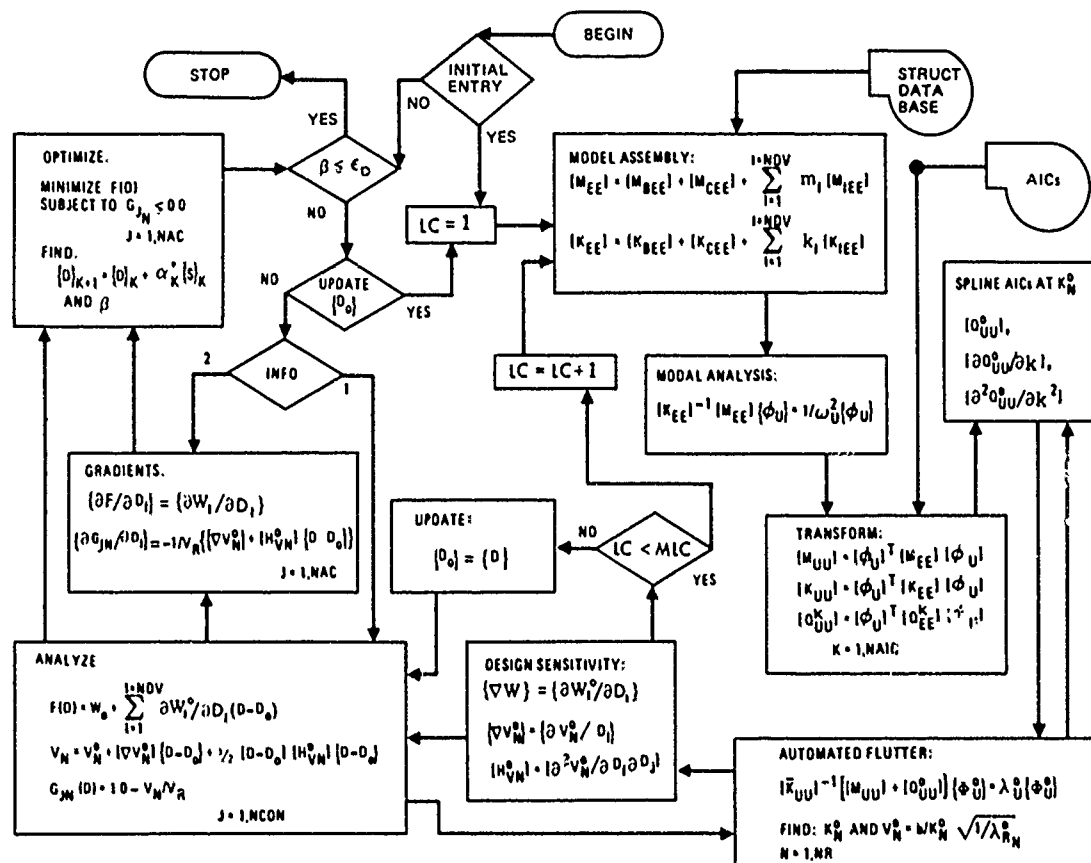


FIGURE 11. FLUTTER OPTIMIZER MAIN PROCESSOR (FLOW PROGRAM)

PROGRAM ARCHITECTURAL DEVELOPMENTS

In the succeeding years, a unique architecture for the FAST-FLOW program evolved. The theory of FAST-FLOW was expressed mainly in terms of matrix operations. The matrix abstraction operations in the FORMAT system were very inefficient. For this reason, a new matrix abstraction program was written for breadboard and checkout purposes. Using this program, functional subroutines can be checked out individually and in operation with other functional subroutines. Nearly 40 array operations can be invoked with direct matrix abstraction in the MATRIX program. These operations include manipulations on real or complex arrays with one, two, or three dimensions. From the beginning, the MATRIX program was designed to perform efficient array operations in compressed vector storage. Using this storage compression scheme, only the non-zero and unique elements are stored and processed.

FAST-FLOW is being developed in a modular fashion using top-down programming. All the modules are developed and tested in place in this system. A data base management system provides the data for this development from the data base. Cross-dependency between modules is eliminated through a system of task supervisors and subtask supervisors communicating through this common data base. This eliminates the need to communicate through common blocks. Each task supervisor is provided with a directory of array names which must be in the data base to perform the task. Failure to locate the required data in the data base results in a call to an error control program. This results in a diagnostic printout, program termination, and the generation of a restart file.

The task supervisor memory is limited to the array names needed to perform the task. The task supervisors locate the input objects and allocate space for the output objects. Scratch space required to perform the function is also allocated by the task supervisors. When all input, output, and scratch space is allocated, the functional routines are called. When the function has been performed, the output objects (arrays) are in the data base and the scratch space is purged. A system of subtask supervisors permits several task supervisors to use the same function. The task supervisors and subtask supervisors can be invoked by either the control program FLOWC or by direct matrix abstraction in MATRIX.

Data base management is achieved by the core and disk file management system of Figures 12 and 13. Each of these systems utilizes a dynamic memory. The core management system of Figure 12 utilizes a central memory in the form of a NAMES table in a common block. This common block is shared by the dynamic memory maintenance subroutines, ALLOC, FINDM, and DELETE. The central memory contains a six-character alphanumeric name and a tri-level name qualifier for each array in the virtual memory work space. The work space is initialized by a call to the REVISE program which sends the request through an assembly language program to the page supervisor of the operating system. This causes the work space to be allocated in one large contiguous block. This space is then cleared and initialized by REVISE. Subroutine ALLOC is responsible for allocating new arrays in the master work vector. The task supervisor allocates a new array by passing an array name, storage mode, and dimensioning information to subroutine ALLOC. This routine updates central memory with these data and reserves space in the master storage vector. The (N1) pointer to the start of information for the requested array is then returned to the task supervisor. The task supervisors can locate previously defined arrays by a call to FINDM. This will cause the data attributes of the array to be returned to the task supervisor. These attributes include the (N1) pointer, the dimensions of the array, and the storage mode.

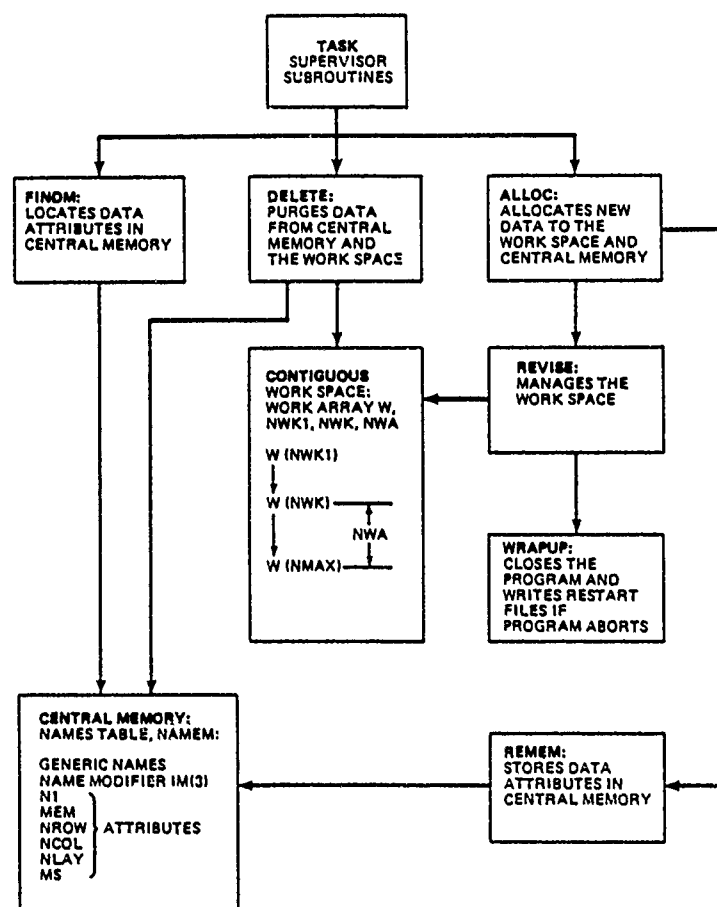


FIGURE 12. CORE MANAGEMENT

The storage mode attribute (MS) identifies the array as real, complex, or integer and the storage compression used to store the array. For sparse matrices, the directory is stored with the data. The memory length attribute (MEM) is then the space required to store both the data and the directory.

A task supervisor may purge an array from the master storage vector by sending the array name to DELETE. This will cause the array name to be removed from central memory and its associated space is then compressed out of the master storage vector. Data residing below the deleted information are moved up in the vector and their (N1) pointers are adjusted in this process.

Figure 13 shows the use of the disk file management system by the task supervisors.

The disk file management system consists of subroutines IOTAPE, IOREAD, and IOWRT. A basic protocol is established by the user communication with the system. The user may identify three types of files to the program, input, output, or scratch files. Input files are read-only files. Any attempt to write on an input file will be inhibited by the disk file manager IOWRT. This will result in a nonfatal error report of the Error Control program. Output files are write first, then read. No data overwrite is permitted on an output file.

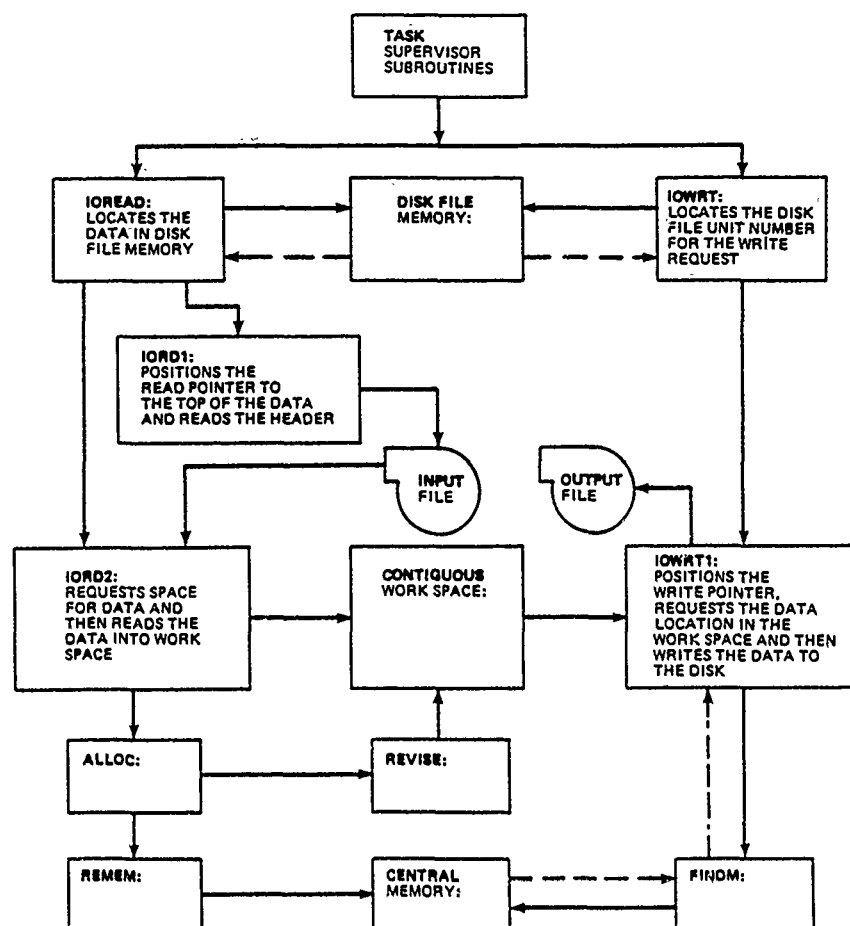


FIGURE 13. USE OF THE DISK FILE MANAGEMENT SYSTEM

Attempts to overwrite data on an output file are inhibited by IOWRT. Input or output files must conform to a sequential or random access file format. Scratch files are write first, then read. Data overwrite is permitted on scratch files and no special file format is required.

In a fashion similar to the dynamic central memory system, the disk file memory uses a dynamic directory. This directory contains the following information for every array on a disk: a six-character alphanumeric array name with a tri-level qualifier and the name of the file on which the array is located. The routine IOTAPE is executed once for each input file that is allocated. This is required to initialize the disk file memory. Then, when a request is made to read a particular array, it can be located in the disk file memory.

The data base management system involves only 11 subroutines. This system is designed to minimize data transfer.

Random access to the vector storage in virtual memory permits data to be used in place without data transfer. Data can be transferred from core to disk or from disk to core by transferring the entire array in one logical record.

Figure 14 shows the overall architecture of the Fully Integrated Flutter Optimization System of FAST-FLOW. Most of this system is now functional. Recently, a general-purpose optimality criteria resizer, OPCRIT, was developed. When checkout is complete, it will be added to the system. Figure 14 shows how a Master Control Program SUBC can select one of several optimizers. The system of Figure 14 provides for either analysis or optimization operation.

In an optimization run, the program operates in a push pull fashion between analysis and optimization functions. Analysis functions are selected by the user directives file. These are then interpreted by the Master Analysis Control Executive ANALC.

8-16

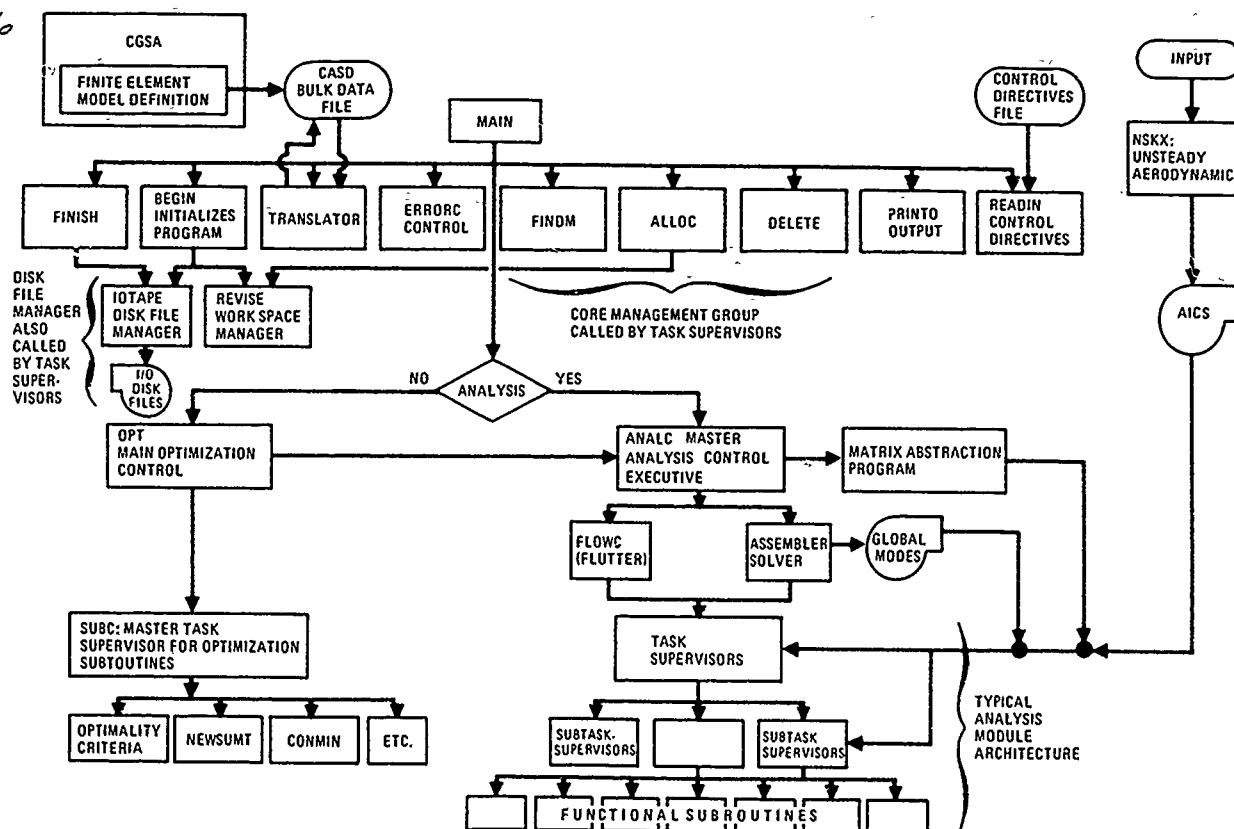


FIGURE 14. FULLY INTEGRATED FLUTTER OPTIMIZATION SYSTEM

CONCLUSIONS

Previous work has shown that flutter optimization is technically practical and feasible. The main emphasis in the FAST-FLOW development is on practical design optimization of complete aircraft configurations. To accomplish this, the development has been directed toward full finite-element idealization rather than beam models. Technical developments in computer hardware and software will allow structural models like that shown in Figure 3 to be used in practical advanced and preliminary design situations of the future.

The recursive nature of the design process will continue to demand efficient approaches to the evaluation of the flutter constraints. For this reason, FAST FLOW incorporates several innovations as well as conventional approaches. These include model reassembly in modal coordinates followed by a modal update. A fully automated flutter analysis using design sensitivities from a previous design cycle tracks the flutter modes dynamically in design space. Second-order Taylor approximations are used to evaluate constraints on both flutter and hump modes in a high-speed design loop. FAST-FLOW provides for structural optimization with constraints emanating from several fuel weights, payload configurations, and wing stores. FAST-FLOW also provides for design sensitivity updates during a fully automated design cycle.

REFERENCES

1. Warren, D. S. and Johnson, J. R., Structural Optimization of a Supersonic Horizontal Stabilizer. Paper presented at the 29th meeting of the Structures and Materials Panel Advisory Group for Aerospace Research and Development, Sept. 28 Oct. 8, 1969, Istanbul, Turkey.
2. McGrew, J. A., Douglas Aircraft Company, "Flutter and Dynamic Response Analyses Program C4EZ," Vol. I and II, MDC J6469, June 1973.
3. Purdy, D. M., Dietz, C. G., and McGrew, J. A., Douglas Aircraft Company, Optimization of Laminates for Strength and Flutter, Air Force Conference on Fibrous Composites in Flight Vehicle Design, Sept. 1972, Douglas Paper 6058.
4. Dodd, A. J., Douglas Aircraft Company, A Survey of the State of the Art in Structural Synthesis, April 1969, DAC-67698.
5. Dodd, A. J., Douglas Aircraft Company, Development of an Optimization Capability in Format, 1970, MDC-J0358. Second Report, 1971, MDC J5053.
6. Dodd, A. J., Douglas Aircraft Company, Static Optimization of Large Structures Using Optimality Criteria, 1980, MDC J7725.
7. Ahlman, A., Gladhill, T., Lee, P., and Tate, B., Douglas Aircraft Company, Computer Aided Structural Design, March, 1977, MDC J7487.

8. Warren, D.S., USAF, Applications Experience with the FORMAT System, Proceedings of the Second Conference on Matrix Methods in Structural Mechanics, 1968, AFFDL-TR-68-150, pp. 839-867.
9. Purdy, D. M. and Dietz, C. G., Douglas Aircraft Company, Optimum Design of Composite Primary Structure Aircraft Components, Oct. 1976, Douglas Paper 6452.
10. Haftka, R. T., Parametric Constraints with Application to Optimization for Flutter Using a Continuous Flutter Constraint, AIAA Journal, Vol. 13, No. 4., April 1975, pp. 471-475.
11. Haftka, R. T., Prasad, B., and Tsach, U., NASA, PARS - Programs for Analyses and Resizing of Structures, April 1979, NASA CR-159007.
12. Gwin, L. B. and McIntosh, S. C., USAF, A Method of Minimum-Weight Synthesis for Flutter Requirements, Parts I and II, June 1972, AFFDL-TR-72-22.
13. Gwin, L. B. and McIntosh, S. C., USAF, Large Scale Flutter Optimization of Lifting Surfaces, Parts I and II, Jan. 1974, AFFDL-TR-73-91.
14. McCullers, L. A. and Lynch, R. W., USAF, Dynamic Characteristics of Advanced Filamentary Composite Structures, Sept. 1974, AFFDL-TR-73-111.
15. Lynch, R. W., Rogers, W. A., and Braymen, W. W., USAF, Aeroelastic Tailoring of Advanced Composite Structures for Military Aircraft - Procedure TSO, June 1976, AFFDL-TR-76-100.
16. Sobieszczanski-Sobieski, J., From a Black Box to a Programming System. Remarks on Implementation and Application of Optimization Methods, Proceedings of a NATO Advanced Study Institute Session on Structural Optimization, Belgium, 1980.
17. Greene, W. H. and Sobieszczanski-Sobieski, J., NASA, Minimum Mass Sizing of a Large Low-Aspect Ratio Airframe for Flutter-Free Performance, May 1980, NASA TM-81818.
18. Kiusalaas, J., NASA, Minimum Weight Design of Structures Via Optimality Criteria, Dec. 1972, NASA TN D-7115.
19. Wilkinson, K. et al, USAF, An Automated Procedure for Flutter and Strength Analysis and Optimization of Aerospace Vehicles FASTOP Theory, Dec. 1975, AFFDL-TR-75-137.
20. Rudisill, C. S., and Bhatia, K. G., Optimization of Complex Structures to Satisfy Flutter Requirements, AIAA Journal, Vol. 9, No. 8, August 1971, pp. 1487-1491.
21. Bathe, K. J., Finite Element Procedures in Engineering Analysis. Englewood Cliffs, N.J.: Prentice-Hall, 1982.
22. Stroud, W. J., Automated Structural Design with Aeroelastic Constraints. A Review and Assessment of the State of the Art. The ASME Structural Optimization Symposium, 1974, AMD, Vol. 7.
23. Vanderplaats, G. N., NASA, CONMIN - A Fortran Program for Constrained Function Minimization, Aug. 1973, NASA TM X-62, 282.
24. Miura, H., NEWSUMT User's Guide, Cosmic-Barrow Hall, University of Georgia, 1977.
25. Vanderplaats, G. N., and Moses, F., Structural Optimization by Methods of Feasible Directions, Computers and Structures, Vol. 3. Elmsford, N.Y.: Pergamon Press, 1973, pp. 739-755.
26. Fox, R. L., Miura, H., and Rao, S. S., NASA, Automated Design of Supersonic Airplane Wing Structures Under Dynamic Constraints, April 1973, NASA-CR-112319.
27. Zoutendijk, G., Methods of Feasible Directions. New York: Elsevier Publishing Co., 1960.
28. Rudisill, C. S., and Bhatia, K. G., Second Derivatives of the Flutter Velocity and the Optimization of Aircraft Structures, AIAA Journal, Vol. 10, No. 12, Dec. 1972, pp. 1569-1572.
29. Bhatia, K. G., An Automated Method for Determining the Flutter Velocity and the Matched Point, AIAA Journal, Vol. 11, No. 1., Jan. 1974.
30. Rudisill, C. S. and Cooper, J. L., An Automated Procedure for Determining the Flutter Velocity, AIAA Journal, Vol. 10, No. 7, July 1973.
31. Cooper, J. L., NASA, A Curve Fitting Method for Solving the Flutter Equation, Dec. 1972, NASA CR-132629.
32. Rommel, B. A., Douglas Aircraft Company, Methods for Optimum Design of Aircraft to Satisfy Flutter Requirements, 1979, MDC J8535.

by I.W.Kaynes and D.E.Fry

Royal Aircraft Establishment
Farnborough
Hants, UK

SUMMARY

Methods have been developed for designing active control systems to alleviate the symmetric loads due to vertical gusts on a flexible aircraft. Techniques for choosing sensor positions and system gains are demonstrated, with the interpretation of results being aided by graphical methods that allow easy assessment of conflicting objectives and system constraints. A relatively simple model shows that loads in continuous turbulence can be alleviated by at least 50%, with ailerons driven by feedback signals from accelerometers at the centre of gravity and on the wing and with pitch stability augmented using the elevators. Manoeuvre loads are also alleviated. The methods are shown to be useful for predicting the potential of active controls at an early stage of design definition. The possibility of slight degradations from a number of sources is assessed, including more complex representations of the aileron actuator and the sensors, aileron rate limitations and different choices of gust model.

1.0 INTRODUCTION

This paper considers the benefits of load alleviation on a large flexible aircraft. Such structural applications of active control technology (ACT) have become operational, with the first system entering service on the Lockheed L1011 (1). This system allowed a more efficient aircraft to be created by extending the wing span of the basic design without the need for expensive modifications to increase its structural strength. This was the most effective solution to the limit load problem in this case.

The application of load alleviation at the initial design stage of a new aircraft potentially offers greater benefits than can be obtained on an existing aircraft. It is necessary to integrate the ACT system design with all the other relevant parts of the initial design process in order to reach an optimum configuration. Careful comparisons must be made between the weight, cost and complexity of an ACT system with alternative designs of the structure which might achieve the equivalent results in a passive manner.

In order to investigate ACT systems at the preliminary stages of design, it is required that the methods employed should not depend upon very detailed mathematical models of the aircraft, although in due course the predictions must be precisely defined on a full dynamic model, such as could be produced from analysis with FLEXSTAB (2). It is desirable that the physical implications of the results should be readily understood, since there are many possible configurations of systems to consider with variables including sensor type and position, motivator characteristics and selection, actuator performance and signal shaping filters.

This study of load alleviation has been based on the mathematical model (3) of a transport aircraft and has been restricted to using only existing control surfaces (elevator and symmetrically operated ailerons) as the active controls. This limitation has precluded investigations of the potential extra benefits which could result from actively controlling new motivators on the wing. No attempt has been made to modify the mathematical model to improve the performance of the active controls. In a fully integrated approach to the initial design of a new aircraft aeroelastic tailoring of the wing structure could both modify the basic loading response of the wing and also improve the effectiveness of the wing mounted control surfaces.

When considering the loading actions on an aircraft, such as gust encounters, manoeuvring and landing, it is often found that extreme gust encounters are the dominant effect on parts of the flying surfaces of large aircraft (the structures of combat aircraft are usually dominated by the manoeuvre loads). If it is possible to reduce some of the gust loads, then the weight of some flying surfaces may be reduced, to a lower limit set by either the extent of alleviation which can be achieved or by the point at which some other loading action becomes more critical to the detail design of the structure. The form of load alleviation investigated here is the reduction of the incremental bending moments at various wing positions produced by vertical turbulence, while monitoring other loads, responses and control surface activity. The main criterion for measuring the alleviation achieved is the amplitude of the load, which is directly applicable to the assessment of the aircraft strength required for encounters with extreme gusts.

The techniques employed in the exercise described here have included both classical control theory (frequency domain) and state space methods (time domain), facilitated by the use of the control simulation package TSIM (4). This is a command structured package which requires the equations of motion as input and then gives ready access to a full range of system analysis techniques. This interactive tool allows the designer to build up a greater understanding of the physical model than is possible with automatic numerical optimisations of the system, and is particularly aided by the graphical presentations of the results.

2.0 TURBULENCE MODELS

As described in the introduction, the objective of this study has been defined as the reduction of the gust loads which define the strength of the wing. It is necessary to refer to the current airworthiness requirements to find the descriptions of the gust environments which are currently the source of

9.2 stressing data for conventional aircraft. With the introduction of ACT, it is quite possible that there are new sensitivities and these may be inadequately described by the current requirements, since these have all been deduced from the measured loading patterns on conventional aircraft. By their nature, requirements tend not to have a great physical realism but cover present aircraft in a way which has been judged as satisfactory from past safety records. Extreme caution is necessary in eroding any of the hidden safety margins; for example, operational measurements (e.g. ref.5) with counting accelerometers were used to define the current 'gust' requirements, but the observations implicitly included manoeuvres and their effect has been combined into the 'gusts'. This emphasises the need to study a broader scope of data than the requirements alone, both to design a gust load alleviation system and also to assess its true effectiveness.

Considering first the current airworthiness requirements for structural design, these fall into the two categories of discrete gusts and continuous turbulence. The simplest forms of discrete gust models with any relevance to the present day are the ramp gusts of fixed length (100 ft. in the UK and 12.5 wing chords in the USA) which were used with simple 'heave-only' aircraft dynamics to convert the counting accelerometer data into the equivalent gust velocities, forming the basis of present day requirements. This class of discrete input has been included in this investigation by way of 1-cosine gusts rising to a maximum and returning to zero, as shown in fig.1a. The application of discrete gust models to aircraft certification in the UK now entails tuning the length of a gust to find the greatest response, the aircraft dynamics now including short period motion and flexibility. However, gust magnitude and gust length are assumed to be uncorrelated and it is not certain that gust data demonstrate this independence.

In the USA the power spectral density approach is now accepted as the main tool for strength assessment by the FAA. This makes the assumption that the turbulence is continuous and the spectral density of the vertical component is given by the von Karman one-dimensional spectrum.

Jones (6) has proposed a statistical discrete gust method (SDG) which addresses some of the shortcomings of both methods. The turbulence is represented as a series of discrete ramp gusts, the magnitude of each varying with its length H according to a $1/3$ power law for gust families of equal probability. The maximum of a response is defined by the greatest peak response to families of 1, 2, 4 or 8 constituent gusts with lengths and spacings chosen to give the largest peak. The magnitudes of the more complex gust families are reduced to allow for the lower probability of such patterns. It is only for lightly damped responses that a family of more than two gusts is the most significant. The SDG and PSD methods are related, for example by the $1/3$ power of H being mathematically connected to the $-5/3$ power of frequency dependence in the von Karman spectrum. However, SDG does have the advantages of time domain gust models, such as allowing some calculations of the behaviour of non-linear systems, with the added benefit of greater realism than the earlier discrete gust models. The initial family of gusts in the SDG method were smooth ramps of the '1-cosine' form (fig.1b) and these form the basic elements in describing most atmospheric turbulence. However, observations of disturbances (e.g. ref.7) suggest that some severe events may result from encounters with vortices. Jones has postulated additional vortex gust families (fig.1c) to describe these events within the framework of SDG (6). These are found to be crucial to the effectiveness of load alleviation, but the realism of the vortex patterns is open to questions as to the magnitude, shape and frequency of occurrence, since the data available on vortices are very sparse.

In the ACT design described in this paper attention has been paid to PSD, SDG and discrete gust models. For some aspects of system design it is convenient to utilise a simple turbulence model based in the frequency domain. Implementation of the turbulence spectrum as a filter applied to white noise requires that it be represented by a rational function. A first order filter was used with a time constant chosen such that, over the frequency range of interest, the band limited white noise spectrum obtained was a reasonable approximation to the von Karman spectrum with a realistic scale length. This representation of the turbulence spectrum was advantageous in that it may be expressed by a single differential equation, with consequent economy during the solution of the equations of motion. At high frequencies the band limited white noise decays with frequency to the power -2 , the same power as the Dryden spectrum.

It should be emphasised that all turbulence models considered here are symmetrical, vertical inputs to an aircraft flying on a level flight path. Real gust loading actions on the wings would also include the responses to gusts in other directions (that is, lateral and longitudinal in addition to the normal gusts) and the different patterns of loading produced by spatial variations of the normal gusts. These effects are likely to represent a greater proportion of the total gust loads for an aircraft with symmetric load alleviation than for an aircraft without such ACT.

3.0 DESIGN APPROACH

The general arrangement of the aircraft is shown in fig.2. Two pairs of control surfaces were modelled for the load alleviation systems, these being the elevator and symmetrically-operated ailerons. The actuators for the surfaces were modelled either as first or second order systems, with parameters chosen to represent the capabilities of currently available hardware.

The loads which were the objective of the gust load alleviation (GLA) were bending moments on the wing at approximately 30% and 60% of the semi-span. These positions were chosen as the inner and outer boundaries of the middle part of the wing which, on many aircraft of this class, is most sensitive to gusts for determining the design strength. It follows that this is the part of the wing likely to benefit from potential weight saving as a result of gust load alleviation. These bending moments are denoted by $BH20$ and $BH40$ and are normalised to give unit response to 1 m/s root mean square continuous turbulence for the datum aircraft.

The mathematical model allowed rigid aircraft freedoms of heave and pitch, forward speed

perturbation and flexible aircraft response in two symmetric elastic modes. The derivation of the model is described in ref.3 and the equations of motion are given in table 1. These were implemented under the simulation package TSIM with allowance for the acceleration and pitch rate sensors to be placed at any points on the wing and fuselage.

It was considered desirable to retain at least the same stability as possessed by the basic aircraft in the whole body and elastic vibration modes. A performance or cost function was now defined: requiring the minimisation of the bending moments with constraints on motivator activity and damping in the rigid aircraft and elastic modes, with the addition of monitoring the wing torques and fuselage accelerations. The means available were the two pairs of control surfaces operated by feedback from acceleration and pitch rate sensors placed at any points on the wing or fuselage. It was possible to utilise a numerical parameter optimisation program for this constrained optimisation problem, but with the large number of choices and freedoms involved this proved to be lengthy and unwieldy. Clearly optimal control theory applied with a large weighting on the bending moments could meet the criteria, but with a control law that would demand the feedback of all the states of the system, including those describing actuators, signal filters and disturbance inputs as well as the rigid and flexible freedoms of the aircraft. Many of these states are not available and so a reduced state or output state feedback reduction of the optimal control law would be required, to give a compromise solution based on state estimators. This requires a great deal of care and human interaction, and thus there is no guarantee that the estimators are chosen in an optimum manner and the unique advantages of the original optimal control law are lost. Moreover, the choice of sensor positions remains to be selected entirely by the designer. It was thus decided to adopt an approach which gave more insight into the physical situation and graphically demonstrated the salient features of the system to enable solutions to be reached interactively by the designer.

In the first stage of basic aircraft stabilisation it was found that a simple feedback of pitch attitude to the elevator effectively eliminated the phugoid oscillation with little effect on other aircraft responses. The basic aircraft with this stabiliser added was regarded as the datum case for later comparisons. To augment the stability of the short period mode it was also sufficient to activate only the elevator, utilising pitch rate feedback in this case and a gain chosen from a point on the root locus which gave a relative damping greater than 0.5 and a higher short period frequency. The eigen values are given in table 2. These changes are known to improve handling qualities with a better transient response to pilot inputs. In general, manoeuvring aspects have not been considered in this paper since it was assumed that appropriate shaping filters on the pilots demands could produce any required modifications to handling characteristics. Although not specifically designed for the task, it is shown in section 6 that the gust load alleviation system can also serve to alleviate manoeuvre loads. These problems have been addressed more fully in a study (8) of active control systems and their structural implications on a combat aircraft, for which manoeuvring flight is inherently more significant. In continuous turbulence the modified short period characteristics were found to reduce greatly the pitching responses and also make a mild improvement to most loads and accelerations.

The aileron was the primary motivator available for alleviating wing loads, but the power of this surface is small in relation to overall gust loading on the wing. This is apparent by examining the control effectiveness in comparison to the wing lift under the linear model: in quasi-steady restrained level flight, it is necessary to apply approximately 60 degrees of aileron to counteract the entire incremental lift of the wing resulting from a gust of 11 m/s. This gust corresponds to a change of 2.5 degrees in the aircraft incidence and would produce an acceleration of 1 g at the centre of gravity of the basic aircraft. However, the most critical gust design loads are likely to be the bending moments on the inboard parts of the wing. Since the aileron is near the wing tip it is more effective in modifying this moment than in changing the overall lift; for the above example, an aileron angle of 30 degrees is required to eliminate the quasi-steady incremental bending moment near the wing root. The aeroelastic reduction of aileron effectiveness is included in these aileron characteristics. These considerations of bending moment on the wing of a restrained aircraft give a guide to the potential alleviation. Rather less alleviation of the bending moments is predicted if the aircraft is allowed freedom to respond in pitch. This is caused by the pitching moment of the aileron, which acts to increase the aircraft incidence and hence the loads, in opposition to the restoring moment from the natural stability of the aircraft.

The output quantity most directly related to the wing loads induced by normal gusts is normal acceleration. The centre of gravity is the position at which accelerometers have been mounted in the past for a good overall indication of turbulence response and loads at the wing root. It was thus an obvious first choice to control the ailerons by feedback of normal acceleration sensed by an instrument mounted on the structure at a point near the centre of gravity. This sensor gives only a general measure of the aircraft heave response and it does not provide adequate information on the pitching and elastic mode responses, these freedoms being wing load constituents that are more important for outboard wing stations. The extensions that suggest themselves are then either to move the sensor to a more effective position for the particular load to be alleviated or to augment the signal by adding another accelerometer at some other position on the aircraft. Both strategies are demonstrated here and the presentation of results allows the best system to be selected for any model of the aircraft and control systems. This is especially useful when investigating the sensitivity of the GLA capabilities to different models of the aircraft, the sensors and the actuator dynamics. In the system design process the continuous turbulence model is the basis for response evaluation and the systems thus defined are later assessed under other turbulence models.

4.0 SYSTEM DEFINITION

A block schematic of the general gust load alleviation system is given in fig.3. Pitch attitude and filtered pitch rate are fed back to the elevator and the outputs from normal accelerometers are filtered and fed to the ailerons. The elevator actuation mechanism is represented by a first order lag.

9-4 First order filters were applied to the pitch rate and acceleration signals. The time constants for these were initially chosen to represent the filters which would be required to reduce the unwanted input resulting from structural responses at frequencies higher than those contributing to the loads. These frequencies also correspond to the higher modes not explicitly described in the aircraft equations of motion, for the same reason. Detailed study showed that benefit could be gained from modifying the filters as part of the design process, for example to affect a pole position. However, more refined use of signal shaping filters was not attempted; this is a field which will be aided by more advanced techniques of pole and zero manipulation.

Gust load alleviation systems were studied for three different levels of actuator and instrumentation modelling, named systems A1, B2, C2. In A1 the aileron actuator is represented by a first order filter with a time constant of 0.05 seconds, whereas for B2 and C2 the actuator is modelled in second order form with damping 0.7 and natural frequency 100 rad/s. The latter value was chosen as an easily achievable frequency for practical use, representing a lower rate capability than the actuators which had been flying for some years in the fly-by-wire Hunter. It was found necessary to increase the time constant of the shaping filter on the signal from the centre of gravity accelerometer from 0.05 to 0.1 seconds. This change was to improve stability at some gain values, thus facilitating the selection of gain values. Both systems A1 and B2 have the assumption that perfect sensors are available to measure the instantaneous acceleration and pitch rate at their mounting points on the structure of the aircraft. System C2 is the same as B2 but with the addition of sensor characteristics: the accelerometer is modelled by a second order filter of damping 0.7 and natural frequency 60 rad/s and the pitch rate gyro is represented by a first order filter with time constant 0.05 seconds.

The first system investigated was the simplified configuration in which the only accelerometer was one at the centre of gravity. For a model of the form of system A1, increasing the gain on this accelerometer up to 10 deg/g reduced the bending moments BM20 and BM40 to 70% and 52% of the datum values of continuous turbulence response. However, this was at the cost of reducing the damping in the second flexible mode from 5.4% to only 2.2%. For the model B2 (including actuator characteristics) there are similar results and the system C2 (incorporating sensor responses) gives the less optimistic load alleviation values of 75% and 62% for BM20 and BM40 respectively.

It is clearly unsatisfactory for a GLA system to cause such a reduction in the damping of a structural mode. The physical mechanism for this tendency towards instability is explained by the shape of the second elastic mode. There is a node on the wing at approximately two-thirds span and this is inboard of the aileron. Deflecting the aileron downwards (for example) will produce an upward acceleration of the whole aircraft in the heave mode and also a distortion in the elastic modes with upward acceleration at the wing tip. At a sensor inboard of the node, however, the acceleration in the second mode will be downward and thus amplified by the control system if this is working to reduce the dominant upward heave acceleration.

A more stable system may be possible if the sensor is moved to fuselage positions other than the centre of gravity. Given two variables in the control system as the sensor position and gain, the technique of plotting contours of responses has been found most indicative of the nature of the compromises to be made in choosing values for these variables. Under the simulation package TSIM the eigen values and continuous turbulence responses were calculated for a small number of gains and sensor positions and these results were then processed to give the contour plots shown in fig.4. The first picture shows the variation of the inner bending moment, BM20. It is seen that for the gain considered the alleviation improves as the gain is increased. The best position for the sensor is slightly forward of the centre of gravity. The outer bending moment, BM40, is shown in fig.4b and demonstrates a clear upper limit to the gain required. For gains above 10 deg/g the alleviation is degraded and a gain must be chosen with a view to achieving the optimum balance between BM20 and BM40 alleviation. For a practical design, this choice would be based on the relative importance of gust loading in defining the structure at these points. The rates of movement of the aileron are illustrated in fig.4c, the units being deg/s for 1 m/s r m s turbulence. All the values are within the capabilities of present day hardware. Fig 4d shows the contours for the minimum damping value in the system eigen values. The least damped mode generally corresponds to the second elastic mode of the aircraft. The damping increases as the sensor is moved forwards of another node, at a position of 12m ahead of the centre of gravity. The fuselage positions which yielded best alleviation are also seen to correspond to the lowest damping and so fuselage positioning is not the source of a GLA system with good damping properties on this model.

In view of the interaction between the GLA system and the second elastic mode, it was considered likely that improved performance could result from mounting a symmetric pair of accelerometers on the wings instead of a single sensor on the fuselage centre line. Responses were calculated for a range of gains on the combined accelerometers with the mounting positions varied across the wing from root to tip near the trailing edge. The results are presented as contour plots in fig.5. The minimum damping contour clearly shows that damping is degraded below the basic aircraft value for all points inboard of the nodal line. However, although the load alleviation and damping are improved for a wing tip position, the cost is that the rate of aileron movement increases dramatically. 3 deg/s per m/s gust input corresponds to the performance limits of typical actuators. Since the model is linear, this may be scaled up for severe turbulence, for example a root mean square value of 4 m/s corresponds to a root mean square aileron rate of 12 deg/s. Under the assumption that the turbulence is Gaussian this implies that the aileron rate would be below 36 deg/s (three standard deviations) for 99.7% of the time in this turbulence patch. A heavy line repeating this upper limit 3 deg/s per m/s aileron rate contour has been superimposed on the plots. By examining the values of the other quantities along this line it is easy to assess the most effective sensor position. This is seen to be at about 0.4 span, with values of 64% and 44% for the loads BM20 and BM40, but this has been achieved with a minimum damping of approximately 3%. This is a lower damping than the basic aircraft and is only a little better than the value reached with a single accelerometer at the centre of gravity.

The next logical step towards defining an efficient system was to combine the good load alleviation properties of accelerometers near the fuselage with the damping improvements from sensors on the outer wing. This adds extra dimensions to the control law design problem, which were reduced by considering

the most extreme system of an accelerometer at the centre of gravity and a symmetric pair of accelerometers near the wing tip trailing edge. Taken individually, these positions have yielded, respectively, the best load alleviation at lowest aileron activity and the most heavily damped control system. 9-5

The design problem in this case is to find the best combination of gains on the two accelerometer channels. Contour plots are shown in figures 6 and 7 for the responses of systems A1 and C2 to a range of gains on the centre of gravity accelerometer (ANZB) and the wing tip accelerometers (ANZW). The bending moment plots, such as figures 6a and 6b, show the load alleviation achieved. The origin represents the pitch stabilised aircraft and moving up the vertical axis shows the effect of increasing the gain on a controller using feedback from the centre of gravity alone. This signal is dominated by the heave acceleration, with no pitching contribution and only small elastic mode components. Adding the feedback from the wing tip sensors contributes both an additional element of heave acceleration and also the new form of response from both the pitching and structural deformation accelerations. The gain on heave acceleration is thus now the sum of ANZB and ANZW and if the pitching and elastic mode contributions were absent then the contours of constant alleviation would consist of lines at 45 degrees to the axes, that is connecting points at which $(ANZB + ANZW)$ is constant. It is seen that this 45 degree line effect dominates the bending moment plots and reductions below the values at the vertical axis intersections represent the improvements resulting from the use of multiple sensors. Both fig.6a and 6b show the same form of a valley at 45 degrees to the axes and sloping down to lower values as the wing tip acceleration gain is increased. If the bending moment at more than one wing station is included in the alleviation objectives then a compromise must be made, because the valleys on the BN20 and BN40 contour plots have different positions (a larger gain is required to alleviate the bending moment nearer the wing root). A conflict arises in that the alleviation of a load is restricted by the aileron rate which may be achieved and this in turn is closely related to the gain on the wing tip acceleration. Fig.6c exemplifies this cost of alleviation: the larger high frequency output from the wing tip signal dominates the demanded aileron rate. The effect on this quantity of increasing gain ANZB is much less than the effect of ANZW and this is shown by the nearly vertical nature of the contours in this figure. Only small gains on the wing tip accelerometers are sufficient to improve the damping (fig.6d) to the level of the basic aircraft, a result which can be attained in conjunction with the acceptable aileron rates. A good insight into the balancing of the system design compromises is obtained from the plots and the choice of gain values can be made as a considered balance of all the benefits and detriments.

For system A1 the gain values chosen for ANZB and ANZW were 9.22 and 3.64, as marked by a cross in fig.5, and these values gave a large reduction of both loads while keeping an aileron activity of 3 deg/s per m/s gust input. For system C2, including the sensors and second order actuator models has reduced the potential load alleviation since the aileron rate activity has been increased. Consequently, a lower value of 2.56 was chosen for gain ANZW in conjunction with an ANZB value of 9.78. The gains for all the systems are summarised in table 3 and the bending moment alleviations are given in table 4. The most notable difference between the three systems is that the second order actuator produces more aileron activity at higher values of the wing tip gain ANZW. This has little bearing on the system definition since the differences are small for low ANZW gains, and such values are dictated by the assumed maximum aileron rate.

5.0 CHARACTERISTICS OF THE LOAD ALLEVIATIONS SYSTEMS

Three gust load alleviation systems have been designed and assessed by reference to their effect on aircraft response to a particular model of continuous turbulence. This input was chosen with regard to convenience for control system design and economy of computation. In this section it is demonstrated that the results obtained are not over-sensitive to changes from the basic mathematical models, allowing the conclusion that a relatively simple model of the controlled aircraft may be used in the initial design stage to indicate the potential of GLA. Factors considered include the number of elastic modes, the sensitivity to other turbulence inputs and non-linear behaviour of the aileron actuators. It has been shown that modelling the sensor and actuator dynamics does not change the fundamental behaviour of the GLA systems, although it does improve the final accuracy.

5.1 Number of elastic modes

The aircraft model in this investigation was reduced from sixteen to two elastic modes by the method of residual stiffness (3). It is possible that some of the discarded higher frequency modes could interact with the control system to cause instability, despite the low frequency low-pass filters applied to the sensor signals. The calculations for the contour plots of fig.7 (system C2) were repeated with six elastic modes explicitly retained in the model. The damping plot is shown in fig.8. By comparison with fig.7d it is seen that there has been little change for small gains on the wing tip accelerometers, but for gains above 6 deg/g there is a reduction of damping and instability is reached at 10 deg/g. As has been discussed above in connection with the effect of actuator models, differences for such large gains are not of practical significance since the aileron rate restriction precludes their use. For gains of 6 deg/g or less on the wing tip accelerometers there was little difference between the contour plots of bending moments or aileron rate for two or six elastic modes. This confirms the adequacy of the two mode model for the initial design. It is always possible that a mode at higher frequency can interact with sensor or motivator position to create stability problems, but it is anticipated that such complications can be handled by signal shaping. This should cause little degradation of the load alleviation, since this mainly results from reducing the loads associated with the short period mode and changing the characteristics of response in the first elastic modes. This is shown by the Bode plots (fig.9) for system C2 with two elastic modes, with the dashed lines representing the datum aircraft.

9-6 5.2 Response to discrete gusts

The load alleviation systems have been designed for continuous turbulence. It is necessary to consider different forms of input in order to check for undue model sensitivities of the load reductions achieved. The additional gusts examined here are discrete gusts described in section 2.

The response of system A1 to a '1-cosine' gust of 40m length is illustrated in fig.10. The datum aircraft responses are shown by the dashed lines. This short gust excites the elastic modes and the diminished excitation and greater damping of the wing bending under the GLA system are indicated by the trace of wing tip acceleration NZW. It is apparent that the bending moments BM20 and BM40 have both been significantly reduced. The amplitude of aileron deflection reaches a peak of 16 degrees and a maximum rate of 200 degrees per second. The only detrimental effects are seen to be a slight increase in the acceleration at the nose (a result of the reduced pitch response) and significant increases in the wing torque TQ40.

The reduction in peak bending moments for this gust is similar to that predicted by the continuous turbulence model. A more complete view is given by considering a range of gust lengths: fig.11 shows the peak responses reached for all systems for 1-cosine gusts from 25m to 400m length. The second row of table 4 gives the overall load alleviations, which are found to be similar to continuous turbulence for BM20 but generally poorer for BM40. These differences are reduced when the gust magnitude is varied in proportion to gust length to the power one-third, as proposed by Jones (6) in the statistical discrete gust theory. When the full SDG model is applied, including families of gusts, the load alleviation is almost identical to the continuous turbulence predictions (table 4), reflecting the mathematical relationship between PSD and SDG discussed in section 2. Jones (6) has postulated a family of vortex gusts of varying diameter and related magnitude (fig.1c). The largest gust velocities occur for a vortex of diameter (length across the core) 30m and for the datum aircraft that also produces the maximum bending moments. This is found to remain true when the load alleviation systems are added and the bending moments are reduced more effectively than was the case for the other forms of turbulence input, as shown in table 4. The time responses for system A1 are shown in fig.12, with the datum aircraft represented by dashed lines. The reduction of the bending moments is apparent. Maximum aileron deflection is less than 10 deg but the aileron rate reaches 200 deg/s, which is possibly excessive for typical hardware.

5.3 Effect of aileron rate limits

A major concern in the application of gust load alleviation to large aircraft is that the aileron power controls may not be able to operate as quickly as required to alleviate rapid loading actions. It has been demonstrated in section 4 that the contour plots of aileron activity allow control law gains to be chosen so that the activity is minimised, but this conflicts with the degree of alleviation which may be achieved. Given the statistical nature of the PSD turbulence model and its method of application, it is possible to state only the frequency with which the aileron rate demand would be expected to exceed any particular level. The potential alleviation of loads would be small if the gains are set at such low values that the demand keeps within the practical capabilities of the power control for all gust encounters anticipated during an aircraft's life. Consequently, it is necessary to examine the effects of saturation of the aileron control. This is modelled here by introducing levels below which the rate demand to the aileron is limited. The sample levels which have been tested are 60 and 120 deg/s, which represent, respectively, the capabilities of a conservatively rated modern actuator and of an actuator typical of those presently used for ACT applications. Since saturation against the rate limit is a non-linear effect, the PSD approach becomes invalid and attention is restricted to analyses in the time domain. These include the SDG method and it should be remembered that the PSD and SDG results were in close agreement for linear systems, suggesting that the methods are indeed modelling similar characteristics of atmospheric motions.

The effects of the aileron rate limits are most severe for short gusts with lengths between 30m and 75m. The system A1, with the first order actuator model produces the greatest aileron rate demands and is thus most influenced by the rate limits. Table 4 shows that alleviation capabilities of the three systems are almost identical under the 60 deg/s limit. The outer wing is more sensitive to rapid aileron movements and so BM40 is more affected by the rate limits than BM20. The differences between turbulence models have been emphasised for BM40; the most pessimistic alleviation is predicted by the 1-cosine gusts, but it is likely that this could be improved by tuning the system if this gust model was significant. A new version of system A1 could be chosen so as to demand less aileron activity by imposing a limit lower than 3 deg/s per m/s in the selection of gains from fig.6. A reduction in the wing tip accelerometer gains would achieve this at the expense of slightly less alleviation of BM20 and reduced damping of the elastic modes.

6.0 MANOEUVRE LOAD ALLEVIATION

Manoeuvring flight had not been considered during the design of the GLA systems. It was assumed that any handling deficiencies or unfavourable loading actions that arose could be offset by controlling the ailerons with signals suitably derived from the pilot inputs. To check the feasibility of this approach the aircraft characteristics were checked for a pull-up manoeuvre. This was defined as a rapid pitch demand reaching a maximum, steady value in 0.1 seconds, acting through the first order model of the elevator actuator to deflect the control surface.

For the basic aircraft this pull-up produced a maximum pitch rate after one second and a maximum acceleration at the centre of gravity (NZB) after two seconds. These times are typical for a rapid manoeuvre; longer time scales are not considered here because it is likely that thrust changes would then be made. Applying the same pilot demand with the GLA system A1 engaged gave lower responses in

pitch rate and acceleration than for the basic aircraft. In order to compare the loads for the same amplitude of manoeuvre, the demand was scaled up by a factor of 1.55 to give aircraft motion very similar to that of the basic aircraft. This could be implemented easily by applying a gain to demand signals when the GLA was operating. The responses are shown in fig.13. 9-7

The bending moments are both reduced to about one-third of the basic aircraft values (as shown by dashed lines). This results from the ailerons responding to the acceleration in the correct manner to reduce the loading near the wing tips and hence achieve the 'classical' form of bending moment relief. The change in load distribution causes the reversal of the outer wing bending moment BM40. The pitching moment from the aileron assists in achieving the demanded pitch rate despite the detrimental effect on overall lift. However, aileron deflection is double that on the elevator of the basic aircraft and this could limit the alleviation available in extreme manoeuvres.

7.0 CONCLUSIONS

Methods of designing active control systems to alleviate the symmetric loads due to vertical gusts on a flexible aircraft have been developed. Based on the control simulation package TSIM, the interpretation of results has been aided by techniques including a pictorial presentation that allows easy assessment of conflicting objectives and system constraints.

A system has been designed to alleviate the incremental bending moments at two wing stations with ailerons driven by feedback signals from accelerometers. It was found that the most effective sensor configuration was one at the centre of gravity and a symmetric pair at the wing tips. The gains for these accelerometers were chosen from contour plots of responses. Compromise values were readily located such that both loads were reduced by at least 50% with aileron activity held to a chosen level. The control laws are compatible with a pitch stabilisation system and stability has been found to be maintained when checked on models including up to six elastic modes. The results are only a little degraded by including a more complex mathematical model of the aileron actuator and models of the response characteristics of the accelerometers and the pitch rate gyro. This supports the application of simple models to estimate the potential of load alleviation systems at the early design stage of an aircraft.

The gust load alleviation systems were designed from continuous turbulence analyses and when checked on the statistical discrete gust method similar alleviation was attained. The alleviation predicted for 1-cosine and vortex discrete gusts were rather less optimistic in some cases. The influence of aileron rate limitations were investigated and the decrease in effectiveness of the load alleviation systems was only significant for the conservative rate limit of 60 deg/s.

The gust load alleviation systems were demonstrated also to make significant reductions in manoeuvre loads, with handling unaffected if the control laws included a simple gain applied to the pilot demand signal.

REFERENCES

<u>No.</u>	<u>Author</u>	<u>Title</u>
1	R.F O'Connell	Design, development and implementation of an active control system for load alleviation for a commercial transport airplane. AGARD R683 (1979)
2	Air Force Flight Dynamics Laboratory	A method for predicting the stability characteristics of control configured vehicles. AFFDL TR 74-91 (1974)
3	I.W.Kaynes	The implementation of the longitudinal equations of motion for a flexible aircraft. RAE Technical Report 83024 (1983)
4	M.J.Corbin J.S.Winter	TSIM - a combined analysis package for the design of flight control systems. RAE Technical Memorandum FS 185 (1978)
5	S.D.Ellis	A presentation of measured aircraft responses in turbulence during civil operations. RAE Technical Report 78113 (1978)
6	J.G.Jones	Modelling of gusts and wind shear for aircraft assessment and certification. Proc. Indian Acad. Sci. (Eng. Sci.) Vol 3, part1, pp 1-30 (1980)
7	A.Burns	On the nature of large clear air gusts near storm tops. RAE Technical Report 72036 (1972)
8	D.E.Fry I.W.Kaynes	The design of ride control and manoeuvre load alleviation control systems for a flexible combat aircraft. RAE Technical Report 82020 (1982)
9	I.W.Kaynes	Gust load alleviation on a flexible aircraft. RAE Technical Report 82063 (1982)

LIST OF SYMBOLS

AIL	symmetric aileron deflection, degrees
ANZB	gain on CG normal acceleration feedback to aileron, deg/g
ANZW	gain on wing tip normal acceleration feedback to aileron, deg/g
BM20, BM40	bending moments at 30%, 60% spanwise positions on wing (factored for unit response in continuous turbulence)
ETA	elevator deflection degrees
e_1, e_2	displacement in elastic modes
G_q	gain on pitch rate feedback to elevator, deg per deg/s
G_0	gain on pitch attitude feedback to elevator, deg/deg
H	gust length, m
NZA	normal acceleration at nose, g
NZB	normal acceleration at centre of gravity
NZW	normal acceleration at wing tip
Q	pitch rate measured on structure near centre of gravity, deg/s
q	pitch rate aircraft, rad/s
SAIL	rate of change of aileron deflection AIL, deg/s
SETA	rate of change of elevator deflection ETA, deg/s
TQ20, TQ40	torques at 30 and 60 spanwise positions on wing (factored for unit response in continuous turbulence)
U_0	parameter defining gust amplitude in SDG method
u	perturbation of aircraft forward velocity, m/s
w	perturbation vertical velocity of aircraft, m/s
WGUST, w_g	vertical gust velocity, m/s
ζ_A	damping of record order aileron actuator
ζ_I	damping of accelerometer
η	elevator deflection, rad
θ	pitch attitude, rad
τ	symmetric aileron deflection, rad

Table 1

EQUATIONS OF MOTION

Aircraft velocity = 250 m/s

$$\begin{aligned}
 \ddot{u} &= -0.0132\ddot{u} + 9.816 \\
 \ddot{w} &= -0.0856\ddot{u} - 0.9903(\ddot{w} + \ddot{w}_g) + 241.7\ddot{q} + 0.9504e_1 = 0.000725e_2 + 21.73e_1 + 18.08e_2 + 6.806\ddot{\eta} + 9.275\ddot{\eta} \\
 \ddot{q} &= +0.000174\ddot{u} - 0.0159(\ddot{w} + \ddot{w}_g) - 0.9883\ddot{q} + 0.0323e_1 + 0.1045e_2 + 0.485e_1 + 3.32e_2 + 1.77\ddot{\eta} + 0.7986\ddot{\eta} \\
 \ddot{e}_1 &= 0.0842\ddot{u} + 0.8897(\ddot{w} + \ddot{w}_g) + 3.03\ddot{q} - 4.205e_1 - 0.5969e_2 - 164.6e_1 - 28.05e_2 + 6.113\ddot{\eta} - 42.03\ddot{\eta} \\
 \ddot{e}_2 &= -0.0292\ddot{u} - 0.1723(\ddot{w} + \ddot{w}_g) + 5.097\ddot{q} - 0.4456e_1 - 2.155e_1 - 2.854e_1 - 430.5e_2 - 20.27\ddot{\eta} - 13.29\ddot{\eta} \\
 \text{NZA} &= -0.00116\ddot{u} - 0.0118(\ddot{w} + \ddot{w}_g) + 0.4032\ddot{q} + 0.0551e_1 + 0.2404e_2 - 0.9548e_1 + 90.65e_2 + 1.39\ddot{\eta} + 1.449\ddot{\eta} \\
 \text{NZB} &= -0.00804\ddot{u} - 0.0850(\ddot{w} + \ddot{w}_g) - 0.2943\ddot{q} - 0.0590e_1 - 0.156e_2 - 2.951e_1 - 26.55e_2 - 0.4182\ddot{\eta} - 1.178\ddot{\eta} \\
 \ddot{Q} &= 57.3\ddot{q} + 1.117e_1 - 0.8757e_2 \\
 \text{NZW} &= -0.0554\ddot{u} - 0.6511(\ddot{w} + \ddot{w}_g) - 5.162\ddot{q} + 3.036e_1 + 1.139e_2 + 112.2e_1 + 152.9e_2 + 4.397\ddot{\eta} + 33.43\ddot{\eta} \\
 \text{BM20} &= -0.0213\ddot{u} - 0.199(\ddot{w} + \ddot{w}_g) - 1.46\ddot{q} - 1.399e_1 - 0.4151e_2 - 334.3e_1 - 23.1e_2 + 4.777\ddot{\eta} - 14.66\ddot{\eta} \\
 \text{BM40} &= 0.00605\ddot{u} - 0.0249(\ddot{w} + \ddot{w}_g) + 0.3829\ddot{q} - 0.2999e_1 + 0.1274e_2 - 377.e_1 - 345.9e_2 - 5.637\ddot{\eta} + 34.06\ddot{\eta} \\
 \text{TQ20} &= 0.3388\ddot{u} + 3.529(\ddot{w} + \ddot{w}_g) - 6.416\ddot{q} - 4.017e_1 + 1.496e_2 - 252.9e_1 + 145.1e_2 + 3.72\ddot{\eta} + 28.08\ddot{\eta} \\
 \text{TQ40} &= 0.3083\ddot{u} + 3.402(\ddot{w} + \ddot{w}_g) + 2.773\ddot{q} - 6.356e_1 + 0.664e_2 - 239.5e_1 - 151.1e_2 - 5.36\ddot{\eta} + 123.2\ddot{\eta}
 \end{aligned}$$

Table 2

EIGEN VALUES

Basic aircraft No active controls					Datum Phugoid suppression only				
Real part	Imaginary part	Frequency Hz	Damping		Real part	Imaginary part	Frequency Hz	Damping	
-1.113	20.691	3.29	0.054	EL 2	-1.113	20.694	3.29	0.054	EL 2
-2.156	12.654	2.01	0.168	EL 1	-2.156	12.653	2.01	0.168	EL 1
-0.901	1.893	0.30	0.430	SP	-0.746	2.445	0.39	0.315	SP
-0.0062	0.0531	0.0085	0.116	PH	-0.0237	-	-	-	PH
-	-	-	-	-	-0.227	-	-	-	PH
-	-	-	-	-	25.072	-	-	-	Elev
Pitch stabilised aircraft Datum configuration plus pitch rate feedback					Load alleviation system A1 First order aileron actuator, perfect sensors				
-1.149	20.846	3.32	0.055	EL 2	-19.526	29.750	4.73	0.549	Ail
-2.192	12.700	2.02	0.170	EL 1	-1.331	20.366	3.24	0.065	EL 2
-2.161	2.103	0.33	0.717	SP	-2.518	7.547	1.20	0.317	EL 1
-0.0240	-	-	-	PH	-2.012	0.355	0.057	0.985	-
-0.182	-	-	-	PH	-0.0233	-	-	-	PH
-29.607	-	-	-	Elev	-0.353	-	-	-	PH
-	-	-	-	-	-12.619	-	-	-	-
-	-	-	-	-	-29.584	-	-	-	Elev
Load alleviation system B2 Second order aileron actuator, perfect sensors					Load alleviation system C2 Second order aileron actuator, sensor characteristics				
-49.817	66.366	10.56	0.600	Ail	-38.622	70.877	11.28	0.479	Ail
-1.116	20.486	3.26	0.054	EL 2	-45.826	40.305	6.41	0.751	Acc
-2.167	9.331	1.49	0.226	EL 1	-0.970	20.203	3.22	0.048	EL 2
-2.107	0.404	0.064	0.982	-	-1.846	8.601	1.37	0.210	EL 1
-0.0233	-	-	-	PH	-27.359	7.648	1.22	0.963	Elev
-0.335	-	-	-	PH	-0.0233	-	-	-	PH
-10.026	-	-	-	-	-0.339	-	-	-	PH
-12.463	-	-	-	-	-1.611	-	-	-	-
-29.570	-	-	-	Elev	-6.717	-	-	-	-
-60.521	-	-	-	-	-9.675	-	-	-	-
-	-	-	-	-	-75.776	-	-	-	-

Key to identifiable modes: EL 1, 2 : elastic modes 1, 2,

SP : short period,

PH : phugoid,

Elev, Ail: elevator, aileron actuators,

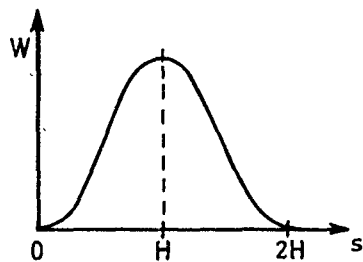
Acc : accelerometer.

Table 3
SYSTEM GAINS AND PARAMTER VALUES

Quantity		Units	Datum	Pitch stabilised	Load alleviation systems		
			Phugoid suppression	Phugoid suppression plus pitch rate feedback	A1 First order actuator perfect sensors	B2 Second order actuator perfect sensors	C2 Second order actuator + sensor models
Feedback values	Pitch attitude to elevator	deg/deg	1	1	1	1	1
	Pitch rate to elevator	deg per deg/s	0	1.2	1.2	1.2	1.2
	CG acceleration to aileron	deg/g	0	0	9.22	10.33	9.78
	Wing tip acceleration to aileron	deg/g	0	0	3.64	1.91	2.56
Filter time constants	CG acceleration	second	0.05	0.05	0.05	0.1	0.1
	Wing tip acceleration	second	0.05	0.05	0.05	0.1	0.1
	Pitch rate	second	0.05	0.05	0.05	0.05	0.05
Aileron actuator model	First order, time constant	second	-	-	0.05	-	-
	Second order, frequency	rad/s	-	-	-	100	100
	Second order, damping	rad/s	-	-	-	0.7	0.7
Elevator actuator model	First order, time constant	second	0.04	0.04	0.04	0.04	0.04
Sensor models	Accelerometer frequency	rad/s	-	-	-	-	60
	Accelerometer damping	-	-	-	-	-	0.7
	Pitch rate gyro	second	-	-	-	-	0.05
	time constant	-	-	-	-	-	-

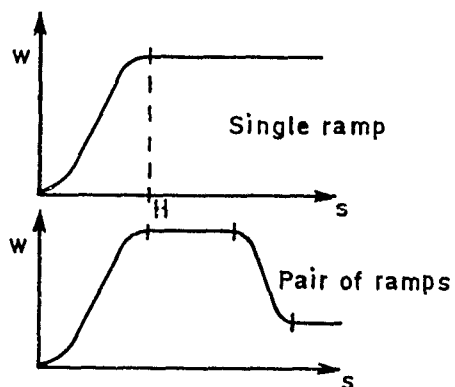
Table 4
LOAD ALLEVIATION PREDICTED VIA DIFFERENT TURBULENCE MODELS

The loads are expressed as a percentage of the datum value for each model										
Load alleviation system			A1	A1	A1	B2	B2	B2	C2	C2
Aileron rate limit, deg/sec			-	120	60	-	120	60	-	120
Turbulence model	Amplitude (m/s)	Form of result	BM20							
Power spectrum	rms=1	rms	49.1	-	-	54.0	-	-	56.0	-
1-cosine gust	20	peak response, all H	51.8	53.1	68.1	56.1	56.1	69.0	57.2	68.4
1-cosine gust	20 (H/50) ^{1/3}	peak response, all H	50.6	50.6	60.6	55.5	55.5	60.2	56.9	60.2
vortex, H=30m	see fig.1c	peak response	45.3	53.6	74.0	51.5	54.8	72.9	51.8	54.6
SDG	see fig.1b	peak response, all gust families	50.4	50.4	62.0	55.3	55.3	61.5	56.7	61.6
BM40										
Power spectrum	rms=1	rms	38.7	-	-	43.4	-	-	49.4	-
1-cosine gust	20	peak response, all H	47.3	63.1	85.3	62.6	62.8	87.1	67.9	87.2
1-cosine gust	20 (H/50) ^{1/3}	peak response, all H	43.8	46.2	73.8	57.8	57.8	75.4	64.9	76.2
vortex, H=30m	see fig.1c	peak response	32.0	42.5	65.0	45.3	47.6	62.0	48.7	51.7
SDG	see fig.1b	peak response, all gust families	39.8	42.9	56.6	49.5	49.5	59.1	55.8	59.3



$$w(s) = \begin{cases} (1 - \cos \frac{\pi s}{2H}) W & , 0 < s < 2H \\ 0 & s \leq 0 \text{ and } s \geq 2H \end{cases}$$

a 1-cosine complete gusts



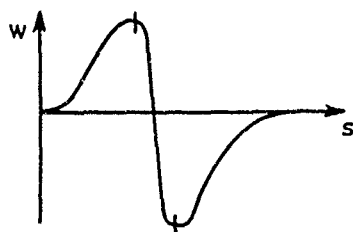
Amplitude of a single gust is given by

$$w(s) = \begin{cases} 0 & , s \leq 0 \\ (1 - \cos \frac{\pi s}{2H}) W(H) & , 0 < s < H \\ W(H) & , s \geq H \end{cases}$$

$W(H)$ is defined here as
 $W(H) = 20 * (H/s_0)^{1/3}$ m/s
 (H in metres)

For gust pair $W(H)$ is multiplied by 0.85,
 for 4 gusts by 0.6 and for 8 gusts by 0.4

b Ramp elements in statistical discrete gust method



c Vortex gust

$$w(s) = \begin{cases} 0 & , 0 \leq s \\ \frac{1}{2} W(H) (1 - \cos \frac{\pi s}{3H}) & , 0 < s < 3H \\ -W(H) \cos \frac{\pi s}{H} & , 3H \leq s \leq 4H \\ -W(H) \exp \left(-\frac{1}{2} \left(\frac{s-4H}{H} \right)^2 \right) & , s > 4H \end{cases}$$

$$W(H) = \begin{cases} 3 H^{1/3} & , H \leq 30 \\ 3 \cdot \frac{30^{4/3}}{H} & , H > 30 \end{cases} \quad \begin{matrix} (H \text{ metres}) \\ (W(H) \text{ m/s}) \end{matrix}$$

Fig 1 Discrete gust models

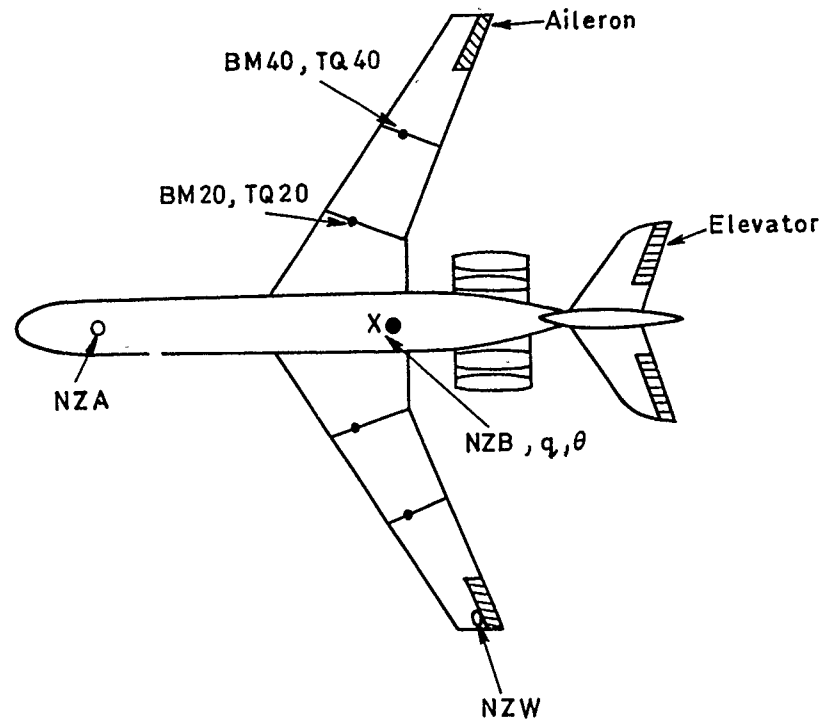


Fig 2 Aircraft layout showing sensors and motivators

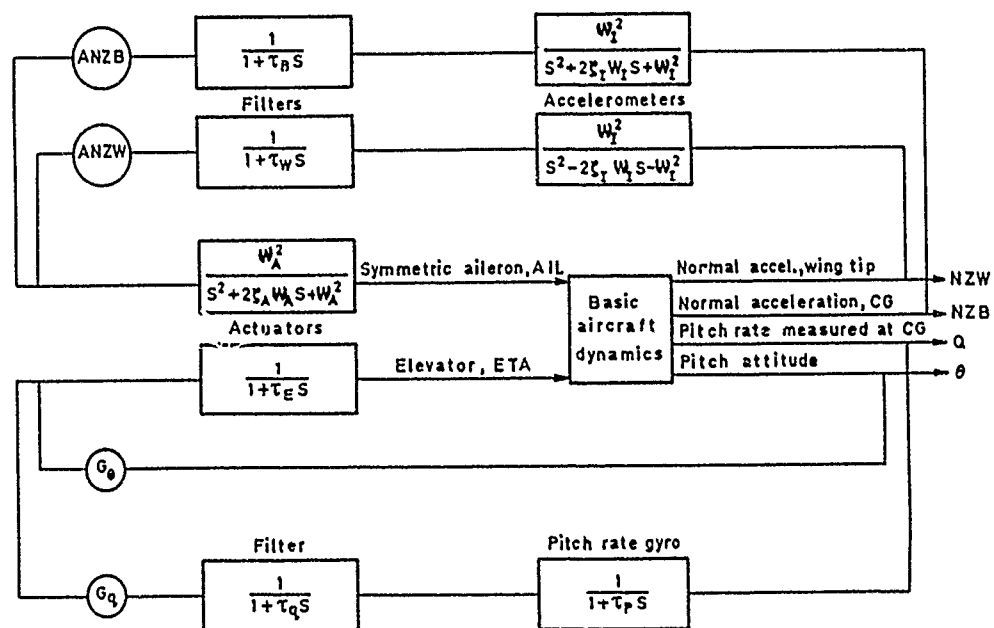


Fig 3 Block schematic for load alleviation system C2

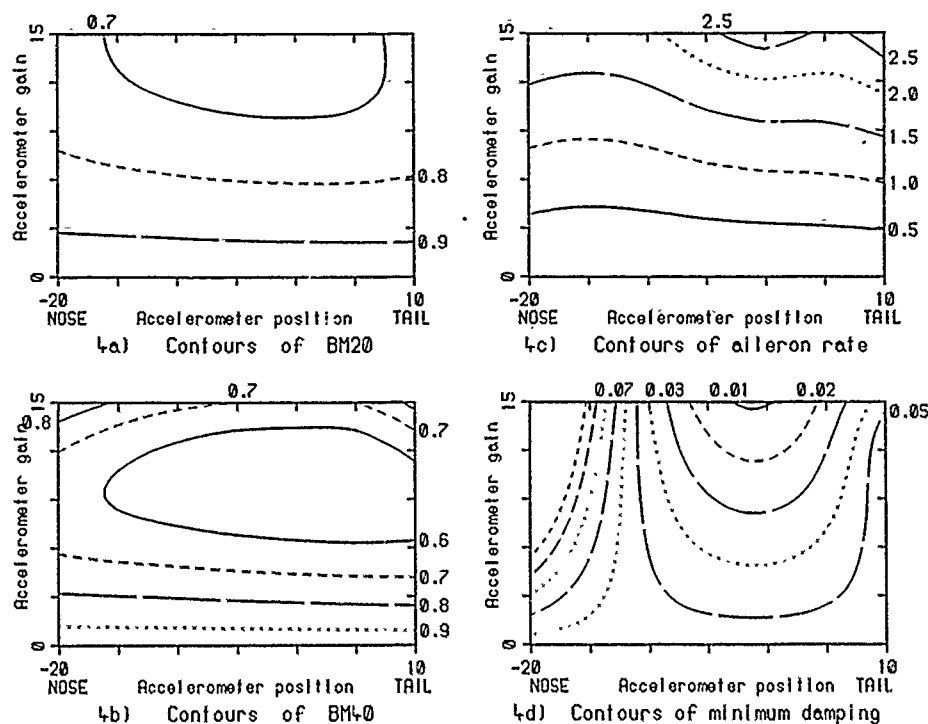


Fig 4 Contours for choice of accelerometer gain and fuselage position in a single accelerometer system

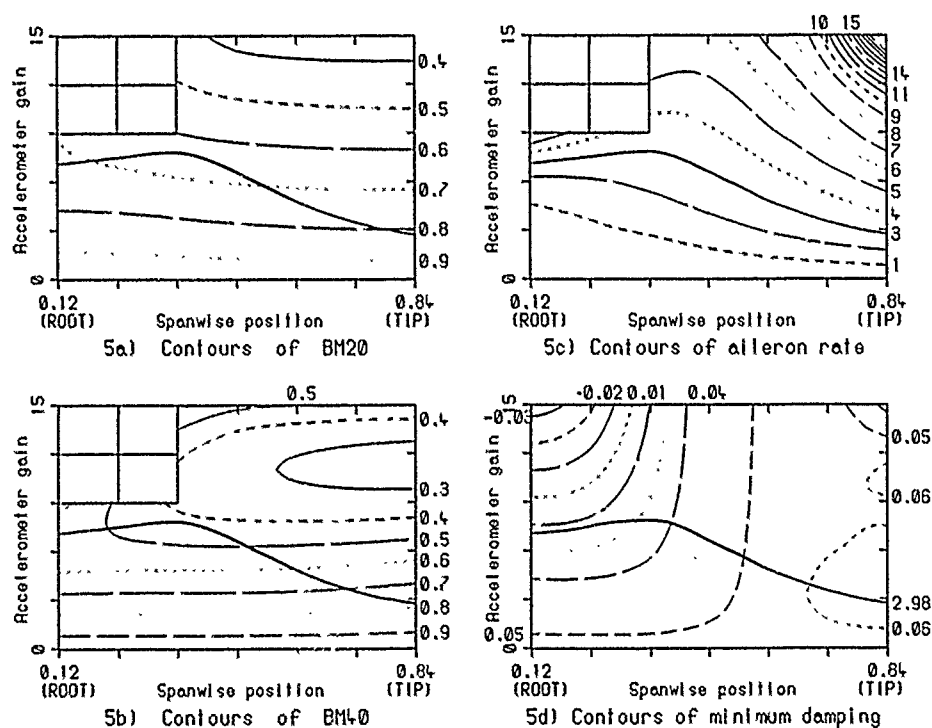


Fig 5 Contours for choice of accelerometer gain and spanwise position for a system with a symmetric pair of sensors on the wing only

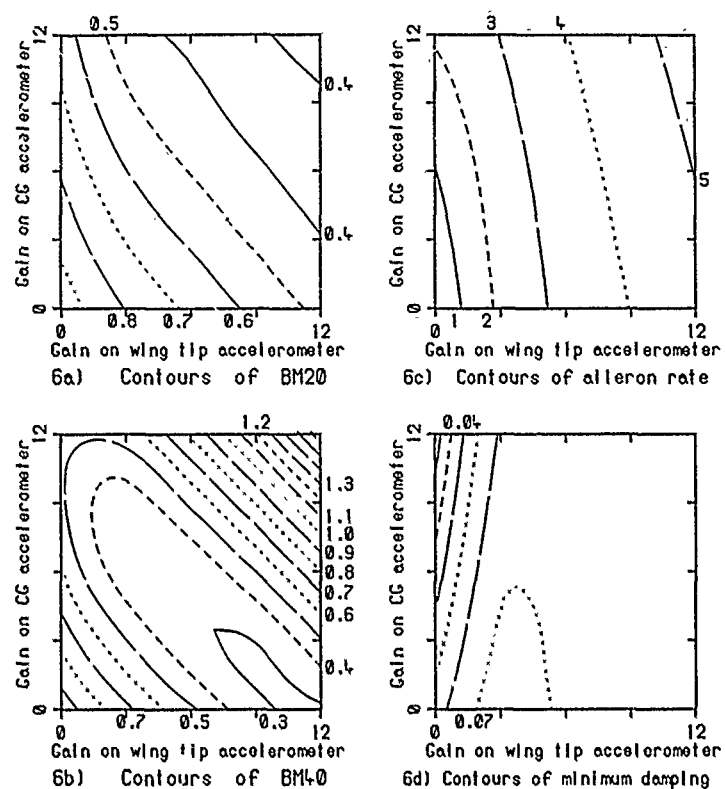


Fig 6 Contours for choice of accelerometer gains in system A1

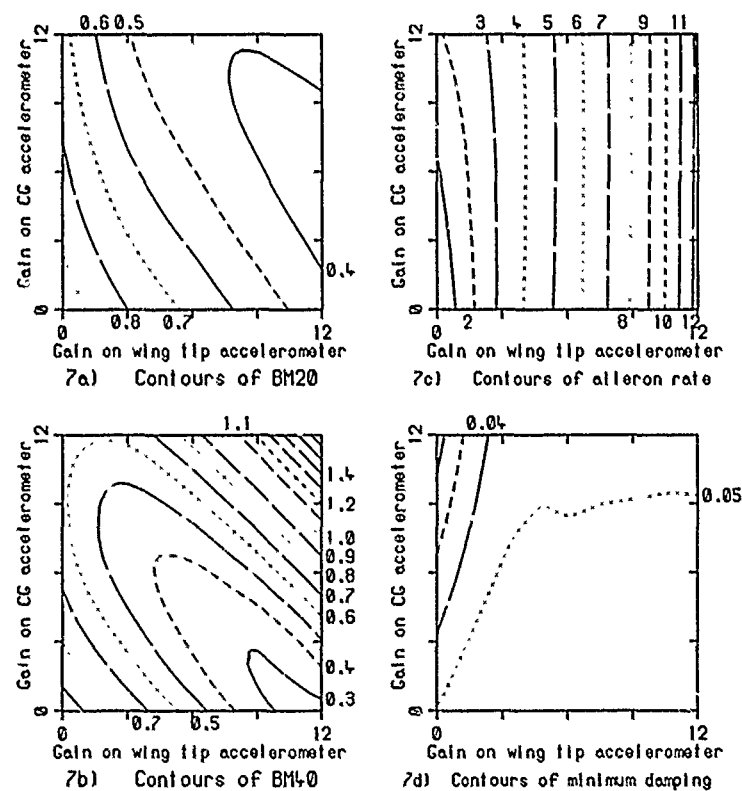


Fig 7 Contours for choice of accelerometer gains in system C2

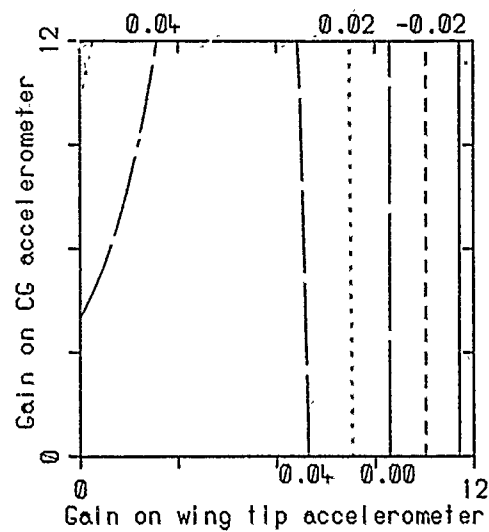


Fig 8 Minimum damping contours for system C2 with six elastic modes

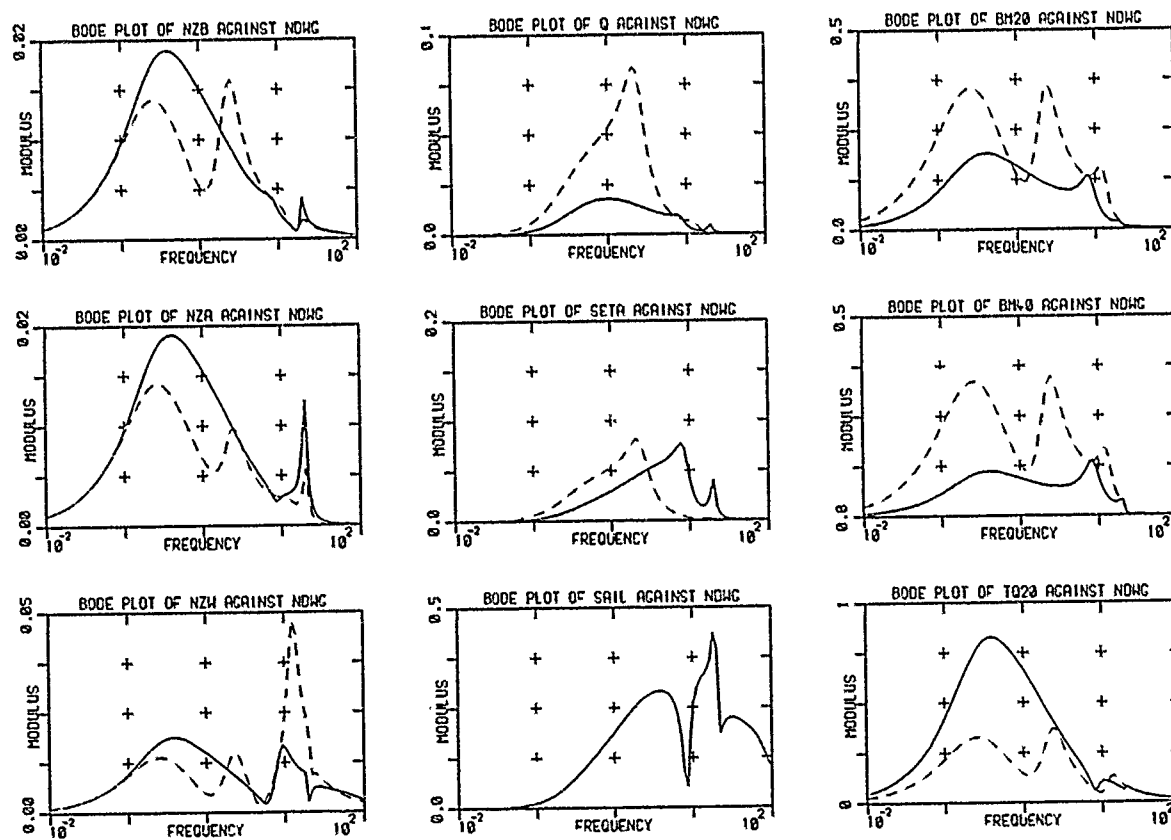


Fig 9 Bode plots for system C2

9-16

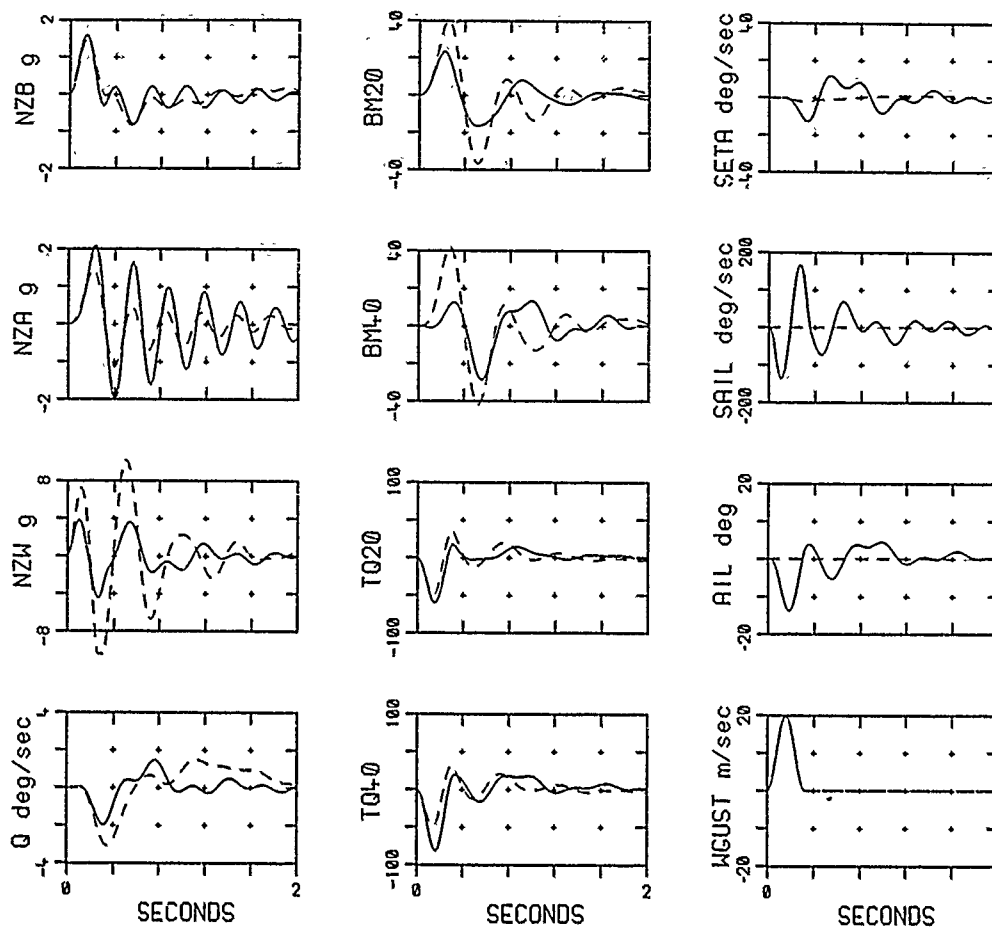


Fig 10 Response of system A1 to a 40m '1-cosine' gust

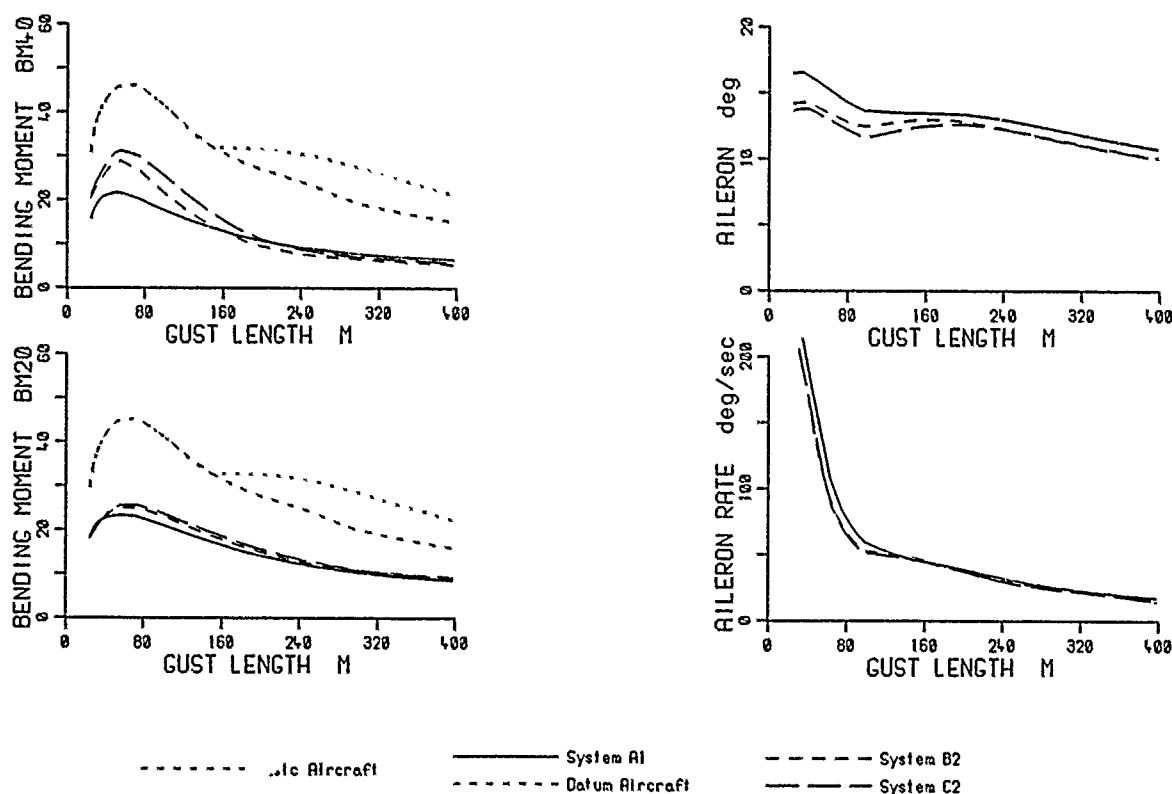


Fig 11 Variation of peak responses with length of 20m '1-cosine' gusts

9-17

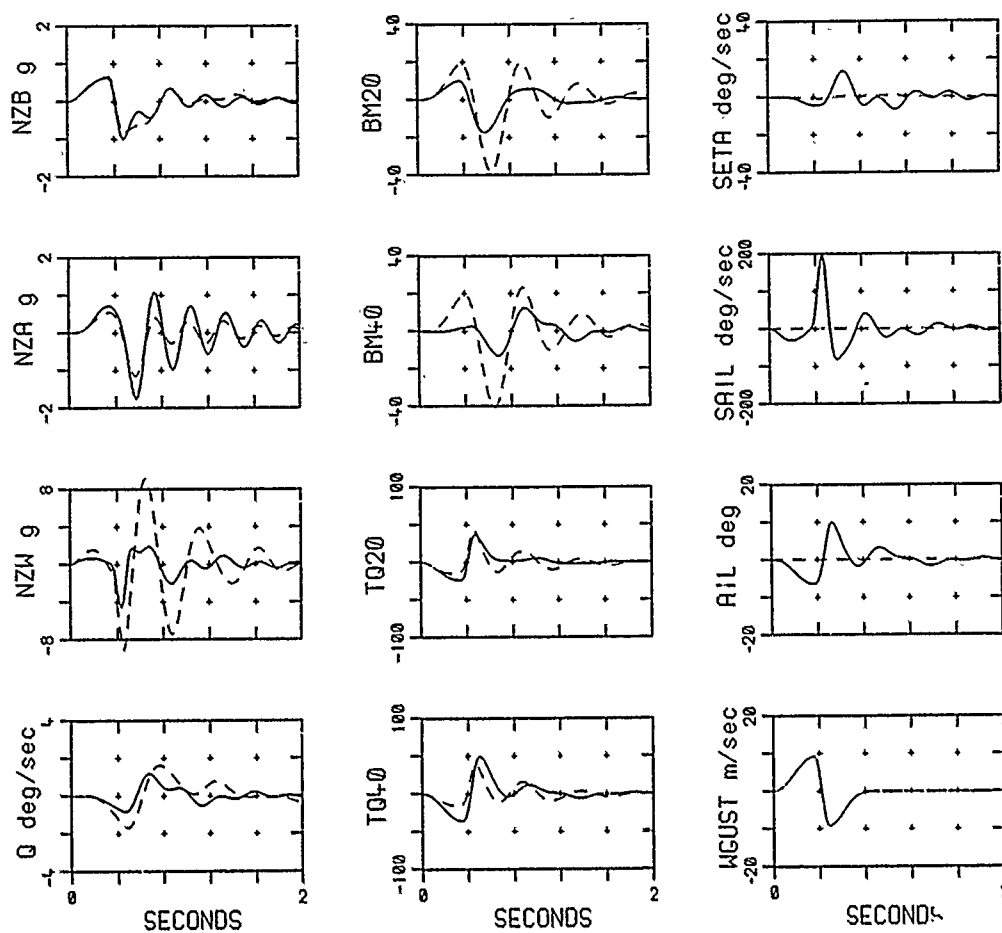


Fig 12 Response of system A1 to a vortex gust

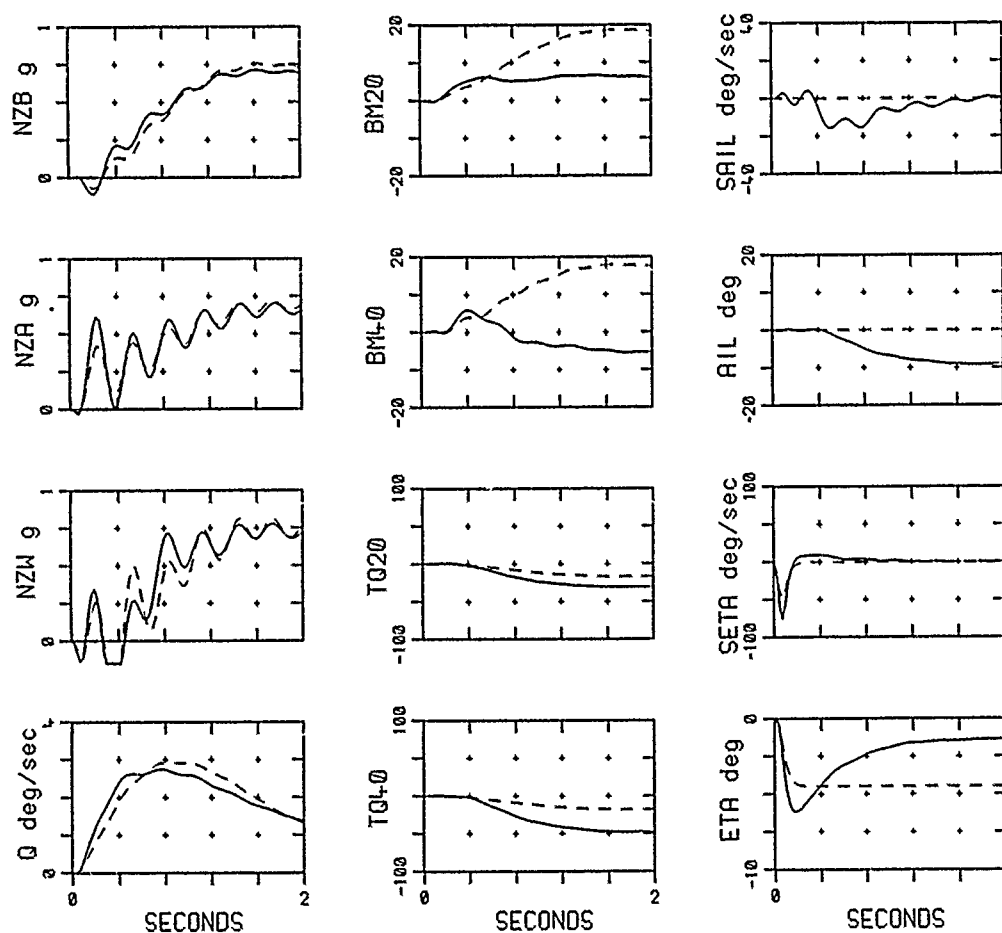


Fig 13 Response of system A1 to a pitch-up manoeuvre

AEROELASTIC DESIGN CONSIDERATIONS IN THE DEVELOPMENT OF HELICOPTERS

by

H. Strehlow, B. Enenkl

MESSERSCHMITT-BÖLKOW-BLOHM GMBH
Postfach 801140
8000 München 80, Germany

SUMMARY

There are a number of aeroelastic phenomena associated with the design of helicopters. The dynamic stability and response characteristics of rotary-wing aircraft are dependent on parameters which have to be defined in the preliminary design phase.

The type of rotor and its control determine largely the aeroelastic behaviour of a helicopter. Of special interest are nowadays hingeless and bearingless rotor systems. Aeroelastic design considerations for these rotor types are discussed. Coupling effects due to geometric nonlinearities and blade root attachments with precone, droop, sweep and offsets are of great importance with respect to the aeroelastic stability and must be considered carefully in a preliminary phase. In addition, stability and vibration problems call for exact blade tuning possibilities, which in turn require an analytical understanding.

Coupling between rotor and fuselage may have significant effects on aeroelastic stability and response. Design parameters related to this complex area are also discussed.

NOTATION

Ω	Rotor speed	ζ_p	Presweep
R	Rotor radius	β_p	Pre flap
r	Radial position ($\bar{r} = r/R$)	β_c	Precone
ω	Natural frequency	ζ_o	Equivalent elastic lead deflection
t	time	β_o	Equivalent elastic flap deflection
ζ	Lead-lag deflection	θ_ζ	Pitch-lead coupling parameter
β	Flapbending deflection	θ_β	Pitch-flap coupling parameter
θ	Torsional deflection	I_θ	Modal inertia of blade torsion
EJ	Bending stiffness	$\phi_{\beta 1}$	First flap bending mode
D	Damping ratio	$\phi_{\zeta 1}$	First inplane bending mode
C_T	Thrust coefficient	$\phi_{\theta 1}$	First torsional mode
σ	Rotor solidity	$\hat{M}_{\beta 1}$	Modal flap bending moment related to first mode
μ	Advance ratio	$\hat{M}_{\zeta 1}$	Modal inplane bending moment related to first mode
TR	Modal transmissibility	NA	Neutral (tension) axis
PA	Pitch axis	NR	Nonrotating
EA	Elastic axis	PLL	Pitch link load
AC	Aerodynamic center		
CM	Center of mass		

10-2 1. INTRODUCTION

The most widespread helicopter configuration uses a single main rotor and a small tail rotor. The type of the main rotor and its control have the most important influence on the aeroelastic behaviour. Figure 1 shows the MBB/KHI BK 117 aircraft with a hingeless rotor system. During the last two decades the hingeless rotor concept and



Fig. 1 BK 117 helicopter (MBB/KHI)

its successor, the bearingless rotor, have found continuously growing interest among helicopter manufacturers and research organizations. A brief historical overview of the development of these advanced rotor concepts is given in Ref. 1 and 2.

In 1960, MBB started a research and development program for a hingeless rotor system with a very stiff hub and fiberglass blades of high bending flexibility, see Ref. 3 and 4. Equipped with this new rotor system the BO 105 helicopter (max. design gross weight 2300 kg) was successfully put into operation in January 1971. In November 1982 the certification of the BK 117 helicopter (max. design gross weight: 2850 kg) with a similar but further refined and improved hingeless rotor system was obtained. The BK 117 aircraft is a joint development product of MBB and KHI in Germany and Japan respectively, see Ref. 5 and 6.

In the past, analytical and experimental investigations have established the important role of aeroelasticity in the design of hingeless and bearingless rotor concepts. The three-ring diagram of Figure 2 (from Ref. 7) represents aerodynamic, inertial and elastic forces and their interactions in different helicopter problem areas.

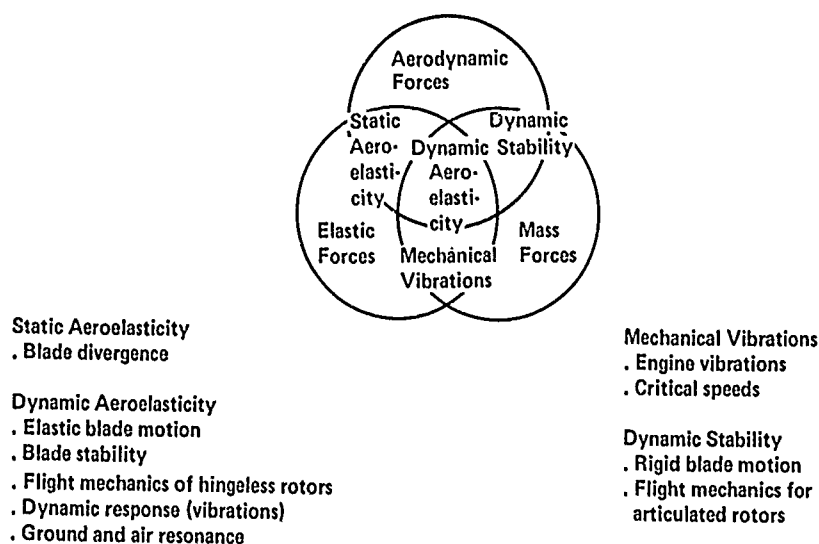


Fig. 2 Triangle of forces at a helicopter

The center area of the diagram indicates the region in which all three types of forces are important. This region, designated "dynamic aeroelasticity", encompasses in the broadest sense all stability and response problems of helicopters with advanced hingeless/bearingless rotors. The complexity of aeroelastic rotor problems is readily explained by the numerous interaction and coupling effects, many of which are inherently nonlinear or are related to timevariant periodic coefficients. Therefore the modelling

and solution of rotary-wing aeroelastic problems is a difficult task, see. Ref. 8. Figure 3 illustrates the numerous rotor blade instabilities which helicopters may

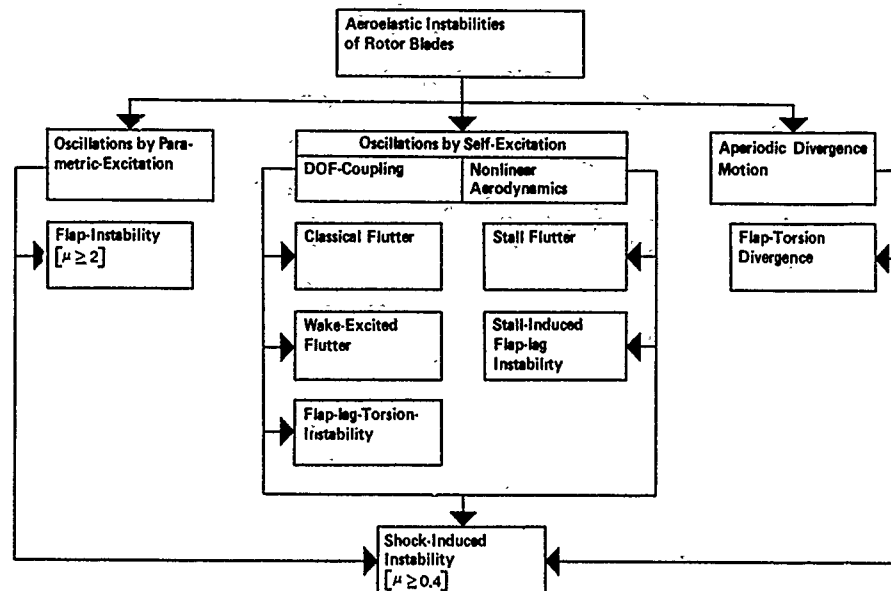


Fig. 3 Overview of rotor blade instabilities

encounter resulting in self-excitation, parametric-excitation or divergence. Especially in high speed flight multivarious instability phenomena due to the extreme variations of the aerodynamic environment of the advancing and retreating rotor blade have been observed in the past. A more detailed discussion of the various aeroelastic rotor blade instabilities that may occur in the operating range of modern helicopters (advance ratio ≤ 0.45) will be given later.

Compared to more conventional articulated and teetering rotor systems the hingeless and bearingless rotors often show quite different aeroelastic stability and response characteristics. Aeroelastic design considerations at MBB for these rotor types are reported and discussed in the following sections, illustrated by appropriate examples. Some aeroelastic coupling effects between rotor and fuselage and related design parameters are considered too.

2. PRELIMINARY AEROELASTIC DESIGN CONSIDERATIONS FOR ROTOR SYSTEMS

This section describes the rationale in selection of key design parameters in the development of hingeless/bearingless main and tail rotor systems.

2.1 BASIC ROTOR CONFIGURATIONS-SELECTION OF BLADE BENDING STIFFNESS

Helicopter rotors are usually classified according to the mechanical arrangement of the hub in order to accommodate the blade flap and lead-lag motion and according to the blade and hub bending stiffness. The so-called hingeless rotor concept is not really hingeless, since only the conventional flapping and lead-lag hinges have been removed but not the feathering hinges for pitch control. Truly hingeless rotors without feathering hinges are called bearingless rotors.

The reason for the design and development of the hingeless MBB main rotor system was the quest for mechanical simplification and improved handling qualities in comparison to fully articulated rotors, see Ref. 9. The MBB hingeless rotor is of the stiff hub type with soft flapwise and soft inplane blades. The main components of the four-bladed rotor are shown in Figure 4. The fiberglass blades are rigidly attached to short hub arms. The rotorhub is made of titanium. The pitch axes of the blades are fixed to the hub arms. The only bearings are those for pitch-control.

These pitch bearings are replaced by a flexural element in the bearingless rotor concept so that further simplification can be achieved. Figure 5 shows an experimental rotor being presently developed at MBB. The experimental configuration uses a standard BO 105 rotor hub with fixed pitch control bearings. The modified blades are attached to a fiberglass flexbeam. Blade pitch is controlled by a torque tube. The MBB bearingless mainrotor concept is of the soft-inplane type.

As an example for an advanced tail rotor system, Figure 6 shows the experimental version of a four-bladed bearingless tail rotor system, see Ref. 10. The design uses a fiberglass bending-torsion flexure to accommodate bending deflections and collective pitch control. For the experimental rotor standard BO 105-tailrotor blades were used in order to reduce the hardware cost. The MBB bearingless tail rotor is also of the soft-inplane type.

10-4

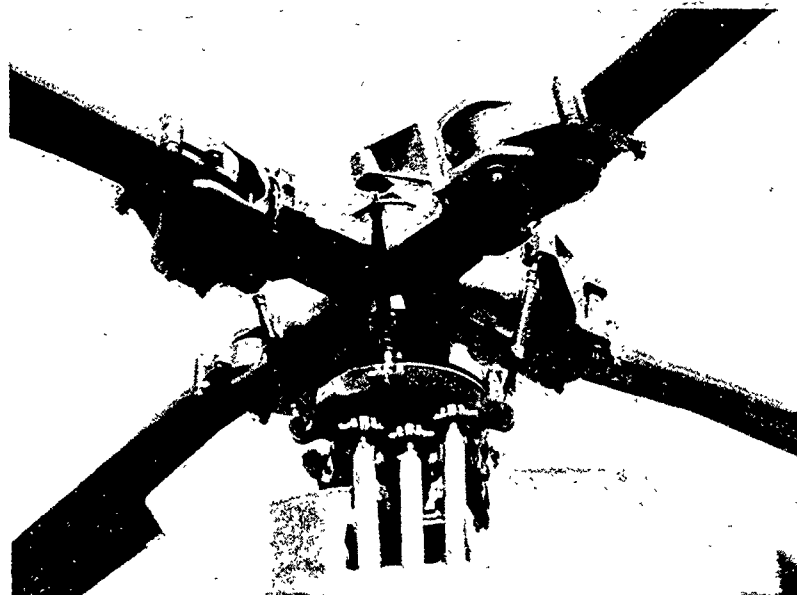


Fig. 4 Soft inplane hingeless main rotor system (BO 105)

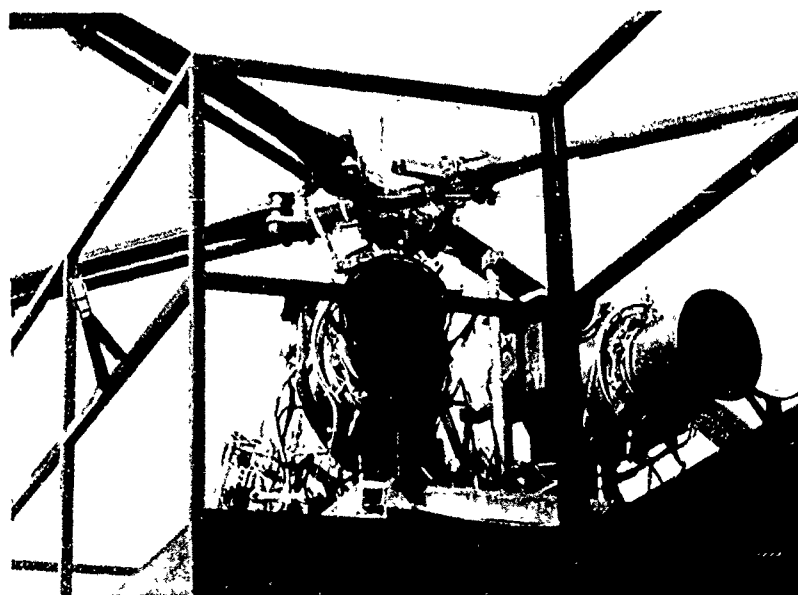


Fig. 5 Soft inplane bearingless main rotor system (experimental)

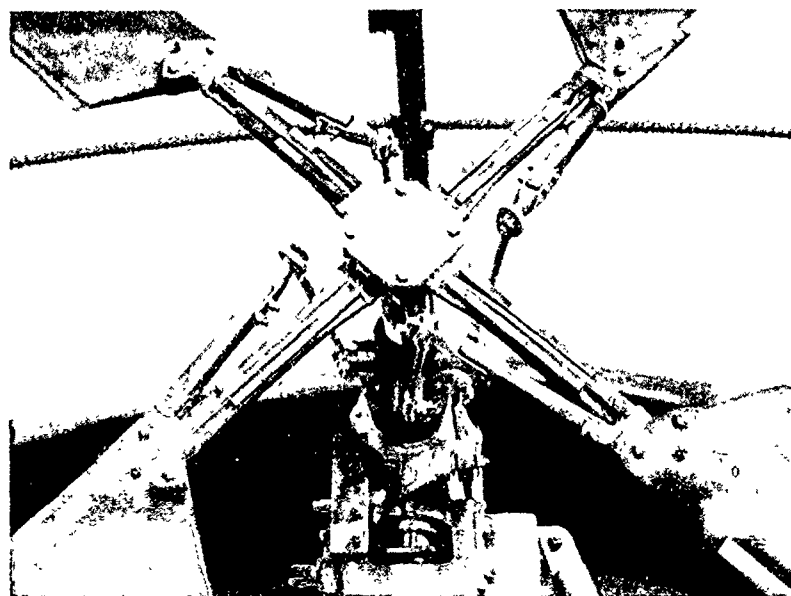


Fig. 6 Experimental bearingless tail rotor system (whirl test)

The selection of flapwise and inplane bending stiffness in the design of hingeless/bearingless rotor systems is crucial with respect to flight dynamics, aeromechanics, and aeroelasticity. For design purposes rotor systems are best characterized by the fundamental flap and lead-lag natural frequencies of the blades at nominal rotor speed, see Ref. 11. 10-5

The modal transmissibilities in Figure 7 show the transfer of cyclic blade root bending moments due to flapwise and inplane 1/rev-moment excitation of the rotating blade for a range of flap and lead-lag blade frequencies, typical for today's main rotor systems.

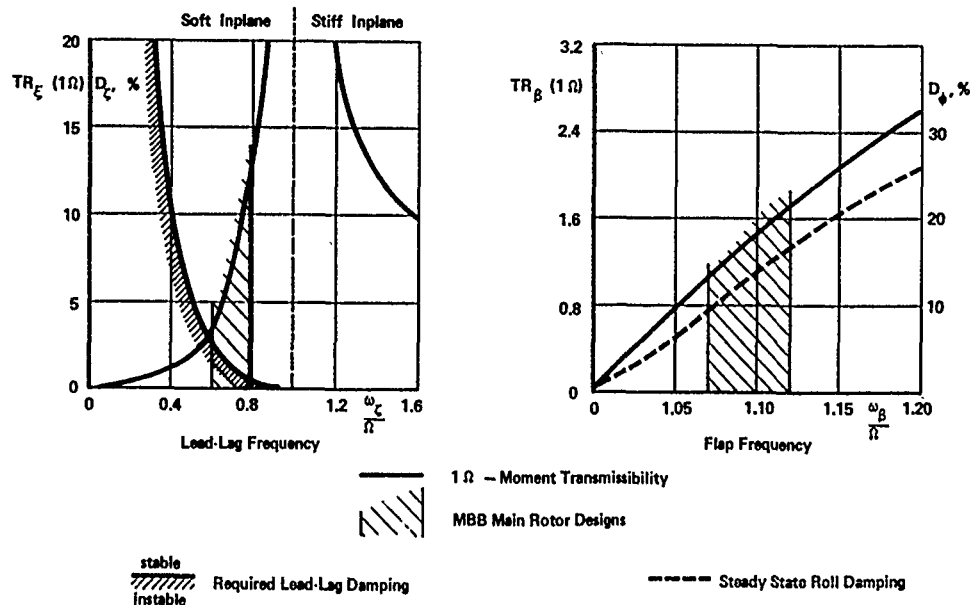


Fig. 7 Key design parameter for main rotors

For hingeless and bearingless main rotor configurations, flapwise soft blades with a fundamental flap bending frequency ω_β in the range of 1.05 to 1.15 Ω are typically selected, distinguished from articulated rotor systems with a blade flap frequency ω_β usually equal or below 1.04 Ω . Here Ω is the nominal rotor speed. It should be noted at this point, that a centrally articulated rotor blade without spring restraints has a natural flap frequency ω_β equal to 1 Ω , arising solely from the centrifugal restoring force. Hingeless and bearingless rotor systems are able to transfer high cyclic control moments from the rotating system via the hub to the fixed-body system. The transformed moments correspond to steady roll and pitch moments. For the damping moments a similar relation exists. Estimates of the body roll damping ratio in the fixed system are plotted in Figure 7 (right) for different flap frequencies. These damping ratios are referred to the roll motion about the center of mass and are calculated for a typical helicopter. The high damping moments of hingeless and bearingless rotor systems are even more important than the high control moments. High damping moments result in a fast and more direct control of the helicopter. The favourable effect of high body roll damping for the aeromechanical rotor stability will be discussed in more detail below.

The selection of the inplane natural bending frequency ω_ζ is in principle at the disposal of the designer. Preliminary design considerations have to take into account the blade stress problem, the aeroelastic lead-lag stability problem of the isolated blade or of the coupled rotor-body system, and the degree of blade motion coupling desired or allowed. High cyclic inplane blade root bending moments may be encountered in flight by 1/rev resonance amplification, shown in Figure 7 (left). The bending moments may be reduced by choosing an inplane frequency well below one per rev. Hingeless and bearingless rotor systems are naturally classified as soft-inplane rotors (blade inplane frequency ω_ζ is below one per rev.) or as stiff-inplane rotors (blade inplane frequency ω_ζ is above one per rev.). Soft-inplane hingeless and bearingless rotor systems are susceptible to a coupled rotor-body instability called ground or air resonance. The required blade lead-lag modal damping for ground resonance stability of helicopters with a relatively stiff landing gear may be estimated from the curve of Figure 7 (left). The calculated damping margins are relevant for a helicopter with a landing gear whose critical mode is body-pitching on ground. It is obvious that the selection of a relatively high inplane frequency ω_ζ (above 0.6 Ω) is necessary, if the required blade inplane damping for stability should be due solely to the "inherent" blade damping capacity. Reducing the inplane frequency is only possible by the provision of an additional lead-lag blade damper. A hingeless rotor with a matched stiffness blade, one that eliminates bending-torsion structural couplings, has a relatively low inplane frequency ω_ζ of about 0.5 Ω . This subject will be discussed below. Blade dampers are always required for articulated rotor systems with a typical inplane frequency ω_ζ of 0.1 to 0.3 Ω . Stiff-inplane configurations cannot become unstable in ground or air resonance. This advantage should not be overestimated due to the fact, that stiff-inplane hingeless and bearingless rotor designs are susceptible to blade flap-lag-torsion instabilities.

Summarizing, the interest in the development of hingeless and bearingless main rotors in the soft-inplane configuration is steadily growing. In contrast to this, the stiff inplane concept still dominates the design and development of hingeless and bearingless tail rotors. An exception is the soft-inplane bearingless tail rotor currently under development at MBB.

2.2 ROTOR DESIGN PARAMETERS THAT AFFECT AEROELASTIC STABILITY AND RESPONSE

One of the most important factors in the design of hingeless and bearingless rotors is the bending-torsion coupling of the blade motion and its effect on aeroelastic and flight dynamic stability characteristics.

The bending of the blade, illustrated in Figure 8, provides moment arms for the aerodynamical and inertial loads. The resultant torsional moment can be expressed solely by the internal bending moments and the corresponding bending curvatures. In terms of the bending stiffnesses, then, the torsional moment on the radial station r is given by (zero pitch):

$$(1) \quad M_\theta(r, t) = - \int_r^R (EJ_\zeta - EJ_\beta) \cdot \zeta'(r, t) \cdot \beta'(r, t) dr.$$

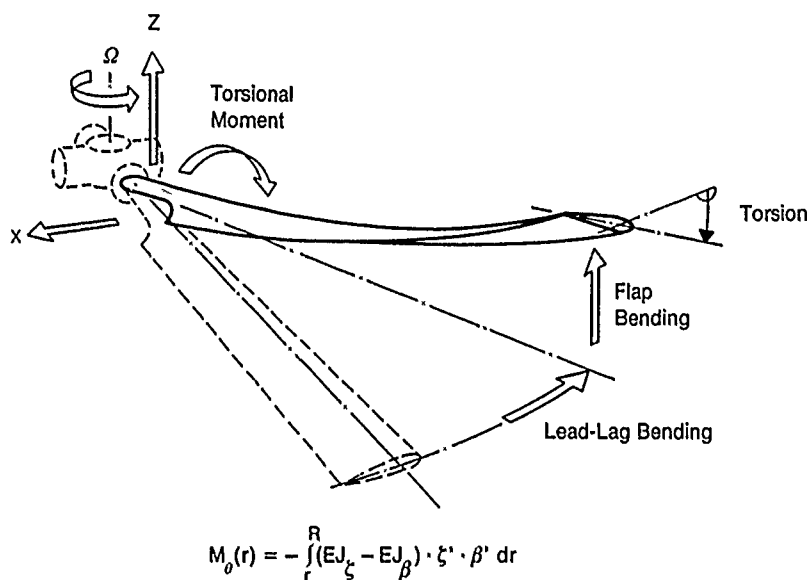


Fig. 8 Elastic bending-torsion coupling of rotor blades

That is, the torsional blade moment (M_θ) due to simultaneous bending in two directions is proportional to the product of the lead-lag (ζ') and flap (β') bending curvature, and is proportional to the difference between the lead-lag (EJ_ζ) and flap (EJ_β) bending stiffness. A complete derivation of Eq. (1) may be found in textbooks (Ref. 12, 13) or in Ref. 14, 15.

The following considerations are applied to blade deflections determined by the fundamental mode shapes. An inspection of Eq. (1) indicates, that the nonlinear torsional moment induced by blade bending will be important mainly at the inner blade portion, where high bending curvatures may be caused by the external blade loads. For typical hingeless and bearingless rotor configurations the chordwise root bending stiffness of the blade is much greater than the flapwise root bending stiffness ($EJ_\zeta > EJ_\beta$). That is, a nose down torsional moment will be induced as indicated in Figure 8. Only in case of a rotor with matched stiffness blades ($EJ_\zeta = EJ_\beta$) this moment vanishes. The torsional blade loads due to bending changes the torsional motion and hence rotor aeroelastic stability and response. These effects are greatest when the pitch bearing is inboard near the rotorhub. A typical example is the MBB hingeless rotor concept with a stiff hub, inboard pitch bearings and control system flexibility, see Ref. 16. In contrast, these coupling effects are greatly reduced or even eliminated, if the pitch bearing is designed to be outboard from the soft hub. The Westland WG-13 Lynx hingeless rotor is a typical example for this concept, where a soft flexural element inboard and a matched stiffness element outboard of the pitch bearing is used for flapping. This design eliminates almost entirely structural bending - torsion coupling, see Ref. 14.

The discussion up to this point has shown that the hingeless rotor concept offers the chance to accommodate aeroelastic coupling effects which may improve or deteriorate the stability and response behaviour of the helicopter. Usually the designer's aim is to stabilize the low damped inplane motion by proper selection of certain geometric blade parameters. There are various geometric parameters, that are used in practical rotor designs and that may produce significant coupling effects. Figure 9 (taken from

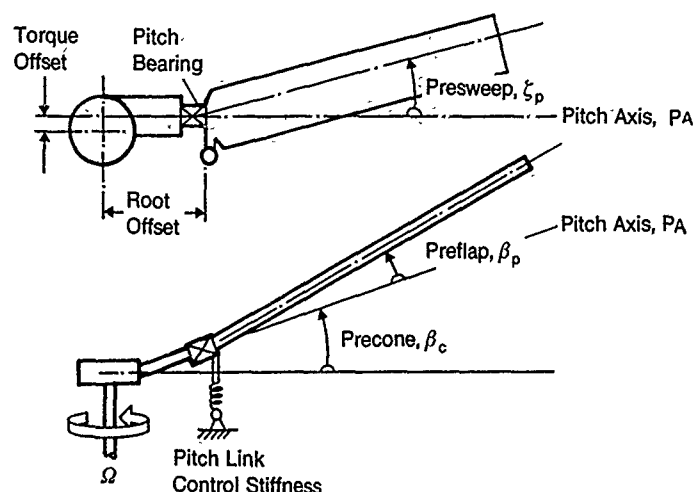


Fig. 9 Geometric configuration parameters of a hingeless rotor blade

Ref. 17) illustrates a hingeless rotor blade with several linear and angular offsets. Blade precone and torque offset are often used to reduce the steady average blade stress from lift and drag loading respectively. But more interesting here, these geometric parameters can also have great influence on the aeroelastic rotor blade stability.

The bending induced torsional blade moments give rise of effective pitch couplings caused by torsional deflections of the blade and of the control system. It is possible to extend the modal analysis of Ref. 14 and to derive an approximate expression for the effective pitch coupling

$$(2) \quad \Delta\theta = \theta_{\zeta} \cdot \Delta\zeta + \theta_{\beta} \cdot \Delta\beta,$$

in which the geometric angular offsets of the pitch axis, that is preflap (negative droop) β_p and prelead (forward sweep) ζ_p , are included. Neglecting torsional dynamics, the resulting expressions for the effective pitch-lead (θ_{ζ}) and pitch-flap (θ_{β}) parameters are:

$$(3) \quad \theta_{\zeta} \approx \frac{\hat{M}_{\theta}}{\omega_{\theta}^2 I_{\theta}} \cdot \beta_0 - \frac{\hat{M}_{\zeta}}{\omega_{\theta}^2 I_{\theta}} \cdot \beta_p$$

$$(4) \quad \theta_{\beta} \approx \frac{\hat{M}_{\theta}}{\omega_{\theta}^2 I_{\theta}} \cdot \zeta_0 + \frac{\hat{M}_{\beta}}{\omega_{\theta}^2 I_{\theta}} \cdot \zeta_p.$$

The elastic steady flap (β_0) and lag (ζ_0) bending deflections are altered by the built-in offsets mentioned before. The first term in Eq.(3) and (4), respectively, is due to the bending induced torsional moment \hat{M}_{θ} , derived from Eq. (1). This negative (nosedown) moment, calculated at the radial position r_0 from the pitch bearing, is approximated by

$$(5) \quad \hat{M}_{\theta}(r_0) = - \int_{r_0}^R \phi_{\theta_1} \cdot (M_{\zeta_1} \cdot \phi_{\beta_1}'' - M_{\beta_1} \cdot \phi_{\zeta_1}'') dr.$$

The second term is due to a torsional moment about the pitch axis, resulting from the transformation of the discrete bending moments \hat{M}_{ζ} and \hat{M}_{β} , at the built-in position of preflap and prelead. These moments are nonzero only for a flexible pitch control system and can be approximated by

$$(6) \quad \hat{M}_{\zeta}(r_0) = \phi_{\theta_1}(r_0) \cdot M_{\beta_1}(r_0) \text{ and } \hat{M}_{\beta}(r_0) = \phi_{\theta_1}(r_0) \cdot M_{\zeta_1}(r_0).$$

Both coupling parameters are inversely proportional to the torsional stiffness ($\omega_{\theta}^2 I_{\theta}$) of the rotating blade.

10-8

As an example, the nose down torsional moment distribution and the total moment are calculated for the BK 117 helicopter by use of equation (5). The result is shown in Figure 10. As discussed before significant torsional moments due to blade bending are produced only at the inner blade radial sections. At the pitch bearing ($r_0/R=0.068$)

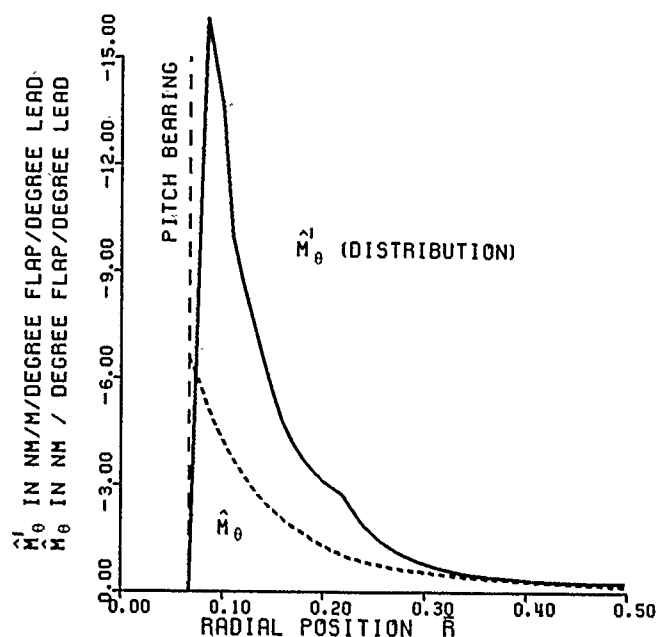
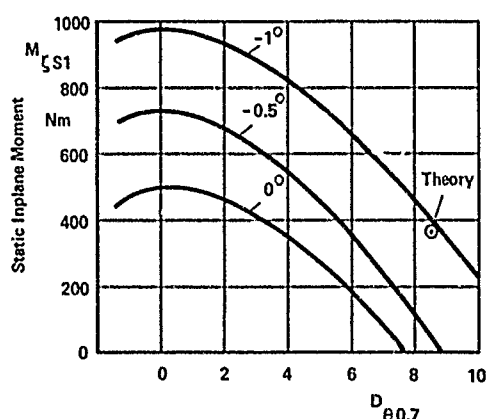
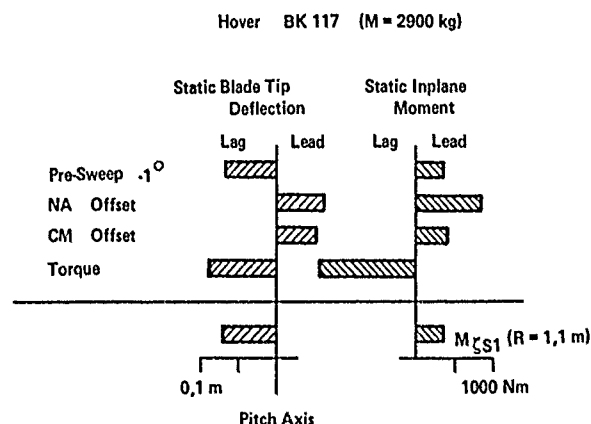


Fig. 10 Torsional moment due to bending for a hingeless rotor blade (BK 117)

the torsional moment has the value $\hat{M}_\theta = -6.6 \text{ Nm/deg/deg} = -2.2 \cdot 10^4 \text{ Nm}$. The corresponding bending moments, defined in Eq. (6), have the values $\hat{M}_\zeta = 2.8 \cdot 10^4 \text{ Nm}$ and $\hat{M}_\beta = 0.93 \cdot 10^4 \text{ Nm}$. The BK 117 hingeless rotor has a built-in precone of $\beta_c = 2.5^\circ$. The orientation of the pitch axis is characterized by $\beta_p = 0$ and $\zeta_p = -1^\circ$ (aft sweep). The resulting elastic equilibrium angles in hover are $\beta_0 = +0.9^\circ$ and $\zeta_0 = +0.1^\circ$. The steady elastic lead angle ζ_0 is measured from the swept blade axis. Figure 11 shows the position of the deflected blade tip measured from the pitch axis due to built-in



Test Results



Analytical Study

Fig. 11 Influence of different offsets on the equilibrium lead-lag bending deflection (BK 117)

sweep, tension and mass center offset and the applied aerodynamic loading (torque). The resulting tip deflections amount to -0.07 m , which is equivalent to -0.9° angular inplane deflection. If the built-in sweep angle is subtracted, the ζ_0 -value noted above is found. The approximate pitch coupling factors of the BK 117 in hover are $\theta_\zeta = -0.2$ and $\theta_\beta = -0.1$. This completes the example.

Numerous investigations (Ref. 2, 16, 18, 19) have shown that favourable pitch coupling parameters for soft-inplane hingeless rotors are: forward inplane bending causing nose down pitch; upward out-of-plane bending causing nose down pitch. These pitch couplings may be achieved by different means shown in the following table.

Condition for Favorable Coupling	Design Provision	Parameter Significance
$\theta_{\zeta} < 0$ for $\beta_o > 0$	Zero Precone	Blade Inplane
	Zero Preflap	
$\beta_p > 0$	Preflap for Soft Control System	Damping
$\theta_{\beta} < 0$ for $\zeta_o > 0$	Torque Offset	Flight Dynamic
	Tension Axis before Mass Axis	
$\zeta_p < 0$	Aft Sweep	Stability
	Aft Sweep for Soft Control System	

The aeroelastic blade stability is significantly influenced by the different blade axes, illustrated in Figure 12. The position of the tension axis was seen to be important for the inplane equilibrium position of the blade. The position of the section shear center

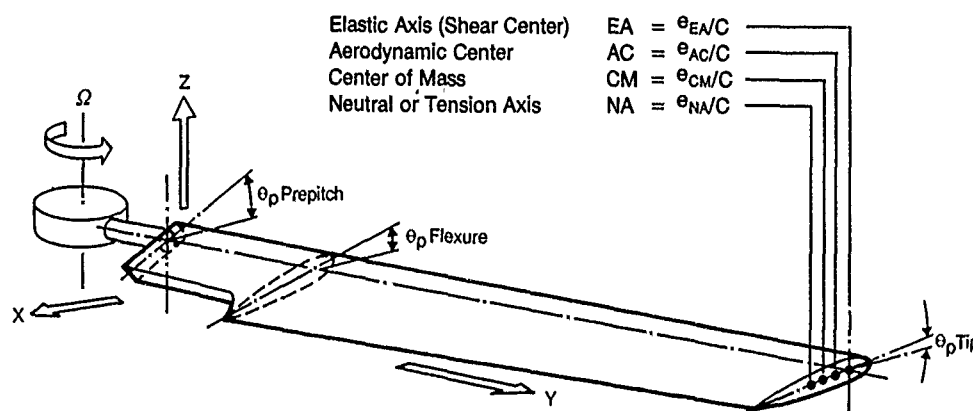


Fig. 12 Rotor blade axes and prepitch/pretwist

is related to structural blade torsion. Blade root torsion about the pitch axes is determined by the control system flexibility. The offset of the section mass center from the aerodynamic center is the key parameter for classical rotor blade flutter. Main rotor blades are usually mass balanced. It has been recognized that chordwise blade balance is also an important parameter in flight dynamics, see Ref. 4. A slightly over-balanced blade produces favorable negative pitch-flap coupling in conjunction with blade torsion/control system flexibility.

Structural coupling between the blade flap bending motion and the blade lead-lag bending motion depends on the blade pitch angle. The pitch is determined by the control setting and the built-in pitch angle, which normally varies along blade span, see Figure 12. The built-in twist must be selected according to aerodynamic considerations, but the orientation of the inboard segment is at the disposal of the designer. Positive prepitch values are found to be stabilizing for soft-inplane hingeless rotor systems. Additional structural coupling effects are caused by hub flexibility (flapwise) inboard of the pitch bearings, see Ref. 17, 18.

The design recommendations, given in this section for soft-inplane hingeless rotors, seem to be applicable also for the soft-inplane bearingless rotor system, see Ref. 20, 21. Of course, the structural and aeroelastic characteristics of bearingless rotors are much more complex and depend highly on the individual design of the flexural element and of the pitch control system.

2.3 BASIC AEROELASTIC ROTOR DESIGN PHILOSOPHY AT MBB

In the past positive experience has been gained at MBB with the soft-inplane hingeless main rotor concept. Using a relatively stiff hub inboard the pitch bearing strong aeroelastic coupling effects are produced by the flexible fiberglass blades. It is the design philosophy at MBB to use these effects for beneficial helicopter stability behaviour, see Ref. 9, 16. The design range of blade inplane and out-of-plane bending frequency selection at MBB is indicated in Fig. 7. Generally, there is a trend to reduce the fundamental main rotor blade flap bending frequency to $(1.06 - 1.08)\Omega$ corresponding to a virtual flapping hinge offset of 8 to 10% R, in order to lower gust and vibration sensitivity and to minimize adverse flight mechanical effects at high speeds. In the

10-10 following table there are summarized different hingeless and bearingless rotor configurations that have been developed or that are presently developed at MBB.

	$\bar{\omega}_\beta$	$\bar{\omega}_\zeta$	β_c	β_p	ζ_p	θ_p	Design Gross Weight - kg
BO 105 Hingeless Main Rotor (Production)	1.12	0.67	2.5°	0°	0°	8° *	2300
BK 117 Hingeless Main Rotor (Production)	1.10	0.66	2.5°	0°	-1°	8° *	2850
BO 105 Hingeless Main Rotor (Modified)	1.12	0.66	0°	2.5°	0°	8° *	2300
BO 105 Bearingless Main Rotor (Experm.)	1.12	0.69	1°	2°	0°	10°	2300
Bearingless Main Rotor (Under Development)	1.07	0.70	0°	2.5°	0°		2100
Hingeless Elastomeric Main Rotor (Under Development)	1.08	0.70	0°	2°	0°		4000
BO 105 Bearingless Tail rotor (Experm.)	1.05 (1.23)	0.76	0°	0°	0°		
Bearingless Tail Rotor (Under Development)	1.04	0.68	0°	0°	0°		

*) for hover

For the purpose of information some key design parameters are given additionally. Figure 13 illustrates two new composite main rotor designs: the elastomeric hingeless rotor and the flexbeam bearingless rotor with a "snubbed" torque tube. Both rotors are

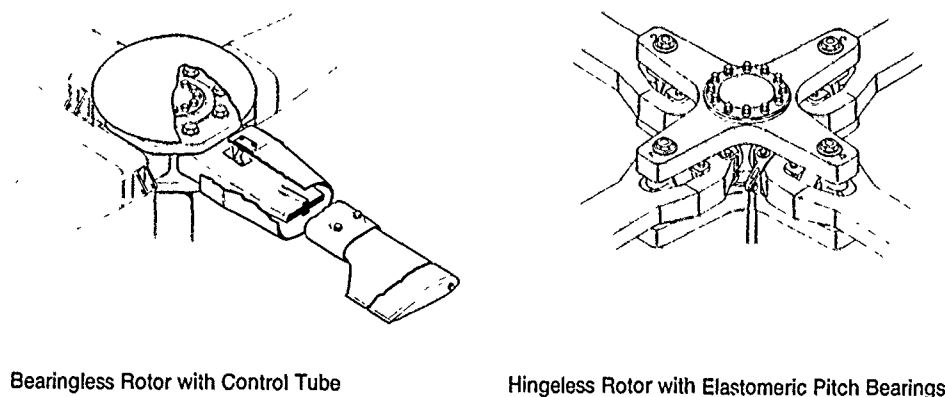


Fig. 13 New composite main rotor designs at MBB

equipped with a small composite material hub for reducing the flap stiffness ("hub stiffness") relative to the BO 105/BK 117 hingeless rotor system. The elastomeric pitch bearing in the hingeless rotor design seems to be ideally suited for helicopter applications, because no lubrication or servicing of any kind is required. The advantages of the bearingless rotor concept - simplicity, reduced weight and drag - seem to be realizable by the new design. Figure 14 shows more details of this rotor.

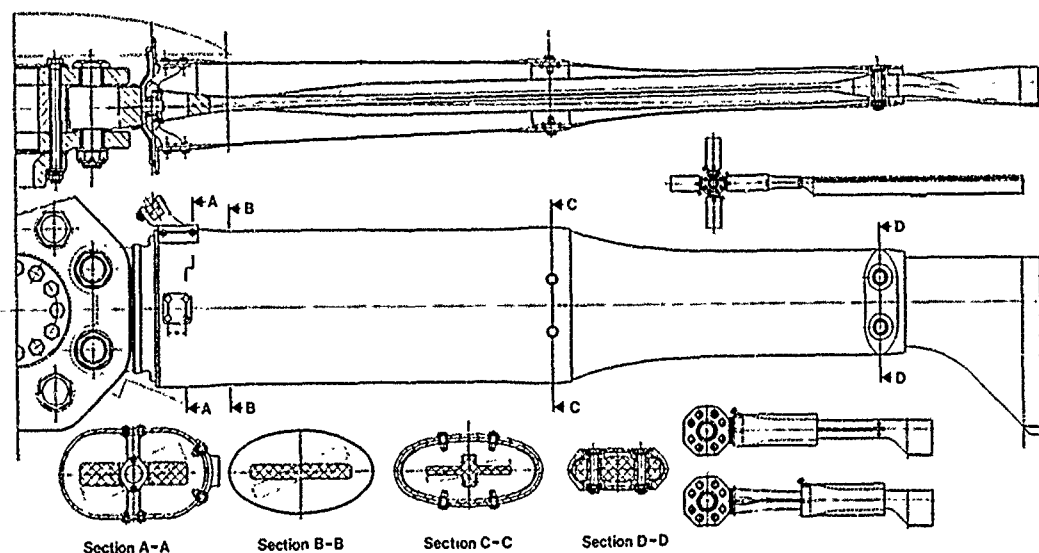


Fig. 14 Composite bearingless main rotor design with flexural single beam element and control tube

The flexural single beam element has a structural "quasi-hinge" to accommodate blade flapping at the inboard section B-B. The torque tube design provides relative low bending stiffness in both directions and allows a simple inspection of the flexbeam. The tube is rigidly attached to the blade (section D-D) and is "fixed" inboard by a snubber, which transmits shear loads to the hub. An alternative design similar to the Boeing Vertol bearingless main rotor (BMR) is shown in Figure 15. This concept uses a double beam flexural element with a simple control rod in the middle of the two flexbeams. It should be noted that Boeing Vertol has successfully flight-tested the BMR on a BO 105 helicopter, see Ref. 21.

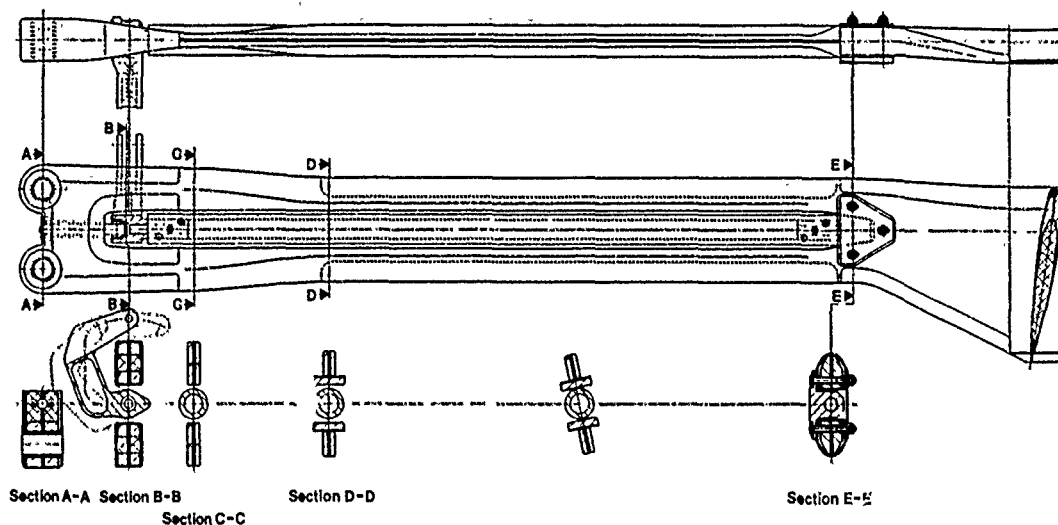


Fig. 15 Composite bearingless main rotor design with flexural double beam element and control rod

The new rotor systems of MBB make extensive use of modern composite material technology, which is believed to be the basis for a successful development of these advanced systems. Therefore extensive research work for composite material are in progress at MBB. But this subject, being of utmost interest for the designer, is beyond the scope of this paper.

3. AEROELASTIC DESIGN OF HINGELESS/BEARINGLESS ROTOR SYSTEMS - SOME ILLUSTRATIVE EXAMPLES

In this section a brief discussion of some illustrative results of soft inplane rotor systems are given with emphasis on the design aspects.

3.1 STRUCTURAL AND DYNAMICAL MAIN ROTOR BLADE DESIGN AND TUNING

The tailoring of the blade bending stiffness to meet the design requirements for the fundamental blade bending natural frequencies is the first step in the development of a new rotor system. Figure 16 presents the flapwise and chordwise bending stiffness distribution for the BK 117 hingeless rotor and the bearingless rotor. Notice that the

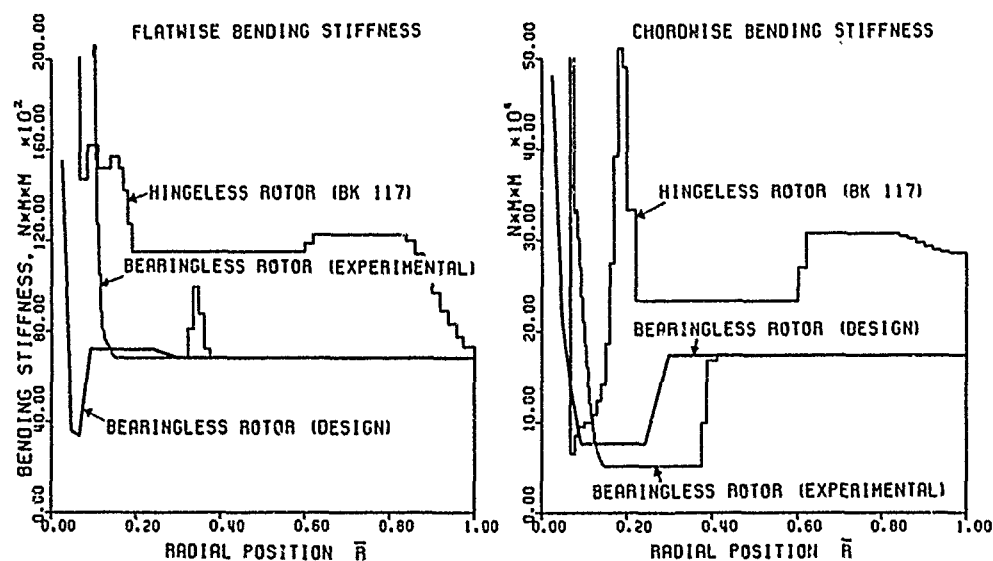


Fig. 16 Blade bending stiffness for hingeless/bearingless rotors

10-12 design gross weight of both rotor systems is different. The plots on the right side of Fig. 16 show that a strong reduction of the chordwise stiffness at the inboard section is needed for a realization of the soft-inplane rotor concept. However, it becomes evident by the plots on the left side of Fig. 16, that the variation of the flap bending stiffness of the blade root is even more extreme if the requirements of lower "hub stiffness" are to be fulfilled. Therefore a structural "quasi flapping-hinge" is provided for the blade root in all new rotor designs. The practical realization of such designs is possible by use of composite materials. The proper selection of the fiber (glass, graphite, kevlar) and the fiber orientation allows easy matching of the required rotor blade stiffness distribution, see Ref. 9. This possibility is always used to provide adequate torsional stiffness to the blades. The torsional stiffness of the BK 117 main rotor blade tip section (0.8 t; 1.0 R) for instance has been increased subsequently by using carbon fiber blade skin.

The BK 117 frequency diagram shown in Figure 17 is typical for MBB's rotor systems with fiberglass blades. The blade is well tuned. Generally resonance of the higher blade bending natural frequencies with the rotor harmonic excitation frequencies (multiple of rotor rotational frequency) must be avoided by special design considerations. Remembering

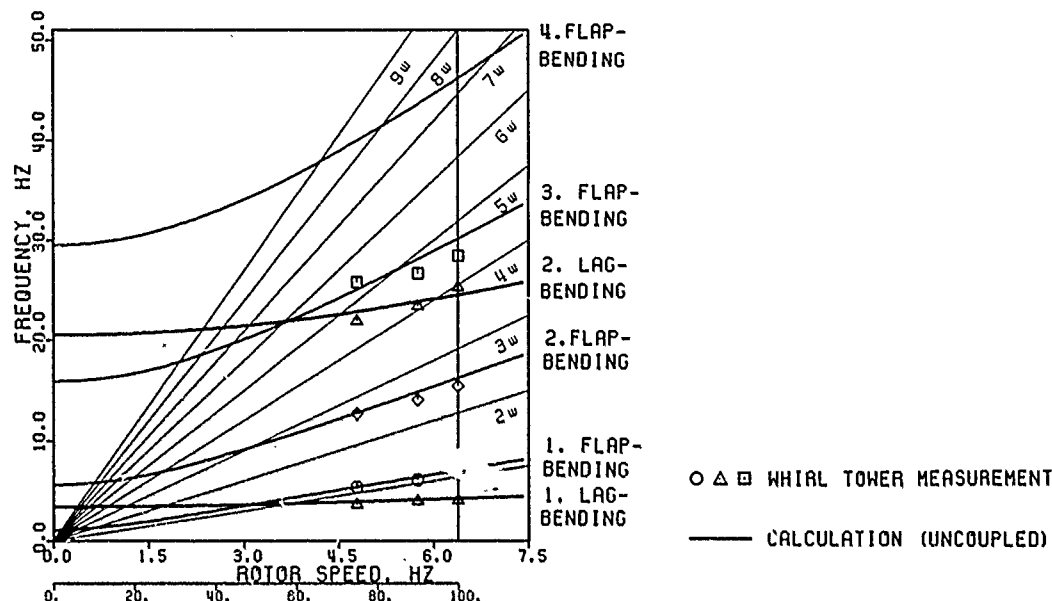


Fig. 17 BK 117 main rotor blade natural frequencies

that the centrifugal stiffening effect determines the flap-bending natural frequencies, proper blade tuning may be achieved effectively by special blade masses, see Ref. 22. Blade tuning for vibration reduction of a N-bladed hingeless or bearingless rotor should be concentrated on those flap-bending modes, that "control" the blade-harmonic N/rev-hub moment excitation in the fixed body frame. Flight tests as well as structural dynamic investigations have confirmed, that the fuselage vibration response is quite sensitive to moment excitation. The fourbladed BK 117 main rotor produces 4/rev, 8/rev ... vibrations. The vibration level of the BK 117 has been improved by reducing the 3/rev- and 5/rev-flap-bending blade moments (rotating frame), that transmit to the hub 4/rev pitch and roll moments (nonrotating frame). From the frequency diagram of Fig. 17 it is easily derived, that the second and third flap-bending mode are of special importance for the vibration problem. The tuning process of the BK 117 rotor blade is illustrated in Figure 18. The modal amplification functions on the right side of the figure show

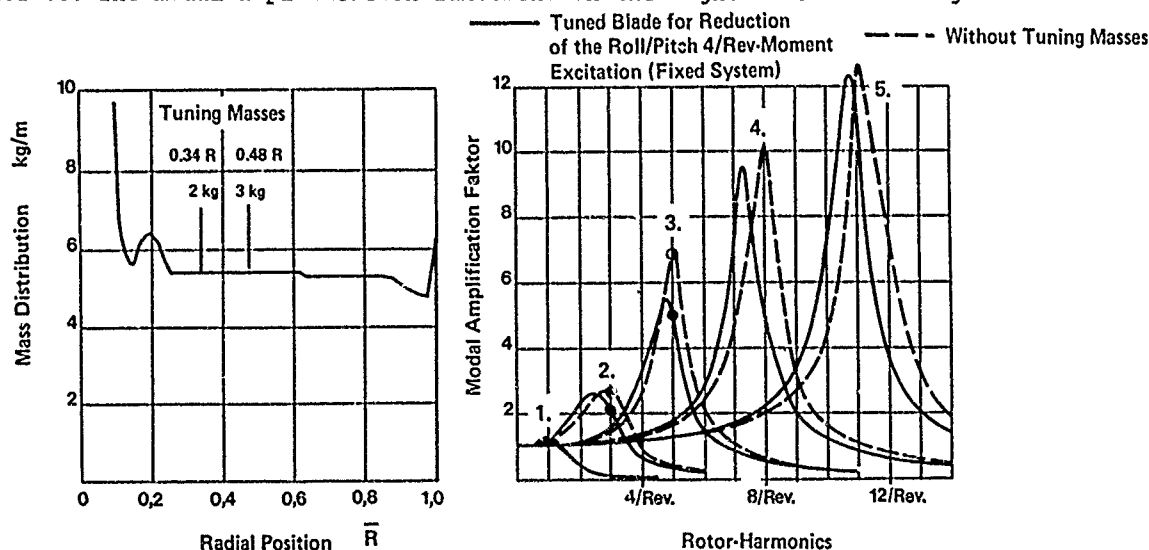


Fig. 18 Influence of tuning masses on the modal amplification factors for flap-bending of BK 117 main rotor blade

the success possible with blade tuning. The final blade mass distribution and the position of the two tuning masses are plotted on the left side of Fig. 18. To complete this section, Figure 19 shows the rotor-harmonic flap-bending moment distribution of the BK 117 near the blade root. The results of Fig. 19 are extracted from level flight tests of the prototype by a special modal analysis technique. A least square fit has been carried out for reducing the scatter of the data. The plots of Fig. 19 show that the 1/rev- and 2/rev-bending moments are clearly causing the highest dynamic blade loads in the hingeless rotor design. Strong resonance amplification of the higher harmonic bending moments are obviously avoided, a result of proper blade tuning described before. The moment peak at a flight speed of about 30 kts is characteristic for many helicopters and is due to rotor wake effects, see Ref. 22.

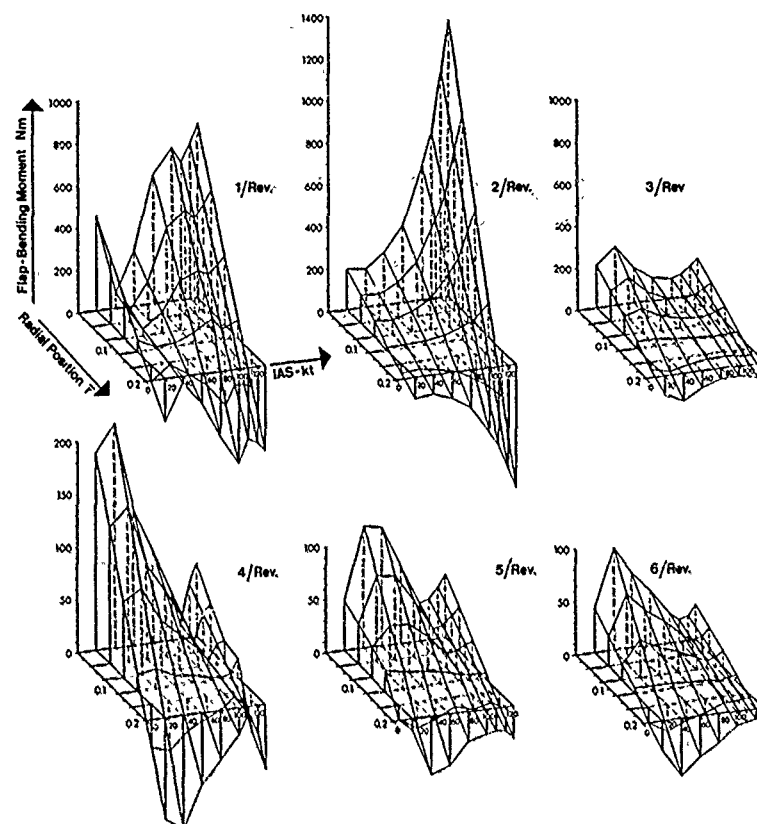


Fig. 19 Rotor-harmonic flap-bending moments vs radial position and flight speed for BK 117 main rotor

3.2 ADVANCED BLADE DESIGN AND RELATED AEROELASTIC STABILITY PROBLEMS

In the introduction, Fig. 3 was presented which gives an overview of rotary-wing aeroelastic instabilities. Classical rotorblade flutter and torsional divergence present no serious problem for mass balanced main rotor blades. Figure 20 presents the torsional frequency of the nonrotating BO 105 rotor blade that is required for stability with

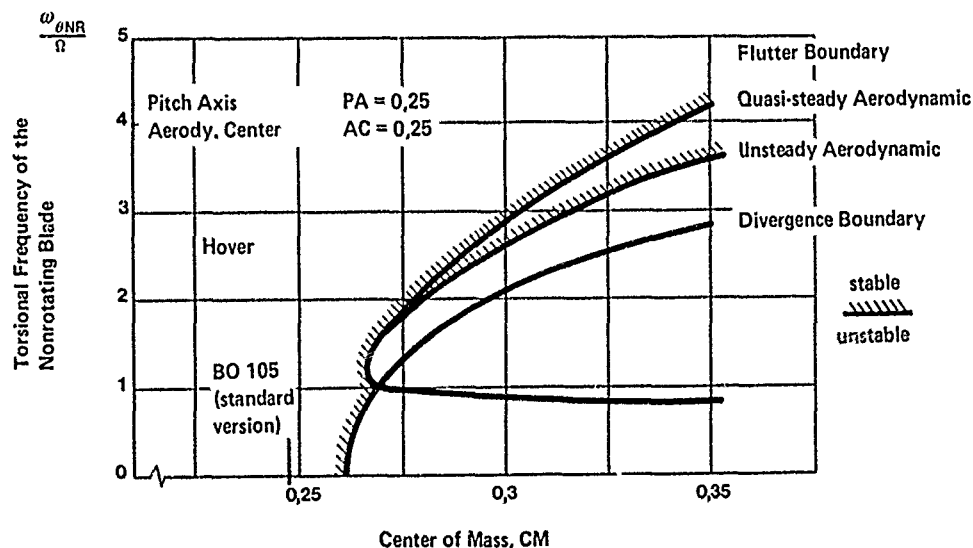


Fig. 20 Effect of rearward CM-position on the BO 105-rotor blade flutter/divergence boundaries

10-14 respect to flutter and divergence in case of a rearward shift of the center of mass (CM). For the chordwise balanced BO 105 blade (CM = 24,8%) flutter or divergence cannot occur. The situation would change for a CM-position aft of the aerodynamic center (AC), which may be the case for tail rotor blades, see next section. In the design of main rotor blades the provision of adequate mass balance is the rule because a minimum weight design is not required. Good autorotative rotor characteristics are achieved only with relatively heavy blades. Actually, the rotor inertia is the key parameter for autorotation.

The flutter/divergence boundaries of Fig. 20 are representative for helicopter main rotor blades in hover. In forward flight the boundary changes slightly but does not become critical for a mass balanced rotor blade, see Ref. 23. Forward flight introduces periodically varying airflow conditions at the advancing and the retreating blade. Figure 21 shows the calculated flutter boundary for a rotor blade with an extreme rearward shift of the center of mass (CM = 0.35). The differences in the flutter results

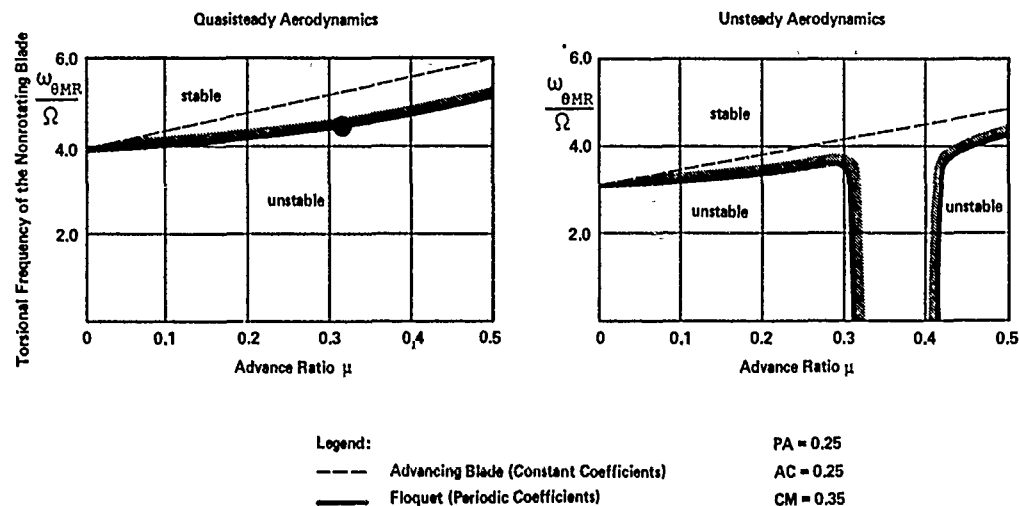


Fig. 21 Investigation of classical flutter in level flight for a rotor blade with extreme rearward shift of the blade center of mass

using quasisteady and unsteady aerodynamics respectively are remarkable. More important for the subject of this section is the result of Figure 22, which illustrates the frequency content of the flutter solution (marked in Fig. 21 by a point). The rotor is able to generate multi-frequency flutter oscillations that are unknown in fixed-wing flutter theory. The occurrence of multi-frequency non-rotor-harmonic blade oscillations is typical for aeroelastic instability phenomena encountered at high forward speeds. Examples will be given later.

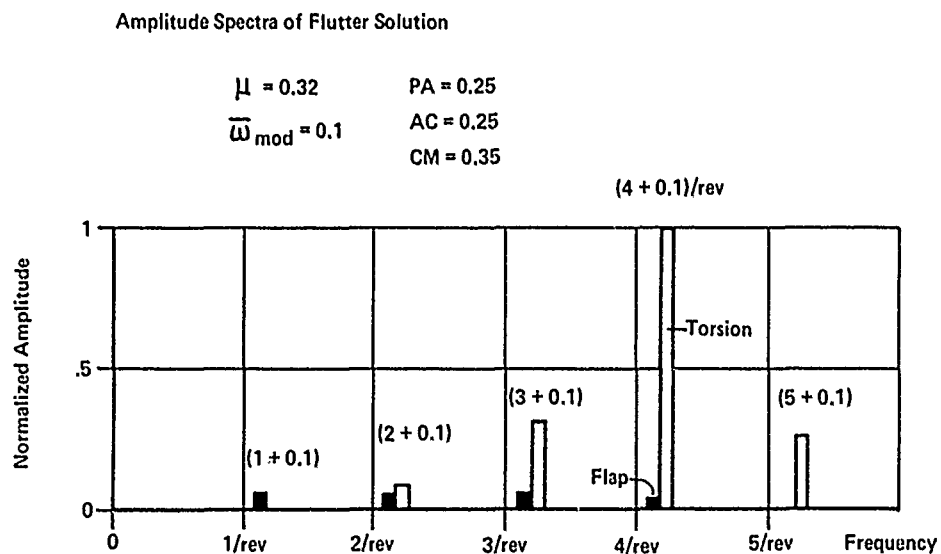


Fig. 22 Typical multi-frequency flap-bending-torsion oscillations at the flutter boundary

Rotor blade wake flutter, noted in Fig. 3, is another instability phenomenon that is unknown in fixed-wing aeroelasticity. Figure 23 shows an advanced geometry blade with swept tips, designed for improvement of the helicopter flight characteristics at high speeds. A detailed discussion of this blade design and flight test results are found in Ref. 24. The flight tests have been performed on a BO 105 helicopter. For the hovering rotor, however, strong torsional blade oscillations have been measured. Figure 24 shows the pitch link load waveform and the corresponding amplitude spectrum in hover. Besides

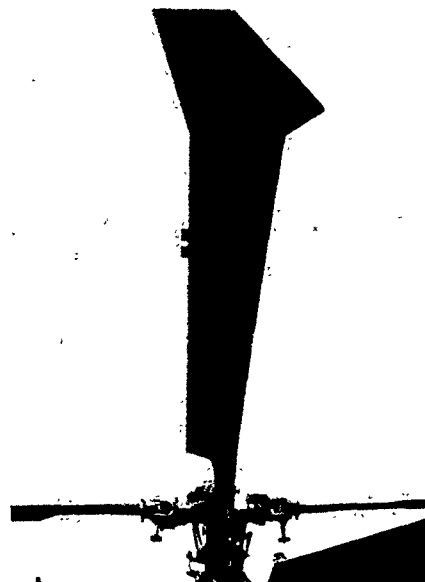


Fig. 23 Advanced swept blade-tip geometry

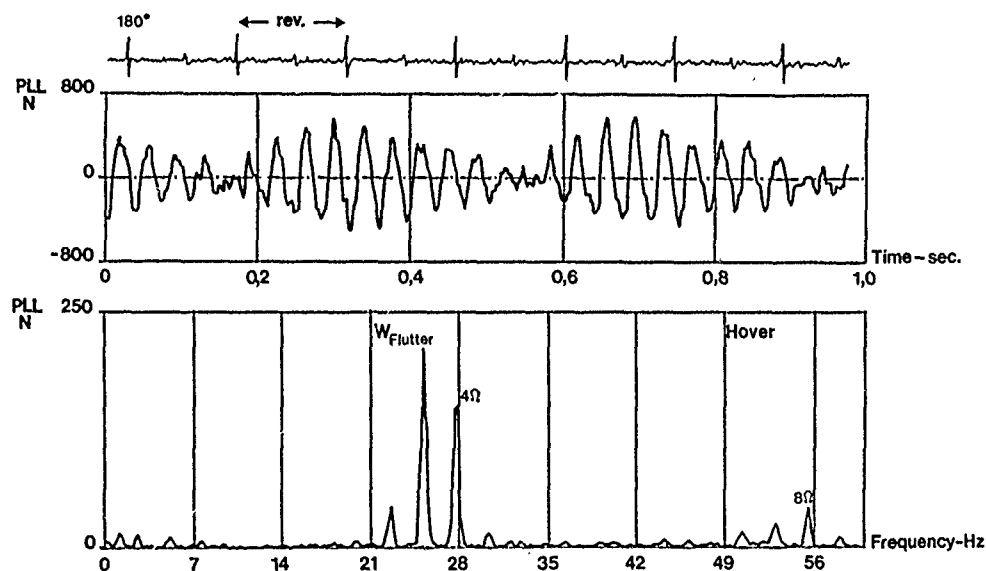


Fig. 24 Wake excited flutter-waveform and amplitude spectrum of control loads with swept wing tips

The 4/rev and 8/rev amplitudes a sharp spike appears at 3.6/rev, which is close to the natural torsional blade frequency. The tested blade was mass-overbalanced with respect to the pitch axis. The extreme forward position of the pitch axis at the swept tip is depicted in Figure 25 on the right side. On the left side of Fig. 25 the aerodynamic

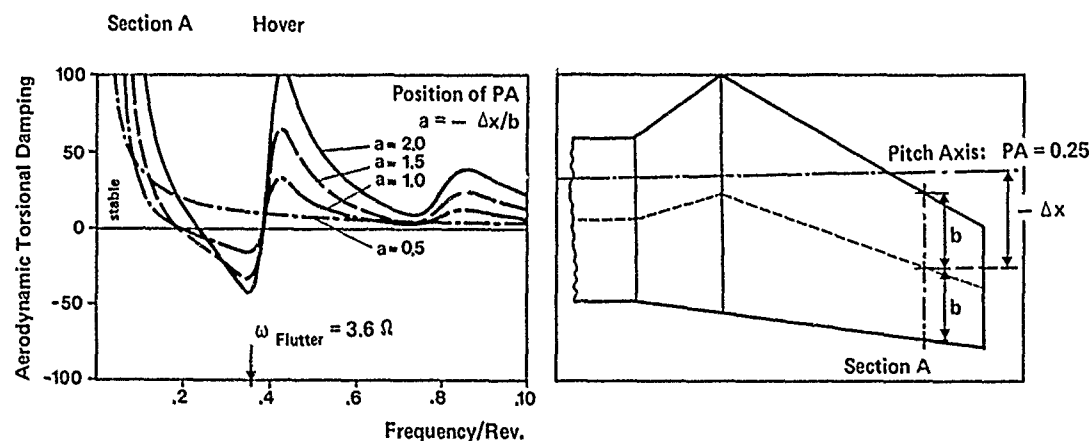


Fig. 25 Negative torsional damping for swept wing tip

10-16

torsional damping is calculated with consideration of wake effects from previous blade passages, see Ref. 25. The position of the pitch axis is characterized by the parameter "a" which is about 1.5 for section A. The torsional damping becomes negative for this value at the measured flutter frequency. It has been concluded that wake-excited flutter was the cause for the torsional oscillations shown in Fig. 24. These oscillations cease completely in forward flight.

An important aspect on the torsional design of a helicopter blade is stall flutter, noted in Fig. 3. A major design objective is to produce a helicopter that has both high maneuver and high forward flight speed capability. Typical stall flutter boundaries are shown in Figure 26. Large spikes in the control loads appearing in the fourth quadrant

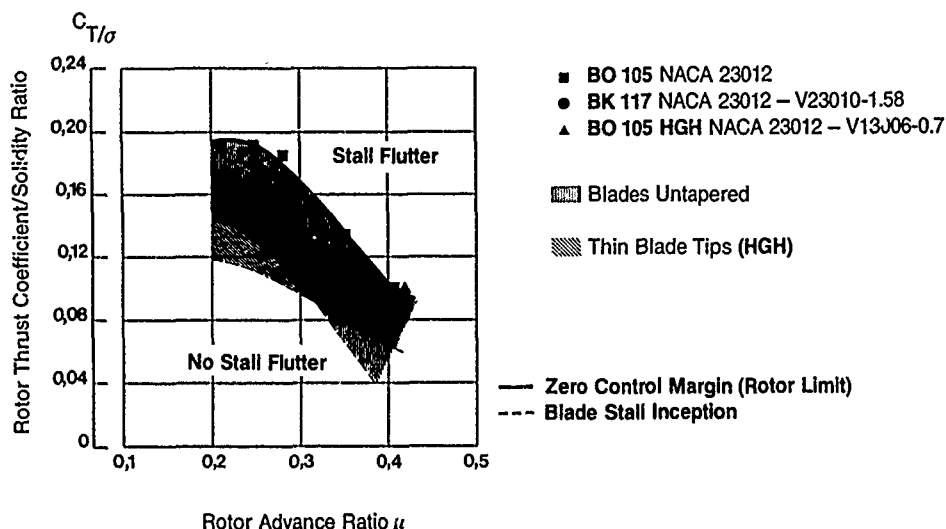


Fig. 26 Stall flutter boundaries (flight test)

of the blade azimuth are usually attributed to stall flutter. A typical control load time history and amplitude spectrum at high rotor thrust is plotted in Figure 27, taken from Ref. 26. The high pitch link loads result from an aeroelastic self-excited pitching

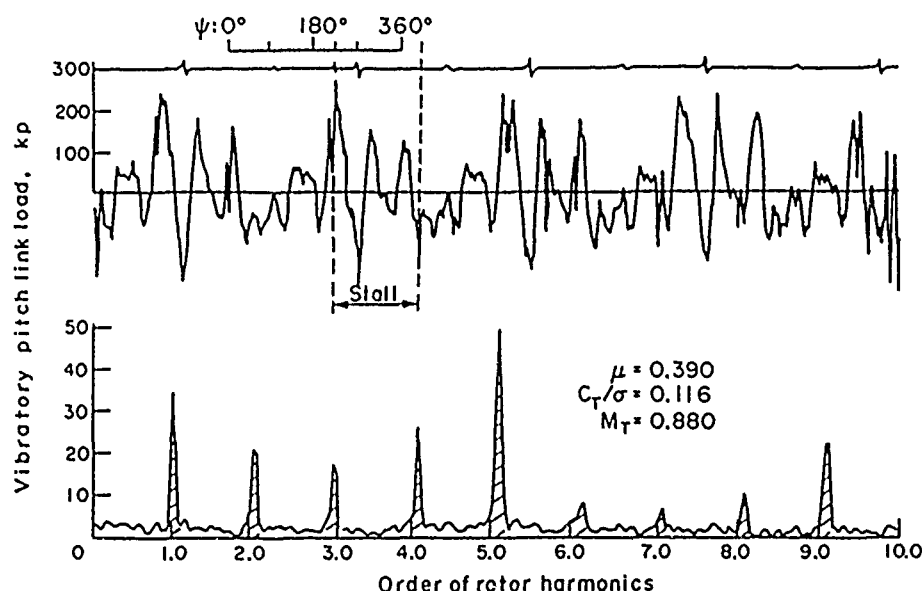


Fig. 27 Waveform and amplitude spectrum of excessive control loads due to stall (thin tip blades)

motion persisting only over small azimuth regions. Consequently the blade motions repeat periodically every revolution, manifested through the higher rotor-harmonic content in the spectrum of Fig. 27. This type of stall-related phenomenon may be better characterized as an excessive response. Strictly, stall flutter is a limit-cycle oscillation whose frequency is determined by the system characteristics (torsional dynamics). Figure 28 - again taken from Ref. 26 - shows a stall-related limit-cycle oscillation, which results in non-rotor-harmonic control loads with distinct frequencies at $(v + 0.2)\Omega$, $v = 0, 1, 2, \dots$. These multi-frequency oscillations are typical for rotary-wing aeroelastic instabilities, pointed out theoretically before. The observed nonlinear limit-cycle oscillations of Fig. 28 cannot be explained exclusively by the generation of negative aerodynamic damping

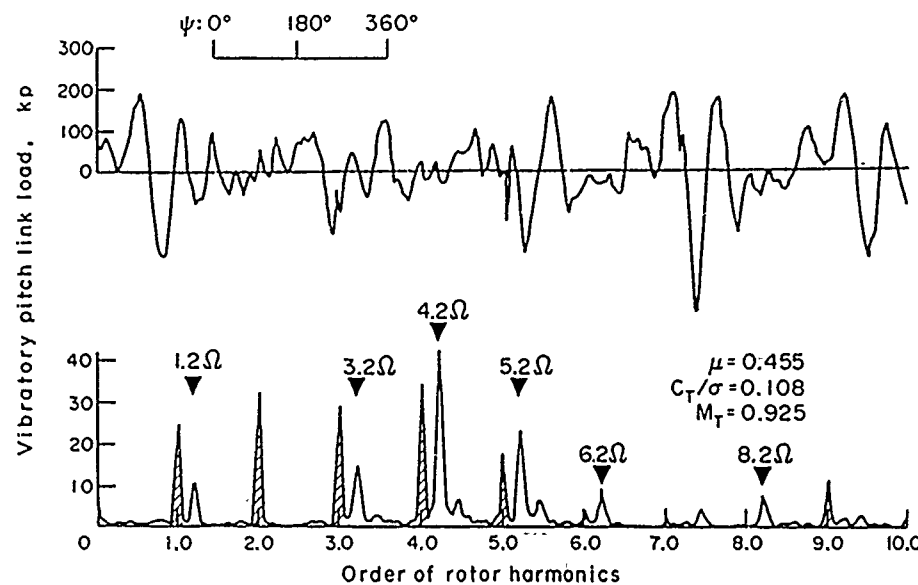


Fig. 28 Waveform and amplitude spectrum of non-rotor-harmonic control loads with thin tip blades

through successive dynamic stall-unstall cycles. Transsonic effects at the advancing blade and the periodically varying aerodynamic environment are supposed to have also great influence. Shock-induced aeroelastic instabilities, noted in Fig. 3, have been observed at high flight speeds for rotor blades with conventional airfoil sections. Figure 29 (from Ref. 26) presents measured pitch link loads from high speed flight tests. The control loads show strong spikes at rotor-subharmonic frequencies $(v + 0.5)\Omega$, $v = 0, 1, 2, \dots$. This complex aeroelastic phenomenon has been investigated in Ref. 26.

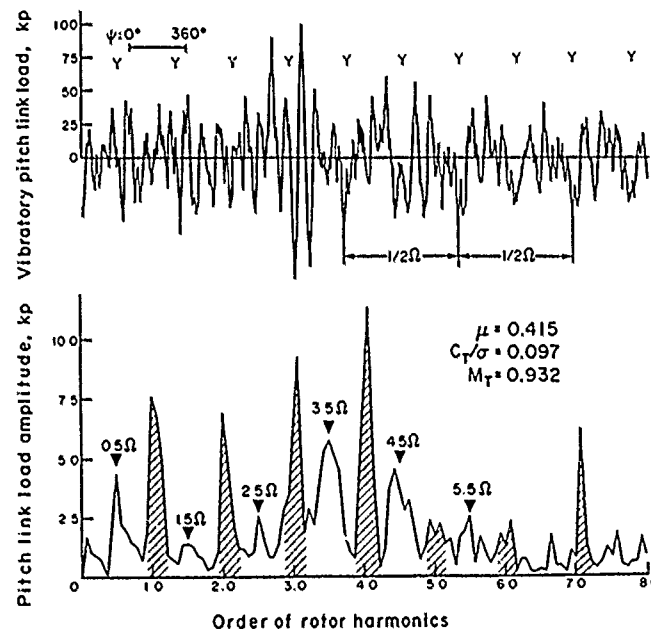


Fig. 29 Waveform and amplitude spectrum of rotor-subharmonic control loads with standard blades

The following explanation has been found: Rapid changes in pitching moments from statically stable to unstable conditions may occur on the advancing blade tips at transonic Mach numbers. These shock-induced nonlinear pitching moments influence the aeroelastic blade response by a motion-independent torsional blade excitation and by a motion-dependent negative aerodynamic torsional stiffness generation. The special nature of azimuthal and spanwise variation of the aerodynamic environment leads to parametric-self-excitation.

Looking back once more to Fig. 3 one will find that in the preceeding discussion, the flap-lag-torsion-instability and the stall-induced flap-lag instability have been omitted. This has been done on purpose, because both instabilities do not pose design problems for MBB's soft inplane main rotor configurations. Summarizing, various design problems due to blade aeroelastic instabilities have been found in the past due to unexpected torsional response and stability behaviour. The discussion has shown that additional research is needed to develop better design concepts that allow an optimal blade torsional tuning.

3.3 STRUCTURAL AND AEROELASTIC DESIGN OF A BEARINGLESS TAIL ROTOR

A composite bearingless tailrotor described above is under development at MBB. The design uses fiberglass bending-torsion-flexure to accommodate bending deflections and collective pitch control. Figure 30 shows a partial view of an experimental version.



Fig. 30 Flexural element and pitch control arms of a bearingless tail rotor (experimental)

The special design of the attachment area to the hub allows low flap stiffness at the inboard region. An integrated viscoelastic damping element is applied to the chordwise flexible part. The design of the pitch horn allows a positive geometrical δ_3 -coupling. It must be noted, that the experimental rotor uses BO 105 standard tailrotor blades. The radial distributions of the bending and torsional stiffness is shown in Figure 31. The increase of the flapwise bending stiffness at about $r = 0.32$ m is due to the stiff attachment of pitch-horn and flexural beam. The distribution of the chordwise bending stiffness is tailored according to the soft-inplane requirements.

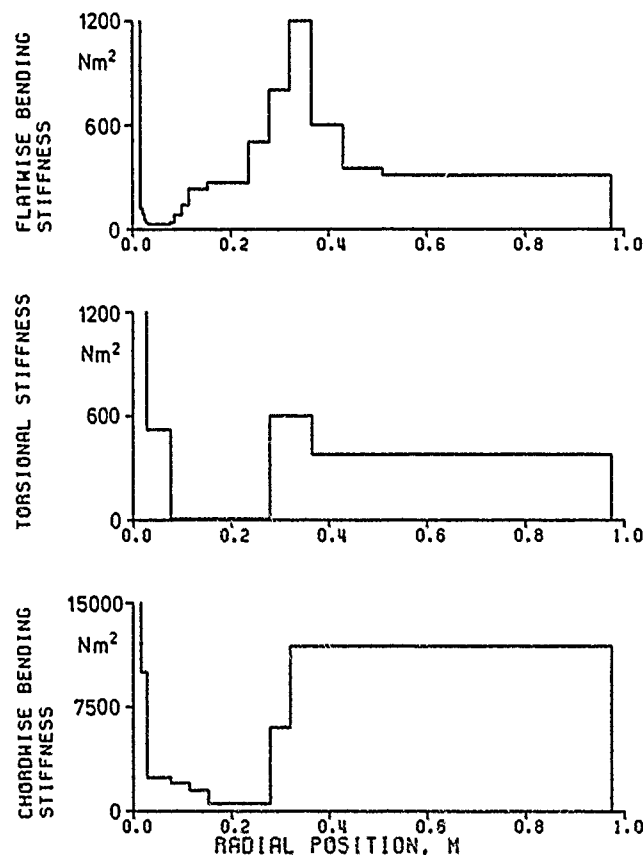


Fig. 31 Stiffness distribution of the bearingless tail rotor (experimental)

Using the data of Fig. 31 the coupled flap-bending torsional natural frequencies were calculated, as shown in Figure 32. The dashed lines mark calculations without aerodynamic forces. The fundamental flap-bending frequency is increased by aerodynamic forces (δ_3 -effect) from 1.05/rev to about 1.23/rev at 100% rpm, while the frequency of the second mode (1. torsion) is considerably decreased. The third mode (2. flap-bending) is only weakly affected. For this mode, the agreement between test and calculation is poor, because the beam model used in the computer program is no longer adequate for this mode. Fig. 32 also contains data of the first lag bending natural frequency computed with an uncoupled beam model. The correlation with test data is fairly good.

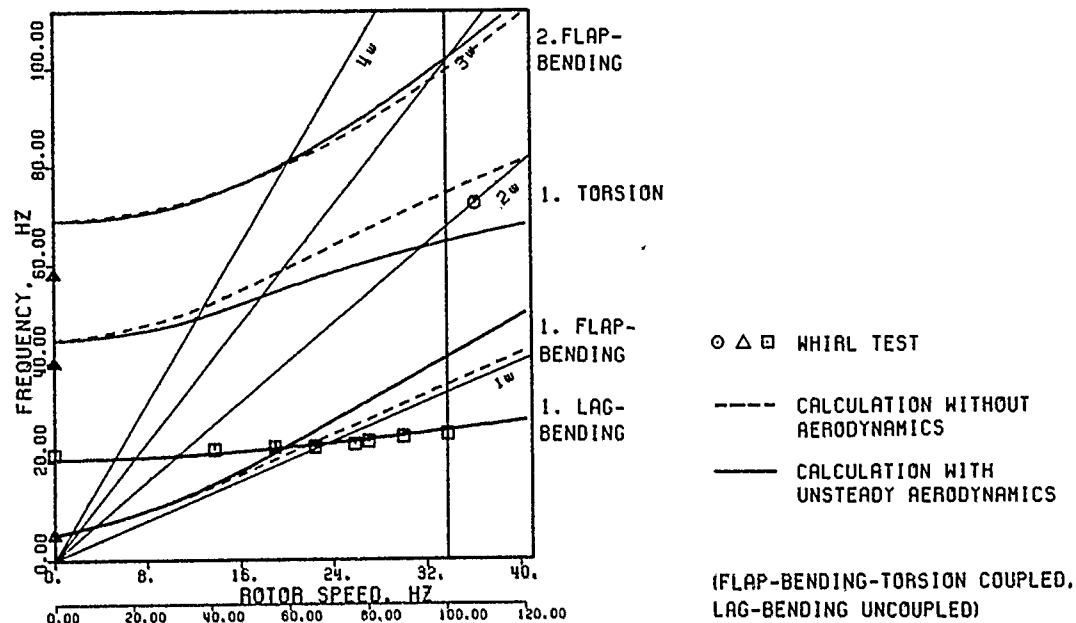


Fig. 32 Bearingless tail rotor (experimental) blade natural frequencies

In Figure 33 and Figure 34 the calculated first and second flap-bending/torsion mode shapes are plotted. The dashed lines indicate shapes at zero rotor speed, while the traced lines apply to nominal rotor speed. The right plot of Fig. 33 shows the effective δ_3 -angle versus rotor speed. In addition the results of an earlier pitchhorn design (pitch-horn 0.017 m shorter) is outlined. The picture indicates a considerable dependence of δ_3 -coupling on geometric design and rotor speed.

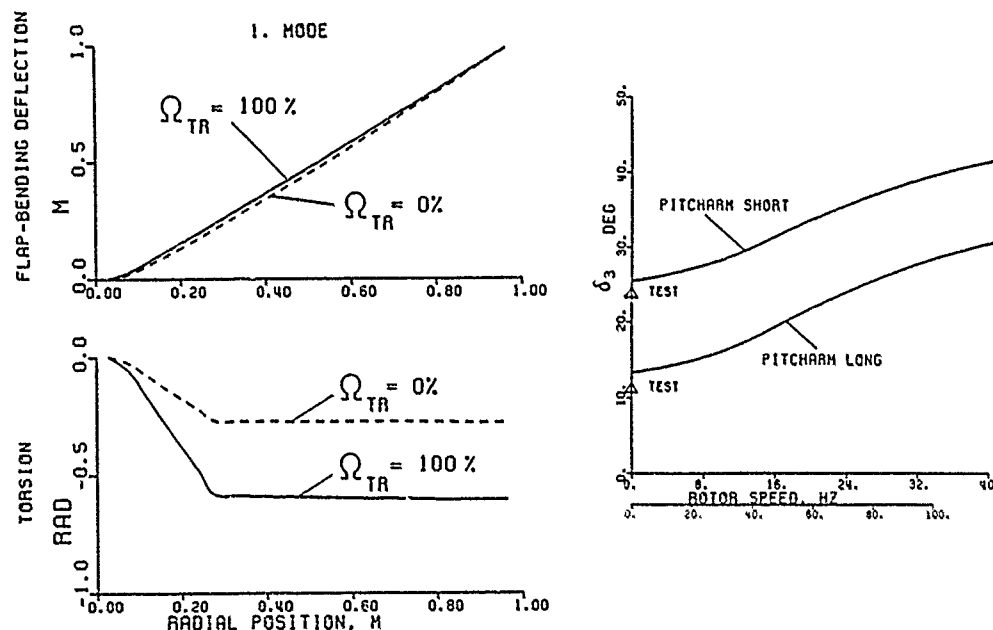


Fig. 33 Coupled bending-torsion mode shape for the bearingless tail rotor (experimental), pitcharm long, 1. mode

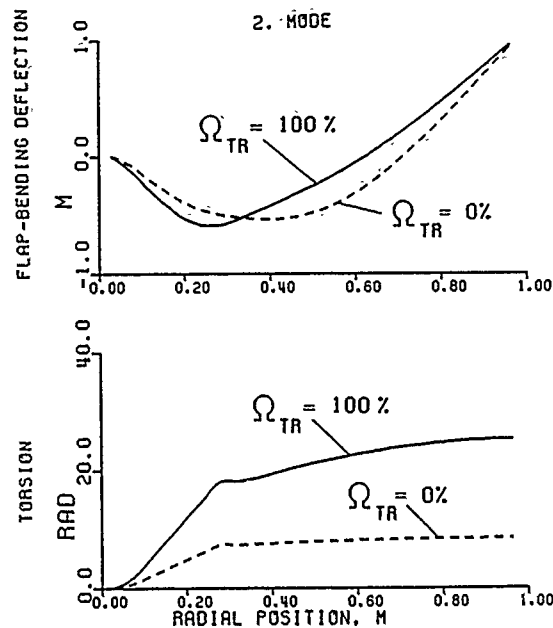


Fig. 34 Coupled bending-torsion mode shape for the bearingless tail rotor (experimental), pitch arm long, 2. mode

The flutter stability is investigated in Figure 35 for different chordwise CM-positions and rotor speeds. The calculated system damping ratios show that the second mode (1. torsion) is quite sensitive to a rearward shift of the center of mass. In addition, this mode is remarkably influenced by the stiffness of the pitch control system. The plot contains the CM-position of the unbalanced experimental tail rotor blade. On the right side of Fig. 35, the damping ratio versus rotor speed is plotted. Flutter is expected at high rotor-speeds outside of the operational range of the tail rotor. The analytical flutter investigations show, that due to the relative low torsional frequency and the high negative pitch-flap coupling, the bearingless tail rotor is sensitive to flutter. Chordwise mass balance may be required for this system.

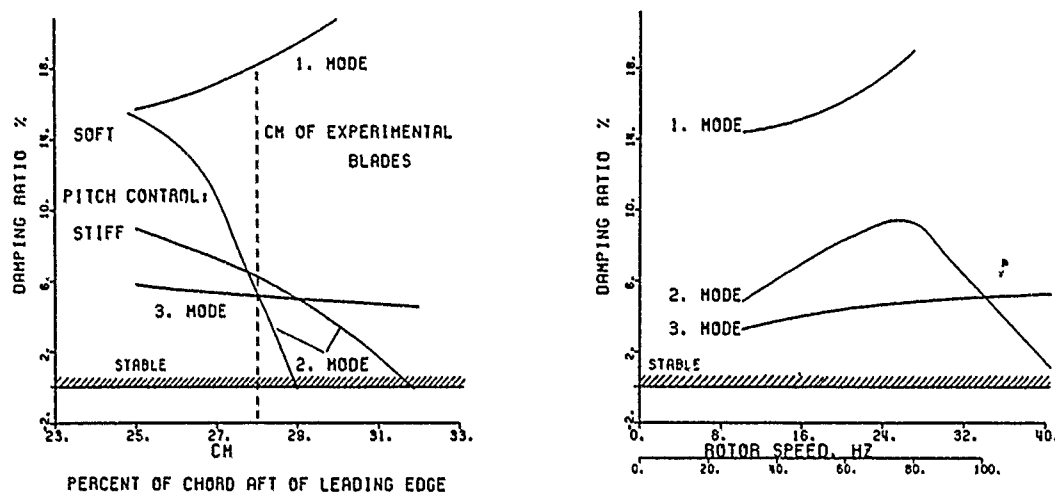


Fig. 35 Tail rotor flutter stability

4. AEROELASTIC DESIGN ASPECTS FOR COUPLED ROTOR-BODY STABILITY AND RESPONSE

The interplay between rotor and fuselage and related aeroelastic design considerations are illustrated by two examples.

4.1 DESIGN EFFORTS FOR IMPROVING ROTOR-BODY AEROMECHANICAL STABILITY

Coupled rotor-body aeroelastic - or more customary - aeromechanical stability of soft-inplane rotors is an important field for design activities. The aeromechanical stability margin depends strongly on the damping of the blade inplane motion. For composite

hingeless and bearingless configurations the inherent material damping and the aerodynamic damping by airfoil drag are normally not sufficient and additional damping sources are required. The damping may be augmented by mechanical damping devices or by blade motion coupling that introduces aerodynamical damping. The BO 105/BK 117 hingeless rotor system uses both means, a "built-in" mechanical blade root attachment damping and favourable aeroelastic motion coupling. It is one of the main features of the BO 105/BK 117 hingeless rotor system that aeromechanical stability on the ground and in air is thus achieved without a discrete voluminous mechanical blade lead-lag damper.

The high mechanical damping capacity of the BO 105/BK 117 rotor blade is illustrated in Figure 36. The rotorblade with the attachment mounting is the actual lead-lag damping "generator". Without tension the measured damping curve is determined mainly by friction forces between the fiberglass rovings and the attachment mounting. With tension the situations is more complex. The resulting damping is somewhat reduced but is still sufficient.

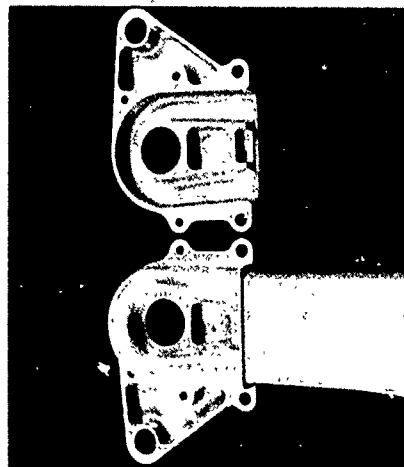
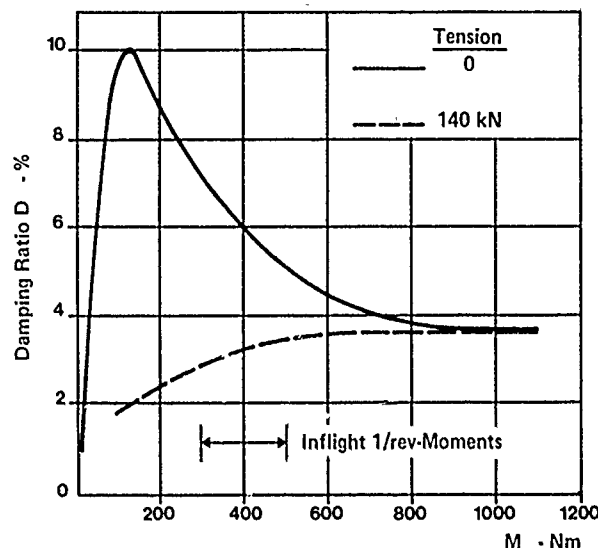


Fig. 36 High mechanical lead-lag damping blade root attachment (BO 105/BK 117 system)

Parallel to the development of the new composite hingeless and bearingless rotor configurations MBB has started a research and development program for elastomeric blade lead-lag damping devices. The following concept has found to be most effective: The damping layer is attached directly to the blade root section and covered by a very stiff plate. Figure 37 (right) shows the experimental bearingless main rotor blade. The elastomeric damper is attached in this case to the flexbeam. The bench test results give an impression of the damping characteristics.

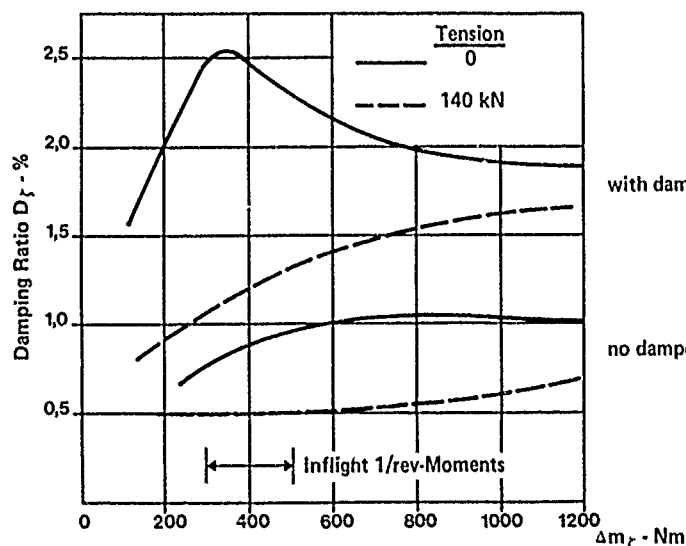


Fig. 37 Experimental investigation of elastomeric blade lead-lag dampers

It has been pointed out before, that a negative pitch-lead coupling factor stabilizes the blade inplane motion. The key design parameters for controlling pitch-lead coupling are precone (β_c) and preflap (β_p). Zero precone has found to be beneficial for lead-lag damping. Whirl tower tests of different rotor configurations are gathered in Figure 38. The results fully confirm the design considerations. Negative pitch-lead coupling increases with thrust for zero precone and built-in preflap. It explains the improved

10-22 damping values of the modified BO 105-hingeless rotor with $\beta_c = 0$, $\beta_p = 2.5^\circ$. These results are important for air resonance stability considerations.

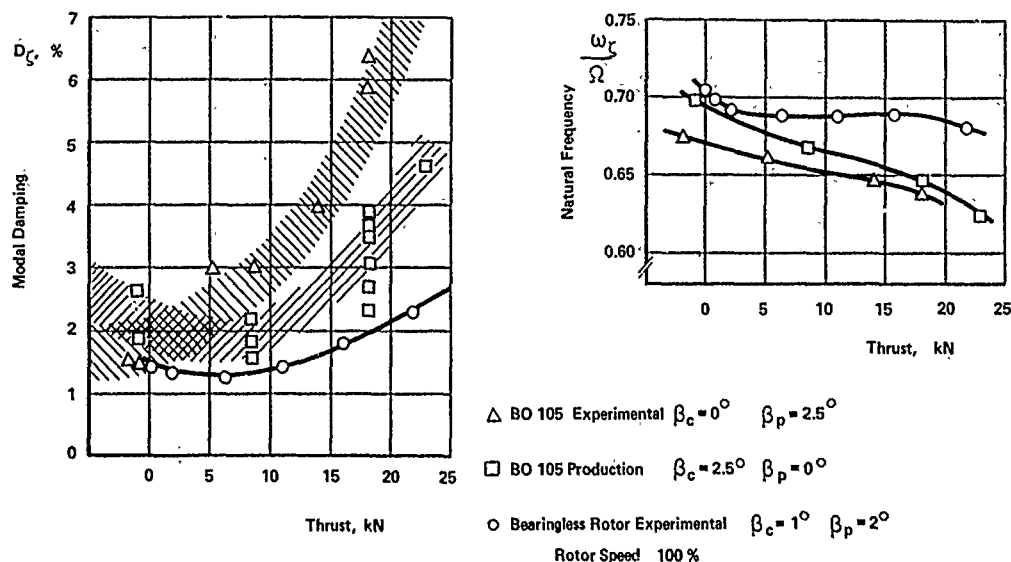


Fig. 38 Influence of precone and preflap on blade lead-lag damping and frequency

For the soft-inplane rotor concept both air and ground resonance are possible, if the rotor driving frequency ($\Omega - \omega_c$) coalesces with a body frequency. Figure 39 shows the critical operating regions of the BK 117 helicopter on ground and in air. Potential instability on the ground is caused by the body fore-and-aft/pitch-mode and in air by the body roll mode. It has been found that a stiff landing gear tuning (the F/A-pitch

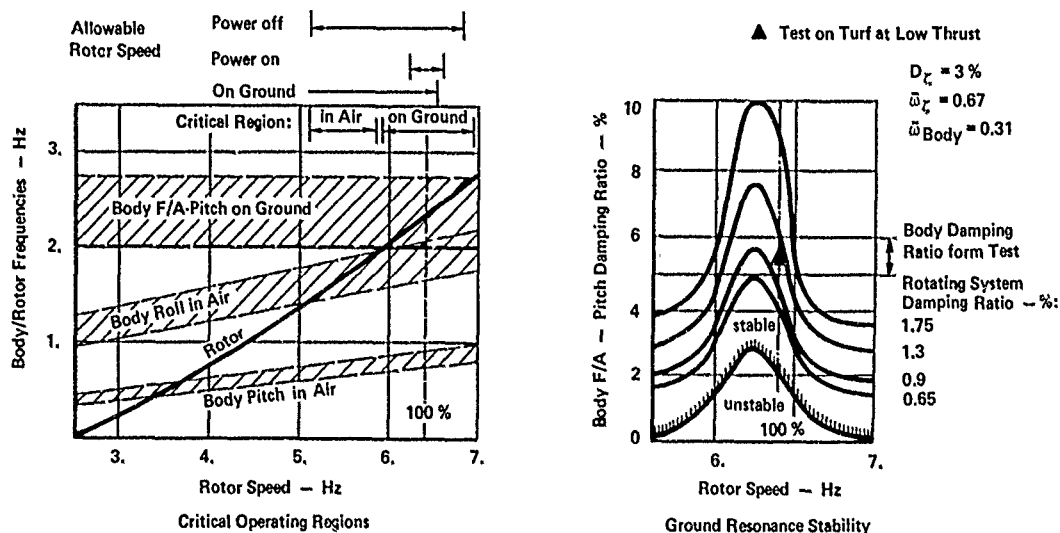


Fig. 39 Ground and air resonance characteristics (BK 117)

mode is the lowest body mode on ground) is advantageous, if the body-roll frequency is well above the operational region. The body roll mode is generally critical for ground resonance due to the small body roll moment of inertia compared to the body pitch moment of inertia. The body roll frequency in air depends on the blade flap-bending stiffness and the body mass/inertia data which are not at the free disposal of the designer. The ground resonance stability margin is presented on the right side of Fig. 39. This example shows that the BK 117 helicopter has an adequate damping margin even for low rotor thrust. The established damping ratio in the rotating system is above 1%. Special ground resonance tests have confirmed this results.

4.2 DESIGN CONSIDERATIONS FOR IMPROVED AEROELASTIC TAILBOOM RESPONSE CHARACTERISTICS

It has been reported in Ref. 6 that the initial configuration of the BK 117 rotor hub and aft-fuselage caused wake induced lateral bending oscillations of the tail boom, known as "tail shake". Figure 40 taken from Ref. 27 illustrates the main interference effects in forward flight. Figure 41 shows some flight test results. It has been found that the high tail boom lateral bending moments are caused by a vortex resonance phenomenon. The first natural bending frequency (ω_{TB}) of the tail boom in lateral direction

is near the vortex shedding frequency (ω_v). A detuning of the tailboom was not possible in this actual case. Wind tunnel and flight tests have shown that a hub cap and the omission of the fuselage spoiler are effective in solving the tail shake problem of the BK 117 helicopter.

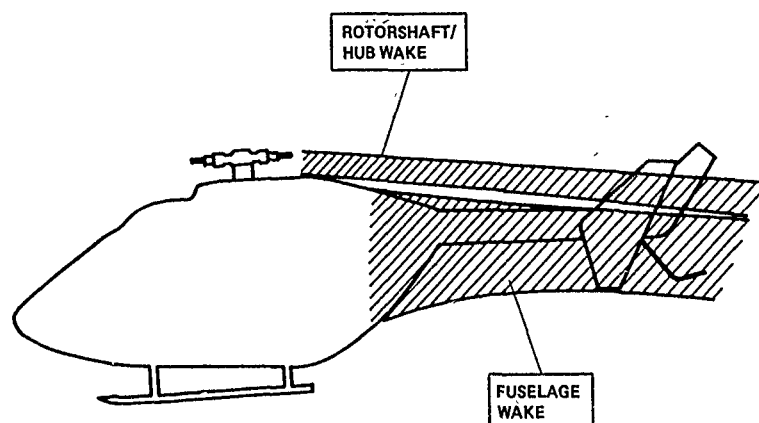


Fig. 40 Main interference effects between fuselage/hub and tail area

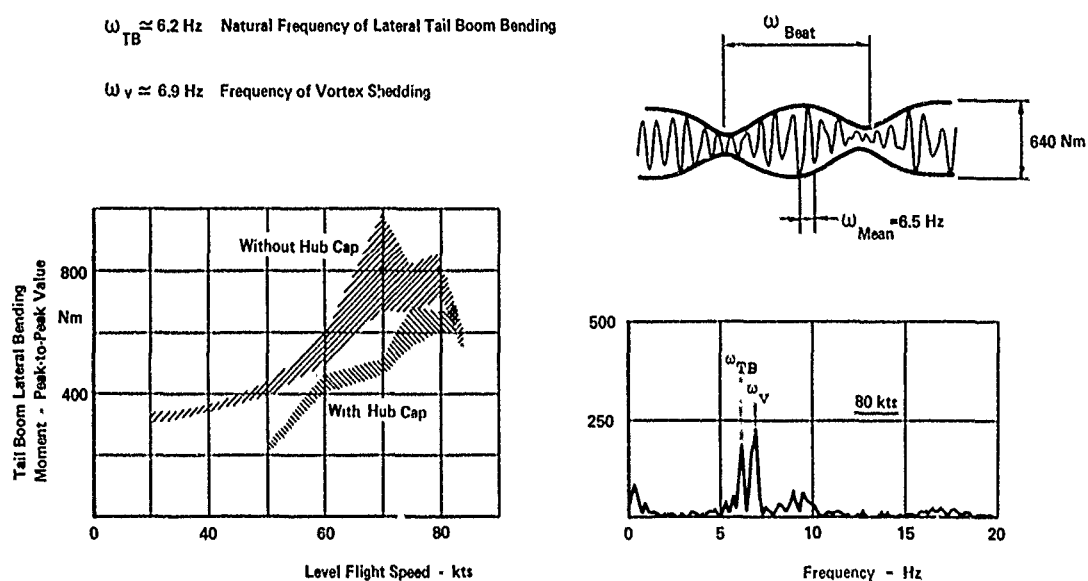


Fig. 41 Tail shake phenomenon

5. CONCLUDING REMARK

The hingeless and bearingless rotor concept is very sensitive to small parameter variations, therefore the various design parameters have to be optimized carefully, considering aerodynamic, dynamic and aeroelastic requirements together.

REFERENCES

1. K.H. Hohenemser Hingeless Rotorcraft Flight Dynamics.
AGARD-AG-197
2. R.A. Ormiston Investigations of Hingeless Rotor Stability.
International Symposium on Aeroelasticity, Nuremberg,
October 5-7, 1981
3. E.F. Weiland Development and Test of the BO 105 Rigid Rotor Helicopter.
J. American Helicopter Soc. Vol. 14, No. 1, January 1969
4. G. Reichert,
H. Huber Influence of Elastic Coupling Effects on the Handling
Qualities of a Hingeless Rotor Helicopter.
39th AGARD FLIGHT MECHANICS PANEL MEETING, Paper 12,
Virginia, 20-23 September 1971
5. E. Weiland,
I. Kagitomi BK 117 a New Helicopter of International Cooperation.
Fifth European Rotorcraft and Powered Lift Aircraft Forum,
Paper No. 10, Amsterdam, September 4-7, 1979
6. H. Huber,
T. Masue Flight Characteristics Design and Development of the
MBB/KHI BK 117 helicopter.
Seventh European Rotorcraft and Powered Lift Aircraft Forum,
Paper No. 35, Garmisch-Partenkirchen, September 8-11, 1981
7. G. Reichert Basic Dynamics of Rotors Control and Stability of Rotary
Wing Aircraft Aerodynamics and Dynamics of Advanced
Rotary-Wing Configurations.
AGARD Paper Reprinted from Lecture Series No. 63 on
Helicopter Aerodynamics and Dynamics
8. P.P. Friedmann Formulation and Solution of Rotary-Wing Aeroelastic
Problems.
International Symposium on Aeroelasticity, Nuremberg,
October 5-7, 1981
9. G. Reichert,
E. Weiland Long Term Experience with a Hingeless/Composite Rotor.
AGARD Flight Mechanics Panel Symposium on Rotorcraft
Design, Paper 11, NASA, Ames, California, May 16-19, 1977
10. H. Huber,
H. Frommlet,
W. Buchs Development of a Bearingless Helicopter Tailrotor.
Sixth European Rotorcraft and Powered Lift Aircraft Forum,
Paper No. 16, Bristol, September 16-19, 1980
11. H. Huber Parametric Trends & Optimization - Preliminary Selection
of Configuration - Prototype Design & Manufacture.
AGARD Paper Reprinted from Lecture Series No. 63 on
Helicopter Aerodynamics and Dynamics
12. W. Johnson Helicopter Theory.
Princeton University Press, 1980
13. A.R.S. Bramwell Helicopter Dynamics.
Department of Aeronautics, the City University, London,
Edward Arnold, 1976
14. R.E. Hansford,
I.A. Simons Torsion-Flap-Lag Coupling on Helicopter Rotor Blades.
Journal of the American Helicopter Society, October 1973
15. D.H. Hodges,
R.A. Ormiston Stability of Elastic Bending and Torsion of Uniform
Cantilever Rotor Blades in Hover with Variable Structural
Coupling.
NASA TN D-8192, April 1976
16. H. Huber Effect of Torsion-Flap-Lag Coupling of Hingeless Rotor
Stability.
29th Annual National forum of the American Helicopter
Society, Preprint No. 731, Washington, D.C., May 1973
17. D.H. Hodges Nonlinear Equations of Motion for Cantilever Rotor Blades
in Hover with Pitch Link Flexibility, Twist, Precone,
Droop, Sweep, Torque Offset, and Blade Root Offset.
NASA TM X-73, 112, May 1976
18. D. H. Hodges,
R.A. Ormiston Stability of Hingeless Rotor Blades in Hover with
Pitch-Link Flexibility.
AIAA Journal, Vol. 15, No. 4, April 1977

19. J.E. Burkam,
Wen-Liu Miao Exploration of Aeroelastic Stability Boundaries with
a Soft-in-Plane Hingeless-Rotor Model.
28th Annual National Forum of the American Helicopter
Society, Preprint No. 610, May 1972
20. D.H. Hodges An Aeromechanical Stability Analysis for Bearingless
Rotor Helicopters.
Journal of the American Helicopter Society, January 1979
21. P.G.C. Dixon,
H.E. Bishop The Bearingless Main Rotor.
Journal of the American Helicopter Society, July 1980
22. G. Reichert,
H. Strehlow Survey of Active and Passive Means to Reduce Rotorcraft
Vibrations.
International Symposium on Aeroelasticity, Nuremberg,
October 5-7, 1981, DGLR-Bericht 82-01
23. G. Reichert The Influence of Aeroelasticity on Stability and Control
of a Helicopter with a Hingeless Rotor.
AGARD 34th Flight Mechanics Panel Meeting, Marseille,
21-24 April 1969
24. H. Huber Helicopter Flight Characteristics Improvement Through
Swept-Tip Rotor Blades.
Fifth European Rotorcraft and Powered Lift Aircraft Forum,
Paper No. 29, Amsterdam- 4-7 September 1979
25. R.G. Loewy A Two-Dimensional Approximation to the Unsteady Aerodyna-
mics of Rotary Wings.
Journal of the Aeronautical Sciences, Vol. 24, Feb. 1957
26. H. Huber,
H. Strehlow Hingeless Rotor Dynamics in High Speed Flight.
First European Rotorcraft and Powered Lift Aircraft Forum,
Paper No. 13, Southampton, September 1975
27. H. Huber,
G. Polz Studies on Blade-to-Blade and Rotor-Fuselage-Tail
Interferences.
AGARD Fluid Dynamics Panel Specialists Meeting on
Prediction of Aerodynamic Loads on Rotorcraft, London,
17-18 May 1982

THE INFLUENCE OF AEROELASTIC STABILITY REQUIREMENTS ON HELICOPTER DESIGN

by
S.P. King
Chief Dynamicist
Westland Helicopters Limited
Yeovil, Somerset
England

SUMMARY

The avoidance of aeroelastic and aeromechanical instabilities is a prime objective of aircraft design, and must be considered throughout the design cycle. Due to lack of data the analysis of instabilities during preliminary design is a difficult task, consequently simple models may be more useful than large and complex analyses. A number of potential instabilities are discussed; blade flutter; main rotor flap-lag stability; tail rotor pitch-flap-lag and the complete aircraft problems of ground and air resonance. In each case a description of the mechanism involved in the instability is given and a simple analytic tool for its investigation is suggested.

Notation

b = Lag mode first moment $= \int_0^R m(r)g(r)dr$
 $e(r)$ = Chordwise cg offset from the feathering axis
 $f(r)$ = Flap mode shape
 $g(r)$ = Lag mode shape
 h = Vertical distance from fuselage cg to rotor hub
 I = Lag mode inertia $= \int_0^R m(r)g^2(r)dr$
 I_f = Fuselage roll inertia about cg
 l = Height of fuselage cg above roll mode centre of rotation
 $m(r)$ = Blade mass distribution
 m_e = Aircraft effective mass at hub
 m_f = Total aircraft mass
 n = Number of blades
 q = Rotor - aircraft mass ratio $= nb^2/m_e I$
 r = Radial position on blade
 R = Rotor radius
 V_T = Tip Speed
 ω_F = Non-dimensional rotor flap mode frequency
 ω_L = Non-dimensional rotor lag mode frequency
 ω_Y = Non-dimensional fuselage mode frequency
 ϕ = Inertia ratio $= 2I_f/In$
 $\theta(r)$ = Torsion mode shape
 ξ_Y = Ratio of critical fuselage damping, relative to ω_Y
 ξ_L = Ratio of critical lag damping, relative to ω_L
 σ_{max} = Peak value of instability, ratio of critical relative to ω_L

1. INTRODUCTION

An important consideration at the preliminary design stage of any new project is the avoidance of aeromechanical instabilities. A number of potential instabilities exist, some being basically single blade phenomena, such as tail rotor flap-lag stability, others consisting of the interaction between the complete rotor system and the fuselage, for example ground resonance. Some of these problems are well understood, others less well, but a feature common to all at the preliminary design stage will be a lack of detailed data for the accurate prediction of stability boundaries and the need to consider a large number of possible configurations. What are required are simple design rules and analyses which may be used to avoid the instabilities. Of course, an understanding of the mechanism involved in the phenomena will be very helpful, not least by indicating which parameters are important and which may be considered of only secondary significance.

At a later stage in a project much more powerful analyses are available which can be used to confirm the stability. An excellent review of the current status of rotary-wing aeroelastic analysis for both stability and response has been given by Friedman in ref. 1. The major disadvantage of using such tools during preliminary design is the lack of understanding gained by their use. After all, it is not of much help to know that a system is unstable if it is not known how to suppress the instability. The other disadvantages are the time required to prepare all the necessary data, and possibly the computer time involved in major parametric variations in a number of design variables.

11-12 The subdivision of rotor aeroelastic stability problems into hub fixed and hub free phenomena is convenient, but artificial, and for a number of problems must be done with care. An example of the importance of hub flexibility on what is essentially a single blade problem is the flap-lag-torsion stability of a supercritical tail rotor where the torsion mode frequency will be a function of the control system stiffness, and this stiffness will depend in turn upon the phase relationship between the motion of the separate blades. This type of effect can couple together a basically single blade problem into a rotor or even complete aircraft problem. If possible however consideration of the motion of a single blade will give the clearest understanding of the mechanism involved in an instability.

A large number of stability problems exist but only a limited number can be considered here. To fix ideas it is assumed that the type of aircraft being designed has a subcritical main rotor, ie fundamental lead-lag mode frequency less than once per rev., and a supercritical tail rotor. Both rotors are assumed to have more than two blades; this does not mean that the problems discussed here do not apply to two bladed rotors but the additional problems due to the lack of polar symmetry with two bladers are not considered.

The hub fixed problems are considered first, followed by the complete aircraft air and ground resonance instabilities. These latter problems do not include the very low frequency flight path stability problems. In each case a description of the phenomenon is given, and guide lines suggested for its avoidance. The type of analytical tools, in terms of degrees of freedom, most useful for preliminary work are also discussed.

2. HUB FIXED PROBLEMS

2.1 Flutter

This is a two degree of freedom instability, the freedoms being flap and torsion, with some mechanism coupling the two motions. The coupling between torsion and flap is aerodynamic; a perturbation in the blade pitch induces changes in the blade lift loads and causes the blade to flap. The coupling between flap and torsion may be of a number of forms, for example chordwise centre of mass offsets from the feathering axis or kinematic pitch-flap coupling due to the orientation of the hinges and control circuit. This problem is very similar to the fixed-wing flutter problem.

A preliminary analysis for flutter is most simply carried out using a two degree of freedom model, with one freedom being rigid blade flapping about an offset hinge (spring restrained for an hingeless rotor) and the other pure rigid body pitching about a feathering bearing. The hinge order should be the same as on the aircraft. Also to be included are chordwise centre of mass and centre of lift offsets from the feathering axis and any kinematic pitch-flap coupling. Using such a simple model stability boundaries similar to those shown in Fig. 1 can be produced. This shows the combinations of torsional stiffness and centre of mass offset which have to be avoided: in this particular case the centre of lift was taken to be on the feathering axis and no pitch-flap coupling was included. Clearly, the simplest way of avoiding the instability is to ensure that the centre of mass is forward of the quarter chord. It is worth pointing out that the inertia term coupling the flap and torsional motion is

$$\int_0^R f(r)\theta(r)e(r)m(r)dr$$

where $f(r)$ is the flap mode shape, $\theta(r)$ is the torsion mode shape, $m(r)$ is the mass distribution and $e(r)$ is the chordwise cg offset. Thus cg offsets in the neighbourhood of the tip are more important than at the root. The results in Fig. 1 are based upon rigid body mode shapes and a constant cg offset.

2.2 Main Rotor Flap Lag Stability

This section is entitled main rotor flap lag stability to distinguish it from the associated problems encountered on supercritical rotors which are discussed below. The instability is sometimes known as a pitch lag instability, but the basic degrees of freedom are flap and lag, with the instability arising from the presence of a kinematic pitch-lag coupling. The effect of this coupling is to induce aerodynamic lift loads in response to blade lag deflections, which cause the blade to flap and via the Coriolis loads induce more lag motion.

This is one of the more simple aeroelastic stability problems, since only rigid body flap and lead-lag degrees of freedom are required, together with the pitch-lag coupling and steady coning angle. Since only two degrees of freedom are involved analytical expressions may be obtained for the stability boundaries, at least for uniform blades in the hover. Simple quasi-steady aerodynamics with constant induced velocity are adequate for a preliminary analysis. Typical stability boundaries for two values of lag frequency are shown in Fig. 2; these results assumed a flap frequency of 1.1 and zero structural lag damping.

One aspect which can degrade main rotor stability in certain flight conditions is the change in kinematic pitch-lag coupling with steady coning angle, steady lag deflection and impressed blade pitch due to changes in the orientation of the track rods. This will be aggravated by the use of short track rods. With hingeless rotors the steady flap and lag deflections tend to be much smaller when compared with articulated values,

consequently the variation in pitch-lag coupling will be less. On the other hand, significant structural coupling between flap and lag may now exist and this can have a powerful effect on stability, although the evidence is that in the complete absence of pitch lag coupling the system remains stable for any value of flap lag coupling, Ref. 2.

2.3 Tail Rotor Buzz and Bang

Accurate prediction of stability boundaries for tail rotors are inherently more difficult than for main rotors due to the very disturbed airflow in certain flight conditions in the vicinity of the rotor. However considerable understanding of the aeroelastic behaviour can be obtained by the use of 'free flow' aerodynamic models; that is to say models which ignore such complicating effects as fin blockage and main rotor wake interaction.

Buzz is probably a flap-lag type of instability which occurs when the lag mode frequency is close to the flap mode frequency. Tail rotors usually have lag mode frequencies greater than once per rev., but to avoid excessive hub and blade loading this frequency must be well below two per rev. As tail rotor incidence is increased the lower flatwise blade stiffness compared with the edgewise stiffness reduces the lag frequency from the zero pitch value. Furthermore, with the large amount of pitch-flap coupling employed on tail rotors to reduce the once per rev. flapping the fundamental flap mode frequency will be well above once per rev. Consequently, unless special care is taken the flap and lag mode frequencies will coalesce at high values of blade pitch. A typical plot of the stability boundary in the ω_F, ω_L plane is shown in Fig. 3. The increase in the size of the unstable region as the pitch increases is due to the increased Coriolis coupling. The results in Fig. 3 were obtained with a constant lift curve slope, quasi-steady aerodynamics and no structural flap lag coupling. This last effect may be another consequence of increasing the blade pitch, due to the fact that the principal axes of the blade will not lie in the rotor plane. Fig. 3 probably explains the basis of the buzz phenomenon seen on some tail rotors and shows that instability is most likely at high values of blade pitch; indeed it is not unknown for the pitch range to be limited by the existence of a buzz phenomenon.

The above explanation of buzz has not involved the blade torsional motion. To investigate the influence of torsion an analysis has been conducted using a three degree of freedom model - rigid body flap, lag and torsion with no structural coupling between these degrees of freedom except for a kinematic pitch-flap coupling. Using this model contour plots of the real part of the least stable mode can be produced. Fig. 4 is a typical result, where the horizontal axis is the non-dimensional lag frequency and the vertical axis is the torsion mode frequency. The contours are equally spaced, with an increment of one in the real part of the root when expressed in radians/second. The flap frequency is 1.06, with 45° of pitch-flap coupling and the blade incidence is 10°. This figure shows an instability centred on the frequency coalescence between flap and lag, region 'A', for high values of torsional stiffness. This instability is very mild and it is suggested that it represents the buzz phenomenon. As the torsional frequency is reduced the region of instability disappears but another region, 'B', appears which seems to be associated with a triple coalescence of the flap, lag and torsion modes.

Figs. 5 to 7 show the stability contours at 15, 20 and 25 degrees of collective pitch respectively; the changes in collective also imply changes in the steady coning and sweep angles, since these are computed by the stability programme. These figures show that as the blade incidence is increased the two regions first of all merge into a single unstable area, but that with further increases in pitch the upper region completely disappears and the lower region becomes much smaller. The reason for this behaviour is the complex nature of the aerodynamic loads on the blade. These loads are based upon look-up tables for the values of the section lift, drag and moment coefficients, taking into account the local Mach number and section properties but without delay effects, i.e. quasi-steady theory. For the results shown in Figs. 4 - 7 the induced velocity was calculated by a vortex ring model using a prescribed wake due to Landgrebe, ref. 3.

The wake model used for the results shown in Figs. 4 - 7 is perhaps rather complex for a preliminary design tool but it has been found that the predicted stability boundary depends upon the model chosen. For example, Fig. 8 gives the stability contours for the same case as Fig. 6 using a prescribed wake due to Kocurek and Tangler (ref. 4); it has been suggested that this may be a more accurate model for blades with aspect ratios typically encountered on tail rotors. It is clear that the basic nature of the results is the same but with some important detailed differences. Similarly, the use of look-up tables for the aerodynamic loads rather than a constant lift curve slope has been found to be important, especially when operating close to the stall boundary. This can be seen by comparing Figs. 6 and 9, which use the same wake model but differ in that Fig. 9 is based upon a constant lift curve slope and drag co-efficient. Finally, Fig. 10 gives the predictions using the simplest model - constant lift curve slope and drag co-efficient and annular momentum theory for the induced velocity. Once again the general characteristics are the same as in Figures 6 and 8, but with significant changes in detail. Because the actual flow through the tail rotor will be complicated by interference from the main rotor and the fin none of the models will precisely describe the flow. Therefore it is important that predictions of tail rotor stability should be treated with caution, with the predicted stability boundaries being well avoided.

The region and degree of instability is further complicated by the effect of a steady axial flow through the rotor. For example Fig. 11 gives the predicted stability at 20 degrees of pitch with an axial flow of $0.03V_T$, which may be compared with Fig. 8

and shows a significant variation from the zero speed case. Other factors which will influence stability are forward flight, which introduces periodic terms into the equations of motion and therefore makes the investigation much more difficult, and structural coupling between flap, lag and torsion. This can radically affect the stability boundaries, as has been shown for example by Ormiston and Hodges, ref. 2. If the major lagwise flexibility is outboard of the feathering hinge, as is likely on a tail rotor, then the coupling between flap and lag will almost certainly change as the blade pitch is changed.

The lower region of instability, 'B' in Fig. 4, is probably the 'bang' instability since it is much more unstable than region A. No structural damping has been included in the calculations, thus in reality the upper unstable region may disappear with the blade becoming marginally stable. Due to the impulsive nature of the aerodynamic loading on the tail rotor this very lightly damped mode will be continually excited in some flight conditions, and therefore generate the large, but not catastrophic loads associated with buzz. The effect of structural damping on region 'B' will be to reduce the extent of, but not to eliminate, the instability.

One aspect which has to be given careful consideration is the placement of the torsional mode frequency. Because the blade will 'see' different stiffnesses at the track rod depending upon the phase relationship between the torsional motion of each blade a number of torsion mode frequencies will exist. These collective, cyclic and asymmetric torsion modes must all be chosen to avoid the unstable regions. This is an example of the flexibility of the hub having an influence upon a basically single blade phenomenon.

The complexity of tail rotor stability problems is such that the accurate prediction of the stability boundaries is a very difficult task, for which simple models are not particularly suited. However, for the rotor used to produce the results shown in Figs. 4 - 11 it is clear that stability should be obtained provided the lag frequency remains above 1.5, the torsion frequency is above 3, no structural couplings are present and the rotor operates below stall. These results are not necessarily applicable to other rotors, all of which will have to be considered on their individual merits. It is recommended that the torsional degree of freedom be included in any analysis of tail rotor stability and that predicted stability boundaries are well avoided.

3. COMPLETE AIRCRAFT INSTABILITIES

3.1 Ground Resonance

Any helicopter with a main rotor fundamental lag mode frequency less than once per rev. is susceptible to ground resonance. The degrees of freedom involved are the lead-lag motion of the rotor blades and any fuselage mode containing in-plane motion of the rotor hub. The instability occurs in the vicinity of a frequency coalescence between the regressing lag mode and the fuselage mode, provided the rotor speed is greater than the fundamental lag frequency; the phase relationships between the couplings are such that a frequency coalescence when the lag mode frequency is greater than the rotor speed does not produce an instability, neither does a coalescence with the progressing lag mode.

Important parameters with regard to ground resonance are lag mode frequency and damping, fuselage frequency and damping and fuselage mode shape. Of lesser significance are flap mode stiffness and aerodynamic loads: ground resonance is a purely mechanical instability which can exist in vacuo, although on some helicopters with only a very marginal degree of instability rotor couplings can be used to stabilize the aircraft via the aerodynamic loads.

Accurate predictions of ground resonance stability characteristics require a fairly extensive mathematical model with flap and lag rotor degrees of freedom and at least four fuselage freedoms - pitch/longitudinal and roll/lateral. Aircraft stability control augmentation systems can also effect ground resonance, and if significant response of these systems are expected at the frequencies associated with ground resonance they must be included in the analysis. (A simpler approach may well be to ensure that the feedback systems are filtered in such a way as not to respond at the frequency of the ground resonance oscillations.) In order to estimate the amount of lead-lag damping required, if any, this type of model is rather too complex; a simpler, even if approximate, analysis is useful.

Fig. 12 shows a simple mathematical model which can be used to investigate ground resonance analytically. This is similar to the Coleman and Feingold model, ref. 5, except that the first elastic lead-lag mode of the rotor is used rather than rigid body rotation about a hinge. Thus the model may be used for hingeless rotors. No aerodynamic terms are included, but structural damping terms are. By applying the transformation to multi-blade co-ordinates, ref. 6, the number of equations of motion can be reduced to three. These are standard equations and are similar to those given by Done in ref. 7.

This set of three second order coupled differential equations are at this stage exact, but difficult to solve analytically. They may be reduced to an approximate set of four first order equations by a technique similar to that given in ref. 7. Without going into details the process may be described as follows. The three second order equations are reduced to six first order equations by treating velocity as a co-ordinate. Next, the uncoupled and undamped rotor and fuselage subsystems are solved separately to produce a set of uncoupled complex mode shapes, with their associated frequencies. For the rotor subsystem these are the progressing and regressing lag modes. If a similarity transformation based upon these uncoupled modes is applied to the damped, coupled fuselage-rotor

system the equations of motion are not completely de-coupled. However, the frequency characteristics as a function of rotor speed are of the form shown in Fig. 13, and in the neighbourhood of the frequency coalescence 'A' the effect of the progressing lag mode can be expected to be small. Consequently by ignoring this mode the system can be reduced to a set of four approximate first order equations, from which analytic results can be deduced.

This technique may also be used to investigate resonances between the fuselage and the progressing lag mode. The result of such an analysis is to demonstrate that the system remains stable. Similarly, intersections between the regressing lag mode and fuselage mode frequencies at rotor speeds for which the lag mode frequency is greater than the rotor speed, 'B' in Fig. 13, also do not lead to instability.

In the neighbourhood of a frequency coalescence such as 'A' the system is unstable, and the following analytical results may be obtained:

With no structural damping the peak value of the instability is given by

$$\sigma_{\max} = \frac{1}{4} \left(\frac{\omega_Y^3}{\omega_L} \right)^{1/2} q \quad (1)$$

where ω_Y = fuselage frequency,

ω_L = lag mode frequency at frequency coalescence = $\Omega - \omega_Y$,

σ_{\max} is expressed in terms of the ratio of critical lag mode damping, ie relative to ω_L , and q is given by

$$q^2 = \frac{nb^2}{m_e I}. \quad (2)$$

The other variables are defined in the notation section.

Including structural damping it can be shown that the amount required to just suppress the instability is

$$\xi_Y \xi_L = \frac{1}{16} \left(\frac{\omega_Y}{\omega_L} \right)^2 q^2 \quad (3)$$

where ξ_Y and ξ_L are the fuselage and lag mode damping, expressed as ratio of critical relative to ω_Y and ω_L respectively.

Other formulae for the width of the unstable region, in terms of rotor speed, and the degree of instability when some, but not sufficient, damping is present may also be derived, but the two expressions given above are the most useful. It is interesting to note that even this approximate approach produces the result that to suppress ground resonance the important parameter is the product of the damping, not the individual values. Indeed the formula for the range of unstable rotor speeds in the case of insufficient damping (not quoted) shows that the range becomes very wide with unbalanced damping, for a constant value of the product of damping. Similar results have been obtained by Ormiston, ref. 8, using a numerical analysis.

To give an indication of the accuracy of the technique Fig. 14 compares the measured peak value of instability for a range of lag stiffnesses on a scale model of the Lynx, ref. 9, with the predictions of Eq. (1). The lag stiffness is given in terms of the non-dimensional lag mode frequency at the scaled normal operating rotor speed. The predicted values of peak instability are slightly greater than the measured, which is not unexpected since Eq. (1) has been derived assuming no structural damping. If the predicted values of instability are reduced by the measured, non-rotating lag damping in each case then the agreement becomes excellent. This result shows that the approximate method may be used with some confidence as a preliminary design tool.

At the project stage little will be known about the undercarriage stiffness and damping, consequently determining the minimum required lead-lag damping to prevent instability will be difficult. One way of overcoming this lack of data is to assume that the undercarriage characteristics are just those which produce the worst possible ground resonance instability. It can be seen from Eq. (3) that more damping is required as the fuselage frequency increases, provided the frequency coalescence still occurs below the maximum possible rotor speed. Thus a pessimistic assumption is that the frequency coalescence occurs at the maximum operating rotor speed.

Increasing the mass ratio q also increases the required damping; thus the combination of a light fuselage and heavy rotor system produces the most unstable situation. On a real aircraft it is unlikely that the fuselage mode involves pure translation of the aircraft, some pitch or roll rotation will be involved. The analysis for the model shown in Fig. 12 may be repeated with a further fuselage degree of freedom included, namely rotation about an axis vertically below the hub, through the aircraft cg and parallel to OY in Fig. 12. It is found that the formulae given above are unchanged provided the effective mass at the rotor hub is used rather than the real aircraft mass, where the effective mass is defined by

11-6

$$m_e = \frac{I_f + \ell^2 m_f}{(h + \ell)^2} \quad (4)$$

and the other variables are defined above.

For a fixed fuselage mass, inertia and height of the rotor above the cg the effective mass may be considered to be a function of the roll centre position of the mode. It can be shown that the minimum value of the effective mass is

$$m_e = \frac{m_f I_f}{I_f + h^2 m_f} \quad (5)$$

Using this value in Eq. (3), together with a value of ω_y which produces a frequency coalescence at the upper limit of rotor speed will result in a level of lag damping which will suppress ground resonance regardless of the roll mode frequency and centre of rotation.

One further result may be of some interest. It is possible to perform a similar analysis to that discussed above for the case where the fuselage has four degrees of freedom - pitch, roll, longitudinal and lateral. It is found that if the fuselage modes are well separated in frequency then each individual frequency coalescence with the regressing lag mode may be considered separately. If however a pitch/longitudinal mode coincides in frequency with a roll/lateral mode then the degree of instability becomes greater. It can be shown that the expression for the mass ratio q becomes in this case:

$$q^2 = \frac{nb^2}{I} \left(\frac{1}{m_e} + \frac{1}{m_e'} \right) \quad (6)$$

where m_e , m_e' are the effective masses in the lateral and longitudinal directions.

If the damping requirement deduced from Eq. (3) is based upon the worst possible fuselage mode shapes and frequencies, ie coalescence with the regressing lag mode at maximum rotor speed, minimum effective mass in both the pitch and roll modes and equal pitch and roll mode frequencies then the aircraft will be stable with any undercarriage configuration. If this level of damping is too large then it becomes necessary to include the actual undercarriage characteristics in the calculations.

As an example of the use of Eq. (3) consider the following typical example:

Aircraft mass	=	3600 kg
Pitch inertia	=	16200 kgm ²
Roll inertia	=	2700 kgm ²
Height from hub to cg	=	1.2 m

The minimum lateral and longitudinal effective masses are 1210 and 2730 kg, respectively. Assume the rotor system has four blades, that the first lagwise moment (b) is 133 kgm and the inertia is 540 kgm². Then the value of q from Eq. (6) is 0.395. Assuming that both the roll and pitch fuselage frequencies are equal and that coalescence occurs at the normal operating rotor speed the required damping levels are shown in Fig. 15, for a range of lag mode frequencies. The reduction in damping requirement as the lag frequency is increased makes the prevention of ground resonance on hingeless rotors a much simpler task compared with conventional articulated rotors.

It must be remembered that this analysis is only approximate and that a number of other parameters may have some influence on the damping requirement. This includes aerodynamic loads, coning angle and pitch-flap-lag couplings.

3.2 Air Resonance

Finally, we consider the problem of air resonance. This instability is closely related to ground resonance, but as the name suggests it occurs in flight, and more especially it is associated with hingeless rotor systems. The 'fuselage' mode in this case arises from the coupling between blade flapping and fuselage pitch and roll motions. This produces one or two modes with significant in-plane hub displacements at frequencies close to that of the regressing lag mode at normal operating rotor speed.

Consider first the simple model shown in Fig. 16 which consists of a single fuselage freedom, roll about the aircraft cg, and blade flapping. By applying the usual transformation to multi-blade co-ordinates the equations of motion may be reduced to three coupled equations. Ignoring the aerodynamic terms these three equations may be solved for the coupled systems natural frequencies, one of which is zero and the other two being given by

$$\omega^2 = -(1 + \omega_F^2) + \frac{1}{2\phi}(1 - \omega_F^2) \pm \sqrt{\{4(\omega_F^2 - 1) + (2 + \frac{1}{2\phi}(1 - \omega_F^2))^2\}} \quad (7)$$

where $\phi = \frac{2I_f}{nI}$,

and the other terms are defined in the notation section.

11-7
Fig. 17 shows the variation of the frequencies with the inertia ratio ϕ and flap mode frequency ω_F . With an infinite fuselage inertia these are the usual progressing and regressing cyclic flap modes, and as the figure shows the progressing mode frequency is almost independent of fuselage inertia. The regressing mode however is very sensitive to the inertia ratio. This mode is often referred to as the 'pendulum' or 'slow gyroscopic' mode.

Fig. 17 may be used to investigate whether air resonance is likely to be a problem for a particular design, simply from a knowledge of the rotor flap and lag frequencies and the airframe pitch and roll inertias. Since typical values of ϕ are 2 - 4 and 10 - 20 for roll and pitch respectively, a frequency coalescence with the regressing lag mode is much more likely to occur with the roll pendulum mode. For example, a value of ω_F of 1.1 and ϕ of 2.0 will result in a resonance with the regressing lag mode if $\omega_L = 0.65$.

The damping in the pendulum mode is fairly large, due to the large amount of aerodynamic damping in the fundamental flap mode, and this has a considerable effect on the frequency of the pendulum mode, as well as the damping. An analysis of the system shown in Fig. 16 with simple aerodynamic lift loads included produces the results shown in Fig. 18, for a range of Lock's numbers. It shows that the effect of the aerodynamic loads is to reduce the pendulum mode frequency, and to introduce significant damping into the mode. For low values of the inertia ratio the value of the real part of the root is approximately 0.25 of the Lock's number, whereas it can be shown that without the fuselage freedom the real part of the regressing flap mode is 0.5 of the Lock's number.

Having established from the undamped results shown in Fig. 17 that air resonance is a potential problem the question then arises as to how much damping will be required in the rotor lead-lag mode to prevent the instability. An accurate prediction cannot be made using the simple techniques discussed in this paper since too many important effects are ignored. What can be shown however is that the amount of damping is likely to be much less than that required to suppress ground resonance. For example, using the same aircraft data as in the section on ground resonance the maximum possible value of q is 0.329 - this ignores the blade flap inertia and assumes that the pendulum mode roll centre is such as to produce the minimum effective mass at the rotor hub. Then, with a lag frequency of 0.65 the damping requirement from equation (3) is

$$\xi_Y \xi_L = 0.002$$

With a Lock's number of 8 and undamped pendulum mode frequency of 0.35 the required lag damping is 0.25% of critical. A more detailed analysis which includes four rigid body fuselage freedoms, rotor flap and lag motions, aerodynamic loads and the steady coning angle gives a predicted lag damping requirement of 0.8% of critical. This is in addition to the aerodynamic lag damping.

It is clear from this analysis that the accurate prediction of air resonance stability will require a more complex model than that discussed here. As well as the importance of coning angle and rotor thrust on the stability rotor couplings can have a powerful effect. The methods will however indicate if air resonance is likely to be a problem.

4. CONCLUSIONS

A number of rotor and complete aircraft instabilities have been discussed, although it must not be considered that the list is by any means complete. Where possible a simple explanation of the mechanism involved in the instabilities has been given, from which the correct design decisions to avoid the problems may be made. It has to be remembered that these rules can only be considered as guides, not definitive statements, and that each case has to be considered in detail. This will almost invariably require extensive computer analysis, including the effects of forward flight and rotor couplings which may result from non-linearities in the rotor system.

REFERENCES

1. Friedman, P.P., "Formulation and Solution of Rotary-Wing Aeroelastic Stability and Response Problems", Paper 3.2, Eighth European Rotorcraft Forum, Aix-en-Provence, France, September 1982.
2. Ormiston, R.A., and Hodges, D.H., "Linear Flap-Lag Dynamics of Hingeless Helicopter Rotor Blades in Hover", Journal of American Helicopter Society Vol. 17, No. 2, April 1972.
3. Landgrebe, A.J., "An Analytical Method for Predicting Rotor Wake Geometry", Journal of American Helicopter Society, October 1969.
4. Kocurek, J.D., and Tangler, J.Z., "A Prescribed Wake Lifting Surface Hover Performance Analysis", Presented at the 32nd Annual Forum of the American Helicopter Society, Washington, D.C., May 1976.
5. Coleman, R.P., and Feingold, A.M., "Theory of Self-Excited Mechanical Oscillations of Helicopters with Hinged Blades", N.A.C.A. Report 1351, 1958.

6. Hohenemser, K.H., and Yin, S.K., "Some Applications of the Method of Multiblade Co-ordinates", Journal of the American Helicopter Society, Vol 17, No. 3, July 1972.
7. Done, G.T.S., "A Simplified Approach to Helicopter Ground Resonance", Aeronautical Journal, May 1974.
8. Ormiston, R.A., "Aeromechanical Stability of Soft Inplane Hingeless Rotor Helicopters" Paper 25, Third European Rotorcraft and Powered Lift Aircraft Forum, Aix-en-Provence, France, September 1977.
9. King, S.P., "Helicopter Ground Resonance. Experimental Validation of Theoretical Results by the Use of a Scale Model", Paper 7.4, Eighth European Rotorcraft Forum, Aix-en-Provence, France, September 1982.

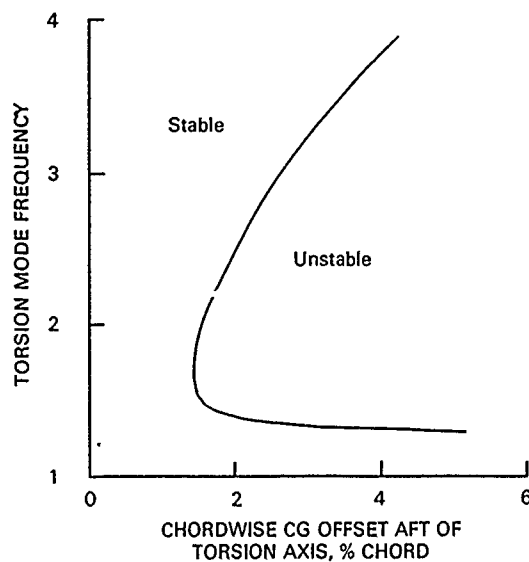


Fig. 1 Flutter boundary
Flap frequency=1.1
No pitch-flap coupling

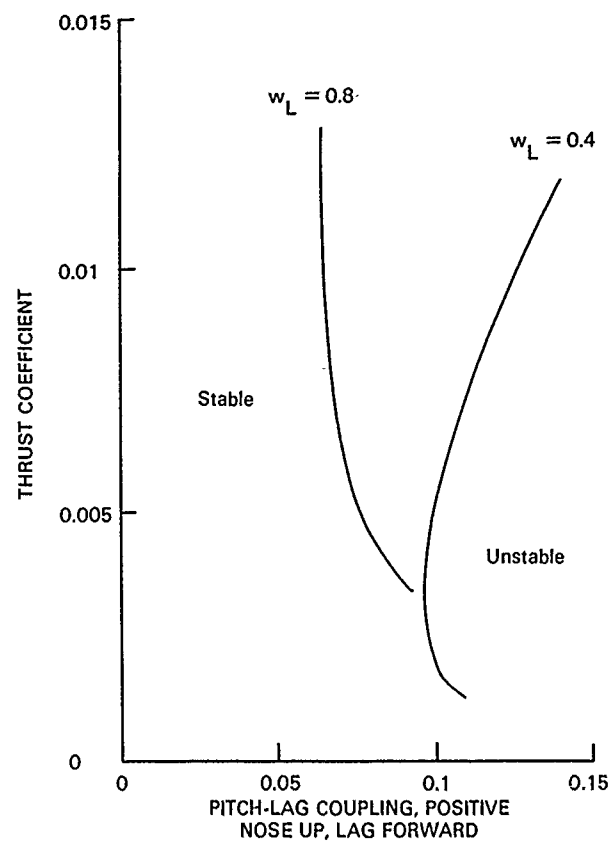


Fig. 2 Flap-lag stability boundaries
Flap frequency=1.1
No flap-lag coupling
Zero structural damping

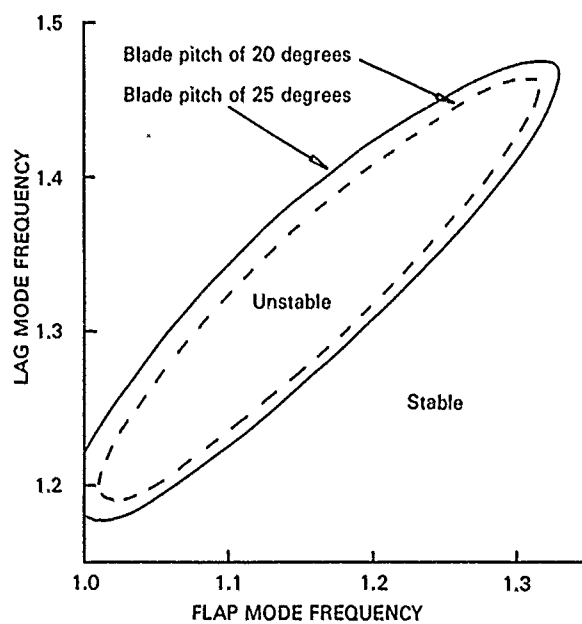


Fig. 3 Tail rotor flap-lag stability
45 degrees of pitch-flap coupling
Zero structural damping

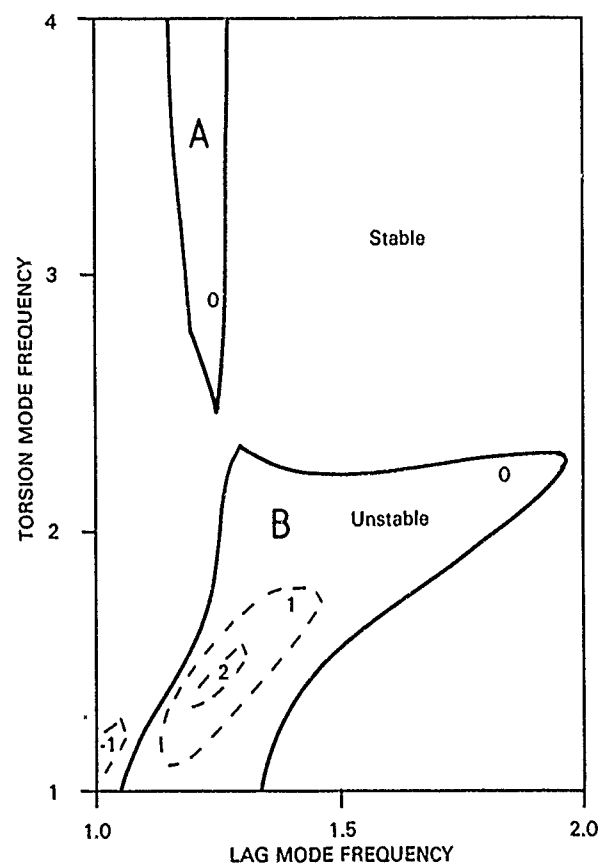


Fig. 4 Tail rotor stability. $\omega_F = 1.06$, $\theta = 10^\circ$
45 degrees of pitch flap coupling
Wake defined by Landgrebe
Look-up tables for airloads

The graph plots Torsion Mode Frequency (Y-axis, 1 to 4) against Lag Mode Frequency (X-axis, 1.0 to 2.0). The plot is divided into 'Stable' and 'Unstable' regions by dashed lines. The 'Unstable' region is located at lower Torsion Mode Frequencies and is bounded by a curve labeled '0' and '1', and a dashed line labeled '2'. The 'Stable' region is the area above and to the right of these boundaries. Several dashed lines are labeled with values: -1, -2, -3, -4, -5, -6, -7, -8, -9, -10, -11, -12, -13, -14, -15, -16, -17, -18, -19, -20, -21, -22, -23, -24, -25, -26, -27, -28, -29, -30, -31, -32, -33, -34, -35, -36, -37, -38, -39, -40, -41, -42, -43, -44, -45, -46, -47, -48, -49, -50, -51, -52, -53, -54, -55, -56, -57, -58, -59, -60, -61, -62, -63, -64, -65, -66, -67, -68, -69, -70, -71, -72, -73, -74, -75, -76, -77, -78, -79, -80, -81, -82, -83, -84, -85, -86, -87, -88, -89, -90, -91, -92, -93, -94, -95, -96, -97, -98, -99, -100.

Fig. 8 Tail rotor stability. $\omega_F=1.06$, $\theta=20^\circ$
45 degrees of pitch flap coupling
Wake defined by Kocurek and Tangler
Look-up tables for airloads

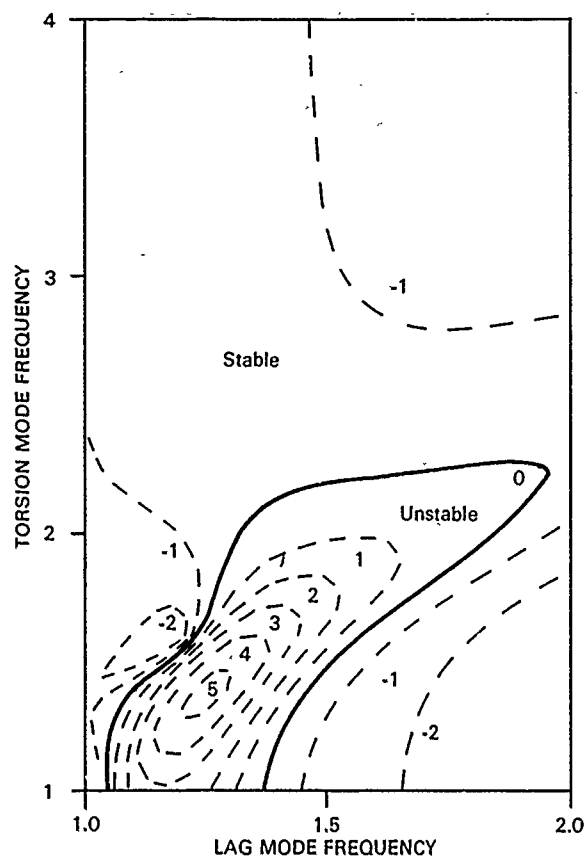


Fig. 9 Tail rotor stability. $\omega_F=1.06$, $\theta=20^\circ$
45 degrees of pitch flap coupling
Wake defined by Landgrebe
Constant Lift curve slope and C_D

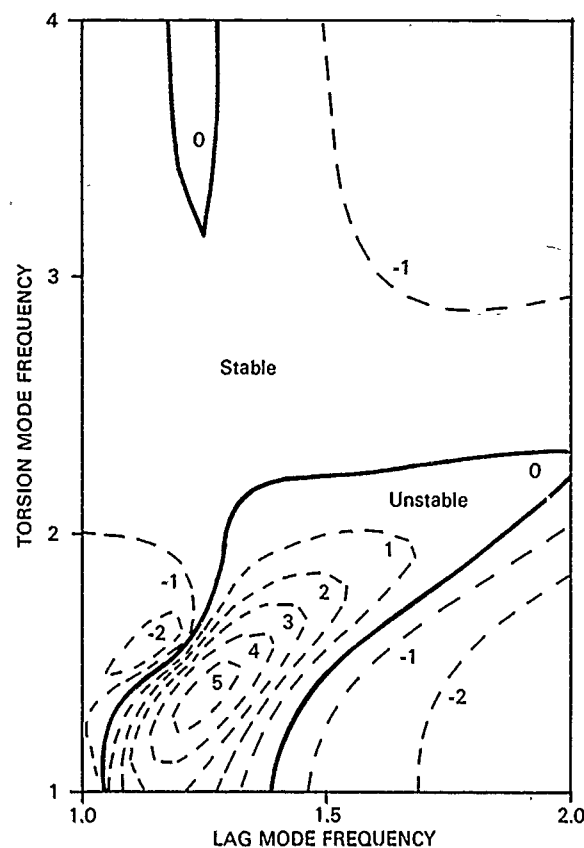


Fig. 10 Tail rotor stability. $\omega_F=1.06$, $\theta=20^\circ$
45 degrees of pitch flap coupling
Wake by annular momentum theory
Constant Lift curve slope and C_D

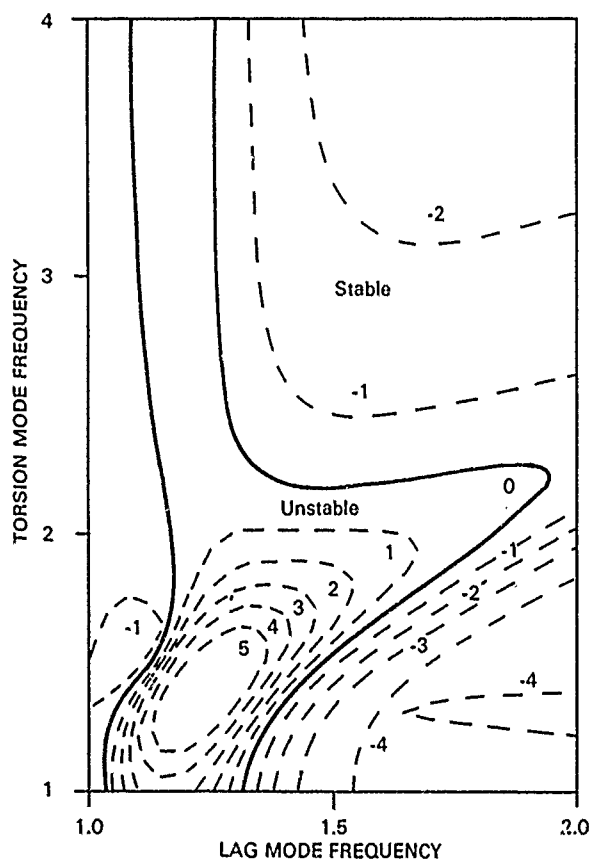


Fig. 11 Tail rotor stability. $\omega_F=1.06$, $\theta=20^\circ$
45 degrees of pitch flap coupling
Wake defined by Kocurek and Tangler
Look-up tables for airloads
Axial flow velocity=0.03 tip speed

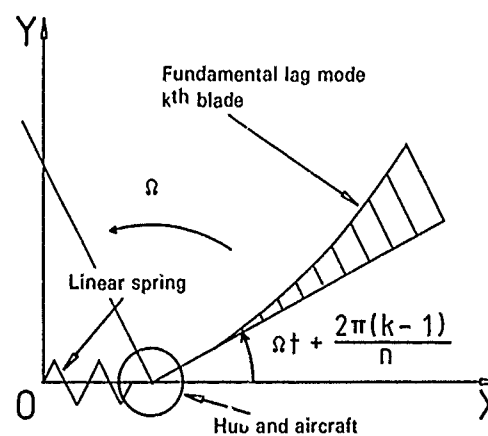


Fig. 12 Simple ground resonance model

11-12

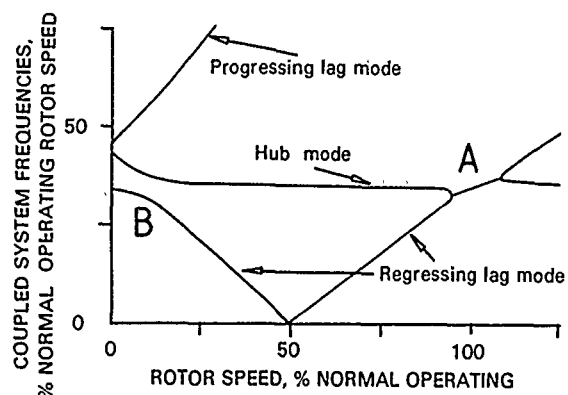


Fig. 13 Variation of simple ground resonance model system frequencies with rotor speed

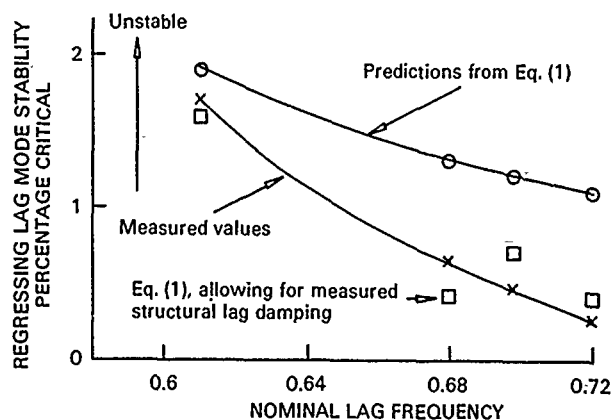


Fig. 14 Comparison of ground resonance stability predictions with test values for a scale model of the Lynx

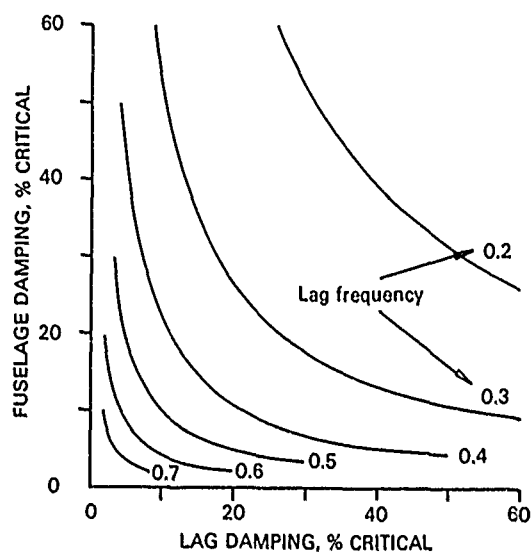


Fig. 15 Variation of fuselage and rotor damping requirements to completely suppress ground resonance for a range of lag mode frequencies

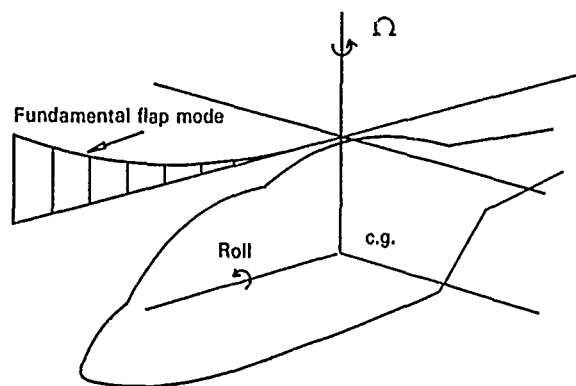


Fig. 16 Simple model for aircraft pendulum mode investigation

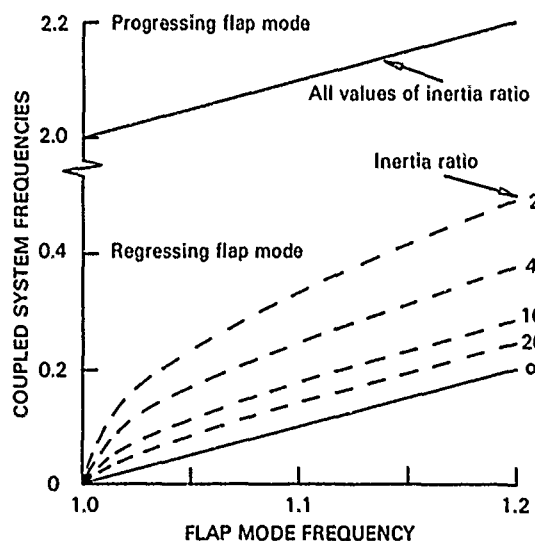


Fig. 17 Variation of aircraft roll and blade flap model frequencies with flap stiffness and inertia ratio

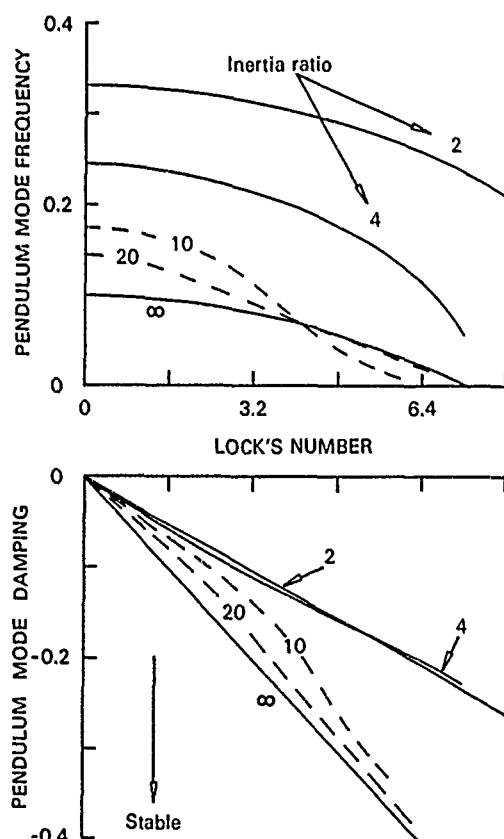


Fig. 18 Variation of pendulum mode frequency and damping with Lock's number for a range of inertia ratios. $\omega_F=1.1$

Wen-Liu Miao
and
Robert H. Blackwell

Sikorsky Aircraft Division
United Technologies Corporation
Stratford, Connecticut 06602
U.S.A.

Summary

The high speed requirement dictates that the rotor design be simple and clean. Elimination of blade articulations as well as pitch bearings and lag dampers is emerging as a candidate technology for such a rotor.

The resulting bearingless type rotor design has to deal with the question of rotor stability and the coupled rotor/airframe stability. The merits of the stiff-inplane design versus the soft-inplane design in light of the stability issues are discussed. The philosophy of introducing blade bending torsion couplings to improve stability characteristics is substantiated.

As vibration potential increases with airspeed exponentially and may become a limiting factor to the speed achievable, reducing vibration should be an integral part of the aeroelastic considerations for high speed rotor. Parameters that can reduce vibrations are discussed generically. Sensitivities of vibration are shown for blade bending and torsion stiffnesses, mass distribution, frequency and mode shape.

List of Symbols

A_{APPROX}	=	induced inflow parameter, $\frac{\pi \sigma}{6} \left[\sqrt{1 + \frac{120}{\pi \sigma}} - 1 \right]$
c	=	blade chord
C_{do}	=	profile drag coefficient
C_L	=	rotor lift coefficient, $L/\pi R^2 \rho (\Omega R)^2$
f	=	aircraft equivalent flat plate area
H	=	vertical distance from fuselage center to junction of fuselage and main rotor pylon
ΔH	=	vertical distance from rotor hub to junction of fuselage and main rotor pylon
i	=	mode number
IF	=	body rotor interference factor, $(\Delta L/R)/(\Delta H/H)$
K_β	=	total flap hinge spring rate at $\theta=0$
$K_{\beta b}$	=	flap spring rate at blade root
$K_{\beta h}$	=	flap spring rate at hub
K_ζ	=	total lead-lag hinge spring rate
$K_{\zeta b}$	=	lead-lag spring rate at blade root
$K_{\zeta h}$	=	lead-lag spring rate at hub
L	=	airload
ΔL	=	horizontal distance from the fuselage nose to the main rotor hub
p	=	non-dimensional flatwise frequency
r	=	blade radial coordinate
R	=	rotor radius
R	=	variable elastic coupling parameter, Fig. 2
x_{AC}	=	blade chordwise aerodynamic center

x_{CG}	=	blade chordwise center of gravity
α_s	=	rotor shaft angle, positive for rotor tilted aft
β_{B-H}	=	built-in flexbeam-to-hub cone angle
β_{BL-B}	=	built-in blade-to-flexbeam cone angle
γ	=	Lock number
δ_{TAB}	=	blade tab deflection, positive for trailing edge up
θ	=	blade pitch angle
θ_{B-H}	=	built-in flexbeam-to-hub pitch angle
θ_{BL-B}	=	built-in blade-to-flexbeam pitch angle
θ_ζ	=	blade pitch-lag coupling
ρ	=	air density
σ	=	rotor solidity
ω	=	frequency
$\omega_{1\beta}$	=	blade first flatwise mode frequency
$\omega_{1\zeta}$	=	blade first edgewise mode frequency
$\bar{\omega}_\zeta$	=	non-dimensional blade edgewise frequency
ω_θ	=	blade torsion frequency
Ω	=	rotor speed

Introduction

There is a continuing need to advance rotor system technology and develop better rotor systems. With the advancements in recent years in the areas of design technology, analytic methodology, material science and technical knowledge in rotorcraft aeroelasticity, the stage is set for a renewed assault on the design of the high speed rotor.

For efficiency at high speed, a rotor design should be simple and aerodynamically clean. Modern rotors certainly are heading in that direction. In recent years, articulated rotors have evolved from three separate hinges in pitch, flap and lag to one coincidental "universal joint". The best example is the elastomeric bearing first used in the rotor system of the U.S. Army/Sikorsky BLACK HAWK helicopter. Westland eliminated both the flap and the lag hinges making a hingeless rotor while retaining the pitch bearing and the lag damper on their WG30. MBB went a step beyond and successfully produced the BO-105 which has a hingeless rotor without a lag damper. Boeing Vertol, after their hingeless rotor YUH-61A entry to the UTTAS competition, developed a Bearingless Main Rotor (BMR) achieving elimination of the flap and the lag hinges, the lag dampers as well as the pitch bearing. Although bearingless rotor designs had been employed successfully for years, notably on the tail rotors of the BLACK HAWK and the S-76 helicopter, the BMR was the first main rotor application. The successful flight demonstration of the BMR under the sponsorship of the U.S. Army Applied Technology Laboratory (AVRADCOM) kindles the renewed effort in designing a simple and clean high speed rotor.

This paper addresses two fundamental issues that the dynamicist or the aeroelastician faces during the conceptual design stage: stability and vibration. In these two areas, the rotorcraft community has made great strides in terms of gaining fundamental understanding in recent years. Based on this analytical, experimental and flight test knowledge, judgments can now be made to provide some logical design criteria for a bearingless type of rotor design.

Rotor Stability Considerations

The very first consideration for a bearingless type of rotor design is the choice of the blade first edgewise mode frequency. With the frequency above 1/rev (or stiff-inplane) it is well known that this type of rotor will not have the problem of coupled rotor/body aeromechanical stability (otherwise known as ground resonance if on the ground, or air resonance if in the air). However, a stiff-inplane rotor has its share of rotor aeroelastic stability concerns as discussed thoroughly by Ormiston and Hodges¹. Figure 1, taken from Reference 1, shows that the soft-inplane rotor is more stable in terms of flap-lag stability than the stiff-inplane design.

12-3

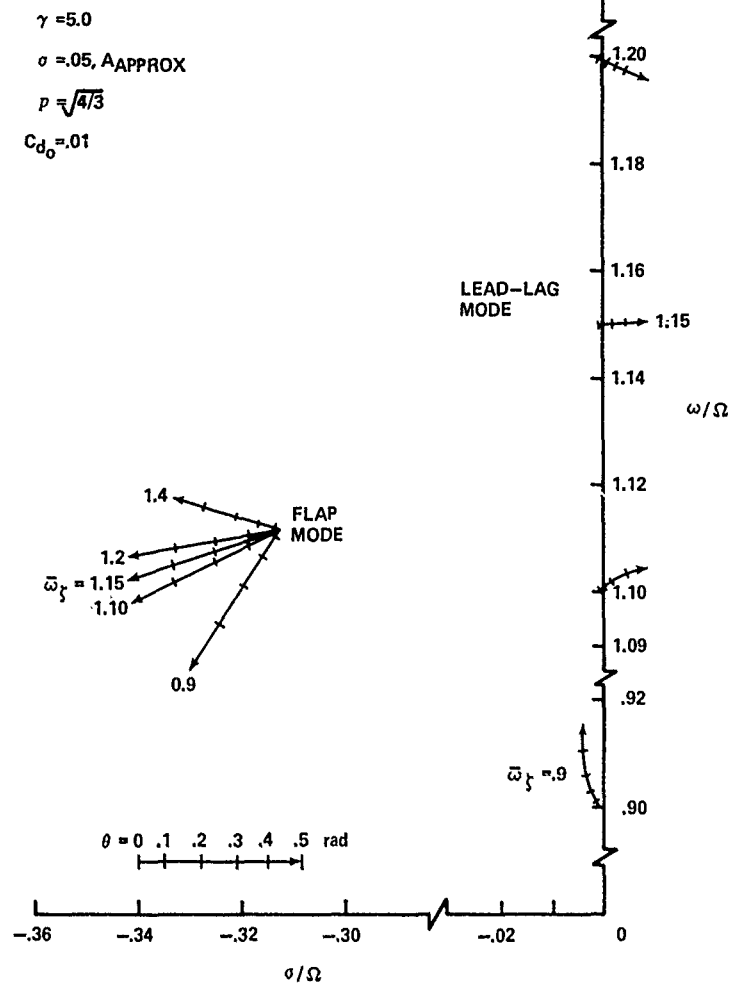


FIGURE 1. STIFF INPLANE ROTOR HAS ROTOR STABILITY PROBLEM.

$$R \equiv \frac{K_{\beta}}{K_{\beta_b}} = \frac{K_{\zeta}}{K_{\zeta_b}}$$

$$K_{\beta} = \frac{1}{\frac{1}{K_{\beta_h}} + \frac{1}{K_{\beta_b}}}, \quad K_{\zeta} = \frac{1}{\frac{1}{K_{\zeta_h}} + \frac{1}{K_{\zeta_b}}}$$

$R = 1$: PITCH I/B OF FLAP AND LAG
 $R = 0$: PITCH O/B OF FLAP AND LAG

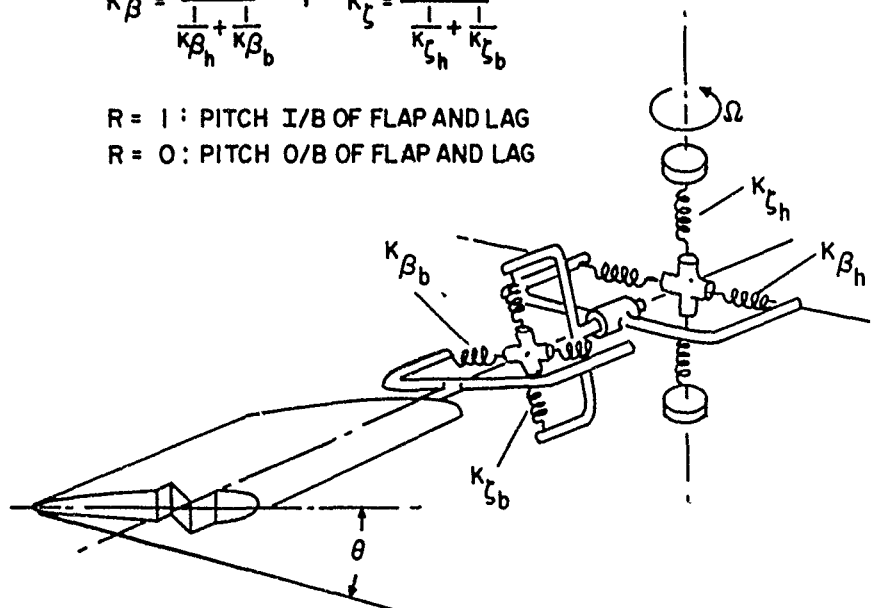


FIGURE 2. DEFINITION OF "R" FACTOR.

The stiff-inplane rotor stability is also very sensitive to the elastic bending-torsion coupling resulting from the difference in the flatwise and edgewise bending stiffness (often referred to as the ΔEI coupling). This elastic coupling is a function of the radial location of the blade pitch bearing with respect to the blade bending element. A pitch bearing that is outboard of the blade bending element will have zero coupling while an inboard pitch bearing will have the full coupling. Ormiston¹ used an R factor to denote the relative distribution of the bending flexibilities inboard and outboard of the pitch bearing. The definition of the R factor is shown schematically in Figure 2. The R factor equals zero for all the bending flexibility inboard of the pitch bearing. With all the bending flexibility outboard of the pitch bearing, the R factor equals one. For a typical bearingless rotor design, the R value falls between zero and one. Figure 3, taken from Reference 1, shows that for the stiff-inplane rotor, depending on the elastic coupling or the R factor, the rotor has an unstable region at high collective pitch angles.

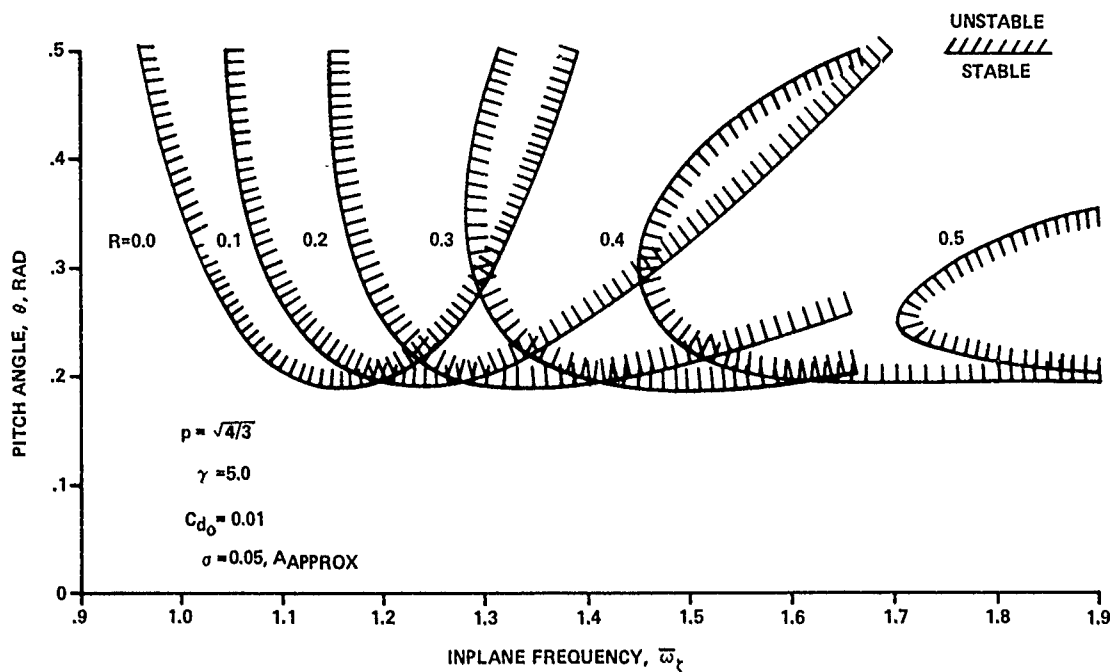


FIGURE 3. STIFF INPLANE ROTOR STABILITY IS SENSITIVE TO ROTOR COUPLINGS.

Introducing pitch-lag kinematic coupling changes stability characteristics of the stiff-inplane rotor drastically for different R values. Figure 4, taken from Reference 1, shows that for the stiff-inplane rotor with an edgewise frequency ratio of 1.4, the pitch-lag coupling that eliminates the instability at one R factor will destabilize the blade at another R value. While for the soft-inplane configuration (edgewise frequency ratio of 0.7), there exists some type of pitch-lag coupling which will cause the rotor stability to be relatively independent of the R value.

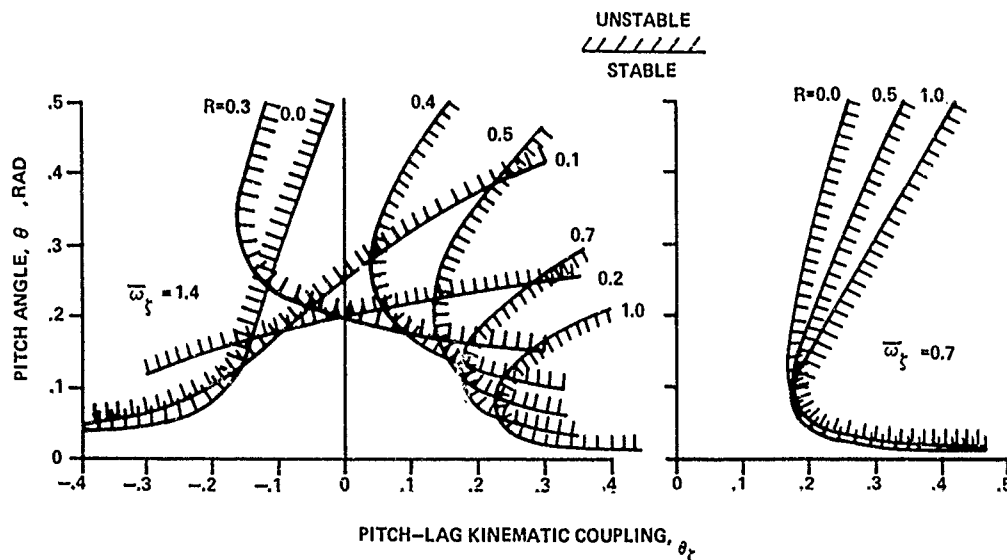


FIGURE 4. SOFT INPLANE ROTOR IS LESS SENSITIVE THAN STIFF INPLANE.

To summarize, although a stiff-inplane rotor offers freedom from coupled rotor/body aeromechanical instability, it has other aeroelastic instability concerns of its own. On the other hand, it has been shown that a soft-inplane rotor can be designed so that it has favorable stability characteristics, e.g., Reference 2. In addition, as shown in Figure 5, a soft-inplane rotor has generally less forced response compared to the stiff-inplane case. A practical frequency range for design is a compromise between the forced response and damping required for stability, and as shown in Figure 5, the frequency range is around 0.7/rev for the soft-inplane design. The ultimate selection of rotor inplane frequency will depend on detailed analysis. However, based on rotor stability and its sensitivities to rotor couplings consideration, the soft-inplane design is preferred.

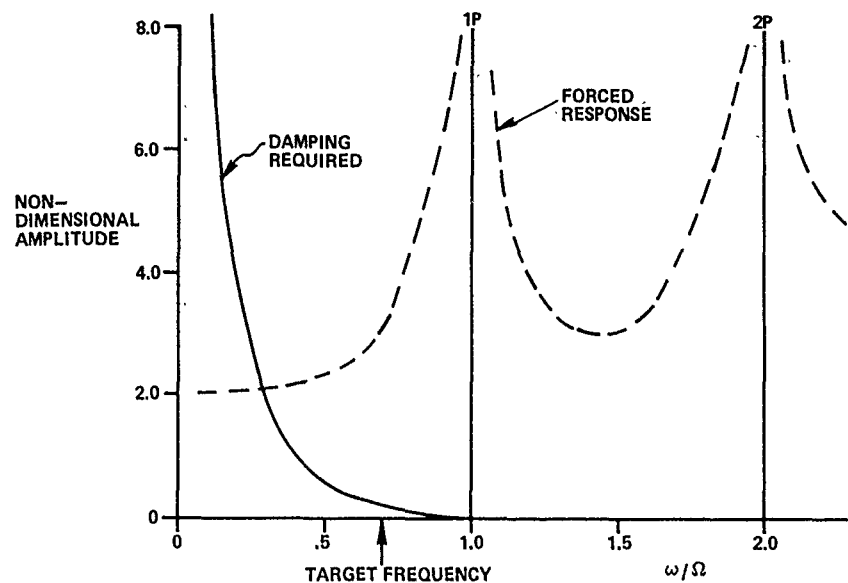


FIGURE 5. CHOICE OF INPLANE FREQUENCY DEPENDS ON DAMPING REQUIRED AND FORCE RESPONSE CONSIDERATIONS.

Rotor/Body Stability Considerations

The coupled rotor/body aeromechanical stability of a soft-inplane bearingless or hingeless rotor has been explored quite extensively during the past ten years²⁻⁶. As discussed in Reference 3, the primary source of damping in the aeromechanical stability mode for the rotor without auxiliary inplane dampers is aerodynamic flap damping. Figure 6, taken from Reference 3, illustrates the inherent damping available as a function of flatwise frequency ratio. Two facts become obvious. First, the choice of flatwise frequency will affect the available damping. Figure 6 suggests that, from the standpoint of aeromechanical stability, it is desirable to have the flatwise frequency as high as possible in order to maximize the potential inherent stability of the coupled rotor/body system. This, in general, will be in conflict with other requirements such as that of low gust sensitivity. Designing a rotor with high flatwise frequency to maximize the available damping for the sake of aeromechanical stability must be weighed against other attributes of the helicopter such as handling qualities, weights etc.

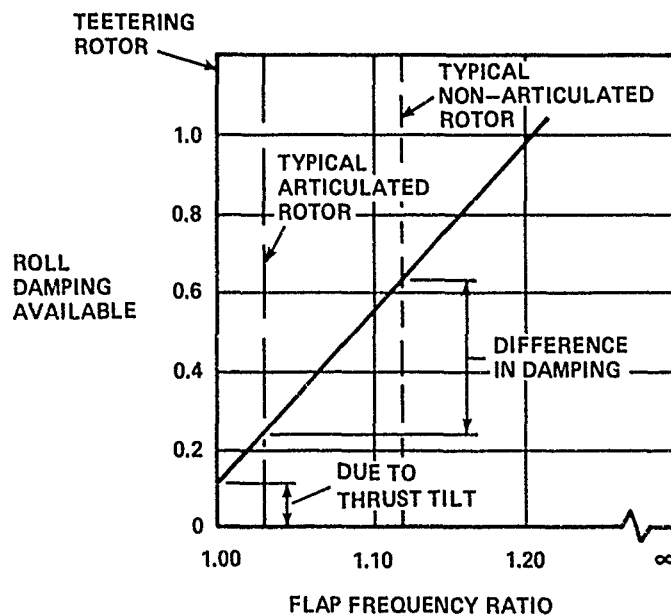


FIGURE 6. SOURCE OF DAMPING FOR AIR AND GROUND RESONANCE.

Because of the importance of the flatwise motion, a means of inducing favorable flatwise response into the aeromechanical stability mode, which consists of primarily the blade inplane motion with body participation, is of utmost importance. The more favorable the flatwise response, the more stable the coupled rotor/body system. The key to a successful high speed rotor design with a soft-inplane bearingless type rotor is then to incorporate favorable couplings to capitalize on this damping source.

There are many design parameters that can be utilized to introduce couplings into the rotor system. Rotating the blade cross sectional principal axes, flatwise and edgewise, about the spanwise pitch axis so that they do not coincide with the inertial axes is one direct way of introducing flatwise and edgewise coupling⁷. For a bearingless type of rotor, this can be accomplished by introducing a flexbeam-to-hub pitch angle and/or blade-to-flexbeam pitch angle. A Froude scaled model of the rotor design reported in Reference 2 was tested for aeromechanical stability with this parameter variation.

The test data shown in Figure 7, taken from Reference 8 test report, are for two configurations. Although both configurations had a resultant blade pitch angle of 9.6° , one configuration achieved this with a beam-to-hub pitch angle of zero and the blade-to-beam pitch angle of 9.6° while the other configuration had a beam-to-hub pitch angle of 12° and the blade-to-beam pitch angle of -2.4° . The latter configuration intuitively possesses more flatwise and edgewise coupling than the former, and, as the test data in Figure 7 show, it is considerably more stable.

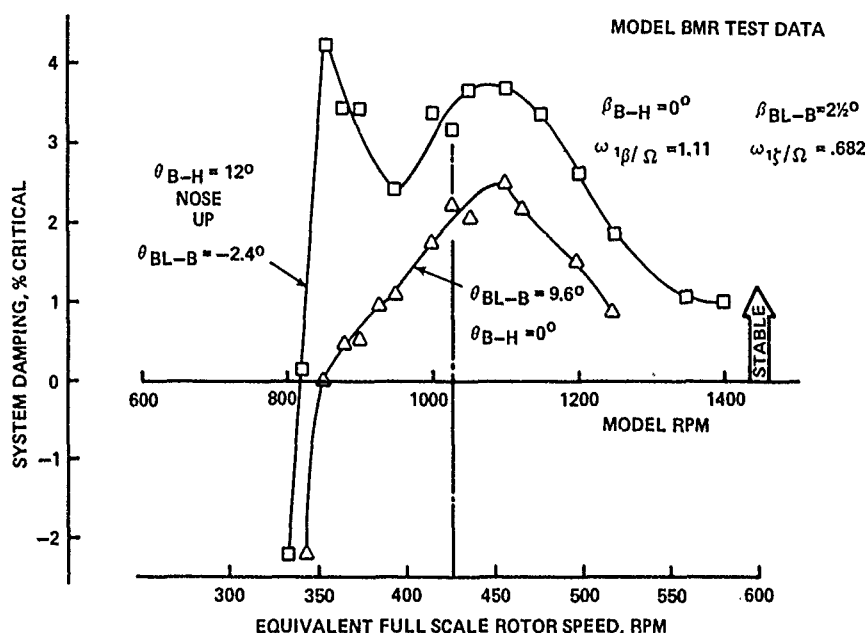


FIGURE 7. EFFECT OF BEAM-TO-HUB PITCH ANGLE ON SYSTEM STABILITY.

Since the flatwise and edgewise motion can be indirectly coupled through torsion (or pitch), pitch-flap and pitch-lag couplings also have impact on stability. A sample of the latter's effect on stability was shown in Figure 4 earlier. Design parameters such as precone, or beam-to-hub cone angle, and droop, or blade-to-beam cone angle, orient the blade pitch axis in space and therefore directly determine the magnitude of pitch-flap on pitch-lag coupling. This is because the perturbational forces acting through the steady vertical offset and the steady forces acting through the perturbational vertical deflection are flap or lag originated, as shown schematically in Figure 8. A similar conclusion can be drawn with respect to the parameter of blade-to-beam sweep angle. Test data shown in Figure 9, also taken from Reference 8, show that a configuration with zero beam-to-hub cone angle is more stable than the configuration with the beam coned up at the hub. This sensitivity is consistent with that reported in Reference 3. With blade pitch motion contributing to the coupling, it is obvious that control system stiffness will also be an important design consideration, as is the location of the pitch arm and pushrod attachment point.

In summary, a successful high speed rotor of the bearingless type design should have beneficial blade pitch-flap-lag couplings(s) incorporated in order to achieve inherent aeromechanical stability. Design parameters to be considered are: beam flatwise stiffness, beam edgewise stiffness, control system stiffness, location of pitch arm and pushrod attachment point, beam-to-hub pitch angle, blade-to-beam pitch angle, beam-to-hub cone angle, blade-to-beam cone angle, and blade-to-beam sweep angle.

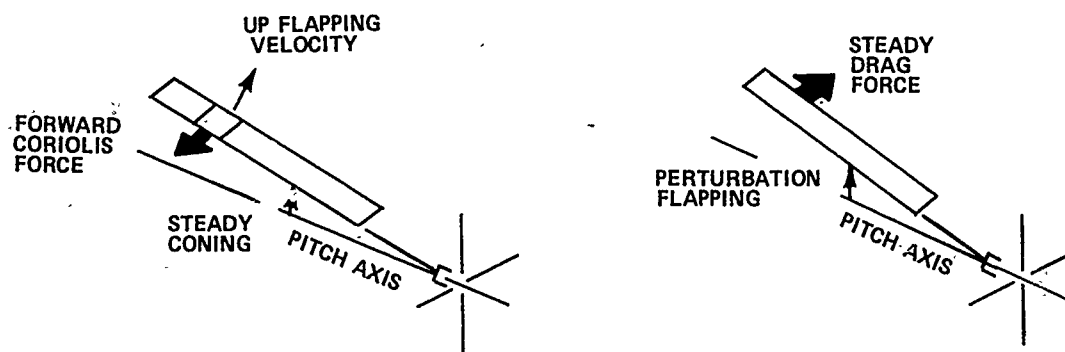


FIGURE 8 SCHEMATICS OF PITCH-FLAP COUPLINGS.

MODEL BMR TEST DATA

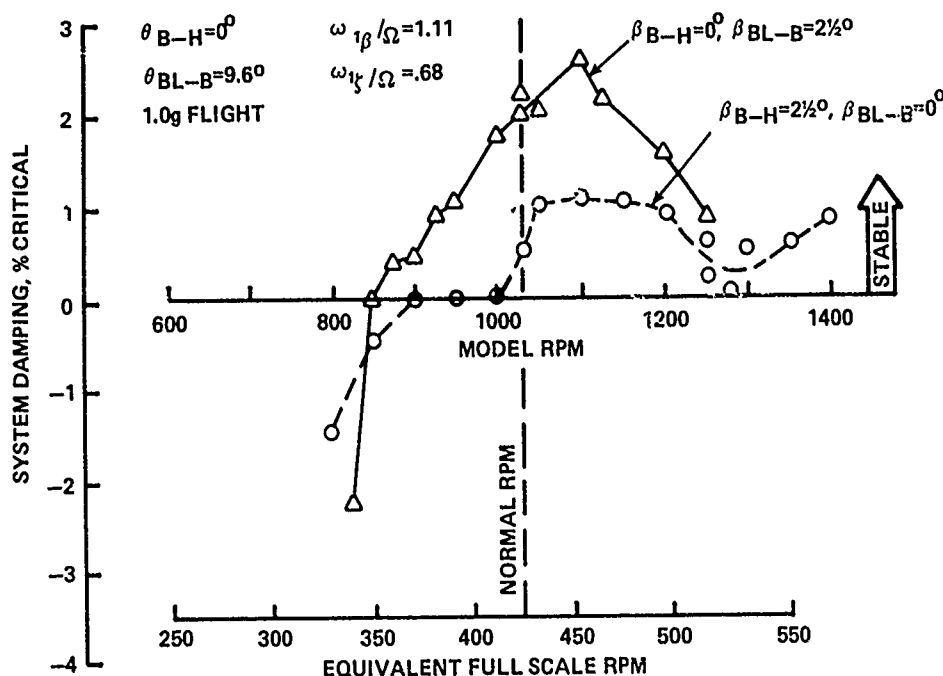


FIGURE 9. EFFECT OF BEAM-TO-HUB CONING ANGLE ON SYSTEM STABILITY.

Factors Affecting Vibration

Having achieved a stable design for the high speed rotor, one's attention will turn to the minimization of vibration. Vibration has been one of the prime causes limiting the speed achievable by the helicopter. There are basically three areas that need attention. First is the airframe dynamics. Theoretically, it is possible to design an airframe such that it will produce a minimum amount of forced response. This can be done either by designing an airframe with sufficient frequency separation of the natural modes from the forcing frequency or by introducing modal cancellations. Neither of these are achieved during the normal course of design and development process. The resulting hub impedance will have a definite impact on the vibration characteristics of the helicopter. Viswanathan and Myers⁹ showed that, by tuning the rotor-pylon mounting impedance, a 75% reduction in the vertical hub shear could be achieved. Flight test results for eight different pylon configurations reasonably confirmed this prediction⁹. Airframe dynamics, in general, will have large impact on the helicopter vibration; however, a full discussion of this is beyond the scope of this paper.

12-8

The second area involves the rotor and airframe interference. As pointed out by Landgrebe, Moffitt and Clark¹⁰, with earlier generations of rotorcraft, neglecting the airframe effect on the rotor flowfield was not critical primarily because the rotor and airframe were well separated. Those authors defined an interference factor as the ratio of the length of the airframe forward of the hub center (nondimensionalized by the rotor radius) to the height of the rotor hub from the junction of the fuselage and main rotor pylon (nondimensionalized by the vertical distance from the fuselage center to the junction of the fuselage and main rotor pylon). The UH-1H has an interference factor of 0.36 while the YUH-61A has a value of 2.8. Figure 10, taken from Reference 10, shows the calculated effect of the airframe on blade section angle of attack distribution at 30% radius. Clear is the pronounced third harmonic content in the increment representing the body induced effect. The resulting vibratory loads are significant. This airframe aerodynamic effect has attracted quite a bit of research activity^{11,12}, but again, a full discussion is beyond the scope of this paper.

The third area deals with the rotor dynamics. Since the main rotor is the prime source of vibration, reducing helicopter vibration by attacking its source has been an attractive idea for many years. Rotor dynamics are affected by parameters such as blade bending stiffness, torsional stiffness, mass distribution, chordwise cg-ac offset etc. Although these parameters have been examined by many researchers over the years, new insights were gained in recent years both by analysis and by test¹³⁻¹⁵. These are discussed in more detail in the next section.

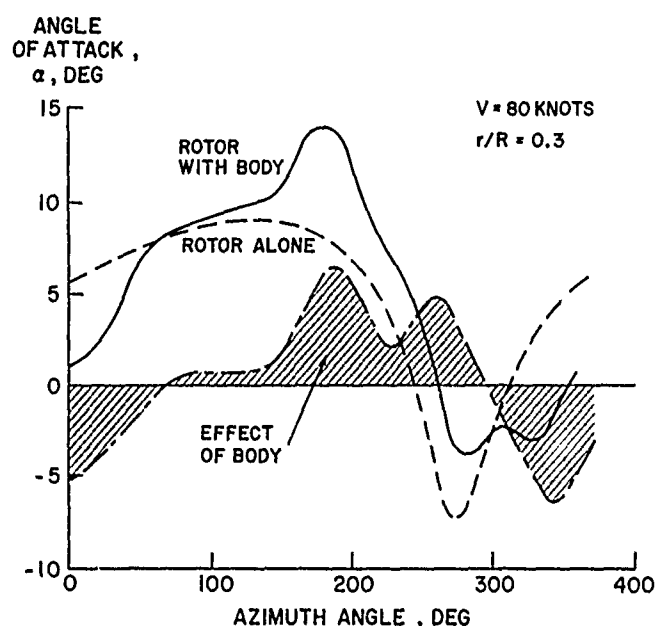


FIGURE 10. BODY EFFECT ON ROTOR ANGLE OF ATTACK DISTRIBUTION.

Vibration Considerations

Designing a rotor for high speed flight and low vibration is indeed a challenge. First, it is well known that the oscillatory components of blade lift increase quickly with airspeed. Older generation helicopters apparently produced fairly tolerable vibration without the vibration control treatment used in current aircraft (e.g. bifilars, absorbers, isolated transmissions and active control systems). The difference is that cruise speeds of 100 knots or less were used. Second, the hingeless rotor which offers advantages in terms of simplicity and low drag tends to aggravate vibration by virtue of the moments applied to the hub. The dynamicist will be further challenged to produce blades with low inherent vibration because approaches involving various hub absorbers (bifilars, pendulums, etc) and even attempts to increase rotor-fuselage separation may be ruled out by their aerodynamic drag implications in high speed flight.

In order to meet this challenge, rotor blades will have to be optimized from a structural dynamics standpoint. As pointed out in Reference 13, vibration considerations have not, in general, played a strong role in shaping current rotor blades. Blade design has been based more on strength, weight and aerodynamic considerations. Except to separate blade natural frequencies from harmonics of rotor speed, the dynamicist has provided little clear guidance to the blade designer. Vibration, if it has turned out to be troublesome, has been attacked by changing fuselage dynamics or adding vibration absorption devices. This situation stems from a lack of systematic data describing the vibration effects of individual blade parameters and from difficulties in reliably predicting vibratory hub loads with state-of-the-art aeroelastic response analyses.

This situation must change if the low vibration high speed rotor is to become a reality. Indeed several manufacturers and universities have begun concentrated work in the area of blade design for low vibration¹³⁻¹⁶.

In the paragraphs which follow, the design of a low vibration high speed rotor will be considered by examining the roles of several key design parameters. The review will be based on recent analytic investigations and on model and full scale test results. Where possible preferred design choices will be suggested and issues remaining to be considered will be highlighted.

Number of Blades - Once the type of rotor system is selected, the next most important decision affecting vibration is the number of blades. The number is based on a tradeoff involving such factors as cost, performance, ballistic survivability and noise. From a vibration standpoint, it is generally accepted that more blades will produce lower vibration. Recent Sikorsky models have borne this out as the four-bladed UH-60A and S-76 devote about 2% of gross weight to vibration control, whereas the six-bladed CH-53D and the seven-bladed CH-53E employ no vibration control hardware.

The beneficial effect of increased blade number follows directly from the fact that the magnitudes of the harmonic airloads decrease with the number of the harmonic. Figure 11, for instance, shows the magnitudes of the harmonic airloads measured at the three-quarter radius position of a CH-53A blade (Reference 17). As shown, the magnitudes of the airload harmonics fall off directly with harmonic number. Insofar as the $n-1$, n and $n+1$ harmonic airloads produce vibration on an n -bladed rotor, Figure 11 suggests that five or more blades should be used for rotors which are to operate at high advance ratio. As advance ratios of 0.4 and 0.5 are approached, five or more blades may become a requirement for a successful low vibration rotor.

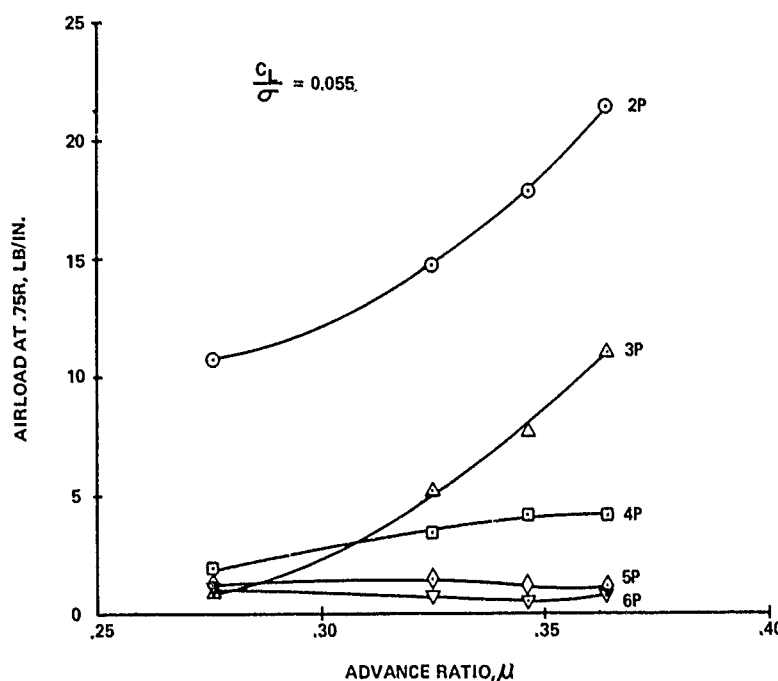


FIGURE 11. MEASURED BUILDUP OF CH-53A BLADE LOADS WITH ADVANCE RATIO.

It is worthwhile to point out that the choice of the number of blades should be made in conjunction with the selection of blade mode frequencies. This issue is illustrated in Figure 12. Shown in the figure are typical blade and rotor mode frequencies for articulated rotors and the excitation frequencies which produce vibration on n -bladed rotors. The obvious rule should be to avoid proximity of the $n-1$, n and $n+1$ harmonics from as many blade modes as possible. As an example, a six-bladed rotor with first edgewise and torsion modes below 5/rev would appear to warrant consideration during preliminary design.

Bending Stiffness - The selection of blade bending stiffness is important for two reasons. First, the stiffness, along with the mass distribution, determines the placement of the bending mode frequencies. Second, the bending stiffness at the root of the blade determines the effective hub offset which has a controlling influence on vibratory root shears and moments.

In designing for high speed flight, the conventional practice of separating blade mode frequencies from rotor speed harmonics will become increasingly important as the magnitude of the harmonic forces increases with advance ratio. In addition to avoiding rotor speed harmonics, the optimal choice of blade bending mode frequencies for minimum excitation should be considered. The advent of composite materials allows stiffness values to be selected which were not practical with metal blades. With regard to effective hub offset, soft root flexures in the flatwise and edgewise directions will minimize the moments transmitted to the hub. The issue here will be to produce a low offset arrangement which is viable from a structural standpoint and which satisfies aeroelastic stability constraints.

12-10

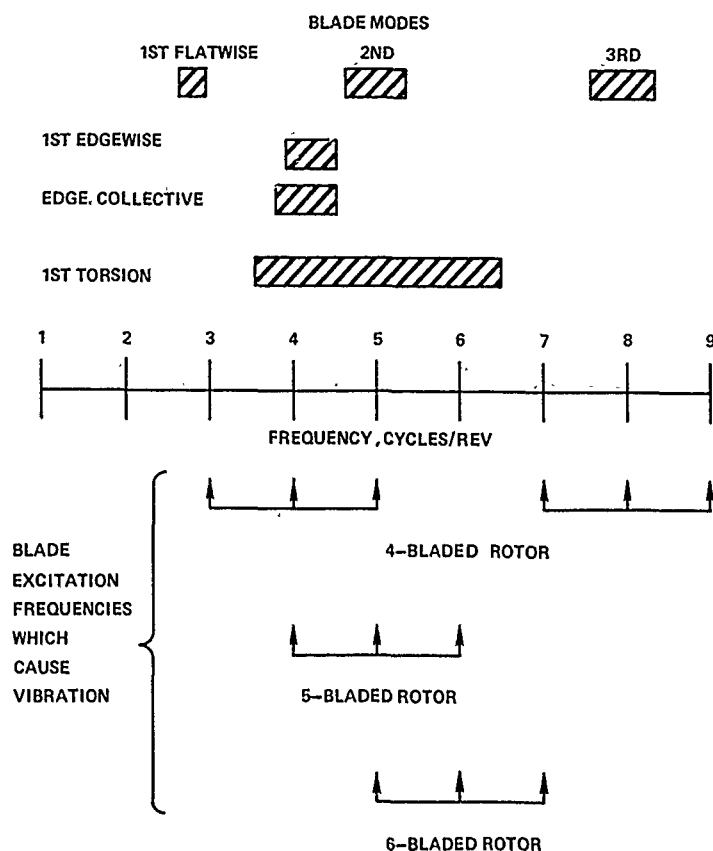


FIGURE 12. CRITERIA FOR SELECTING NUMBER OF BLADES AND BLADE MODE FREQUENCIES.

Spanwise Mass Distribution - References 13 and 14 explore the effect of blade spanwise mass distribution on the vibratory forces applied to the hub on an articulated rotor. Reference 14 demonstrates that significant reductions in root forces can be achieved by changing the spanwise mass distribution. The mechanism outlined is that the mass distribution alters the bending mode shapes in such a way as to reduce generalized airloading at particular rotor harmonics.

Figure 13, taken from Reference 14, illustrates the change in flatwise mode shapes produced by adding a 10 lb tip mass to an S-76 rotor blade. It is shown that these small changes can make the mode shape much more orthogonal to the airload distributions present at particular forcing frequencies. Figure 14, also from Reference 14, shows the predicted vibratory hub loads reductions to be achieved with the tip weight. The change in the mode shape of the first two flatwise modes has substantially reduced the 4/rev vertical root shear associated with these modes.

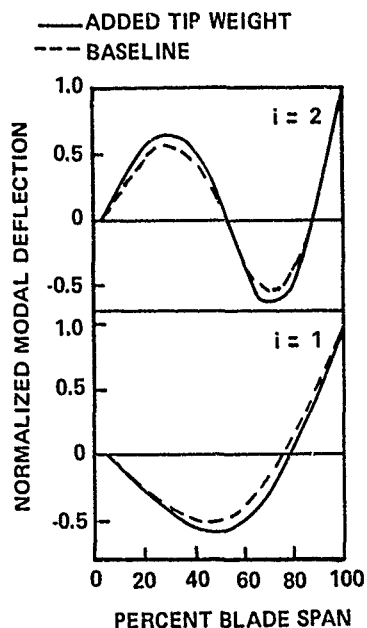


FIGURE 13. EFFECT OF 10LB TIP WEIGHT ON S-76 BLADE FLATWISE MODE SHAPES.

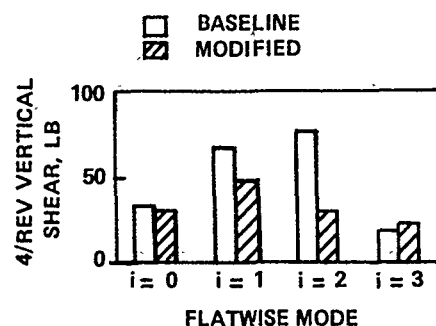


FIGURE 14. PREDICTED CHANGE IN 4 PER REV ROOT VERTICAL SHEAR CONTRIBUTION OF EACH FLATWISE MODE.

Reference 13 considered adding mass to the UH-60A blade. In that case, the analysis predicted that mass added at midspan would reduce vibratory hub loads. Figure 15, taken from Reference 13, illustrates these results. Clearly the best mass distribution depends upon the other properties of the blade and the flight condition. It is premature to speculate on what types of mass distribution will be appropriate to a given high speed rotor blade, but the results illustrated above suggest that this is a parameter which may afford significant vibration benefits.

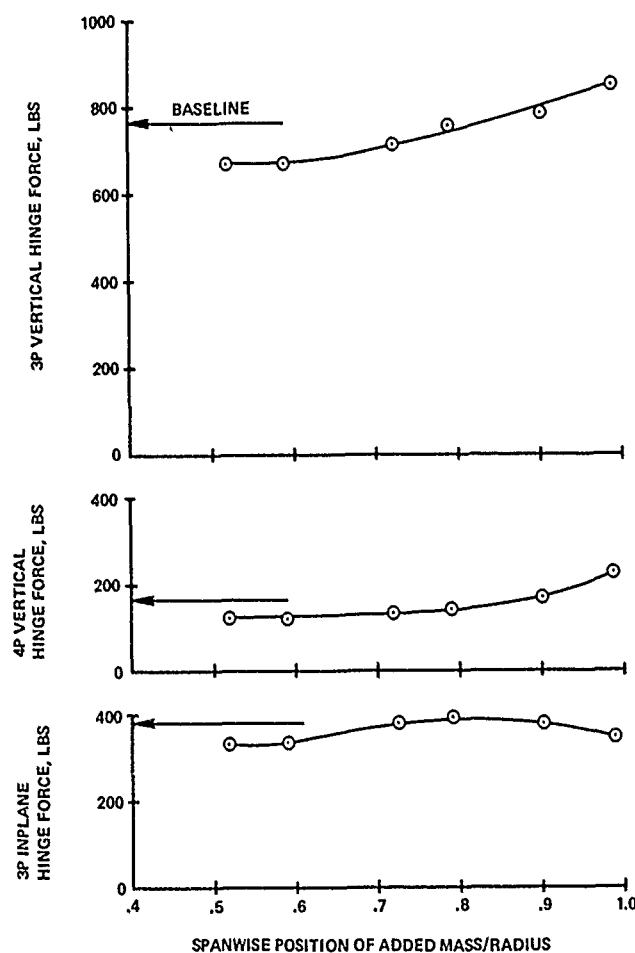


FIGURE 15. PREDICTED EFFECT OF ADDING 10 LB CONCENTRATED MASS ON UH-60A VIBRATORY HUB SHEARS; $V = 145$ KN, $L = 17,500$ lb.

Blade Chordwise Center of Gravity to Aerodynamic Center Offset - Chordwise offset of the c.g. and a.c. can be expected to produce coupling between torsional and flatwise bending response. Ideally, vibratory shear forces applied to the blade (at n/rev , for instance) would produce a torsional response (at n/rev) which would alter the angle of attack in such a way as to null the original airload. Provided this coupling can be arranged without compromising aeroelastic stability, it should be an effective means of reducing vibratory hub loads. Reference 18 predicted that significant (3 to 1) reductions in vibratory root shear could be produced by blades having chordwise c.g.s. in the region of 18 to 20 percent chord and blade torsional frequencies placed near the excitation frequency. Analytic results presented in Reference 13 appear to confirm the potential benefit of this coupling. Figure 16, taken from Reference 13, depicts the predicted reduction in 3/rev vertical vibratory shear on a UH-60A blade operating at 145 knots. With a c.g. five-percent of chord forward of the a.c. and the torsion frequency placed close to 3/rev, 45 percent reductions in 3/rev shear are predicted.

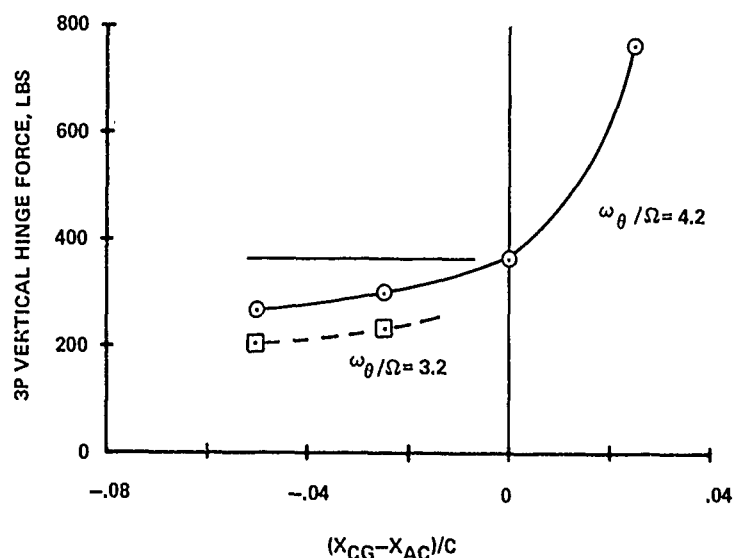


FIGURE 16. PREDICTED EFFECT OF CHORDWISE CG - AC OFFSET ON UH-60A VIBRATORY HUB SHEARS; $V = 145 \text{ KN}$, $L = 17,500 \text{ LBS}$.

Introducing this coupling embodies a certain amount of risk. In addition to stability considerations, its effectiveness for reducing vibration over a range of flight conditions, the resultant control loads and the effect on performance and handling qualities will have to be considered. If it can be made to work, however, this approach could provide passively some of the vibration reduction benefits sought through higher harmonic control systems.

Blade Twist - Blade twist affects vibratory hub loads in two ways. First, the twist alters the basic airloads applied to the blade. Second, twist increases the coupling between flatwise and edgewise response. Linear aerodynamic theory shows that blade flatwise airloads at 2/rev, 3/rev and 4/rev include components which are proportional to twist angle times advance ratio squared. (See Reference 19, for example). It is further believed that the advancing tip of a high twist blade experiences impulsive lift, drag and pitching moment due to a negative angle of attack and that this impulse translates into increased higher harmonic blade response and increases vibration. Conclusive data, however, are scarce. Analytic results reported in Reference 13 showed no clear trends of vibratory root forces with changes in twist. Figure 17, taken from Reference 13, shows results for a UH-60A rotor operating at 145 knots and 175 knots.

The vibration implications of twist on the high speed blade are, therefore, uncertain. Because the answer may depend upon the details of the advancing tip loading which is difficult to model analytically, the final decision may have to be based on model or full scale rotor tests.

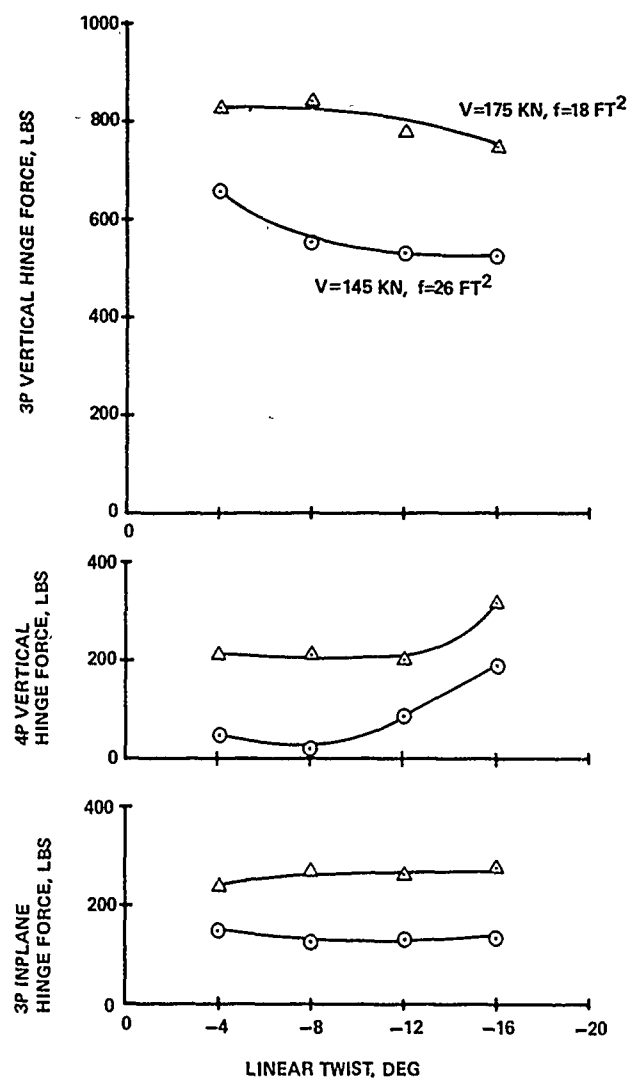


FIGURE 17. PREDICTED EFFECT OF TWIST ON VIBRATORY ROOT SHEARS.

Tip Sweep - Tip sweep alters vibration in two ways. First, sweep changes the lift and drag forces at the tip which are important sources of blade mode excitation and second, sweep may alter the blade dynamic twist, thereby changing airloads all along the blade. The concept of using sweep (and airfoil characteristics to be discussed next) in conjunction with blade torsional properties to control blade dynamic twist was studied in References 20 and 21. It was predicted that tip sweep in conjunction with low torsion stiffness would favorably affect vibration. Model test results from Reference 21 showed benefits for both reduced and conventional stiffness blades. Figures 18 and 19, taken from Reference 13, illustrate the reductions. These results were measured on an articulated model. The mechanism suggested in Reference 13 is that torsional response produced by the airloads at the tip produced a general smoothing of the vibratory flatwise excitation. The response of each of the first three flatwise modes was reduced. Such a mechanism would apply equally well to bearingless blades. Based on these results and the inherent performance advantages of swept tips at high Mach numbers, tip sweep appears to be a valuable element for the low vibration high speed rotor. Because the test results above showed vibration reduction for both soft and conventional torsional stiffness blades, the role of torsional response is not completely clear and should be considered further.

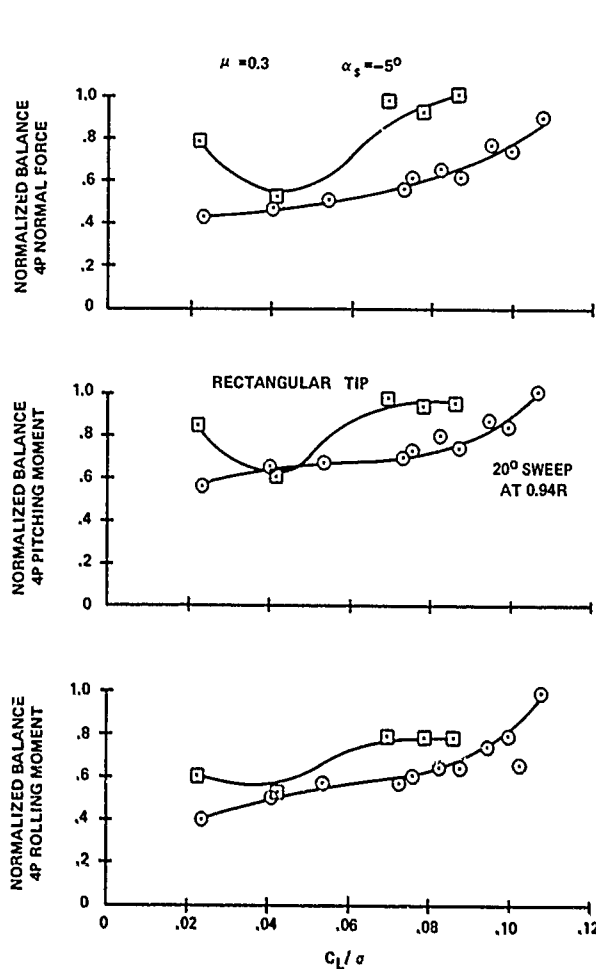


FIGURE 18. COMPARISON OF VIBRATORY HUB LOADS FOR ACR BLADES WITH RECTANGULAR AND SWEEP TIPS.

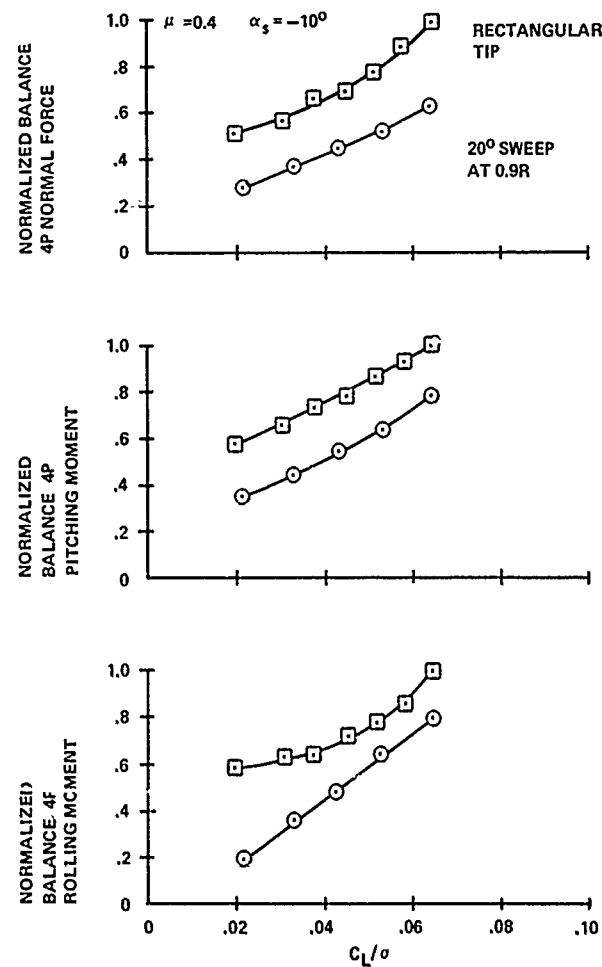


FIGURE 19. COMPARISON OF VIBRATORY HUB LOADS FOR BASELINE BLADES WITH RECTANGULAR AND SWEEP TIPS.

Airfoil - Airfoil pitching moments, like tip sweep, produce a dynamic twisting of the blade which can introduce higher harmonic airloads. The Aeroelastically Conformable Rotor Work discussed in Reference 21 predicted a trend for reduced vibratory hub loads on blades which had tabs deflected to produce noseup section pitching moment relative to that of a baseline cambered airfoil. Apparently the change in advancing blade twist produced by the tab deflection altered that angle of attack distribution on the advancing blade in such a way as to minimize fluctuations in high Mach number pitching moments. The resulting elastic twist and flatwise airload time histories were smoother. Model test results presented in Reference 21 and reproduced as Figures 20 and 21 confirmed that the reduced camber (noseup section pitching moment) caused a reduction in the vibratory forces applied to the model rotor hub.

These results suggest that the airfoils to be used on future-generation high speed rotors should be scrutinized for their impact on vibration. There will likely be a tendency to employ a more highly cambered airfoil inboard on the blade to achieve the high $c_{l,max}$ values necessitated by high speed flight. The torsional response and the angle of attack fluctuations produced by the airfoil should be considered in the selection process.

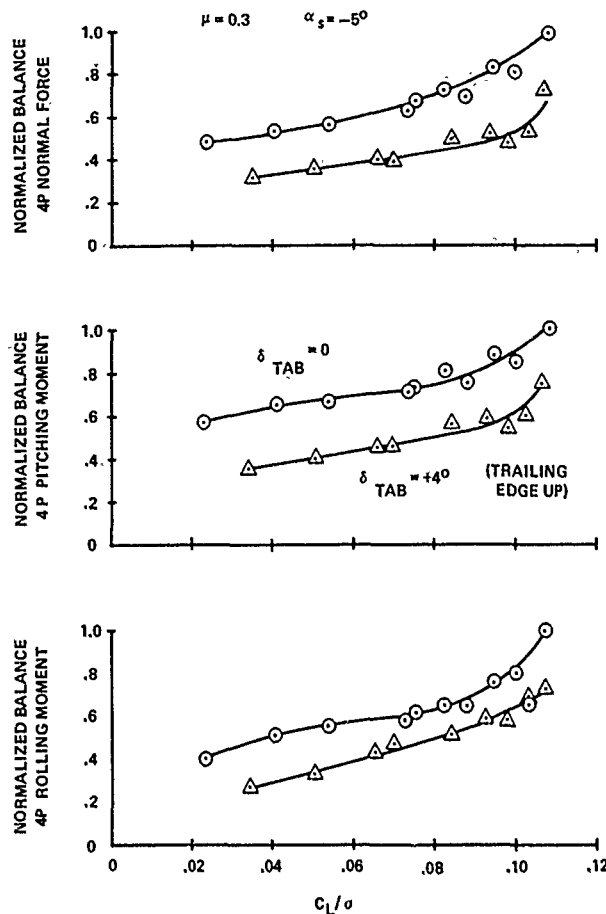


FIGURE 20. COMPARISON OF VIBRATORY HUB LOADS FOR BASELINE BLADES WITH AND WITHOUT TAB DEFLECTION.

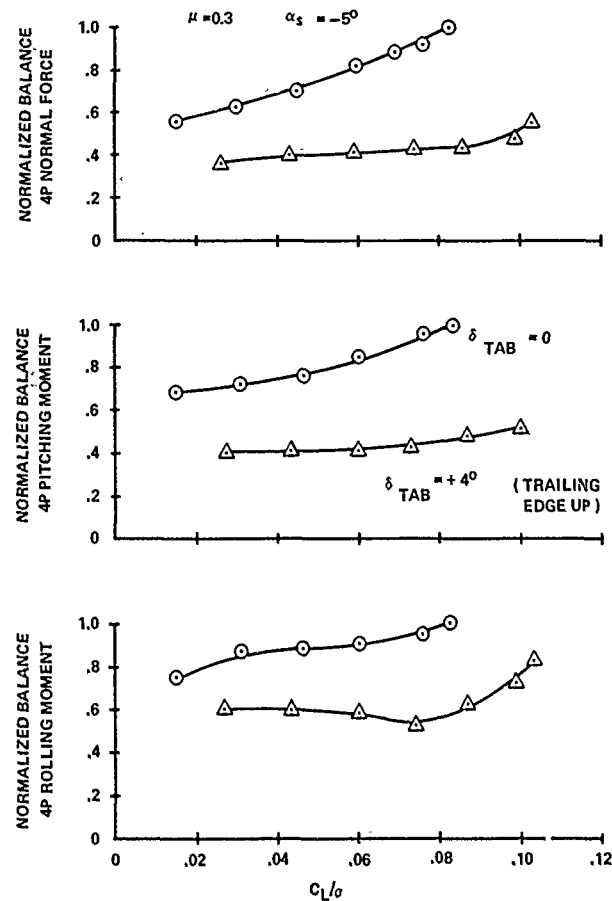


FIGURE 21. COMPARISON OF VIBRATORY HUB LOADS FOR ACR BLADES WITH AND WITHOUT TAB DEFLECTION.

Concluding Remarks

The prevailing design philosophy for avoidance of aeroelastic instability of the rotorcraft has been to avoid frequency coalescence and modal coupling. In addition, lag dampers are used to provide sufficient damping in the edgewise direction. With increased understanding in the physical nature of the rotor system stability, the design philosophy is changing to the one that introduces coupling deliberately among blade bending responses in two planes and blade torsional response. This incorporation of beneficial couplings provides a greater freedom in the design of a bearingless type rotor, the most likely candidate for a high speed rotor. Also, the understanding of the physics of the stability phenomena enables the designer to eliminate the lag damper, a definite plus in the performance consideration of a high speed rotor.

Recent research indicates vibration can be reduced by control of elastic twisting either through aerodynamic design or through incorporation of blade couplings utilizing blade stiffness and mass distributions as well as tip shapes. Although the studies performed to date have addressed the articulated rotor, the results should be applicable to the bearingless rotor as well. Of course, the need to quantify these sensitivities for the bearingless rotor does exist. A more important question that needs to be answered is "Are the couplings that are desirable for vibration reduction are also beneficial in terms of stability?"

References

- 1) Ormiston, Robert A. and Hodges, Dewey H., "Linear Flap-Lag Dynamics of Hingeless Helicopter Rotor Blades in Hover", Journal of the American Helicopter Society, April 1972.
- 2) Staley, J. A., Gabel, R. and McDonald, H. I., "Full Scale Ground and Air Resonance Testing of the Army/Boeing Vertol Bearingless Main Rotor", Presented at the 35th Annual National Forum of the American Helicopter Society, No. 79-23, May 1979.
- 3) Burkam, John, E. and Miao, Wen-Liu, "Exploration of Aeroelastic Stability Boundaries with a Soft-In-Plane Hingeless - Rotor Model", Journal of the American Helicopter Society, October 1972.
- 4) Ormiston, Robert A., "Aeromechanical Stability of Soft-In-Plane Hingeless Rotor Helicopters", Paper No. 25, Presented at the Third European Rotorcraft and Powered Lift Aircraft Forum, Sept. 7-9, 1977, Aix-En-Provence, France.
- 5) Bousman, William G., "An Experimental Investigation of the Effects of Aeroelastic Couplings On Aeromechanical Stability of a Hingeless Rotor Helicopter", Journal of the American Helicopter Society, January 1981.
- 6) Baldock, J.C.A., "Some Calculations for Air Resonance of a Helicopter With Non-Articulated Rotor Blades", RAE Technical Report 72083, August 1972.
- 7) Ormiston, Robert A., "Concepts for Improving Hingeless Rotor Stability", Proceedings of the American Helicopter Society Mideast Region Symposium on Rotor Technology, August 1976.
- 8) Chen, C., Staley, J. A., Miao, W. and Harris, F. D., "Aeroelastic Stability Test Results for a 1/5.86 Scale Model of a Bearingless Main Rotor System on the B0-105 Helicopter", Boeing Vertol Company Report D210-11245-1, June 1977.
- 9) Viswanathan, Sathy P. and Myers, Alan W., "Reduction of Helicopter Vibration Through Control of Hub-Impedance", Journal of the American Helicopter Society, October 1980.
- 10) Landgrebe, Anton J., Moffitt, Robert C., and Clark, David R., "Aerodynamic Technology for Advanced Rotorcraft - Part II", Journal of the American Helicopter Society, July 1977.
- 11) Wilby, P. G., Young, C. and Grant, J. "An Investigation of the Influence of Fuselage Flow Field on Rotor Loads, and the Effects of Vehicle Configuration", Presented at the Fourth European Rotorcraft and Powered Lift Aircraft Forum, September 13-15, 1978, Stresa, Italy.
- 12) Sheridan, Philip F. and Smith, Robert P., "Interactional Aerodynamics - A New Challenge to Helicopter Technology", Presented at the 35th Annual National Forum of the American Helicopter Society, May 1979.
- 13) Blackwell, R. H., "Blade Design for Reduced Helicopter Vibration", Presented at the American Helicopter Society Northeast Region National Specialists' Meeting On Helicopter Vibration, November 1981, Hartford, CT
- 14) Taylor, R. B., "Helicopter Vibration Reduction by Rotor Blade Modal Shaping", Presented at the 38th Annual Forum of the American Helicopter Society, Anaheim, CA, May 1982.
- 15) Friedmann, P. and Shanthakumaran, P., "Optimum Design of Rotor Blades for Vibration Reduction in Forward Flight", to be Presented at the 39th Annual Forum of the American Helicopter Society, St. Louis, MO, May 1983.
- 16) Peters, D. A., et al, "Design of Helicopter Rotor Blades for Desired Placement of Natural Frequencies", to be Presented at the 39th Annual Forum of the American Helicopter Society, St. Louis, MO, May 1983.
- 17) Beno, E. A., "CH-53A Main Rotor and Stabilizer Vibratory Airloads and Forces", SER-65993, NASC Report, Naval Air System Command, Washington, DC, June 1970.
- 18) Miller, R. H. and Ellis, C. W. "Helicopter Blade Vibration and Flutter", Journal of the American Helicopter Society, Vol. 1, No. 3, July 1956.
- 19) Landgrebe, A. J., "Simplified Procedures for Estimating Flapwise Bending Moments on Helicopter Rotor Blades," NASA CR-1440, October 1969.
- 20) Blackwell, R. H., "Investigation of the Compliant Rotor Concept," USAAMRDL-TR-77-7, Eustis Directorate, U.S. Army Air Mobility Research and Development Laboratory, Fort Eustis, VA, June 1977.
- 21) Blackwell, R. H. and Frederickson, K. C., "Wind Tunnel Evaluation of Aeroelastically Conformable Rotors", USAAVRADCOM TR-80-D-32, Applied Technology Laboratory, U.S. Army Research and Technology Laboratories, January 1981.

ANALYSE PRÉVISIONNELLE DU COMPORTEMENT AÉROÉLASTIQUE DES ROTORS ARRIÈRE

par

G. GENOUX et G. BLACHÈRE

Société Nationale Industrielle Aérospatiale

Marignane Cédex

13725

France

RÉSUMÉ

Une connaissance relativement précise du comportement aéroélastique des rotors d'hélicoptères est nécessaire pour les dimensionner au mieux et avec le maximum de sécurité.

Dans le cas des rotors arrière, la prévision de leur comportement est complexe en raison de l'environnement dynamique, aérodynamique et de leurs conditions particulières de fonctionnement (plage de pas, vrillage important, régime,...).

La représentation complète du comportement du rotor anticouple et de la structure hélicoptère est très difficile à modéliser au stade prévisionnel ; aussi l'approche consiste-t-elle, malgré des limitations inhérentes à cette démarche, à créer un ensemble de modèles spécialisés, adaptés aux types de rotors étudiés, de taille raisonnable et permettant une analyse prévisionnelle des problèmes les plus importants. Ce papier décrit certaines méthodes utilisées à l'Aérospatiale pour l'étude et la mise au point aéroélastique des rotors arrière, ainsi que leur application à différents concepts (rotors articulés, rotor à lame, fenestron).

NOTATIONS

Ω_{RP}	Régime de rotation du rotor principal
Ω_{RA}	Régime de rotation du rotor arrière
b	Nombre de pales du rotor
n	Numéro d'harmonique
ω_{Fi}	Fréquences propres du fuselage
ω_{RAi}	Fréquences propres du rotor arrière
ω_T	Fréquence fondamentale de trainée
ω_{To}	Fréquence fondamentale de torsion
R	Rayon du rotor
\emptyset	Diamètre du rotor
c	Corde de la pale
\emptyset	Pas au manchon
$\emptyset_{0,7R}$	Pas à 0,7R
α	Amortissement modal réduit
X_g	Centrage en corde de la pale
d	Déport du balancier
a_o	Conicité
α_D	Basculement du disque
C_z	Coefficient de portance
C_{mo}	Coefficient de moment à portance nulle
C_T	Coefficient de traction
C_D	Coefficient de trainée
τ	Densité de l'air
M	Nombre de mach
M_{DT}	Mach de divergence
T	Variable temporelle
(x, y, z)	Trièdre de référence du rotor
	x direction longitudinale de l'hélicoptère
	y direction latérale de l'hélicoptère
	z direction verticale de l'hélicoptère

1. INTRODUCTION

Bien que la fonction à assurer soit plus simple que pour les rotors principaux, les rotors arrière donnent naissance à de nombreux problèmes aéroélastiques, certains analogues à ceux des rotors principaux et d'autres spécifiques dus à un effet d'échelle, aux technologies utilisées, aux conditions de fonctionnement (plage de pas importante, régimes élevés), à des liaisons cinématiques particulières (liaison K)... Par ailleurs l'environnement aérodynamique et dynamique des rotors arrière est relativement complexe et rend très difficile au stade de la conception une modélisation complète et générale de leur comportement aéroélastique.

Aussi, notre approche consiste à créer des modèles spécialisés adaptés aux types de rotors étudiés, de taille raisonnable, en tirant parti de notre expérience propre et de celle d'autres constructeurs.

Après une description des différents concepts développés par l'Aérospatiale que ce soit au titre de la série ou d'une évaluation "recherche", nous rappellerons brièvement les méthodes de calcul utilisées pour la détermination des caractéristiques propres (fréquences, amortissement) du rotor isolé ; les critères généralement retenus pour le positionnement des fréquences propres seront indiqués ainsi que certaines instabilités ayant fait l'objet d'une étude particulière et/ou d'essais.

Ensuite, sera abordé le difficile problème de l'étude des vibrations forcées (réponse et stabilité aéroélastique) pour le rotor en vol d'avancement, bien que d'expérience cette configuration ne soit pas critique dans l'étude d'un rotor arrière.

Une dernière partie traitera des couplages entre le rotor et la structure et sera illustrée par quelques instabilités typiques de l'hélicoptère.

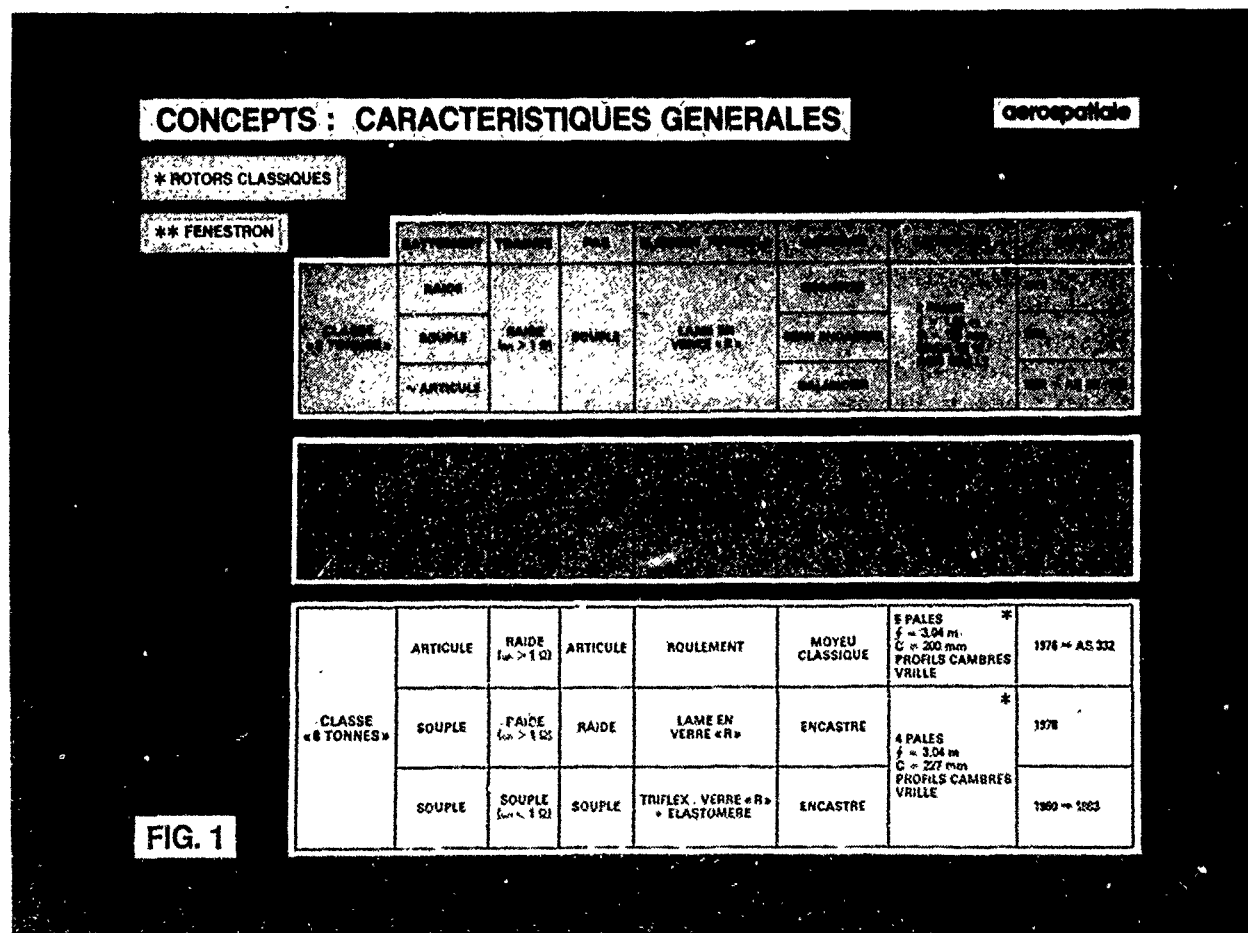
2. LES CONCEPTS DE ROTOR ARRIÈRE

Comme pour les rotors principaux, de nouvelles technologies sont apparues pour les rotors de queue d'hélicoptère.

Durant les dix dernières années l'Aérospatiale a étudié différents concepts de rotor pour équiper des appareils dans la gamme 2T, 4T ou 8 tonnes.

Tous ces rotors ont un point commun qui est l'utilisation des matériaux composites permettant une meilleure optimisation aérodynamique et dynamique, ainsi qu'une grande simplification du moyeu par la suppression de tout ou partie des articulations mécaniques classiques.

Les caractéristiques générales des différentes formules évaluées qui serviront à illustrer certains problèmes aéroélastiques sont présentées fig. 1.



• Classe 2T

Pour la gamme des appareils de 2T, trois types de concepts ont été examinés, différant essentiellement par leur mode de liaison au mât (encastré, semi encastré, balancier).

Il s'agit de rotors à lame bipale constitués d'une lame en verre souple en flexion et en torsion, liant 2 pales opposées ; la commande de pas pour contrôler la portance du rotor se fait par l'intermédiaire d'une manchette s'appuyant sur 2 paliers localisant l'axe de pas et l'articulation de battement.

La version balancier a été développée pour une application sur l'"Ecureuil" ; les deux autres, dans un cadre recherche en utilisant les mêmes pales pour réduire les coûts de développement.

Certains détails de montage sont indiqués fig. 2, 3 et 4 pour les versions "semi encastré" et en "balancier".

ROTOR SEMI ENCASTRE

aérospatiale



FIG. 2

ROTOR EN BALANCIER ECUREUIL

aérospatiale

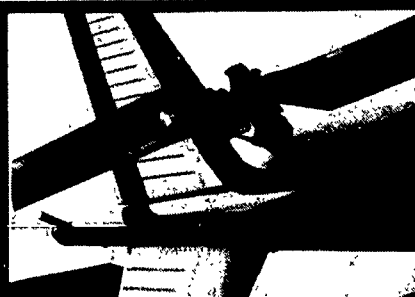


FIG. 3

ROTORS A LAME BIPALE : CLASSE "2T"
(DETAILS DE MONTAGE)

aérospatiale

PALE : TECHNOLOGIE VERRE - MOUSSE

MONTAGE SEMI-ENCASTRE

MONTAGE EN BALANCIER

PALIER SEC

MASSSES CHINOISES

LAME EN VERRE

PALIER ELASTOMERE

MANCHETTE

ARTICULATION DE BALANCIER
SUR PALIER ELASTOMERE

PALIER ELASTOMERE

FIG. 4

13-4 • Classe 4T

La solution de rotor arrière, caréné par une veine structurale et baptisée "Fenestron" a été adoptée pour la première fois en 1968 sur la SA 341 Gazelle en lieu et place du rotor arrière classique.

Depuis, cette solution a été reconduite sur plusieurs appareils de l'Aérospatiale, compte tenu de son intérêt sous l'aspect sécurité au sol ou près du sol, avec des améliorations notables par rapport à la définition initiale, en particulier sur le rendement aérodynamique en vol stationnaire et le devis de masse ; ces gains étant dus pour une large part à l'utilisation des matériaux composites.

La philosophie générale qui se dégage des travaux effectués à l'Aérospatiale, tend à montrer que cette solution est intéressante pour les machines de faible et moyen tonnage jusqu'à 6 T environ. C'est donc la solution qui a été retenue pour l'AS 365 N₁.

Dans ce cas le rotor est constitué de 11 pales ; chaque pale comporte un longeron en Kevlar qui se prolonge dans la zone centrale du moyeu, par un faisceau bobiné assurant la reprise des efforts centrifuges et dont la souplesse en torsion permet la commande de pas.

Le pied de pale quand à lui, est encastré sur un double palier autorisant la commande en pas et équilibrant les moments de flexion.

L'illustration de ce concept est donnée fig. 5, 6 et 7.

FENESTRON 365 N1

aérospatiale

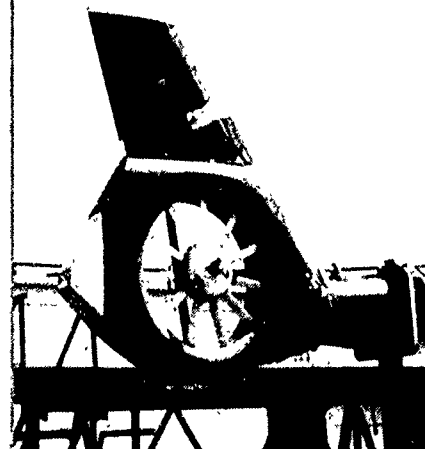


FIG. 5

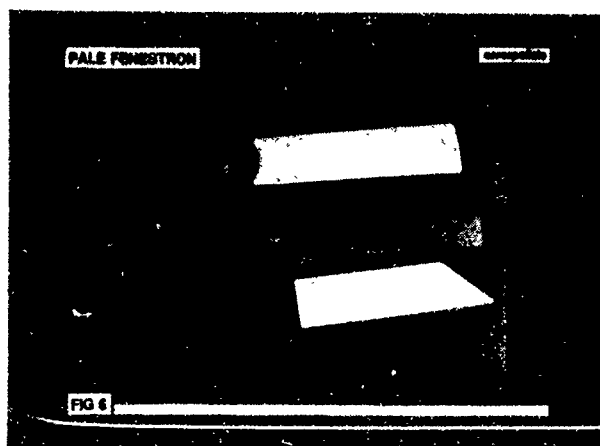


FIG. 6

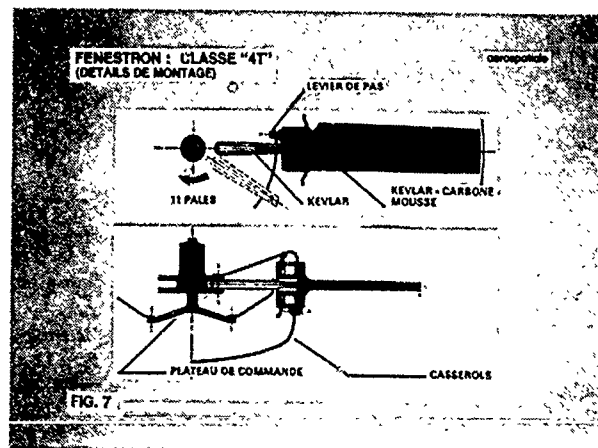


FIG. 7

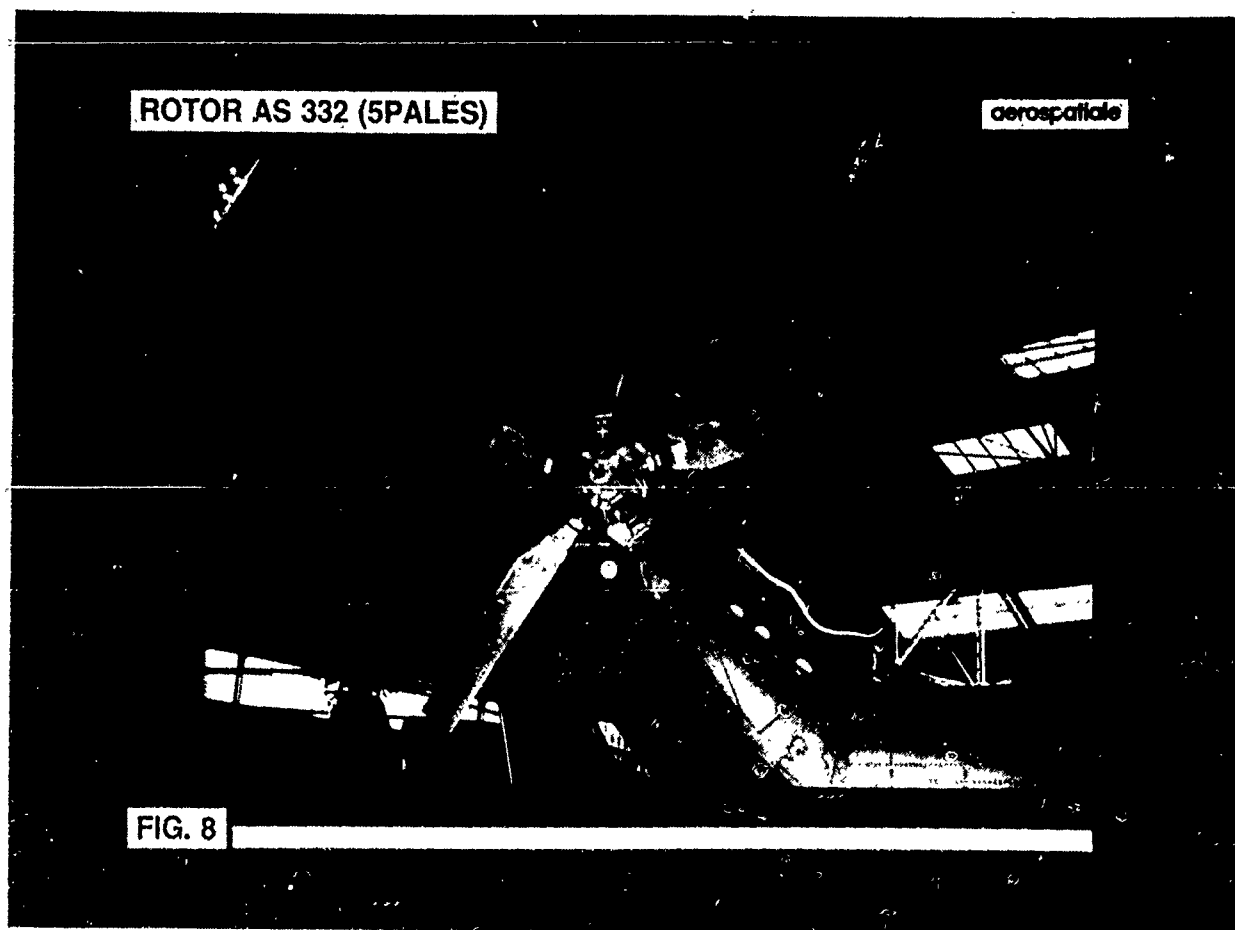
• Classe 8T

Pour les appareils de tonnage plus important, le problème de la sécurité au sol se pose moins en raison de la position généralement très surélevée du rotor arrière, ce qui réduit en outre l'inclinaison latérale de l'appareil qui a tendance à augmenter avec le tonnage, toutes choses égales par ailleurs.

Aussi, l'Aérospatiale a-t-elle poursuivi également ses recherches sur les rotors classiques.

Pour cette classe d'appareil, trois types de rotor ont été développés.

L'un d'eux, un rotor classique avec des articulations mécaniques (pas, battement) comprend cinq pales de technologie composite et a été choisi dès l'origine pour équiper l'AS 332 (Fig. 8).



Les deux autres ont été développés à titre recherches ; il s'agit :

- d'un rotor quadripale utilisant comme élément souple en battement et en torsion, une lame en fibres de verre unidirectionnelles (fig. 9 et 11),
- d'un rotor quadripale "Triflex" dont l'élément torsible est réalisé à partir de filaments de verre noyés dans un élastomère polyuréthane ou silicone (fig. 10 et 11).

ROTOR A LAME (4 PALES)

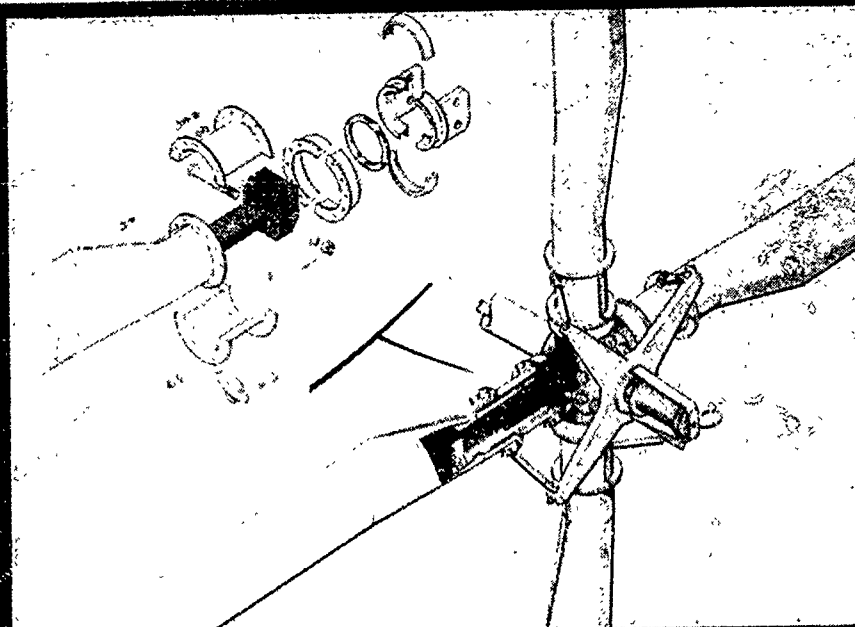


FIG. 9

13-6

ROTOR TRIFLEX (4 PALES)

aérospatiale

**FIG 10****ROTORS QUADRIPALE : CLASSE "8T"
(DETAILS DE MONTAGE)**

aérospatiale

PALE : TECHNOLOGIE VERRE - CARBONE - MOUSSE

ROTOR A LAME

ROTOR TRIFLEX

LAME EN VERRE

ATTACHE
FEUILLETÉE

MANCHETTE

PALIER SEC OU
ÉLASTOMÈREPALIER SEC OU
ÉLASTOMÈRE

ÉLASTOMÈRE

VERRE

FIG. 11

3. ÉTUDE DES CARACTÉRISTIQUES PROPRES (fréquences, amortissements) DU ROTOR ISOLÉ

Une des principales étapes dans la définition d'un rotor arrière consiste en l'étude des caractéristiques propres (fréquences propres, amortissement) du rotor isolé, c'est-à-dire limité à la pale et au moyeu, en configuration de vol stationnaire.

En effet la prévision correcte de ces caractéristiques permet :

- le bon positionnement des fréquences à partir d'un certain nombre de critères.
- d'examiner certaines problèmes de stabilité linéaire du rotor et les couplages.

Avant d'aborder ces deux points nous précisons donc les hypothèses concernant ce type de calcul.

3.1. Méthode de calcul

3.1.1. Hypothèses générales

La méthode utilisée a été présentée dans la référence 1 et le lecteur intéressé pourra s'y reporter.

Elle consiste à définir un mode propre comme un des mouvements libres de la pale autour de sa position d'équilibre dans l'hypothèse des petits déplacements linéarisés.

Le calcul comporte alors deux parties :

- détermination de l'état statique, problème non linéaire résolu par une méthode d'intégration numérique pas à pas itérative.
- détermination de la pulsation et de l'amortissement de chacun des modes par résolution de l'équation caractéristique du système différentiel linéarisé autour de l'état statique.

Les forces aérodynamiques sont incluses directement dans l'écriture des équations du mouvement des pales, de sorte que les amortissements sont obtenus directement pour chaque mode, sans qu'il soit nécessaire comme c'est le cas pour d'autres méthodes d'exprimer le mouvement libre comme une combinaison linéaire de modes propres calculés dans le vide.

La précision du résultat dépend alors de la discrétisation de la pale et non du nombre de modes retenus pour caractériser le mouvement.

Le schéma aérodynamique est quasi stationnaire avec utilisation des caractéristiques bidimensionnelles de profils mesurées en soufflerie (fichier de polaires). Quant à la vitesse induite elle est calculée par la méthode des anneaux.

Pour la partie dynamique de l'étude, il est également possible d'utiliser des forces aérodynamiques bidimensionnelles instationnaires en fluide parfait.

Chaque constituant du rotor (pale, moyeu, chaîne de commande) est discrétisé en éléments pesants du type poutre hétérogène sans gauchissement.

Aux extrémités (nœuds) de chaque élément un certain nombre de conditions aux limites portant sur les déplacements ou leurs dérivées et les efforts peuvent être introduites (articulations, encastrements, amortissements,...).

Les éléments sont repérés dans un référentiel prenant en compte les précalages éventuels (prétraînée, préconicité, pas,...) et sont décrits par des données locales du type :

- élastiques (raideurs, axes principaux, centre neutre, centre de torsion, centre de cisaillement)
- massiques (masses, centre de gravité, axes d'inertie, moments d'inertie)
- géométriques (loi de vrillage, axes géométriques, évolution de la forme).

3.1.2. Hypothèses particulières

Le modèle général décrit précédemment doit être aménagé pour prendre en compte certains caractères particuliers des concepts développés.

Plus précisément, il s'agit :

— sur les rotors à lame

- de l'introduction du vrillage important et non linéaire de la partie torsible.
- de l'analyse du système hyperstatique en flexion et torsion de la zone interne constituée par la lame, la manchette, le palier et la chaîne de commande.

Pour la torsion le modèle tient compte pour la lame de l'équilibre des efforts de cisaillement et des contraintes normales (rappel filaire, raccourcissement axial, flexion différentielle).

Par ailleurs le couplage battement/torsion, réduit en raison de la présence du palier, est également représenté.

Différentes conditions aux limites sont également introduites pour représenter les montages encastré, semi encastré et articulé au niveau de la liaison mât-pale, ou l'effet d'une impédance de la structure

- 13-8 — sur le rotor à élément torsible type Triflex, une analyse similaire à la précédente doit être faite, mais avec une modélisation spécifique concernant le bras souple et intégrant la loi de comportement de chaque fil.

Actuellement les calculs sont faits sans prendre en compte l'élastomère qui intervient peu sur les caractéristiques élastiques dans la plupart des configurations où l'ensemble des fils est tendu.

Quant au calcul de l'amortissement interne, il fait l'objet d'études en cours sur une base semi expérimentale.

— sur le rotor articulé classique type AS 332, la modélisation du moyeu repose sur une base expérimentale facilitée par le fait qu'il s'agit d'une évolution par rapport à un moyeu existant AS 330 qui a constitué une bonne référence expérimentale pour prédire les lois de comportement du moyeu AS 332. Cette identification par essais était indispensable, compte tenu du rôle important du moyeu sur la position des fréquences propres (voir figure 12) et de la très grande difficulté d'une modélisation par calculs de ces éléments et en particulier de la batterie de roulements d'incidence.

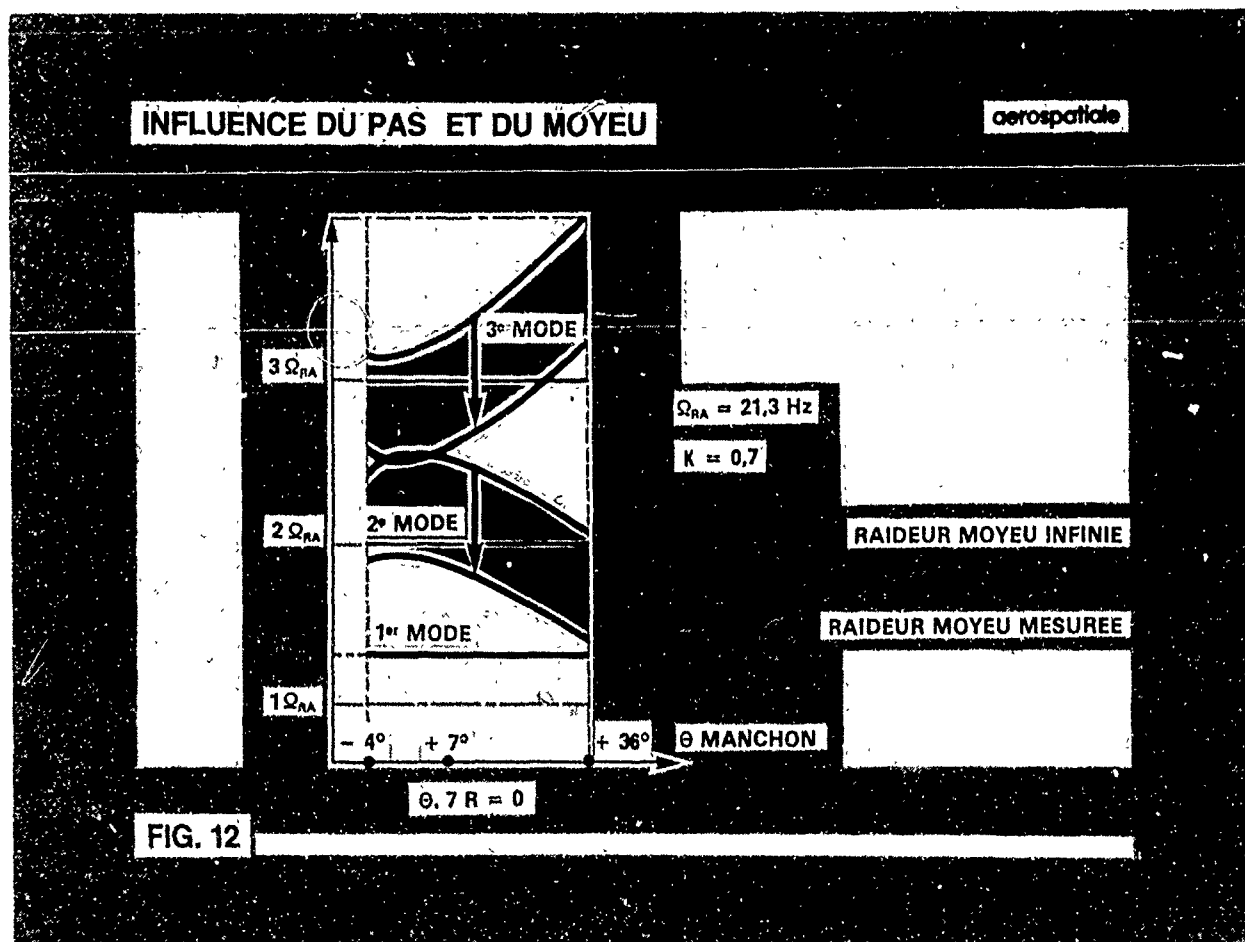


FIG. 12

— sur le rotor fenestron, les principes de modélisation sont les mêmes que ceux des rotors à lame. Par contre au niveau de la "casserole" une modélisation par éléments finis a été faite de façon à introduire des raideurs équivalentes (en pratique importantes) au niveau des paliers.

3.2. Positionnement correct des fréquences propres

Il s'agit de s'assurer dans la mesure du possible du positionnement correct des fréquences propres du rotor arrière par rapport aux différentes sources d'excitations et cela sur :

- une plage de fréquence s'étendant de 0 à ≈ 100 Hz pour les rotors classiques et de 0 à ≈ 200 Hz pour les fenestrons.
- une plage de régime correspondant sensiblement à $\Omega_{RA} \pm 20\%$.
- une plage de pas relativement importante et caractéristique des rotors arrière de -15° à $+35^\circ$ environ.

Les critères généralement retenus sont :

- placement correct des modes du rotor arrière (ω_{RAI}) par rapport aux harmoniques de l'excitation ($k\Omega_{RA}$) en gardant une marge suffisante pour réduire l'amplification due à la proximité d'une résonance, en particulier pour les modes peu amortis ou très couplés.
- placement correct des modes ω_{RAI} entre eux pour réduire les couplages aéroélastiques.
- séparation des modes ω_{RAI} de :

ω_{Fi} pour les modes en y

$|\omega_{Fi} \pm \Omega_{RA}|$ pour les modes coplanaires (x, z)

et en particulier pour les modes fuselage (ω_{Fi}) à basse fréquence.

- éviter la proximité du $2\Omega_{RA}$ pour les modes ω_{RAI} pour minimiser la réponse en $2\Omega_{RA}$ due :

- aux effets de Coriolis

- à un dérèglement du rotor excitant la structure en $1\Omega_{RA}$.

- séparation correcte des modes ω_{RAI} de :

$\Omega_{RP} \pm \Omega_{RA}$ pour les modes en y

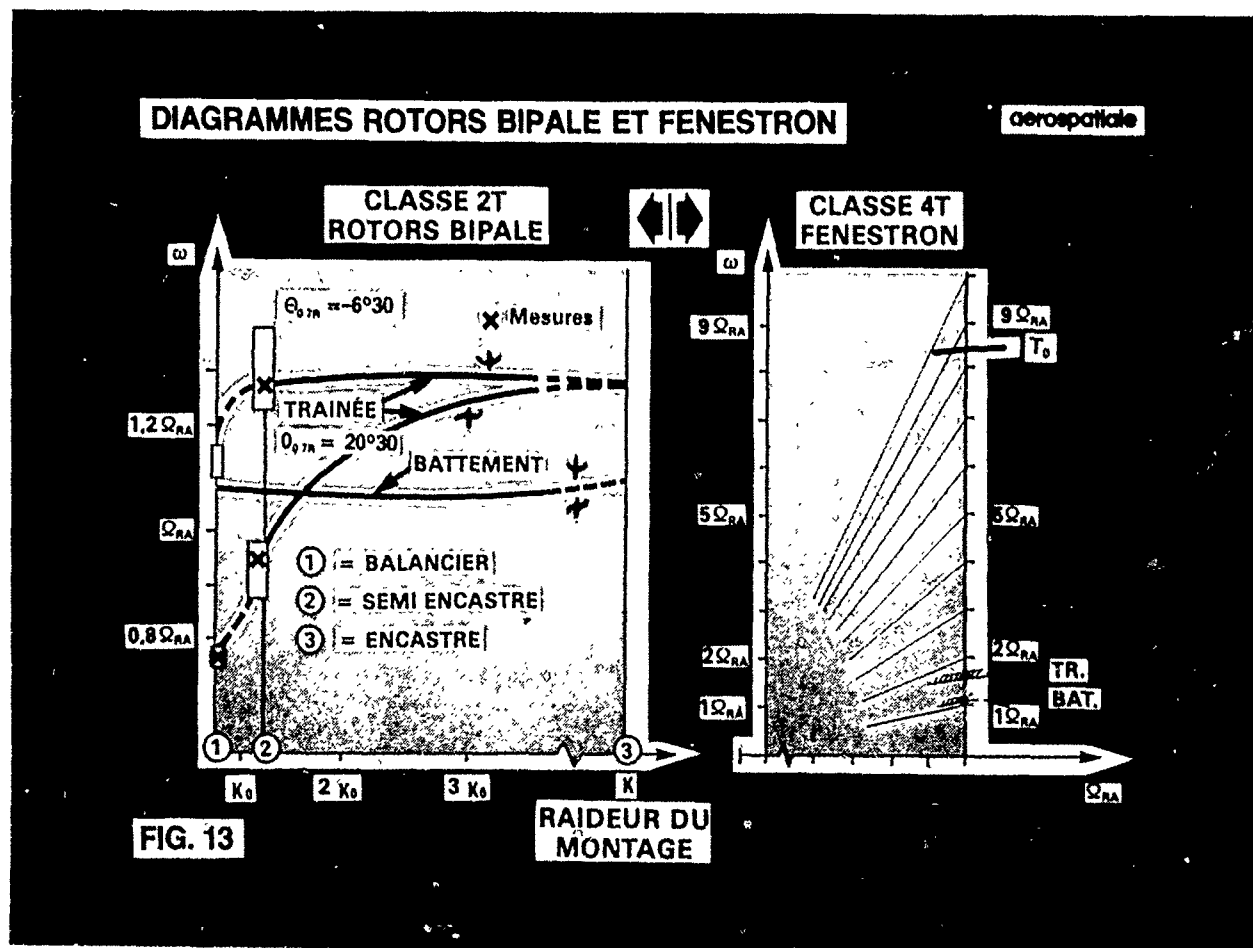
nb $\Omega_{RP} \pm \Omega_{RA}$ pour les modes coplanaires (x, z)

pour minimiser les réponses aux excitations du rotor principal encore qu'à notre connaissance le seul phénomène qui puisse apparaître soit lié à l'interaction entre les vibrations en $b\Omega_{RP}$ et une vibration en Ω_{RA} due à un balourd élevé.

- séparation correcte des modes ω_{RAI} des excitations aérodynamiques dues aux interactions comme par exemple celles induites à petit pas par les bras support de BTA du fenestron et les pales.

L'ensemble de ces exigences est souvent difficile voire impossible à concilier et un compromis doit être trouvé qui ne se résume pas seulement à des actions sur les caractéristiques du rotor isolé, mais également sur celles du moyeu et de la structure.

Nous limiterons donc cette partie, à une présentation des diagrammes de fréquences caractéristiques des concepts expérimentés avec quelques points expérimentaux mettant en évidence un bon recoupe-ment calculs-mesures.



— Évolution des modes propres symétriques et antisymétriques d'un rotor bipale en fonction des conditions de liaison au moyeu.

— Diagramme de fréquences propres d'un fenestron.

DIAGRAMMES ROTOR TRIFLEX ET ROTOR ARTICULE

aérospatiale

ROTOR QUADRIPALE TRIFLEX

ROTOR ARTICULÉ (5 PALES)

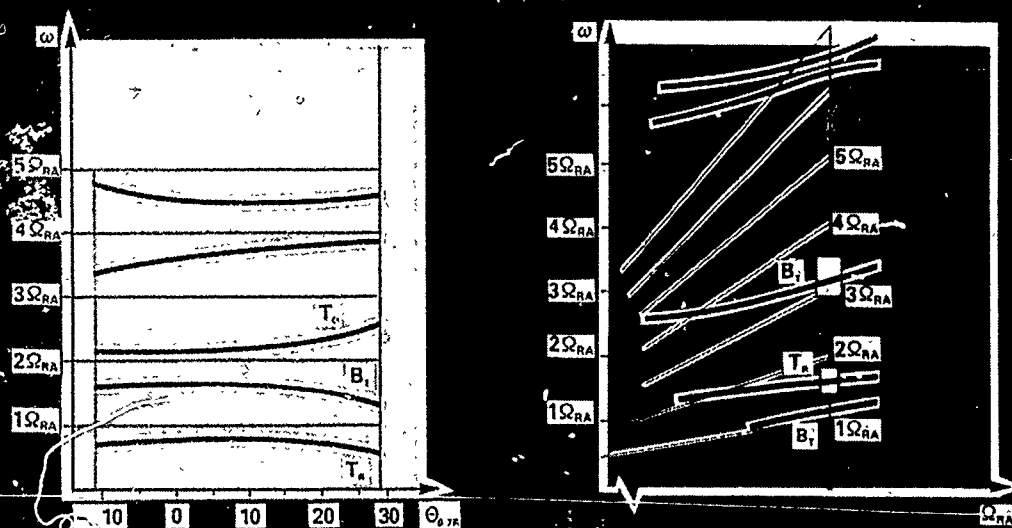


FIG. 14

- Évolution en fonction du pas, des modes propres d'un rotor quadripale Triflex.
- Diagramme de fréquences propres du rotor arrière 5 pales, articulé de l'AS 332.

ROTOR A LAME QUADRIPALE

aérospatiale

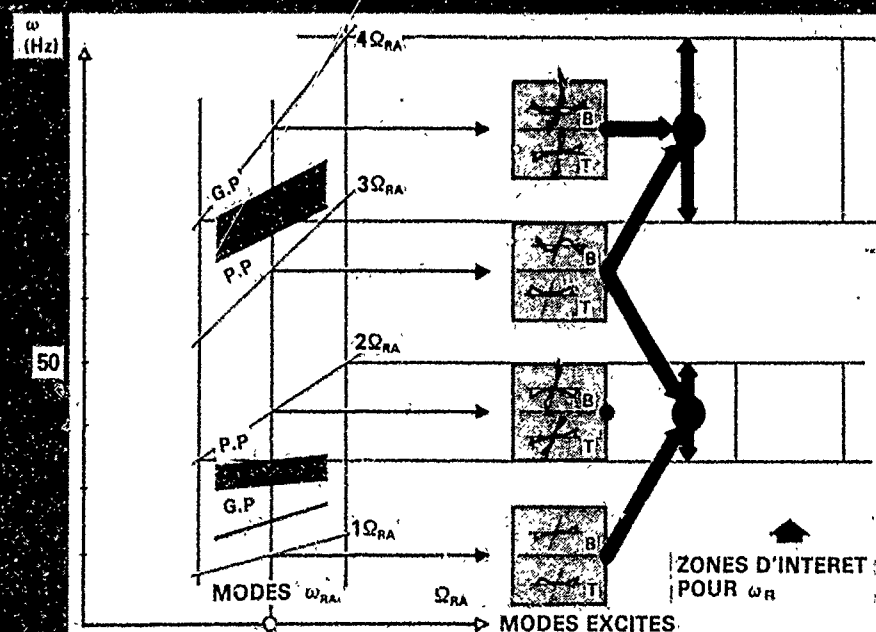


FIG. 15

- Position des fréquences propres d'un rotor à lame quadripale et définition des zones d'intérêt pour les modes fuselage.

3.3. Etude des instabilités - rotor isolé

Le programme de calcul décrit précédemment, et adapté aux différents concepts, permet de traiter les différents type d'instabilité linéaire qu'on peut rencontrer sur un rotor arrière, car il tient compte implicitement de tous les couplages.

Il permet donc de traiter les cas d'instabilité classiques mettant en jeu les trois degrés de liberté qui caractérisent le mouvement de la pale et qui sont fortement couplés par les paramètres de construction du rotor.

Toutefois, suivant la nature du problème et afin de limiter les temps de calcul, des modèles simplifiés basés sur une représentation modale d'un nombre réduit de degrés de liberté sont mis en œuvre pour faciliter certaines études paramétriques au moment de la conception.

Il sort du cadre de cette présentation de faire une étude exhaustive des différents types d'instabilité, néanmoins il nous paraît intéressant de donner quelques indications sur certains aspects prévisionnels où le calcul a pu être validé par l'expérience tel le couplage battement-trainée.

De plus certains problèmes qui nous ont paru critiques à la conception, tels le couplage battement-torsion seront abordés sans pouvoir donner cette identification.

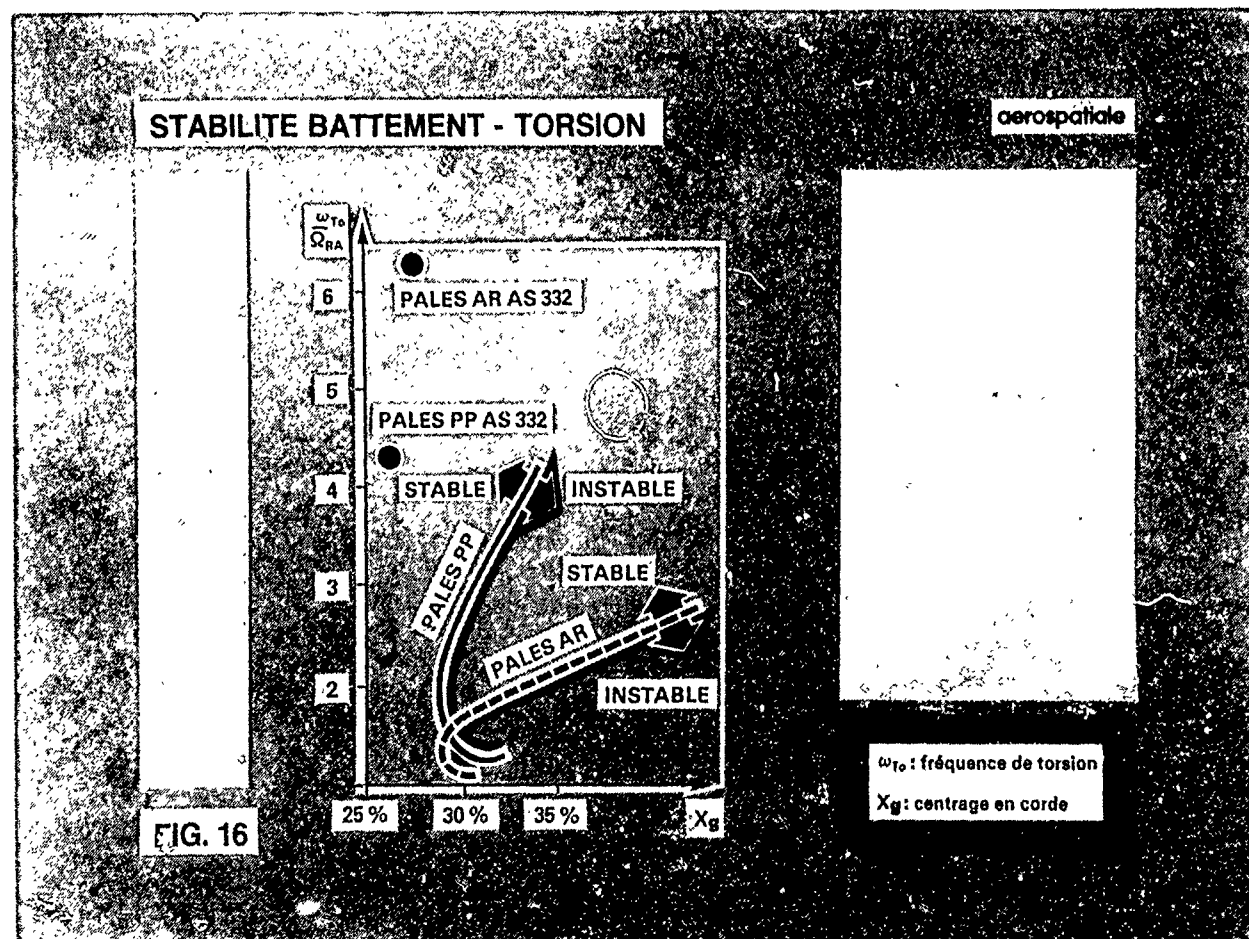
Des remarques seront également faites sur des raisons possibles qui font que les rotors arrière ne rencontrent pas certaines instabilités.

3.3.1 Instabilité battement-torsion

Ce problème s'apparente au flottement des ailes et son mécanisme est bien connu.

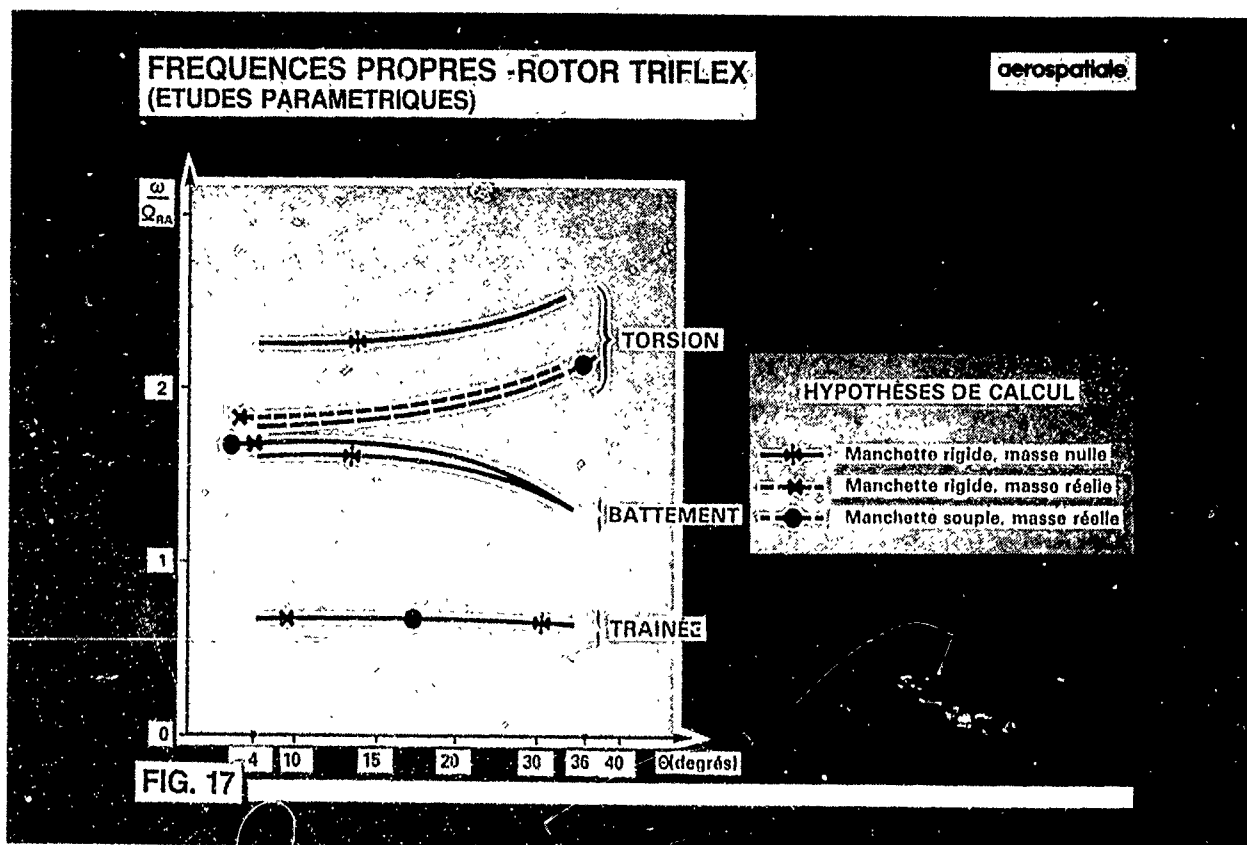
Le mouvement de battement génère des efforts d'inertie et des efforts aérodynamiques qui engendrent successivement un mouvement de torsion, un vrillage de la pale, une incidence aérodynamique, des efforts aérodynamiques, un mouvement de battement, etc.

A technologie donnée, les rotors arrière sont moins sensibles à ce type de couplage que les rotors principaux ainsi que le montre la fig. 16, dans le cas de l'AS 332, en prenant comme paramètres la fréquence réduite de torsion et le centrage en corde.

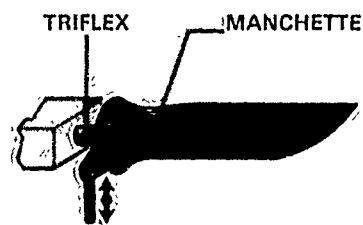
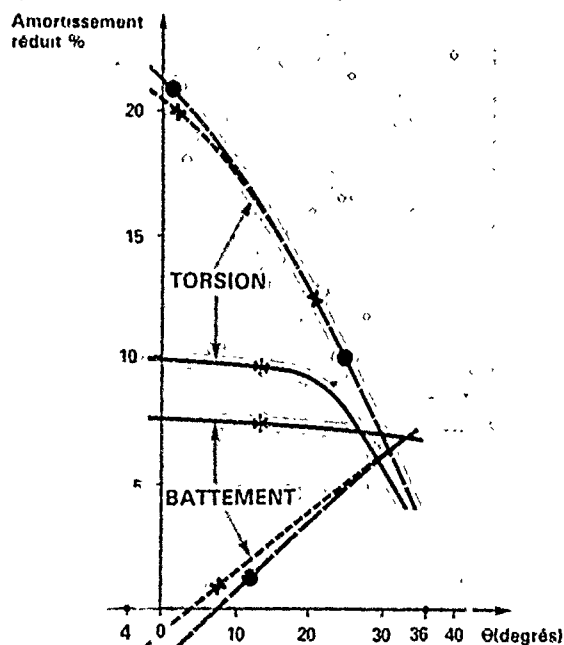


13-12 Expérimentalement ce problème n'a jamais été rencontré à l'Aérospatiale malgré la diversité des concepts.

Un exemple de cette sensibilité à ce type de couplage est présenté sur les fig. 17 et 18 qui montrent l'influence des caractéristiques de masse et de raideur de la manchette sur les fréquences propres et l'amortissement des modes d'une des versions étudiées du rotor "Triflex".



**COUPLAGE BATTEMENT - TORSION
(ETUDES PARAMETRIQUES)**



3.3.2. Instabilité battement-traînée

Les conditions d'obtention de ce type d'instabilité peuvent être rencontrées sur les rotors arrière "stiff in plane" en raison de :

- La position des 2 premiers modes situés en général dans la plage $[1 \Omega_{RA}, 2 \Omega_{RA}]$
- Le couplage de ces 2 modes par :
 - le pas qui varie sur une plage importante
 - les effets de Coriolis battement \rightleftharpoons traînée
 - le vrillage qui est relativement important pour optimiser les performances.

Par ailleurs des termes de couplage supplémentaires peuvent intervenir tels que liaison K, centrage en corde, préconicité, ... et c'est en général sur ces termes là, qu'il est le plus simple de jouer.

Dans le cas de l'AS 332 une étude paramétrique assez large a été effectuée, sur les principaux paramètres de définition du rotor lequel pouvait présenter ce risque en raison de :

- la souplesse du moyeu rapprochant (à grand pas) les 2 premiers modes (battement et traînée)
- l'effet déstabilisant du vrillage de la pale.

Il a été trouvé que compte tenu des différentes contraintes de définition, le paramètre le plus efficace, pour augmenter l'amortissement à grand pas du mode de traînée, était d'avoir une liaison K aussi réduite que possible tout en restant compatible avec les exigences de résistance en 1Ω en battement.

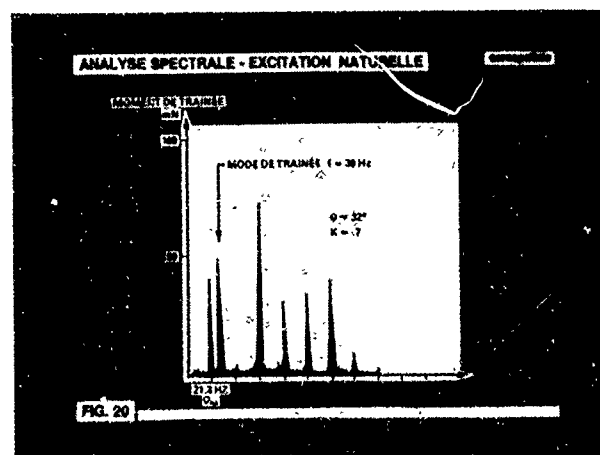
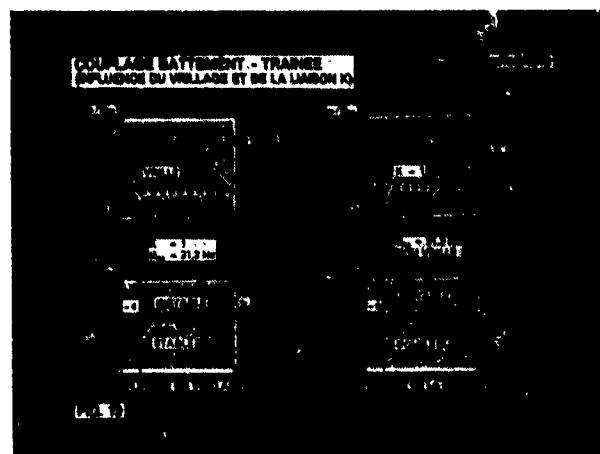
La figure 19 illustre quelques résultats de calcul issus de cette étude.

Quant à la valeur retenue par la liaison K ($K = 0,7$), elle a été déterminée expérimentalement lors d'essais au banc-tournant qui avaient pour but de :

- confirmer le positionnement des fréquences propres,
- mesurer l'amortissement du 2^e mode à prédominance traînée, en fonction du pas et de la valeur de la liaison K.

La détermination par essais des fréquences propres s'est faite par :

- analyse des réponses au croisement des harmoniques lors des montées en régime et des excursions en pas à régime donné,
- analyse spectrale des signaux en excitation naturelle (voir fig. 20).



13-14

Pour la détermination de l'amortissement, le rotor est excité par un vérin permettant le réglage du pas et délivrant une excitation à fréquence variable des pales en phase. L'analyse de la courbe de réponse (voir fig. 21) permet de définir l'amortissement et la fréquence du mode. Cette approche expérimentale est détaillée dans la référence 2. La figure 22 fournit quelques résultats expérimentaux qui se recourent correctement avec les prévisions.

MESURE DE L' AMORTISSEMENT

aérospatiale

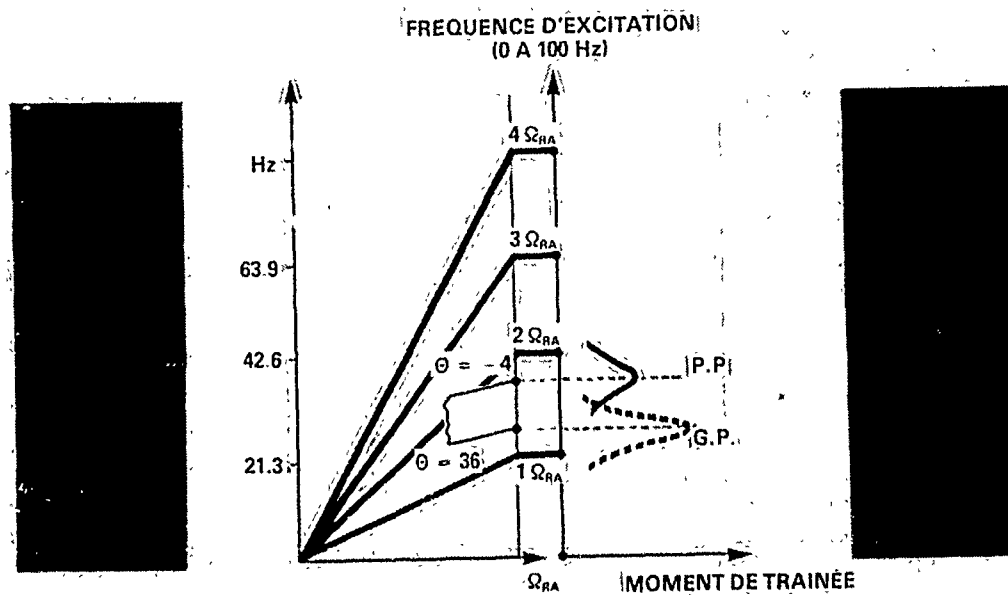


FIG. 21

DIAGRAMME DE FREQUENCES
(CALCULS - ESSAIS)

aérospatiale

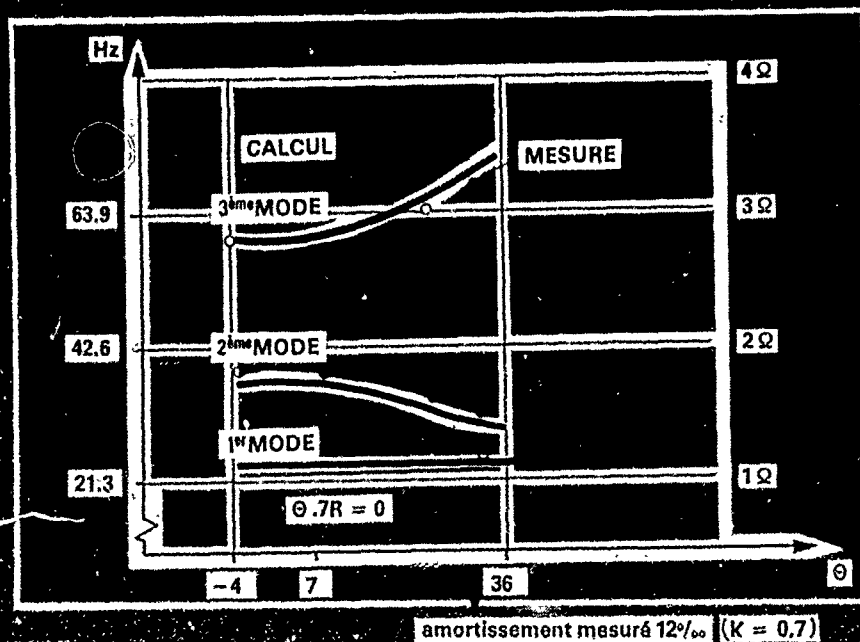


FIG. 22

amortissement mesuré 12‰ (K = 0.7)

3.3.3. Le "Weaving"

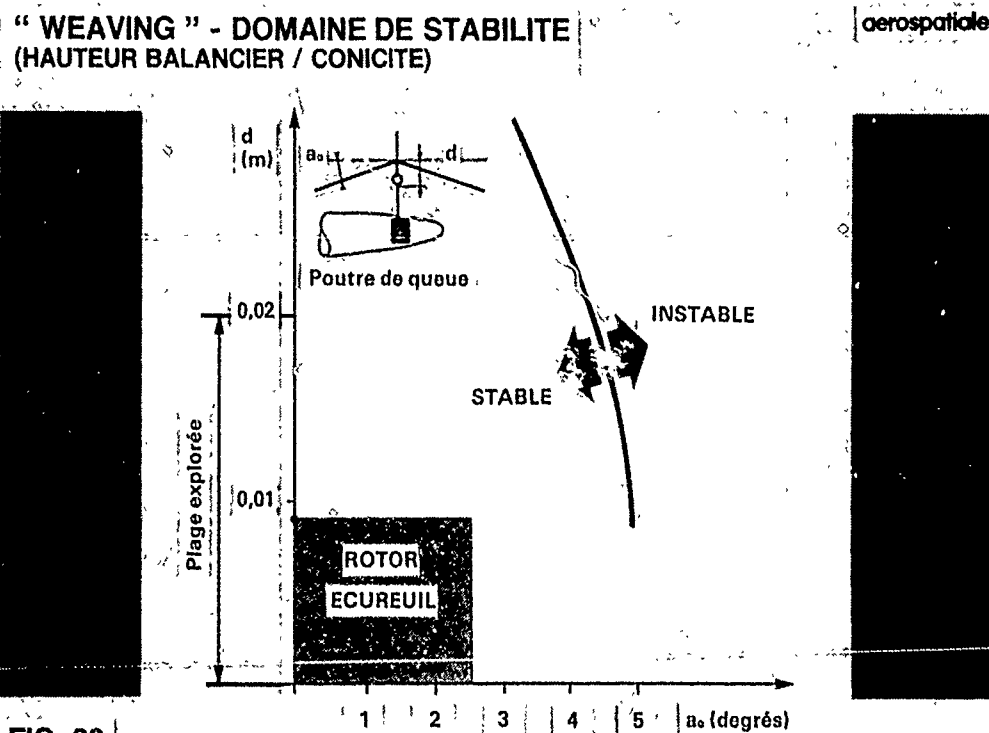
C'est une forme d'instabilité particulière des rotors bipales en balancier ou plus précisément des rotors dont les pales sont couplées structuralement par le moyeu et dont l'angle de pas peut varier à cause de la souplesse de la commande. Elle s'apparente au couplage pas-battement mais en prenant en compte le rotor complet, et conduit à un phénomène d'ondulation du bipalè.

Son mécanisme est connu et fait intervenir des paramètres principaux comme l'angle de conicité et le déport du balancier mais également des paramètres secondaires comme la liaison K, le centrage en corde, les effets de décrochage...

Du point de vue du concept, un faible déport de l'axe du balancier et une limitation de la conicité assurent une bonne stabilité à de tels ensembles.

L'illustration en est donnée sur le fig. 23 qui présente le domaine de stabilité théorique d'un rotor arrière du type écureuil, en fonction de la conicité et du déport du balancier.

En phase prototype, et sur les bases de cette étude, une expérimentation au sol et en vol a été réalisée en faisant varier le déport sans toutefois aller jusqu'aux limites de stabilité.



13-16 4. ÉTUDE DU VOL D'AVANCEMENT

L'étude du rotor en vol d'avancement permet de :

- s'assurer de l'état de stabilité du système,
- caractériser le niveau de charges.

4.1. Stabilité

Des phénomènes aérodynamiques non linéaires apparaissent à grande vitesse sur les pales.

On distingue en général :

a) le flottement de décrochage résultant

- des conditions de fonctionnement (C_z élevé) en pale reculante,
- des effets de compressibilité en pale avançante,
- de l'interaction tourbillonnaire.

Ce phénomène se traduit par un mouvement oscillatoire se reproduisant à chaque tour.

b) la génération de sous harmoniques apparaissant lorsque l'extrémité devient supercritique (onde de choc).

Dans les deux cas, les oscillations peuvent s'interpréter comme des réponses à "amplitude limite" ou comme un début d'instabilité d'un système mécanique à coefficients périodiques et pour l'analyser il est nécessaire de connaître le mouvement réel (solutions transitoires et réponses aux excitations).

Ces problèmes sont à notre connaissance peu fréquents sur les rotors arrière et ils intéressent surtout les rotors principaux. Pour le flottement de décrochage on peut en trouver les raisons dans :

- le choix des profils de rotor arrière, optimisés pour le stationnaire, et pour lesquels on privilégie le $C_{z_{MAX}}$ au détriment du M_{DT} à l'inverse des profils de rotor principaux (voir fig. 24)

- des incidences de fonctionnement plus faibles que sur les rotors principaux à cause du délestage dû à la dérive, mais aussi parce que le rotor arrière n'assure en général pas de traction. Ce dernier point est illustré par la planche 25, qui indique les domaines de fonctionnement respectifs des rotors.

L'analyse de ces problèmes, nécessite de toute façon une modélisation aérodynamique sophistiquée prenant en compte les caractéristiques instationnaires dans les domaines linéaire et décroché de l'écoulement.

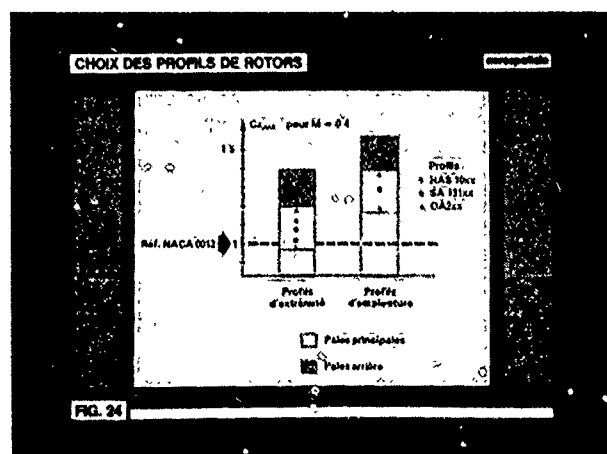


FIG. 24

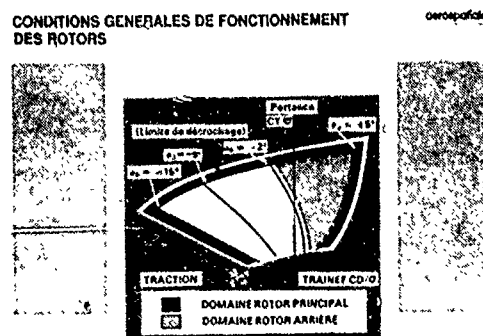


FIG. 25

4.2 Calcul des charges

Pour le calcul des charges en vol d'avancement, l'Aérospatiale utilise deux méthodes principales décrites dans la référence 3.

L'aérodynamique utilisée est quasi-stationnaire et exploite les fichiers de polaire, la vitesse induite est calculée par les formules de Meyer Drees.

La recherche de la solution stationnaire (réponse aux excitations) se fait :

- par une méthode modale supposant de petits mouvements autour de l'état statique

ou

- par la méthode des azimuts, qui est une méthode d'intégration directe, ne comportant pas la limitation précédente.

En réalité ces méthodes sont peu utilisées au niveau prévisionnel sur les rotors arrière, car le champ des vitesses locales est mal connu et d'autre part elles apportent peu au niveau du dimensionnement car les configurations les plus sévères sont les arrêts de virage, les caps au vent...

Elles peuvent être quelquefois utilisées pour certaines études comparatives menées pour minimiser les réponses au voisinage des harmoniques de l'excitation.

5. COUPLAGE ROTOR-STRUCTURE

13-17

Sous l'aspect prévisionnel, nous disposons d'un programme général d'étude des couplages entre un rotor et une structure connectant les bases modales tronquées du rotor isolé supposé dans le vide, de la structure et les excitations aérodynamiques fondées sur une représentation par polaires du profil. Jusqu'à présent les calculs dynamiques de structure sur plan ne fournissent pas des éléments suffisamment précis pour l'étude de ces couplages.

Nous préférons donc procéder à une identification expérimentale de la structure avant vol et étudier les couplages à ce stade.

Par ailleurs, nous avons développé des modèles spécialisés validés par l'expérience à l'occasion de problèmes particuliers et nous les appliquons pour faire des études paramétriques.

5.1 Instabilité en parapluie

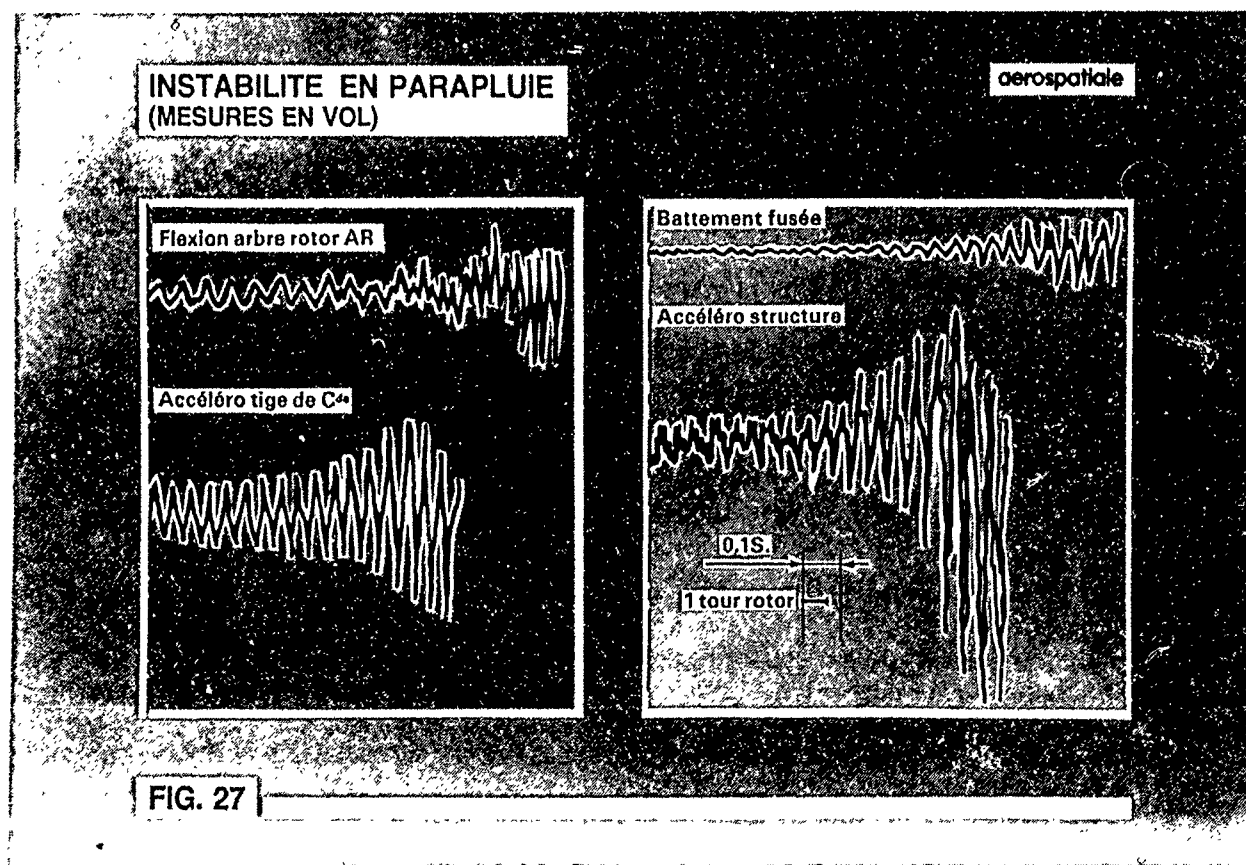
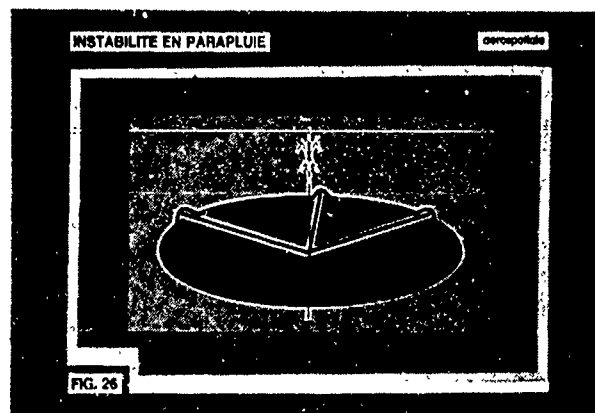
Cette instabilité se caractérise par un mouvement de battement en phase (voir fig. 26) de l'ensemble des pales couplé avec un mouvement de la structure suivant l'axe de rotation du rotor et/ou un mouvement de commande suivant le même axe.

La fréquence du phénomène est la même sur le rotor et sur la structure et n'est pas en général une harmonique du régime.

Ce problème a été rencontré en 1963, lors des essais du rotor de queue prototype (de conception classique) de l'AS 321 pendant la phase de coupure de la servocommande simple corps.

La conséquence directe, étant une diminution de la raideur de la chaîne de commande.

L'allure générale des signaux en axes fixes et en axes tournants est donnée fig. 27.



13-18

Dans ce cas précis le passage en servo double corps a permis d'éliminer définitivement le problème. Par la suite un modèle de calcul simplifié a été établi en introduisant le mouvement de battement des pales, le mouvement de pas induit par la commande, le mouvement de la tête rotor ; son application au cas considéré rend compte assez correctement de cette instabilité et montre que la rigidité de commande était le paramètre fondamental (voir fig. 28).

Toutefois le bon recouplement observé est dû à la caractérisation précise des différents éléments (impédance transversale de la poutre de queue, raideur de la chaîne de commande...). Au niveau purement prévisionnel il en irait différemment, et il faut s'entourer de marges suffisantes.

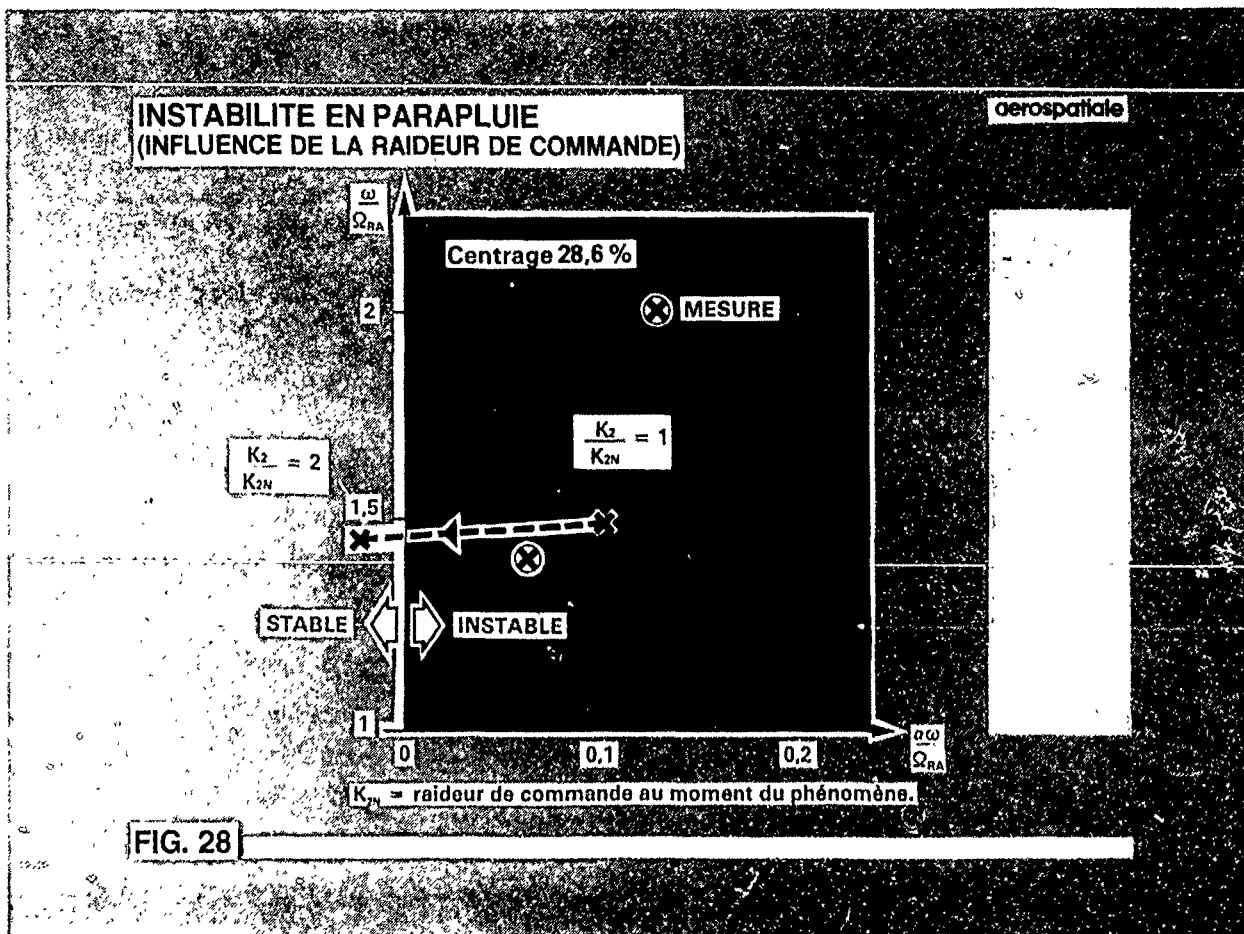


FIG. 28

5.2 Instabilité en assiette

Cette instabilité se caractérise par un mouvement coplanaire de la tête rotor associé à des mouvements de battement antisymétriques, des mouvements de traînée des pales et par un mouvement de flexion de la commande.

Les fréquences du phénomène en structure et sur les pales sont décalées de Ω_{RA} ($\omega_F = \omega_{RAI} + \Omega_{RA}$) et ne sont pas en général des harmoniques du régime.

L'amortissement du mode couplé battement-traînée est la caractéristique de l'instabilité.

Ce phénomène a été rencontré en utilisation sur l'AS 330 pour certaines configurations de cap au vent ; il est dû dans ce cas à une augmentation du jeu en utilisation au niveau de la tige de commande qui modifie la fréquence du mode araignée qui est par ailleurs fonction de la sortie de la tige, donc du pas.

Le modèle de calcul prend en compte tous les éléments qui viennent d'être évoqués, ainsi que l'influence de la structure.

La figure 29, montre l'influence du pas, de la rigidité de commande (tige, araignée) et de la liaison K sur le domaine de stabilité.

Quant aux options retenues pour résoudre ce problème, elles sont :

- augmentation de la fréquence du mode structure par diminution de la longueur de l'arbre,
- réduction et surveillance des jeux aux appuis de la tige de commande.

Ce type d'instabilité est maintenant maîtrisé et les essais en vol sur des concepts analogues se font en simulant le vieillissement des appareils en utilisation.

INSTABILITE EN ASSIETTE

aérospatiale

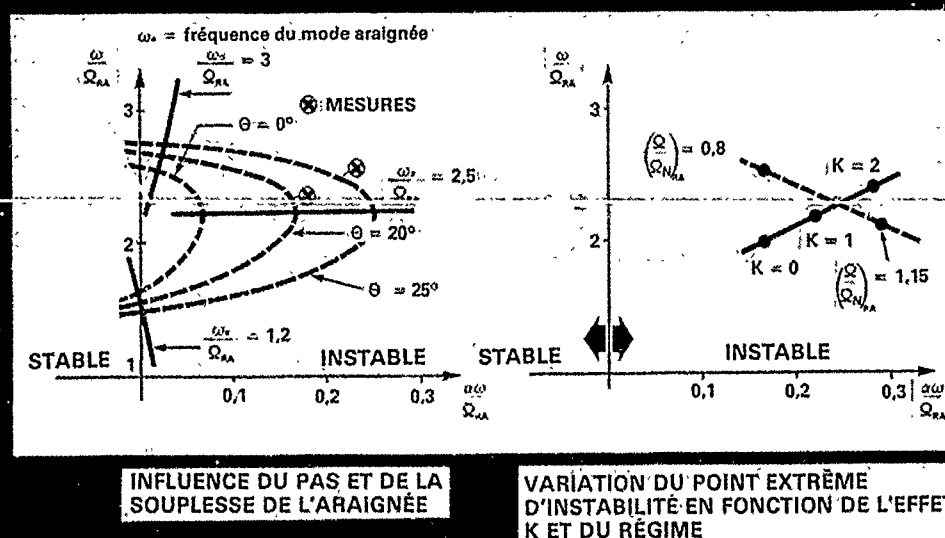


FIG. 29

5.3 Instabilité des rotors "soft in plane"

Si les rotors "soft in plane", c'est-à-dire à fréquence de traînée $< 1 \Omega_{RA}$ sont intéressants à plus d'un titre (efforts de commande, contraintes pales et moyeu, masses réduites...), ils présentent des risques élevés d'instabilité du type résonance air et sol.

Ce problème est bien connu et maîtrisé dans le cas des rotors principaux, mais pour les rotors arrière la plage de couplage rotor/structure est bien plus importante (dans le rapport des régimes à isoposition du mode de traînée) comme le montre la figure 30.

Les solutions à ce problème sont :

- éviter des modes structure à fort déplacement du rotor arrière dans son plan, dans la plage de fréquence 0,8 à $1,2 \Omega_{RA}$.

- avoir un amortissement suffisant sur le rotor et la structure.

Dans le cadre du programme d'évaluation technologique d'une solution Triflex, le premier niveau où ce risque d'instabilité apparaît se situe à la phase d'essais de caractérisation dynamique (fréquences, amortissement) du rotor au banc tournant.

L'étude du couplage rotor-structure a été faite dans ce cas à partir des données expérimentales de la structure du banc ; un mode structure ($\omega_f \approx 7,4$ Hz, amortissement $\approx 20 \text{ }^\circ/\infty$) a été identifié comme créant les conditions de résonance sol dans le domaine d'essai prévu.

Le diagramme fig. 31 montre à titre d'exemple, la stabilité de l'ensemble en fonction du régime et à partir d'une estimation concernant l'amortissement structural des pales en traînée ($\approx 50 \text{ }^\circ/\infty$).

Dans ce cas précis, la situation n'est pas critique dans la mesure où les moyens d'action sont nombreux et en particulier :

- déplacement de la fréquence structure par haubannage du banc,
- et/ou utilisation des moyens de réglage prévus sur le rotor (paliers de différentes raideurs avec plusieurs valeurs d'amortissement).

RESONANCE SOL COMPARAISON DES ZONES DE COUPLAGE ROTOR PRINCIPAL ET ROTOR ARRIERE

aerospatiale

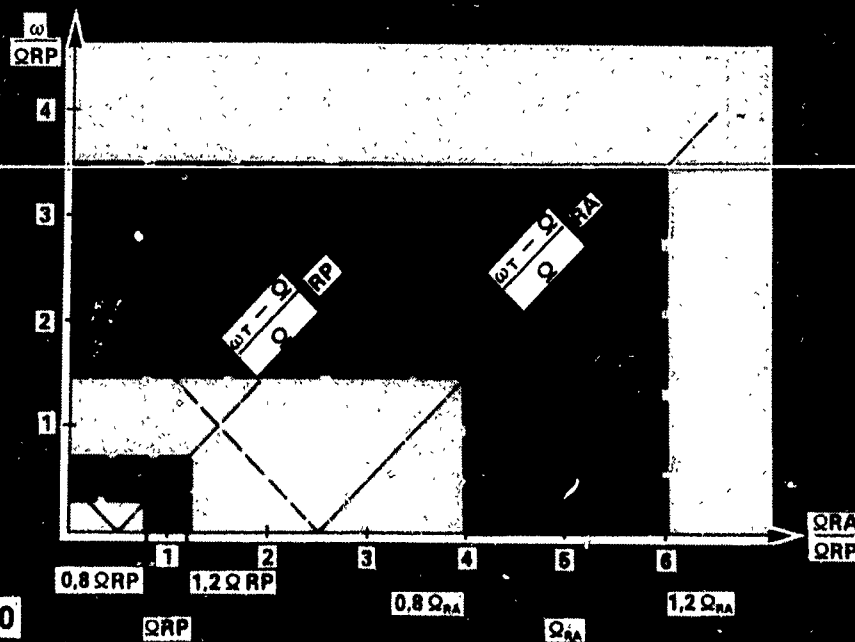


FIG. 30

"RESONANCE SOL" ROTOR TRIFLEX AVANT MODIFICATIONS DU BANC (PETIT PAS)

aerospatiale

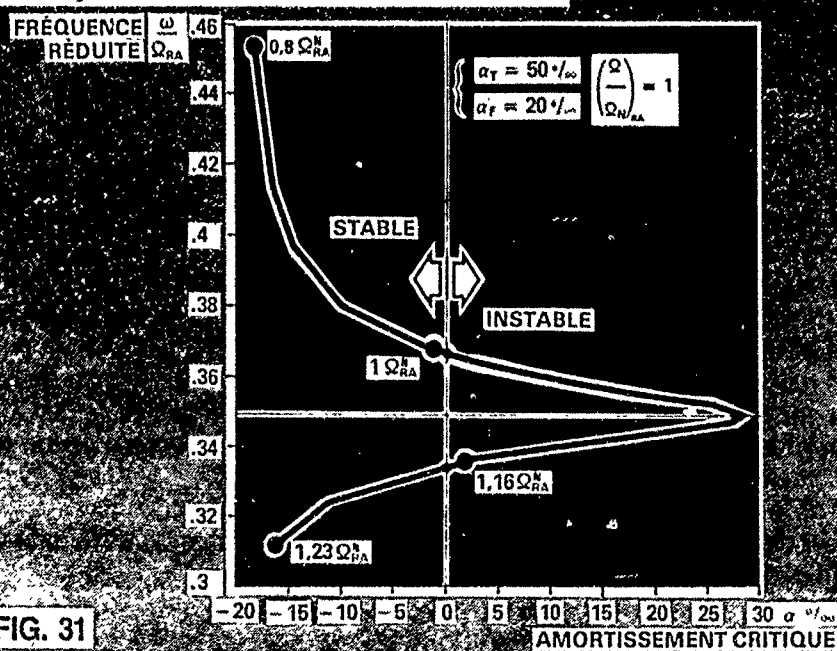


FIG. 31

5.4. Modulation de couple

Ce type de phénomène résulte d'un couplage entre les mouvements en traînée des pales en phase, la torsion de la transmission et l'ensemble de régulation du moteur.

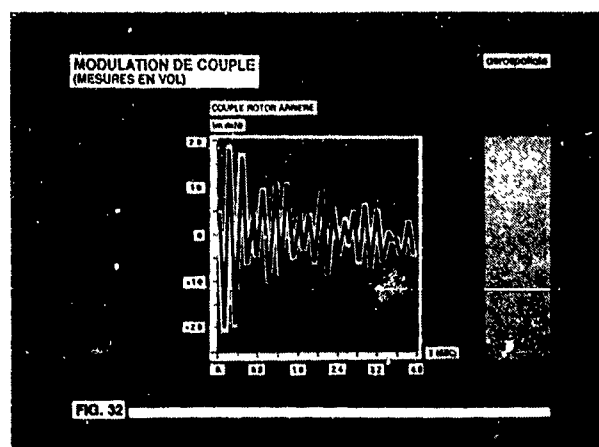
Il se traduit en particulier par une modulation du couple rotor arrière.

Une illustration en est donnée sur la figure 32, qui représente l'allure des signaux enregistrés pendant le phénomène lors des essais prototypes du fenestron de l'AS 365 N₁. Ces oscillations faiblement amorties, apparaissent à des fréquences de 4,4 Hz et 5,8 Hz pour des conditions de vol particulières (grande vitesse, dérapage, forte augmentation de pas).

La modélisation de cette instabilité fait appel à des programmes de simulation où les effets non linéaires de la régulation moteur sont pris en compte.

Parmi les différentes solutions envisagées, c'est le raidissement de la transmission qui a été retenu et qui permet une réduction sensible et suffisante des contraintes par diminution du couplage entre la régulation et le rotor arrière.

La figure 33 présente les résultats du calcul de simulation. Ce type de problème n'est pas particulier au fenestron et peut se rencontrer avec des rotors classiques.



MODULATION DE COUPLE
(REPONSE CALCULEE A UN ECHELON)

aérospatiale

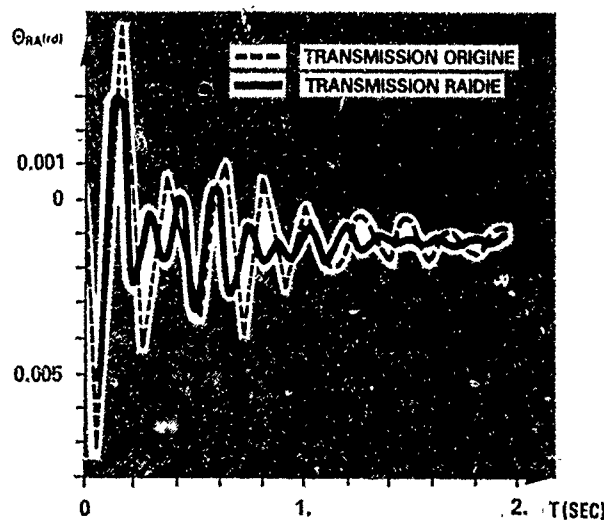


FIG.33

6. CONCLUSIONS

Les exemples traités dans cette présentation montrent que l'analyse du comportement aéroélastique des rotors arrière est délicate, dans la mesure où les facteurs d'instabilité sont très nombreux et pour certains, difficilement accessibles au calcul lors de la phase de conception.

A ce stade il est illusoire de pouvoir modéliser correctement des raideurs de roulement, des chaînes de régulation, des jeux de montage, des modes structure et leur amortissement... pour reprendre certains des exemples traités.

Cette complexité rend vaine, de notre point de vue, une approche prévisionnelle utilisant un programme général qui nécessiterait une modélisation complète de la plupart des composants de l'hélicoptère (rotor, chaîne de puissance, transmission, régulation, structure...) et qui serait d'un emploi délicat. Nous pensons qu'il est préférable, malgré des limitations inhérentes à cette démarche ("troncature" du domaine d'étude) d'utiliser des modèles particuliers dont on a vérifié la validité lorsqu'on a pu dans certains cas leur associer les phénomènes physiques.

Bien que cette démarche se soit révélée satisfaisante d'un point de vue pratique, un effort de recherche est actuellement en cours pour accéder à une meilleure prévision dans le cas du vol d'avancement et dans l'identification des structures.

LISTE DES RÉFÉRENCES

Réf. 1. J.P. LEFRANCO - B. MASURE. «A complete method for computation of blade mode characteristics and responses in forward flight». Seventh European Rotorcraft and Powered Lift Aircraft Forum.

Réf. 2. J.P. COSTON. «Methods of digital signal analysis applied to the study of dynamic systems in helicopters». Paper 48. Fifth European Rotorcraft and Powered Lift Aircraft Forum.

Réf. 3. B. MASURE et A. VUILLET. « Méthodes de calcul des charges sur rotor utilisées à l'Aérospatiale et recoupements expérimentaux » - AGARD 1982.

14-1

THE ROLE OF AEROELASTICITY IN THE PRELIMINARY DESIGN OF HELICOPTER ROTORS

by

V. GIAVOTTO, M. BORRI

Aerospace Department - Politecnico di Milano
Via Golgi, 40 - 20133 MILANO - Italy

and

A. RUSSO, A. CERIOTTI

Costruzioni Aeronautiche G. AGUSTA S.p.A.
21047 CASCINA COSTA DI SAMARATE (Varese) - Italy

SUMMARY

The design of a helicopter rotor is a complex process, in which aeroelastic aspects are involved practically at all stages. As the integration of the different models employed in the design needs to be rationalized, integrated computation system shall be developed, whereby aeroelasticity can be taken into account since the earliest stages.

This paper shows the first significant results of a development activity of this kind carried out by AUGUSTA in cooperation with POLITECNICO of Milano.

1. INTRODUCTION

The role played by aeroelasticity in the preliminary design of a helicopter rotor is being regarded ever more as considerably significant, although its bounds do not appear to be easily definable yet. The purpose of this paper is to help in a discussion which will take several years to be settled.

In all its aspects rotor dynamics is a deeply aeroelastic phenomenon, and actually aeroelasticity enjoys a potential role in all design evaluations, such as performance analysis, load prediction, stability analysis, etc.

The development of a new helicopter may often involve high economic burdens and risks and requires an ever more precise and ample preliminary design; such preliminary design must allow adequate consideration of all interactions between subsystem and, as far as possible, the attainment of final conclusions.

In other words the preliminary design shall be an interdisciplinary optimization process, requiring a sound management structure to harmonize different criteria, such as mission, performances, handling qualities, noise and vibrations, etc. In this process the aeroelastic analysis can be a focal reference.

2. THE PRELIMINARY ROTOR DESIGN

Traditionally the preliminary design consists of the following stages (Fig. 1):

- Aerodynamic Rotor Design
- Aerodynamic Blade Design
- Dynamic Rotor Design.

Performance criteria [1,2] prevail in the Aerodynamic Rotor Design Stage, which is mainly intended for the definition of the three basic rotor parameters, i.e. disc loading, rotor tip speed, and rotor solidity. In this stage mathematical optimization processes may be particularly helpful, provided both objectives and constraints can be correctly defined.

The main function of the Aerodynamic Blade Design is rather the selection or the design of profiles, twist, and blade plan form. Regarding the aerodynamics of the blade, the two dimensional scheme is still the most largely employed; usually it is duly corrected for sweep angle and dynamic separation.

These problems have not been completely settled yet, and this brings about a considerable scatter in the analysis methodology. Some very good reviews of the state of the art have recently been issued, such as Friedman's [3] very extensive one, whereas Beddes, McCrosky and Gangwani [4,5,6] have provided a precise definition of the non-stationary effects and of separate flows. Table 1 [from ref.5], which briefly outlines the main effects affecting the phenomenon concerned, emphasizes the extent to which some of these effects have not been investigated yet.

14-2

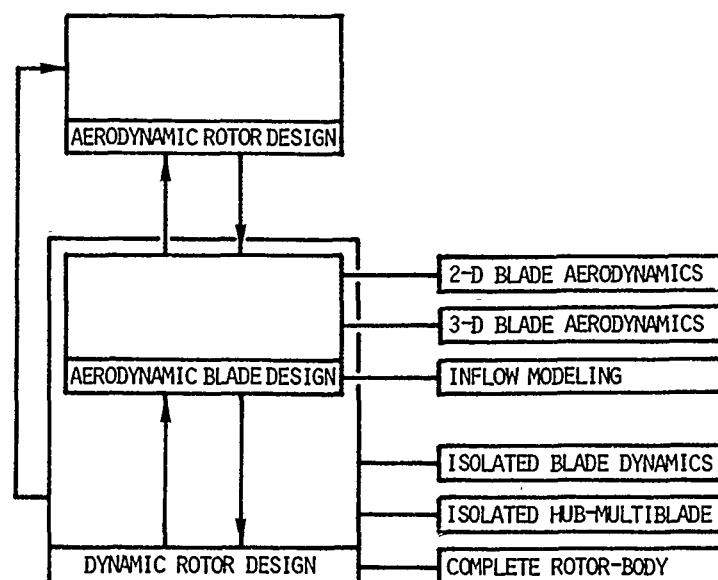


Fig. 1 - Classical approaches in the design of a main rotor

TABLE 1 - IMPORTANCE OF DYNAMIC STALL PARAMETERS
(from Ref. 5)

STALL PARAMETER	EFFECT
Airfoil shape	Large in some cases
Mach number	Small below $M_\infty \sim 0.2$ Large above $M_\infty \sim 0.2$
Reynolds number	Small (?) at low Mach number Unknown at high Mach number
Reduced frequency	Large
Mean angle, amplitude	Large
Type of motion	Virtually unknown
3-dimensional effects	Virtually unknown
Tunnel effects	Virtually unknown

It seems that the three-dimensional methods effectively employed for fixed wings [7,8] cannot be easily transferred for rotary wings. A limited application of three-dimensional models was carried out for the study of vortex-blade interaction [9,10,11], as well as for the study of the tip area, by which, as it is well-known, performances can be considerably affected [12].

Another peculiar aspect of the aerodynamics of a rotary wing is the requirement for the modelling of the induced flow field. As the basic works of Langrebe already showed [13, 14], for an accurate solution of this problem the actual form of blade wake shall be determined. Moreover decisive effects [15, 16] may be brought about by the interference with fuselage.

The Dynamic Rotor Design stage fundamentally requires an aeroelastic approach, namely an interdisciplinary one, synthetically including the different spheres of competency. The approaches that are usually employed in the analysis can be classified as follows [17]:

- Isolated Blade Dynamics
- Isolated Hub-Multiblade Dynamics
- Complete Rotor-Body Dynamics.

The Isolated Blade scheme allows an initial analysis of many stability problems and the prediction of loads.

When blade interactions, such as those due either to controls flexibility or to aerodynamic interferences, must be taken into account, the Isolated Hub-Multiblade scheme shall instead be taken on. Such scheme allows also the analysis of whirl instability and of some effects of blade asymmetry.

Finally the Complete Rotor-Body scheme is the most thorough one, allowing the analysis even of the phenomena (e.g. air resonance and ground resonance) that could not possibly be analyzed by the former schemes. It is also utilized for the refinement of the analyses carried out by means of simpler schemes. Based on this approach different computation models with different approximation levels were developed [19, 20]. Besides being used for the design operation, such models can also be helped for flight tests analysis, e.g. through parametric identification processes [18].

In the traditional approach the various design stages occur in sequence according to a logical progress, starting from an overall outline to an ever more detailed definition. However since the optimizing process needs to be pushed as much as possible, generally several design iterations are required, then all stages or some of them shall be passed through again.

Clearly the entire rotor design process could be made more rational and effective by a unified computation system that would be able to integrate the different complexity levels and the different disciplinary approaches. As an additional advantage, such a computation system, which appears to be feasible on the basis of the present state of knowledge and technology, would be a common data base and a focal point for all design teams.

3. ROTOR AEROELASTICITY

One of the basic characteristics of the rotary wing aeroelastic analysis is that non-linear effects must be taken into account; the latter are mainly due to geometrical non-linearities in terms of inertia and elasticity, and to constitutive non-linearities in the aerodynamic field. Moreover the forward flight and cyclic pitch bring about periodical variations in the coefficients of equilibrium equations. The problem is non-linear to such an extent that stability substantially depends upon the trim solution it is related to. Therefore, prior to any stability analysis, the determination of the trim solution shall be carried out in a non-linear mode.

Different complexity and sophistication levels for the models, namely for the structural, inertial, and aerodynamic operators [21, 22], were employed. Some simplification cannot be avoided, and the attempts of gathering partial models together do not always lead to quite consistent formulations.

The approach presented by Dat [23] and developed by Costes [24] is certainly a unitary one based on a consistent formulation. It is founded on the determination of the acceleration potential of the aerodynamic field, and it can also take separate flows on the blade into account. Much work has been done and more will be done in this field for the attainment of ever more effective design tools.

4. DEVELOPMENT OF INTEGRATED METHODS

In order to meet the requirements evidenced above AUGUSTA has undergone the development of integrated computation methods, within its cooperation activity with the Aerospace Engineering Department of the Politecnico of Milan. The final aim of this activity is the accomplishment of a computation system for the analysis of helicopter dynamics, to be employed effectively at different levels of complexity and integration, and thus to be a unified tool for all design stages and requirements. To this end a high modularity is required to enable the selection of structural and aerodynamic models with different complexity. The computation system shall also be arranged for the integration with new moduli.

As far as structural modelling is concerned, the system uses a finite element scheme, organized in terms of substructures.

The aerodynamic models available for use shall range from two dimensional approximation to the most sophisticated schemes with fuselage interaction and free wake.

As other authors already stressed [26, 26], the achievement of these goals is neither easy nor quick, it may show unexpected difficulties, and does in any case require a considerable engagement of resources. The development involved shall therefore be based on a firm foundation and faced with utmost care.

14-4

The activity so far performed has led to the formulation of a new anisotropic beam theory, which has been implemented in ANBA2 Computer Program [27], and to the development of a formulation of rotor dynamics with space-time finite elements, which has been implemented in STAHR Program [28, 29].

ANBA2 PROGRAM

Starting from the two-dimensional Finite Element idealization of the cross section of a beam and by the exact integration along beam axis, ANBA2 Program (ANisotropic Beam Analysis) can supply the following data:

- the mass and stiffness matrices of the section, with due consideration of all possible couplings e.g. bending-torsion, shear tension, etc., that can be achieved with anisotropic materials;
- all components of stress including interlaminar stresses corresponding to prescribed values of resultant forces and moments, apart from extremity effects;
- extremity eigensolutions in terms of displacements, stresses, and diffusion lengths.

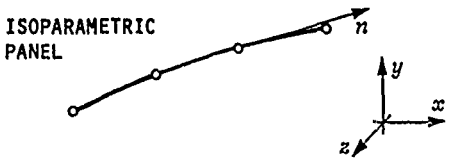
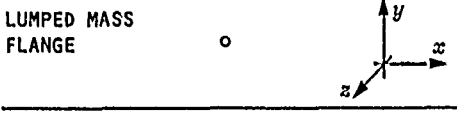
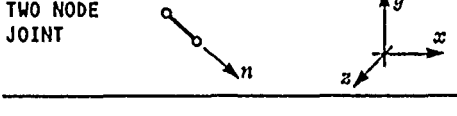

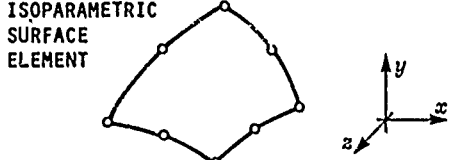
ELEMENT	STRESS COMPONENTS	NODES
ISOPARAMETRIC PANEL 	σ_z, τ_{zn}	2 TO 4
LUMPED MASS FLANGE 	σ_z	1
TWO NODE JOINT 	τ_{zn}	2
LAMINA 	ALL : $\sigma_x, \sigma_y, \sigma_z$ $\tau_{xy}, \tau_{yz}, \tau_{zx}$	2 TO 4 COUPLES
ISOPARAMETRIC SURFACE ELEMENT 	ALL : $\sigma_x, \sigma_y, \sigma_z$ $\tau_{xy}, \tau_{yz}, \tau_{zx}$	3 TO 8

Fig. 2 - Beam cross section Elements in Program ANBA2

The elements that are available for the section idealization are indicated in Fig. 2 (from [27]). It should be noted that the lamina element, which can be very small in thickness and have a full three dimensional stress state, can be employed to divide a laminate into its laminae and interlaminar layers.

As far as materials are concerned, the program can take every type of unhomogeneity and anisotropy into account, and it may also be an advanced and easy-to-use tool for isotropic beam analysis. The effectiveness of this approach mainly depends on the fact that discretization occurs on the section only. For inst., an idealization having 500-1.000 degrees of freedom on the section leads to a problem of medium-small size; however it enables the performance of a detail analysis that three-dimensional schemes would make absolutely impossible.

ANBA2 Program was already employed also as analysis modulus in optimization process for composite blade sections.

Moreover isoparametric beam elements were developed, which would make use of the results of ANBA2 Program and could take any possible coupling and geometric non-linearity into account. Besides all this will be the basic tool for facing aeroelastic tailoring problems.

STAGR PROGRAM

In the present version STAGR Program (Stability and Trim Analysis of Helicopter Rotor) can analyze isolated blade schemes.

The structural idealization makes use of the isoparametric finite elements mentioned above. The articulation and control linkage up to the swash plate can be modelled by a series of links and/or viscous elements that are assembled, with the Finite Element technique, through the use of Lagrange multipliers.

The control variables consist in the position and orientation of the swash plate; in this way the actual geometry of the couplings (e.g. pitch-flap, pitch-lag, etc.) having a basic significance for stability, can correctly be taken into account.

For the attainment of a unified formulation, suitable both for the trim analysis of a periodical solution and for the stability of a trim solution, STAGR Program makes use of a Finite Element discretization also of the time domain. Such discretization starts from the Hamilton principle, in the weak form, extended to non-conservative system [30].

$$\int_{t_I}^{t_F} (\delta T + \delta U + \delta L_e) dt = \sum_{i=1}^n \delta q_i p_i \quad \left| \begin{array}{l} t_F \\ t_I \end{array} \right. \quad (1)$$

where δ is the synchronous virtual change
 T is the kinetic energy
 U is the work function of conservative forces only
 δL_e is the virtual work of non-conservative forces
 q_i ($i=1,2,\dots,n$) are generalized coordinates
 and $p_i = \frac{\delta T}{\delta \dot{q}_i}$ (2) are the generalized momenta;

finally t_I and t_F are the extremes of the time interval considered.

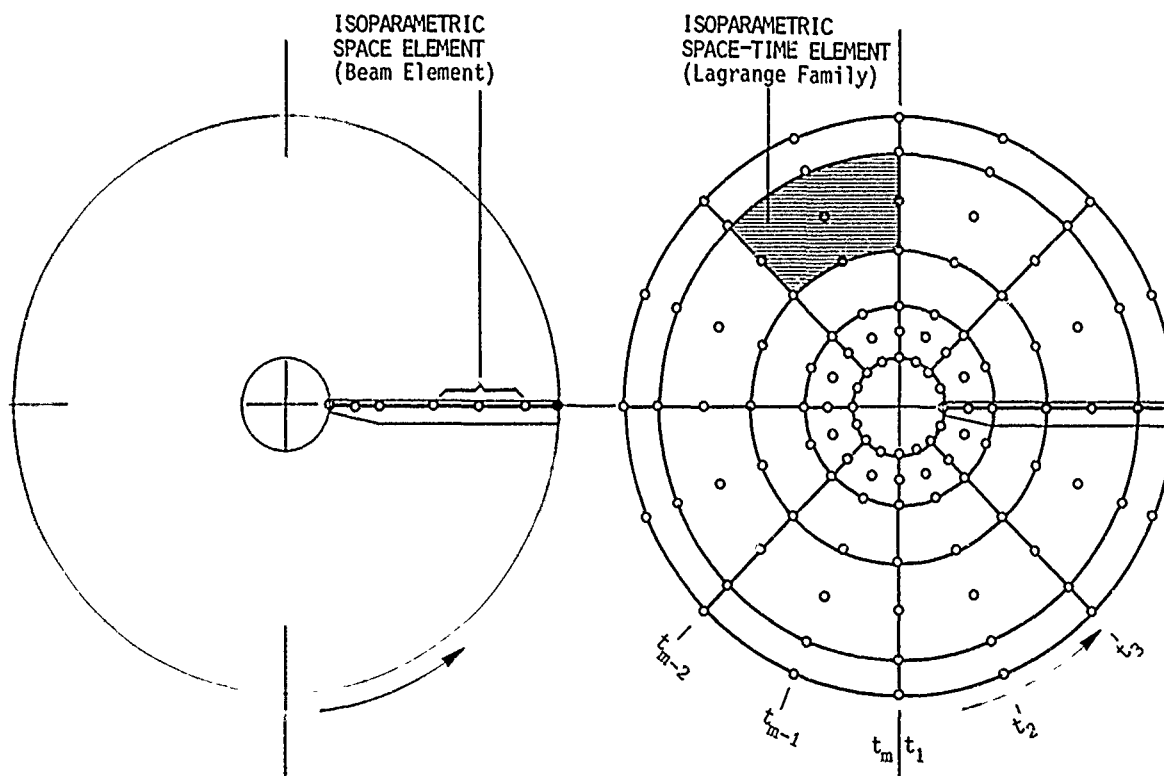


Fig. 3 - The concept of Space-Time Finite Elements in Rotor Dynamics

The discretization of the time domain consists in the assumption of the following coordinate values as unknowns.

$$\bar{q}_{ik} = q_i(t_k) \quad (3) \quad (i=1, 2, \dots, n) \quad (k=1, 2, \dots, m)$$

at m discrete time values, where clearly $t_1 = t_I$ and $t_m = t_F$.

Through the Finite Element method, instants t_k are connected by time elements (Fig. 3) in groups of 2, 3, or 4 consecutive values. Inside each element the coordinates q_i are expressed as functions of \bar{q}_i unknowns of the same element, by means of suitable interpolating functions.

By assuming one revolution of the mast as $t_I - t_F$ interval, through the above formulation the problem becomes like a usual Finite Element static (non-linear) analysis. Thereby the entire technology of finite element programs can be utilized profitably. Particularly the automatic assembling, solution, and substructuring algorithms can be employed directly, and data and program organization can follow well-established schemes.

Periodical solutions (trim solutions) are obtained directly through the setting of equality constraints between unknowns \bar{q}_i and \bar{q}_{im} [28, 29, 30].

The Floquet stability analysis is performed through the study of the eigenvalues of the connection problem regarding \bar{q}_{i1} and \bar{q}_{im} , by means of the tangent matrices related to small motions around a trim solution [28, 29, 30]. These matrices are the same as those required for the computation of the trim solution through the Newton-Raphson method. In the present version STAHR Program takes on a prescribed inflow distribution and simply employs two-dimensional aerodynamics, with the usual corrections for sweep, compressibility, unsteadiness, and dynamic stall.

The STAHR version which is operating at present has proved to have the flexibility, versatility, and easy-use characteristics as expected.

5. FUTURE DEVELOPMENTS

According to the present planning it will take the next four years to complete the computation system being developed. Through the implementation of substructure technique the present procedure shall be extended initially to the consideration of the complete rotor (several blades, hub, and suspension) and subsequently to the complete helicopter (rotor plus fuselage).

As far as aerodynamics is concerned, the plan provides the development and the implementation of moduli that, being based on consolidated theories, will allow the improvement of the modelling of the induced velocity field and of the most important three-dimensional effects.

6. CONCLUSIONS

The development of integrated computation system for rotor design seems feasible and promises considerable advantages.

The results so far obtained in this field from the cooperation activity between AUGUSTA and POLITECNICO of Milano are already significant, though partial. The theory of the anisotropic beam and the use of space-time finite elements in rotor dynamics, which are already implemented in computation programs, are a firm basis for future developments.

It would however be desirable that the same levels of generality and completeness be reached also by aerodynamic modelling.

REFERENCES

14-7

- [1] STEPNIIEWSKI W.Z.: Basic Aerodynamics and Performance of the Helicopter
AGARD LS 63 - 1973
- [2] HUBER H. : Parametric Trends and Optimization, Preliminary Selection of Configuration, Prototype design and Manufacture. AGARD LS 63 - 1973
- [3] FRIEDMAN P.P.: Formulation and Solution of Rotary Wing Aeroelastic Problems.
International Symposium on Aeroelasticity - Nuremberg 1981
- [4] BEDDOES T.S.: Representation of Airfoil Behaviour AGARD CP 334 - 1982
- [5] McCROSKEY W.J.: The Phenomenon of Dynamic Stall. Von Karman Institute - Lecture Series on Unsteady Airloads and Aeroelastic Problems in Separated and Transonic Flow. Rhode Saint Genèse - Belgium 1981
- [6] GANGWANI S.T.: Prediction of Dynamic Stall and Unsteady Airloads for Rotor Blades.
37th Annual Forum of A.H.S. - New Orleans - Louisiana 1981
- [7] McNEAL SCHWENDLER CO.: MSC/NASTRAN Aeroelastic Supplement 1979
- [8] MORINO L. : A General Theory of Unsteady Compressible Potential Aerodynamics.
NASA CR 2464 - 1974
- [9] ARIELI R., TAUBER M.: Computation of the Transonic Flow about lifting Rotor Blades
AIAA Atmospheric Flight Mechanics Conference - Boulder Colorado 1979
- [10] CARADONNA F.X., PHILIPPE J.J.: The Flow over a Helicopter Blade tip in the Transonic Regime, VERTICA Vol.2 n° 1 - 1978
- [11] TAUBER M.E., HICKS R.M.: Computerized Three Dimensional Aerodynamic Design of a Lifting Rotor Blade.
36th Annual Forum A.H.S. Washington D.C. 1980
- [12] DADONE L.: The Role of Analysis in the Aerodynamic Design of Advanced Rotors
AGARD CP 334 - 1982
- [13] LANDGREBE A.J.: An Analytical Method for Predicting Rotor Wake Geometry, J.A.H.S.
october 1969
- [14] LANDGREBE A.J.: The Wake Geometry of a Hovering Helicopter Rotor and its Influence on Rotor Performance. J.A.H.S. october 1972
- [15] CLARK D.R., MASKEW B.: Calculation of Rotor Airframe Interference for Realistic Configuration. 8th European Rotorcraft Forum. Aix en Provence 1982
- [16] HUBER H., POLZ G.: Studies on Blade to Blade and Rotor-Fuselage-Tail Interferences
AGARD CP 334 - 1982
- [17] HOENEMSER K.H.: Hingeless Rotorcraft Flight Dynamics. AGARD AG 197 - 1974
- [18] KALETA J.: Rotorcraft Identification Experiences. AGARD LS 104 - 1979
- [19] HOODGES D.H.: Aeromechanical Stability of Helicopter with Bearing-less Main Rotor
NASA TM 78459 - 1978
- [20] WARBRODT W., FRIEDMAN P.P.: Formulation of Coupled Rotor Fuselage Equations of Motion.
VERTICA Vol.3 n° 3 - 1979
- [21] LOEWY R.G.: A Two-Dimensional Approximation to Unsteady Aerodynamics of Rotary Wings. Journal of Aeronautical Science Vol. 24 - 1957
- [22] PETERS D.A., GAONKAR G.H.: Theoretical Flap-Lag Damping with Various Dynamic Inflow Models. J.A.H.S. Vol.25 n° 3 - 1980
- [23] DAT R.: Aeroelasticity of Rotary Wing Aircraft. AGARD LS 63 - 1973
- [34] COSTES J.J.: Equilibre Aeroelastique d'un Rotor d'Helicoptère en Présence de Forces

Aérodynamiques non linéaires. La Recherche Aérospatiale n°5 - 1982

- [25] KERR A.W., STEPHENS W.B.: The Development of a System for Interdisciplinary Analysis of Rotorcraft Flight Characteristics.
AGARD AG 334 - 1982
- [26] ARCIDIACONO P.J., SOPHER R.: Review of Rotor Loads Prediction Methods.
AGARD CP 334 - 1982
- [27] GIAVOTTO V. et Al.: Anisotropic Beam Theory and Application. Computer and Structures
Vol. 16 N° 1-4 - 1983
- [28] BORRI M., LANZ M., MANTEGAZZA P.: A General Purpose Program for Rotor Blade Dynamics.
7th European Rotorcraft Forum Garmish-Partenkirchen 1981
- [29] BORRI M., LANZ M., MANTEGAZZA P., ORLANDI D., RUSSO A.: STAHR: A Program for Stability and Trim Analysis of Helicopter Rotors.
8th European Rotorcraft Forum, Aix en Provence 1982
- [30] BORRI M., LANZ M., MANTEGAZZA P.: Helicopter Rotor Dynamics by Finite Element time Discretization. L'Aerotecnica Missili e Spazio Vol.60 - Dicembre 1981.

AEROELASTICITE ET OPTIMISATION EN AVANT-PROJET

C. PETIAU et D. BOUTIN

AVIONS MARCEL DASSAULT-BREGUET AVIATION
78, quai Carnot
92214 - SAINT-CLOUD

1 - AVANT PROPOS

Nous présentons une procédure développée aux AMD-BA visant à effectuer les analyses structurales statiques et dynamiques aussi complètes que possible au stade des avant-projets.

L'analyse s'effectue en quelques semaines à partir d'un plan 3 vues de l'avion, des lois d'épaisseurs relatives des voilures, d'une définition sommaire de l'architecture interne, du choix des matériaux et de la technologie de construction.

Les calculs d'avant-projet comportent pour chaque version étudiée les tâches suivantes :

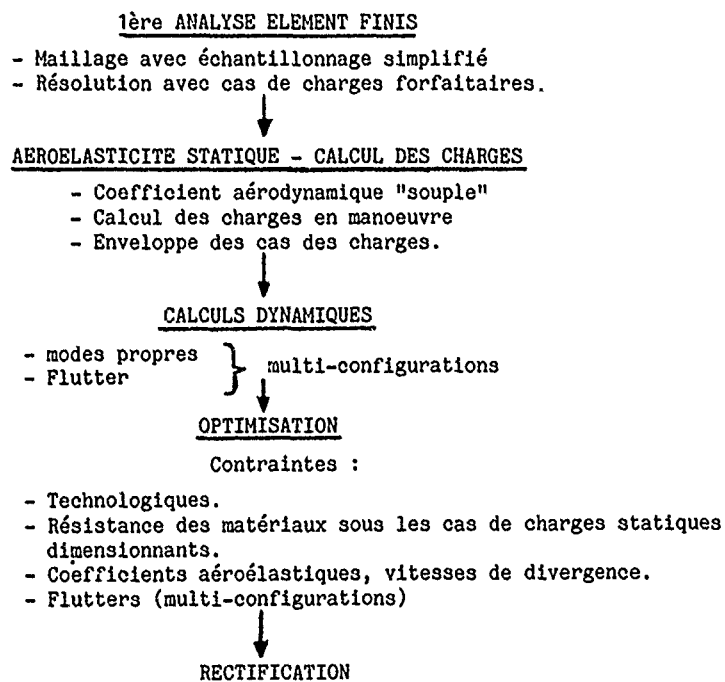
- Une première analyse éléments finis de dégrossissage avec un échantillonnage et des charges simplifiées.
- Une analyse des problèmes d'aéroélasticité statique, le calcul des charges en tenant compte de l'aéroélasticité, et la recherche automatique des chargements enveloppes.
- Des calculs de flutter avec recherche des configurations critiques d'emport de charges extérieures.
- L'optimisation automatique de l'échantillonnage, fournissant la masse de structure minimale satisfaisant aux contraintes de tenue statique, de limitations de l'aérodistorsion et des vitesses de flutter.

L'ensemble de ces travaux est effectué avec notre logiciel ELFINI ; pour répondre aux impératifs de rapidité des analyses d'avant-projet, nous avons dû améliorer sensiblement les procédures d'élaboration de données interactives, les techniques de gestion des cas de charges aéroélastiques et surtout notre méthode d'optimisation pour prendre en compte simultanément les multiples configurations d'emport de charges.

Pour illustrer notre procédure, nous donnons un aperçu de son application à l'avant-projet d'un avion de combat à voilure en matériaux composites.

2 - DESCRIPTION DE LA METHODE2.1 - Organisation générale

Nous résumons sur le tableau ci-dessous les tâches intervenant dans le processus d'optimisation d'un avant projet de structure d'avions de combat. On s'appuie sur un maillage d'éléments finis de l'ordre de 1500 à 3000 Noeuds.



L'ensemble de ces opérations est effectué par notre logiciel ELFINI dont l'organigramme est présenté planche I.

2.2 - 1ère analyse éléments finis statiques

Elle est effectuée sur un schéma d'éléments finis relativement simplifié avec des échantillonnages constants par zone et des cas de charges forfaitaires ; pour bénéficier d'un transfert automatique des charges aérodynamiques sur le schéma structural, l'ensemble des surfaces portantes doit être représenté.

Cette phase permet d'appréhender les points sensibles du dimensionnement statique.

Le schéma est réalisé par notre méthode topologique qui permet de décrire systématiquement par "pavé" de propriété constante dans un espace d'indices, les différentes propriétés du maillage (connection des noeuds par les éléments, géométrie, caractéristiques des éléments, etc....).

La méthode topologique intervient non seulement dans le maillage mais encore dans toutes branches du système ELFINI en tant que moyen d'accès au modèle.

Le module de maillage topologique de ELFINI est relié à notre système de CAO tridimensionnel CATIA.

Du point de vue informatique, ces travaux peuvent être exécutés au gré de l'utilisateur en mode interactif, en "batch" où, ce qui est le plus adapté à l'avant-projet, par une procédure hybride dite "Batch interactif" sur laquelle nous reviendrons.

2.3 - Aéroélasticité statique et calcul des charges

Pour ces calculs, en avant-projet, il faut répondre à trois impératifs apparemment contradictoires :

- Nécessité d'une précision de l'estimation des charges d'une qualité équivalente à celle du calcul des contraintes par Eléments Finis.
- Sophistication devant rester homogène avec les hypothèses simples des calculs d'aérodynamiques linéarisés recalés sur les essais de soufflerie disponibles au moment de l'avant-projet.
- Délais de préparation des données et coût ordinateur réduit.

Nous avons réalisé ce compromis dans la branche "CHARGE" de notre logiciel ELFINI dont le principe est détaillé en annexe.

Dans une phase initiale, nous effectuons la partie la plus importante des calculs indépendamment du couplage aéroélastique et des hypothèses de recalage empiriques de l'aérodynamique, ce sont :

- Les calculs théoriques des pressions dues à des effets aérodynamiques unitaires par des méthodes de singularité (quelques dizaines de formes élémentaires).
- La résolution du modèle éléments finis pour des chargements de bases (quelques centaines) décomposés en charges unitaires de pression, d'inertie et d'efforts locaux.

De ces calculs, on extrait des opérateurs "concentrés" :

- Chargements de pression des effets aérodynamiques unitaires décomposés dans les charges de base.
- Lissage des déformées sous les charges de base dans les formes aérodynamiques unitaires.
- Efforts généraux et contraintes aux points sensibles pour les chargements de base.

A partir de ces opérateurs, on obtient par des calculs de faible volume :

- Les coefficients aérodynamiques avion souple.
- Les réponses en manoeuvre par intégration des équations de la mécanique du vol.

Les recalages empiriques de l'aérodynamique et les configurations massiques aux points de vol considérés sont définis au début de cette deuxième phase, qui peut s'effectuer en mode interactif.

Des modules spécialisés permettent de visualiser les limites du domaine de vol et recherchent automatiquement les cas dimensionnants par balayages de manoeuvres types.

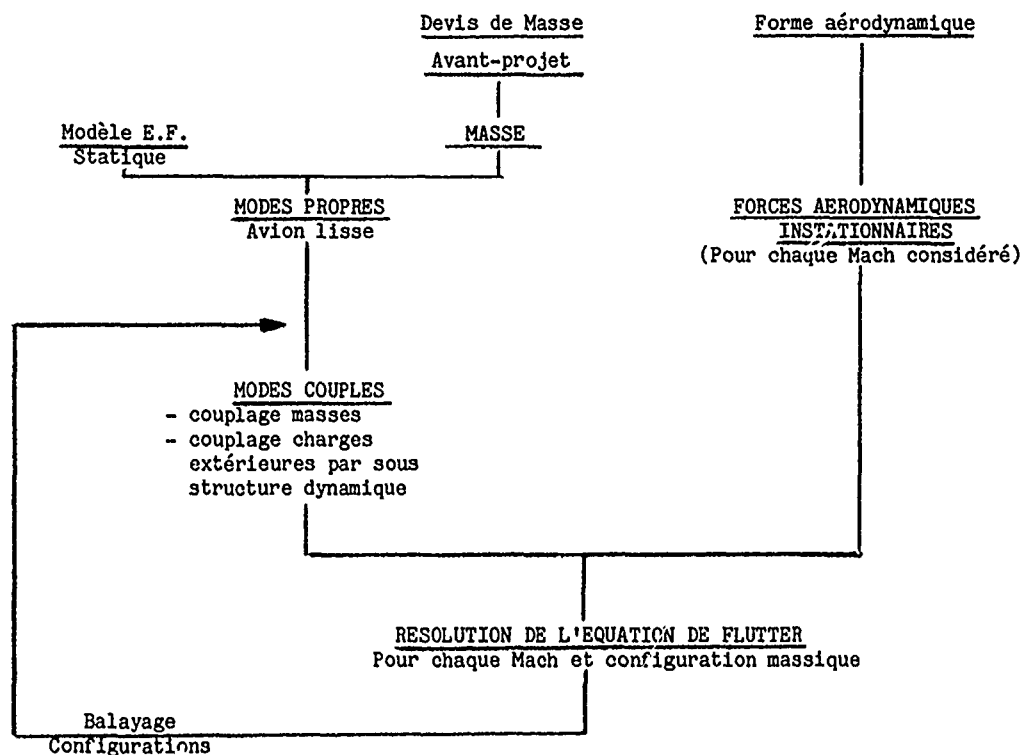
Le choix des manoeuvres étudiées résulte des clauses techniques et de l'expérience acquise.

Ces calculs permettent de tabuler pour chaque configuration de vol les opérateurs reliant les contraintes des zones sensibles aux paramètres de la mécanique du vol quasi rigide ; ces opérateurs permettent de prendre en compte aisément les contraintes structurales pour la mise aux points des commandes de vol électriques.

2.4 - Premières analyses de flutter

Ces calculs qui s'effectuent sur le premier maillage de la structure visent à dégager les tendances au flottement de la formule envisagée ; on balaye les principales configurations de masse et d'emport de charges extérieures pour sélectionner celles qui seront contrôlées dans les itérations de l'optimisation.

Nous résumons les étapes du calcul sur l'organigramme ci-dessous :



Comme pour l'aéroélasticité statique les calculs coûteux sont rassemblés dans les phases initiales les calculs de modes propres et de forces aérodynamiques instationnaires.

A partir de là, le balayage des configurations d'emport de charge est rapide en procédant au couplage par une méthode de sous structure dynamique.

2.5 - Optimisation

On utilise le module d'optimisation de ELFINI, déjà présenté dans les références 2 et 3, c'est la clef de voûte de l'analyse rapide en avant projet ; il assure la recherche automatique de l'échantillonnage conduisant à une masse structurale minimale.

Les paramètres de l'optimisation sont des facteurs multiplicatifs de l'échantillonnage de groupes d'éléments finis ; pour les matériaux composites, ce sont les nombres de plis par direction sur des groupes d'éléments finis.

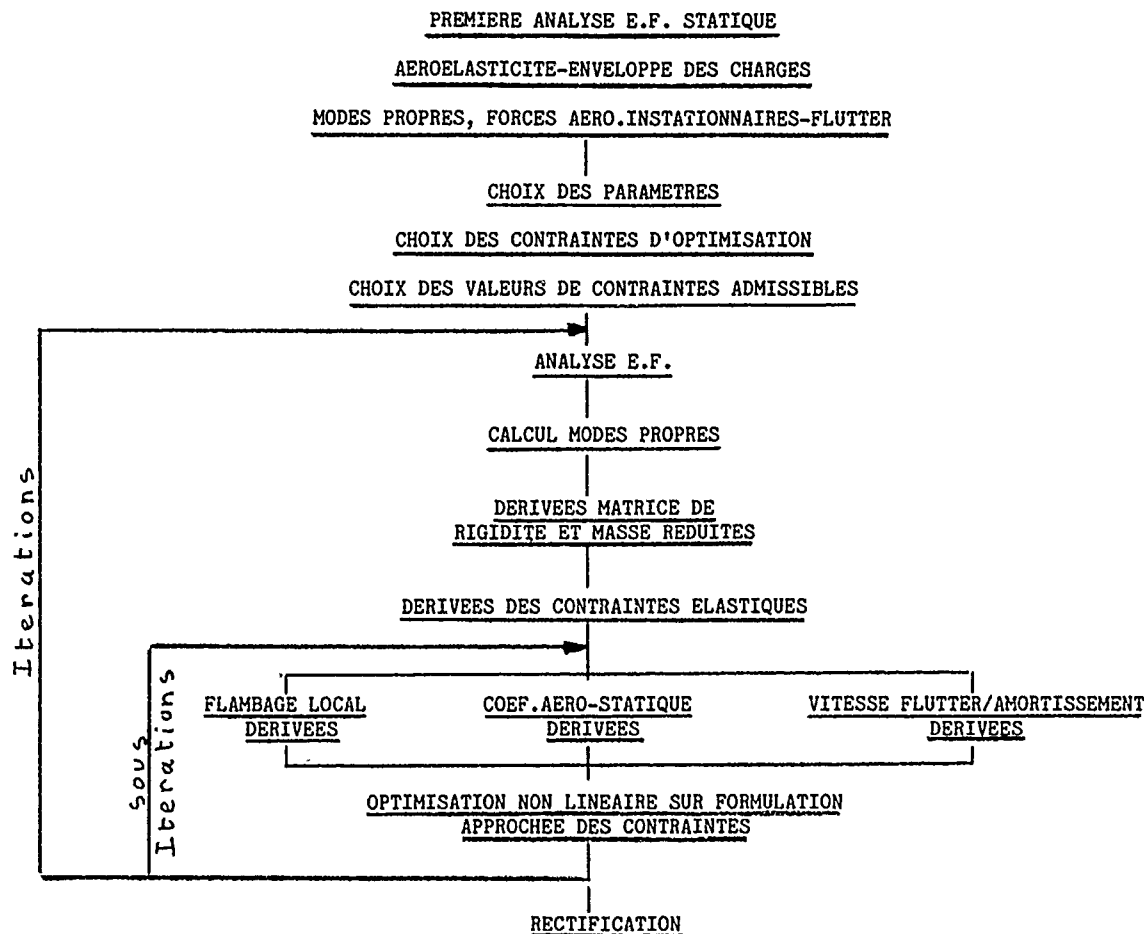
Les contraintes d'optimisation prises en compte sont des types suivants :

- Minimum technologique sur les épaisseurs, limitation des variations entre paramètres voisins.
- Limitation en déformation, efforts locaux, contrainte élastique, critère de rupture divers, flambage local des métalliques et composites avec éventuellement effets de plasticité, cela sous des chargements statiques multiples.
- Limitation sur les variations aéroélastiques des coefficients aérodynamiques, des vitesses d'inversion de gouverne et de divergences statiques.
- Limitation sur les vitesses de flutter et les amortissements aérodynamiques pour diverses configurations de masse et d'emport de charge.

L'outil d'optimisation utilisé aujourd'hui permet la prise en compte de plus de 500 paramètres et de plusieurs milliers de contraintes.

Pour étudier simultanément plusieurs configurations de masse et de rigidité, on gère parallèlement plusieurs modèles dont les paramétrages sont communs.

L'organigramme de l'optimisation est le suivant :



- Réponse des contraintes à une variation de paramètres imposée directement.
- Optimisation pour une petite variation des contraintes admissibles.

le module de "rectifications" procède à partir des tables de dérivées partielles de contraintes : on donne en conversationnel, l'influence des retouches de dessin sur les contraintes, ou inversement celle des variations de contraintes admissibles sur les échantillonnages optimaux.

Les principes théoriques et le fonctionnement précis de notre module d'optimisation sont exposés en détail dans la référence 3.

2.6 - Procédures d'exécution des travaux, coût ordinateur, délais d'exécution

En dehors des phases coûteuses, résolutions des éléments finis, calcul des modes propres et optimisation, pour lesquels la procédure d'exécution en batch est normale, nous nous sommes posés le problème du degré d'interactivité nécessaire à l'élaboration et la manipulation des modèles d'avant-projet.

C'est une procédure dite "Batch interactive" qui s'est dégagée à l'usage ; les données sont générées sur un écran alphanumérique à l'aide d'un éditeur de texte et exécutées en temps réel par "courtes rafales" sur une console Tektronix ; le programme donne la main à l'utilisateur à la fin de chaque séquence ; on peut alors effectuer les visualisations de contrôle en mode interactif pur et éventuellement modifier le fichier de données sur l'écran alphanumérique ; l'opérateur continue ou recommence l'exécution à partir de n'importe quel point.

Dans cette procédure, l'inconvénient de ne pas disposer, comme en interactif pur, de l'aide d'un menu est largement compensée par la possibilité de générer les données par modification de fichier modèle, ce qui est très appréciable quand il faut suivre toutes les évolutions d'une formule en avant-projet.

A ce niveau on profite aussi largement des facilités de l'adressage topologique qui rend les données de l'aéroélasticité et de l'optimisation peu sensibles aux modifications du modèle Eléments finis.

La première optimisation d'une nouvelle formule d'avion par notre procédure demande un délai de 4 à 8 semaines pour une équipe de trois personnes entraînées ; ces temps se raccourcissent notablement pour l'analyse des évolutions.

Le temps ordinateur dépend de la complexité des schémas éléments finis et aérodynamiques utilisés ; il est relativement faible dans les phases d'analyse préliminaire (moins d'une heure CPU d'IBM 3081 pour l'exemple présenté au §.3) ; l'optimisation proprement dite demande elle plusieurs heures CPU par exécution il faut compter qu'elle doit être relancée pratiquement tous les soirs pendant la phase active de l'avant-projet pour l'étude des variantes.

3 - EXEMPLE : AVANT-PROJET D'AVION DE COMBAT

Nous donnons ici un aperçu de l'application de la procédure à l'étude d'un avant-projet d'avions de combat de formules delta-canard comportant une voilure en matériaux composites ; les planches présentées illustrent plusieurs variantes de ce projet.

3.1 - Analyses initiales

Nous présentons planche 2 le modèle d'éléments finis simplifié de l'avion complet comportant 11 737 degrés de liberté et constitué pour l'essentiel d'éléments finis à interpolation linéaire.

Les caractéristiques du calcul d'aéroélasticité et de charges sont résumées sur le tableau ci-dessous :

Nombre de formes aérodynamique de base	Sym.	54
	Antisym.	81
Nombre de chargements de base total	Sym.	249
	Antisym.	292
Nombre de points sensibles		250
Nombre de configurations massiques considérées		7
Nombre de Machs considérés		9
Nombre d'altitudes		10
Nombre de types en manoeuvre		5
Nombre de cas enveloppe		6

Nous présentons planches 3 à 10 quelques visualisations caractéristiques issues de ces calculs.

Les calculs de modes et de flutter ont été effectués pour 9 configurations d'emports de charges dont 3 ont révélé un flutter latent (voir planche 15).

3.2 - Optimisations

Elles ont porté indépendamment sur le caisson de voilure, la partie centrale du fuselage et la dérive, nous donnons ici un aperçu de l'étude du caisson de voilure.

Pour limiter le volume des calculs, le fuselage et les charges extérieures sont couplés à la voilure par une méthode de super éléments statiques et dynamiques.

Les calculs statiques sont menés sur une seule configuration élastique calculée parallèlement avec des conditions aux limites symétriques et antisymétriques (au travers du super élément fuselage) on prend en compte les 6 chargements enveloppe.

Les calculs dynamiques sont menés avec les 3 configurations élastiques et massiques ayant montré des flutters latents.

L'optimisation met en jeu 304 paramètres portant sur :

- Le nombre de couches de fibres de carbone dans 4 directions imposées (0° , $\pm 45^\circ$, 90°) sur les panneaux d'intrados et d'extrados (voir planches 10 à 12).
- Les sections des semelles de longeron et de nervure.
- Les âmes de longeron et de nervure.

La masse totale paramétrée par 1/2 voilure est initialement de 312 kg.

On prend en compte 676 contraintes d'optimisation des types suivants :

- 243 critères de rupture dans les fibres.
- 172 critères de flambage de maille (2 modes de flambage sont contrôlés par maille).
- 5 vitesses de flutter et 60 amortissements aéroélastiques.
- 1 efficacité des gouvernes en roulis.
- 195 contraintes Technologiques portant sur les épaisseurs minimales, les proportions en fibres dans chaque direction et les pentes d'épaisseurs.

Le point de départ correspond à un échantillonnage constant à 19 couches de 0,13 mm d'épaisseur dans chaque direction ; l'optimisation a été conduite en introduisant les contraintes en 3 phases successives.

- 1 - Optimisation aux seules contraintes statiques.
- 2 - Addition des contraintes technologiques.
- 3 - Addition des contraintes de Flutter.

La convergence est toujours atteinte en moins de 5 itérations.

L'évolution de la masse paramétrée et de quelques contraintes significatives est présentée planche 14.

Les nappages optimums successifs des fibres sont présentés planches 10 à 13 ; on remarquera le coût relativement élevé des contraintes dites technologiques qu'on a choisi volontairement très conservatives.

Nous présentons des courbes d'amortissement aéroélastique des modes propres qui caractérisent deux façons de contrôler le flutter.

- Flutter "sec" planche 15, simplement déplacé en vitesse par l'optimisation (contrainte sur la vitesse de Flutter).
- Flutter "mou" planche 16, disparaissant dans l'optimisation qui doit donc être contrôlé par des contraintes portant sur les amortissements à vitesse donnée (voir réf.3).

Pour illustrer les possibilités du module interactif de rectification, nous montrons planches 17 à 18, l'influence de variation de contraintes admissibles sur l'échantillonnage optimal.

Les contraintes d'aéroélasticité statique n'étaient pas en butée dans ces premiers calculs, nous avons dû augmenter la sévérité de cette contrainte pour faire apparaître leur influence sur la masse optimale (voir planche 18).

4 - CONCLUSIONS - DEVELOPPEMENTS

La méthode de travail présentée permet d'évaluer en quelques semaines une formule structurale avec une équipe réduite ; la procédure étant mise en place, on peut analyser les évolutions du projet avec des délais de l'ordre de la journée, l'optimisation étant particulièrement bien adaptée aux comparaisons iso-critère des variantes de structure.

Dans notre approche, les outils d'analyse de l'avant-projet sont basiquement les mêmes que ceux utilisés pour la justification fine de la structure, la différence n'apparaît que dans le mode d'utilisation qui est allégé en avant-projet ; en pratique l'évolution dans le raffinement du modèle est continue au fur et à mesure que se précise le dessin et qu'arrivent les résultats de soufflerie pour les charges.

En dépit des apparences, la méthode est bien adaptée à la coordination de projets en coopération ; en effet, outre une première idée du dimensionnement et un verrouillage partiel des problèmes d'aéroélasticité, le modèle simplifié général qu'on obtient, fournit dès le début du projet des conditions aux limites correctes pour les calculs raffinés des tronçons par les coopérateurs. En retour, le maître d'oeuvre actualise son modèle simplifié à partir des calculs détaillés des coopérateurs pour mener les calculs définitifs d'aéroélasticité et de flutter. A ce propos nous avons mis au point une méthode d'identification structurale qui permet d'effectuer cette opération automatiquement.

A l'intérieur du cadre actuel, le développement de la méthode se fait de façon continue en profitant des progrès des disciplines mises en jeu et de l'accroissement de performances des ordinateurs ; nous soulignons cependant deux points importants :

- Les techniques d'élaboration de données interactives et de visualisations.

Grâce aux possibilités dégagées par la nouvelle génération d'écran "Raster Vidéo" à définition fine, nous transformons progressivement notre procédure "Batch interactif" en un système de "Langage procédural" qui allie l'aide d'un menu au moment de la première rédaction d'une famille de données aux facilités de récupération des historiques pour le calcul des évolutions.

- Contraintes technologiques dans l'optimisation des composites.

Les nappages optimaux en composites dégagés par notre méthode laissent quelquefois perplexer le dessinateur de bureau d'études au moment de la réalisation ; nous sommes donc amenés à chercher une formulation claire des contraintes technologiques du drapage des fibres en particulier dans le contexte de l'utilisation de machines à draper.

Un problème essentiel reste encore ouvert, c'est l'intégration de l'optimisation structurale dans les autres disciplines, en particulier :

- L'aérodynamique et les performances.

Actuellement la liaison est faite par le contrôle des déformations aéroélastiques qui permet théoriquement l'optimisation des profils pour 2 points du domaine de vol. On peut aller beaucoup plus loin, en effet nous sommes capables de calculer les variations de masse induites par les changements de forme aérodynamique.

- Qualité de vol.

Aujourd'hui elles sont prises en compte de façon assez forfaitaire dans l'optimisation structurale par les limitations de variation des coefficients aérodynamiques ; en fait il y a interaction complète entre la conception des commandes de vol électriques, les charges de dimensionnement et l'aéroélasticité.

L'étude de cette optimisation pluridisciplinaire commence par une formulation mathématique explicite du problème, en particulier il faut définir ce qu'est la fonction objectif à minimiser pour obtenir un avion optimal.

REFERENCES

- 1 - C. PETIAU : Méthode de Maillage Topologique dans ELFINI.
Journées sur la génération automatique et la visualisation des maillages
E.D.F - GAMNI - INRIA.
- 2 - C. PETIAU et G. LECINA : Eléments finis et optimisation des structures aéronautiques.
Agard Conferences Proceedings N° 280 : The use of computer as a design tool.
MUNICH 1975.
- 3 - G. LECINA et C. PETIAU : Optimization of Aircraft Structures.
Foundations of Structural Optimization Approach Edited by A.J. Morris.
1982 John Wiley & Sons Ltd.

ANNEXE :

EQUATIONS DE BASE DU COUPLAGE AEROELASTIQUE

I - PHASES PREALABLES (Batch)

- Aérodynamique théorique : champs de pression discrétisés

$$K_P = K_{P_0} + \left[\frac{\partial K_P}{\partial q_1} \right] q_1 + \left[\frac{\partial K_P}{\partial q_0} \right] q_0$$

q_1 effets aérodynamiques rigides (Incidence, X braquage de gouvernes, etc.)
 q_0 Déformée des surfaces portantes exprimées dans une base de monômes

(q_1 et q_0 de rang quelques dizaines)

- Equation du moment de l'avion quasi rigide

$$F_{COG} = \frac{1}{2} \rho V^2 \{ [C_{r1}] q_1 + [C_{r0}] q_0 + C_{r0} \}$$

Les coefficients aérodynamiques $[C_{r1}]$, $[C_{r0}]$ et C_{r0} sont les torseurs résultants des champs de pression

- Chargement du modèle Eléments finis

$$F = [P] f \quad P = [P_{ano}, P_{inertie}, P_{autres}] \quad \text{chargements de base}$$

- Resolution éléments finis (sur C.L. isostatique)

$$X = [K]^{-1} F \Rightarrow \text{Déformées de base} \quad B = [K]^{-1} P$$

- Opérateurs "concentrés"

$$\text{Contraintes et efforts aux points sensibles } \sigma = \left[\frac{\partial \sigma}{\partial x} \right] X \Rightarrow \left[\frac{\partial \sigma}{\partial f} \right] = \left[\frac{\partial \sigma}{\partial x} \right] [B]$$

$$\text{Torseur résultant et mouvement rigide } \left[\frac{\partial F_{COG}}{\partial f} \right], \left[\frac{\partial R_{COG}}{\partial f} \right] \quad (\text{Pour chaque masse de base})$$

- Chargement aérodynamique décomposé dans les chargements de base

$$f_{ano} = [R] K_P \Rightarrow \frac{\partial f}{\partial q_1} = [R] \left[\frac{\partial K_P}{\partial q_1} \right], \quad \frac{\partial f}{\partial q_0} = [R] \left[\frac{\partial K_P}{\partial q_0} \right]$$

$$\text{Lissage des déformées E.F. dans les formes aérodynamiques } q_0 = [L] X \Rightarrow \left[\frac{\partial q_0}{\partial f} \right] = [L] [B]$$

II - PHASES REPETEES (INTERACTIVES)

- Recalage empyrique de l'aérodynamique (identification sur résultats de soufflerie, "expérience")

$$\Rightarrow \left[\frac{\partial f}{\partial q_1} \right]_{\text{réale}}, \left[\frac{\partial f}{\partial q_0} \right]_{\text{réale}}$$

- Calcul des charges d'inertie dans les configurations envisagées (combinaisons linéaires des effets d'inerties élémentaires)

$$\Rightarrow \left[\frac{\partial f}{\partial g} \right]$$

- Charge aérodynamique de base équilibrée par les effets d'inerties

$$\Rightarrow \left[\frac{\partial f}{\partial q_1} \right]_{\text{équilibre}} = \{ I - \left[\frac{\partial f}{\partial g} \right] [L]^{-1} \left[\frac{\partial F_{COG}}{\partial f} \right] \} \left[\frac{\partial f}{\partial q_1} \right]_{\text{réale}}$$

$$\left[\frac{\partial f}{\partial q_0} \right]_{\text{équilibre}} = \{ I - \left[\frac{\partial f}{\partial g} \right] [L]^{-1} \left[\frac{\partial F_{COG}}{\partial f} \right] \} \left[\frac{\partial f}{\partial q_0} \right]_{\text{réale}}$$

- Calcul des coefficients aérodynamiques avion souple

Elimination des effets souples

$$q_0 = \frac{1}{2} \rho V^2 \{ A_0 + [A_1] q_r + [A_2] q_0 \} + A_{\text{autre}}$$

$$[A_1] = \left[\frac{\partial q_0}{\partial q_r} \right] \left[\frac{\partial L}{\partial q_r} \right]_{\text{équilibre}} \quad [A_2] = \left[\frac{\partial q_0}{\partial q_0} \right] \left[\frac{\partial L}{\partial q_0} \right]_{\text{équilibre}}$$

(Plus correction du mouvement rigide)

$$\Rightarrow q_0 = \frac{1}{2} \rho V^2 \{ [M] q_r + M_0 \} + A_{\text{autre}}$$

$$M = [D]^{-1} [A_1] \quad [D] = I - \frac{1}{2} \rho V^2 [A_2]$$

La singularité de $[D]$ exprime la divergence statique.

. Coefficient aérodynamique apparent

$$[C] = [C_0] + \frac{1}{2} \rho V^2 [C_0] [M]$$

$$C_0 = C_{0r} + [C_0] \left\{ \frac{1}{2} \rho V^2 M_0 + M_{0, \text{autre}} \right\}$$

- Contraintes et efforts unitaires aéroélasticité éliminée

$$\left[\frac{\partial \sigma}{\partial q_r} \right] = \left[\frac{\partial \sigma}{\partial L} \right] \left\{ \left[\frac{\partial L}{\partial q_r} \right] + \frac{1}{2} \rho V^2 \left[\frac{\partial L}{\partial q_r} \right] [M] \right\}$$

- Calcul de manoeuvre avion quasi rigide

. Equation mécanique du vol avec $[C] \Rightarrow q_r(t)$

. Contrainte et effort en manoeuvre aux points sensibles

$$\sigma(t) = \sigma_0 + \frac{1}{2} \rho V^2 \left[\frac{\partial \sigma}{\partial q_r} \right] q_r(t)$$

- Enveloppe automatique des charges, Principes :

- . Un cas de charge est déclaré enveloppe si il conduit à une valeur extrême de contrainte (A une tolérance près) sur au moins 1 point sensible de la structure.
- . On cherche le nombre minimum de cas de charge tel que en chaque point sensible les valeurs extrêmes des contraintes soient atteintes pour au moins un cas de charge (A la tolérance près).
- . L'élargissement de la tolérance permet de réduire le nombre de cas enveloppe.
- . Le processus est associatif.

- Retour aux Eléments Finis pour les cas enveloppe.

- . En charge
- . En déplacement

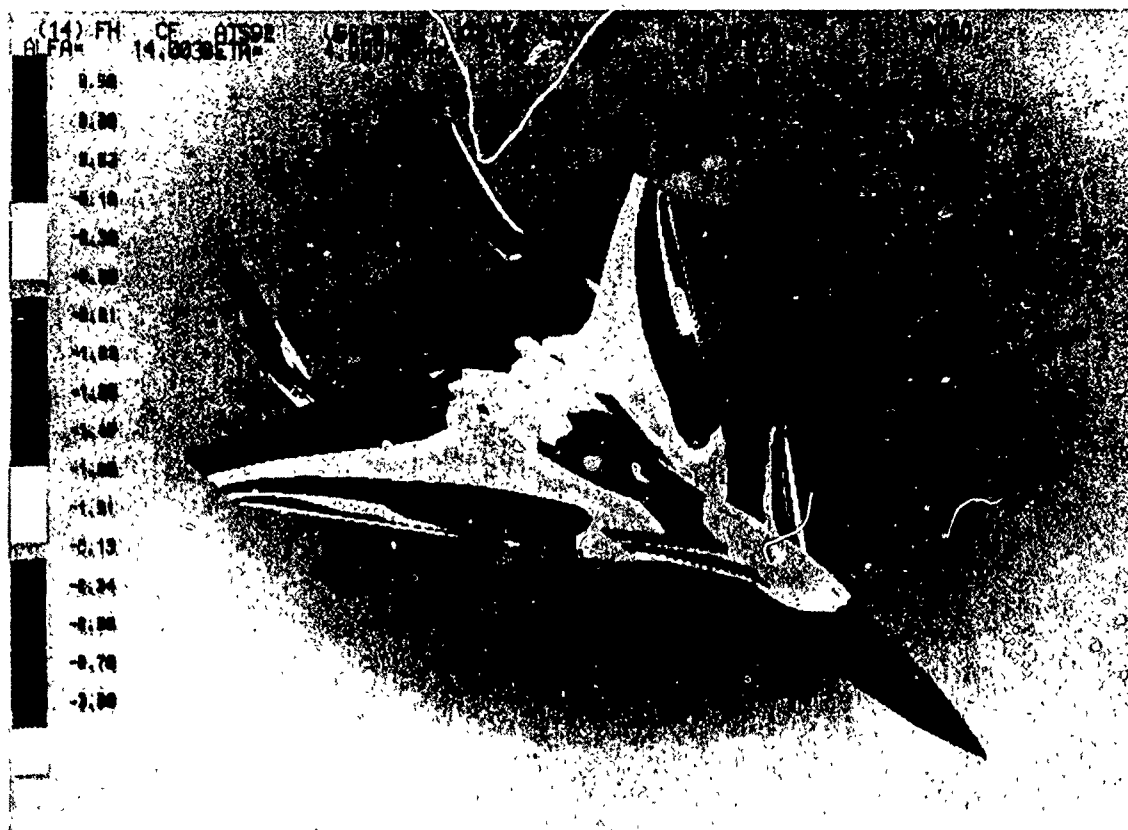


PLANCHE 4

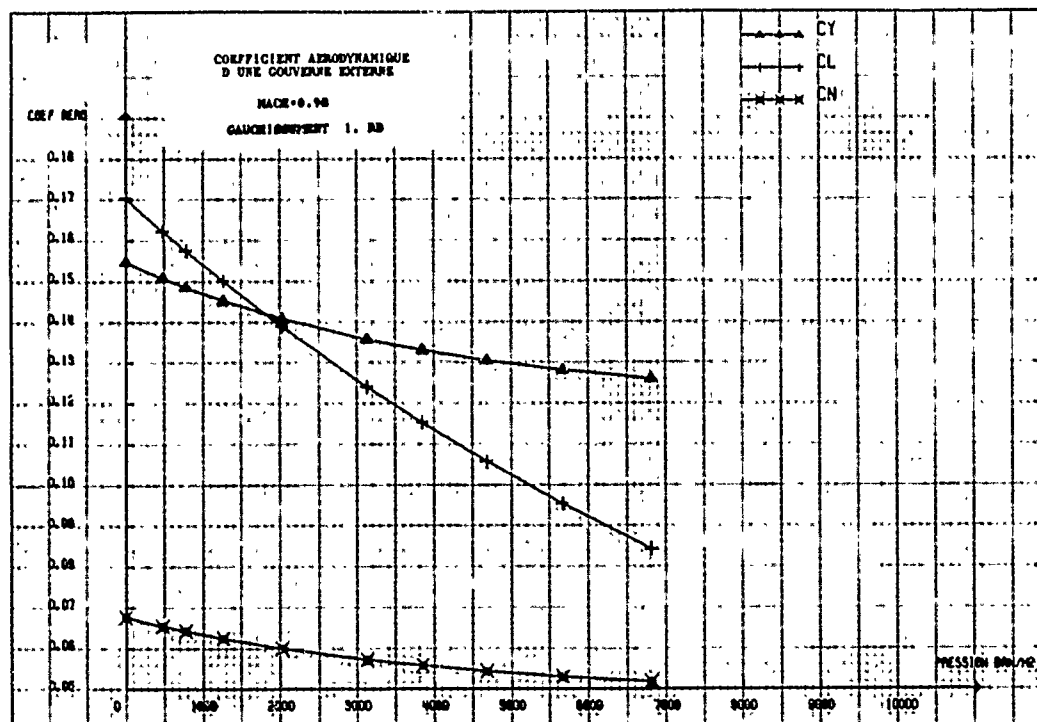


PLANCHE 5

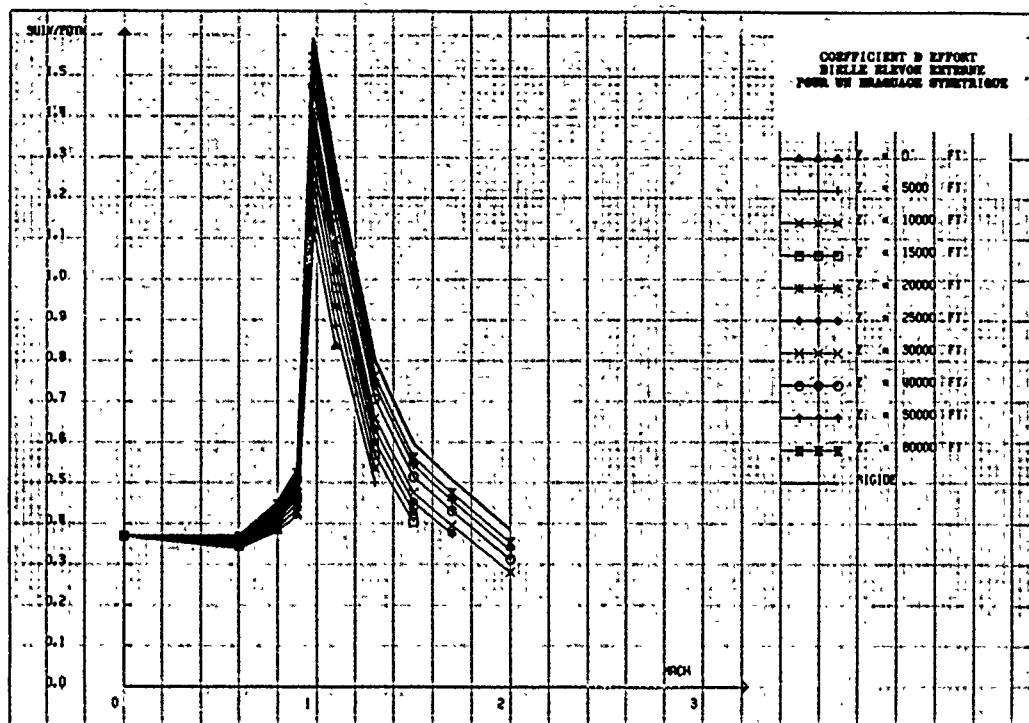


PLANCHE 6

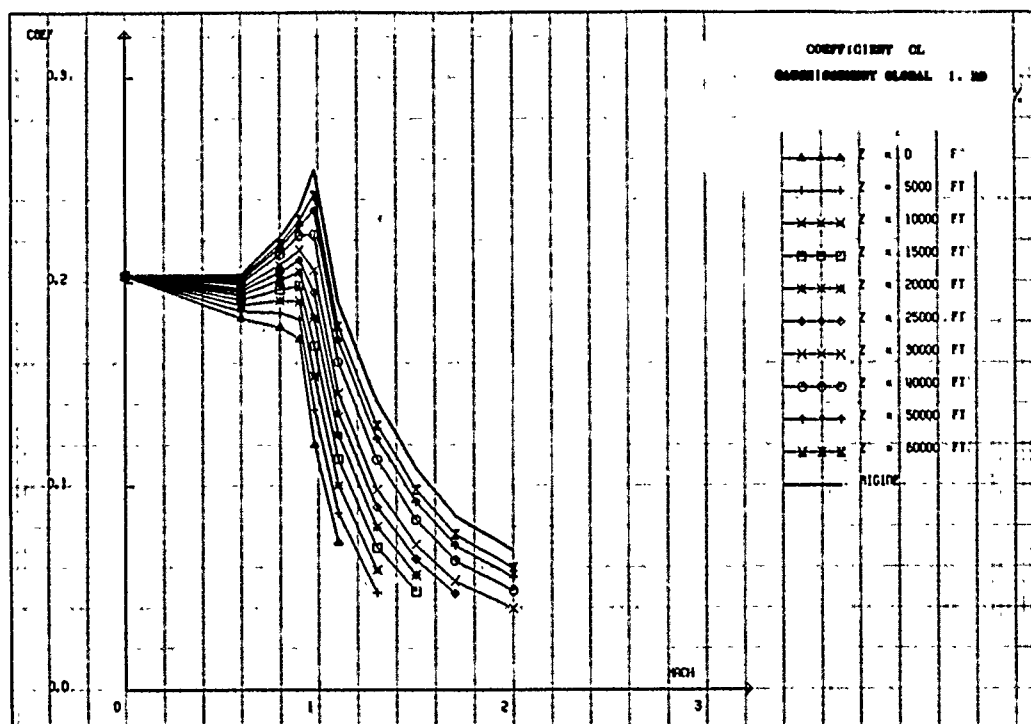


PLANCHE 7

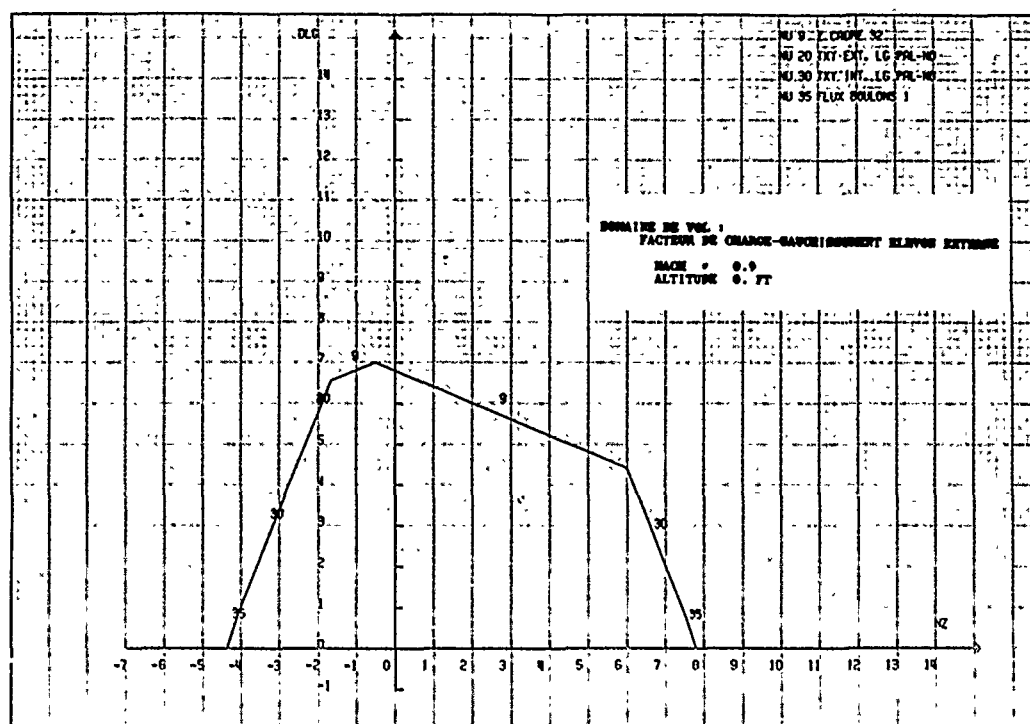


PLANCHE 8

MANOEUVRE ENVELOPPE
 FACTEUR DE CHARGE + ROULIS STABILISE
 (CHARGE LIMITE)

MACH 0.9
 Z = 0 FT

MACH 0.9
 Z = 30000 FT

MACH 0.9
 Z = 40000 FT

KP SUR VOILURE

DEFORMEES LIMITE

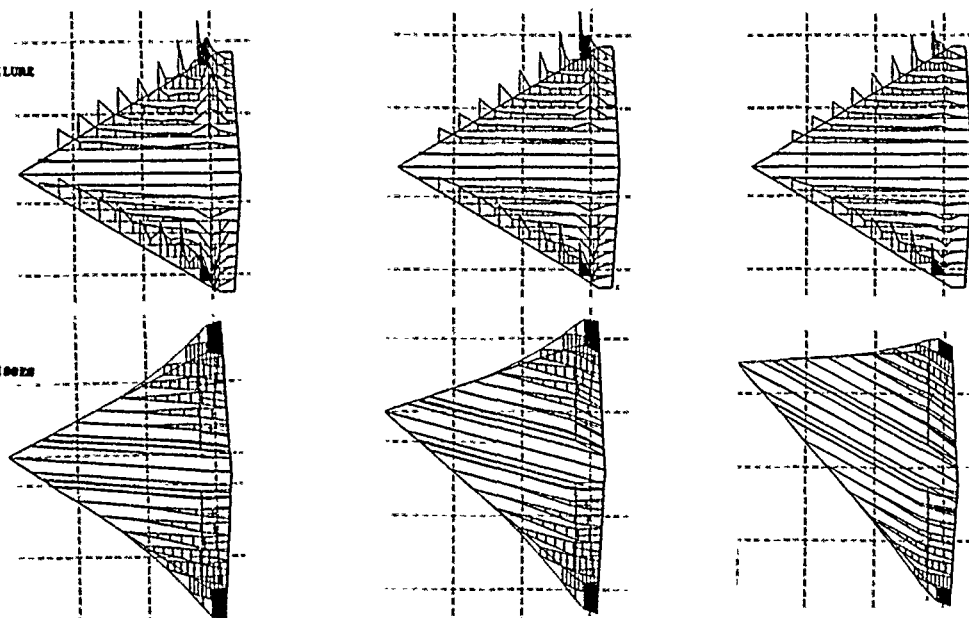


PLANCHE 9

FLUX DE CONTRAINTES PRINCIPALES
REVETEMENTS INTRADOS

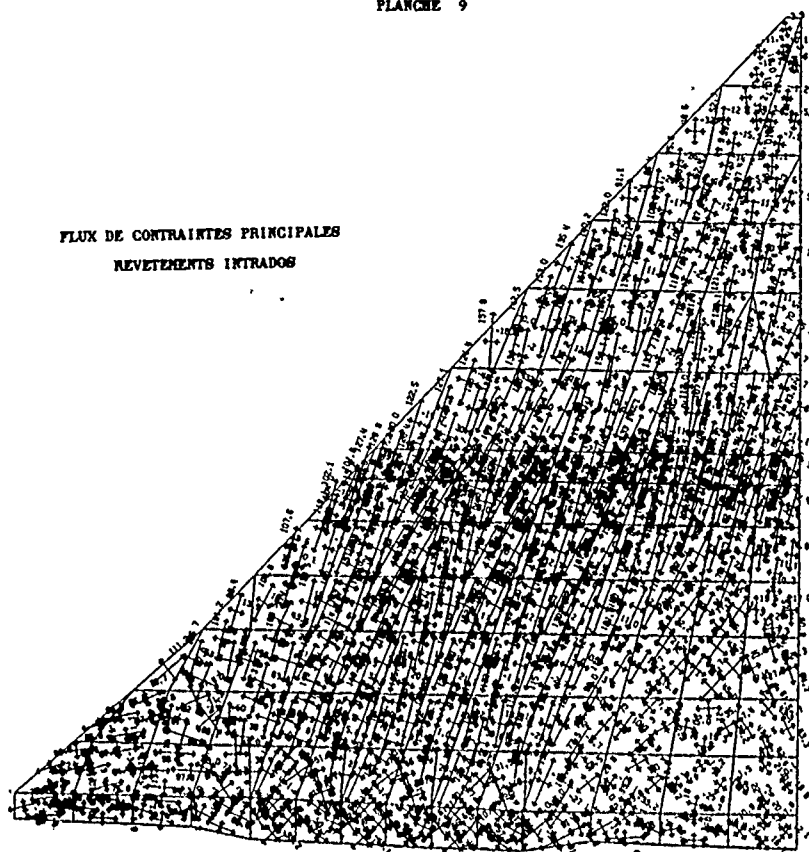
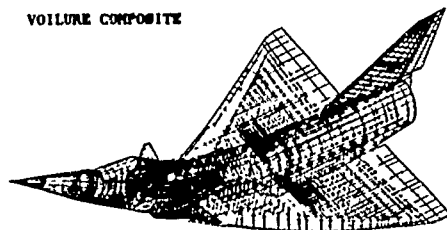


PLANCHE 10

MODES SYMETRIQUES

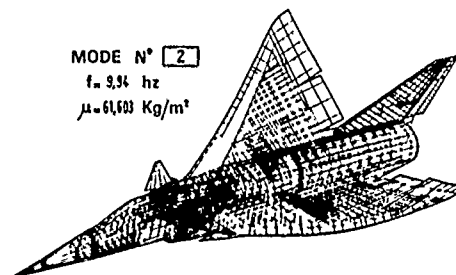
AVION DE COMBAT
VOILURE COMPOSITE



MODE N° 1
 $f = 8,01 \text{ Hz}$
 $\mu = 75,84 \text{ Kg/m}^3$

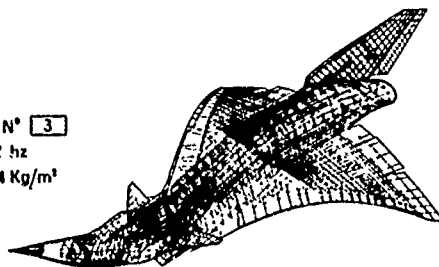
MODE N° 2

$f = 9,94 \text{ Hz}$
 $\mu = 61,603 \text{ Kg/m}^3$



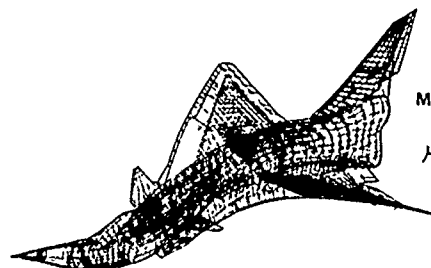
MODE N° 3

$f = 17,62 \text{ Hz}$
 $\mu = 783,28 \text{ Kg/m}^3$



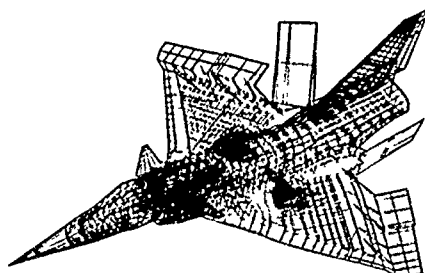
MODE N° 4

$f = 24,88 \text{ Hz}$
 $\mu = 147,87 \text{ Kg/m}^3$



MODE N° 6

$f = 31,18 \text{ Hz}$
 $\mu = 423,83 \text{ Kg/m}^3$



MODE N° 5
 $f = 28,32 \text{ Hz}$
 $\mu = 389,62 \text{ Kg/m}^3$

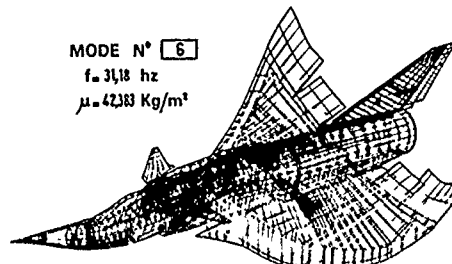


PLANCHE 11

RAFFAGE OPTIMUM

CONTRAINTES SUIVIES :

- * LIMITATIONS TECHNOLOGIQUES DE RAFFAGE
- * CONTRAINTES DE TENUES STATIQUES
- * FLAMBAGE

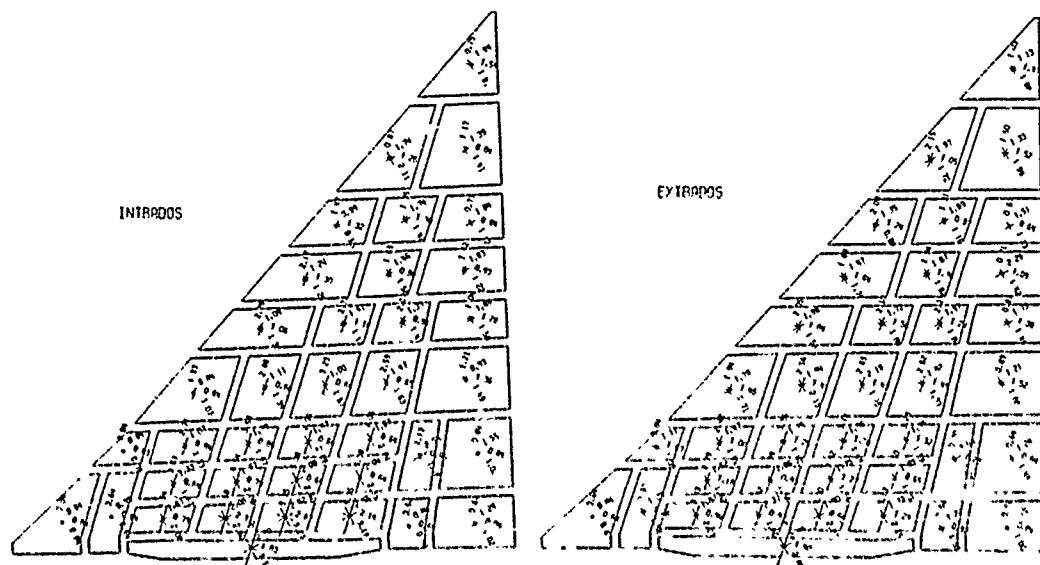


PLANCHE 12

RAFFAGE OPTIMUM

CONTRAINTES SUIVIES :

- * LIMITATIONS TECHNOLOGIQUES DE RAFFAGE
- * CONTRAINTES DE TENUES STATIQUES
- * FLAMBAGE
- * VITESSE DE FLUTTER

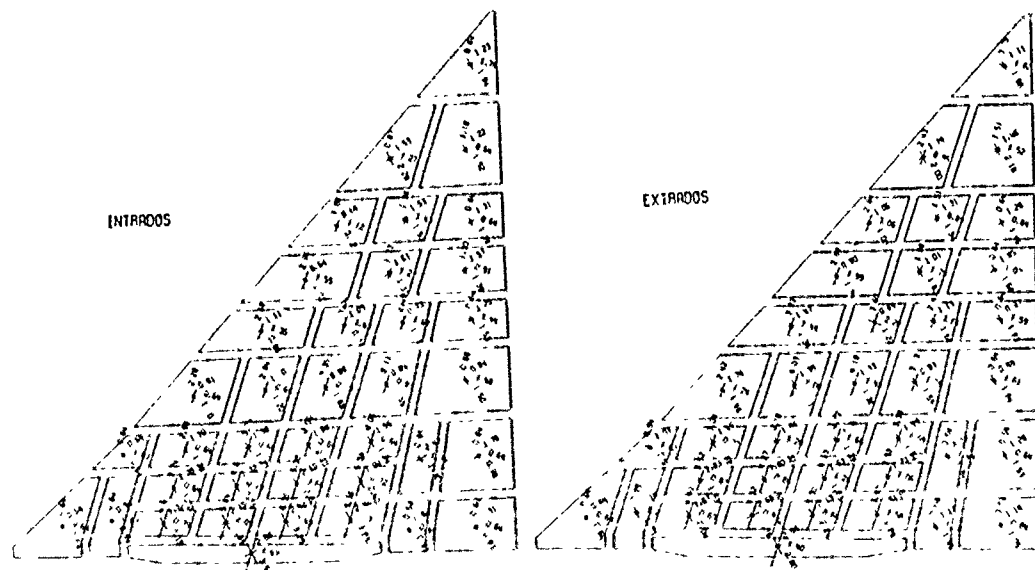
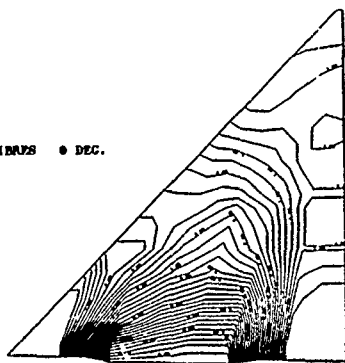


PLANCHE 13

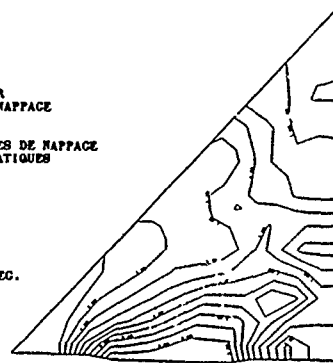
FIBRES 0 DEG.



NAFFAGE OPTIMUM
TRACE DES COURBES 100-EPAISSEUR
DANS CHAQUE DIRECTION DE PLIS DU NAFFAGE

CONTRAINTES SUIVIES :
* LIMITATIONS TECHNOLOGIQUES DE NAFFAGE
* CONTRAINTES DE TENSEURS STATIQUES
* FLAIBAGE
* VITESSE DE FLUTTER

FIBRES +45 DEG.



FIBRES 90 DEG.



FIBRES -45 DEG.

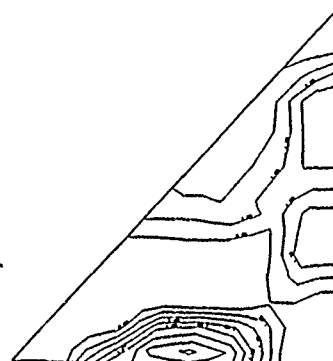


PLANCHE 14

CONVERGENCE EN MASSE

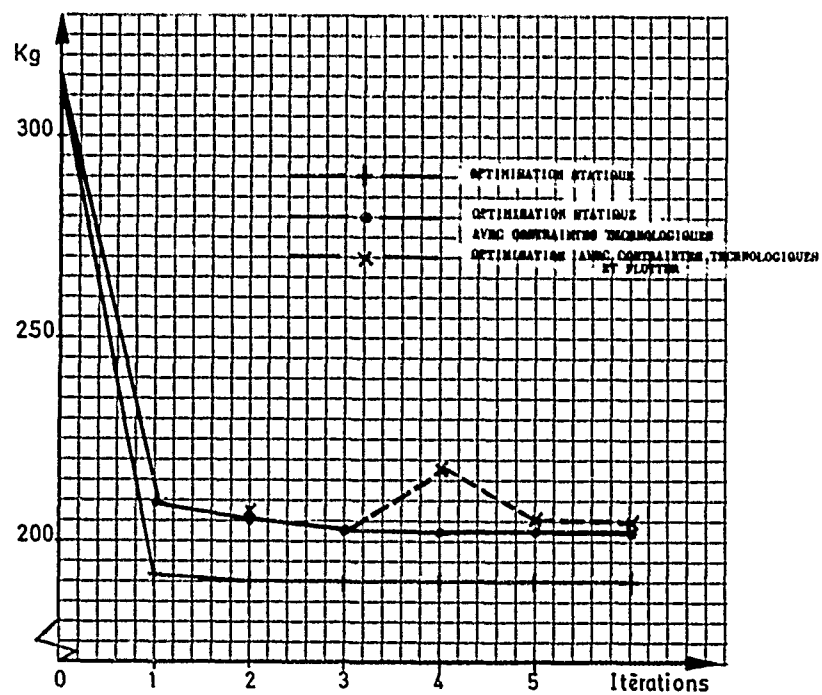
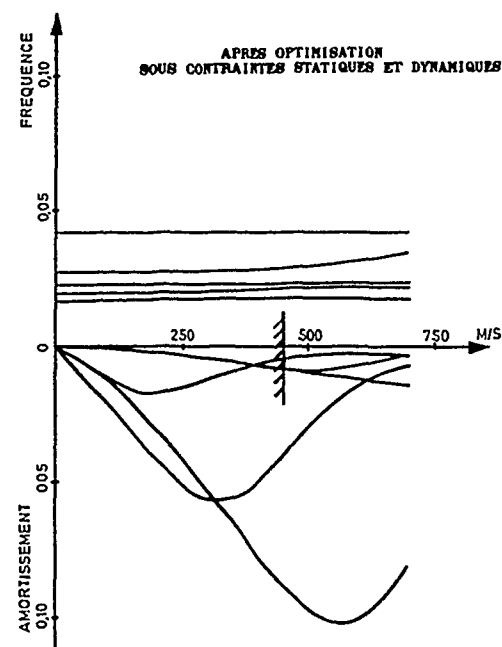
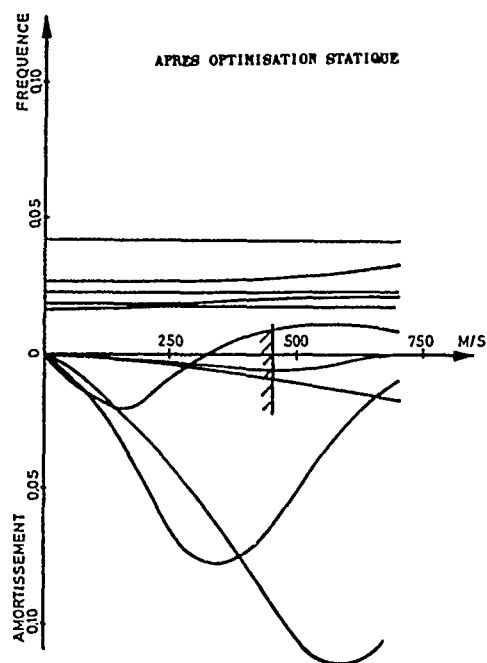


PLANCHE 15

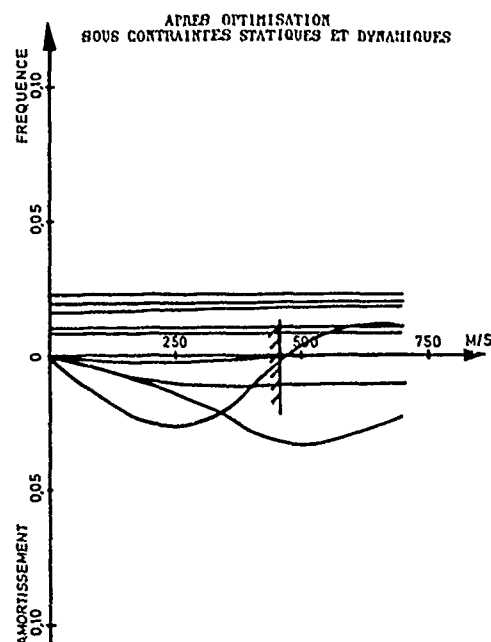
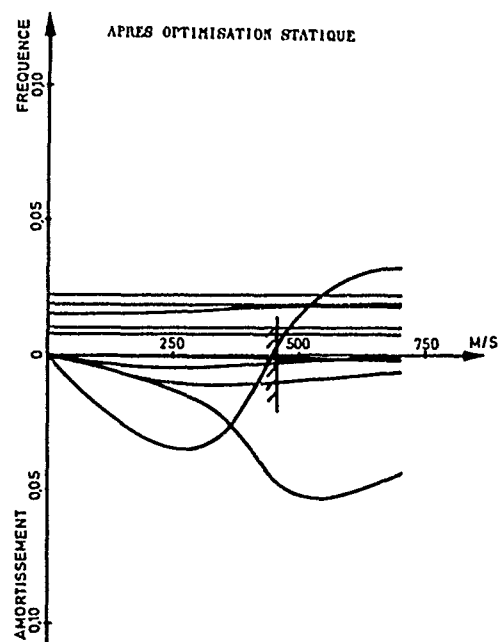
FLUTTER 'MOU' CONTROLE



CONFIGURATION 1

PLANCHE 16

FLUTTER 'REC'



CONFIGURATION 2

PLANCHE 17

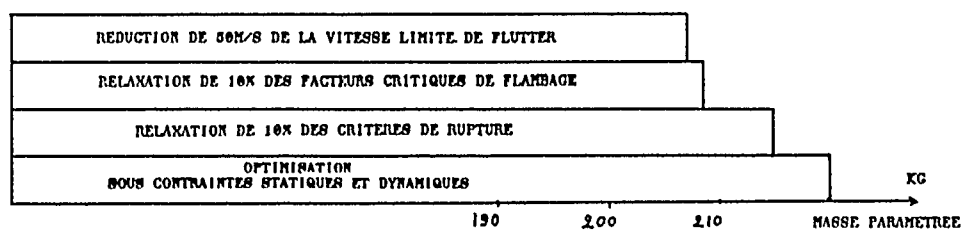
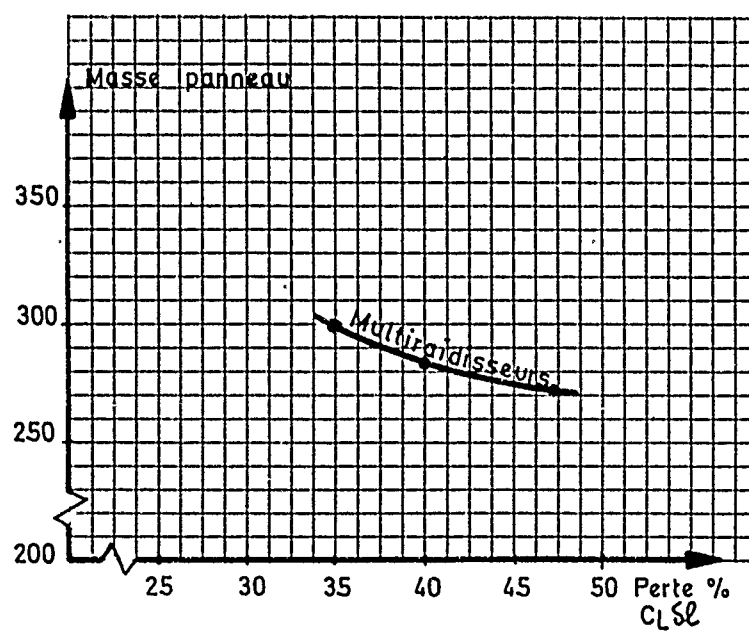
RECTIFICATION
INTERACTIVE

PLANCHE 18

EVOLUTION DES PERTES AEROELASTIQUES
EN FONCTION DE LA MASSE
APRES OPTIMISATION
SOUS CONTRAINTES STATIQUES ET DYNAMIQUES

AEROELASTIC CONSIDERATIONS IN PRELIMINARY DESIGNOF A MILITARY COMBAT AIRCRAFT

by

M. ORMEROD, Principal Dynamics Engineer

and

D. G. GIBSON, Senior Aerodynamicist

British Aerospace PLC
Aircraft Group
Warton Division, Warton Aerodrome,
Preston, Lancashire,
England.

ABSTRACT

This report gives an outline of the aeroelastic considerations taken into account during the early stages of a modern combat aircraft design. It describes the manner in which the aerodynamic performance requirements are balanced against what can be achieved by structural optimisation. At the same time, flutter characteristics are established in such a way that as many as possible of the design features that are potentially critical for flutter are identified.

It is shown that these procedures can produce structure that achieves the selected performance targets and give adequate fundamental (bending/torsion) flutter speeds. However, there are significant secondary effects associated with items such as tip missiles, control surface actuation and underwing stores that have to be treated carefully if meaningful design advice is to be given before the design is frozen.

1. INTRODUCTION

The overall objective is to ensure that the aircraft has adequate quasi-static aeroelastic properties for stability and strength, and does not flutter, within the required flight envelope. This is a continuing activity that keeps going throughout the life of the aircraft from initial project study through to the final release to service. During the early part of an aircraft development programme, the emphasis is placed very much on identifying potential aeroelastic problems. The sensitivity of the underlying mechanisms to changes in all uncertain parameters must then be established. It is important to ensure that the design recognises and reacts to these by setting appropriate formal requirements before the structural configuration is frozen. This report details the way in which we approach this task at BAe Warton.

The selection of static stiffness criteria is described for the various forms of surface. This is part of the basic sizing assumptions made in the configuration design process. The routine solution of the structure to satisfy these targets allows aerodynamic stability work and structural definition to proceed in parallel in the confidence that the design point requirements will be met.

Three methods of flutter assessment are described in the order that they are applied: the use of standard specifications and basic rules of thumb; automated structural optimisation procedures with flutter constraints; and direct flutter calculations. Some results from a recent combat aircraft flutter assessment are shown highlighting the different approach required in early project calculations to those needed for formal clearance demonstration.

2. QUASI-STATIC CONSIDERATIONS2.1 Fundamental Considerations

There are four major aspects of the design and performance of an aircraft that have a considerable influence on the required overall effects of quasi-static aeroelasticity.

These are not in order of importance but of complexity, figure 1 illustrates the overall effects of distortion under balanced conditions.

a) "Rigid Body" Stability

The changes in aircraft "rigid body" stability characteristics as a result of steady aeroelastic distortion, for example, the effect on pitch stability as a result of aerodynamic centre movement.

b) Aircraft Control

If the basic control powers are reduced by increasing dynamic pressure, there are two

16-2 possible consequences.

Firstly, the pilot may be unable to produce sufficient disturbance of the aircraft. In addition, and especially when active control technology is being used, the control system may also be unable to provide sufficient "shaping" of the aircraft response which results in undesirable motion, up to the level of actual loss of control.

c) Structural Strength Requirements

One outcome of (b) above is that with controls with low aeroelastic efficiencies (flex/rigid ratios) the amount of control deflection, in the aerodynamic sense, to provide the required rotation moments on the aircraft is increasing and obviously, with it, the amount of hinge moment applied to the surface, and control surface strength required.

d) Drag

There are both first and second order effects on aircraft drag.

There is the direct effect of the distortions due to applied loads for the trimmed aircraft which changes the aerodynamic loadings and produce direct changes in pressure distributions and hence in drag due to lift.

With significant structural distortion the direction of the resultant forces from the pressure distributions are also changed, with a consequent further change in the total drag force.

The basic objective throughout the evolution of the aircraft design is to minimise the adverse effect of structural properties on the aerodynamic performance and weight of the structure. In order to satisfy this requirement, criteria to be met have to be devised in order to provide both rational and reasonable constraints on the structural properties of the aircraft.

2.2 Constraints on Structural Properties

- a) Requirements - In the early design stages of an aircraft, the usual problem that effects all areas applies to the structural properties that is that with inadequate definition (because the configuration is being defined) the desired structural properties have to be designed in.

Fortunately, as a result of the advent of structural optimisation procedures, to obtain minimum weight structures, which are sufficiently reliable and economical for routine use, the task of controlling the aerodynamic effects of the structural properties appears to have become manageable, or at least reached the stage where the task appears reasonable.

- b) Derivation of Criteria - As in all design stages the task of setting adequate criteria is that of reconciling the desirable aims of perfection with the practical reality of simple straight forward criteria.

In particular, the fact that the end results required are for the total configuration and, in general, simple constraints that are independent of the rest of the configuration, are required to allow independent design of the pieces is a major consideration.

2.3 Application to lifting surfaces

We regard the lifting surfaces as falling into one of three categories, dependent on method of attachment and intended use. The three categories are:

- a) Spigotted all-moving tails - stabilisers attached to the aircraft by rotating spigot fitting with the whole surface used for control.
- b) Fully fixed tails - usually fins and rudders but horizontal surfaces with flaps also fall into this category.
- c) Wings - major lifting surface firmly attached to the fuselage.

Proceeding to consider these types in more detail, they have the following characteristics:

- a) Spigotted surfaces are, in general, sensitive to operating mechanisms flexibility, and not to actual panel flexibility and, as a result are sized to strength only criteria with an actuation/attachment stiffness requirement.

Figure 2 illustrates the basic properties of this type of surface.

- b) Fin (or horizontal tail) size is determined among other considerations, by the dual requirements of adequate stability and adequate control at high equivalent airspeeds.

To obtain this level of effectiveness, criteria for both sideslip and rudder angle loadings (for a fin) are set for a high Mach/high EAS point on the basis of previous achieved levels of efficiency, and the structure optimised to achieve this level of efficiency with fixation at a major rear fuselage frame.

This is possible, in general as a consequence of having both an identifiable load path from the fin to the main centre fuselage, and that load distribution does not materially affect the fin result. There is a complementary requirement for stiffness on the front fuselage which is also assumed in the sizing process. 16-3

Figure 3 illustrates the effects being balanced during the optimisation process.

- c) Wings in general have two important characteristics. They are attached to the fuselage over a significant length, Tornado and F111 being notable exceptions; and are required to provide both the aircraft speed and lift performance together with some roll control power from wing mounted flap or spoiler surfaces.

With "slender" aircraft, the shape of the wing under 'normal' acceleration is determined more and more by the way the aircraft is balanced by flaps and/or horizontal surfaces and the resulting longitudinal vertical displacement of the fuselage a definition that is not usually available when preliminary wing sizing is carried out. This indeterminacy has resulted in concentration on the antisymmetric requirements in that aileron roll power is an identifiable requirement where fuselage effects are not as large. The required roll effectiveness is derived from required "time to bank angle" manoeuvrability specifications. Calculation of aileron "effectiveness" (fixed root) still requires an assumption of fuselage effects and the roll damping effects. Current BAE practice is to use an optimisation based on steady roll rate, which allows the structure to trade damping efficiency for control effectiveness, in order to achieve the minimum weight structure, also because the damping and forcing moments are equal at the aircraft centreline, the effects of the wing attachment fittings flexibility on the stiffness required from the wing is minimised. Figure 4 illustrates the overall effects that the optimisation has to consider, and the way in which they may be exchanged. It should be noted that although similar to the cases used for the fin, damping loss is traded against flap loss, instead of a minimum efficiency for both effects. Conflict between this criterion and the requirement that exists for washout under high load, results in a choice being made on the selection of the more important criterion.

3. FLUTTER ASSESSMENT PROCEDURES

To meet the objectives, the methods employed must be rapid and flexible so that a wide range of structural configurations can be studied without prohibitive expenditure on manpower, and computer time. Three assessment procedures are available.

3.1 Previous experience

In general, the wide range of experience gathered throughout the world over the past 60 years or so has been distilled into requirement documents such as MIL 8870, and Av/P/970. These carry considerable weight with the procuring authorities and make a sensible base for early design advice. Typical examples are Control Surface rotation stiffness and backlash which are tightly specified. They ensure that actuator mechanisms with, for instance, complicated bell crank mechanisms are monitored very closely if not killed at birth.

Previous experience has also provided a set of simple rules of thumb which, in general, but not always, produce a design which is relatively free from flutter.

- a) Make everything as stiff as possible, although there may be some advantage in flexible underwing store pylons which could decouple the wing and store modes.
- b) Maximise bending/torsion frequency separation. This usually means aiming for high torsion stiffness.
- c) Although sweep, taper and aspect ratio are usually dictated by other considerations given the choice high values of the first two and a low value of the third are beneficial.
- d) Place all equipment close to the leading edge rather than the trailing edge. If rearward scanning sensors are required in, say, the trailing edge, try to compensate by mounting the control equipment etc on the leading edge.
- e) Ensure all underwing and wing tip mounted store cg's are kept as far forward as possible

Some of the older criteria based on ensuring that the torsion mode frequency is sufficiently high rarely work reliably for the low aspect ratio aerodynamic surfaces typical of modern combat aircraft.

3.2 Optimisation with flutter constraints

It is now possible to size aerodynamic surface structures using optimisation techniques that respect flutter criteria (Ref 1 for instance). These split the optimisation process into two parts. The first follows the traditional strength criteria yielding a first standard of structure. The second works to flutter criteria. These two procedures are followed iteratively until a structure satisfying both sets of requirements, results.

Although these procedures will be developed further, used more often and over a wider range of structural types in the future, care is required. Our experience suggests that:

- a) For typical combat aircraft wings with low aspect ratio, fixed root and trailing edge controls the strength/static aeroelastic designed wing has more than adequate fundamental bending/torsion flutter margins. Provided the simple frequency criteria for the control surfaces set by MIL SPEC/Av/P/970 are met, flutter associated with trailing edge flaps should also be avoided.

Thus, problems with the wing are most likely to occur for externally mounted stores. The specifications for most modern combat aircraft include a wide range of tanks and air-to-air missiles both underwing and on the wing tip. Often there are fall-out requirements for a large number of air-to-ground stores. The computing time and costs alone preclude the use of current optimisation methods to cover all the possible combinations of these stores.

- b) For all moving tailplanes, fins and foreplanes controlled by hydraulic actuators, flutter can be a serious problem. Our limited experience of using structural optimisation routines with flutter constraints in a case such as this has lead to the following tentative conclusions.

The flutter mechanisms involved are sensitive primarily to mass changes on the surface structure and stiffness changes in the actuation system or the mounting spigot. MIL SPEC and Av/P/970 already require high values of mounting stiffness and it is difficult and costly to increase these significantly. Thus the only realistic parameter that is available is mass balance. This can be specified more economically via direct flutter calculations - see below.

Flutter derivatives (rates of change of flutter speed with mass and stiffness) must be treated with caution. Figure 5 shows an example of a tailplane flutter where the initial set of flutter derivatives indicate that mass should be concentrated the leading edge tip. However, even relatively small changes in mass at this point give subtle changes in the mode shapes and thus change the flutter coupling mechanism. In the end, the most weight-effective solution was to add a large concentrated mass at a point that initially had negative derivatives.

- c) The strength/static aeroelastic requirements for a fin rudder give a different overall stiffness distribution to the wing. In general the flutter margins are lower than the wing but are still adequate.

Thus, although formal optimisation procedures with flutter constraints should ensure that severe basic bending torsion flutters do not occur they are unlikely to change significantly the design of the fundamental torsion box structure.

Furthermore, uncertainties associated with crucial parameters such as control surface actuator impedance and transonic unsteady aerodynamics mean that the results cannot be taken at face value. Sensitivity studies, as described below, are still essential.

3.3 Specific Flutter Assessment

Modern computing capacity and speed is such that the complex calculations associated with flutter assessment can now be conducted quickly and reasonably accurately. It is still not possible to do a full flutter investigation covering all required aspects of the design, but by careful formulation of procedures and selection of configurations and conditions, insight into the mechanisms can be gained. This allows meaningful conclusions to be drawn and useful design advice to be given. We use the following procedures, believing that they form an adequate base for this.

- a) For the structure, the routines used to generate the structural sizes during the strength/stiffness optimisation process also yield a full stiffness matrix and structural mass distribution for the primary and secondary aerodynamic surfaces. This structure is broken down into sub-structures and then put into a branch mode form such that parameters that are known to be flutter sensitive or are uncertain are isolated and can be easily changed.
- b) "Discrete Load Modes" (ref 2) are included where local structural distortions are likely to play a significant part in the coupling between branch items (wing/pylon interface, for instance).

If the structural components are represented in this way the unsteady aerodynamic forces need only be generated once for each Mach number.

- c) Unsteady Aerodynamic calculations are limited to one subsonic and one supersonic Mach number ($M = 0.8$ and $M = 1.2$). Flutter investigations are limited to S.L. conditions only. Reductions in flutter speed from transonic effects are taken into account by an additional factor of 1.1 on the required flight envelope speed terms in the Mach number range 0.8 to 1.2 (e.g. fig 6).
- d) The unsteady aerodynamics for underwing stores are omitted. However, the tip missile

165
16-5

aerodynamics must be included. These can be generated quickly and with sufficient accuracy in the following way:

Extend the wing out to the outer surface of the tip missile in the basic wing aerodynamic calculation and factoring the resulting aerodynamic lift forces on the extended area to zero. Add in measured or calculated aerodynamic forces for the rigid missile. Comparison with wind tunnel measured values for the F5 (ref 3) showed reasonable agreement.

- e) Flutter calculations are made in general at constant frequency parameter. Computer programs have been developed which calculate the variation of modal frequency and damping with different structural parameters as well as with airspeed. We also use extensively the root-following routines of Baldock and Niblett (ref 2). This allows us to derive flutter speed contours for a wide range of structural stiffness, mass, inertia and c.g. parameters.

We have applied this procedure during a recent combat aircraft study.

3.4 Results

- a) Wing - For the wing the branch modes chosen included torsion box primary modes, two trailing edge flap rotation modes, fixed hinge flap modes, tip missile pitch wing/pylon "discrete load modes" and fixed root pitch and roll modes for each underwing pylon. Unsteady Aerodynamics were calculated for wing, flap rotation, flaps, discrete load and tip missile modes only.

Basic flutter speed calculations indicated that for nominal parameter values, no flutter problems were expected for the clean wing (fig 2). Root following routines were used to plot flutter contours for inboard and outboard flap stiffnesses (fig 7). These show clearly that margins are high over all reasonable combinations - Note, as expected, zero actuator stiffness gives a severe flutter - a serious problem if the actuator fails or if there is significant backlash.

If the tip missile is included, then basic bending/torsion flutter speeds reduce markedly. There are two sources: (1) the inertia of the store reducing the fundamental torsion mode frequency, and (2) the presence of the missile strengthens the wing tip aerodynamics (fig 8a). Again the root following routines were employed this time to assess the trade off between tip missile attachment stiffness and the missile fore/aft c.g. position (fig 8b).

When underwing stores are added, the large number of possible combinations of stores precludes a full assessment of each. However, a baseline set of configurations representing the most important configurations and covering a reasonable range of mass and c.g. were chosen. Flutter studies again concentrated on understanding fundamental coupling mechanisms and establishing sensitivities. Figure 9 shows typical combinations of parameters that could give serious problems.

- b) Fin/Rudders - For the fin, the structural model was set up with branch modes representing the primary torsion box, rigid rudder rotation and the rudder. Basic bending torsion flutter is well outside the required flight envelope but a coupling between the 3rd primary mode and the rudder mode is potentially a problem (fig 10). The flutter is not sensitive to realistic changes in actuator stiffness (fig 11). Bearing in mind uncertainties about transonic effects, this flutter would require very careful monitoring.

Actuator failure (to zero or very low stiffness) results in a mild low speed flutter.

Neither of these problems can be easily cured by realistic levels of mass balance. The flutters are relatively mild however and could be cured by the addition of extra damping in the rudder rotation mode.

- c) Foreplane - For the foreplane, the branch modes used included fixed root modes for the main structure and two rigid foreplane modes-spagot rotation and spagot bending. Contour plots of flutter speed against spagot bending and rotation stiffness indicates immediately the importance of the rotation mode and hence sensitivity to actuator impedance and attachment stiffness (fig 12).

Studies of the effect of mass balance show that the optimum position is at the tip leading edge.

3.5 Design Recommendations

Based on the detailed results obtained from these calculations, a re-issue of design requirements can be made. In this case specific requirements were issued for:

- (a) Control surface actuator impedance and local attachment structure stiffness for the wing flaperons, foreplane, and rudder. In general these confirm the requirements of MIL SPEC and Av/P/970.
- (b) Tip missile c.g. position. This was chosen (from fig 8) so that the flutter became independent of local attachment structure stiffness.
- (c) because of doubts about the transonic behaviour of the rudder and flaperons, space provision was recommended for rotary dampers.

(d) Provision only for up to 4 Kg mass balance in the foreplane.

(e) Underwing store c.g. position and pylon stiffness values.

4. CONCLUSIONS

The availability of powerful modern computers allows the simultaneous consideration of strength, static aeroelastic, and flutter in a structural optimisation process during the early design phase of an aircraft.

- a) The availability of structural optimisation procedures including quasi-static aeroelastic constraints has increased dramatically the confidence in being able to achieve particular aero structural properties.
- b) The most immediate increase in knowledge of techniques are required in the sphere of setting criteria for aero-structural properties that represent simply the total restraints that are desired to be applied. To put it another way, exploration of the best way to apply the possible, in order to achieve the desirable.
- c) Present work and capability is mainly applied to the case of obtaining the best aero-structural results from a particular configuration. Considerable exploration seems necessary in order to optimise the configuration at the stage before a finite structural definition is possible.
- d) The strength and static aeroelastic requirements for a modern combat aircraft structure are such that coupling between fundamental bending and torsion modes is unlikely to cause serious fundamental flutter problems for the basic fixed-root wing, fin or tailplane/foreplane. Problems are more likely for all-moving surfaces, controls and externally mounted equipment. In these cases, the flutters are sensitive to parameters that are difficult to specify precisely in the early stages of an aircraft development. Transonic effects are imperfectly understood and cannot be predicted with confidence. Nevertheless, modern computing methods, speed and access mean that a substantial appreciation of flutter characteristics can now be gained quickly and economically. These can be used to identify potential coupling mechanisms, and their sensitivity to uncertain parameters. Appropriate design requirements can then be set. Where significant doubts remain, a full ground and flight test programme can be planned.

REFERENCES:

1. Structural Optimisation of Advanced Aircraft Structures
12th ICAS Congress Meeting - October 1980
2. Calculation Methods for the Flutter of Aircraft Wings and
External Stores
Ll. T. Niblett and J. C. A. Baldock - AGARD-CP-162 - 1974
3. Transonic Wind Tunnel Tests on an Oscillatory Wing with
External Stores
H. Tijdeman et al - AFFDL-TR-78-194 - December 1978

QUASI-STATIC AEROELASTIC DISTORTION

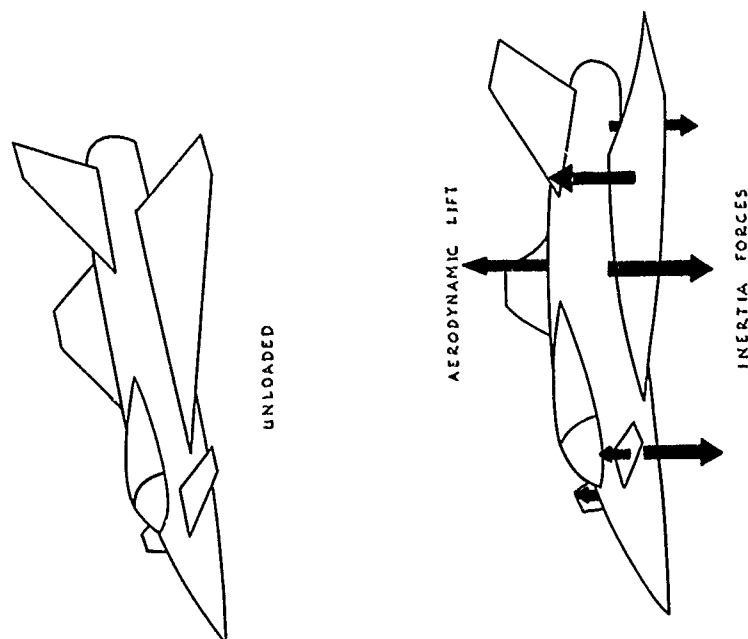
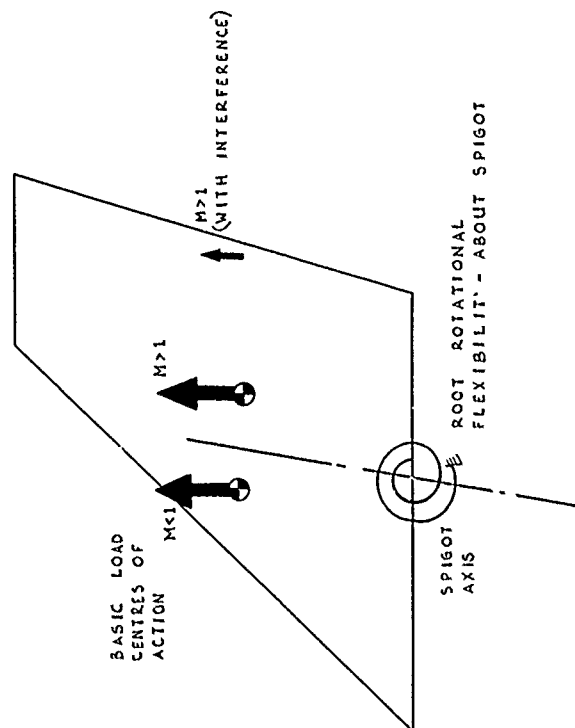


FIG 1

FIG. 2

ALL MOVING SURFACE (SPIGOTTED)

BASIC LOAD CASES FOR STIFFNESS:-
AIRCRAFT INCIDENCE - ANGLE OF ATTACK
OR PANEL ROTATION.



AEROELASTIC PROPERTIES DOMINATED
BY ACTUATION SYSTEM STIFFNESS
MODIFIED BY PANEL STIFFNESS PROPERTIES.

FIG 4

WING

STIFFNESS LOAD CASE:-
AILERON REACTED BY ROLL RATE (DAMPING)
TO EXCEED A TARGET VALUE OF ROLL RATE.

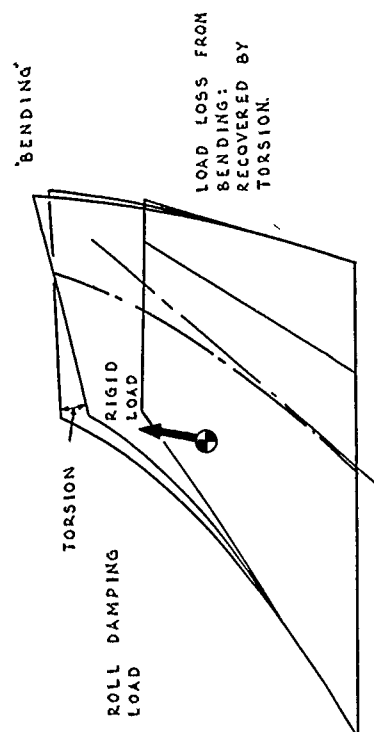
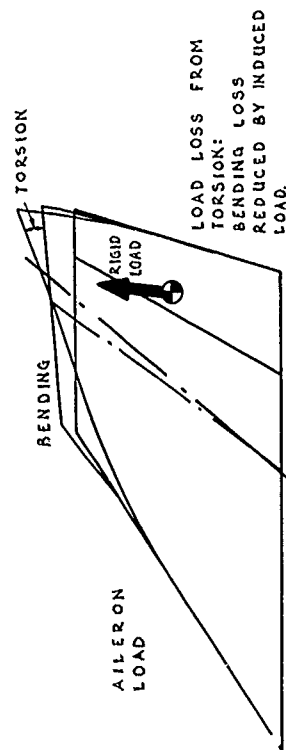


FIG 3

FIXED FIN OR TAILPLANE

BASIC LOAD CASES FOR STIFFNESS (FIN) :-

SIDESLIP ANGLE } EFFICIENCIES
RUDDER ANGLE } \gg TARGET VALUE

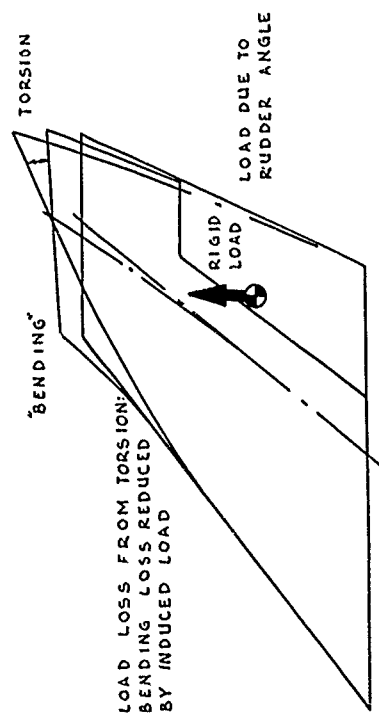
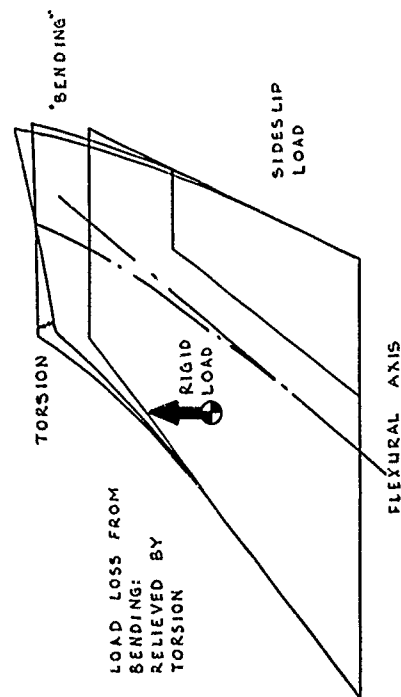


FIG 5

MASS BALANCE OPTIMISATION ON AN ALL-MOVING TAILPLANE

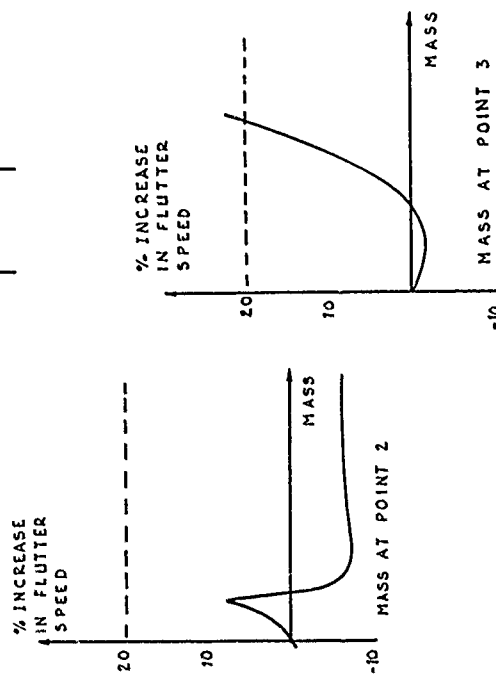
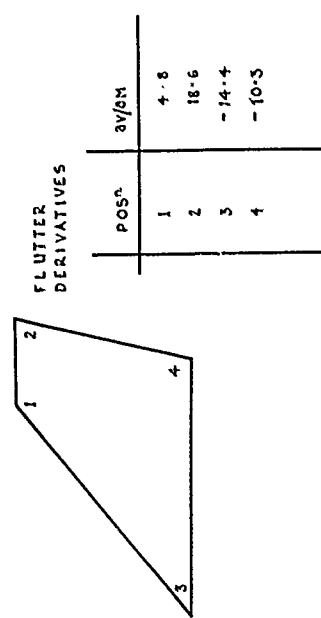


FIG. 6

CLEAN WING FLUTTER

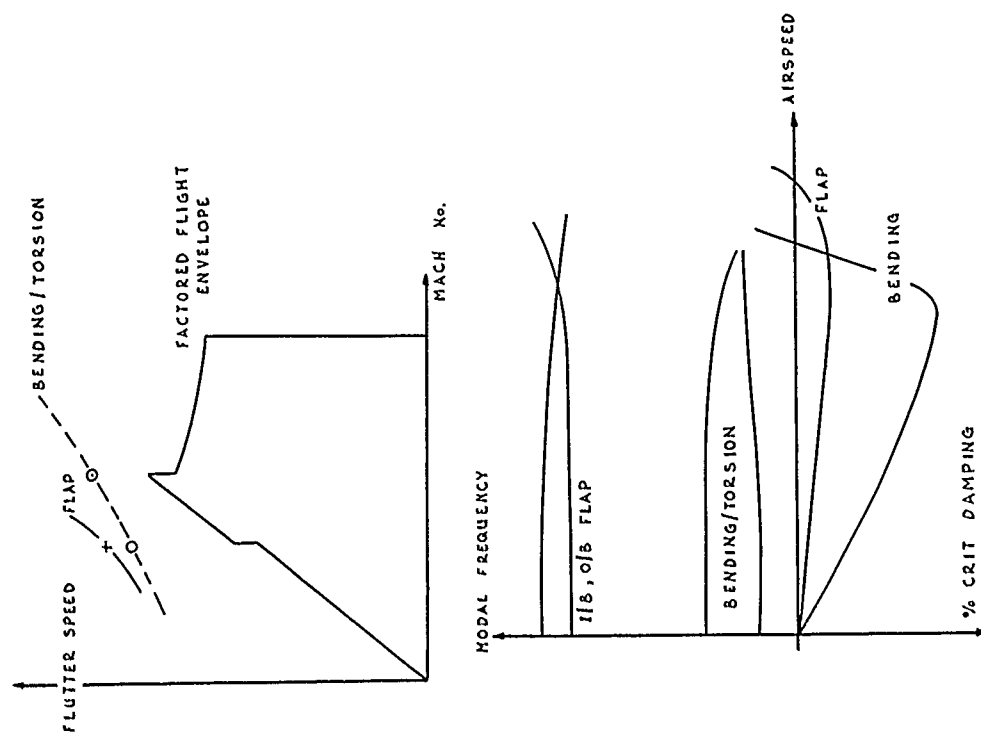


FIG. 8

WING FLUTTER WITH TIP MISSILE

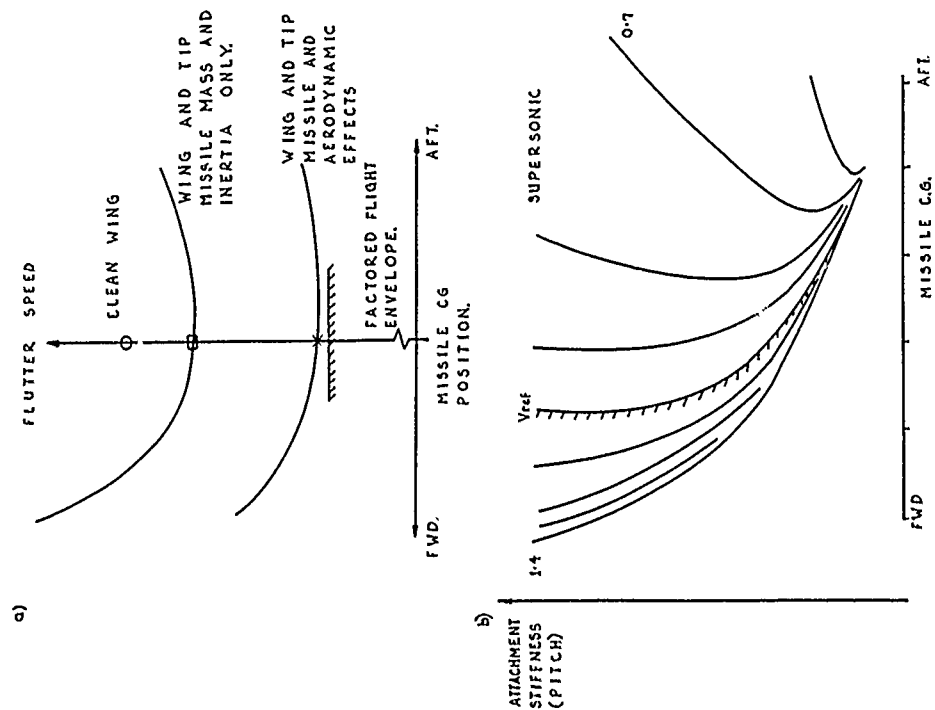


FIG. 7

EFFECT OF ACTUATOR STIFFNESS

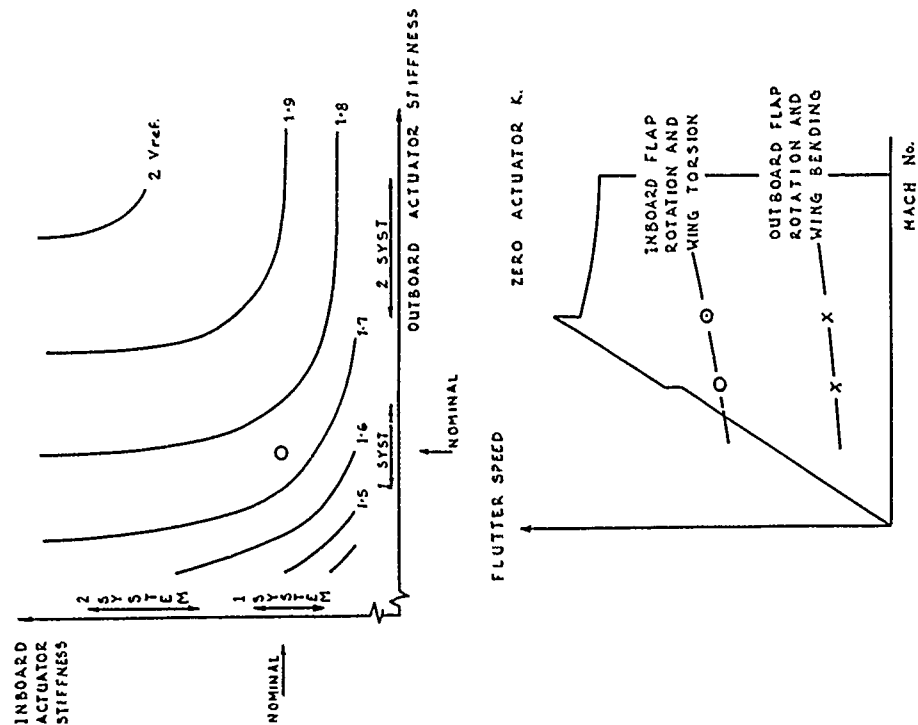


FIG. 10

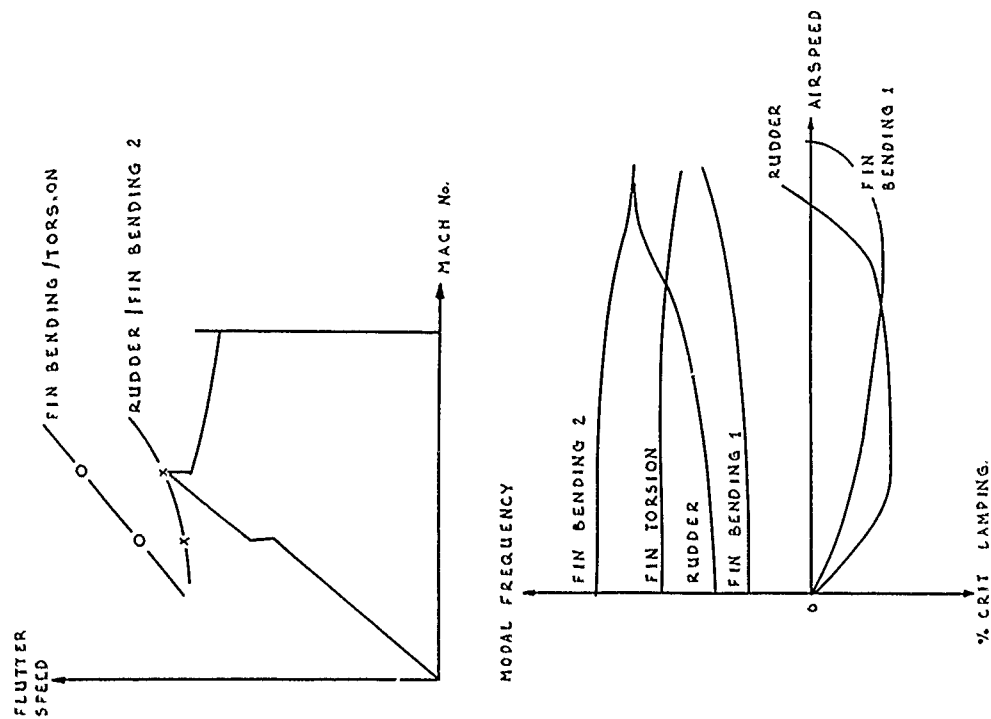
FIN FLUTTER

FIG 9

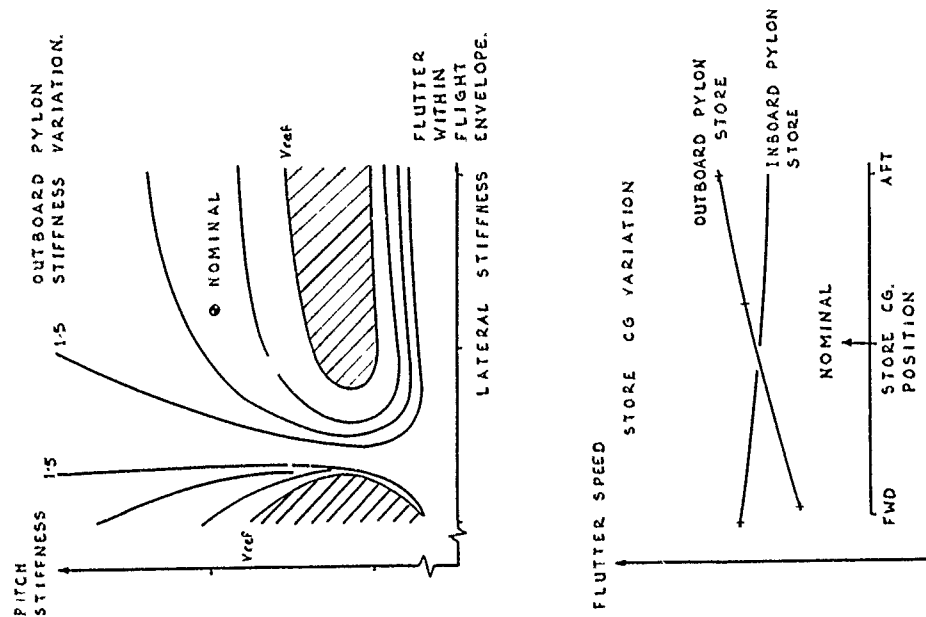
UNDERWING STORE FLUTTER

FIG. 12

ALL MOVING FOREPLANE FLUTTER

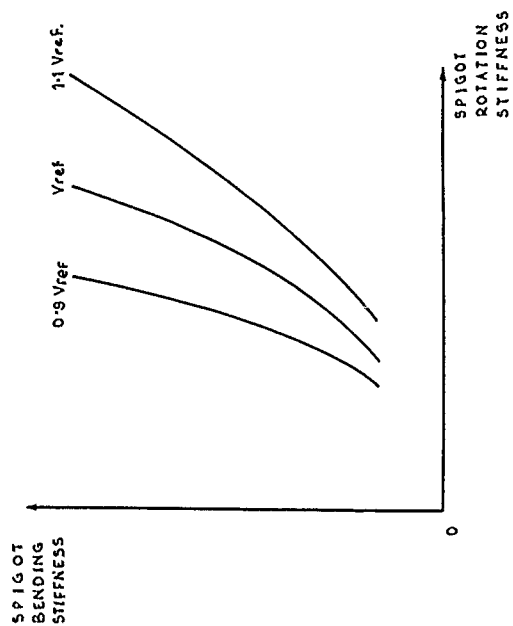
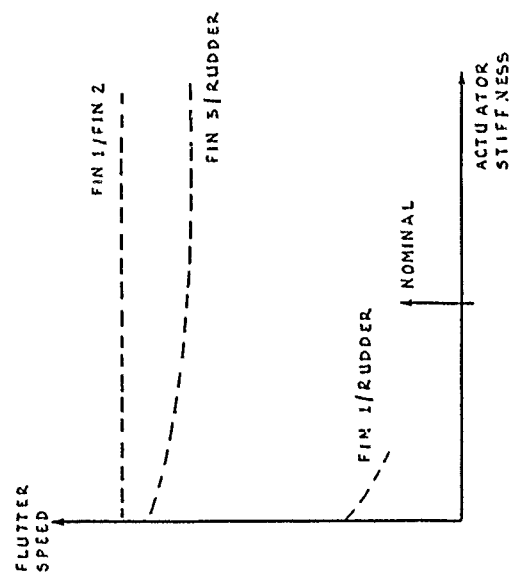


FIG. 11

EFFECT OF RUDDER ACTUATOR STIFFNESS



PRELIMINARY DESIGN OF AIRCRAFT USING STRUCTURAL
OPTIMIZATION METHODS

by

H. Gödel
G. Schneider
H. Hörnlein

Messerschmitt-Bölkow-Blohm GmbH.
Airplane Division
P.O. Box 801160, 8000 Munich 80
W.-Germany

SUMMARY

Weight minimized surfaces of a modern high performance aircraft have to fulfil statical, dynamical and aeroelastical requirements such as high manoeuvrable aircraft, high control surface effectiveness, no flutter in the mission domain. To meet these requirements it is necessary to improve the optimization procedures and applicate them even in the preliminary design phase of an aircraft to become acquainted with the influence of the main design parameters.

The presented paper deals with the activities at MBB in the field of structural optimization.

The theoretical background of the optimization will be described with special regard to the constraints such as stresses, deflections in conjunction with control surface effectivenesses, flutter speed and side limits. Flutter speed optimization is based on an optimality criterion including physical facts whereas for the other constraints mathematical programming procedures are used.

By means of well-known test examples, a vertical tail structure and a simplified wing structure the capabilities of the applied optimization program systems are shown and results are presented.

INTRODUCTION

Computer program systems for both structural analysis and optimization of flexible aerodynamic surfaces are in use already for some years. These programs enable the design engineers to do quite complex investigations even in the preliminary design phase of an aircraft. A great deal of automated methods for analyzing airframe structures for strength and aeroelastic behaviour have been developed. Many analysis programs are being supplemented with automated resizing procedures. Making practical use of this structural optimization technology, it is necessary to have some kind of interdisciplinary structural design analysis system. Highly manoeuvrable fighter aircraft will be strongly influenced by advanced technologies in structures, aerodynamic configurations and digital control systems. The design of advanced digital flight control systems needs an excellent knowledge of the elastic behaviour of the aircraft such as elastic derivatives, control surface effectivenesses and vibration modes.

The structural optimization procedures are based on a given aerodynamic and structural concept. The aeroelastic efficiency of a thin wing-flap structure is the result of the interaction between these two disciplines. The main advantage of this kind of complex structural analysis is the handling of aerodynamics, loads, structural analysis and aeroelasticity simultaneously, to get quickly numerical results for the first design phase. Optimization procedures are also used to obtain trend information for further development.

NEW AIRCRAFT DESIGN CONCEPT

The primary objective of new fighter aircraft design studies is to improve transonic and supersonic performance. For aeroelastic considerations, it is very important to know new aerodynamic design as well as structural design concepts.

Aerodynamic Design Concept

A very interesting paper about "Transonic Fighter Design Using Numerical Optimization" has been reported by P.V. AIDALA [1]. The preferred aerodynamic design concept is very similar to the aircraft design shown in Fig. 1.

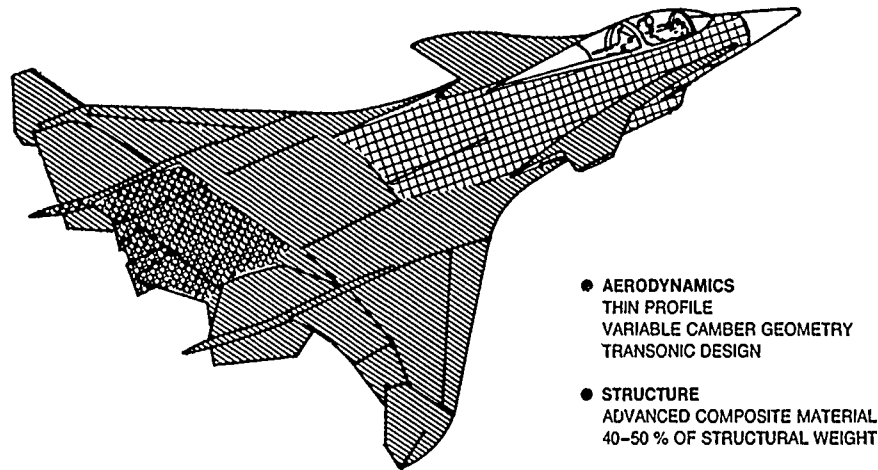


FIG. 1 NEW FIGHTER DESIGN CONCEPT

A wing-body-canard configuration promises to meet the performance requirements, specified at supersonic cruise speed and at a transonic cruise and manoeuvre speed of about Mach 0.9. The wing design employs screwed-hinge variable camber geometry to provide appropriate wing section slopes at different flight conditions. It should be mentioned that most of the aerodynamic design analyses are performed with the assumption of a rigid structure. No aerodynamic changes to wing box twist are assumed.

The structural design of a variable camber wing has important aerodynamic design constraints. For instance, profile thickness, required leading and trailing edge flaps geometry are limitations for the wing box geometry. Now, the structural designer has to fulfil both strength and stiffness requirements under special regard to a minimum weight design.

Structural Design Concept

Many investigations about structural design concepts for new fighter aircraft have been presented in different papers [2], [3]. The objective of these studies was to define the benefits of the application of advanced composite materials. During the last ten years a growing usage of composite structures is obvious. For example, on the F-15 1% of its structural weight is composite material, the F-18 has 9.5% composites, and the YAV-8B V/STOL has almost 19% composites. Advanced composites may comprise 40-50% of the structure of future military aircraft. Beyond the weight and cost-reduction benefits obtained by substituting advanced composites instead of conventional materials, structural performance benefits can be realized from the increased ability to tailor a structure to meet different design requirements. The use of anisotropic composite material with special fibre orientation angles provides a coupling between the strains ϵ_x , ϵ_y and ϵ_{xy} . The structural behaviour due to certain fibre angle orientations is tried to show in a global way in Fig. 2. The acquaintance with the relations between airloads and the change of the angle of attack as well as camber angles is necessary solving aeroelastic problems.

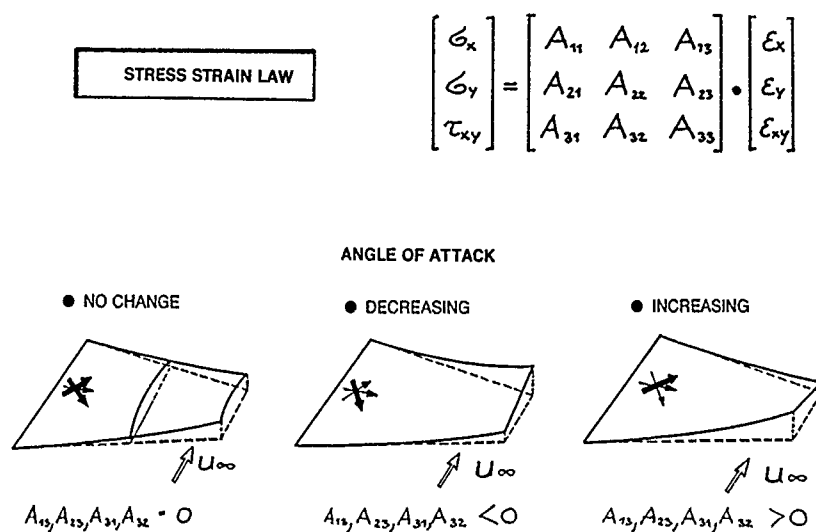


FIG. 2 BEHAVIOUR OF COMPOSITE MATERIAL

STRUCTURAL OPTIMIZATION

A historical review of structural optimization technology and a discussion of methods available in the industry is given in an excellent paper [4] of W. LANSING, E. LERNER and R.F. TAYLOR. It is shown that algorithms for addressing strength and flutter requirements are developed for practical use. The fully stressed design has shown to be a valuable approach to efficient structural design with a large number of elements. Analytical flutter velocity derivatives are used in the development of large scale strength and flutter optimization procedures. In the following two optimization program systems will be described. The first one is the program system ASAT which is an extended version of the well-known program FASTOP. An application is demonstrated in Reference [5]. The second program system is the aeroelastic tailoring and structural optimization procedure TSO.

Structural Optimization by ASAT

A computer software system called ASAT (Automatische Struktur Auslegung von Tragflächen) exists at MBB which allows an automatic design of minimum weight structures. During a cooperation program in 1977 with the U.S. Air Force Flight Dynamics Laboratory, the FASTOP computer system has been received by MBB in exchange for computer programs developed by MBB. During last years the structural dynamic group has further refined this program, by adding a static aeroelastic part to it and has also improved the optimization procedure concerning deflection constraints. This new system is now called ASAT. The program system ASAT consists of several modules such as

- static load and weight calculation (ALAM),
- deformation and stress analysis based on a finite element system (ASAM),
- vibration calculation (AVAM),
- unsteady aerodynamic forces and flutter analysis (AFAM),
- optimization procedures to meet stress, deflection and flutter constraints (ASOM, AFOM),
- transformation procedures to handle different types of grids (ATAM), see Fig. 3.

The static aeroelastic module (AEP) has been developed for recalculations of the static loads which depends on elastic deformations, too. For static analysis the so-called nodal stress method is implemented in the ASAM module. This method enables the optimization engineer to perform static analyses with a rather crude grid and element system which may have an important time saving effect in the preliminary design phase. In the following the properties of optimization constraints are discussed and some equations are given.

17-4

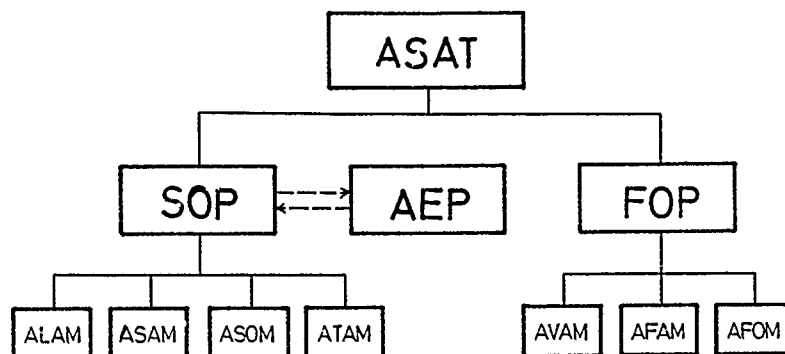


FIG. 3 FLOW CHART OF PROGRAM SYSTEM ASAT

The specialist who is engaged in structural optimization problems at first has to decide the objective function and the design space. Considering optimization using the ASAT program system the weight of the structure will be considered as the objective function. For discussion of possible design variables a design parameter hierarchy is mentioned in the publications of SCHMITT/MALLET [6] and SHEFFEY [7]. The program system in mind is able to resize finite element thicknesses or cross-section areas, only. Optimization of geometry, topology or structure types is of much higher level as optimization of dimensions.

The design variables X_i , $i \in N := \{1, \dots, n\}$ of the n elements describe the whole structure $X \in \mathbb{R}^n$. All other parameters remain unchanged during the optimization process.

The aim of the optimization task is to minimize the weight (W) of the structure whilst taking into account constraints such as stresses (σ), deflections (δ), flutter speed (V_f) and side limits (\underline{x} , \bar{x}).

$$\begin{aligned} &\text{Minimize } W(x) \\ &\text{Subject to } x \in M \quad (\text{domain of feasible design}) \end{aligned} \quad (1)$$

$$\text{where } M := \{x \in \mathbb{R}^n \mid \sigma(x) \leq \tilde{\sigma}, \delta(x) \leq \tilde{\delta}, \tilde{V}_f \leq V_f(x), \underline{x} \leq x \leq \bar{x}\}$$

$$\sigma: \mathbb{R}^n \rightarrow \mathbb{R}^{p \times l}, \quad \delta: \mathbb{R}^n \rightarrow \mathbb{R}^{q \times l}, \quad V_f: \mathbb{R}^n \rightarrow \mathbb{R}_+$$

$$\begin{aligned} p & \text{ number of stress constraints} & P &:= \{1, \dots, p\} \\ q & \text{ number of deflection constraints} & Q &:= \{1, \dots, q\} \\ l & \text{ number of load cases} & L &:= \{1, \dots, l\} \end{aligned}$$

The objective function is a linear function of the design variable x . Because of the bijective relation $m_i = \sum_j s_{ij} t_j$ the variable x_i can represent the weight $x_i := m_i$ or the dimension of the element $x_i := t_i$

$$W(x) = \begin{cases} \sum_{i \in N} s_i t_i = \langle s, t \rangle & \Rightarrow \nabla W = s \in \mathbb{R}^n \\ \sum_{i \in N} m_i = \langle 1, t \rangle & \Rightarrow \nabla W = 1 \in \mathbb{R}^n \end{cases} \quad 1 := (1, 1, \dots, 1) \quad (2)$$

All constraints are highly non-linear functions of the design variable x , however, efficient and well-known solution procedures are available for the analyses.

In the last years optimization procedures have been established which can be divided into two groups. On the one hand procedures have been developed on the basis of "optimality criterion" [8], [9], [10]. For this kind of optimization physical facts of the constraints have to be included. On the other hand methods called "mathematical programming" are used. However, both groups have obtained comparable results. The state of the art might possibly be described as undecided. The program system ASAT contains three different types of redesign formulae which belong to these two groups.

For the stress constraints the classical stress ratio method (SRM) is used.

$$t_i^{v+1} := t_i^v \cdot G(t^v) / \tilde{\sigma}_i \quad ; \quad i \in N, \quad v = 1, 2, \dots \quad (3)$$

RAZANI [11], POPE [12] and others have shown, that the "best" fully-stressed design (FSD) - if it exists [13] - can be close to the true minimum weight design. The high rate of convergency is the most important advantage using this procedure and the main reason for application.

For deflection constraint handling the so-called deflection gradient method (DGM) has been developed by MBB and implemented in ASAT. Starting with a given structure \bar{t}^v the scaling factor $\beta := \max \{ \delta_i(\bar{t}^v) / \tilde{\delta}_i \mid i \in Q \}$ applied to the structure provides a new structure $t^v := \beta \cdot \bar{t}^v$. With the parameter p_R the structure t^v will be relaxed to $t_R^v := (1 - p_R) \cdot t^v$ and the relation $\delta_i(t_R^v) \leq \tilde{\delta}_i, i \in Q$ gives the set of violated constraints $QR \subset Q$, which is used in the next resizing step, see Fig. 4.

$$\bar{t}^{v+1} := t^v + \Delta t^v \quad ; \quad v = 1, 2, \dots \quad (4)$$

In order to compute the iteration step Δt^v the constraints $\tilde{\delta}$ will be more limited by the parameter $p_s \Rightarrow \tilde{\delta}^s := (1 - p_s) \tilde{\delta}$. Using the linearized deflection function $\delta_i(t) \approx \delta_i(t^v) + (t - t^v)^T \nabla \delta_i(t^v)$ the modified constraint $\tilde{\delta}_i^s$ will be fulfilled by gradient travel. $t_\alpha := t^v + \alpha_i \nabla \delta_i(t^v)$. This results in

$$\delta_i(t^v) + \alpha_i \|\nabla \delta_i(t^v)\|^2 \leq \tilde{\delta}_i^s \Rightarrow \alpha_i, \quad i \in QR \quad (5)$$

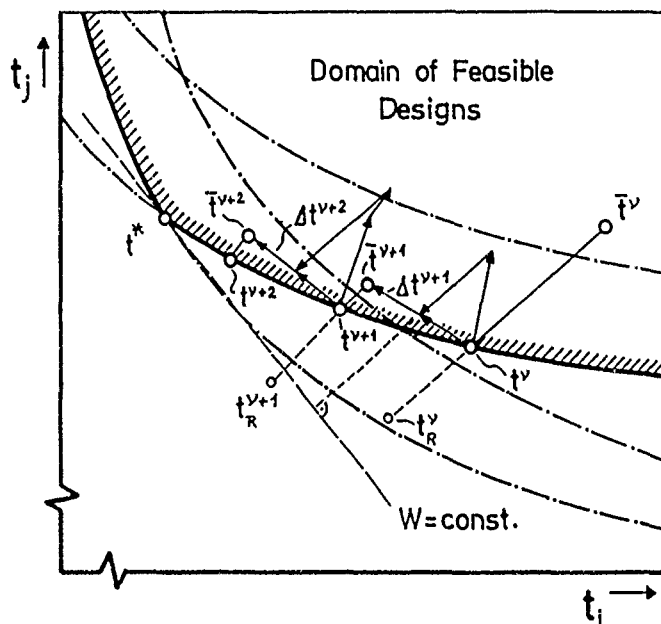


FIG. 4 GENERAL OPTIMIZATION PROGRESS

The combined gradient step

$$g^v := \sum_{i \in QR} \alpha_i \nabla \delta_i(t^v) \quad (6)$$

leads to a structure which fulfils $\tilde{\delta}^s$. Changing the structure in steepest descent direction $(-\nabla W)$, a lower weight will be obtained. So we can write

$$\Delta t^v = \lambda (g^v - \gamma \nabla W) \quad (7)$$

17-6

where $\gamma = \|\nabla W\|$, and α controls the step size. Step size controlling becomes very important and the influence on the optimization convergence increases if we have no convex progress of the constraints. Even for a two bar truss under normal loading and normal deflection constraints step size controlling is necessary, see Fig. 5.

To prove the usefulness of the implemented deflection gradient method some well-known examples have been investigated and results are depicted in Fig. 6, 7 and 8. It can be seen that this method provides comparable results. Comparison data of the examples are available from [14] and [15].

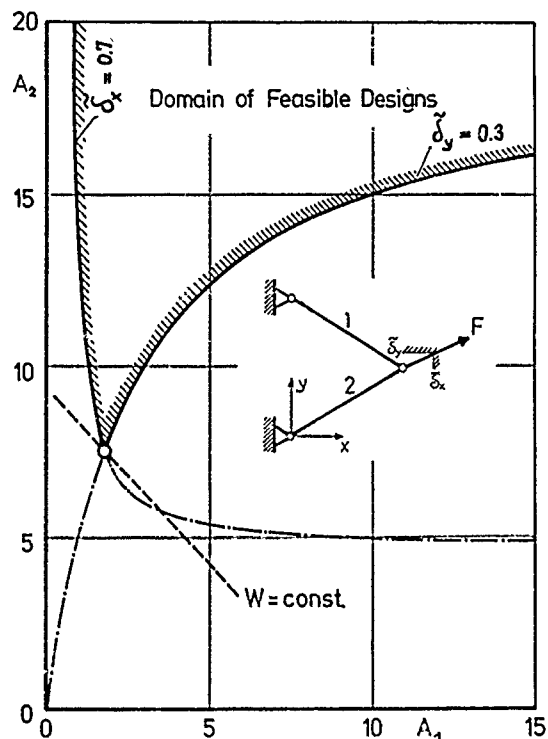


FIG. 5 DEFLECTION CONSTRAINTS ON A SIMPLE TWO BAR STRUCTURE

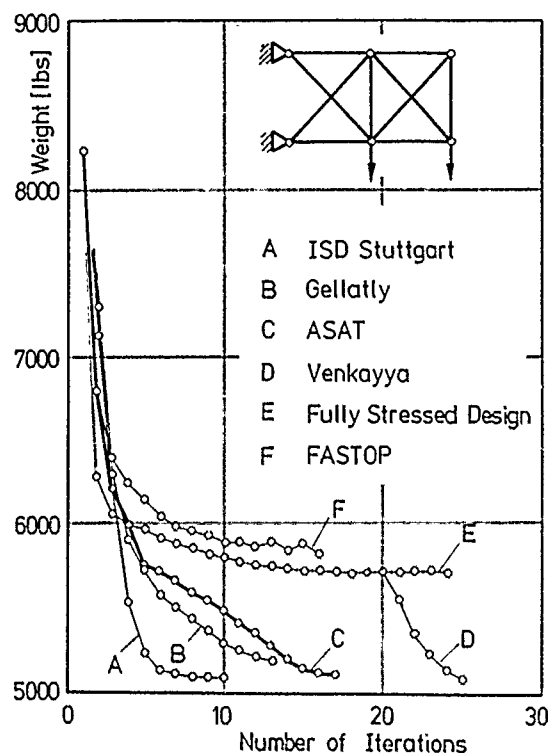


FIG. 6 COMPARISON OF OPTIMIZATION METHODS APPLIED TO A STRESS AND DEFLECTION CONSTRAINED TEN BAR TRUSS

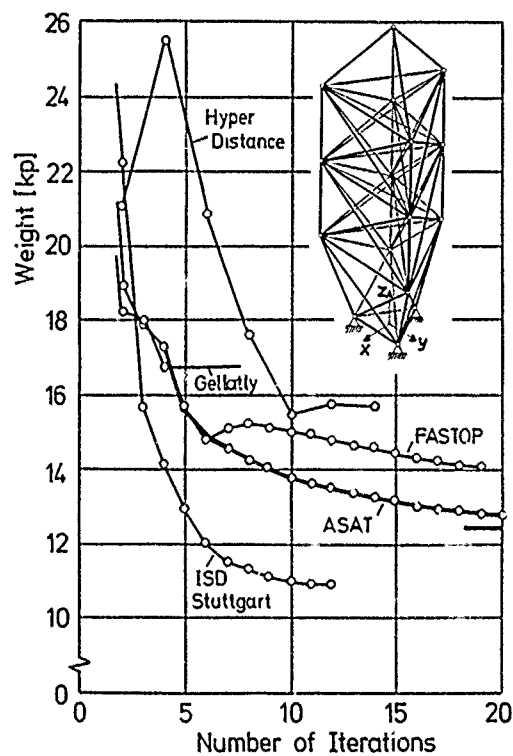


FIG. 7 COMPARISON OF OPTIMIZATION METHODS APPLIED TO A STRESS AND DEFLECTION CONSTRAINED SATELLITE STRUCTURE

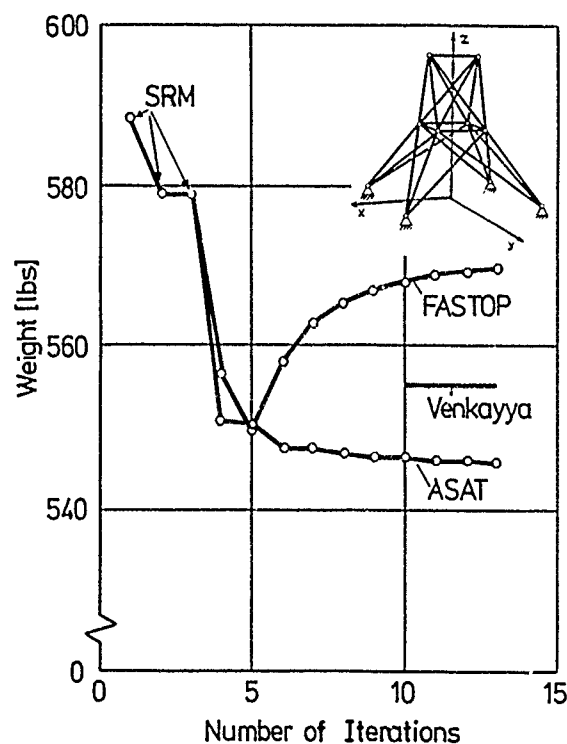


FIG. 8 COMPARISON OF OPTIMIZATION METHODS APPLIED TO A STRESS AND DEFLECTION CONSTRAINED TRANSMISSION TOWER

For optimization with special regard to flutter speed constraint the so-called velocity derivative ratio method (VDRM) is applied. The VDRM is a typical method of the kind of optimality criterion. The optimality criterion

$$\partial V_f(m^*) / \partial m_i = \text{const} ; i \in N \quad (8)$$

results immediately from the KUHN-TUCKER relation. Extensive comparisons made in [16] resulted in the redesign formula of the VDRM

$$m_i^{v+1} := m_i^v \left(\frac{\partial V_f(m^v) / \partial m_i}{(\partial V_f / \partial m_i)_{\text{target}}} \right)^{1/2} ; i \in N, v=1,2,\dots \quad (9)$$

The target velocity derivative $(\partial V_f / \partial m_i)_{\text{target}}$ will be found iteratively using

$$\Delta V_f \doteq (m^{v+1} - m^v)^T \nabla V_f(m^v) ; v=1,2,\dots \quad (10)$$

and $|\Delta V_f - \Delta V_{f \text{ des}}| < \Delta \quad (11)$

where $\Delta V_{f \text{ des}}$ represents a desired gain of flutter speed, and Δ stands for a chosen accuracy. The formulae for the calculation of the flutter velocity derivatives are deduced in the publication of RUDISILL and BHATIA [17]. In order to illustrate the optimization procedure in view of stress and flutter constraints a simplified structural model was chosen [5], see Fig. 9. The surface is cantilevered, the thickness to chord ratio is constant 5%, two aerodynamic load cases were defined. The optimization process is best explained by Fig. 11.

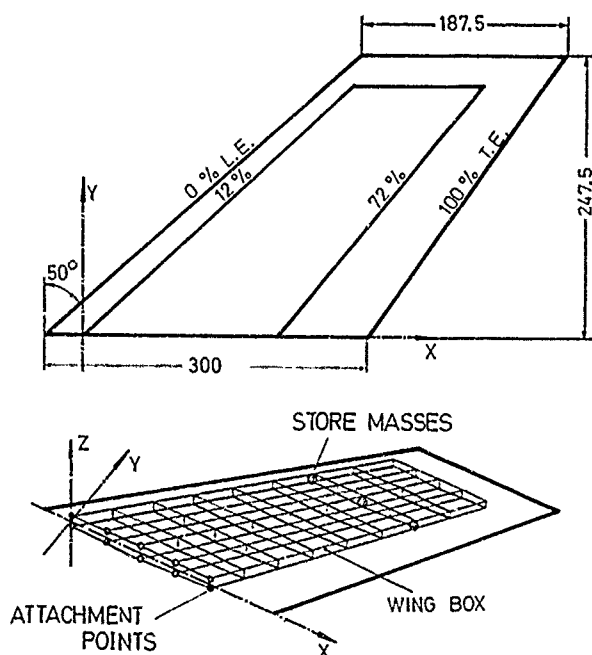


FIG. 9 GEOMETRY AND IDEALIZATION OF A CANTILEVERED WING

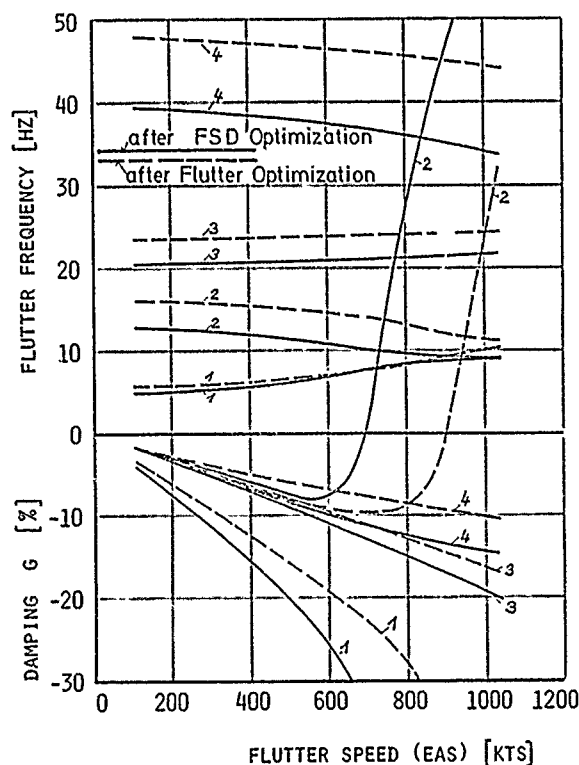


FIG. 10 RESULTS OF FLUTTER ANALYSES

17-8'

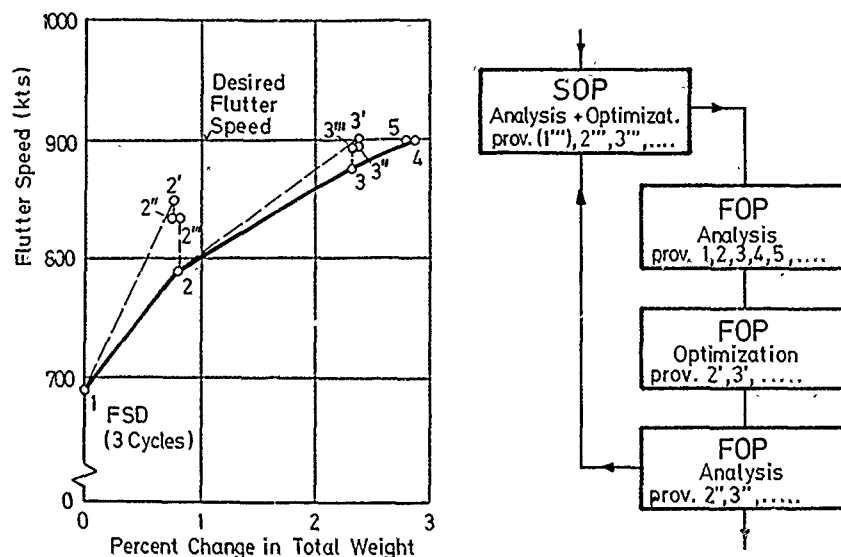


FIG. 11 HISTORY OF STRENGTH AND FLUTTER REDESIGN STUDY

A flutter speed is calculated for the initial fully stressed design (FSD) being 700 kts. After five iteration steps the desired flutter speed of 900 kts is reached with an increase of less than 3% of total weight. The loss of flutter speed from 2' to 2 and 3' to 3 is caused by linearizing effects of the optimization procedure and also by the change of vibration modes. Fig. 10 shows the result of the flutter analyses at iteration point 1 and 5 of Fig. 11. The flutter speed increase results mainly from the frequency separation of mode 1 (bending) and mode 2 (torsion).

Vertical Tail Optimization by ASAT

An optimization analysis in view of both vertical tail and control surface effectiveness was performed. Efficiency calculations done for a stress designed vertical tail provided values which fulfilled 50-60% of the requirements, being $\beta = 0.9$ for vertical tail side effectiveness and $\xi = 0.6$ for control surface effectiveness. Hence, a stiffness designed vertical tail structure was taken as basis of the deflection constraint optimization. For efficiency calculation of this structure the capabilities of ASAT were used. The chosen structural grid is shown in Fig. 12. The anisotrope material of the structure was represented by four separate layers, each layer associated with a certain fibre orientation. Different fibre orientations for the primary surface and for the rudder were used. After some changes of the structure and improvements caused by experiences a vertical tail structure was found which fulfilled the above mentioned requirements. This structure in conjunction with the aeroelastic deformations which represent the deflection constraints was the basis of the optimization calculation.

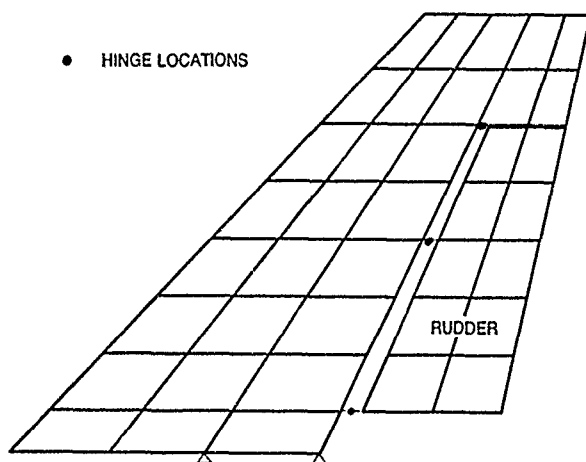


FIG. 12 STRUCTURAL GRID OF VERTICAL TAIL

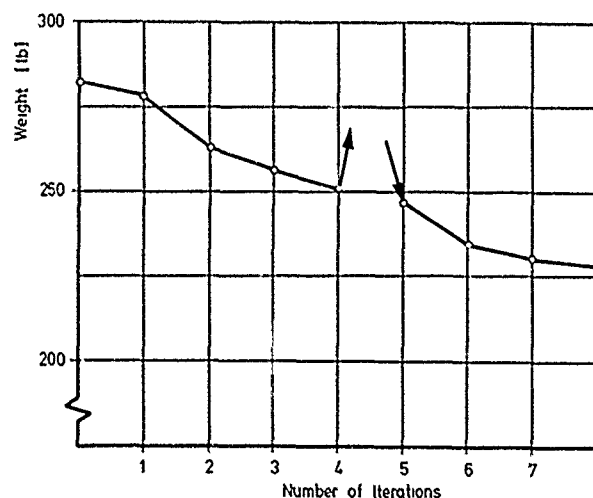


FIG. 13 HISTORY OF OPTIMIZATION FOR A DEFLECTION CONSTRAINED VERTICAL TAIL

Optimization was done only in view of deflection constraints and results of the calculations are shown in Fig. 13, 14 and 15. From Fig. 13 it can be seen that a reduction of 20% of the structures weight was obtained, even for a structure which has been defined by practical experience. Between the iteration steps four and five a simplified step size controlling procedure was applied. Fig. 14 and 15 show for two load cases the aeroelastic deformations and the pressure distributions of the loads due to rigid and elastic structure. In Fig. 14 a constant angle of attack for the whole surface was applied for load case 1 whereas in Fig. 15 a constant rudder rotation was the base for load case 2. Both load cases were defined at Mach number 1.8. Calculations made for the redesigned structure provided nearly the same efficiency values as for the initial design. Violating some stress constraints it should be possible to correct them with an insignificant increase of the weight.

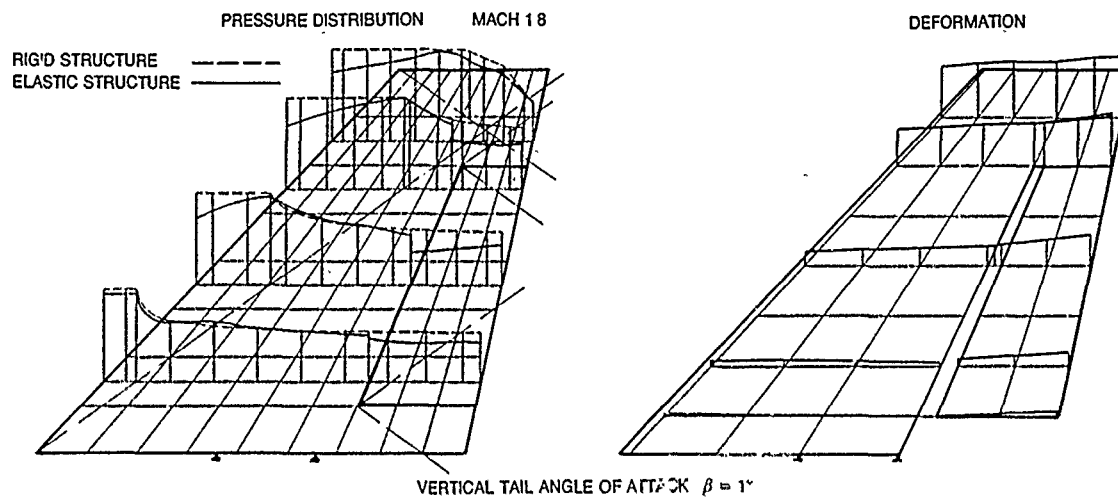


FIG. 14 PRESSURE DISTRIBUTION AND DEFORMATION OF VERTICAL TAIL

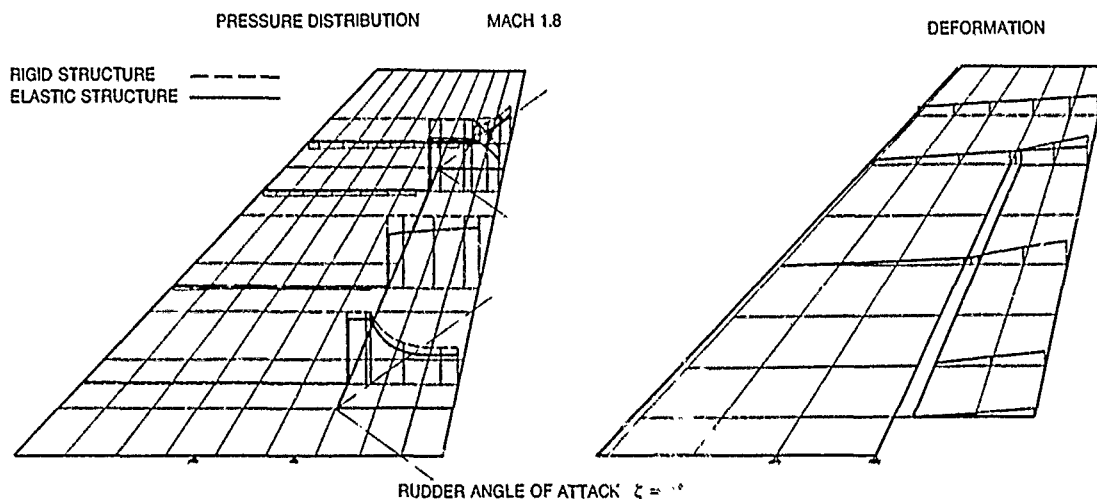


FIG. 15 PRESSURE DISTRIBUTION AND DEFORMATION OF VERTICAL TAIL

Structural Optimization by TSO

The best known procedure which is intended to address the "total design" problem by combining aerodynamic static aeroelastic, flutter and structural calculations and allowing a number of objective functions is the TSO Program (Aero elastic Tailoring and Structural Optimization Procedure). The development of TSO was motivated by the growing use of advanced composites and the desire to achieve the most effective use of these materials. It was necessary to develop a total design coupling the advantages of composite materials with aerodynamic planform and airfoil requirements to achieve the maximum benefit from these technologies [18]. Applied structural optimization procedures depend very much on the type of the aerodynamic and structural model.

Aerodynamic Mathematical Model

The TSO and ASAT program systems have nearly the same mathematical procedures to obtain steady state aerodynamic forces. The planform is subdivided into an arbitrary number of small trapezoidal panels. Aerodynamic influence coefficients corresponding to these panels are computed using either subsonic vortex-lattice theory or the supersonic

17-10

source distribution theory. Unsteady aerodynamics routines for flutter optimization, based on linearized potential flow theory, are included. In both programs there are implemented a subsonic doublet-lattice program and a supersonic Mach-box program for flutter analyses.

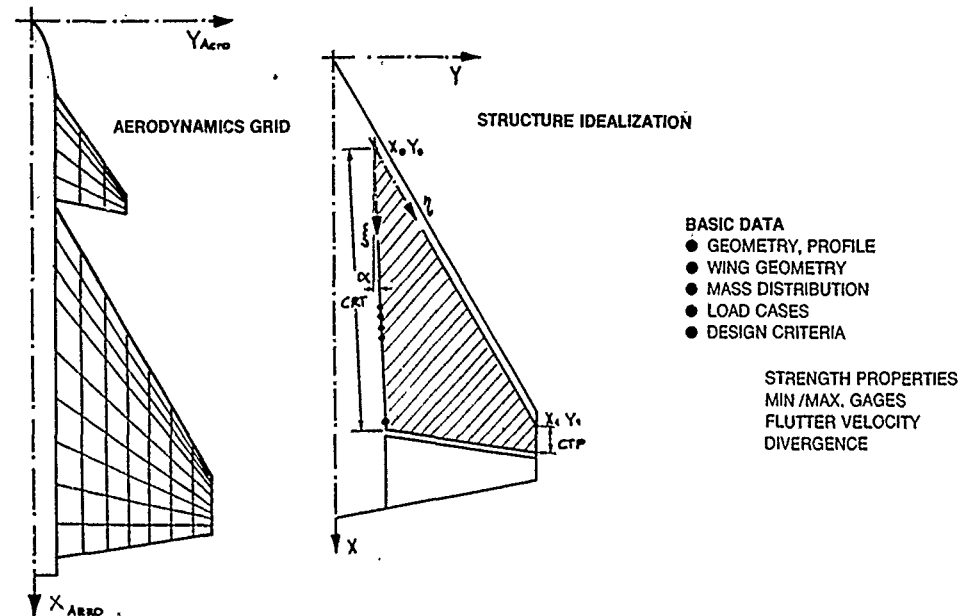


FIG. 16 TSO-MODEL

Structural Mathematical Model

The TSO structural procedures consider only the wing skin thickness distribution. The plate-type representation of the primary structure of a lifting surface allows the treatment of both spanwise and chordwise variations in cover material distributions. The plate is defined as a trapezoid with its overall depth expressed in polynomial form as a function of trapezoidal coordinates ξ and η . For composite cover skins, the plate covers consists of up to three layers, where each layer represents a specific fibre orientation, see Fig. 16 and 17. The elastic deflections of the wing box are expressed in terms of products of chordwise and spanwise deformation shapes represented by Legendre polynomials. The coefficients are the generalized coordinates of the structure, and stiffness and mass matrices are generated in terms of these coordinates. All subsequent computations for strength, flutter and static aeroelasticity are transformed into this generalized coordinate system. This procedure is the key to the significant speed advantage of TSO against conventional finite element methods. A further advantage using TSO is the capability of optimization in view of different objective functions such as weight, pressure distribution, rudder efficiency, 1st mode shape, flutter velocity and deformations.

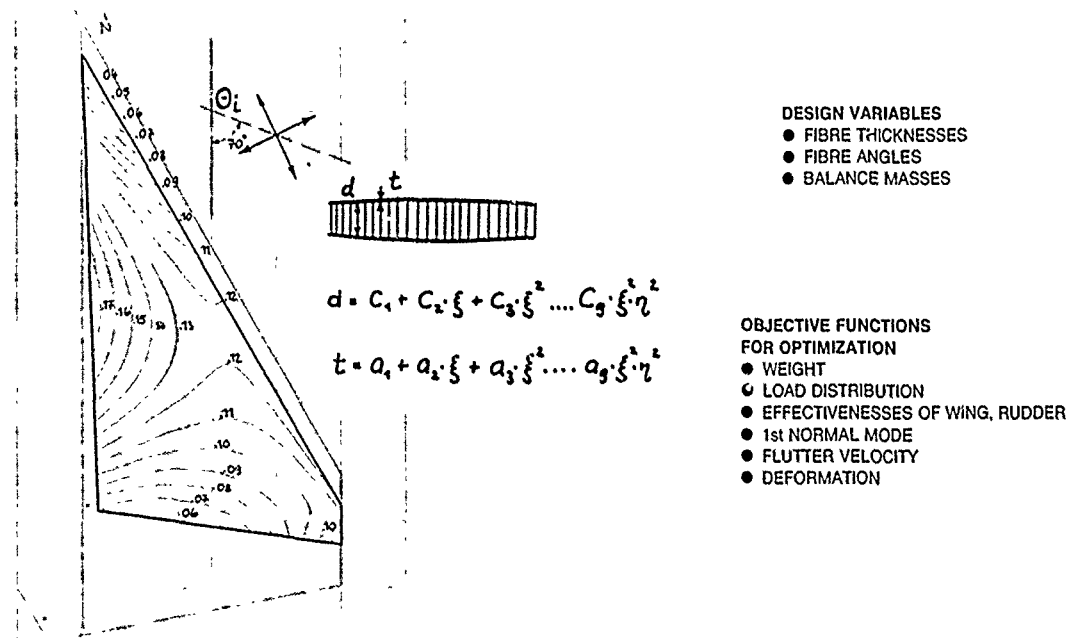


FIG. 17 TSO STRUCTURAL MODEL

The main limitation of plate model idealization is the inability to account for structural discontinuities as cut-outs. Another shortcoming is the inability to account for the substructure as ribs and spars which may be important in relatively thick wing design. Despite its deficiencies in structural modelling, the results of TSO computer runs are accurate enough for the preliminary design of thin wings. A typical application of the TSO program for "Aeroelastic Tailoring in Aircraft Design" has been demonstrated by W. TRIPLETT in Ref. [19].

TSO Optimization of Roll Effectiveness

During a cooperation program between McDonnell-Douglas and MBB a delta wing structure was investigated with the TSO program system mainly in view of control surface effectiveness. Control surface effectiveness requirements are important design objectives for highly manoeuvrable fighter aircraft and also roll performance must be analyzed already in the preliminary design studies. Some variations [20], [21] of different design variables were performed to find out possibilities to improve the aeroelastic behaviour of the composite wing box. Main results of three TSO runs are shown in Tab. 1. The first run represents the roll effectiveness of the initial basic design. In a second run, all three fibre directions θ_1 , θ_2 , θ_3 were varied with the same angle for improving effectiveness keeping the weight constrained, but no significant change could be seen. Varying only one fibre direction θ_1 ("zero degree layer"), a considerable increase of 28% in roll effectiveness was found. A first survey of these preliminary trend studies shows that a promising way to improve roll effectiveness of composite wing boxes would be to turn the main fibre direction towards trailing edge. The second step might possibly be to put an additional material in the mid span area of the wing box in case of a tip aileron.

Calculation	1st Run	2nd Run	3rd Run
Constant	$\theta_1 - \theta_3, a_1 - a_{27}$	$a_1 - a_{27}$	$\theta_2, \theta_3, a_1 - a_{27}$
Variable	- . -	$\theta_1, \theta_2, \theta_3$	θ_1
θ_1 (0° Layer)	68 .°	59.4 °	38.1 °
θ_2 ($\pm 45^\circ$ Layer)	68 .°	59.4 °	68 .°
θ_3 (90° Layer)	158 .°	149.4 °	158 .°
Skin Weight	692. LBS	692. LBS	692. LBS
Roll effectiveness M = 0.9	0.527	0.533	0.675 !
Z _{TIP} 9 g-Load Case $\alpha_{TIP} s = 5.3$ m	16. inch -2.2 °	15.8 inch -2.17 °	14.9 inch -1.6 °
Flutter Velocity/frequency M = 0.9	1800 KTS /23.6 Hz	1870 KTS /24. Hz	no flutter

TAB. 1 TSO OPTIMIZATION OF ROLL EFFECTIVENESS

In 1983 MBB has received the TSO computer program system from AFWAL, Ohio, in exchange for computer programs developed by MBB. This computer program will be tested now and used for optimization investigations in the preliminary design phase of advanced fighter aircrafts.

CONCLUSION

Highly manoeuvrable and transonic fighter design concepts with variable camber and roll effectiveness requirements indicate an increasing need of static aeroelastic design studies. The usage of advanced composite materials has a great potential to satisfy structural design requirements.

In the present paper the activities at MBB in the field of structural optimization are exposed and the usefulness and efficiency of the implemented optimization methods are demonstrated by some examples. It has been shown that the program system TSO is an useful tool during the preliminary design phase whereas ASAT can be used during early design stages as well as for the advanced design.

The structural dynamic engineer has to detect in the early design phase discrepancies in design requirements and actual design data of a given concept. He also has to work out proposals for improved design concepts because of his knowledge of the interaction between aerodynamics and structures. In order to meet these requirements new methods have to be developed which are able to consider new design concepts and procedures.

REFERENCES

- /1/ AIDALA, P.V. Transonic Fighter Design Using Numerical Optimization
ICAS Paper No. 80-2.1, Grumman Aerospace Corporation
- /2/ SELLARS, R.J. Sophisticated Aircraft Structure Development Combat Aeroplanes
TERRY, G. Aeronautical Journal, Sept. 1981
- /3/ BANNINK, E. Advanced Design Composite Material Aircraft Study
HADCOCK, R. Journal of Aircraft, Vol. 15, No. 10, October 1978
FORSCH, H.
- /4/ LANSING, W. Application of Structural Optimization for Strength
LERNER, E. and Aeroelastic Design Requirements
TAYLOR, R.F. AGARD Structures and Materials Panel,
Voss, Norway, Sept. 1977
- /5/ GÜDEL, H. Application of a Structural Optimization Procedure
SCHNEIDER, G. for Advanced Wings
AGARD Report No. 691, January 1981
- /6/ SCHMITT, L.A. Structural Synthesis and Design Parameter Hierarchy
MALLET, R.H. Proc. ASCE, J. Struct. Div. 89, 269-299 (1963)
- /7/ SHEFFEY, C.F. Optimization of Structures by Variation of Critical
Parameters
Proc. 2nd Nat. Conf. on Electronic Computation of
the Struct. Div. ASCE, Pittsburgh, 133-144, 1960
- /8/ PRAGER, W. Optimality Criteria in Structural Design
MARCAL, P. AFFDL-TR-70-166, May 1971
- /9/ GELLATLY, R.A. Optimum Structural Design
BERKE, L. AFFDL-TR-70-165, February 1971
- /10/ VENKAYYA, V. Design of Optimum Structures
Computers and Structures, 1, No. 1/2, 265-309, 1971
- /11/ RAZANI, R. The Behaviour of the Fully-Stressed Design of
Structures and its Relationship to Minimum Weight
Design
AIAA J., 3, December, 2262-2268, 1965
- /12/ POPE, G. The Design of Optimum Structures of Specified
Basis Configuration
Int. J. Mech., Sci., 10, 251-265, 1968
- /13/ PATNIAK, S. Behaviour and Design of Pin Connected Structures
DAYARATNAM, P. Int. J. Num. Meth. Engrg., 2, 577-595, 1970
- /14/ MLEJNEK, H.P. Untersuchung und Weiterentwicklung einiger Ver-
BÜHLMEIER, J. fahren zur optimalen Dimensionierung von Trag-
MAI, M.M. werken
ISD-Bericht Nr. 159, Stuttgart, Juli 1974

- /15/ VENKAYYA, V.B.
KHOT, N.S.
REDDY, V.S.
Energy Distribution in an Optimum Structural Design
AFFDL-TR-68-156, March 1969
- /16/ WILKINSON, K.
LERNER, E.
TAYLOR, R.F.
Practical Design of Minimum Weight Aircraft Structures for Strength and Flutter Requirements
J. Aircraft, Vol. 13, No. 8, 1976
- /17/ RUDISILL, C.S.
BHATIA, K.G.
Optimization of Complex Structures to Satisfy Flutter Requirement
AIAA J. Vol. 9, August 1971
- /18/ LYNCH, R.W.
ROGERS, W.A.
Aeroelastic Tailoring of Composite Material to Improve Performance
General Dynamics Corporation, Fort Worth, Texas
- /19/ TRIPLETT, W.E.
Aeroelastic Tailoring Studies in Fighter Aircraft Design
AIAA Paper 79-0725
- /20/ TRIPLETT, W.E.
Joint McAir - MBB Activities on Aeroelastic Tailoring
MEMO 236-5936, 9 May 1978
- /21/ SCHNEIDER, G.
Schwingungsrechnung und Aeroelastic Tailoring für den klaren Flügel
MBB-TN-FE171/5-78

18-1
18-1

A FLUTTER OPTIMIZATION PROGRAM FOR COMPLETE AIRCRAFT
STRUCTURAL DESIGN

by

Sidney Siegel
North American Aircraft Operations
Rockwell International, El Segundo, California

SUMMARY

A new computer program for flutter optimization has been developed and successfully used to accurately account for the interactive aerodynamic and structural effects of the complete aircraft. The program is both cost- and time-effective when compared with alternate available approaches and can be used from preliminary through advanced design stages. To insure that strength requirements are met, the optimization program starts with the strength design and automatically performs an iterative solution to raise the complete aircraft flutter speed. During each cycle of iteration, local areas of structure are stiffened by applying the criterion of constant strain energy density in the flutter mode to obtain near-minimum weight solutions. This program has successfully analyzed recent complete aircraft designs to provide adequate structure for flutter safety.

NOTATION

b	semichord
C_B	box beam width
CG	center of gravity
CP	control point
d	strip mass EA to CG distance
D_R	coordinate transformation matrix
DOF	degrees of freedom
e	beam element potential energy
e_{av}	average PED
e_{avav}	average PED that exceeds e_{av}
e_v	PED that exceeds e_{avav}
EA	elastic axis
EI	bending stiffness constant
f_F	solution flutter frequency
g_F	solution flutter damping
GJ	torsion stiffness constant
$I_{\theta\theta}$	strip mass moment of inertia about θ axis through CG
$I_{\phi\theta}, I_{\theta\phi}$	strip mass product of inertia
$I_{\phi\phi}$	strip mass moment of inertia about ϕ axis through CG
k	reduced frequency of unsteady aerodynamics
K_R	beam element relative stiffness matrix
K_{RR}	overall relative stiffness matrix

18-2

K_{SG}	overall semiglobal stiffness matrix
l	beam length
L	bending moment
m_s	strip mass
M	torsion moment
M_C, M_G	complete and global mass matrices
p_F, \bar{p}_F	flutter mode relative deflections and complex conjugate
P_F	flutter mode loads
PED	potential energy density
q_F	flutter dynamic pressure
q_R, q_{SG}, q_G	relative, semiglobal, global DOF
q_m	generalized flutter DOF
q_o	rigid body DOF
Q_R, Q_{SG}, Q_G	relative, semiglobal, global forces
t	box beam depth
v_F	solution flutter speed
V_m	solution flutter eigenvectors
v_{req}	required flutter speed
V_{SG}, V_G	orthogonal modes in semiglobal and global DOF
z	beam displacement
Z	shear force
θ	beam twist angle
λ	complex eigenvalue
λ_i	relative beam sweep angle
λ_m	solution flutter eigenvalue
τ	beam element skin gage
ϕ	beam bending angle
ω	modal frequency
ω_v	solution vibration modal frequencies

1. INTRODUCTION

Minimizing structural weight is an essential aspect of today's high-speed aircraft in order to obtain maximum performance at minimum cost. Significant weight reductions can be achieved by optimizing the structure to meet flutter requirements and still be consistent with other constraints such as strength requirements. Many methods and associated computer programs have been developed during the past 15 to 20 years to achieve this goal. Ashley (1) has cited many of the methods in current use. Other methods may be extant, but, because of proprietary considerations, they may not have been published. In general, the publicized methods and associated programs have been limited to the optimization of a single lifting surface using finite element methods. One exception to the use of finite element methods is the use of beam element methodology of Siegel (2), also cited by Ashley (1). The primary advantage of beam element over finite element methodology lies in the reduced number of degrees of freedom required for the mathematical model to adequately represent the structure. Not only does the reduced number of degrees of freedom lead

to reduced computer time and cost, but also to fewer errors in setting up the mathematical model. Additional time and cost savings are achieved by Siegel (2) using modified strip theory aerodynamic forces in lieu of lifting surface theories. Use of modified strip theory in flutter analyses has been shown by Yates (3) and others to yield fairly close correlations with experimental flutter results primarily for medium to high aspect ratio lifting surfaces.

The time- and cost-saving advantages of the beam element methodology and strip theory are offset by some restrictions, which should be considered in their use. These restrictions are primarily the limitation to medium to high aspect ratio lifting surfaces and loss of capability in representing structural elements in fine detail. Since aircraft are still designed with relatively large aspect ratios, and since the flutter phenomenon is not normally concerned with every nut, bolt, and rivet of the structure, the method of this paper has adequate applicability for current aircraft design, as dramatically demonstrated for the B-1 tail and described in the illustrative example.

The method presented here, to optimize the structure of several lifting surfaces of a complete aircraft by beam element methodology, is a refined extension of the single lifting surface of Siegel (2). The criterion of constant strain or potential energy density throughout the deformed structure in the critical flutter mode is retained for minimizing structural weight in obtaining the required flutter speed. The method has been successfully demonstrated in the wind tunnel using B-1 flutter models that incorporated the optimized structure. Subsequently, the B-1 successfully demonstrated flutter stability during its flight-test program. The optimization method is described and the derivation of the mathematical model is given. An example using the results calculated for the B-1 is given to illustrate the method.

2. DESCRIPTION OF METHOD

The structural optimization method described in this paper has been programmed for the computer to provide classical flutter and divergence stability up to a required speed, v_{req} , for a complete aircraft. The program, which can iterate to the desired structure in one computer run, is called Beam Element Flutter Optimization (BEFO). During each iteration cycle, the complete flutter analysis is performed by BEFO using automatically calculated structural changes needed to raise the flutter speed. These incremental structural changes are based on the concept that the most efficient structure is one that provides constant strain or potential energy per unit structural volume (PED) throughout the deformed structure in the flutter or divergence mode. The flow chart of Figure 1 summarizes the various elements of the BEFO program.

The program BEFO normally begins with the strength-required structure of the aircraft or with a structure that has been determined by test or analysis to be deficient for flutter stability. In the context of this paper, flutter stability also implies divergence stability. The structure is idealized by box beam elements lying along the assumed elastic axis for each aircraft component defined in the analysis. These components may include the fuselage, wing, horizontal stabilizer, vertical stabilizer, and any other structural appendage considered significant for flutter. The structure is synthesized to yield global stiffness and mass matrices from which a sufficient number of normal modes are calculated for use in the flutter analysis. In the case of a free-free aircraft, the symmetric and antisymmetric modes must be evaluated separately for optimization. The modal flutter equations are solved for the classical parameters of damping and frequency versus speed using the "k" method. The BEFO program automatically finds the flutter mode that just goes unstable at the lowest speed and calculates the PED of the individual beam elements in that mode. The stiffness of those beam elements that exhibit the larger PED's are automatically adjusted to increase the flutter speed. The new structural stiffnesses and masses are then incorporated into the mathematical model, and the process is repeated until v_{req} is reached.

The BEFO program has two options for determining the PED of each beam element. One option sums the bending and the torsion PED's together to yield one PED per beam. This summed PED option is mainly applied to a metal structure for which both the bending and torsion stiffness properties are adjusted by the same amount. A second option of the program keeps track of the beam element bending and torsion PED's separately so that the bending stiffness may be adjusted differently from the torsion stiffness. This second option is useful for those structures that may be amenable to variations in EI to GJ ratios as in the case of advanced composite materials with 0,±45 degrees ply layups or of metal structures particularly designed for this effect.

3. MATHEMATICAL MODEL

The mathematical model used for BEFO, while similar to that used in the optimization program described by Siegel (2), contains enough changes and differences to warrant a new description as applied to the complete aircraft. The mathematical model is composed of three types of degrees of freedom (DOF): the relative DOF (q_r), the semiglobal DOF (q_{sg}), and the global DOF (q_g). The q_r refer to the DOF of the structural elements of the system, which are fixed at one end and free at the other end. The q_{sg} refer to the DOF of the aircraft relative to a fixed point, which is sometimes referred to as the reference point. Two additional types of DOF are used in the expressions for the vibration mode analysis. These are the global or the absolute DOF (q_g) and the rigid body DOF (q_0). The usage of these types of DOF is explained in the following paragraphs.

The structural stiffness of each aircraft component is primarily represented by beam elements of rectangular cross section. The stiffness properties of these beam elements are described in terms of their bending and torsional stiffnesses (EI and GJ) with respect to an assumed elastic axis (EA). The EI and GJ

18-4

values are assumed to vary quadratically while the geometric properties are assumed to vary linearly span-wise along each beam element. Figure 2 shows a typical representation of a lifting surface structure with 11 structural elements, 10 of which are beam elements and one is a stiffness insert to simulate the inboard actuator stiffness for the all-movable surface.

Control points (CP) are used to define the location of the DOF for each structural element. In Figure 2, 11 CP are used for the 11 structural elements. CP 1 is assigned to the root, which contains the actuator stiffness; and CP 2 is assigned to the structure between CP 1 and CP 2. The remaining CP's that lie along the EA, are assigned to the beam elements outboard of CP 2. The relative angles between the CP's are designated by λ_i . Figure 3 shows a typical beam element of length, 1, with its cross-sectional geometry at the outboard end having the box depth (t) the box width (C_B) and the skin thickness (τ). In addition to these geometric properties, the EI and the GJ at the inboard end, middle, and outboard end of each beam are used to define the beam element stiffness.

The mathematical model of the structure is developed from a third-order stiffness matrix, K_R , which is determined for each beam element cantilevered at its inboard end in terms of relative deflections and forces (Figure 4) at its outboard end, as shown by Eq.(1).

$$Q_R = \begin{Bmatrix} Z \\ L \\ M \end{Bmatrix}_R = K_R \begin{Bmatrix} z \\ \phi \\ \theta \end{Bmatrix}_R = \begin{bmatrix} Z/z & Z/\phi & 0 \\ L/z & L/\phi & 0 \\ 0 & 0 & M/\theta \end{bmatrix} \begin{Bmatrix} z \\ \phi \\ \theta \end{Bmatrix}_R = q_R \quad (1)$$

where z, Z = bending translation, shear force

ϕ, L = bending slope, bending moment

θ, M = twisting angle, twisting moment

The elements of K_R can be expressed as quadratic functions of the beam inboard end, middle, and outboard end stiffness properties derived from basic bending and torsion beam theory as shown in Appendix A. First, the flexibility terms of Eq.(2) must be determined.

$$\left. \begin{aligned} z/Z &= 1^3/60 [9(EI)_1^{-1} + 12(EI)_2^{-1} - (EI)_3^{-1}] \\ z/L &= \phi/Z = 1^2/6 [(EI)_1^{-1} + 2(EI)_2^{-1}] \\ \phi/L &= 1/6 [(EI)_1^{-1} + 4(EI)_2^{-1} + (EI)_3^{-1}] \\ \theta/M &= 1/6 [(GJ)_1^{-1} + 4(GJ)_2^{-1} + (GJ)_3^{-1}] \end{aligned} \right\} \quad (2)$$

where $(EI)_1, (GJ)_1$ = stiffness at the inboard beam end

$(EI)_2, (GJ)_2$ = stiffness at the middle of the beam

$(EI)_3, (GJ)_3$ = stiffness at the outboard beam end

The terms of Eq.(2) can be expressed in matrix form, as shown by Eq.(3).

$$\begin{Bmatrix} z \\ \phi \\ \theta \end{Bmatrix}_R = \begin{bmatrix} z/Z & z/L & 0 \\ \phi/Z & \phi/L & 0 \\ 0 & 0 & \theta/M \end{bmatrix} \begin{Bmatrix} Z \\ L \\ M \end{Bmatrix}_R \quad (3)$$

The elements of the matrix in Eq.(1) can now be written directly in terms of the elements of Eq.(3), as follows:

$$\left. \begin{aligned} Z/z &= (\phi/L)B \\ L/z &= Z/\phi = -(\phi/Z)B \\ L/\phi &= (z/Z)B \\ M/\theta &= (\theta/M)^{-1} \end{aligned} \right\} \quad (4)$$

where $B = 1.0 / [(z/Z)(\phi/L) - (\phi/Z)^2]$

The K_R of Eq.(1) are synthesized for a component by a coordinate transformation matrix (D_R) to form the semiglobal stiffness matrix (K_{SG}). For a component with three beam elements, D_R has the following form: 18-5

$$q_R = \begin{Bmatrix} z_1 \\ \phi_1 \\ \theta_1 \\ z_2 \\ \phi_2 \\ \theta_2 \\ z_3 \\ \phi_3 \\ \theta_3 \end{Bmatrix}_R = \begin{bmatrix} 1 & 0 & 0 & 0 & 0 & 0 & 0 & 0 & 0 \\ 0 & 1 & 0 & 0 & 0 & 0 & 0 & 0 & 0 \\ 0 & 0 & 1 & 0 & 0 & 0 & 0 & 0 & 0 \\ -1 & -l_2 c \lambda_2 & -l_2 s \lambda_2 & 1 & 0 & 0 & 0 & 0 & 0 \\ 0 & -c \lambda_2 & -s \lambda_2 & 0 & 1 & 0 & 0 & 0 & 0 \\ 0 & s \lambda_2 & -c \lambda_2 & 0 & 0 & 1 & 0 & 0 & 0 \\ 0 & 0 & 0 & -1 & -l_3 c \lambda_3 & -l_3 s \lambda_3 & 1 & 0 & 0 \\ 0 & 0 & 0 & 0 & -c \lambda_3 & -s \lambda_3 & 0 & 1 & 0 \\ 0 & 0 & 0 & 0 & s \lambda_3 & -c \lambda_3 & 0 & 0 & 1 \end{bmatrix} \begin{Bmatrix} z_1 \\ \phi_1 \\ \theta_1 \\ z_2 \\ \phi_2 \\ \theta_2 \\ z_3 \\ \phi_3 \\ \theta_3 \end{Bmatrix}_{SG} = D_R q_{SG} \quad (5)$$

The D_R matrix is automatically calculated by BEFO for continuous beam elements of a component, given the length and relative sweep angle of each element.

By using the principle of equal work, the D_R matrix of Eq.(5) and its transpose (D_R^T) are used with the K_R 's of Eq.(1) to obtain the semiglobal stiffness matrix (K_{SG}) as shown in Eq.(6).

$$Q_{SG} = D_R^T K_{RR} D_R q_{SG} \quad (6)$$

where Q_{SG}, q_{SG} = semiglobal forces and DOF

$$K_{SG} = D_R^T K_{RR} D_R$$

$$K_{RR} = \begin{bmatrix} K_{R1} & 0 & 0 \\ 0 & K_{R2} & 0 \\ 0 & 0 & K_{R3} \end{bmatrix}$$

The attachment of one component to another in order to tie the complete aircraft together is achieved by calculating the appropriate elements of the D_R matrix. A specific example of a D_R matrix is shown in Appendix B to illustrate the method for a wing of two beams with a trailing edge control surface. The control surface has two hinge points. The inboard hinge has an actuator supported from the wing.

The inertial forces of the mathematical model are expressed in terms of the absolute coordinate system and include both structural and nonstructural masses. These forces may be expressed as strip mass matrices for each CP of the model, as shown in Eq.(7) for the i th CP.

$$\begin{Bmatrix} Z_i \\ L_i \\ M_i \end{Bmatrix}_C = \omega^2 \begin{bmatrix} m_s & 0 & dm_s \\ 0 & I_{\phi\phi} & I_{\phi\theta} \\ dm_s & I_{\theta\phi} & I_{\theta\theta} \end{bmatrix}_i \begin{Bmatrix} z_i \\ \phi_i \\ \theta_i \end{Bmatrix}_C \quad (7)$$

where Z_i, z_i = shear force and displacement

L_i, ϕ_i = rolling moment and angle

M_i, θ_i = pitching moment and angle

m_s = strip mass

$I_{\phi\phi}$ = rolling moment of inertia about an axis perpendicular to the local EA through the strip center of gravity

$I_{\theta\theta}$ = pitching moment of inertia about an axis parallel to the local EA through the strip center of gravity

$I_{\phi\theta} = I_{\theta\phi}$ = product of inertia

d = distance from the local EA to the strip center of gravity

The complete mass matrix (M_C) is a combination of the strip mass matrices.

The vibration equations of motion for a system with free-free boundary conditions can be written in terms of the complete mass matrix (M_C), the semiglobal stiffness matrix (K_{SG}), and the rigid body modes (D_O) as follows:

$$K_{SG} q_{SG} = \omega^2 M_G q_{SG} \quad (8)$$

where $M_G = M_C S$

$$S = I - D_O M_{OO}^{-1} D_O^T M_C$$

$$M_{OO} = D_O^T M_C D_O + M_O$$

M_O = rigid body mass matrix associated with the reference or fixed point for masses not included in M_C

I = identity matrix

ω = modal frequency

q_{SG} = semiglobal degrees of freedom

The cantilever condition occurs when $M_C = M_G$.

The total motion for the free-free structure (q_G) is a combination of q_{SG} and the rigid body modes amplitudes, as shown in Eq. (9).

$$q_G = q_{SG} + D_O q_O = S q_{SG} \quad (9)$$

$$\text{where } q_O = -(D_O^T M_C D_O + M_O)^{-1} D_O^T M_C q_{SG}$$

The solution to Eq. (8) is a set of orthogonal modes (V_{SG}) and frequencies (ω_V). The free-free modes (V_G) then become

$$V_G = S V_{SG} \quad (10)$$

4. FLUTTER ANALYSIS

The flutter analysis of BEFO uses the orthogonal modes of Eq. (8) to obtain the free-free flutter equations of motion expressed in Eq. (11).

$$\lambda q_m = \omega_V^{-2} Q_G q_m \quad (11)$$

where λ = complex eigenvalue

q_m = complex generalized flutter DOF

$$Q_G = V_G^T \bar{M} I_O V_G$$

$$\bar{M} = M_G + A$$

A = aerodynamic force matrix for a given reduced frequency

$$I_O = I - D_O (M_{OO} + D_O^T A D_O)^{-1} D_O^T \bar{M}$$

The non-free-free condition occurs when $I_O = I$. The original DOF of the system may be obtained by using the appropriate transformation as shown in Eq. (12).

$$(q_G)_F = I_O V_G q_m \quad (12)$$

Up to 40 of the modes calculated from Eq.(8) are selected to be used for the flutter analysis. A rule of thumb criterion for selecting the modes is to use at least three bending and two torsion modes for each major component in the analysis. A feature included in BEFO to help select significant modes for the flutter analysis is the calculation of the potential energy distribution in each mode by DOF, by component, and by type, whether bending, torsion, root, in-plane, or other type of energy. Quick visual observation of the potential energy distribution, after an initial vibration analysis run, can yield valuable insight into the type of modes to be selected for the flutter analysis. By identifying the appropriate mode numbers in the BEFO input data, unnecessary modes can be deleted and computer time conserved. The selection process in BEFO also permits the effect of mode deletion on flutter speed and on optimization to be investigated.

The solutions of Eq.(11) are the generalized complex flutter vectors (V_m) and complex roots (λ_m). The flutter speeds (v_F), flutter frequencies (f_F), and dampings (g_F) can be extracted from the roots as shown in Eqs.(13).

$$\left. \begin{aligned} v_F &= (b/k)/\sqrt{(\lambda_m)_{\text{real}}} \\ f_F &= 1/\sqrt{(\lambda_m)_{\text{real}}} \\ g_F &= (\lambda_m)_{\text{imag}}/(\lambda_m)_{\text{real}} \end{aligned} \right\} \quad (13)$$

where b = reference semichord length

k = reduced frequency, $\omega b/v$

Only the roots or eigenvalue solutions to Eq.(11) are required except at the critical k -value for which one eigenvector or flutter vector is also calculated. The critical k -value is automatically determined to be the one for which one of the flutter modes goes unstable at the lowest speed below the reference or required speed. This critical flutter vector is used to calculate the energy density distribution for optimizing the structure at minimum weight.

A range of k -values is automatically selected by BEFO for which to calculate the solutions to Eq.(11). This range is determined by the frequency range of the input modes and the reference or required speed, v_{req} . The minimum and maximum k -values are determined as shown in Eqs.(14).

$$\left. \begin{aligned} k_{\min} &= (\omega_v)_{\min} b/(1.5v_{\text{req}}) \\ k_{\max} &= (\omega_v)_{\max} b/(0.25v_{\text{req}}) \end{aligned} \right\} \quad (14)$$

The flutter solution begins with k_{\max} to yield solution results at the lower speeds and proceeds towards the k_{\min} value until the solution speeds exceed v_{req} or until the solutions for k_{\min} have been evaluated. The k -value that contains an unstable mode with the lowest speed is automatically determined; if the damping (g_F) is not between $g = 0$ and $g = 0.002$, additional solutions are obtained until the g -value is within the desired range. The point at which the critical flutter mode just goes unstable, $g = 0$, at the lowest speed is the critical k -value solution.

5. STRUCTURAL OPTIMIZATION

The potential energy density distribution is used as the criterion in BEFO to determine where and by how much to stiffen the structure to achieve the required flutter speed. The potential energy for each beam element of the mathematical model, e , is a function of both the bending and torsion deformations of the structure in the critical flutter mode and can be expressed as the product of the complex conjugate of the relative deflections, \bar{p}_F , and the loads, p_F , as shown in Eq.(15).

$$e = \bar{p}_F p_F \quad (15)$$

where $p_F = D_R \bar{V}_G (q_m)_C$

\bar{p}_F = complex conjugate of p_F

$(q_m)_C$ = critical flutter vector of Eq.(11)

The loads, p_F , can be described in terms of the beam element stiffnesses to yield the expression of Eq.(16).

$$e = \bar{p}_F K_{RR} p_F \quad (16)$$

The matrix product on the right side of Eq.(16) is performed so as to evaluate the energies for the combined three DOF for each beam or for the bending DOF and the torsion DOF separately.

18-8

The potential energies of Eq.(16), when divided by their associated structural volumes, become the potential energy densities (PED) that are used as a basis for modifying the structure to meet the required flutter speed at minimum weight. The beams with the higher PED for the system that has an inadequate flutter speed are stiffened by increasing their skin gages. The stiffening process is automatically performed in increments to approach constant PED throughout the deformed structure while increasing the flutter speed. The new stiffness and associated increased mass are incorporated into the mathematical model, and the vibration and flutter analyses are redone. The whole process is repeated until v_{req} is reached.

The new skin gage (τ_{new}) for resizing is calculated by using the formula of Eq.(17).

$$\tau_{new} = \tau_{old} (v_{req}/v_F)^2 \sqrt{e_v/e_{avav}} \quad (17)$$

where e_v = PED for a beam element that exceeds e_{avav}

e_{avav} = average of the PED that exceeds e_{av}

e_{av} = average of beam element PED

Eq.(17) is an empirical approach to increasing skin gages and thereby increasing stiffness in the optimum structural areas and ultimately increasing flutter speed. The first factor, that of raising the speed ratio to the second power, reflects the effect of a change in speed with a change in stiffness. The square root of the PED ratios, as the second factor on the skin gage, is used to select the beam elements with the higher, and therefore the more significant, PED and to effect an appropriate incremental change in flutter speed.

6. PROGRAM CAPABILITIES AND LIMITATIONS

The flutter optimization program, BEFO, as presently constituted in FORTRAN for the CDC 7600, can handle separate components, multiple components, or a complete aircraft. The boundary conditions may be cantilever, with flexible root condition, or free-free. Rigidly attached or sprung stores may be included in the system. Structural redundancies are conveniently handled through the global-to-relative DOF transformation matrix, D_r . The EA's of the various components can have multiple sweep changes. The number of structural elements in the mathematical model is limited only by the present DOF dimension of 165 and computer capacity. Up to 40 flexible modes are allowed for use in the flutter analysis, while up to 165 modes may be calculated in the vibration analysis.

BEFO has certain built-in restrictions so as to stay within practical limits. The beam element skin gages are restricted from exceeding 25 percent of the box depth for the option that maintains the original EI-to-GJ ratios. Another restriction requires that the initial design structure yield a flutter speed that is at least 50 percent of v_{req} . While an unlimited number of iterations is possible, BEFO is currently limited to 15 iterations in order to keep down computer costs. Experience has shown that no more than 10 iterations are required to resolve most structures.

7. ILLUSTRATIVE EXAMPLE

The B-1 was the first flying aircraft to be optimized during its design period through the methods described in this paper. Siegel (2) has shown how the various components of the B-1, the wing, the horizontal stabilizer, and the vertical stabilizer were optimized using the predecessor program to BEFO called STROP. Because of its ability to rapidly achieve the flutter-optimized structure, STROP was able to interact with the design process of the B-1 and to instigate changes early enough to prevent expensive and time-consuming design changes that would have been required later.

An early example of the efficacy of the method, as related to the B-1, occurred in 1972 when a wind tunnel flutter model of the tail experienced an explosive type of flutter at a dynamic pressure about 50 percent below that required. The model, which was tested at high subsonic speeds, consisted of the combined horizontal and vertical stabilizers. A second tail model that was tested for verification yielded essentially the same flutter result. This test result became an immediate concern as it was recognized that the tail structure had a serious deficiency. The STROP program, which was limited to optimizing a single component, was quickly updated to accommodate both stabilizers. Within a few months, the program was modified and checked out, and the corrected structure was determined and incorporated in the design. The main structural boxes of both the horizontal and vertical stabilizers were stiffened in their midspan regions. This flutter optimization was achieved with about 8 percent of the structural weight that would have been required if the stiffness had been increased by the preoptimization method, the ratio of the required dynamic pressure to the flutter dynamic pressure. Within 9 months after the flutter occurrence, the new design was incorporated into subsonic, transonic, and supersonic flutter models and successfully tested to adequate speed margins in all three speed regimes. The optimized design as incorporated into the full-scale aircraft, which has subsequently demonstrated flutter stability throughout the flight envelope in the flight-test program.

Now, with BEFO, the capability to optimize the complete aircraft has become available. The program was used to optimize the complete B-1, a large variable sweep aircraft. This example started with the stiffness and mass data of the current design for the antisymmetric heavy weight condition. In order to properly

exercise the program, the required speed was increased beyond the original value. Figure 6 shows the beam element model, in top and side views, that was used for the antisymmetric case. In this model, 11 beam elements represented the fuselage structure; 11 beam elements and two pivot elements represented the wing structure; nine beam elements, one actuator element, and one inboard structural element represented the horizontal stabilizer structure; nine beam elements and one root element represented the vertical stabilizer structure; and four elements represented the nacelle with its two engines. The control points (CP) between which the beams and other structural elements were located are represented by the small solid circles in Figure 6 and are numbered from 1 to 50 with a reference point at R. Figure 7 lists the number and type of DOF at each CP, totaling 156 DOF. The aerodynamic surfaces are sketched in Figure 6 to reflect their approximate areas.

The flutter analysis, which contained 30 modes, was evaluated at a critical flight condition. The frequencies of these modes calculated in vacuo are listed in Figure 8 for the initial vibration analysis of the base case and the subsequent five iterations. The vibration and flutter solutions, the associated optimizations for the base case, and the five iterations were calculated in one overnight computer run at an approximate cost of \$275 on the CDC 7600.

The number of modes selected for the flutter analyses were obtained from a prior vibration analysis computer run. Previous experience had shown that an adequate number of modes should include most of the modes up through horizontal stabilizer second torsion (H2T). For this example, 43 modes were calculated to include H2T, and 13 modes of the 43 were deleted because of their negligible effect on the critical flutter speeds.

From the base case flutter solution, the critical mode was determined to be horizontal stabilizer first torsion (H1T), and the larger PED's were calculated by BEFO to be associated with the beam elements of the horizontal stabilizer between 25 and 70 percent span, as indicated by the percent stiffness increases of Figure 9 for the first iteration. The skin gages and consequently stiffnesses and masses of the appropriate beam elements were increased accordingly. The in-plane as well as the out-of-plane DOF were adjusted to reflect the mass changes to yield about 0.7 percent increase in the structural weight of the tail. The new condition was analyzed for its vibration modes, and the subsequent flutter analysis used the automatically selected modes indicated in Figure 8. This first iteration yielded, as shown in Figure 10, a 7 percent increase in flutter dynamic pressure (q_F), with the same mode being critical (H1T) as for the base case. Iterations 2 and 3 followed yielding a total increase of 24 percent in q_F for a 2.7 percent increase in tail mass with H1T still being critical.

After the third iteration stiffness and mass changes, a lowly damped fuselage third bending mode (F3B) was calculated as being critical with a slightly lower flutter speed than for the H1T mode. The larger PED's now appeared on the wing as well as on the horizontal stabilizer, and both surfaces were stiffened as shown in Figure 9. The fourth iteration yielded a similar flutter picture, and the wing and horizontal stabilizer were both stiffened again, yielding flutter speeds that exceeded the required speed. Figure 10 shows the increases in q_F with increases in structural weight for the five iterations. The final results show that structural weight increases of 4.1 percent for the tail and 2.1 percent for the wing yielded 48 percent increase in q_F .

8. CONCLUSIONS

The flutter optimization method presented here has been demonstrated on the B-1 as being a successful and useful tool for determining minimum weight structure consistent with strength-sized structure. The method has been developed and used to optimize complete aircraft. Because of the rapidity in using the method, the essential interaction with aircraft design has been achieved. The computer program of the method, BEFO, is considered efficient and accurate because of the minimal computer cost in the performance of the complete vibration and flutter analyses during each iteration cycle. BEFO, as presently constituted, is considered to be limited to medium to high aspect ratio lifting surfaces because of the use of modified strip theory. However, this limitation could be eliminated, but with increased computer cost, by incorporating lifting surface aerodynamic theories.

9. REFERENCES

1. Ashely, H., "On Making Things the Best-Aeronautical Uses of Optimization," Journal of Aircraft, Volume 19, Number 1, January 1982, pp. 5-28
2. Siegel, S., "A Flutter Optimization Program for Aircraft Structural Design," AIAA Paper No. 72-795, August 1972
3. Yates, E.C., Jr, Wynne, E.C., Farrer, M.G., and Desmarais, R.N., "Prediction of Transonic Flutter for a Supercritical Wing by Modified Strip Analysis," Journal of Aircraft, Volume 19, Number 11, November 1982, pp. 999-1004

Appendix A

BEAM ELEMENT STIFFNESS MATRIX

Assume that the inverses of EI and GJ vary quadratically along the beam length, 1. Let r_0 be $(EI)^{-1}$ at the beginning of the beam ($y = 0$), r_1 be $(EI)^{-1}$ at midspan ($y = 1/2$), and r_2 be $(EI)^{-1}$ at the end of the beam ($y = 1$). The general equation for the quadratic is:

$$r = ay^2 + by + c \quad (A1)$$

To solve for the coefficients of Eq.(A1), substitute known values and express the set of equations in matrix form.

$$\begin{Bmatrix} r_0 \\ r_1 \\ r_2 \end{Bmatrix} = \begin{bmatrix} 0 & 0 & 1 \\ 1^2/4 & 1/2 & 1 \\ 1^2 & 1 & 1 \end{bmatrix} \begin{Bmatrix} a \\ b \\ c \end{Bmatrix} \quad (A2)$$

Invert the matrix of the right side of Eq.(A2) to yield the coefficient values.

$$\begin{Bmatrix} a \\ b \\ c \end{Bmatrix} = \begin{bmatrix} 2/1^2 & -4/1^2 & 2/1^2 \\ -3/1 & 4/1 & -1/1 \\ 1 & 0 & 0 \end{bmatrix} \begin{Bmatrix} r_0 \\ r_1 \\ r_2 \end{Bmatrix} \quad (A3)$$

$$\text{where } a = 1^{-2} (2r_0 - 4r_1 + 2r_2)$$

$$b = 1^{-1} (-3r_0 + 4r_1 - r_2)$$

$$c = r_0$$

From theory for a cantilever beam of length, 1, undergoing bending due to a moment, L, and a shear force, Z, at the end of the beam, Eq.(A4) applies.

$$\frac{d^2z}{dy^2} = (EI)^{-1} [L + Z(1-y)] \quad (A4)$$

Using the quadratic expression of Eq.(A1) for $(EI)^{-1}$ yields

$$\frac{d^2z}{dy^2} = (ay^2 + by + c) [L + Z(1-y)] \quad (A5)$$

Separate the variable, y, on the right hand side of Eq.(A5).

$$\frac{d^2z}{dy^2} = aZy^3 + (aZ1 + aL - bZ)y^2 + (bZ1 + bL - cZ)y + c(L + Z1) \quad (A6)$$

Integrate once and apply the conditions $dz/dy = 0$ at $y=0$ and $dz/dy = \phi_1$ at $y=1$.

$$\frac{dz}{dy} = -aZy^4/4 + (aZ1 + aL - bZ)y^3/3 + (bZ1 + bL - cZ)y^2/2 + c(L + Z1)y + C_1 \quad (A7)$$

The constant of integration, $C_1 = 0$ at $dz/dy = 0$; and the bending slope at the end of the beam becomes

$$\phi_1 = (a1^3/3 + b1^2/2 + c1)L + (a1^4/12 + b1^3/6 + c1^2/2)Z \quad (A8)$$

Integrate a second time and apply the conditions $z = 0$ at $y = 0$ and $z = z_1$ at $y = 1$.

$$z = -az^5/20 + (aZ + aL - bZ)y^4/12 + (bZ + bL - cZ)y^3/6 + c(L + Z)y^2/2 + C_2 \quad (A9)$$

The constant of integration, $C_2 = 0$ at $z = 0$; and the deflection at the end of the beam becomes

$$z_1 = (aL^4/12 + bL^3/6 + cL^2/2)L + (aL^5/30 + bL^4/12 + cL^3/3)Z \quad (A10)$$

Express Eq. (A8) and Eq. (A10) as a matrix equation and drop the subscript 1.

$$\begin{Bmatrix} z \\ \phi \end{Bmatrix} = \begin{bmatrix} aL^5/30 + bL^4/12 + cL^3/3 & aL^4/12 + bL^3/6 + cL^2/2 \\ aL^4/12 + bL^3/6 + cL^2/2 & aL^3/3 + bL^2/2 + cL \end{bmatrix} \begin{Bmatrix} Z \\ L \end{Bmatrix} \quad (A11)$$

Eq. (A11) represents the influence coefficients for the deflection (z) and bending slope (ϕ) of a cantilever beam undergoing a shear force (Z) and a moment (L) at the free end of the beam. Substituting the expressions for the coefficients a , b , and c from Eq. (A3) yields the matrix expression of Eq. (A12).

$$\begin{Bmatrix} z \\ \phi \end{Bmatrix} = \begin{bmatrix} (9r_0 + 12r_1 - r_2)L^3/60 & (r_0 + 2r_1)L^2/6 \\ (r_0 + 2r_1)L^2/6 & (r_0 + 4r_1 + r_2)L/6 \end{bmatrix} \begin{Bmatrix} Z \\ L \end{Bmatrix} \quad (A12)$$

The inversion of the influence coefficient matrix of Eq. (A12), which is most conveniently accomplished after the matrix elements have been determined, gives the equivalent bending stiffness matrix for the cantilever beam assuming a quadratic distribution of $(EI)^{-1}$. The torsional stiffness term can be obtained by inverting the 2,2 element of Eq. (A12) after substituting $(GJ)^{-1}$ for $(EI)^{-1}$.

For a beam of constant EI and GJ along its length, Eq. (A12) reduces to Eq. (A13), after including the torsion term.

$$\begin{Bmatrix} z \\ \phi \\ \theta \end{Bmatrix} = \begin{bmatrix} L^3/(3EI) & L^2/(2EI) & 0 \\ L^2/(2EI) & L/(EI) & 0 \\ 0 & 0 & 1/(GJ) \end{bmatrix} \begin{Bmatrix} Z \\ L \\ M \end{Bmatrix} \quad (A13)$$

The corresponding stiffness matrix for Eq. (A13) is shown in Eq. (A14).

$$\begin{Bmatrix} Z \\ L \\ M \end{Bmatrix} = \begin{bmatrix} 12EI/L^3 & -6EI/L^2 & 0 \\ -6EI/L^2 & 4EI/L & 0 \\ 0 & 0 & GJ/L \end{bmatrix} \begin{Bmatrix} z \\ \phi \\ \theta \end{Bmatrix} \quad (A14)$$

Appendix B

TRANSFORMATION MATRIX FOR TWO COMPONENTS

An example of a transformation matrix relating the semiglobal DOF to the relative DOF is presented for two attached components, as shown in Figure 5. The figure shows a wing cantilevered at the inboard end of the first of two beam elements along the LA. A trailing edge control surface is attached through hinge points by one beam element between CP 5 and CP 6. The transformation can be expressed as follows:

$$\begin{bmatrix} z_1 \\ \phi_1 \\ \theta_1 \\ z_2 \\ \phi_2 \\ \theta_2 \\ z_3 \\ \phi_3 \\ \theta_3 \\ z_4 \\ \phi_4 \\ \theta_4 \\ z_5 \\ \phi_5 \\ \theta_5 \\ z_6 \\ \phi_6 \\ \ell_6 \end{bmatrix}_R = \begin{bmatrix} 1 & 0 & 0 & & & & & & \\ 0 & 1 & 0 & 0 & 0 & 0 & 0 & 0 & \\ 0 & 0 & 1 & & & & & & \\ -1 & -l_2 & 0 & 1 & 0 & 0 & & & \\ 0 & -1 & 0 & 0 & 1 & 0 & 0 & 0 & \\ 0 & 0 & -1 & 0 & 0 & 1 & & & \\ -1 & 0 & -l_3 & & 1 & 0 & 0 & & \\ 0 & -C_H & -S_H & 0 & 0 & 1 & 0 & 0 & \\ 0 & S_H & -C_H & & 0 & 0 & 1 & & \\ & & & -1 & 0 & -l_4 & & 1 & 0 & 0 \\ & & & 0 & -C_H & -S_H & 0 & 0 & 1 & 0 \\ & & & 0 & S_H & -C_H & & 0 & 0 & 1 \\ & & & & & & -1 & 0 & -l_5 & \\ & & & & & & 0 & -C_C & -S_C & 0 \\ & & & & & & 0 & S_C & -C_C & 0 \\ & & & & & & & & & -1 & 0 & -l_6 \\ & & & & & & & & & 0 & -C_C & -S_C \\ & & & & & & & & & 0 & S_C & -C_C \\ & & & & & & & & & -1 & -l_7 & 0 \\ & & & & & & & & & 0 & -1 & 0 \\ & & & & & & & & & 0 & 0 & 1 \end{bmatrix} \begin{bmatrix} z_1 \\ \phi_1 \\ \theta_1 \\ z_2 \\ \phi_2 \\ \theta_2 \\ z_3 \\ \phi_3 \\ \theta_3 \\ z_4 \\ \phi_4 \\ \theta_4 \\ z_5 \\ \phi_5 \\ \theta_5 \\ z_6 \\ \phi_6 \\ \theta_6 \end{bmatrix}_{SG}$$

where $C_H = \cos \lambda_H$

$S_H = \sin \lambda_H$

$C_C = \cos \lambda_C$

$S_C = \sin \lambda_C$

l_i = length of associated beam

18-13

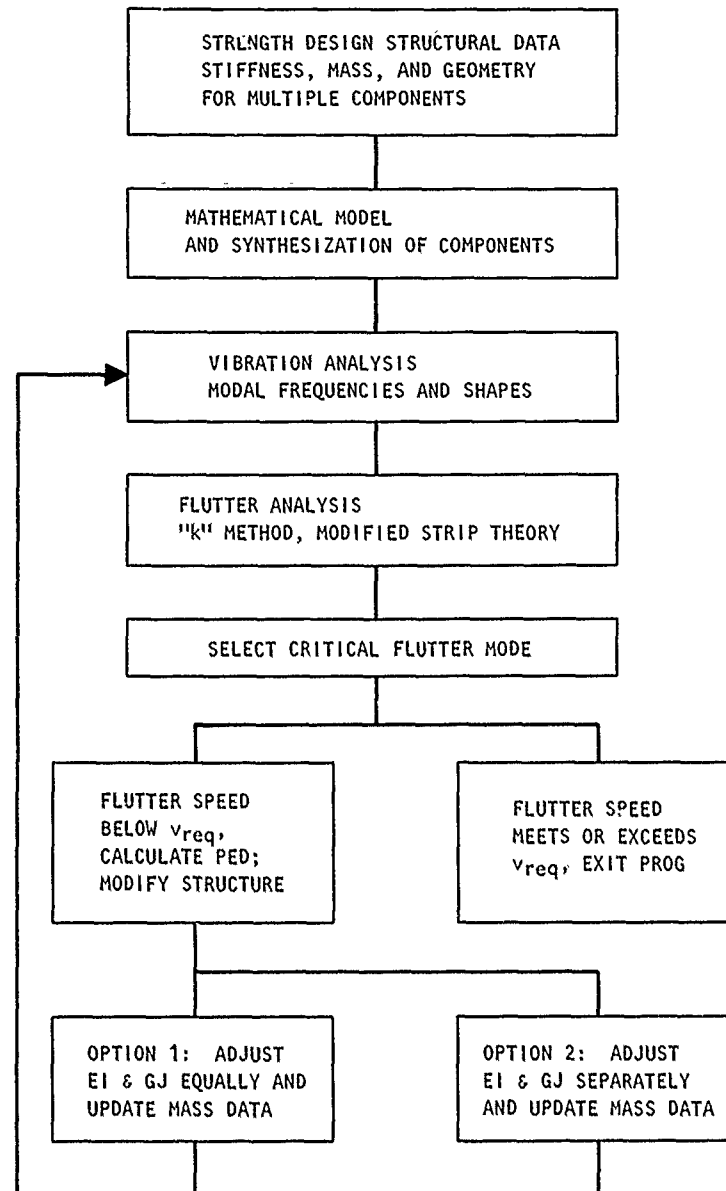


Figure 1. BEFO Flowchart

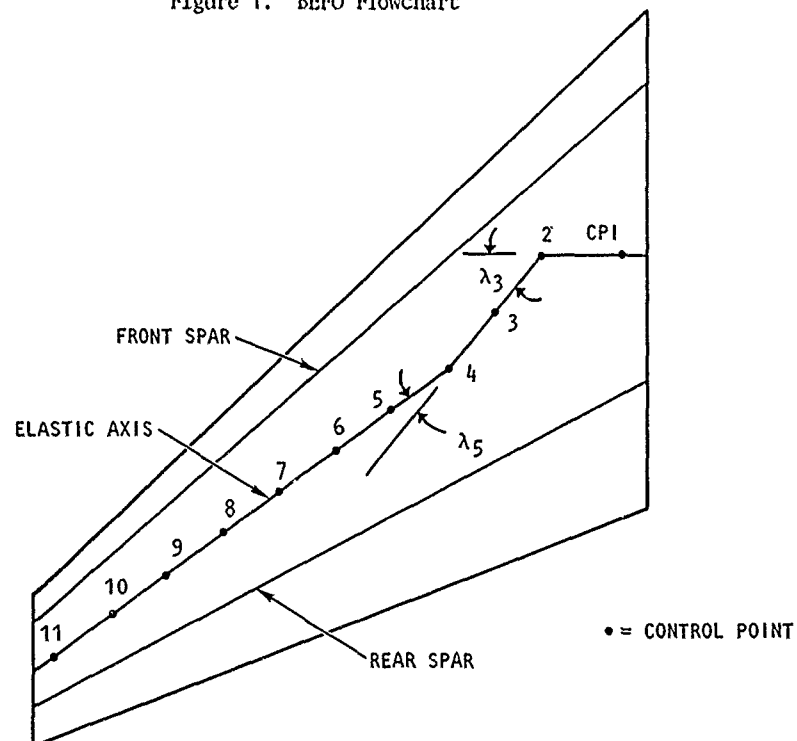


Figure 2 All Movable Surface: Typical Box Beam Representation

18-14

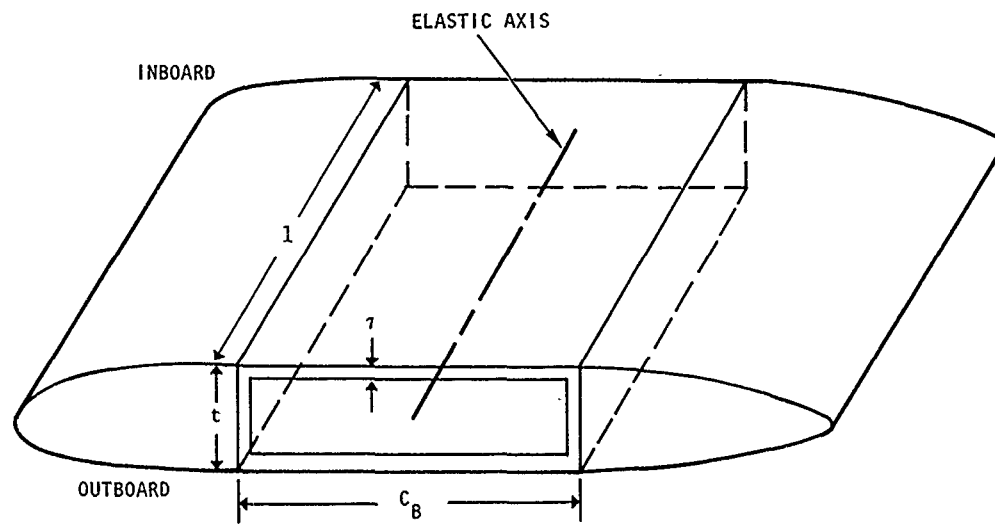


Figure 3. Typical Beam Element Geometry

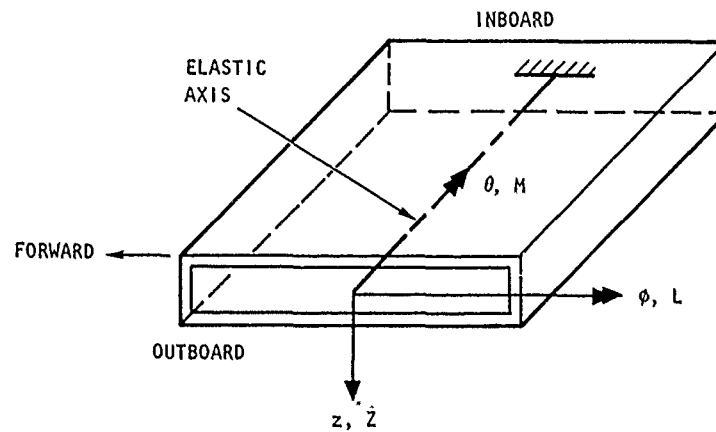
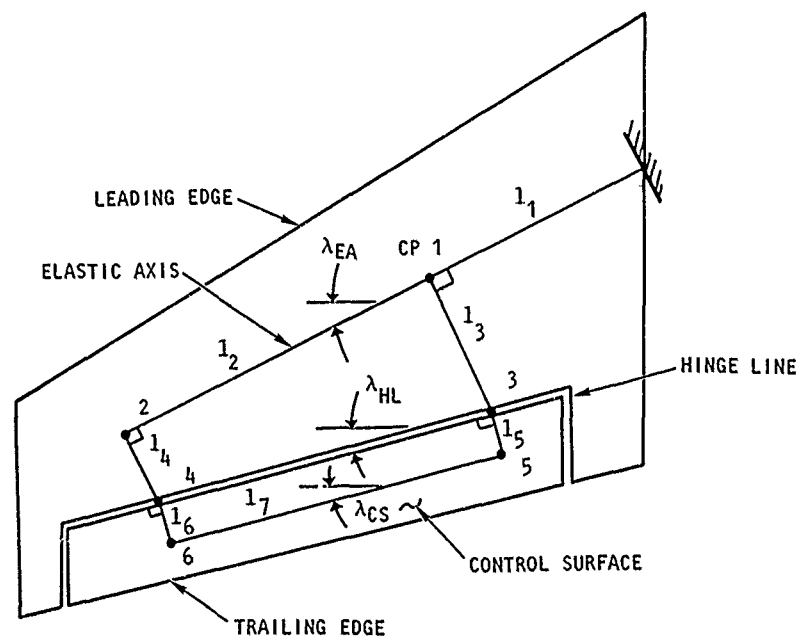


Figure 4. Beam Element Degrees of Freedom and Forces



$$\lambda_H = \lambda_{HL} - \lambda_{EA}$$

$$\lambda_C = \lambda_{CS} - \lambda_{HL}$$

Figure 5. Two Component Model - Wing and Control Surface

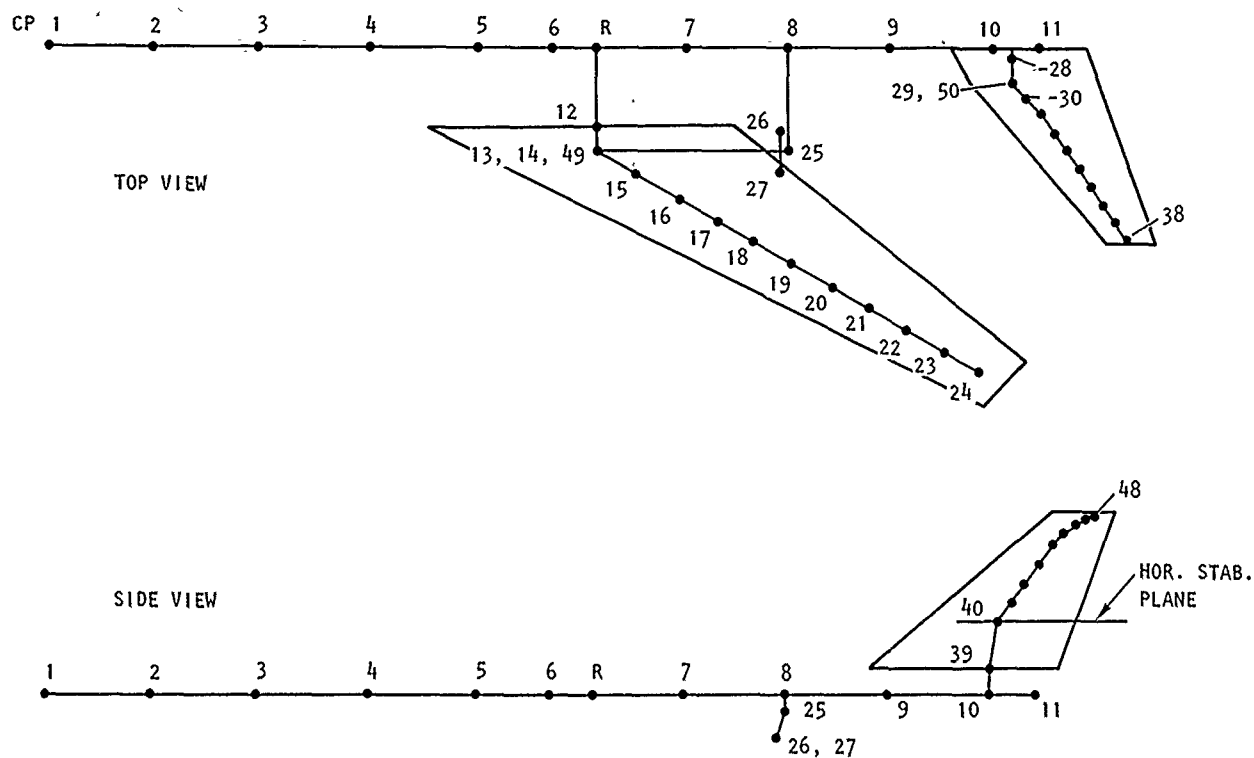


Figure 6. Complete Aircraft Beam Element Model

CONTROL POINT NUMBER	COMPONENT	DOF FOR ANTIS. CASE	NO. OF DOF
1-11	FUSELAGE	y, ψ, ϕ	33
12-24	WING	z, ϕ, θ	39
25	NACELLE	y, z, ϕ, θ	4
26	INBOARD ENGINE	y, z, ϕ, θ	4
27	OUTBOARD ENGINE	y, z, ϕ, θ	4
28-38	HORIZONTAL STABILIZER	z, ϕ, θ	33
39-48	VERTICAL STABILIZER	y, ϕ, ψ	30
49	WING IN-PLANE	x, y, ψ	3
50	HORIZ. STAB. IN-PLANE	x, y, ψ	3
R	REFERENCE POINT	y, ϕ, ψ	3
			<hr/> 156
<p> x = TRANSLATION FORE AND AFT y = TRANSLATION LEFT AND RIGHT z = TRANSLATION UP AND DOWN ϕ = ROTATION ABOUT LINES PERPENDICULAR TO COMPONENT REFERENCE LINE θ = ROTATION ABOUT COMPONENT REFERENCE LINE IN HORIZONTAL PLANE ψ = ROTATION ABOUT COMPONENT REFERENCE LINE IN VERTICAL PLANE </p>			

Figure 7. Global DOF of Complete Aircraft Model

18-16

FREQUENCIES IN HZ							
NO.	MODE ID	BASE	ITER 1	ITER 2	ITER 3	ITER 4	ITER 5
1	W1B	2.41	2.41	2.41	2.41	2.40	2.40
2	F1T	2.97	2.97	2.97	2.96	2.96	2.95
3	W	3.73	3.73	3.73	3.73	3.73	3.72
4	H1B	4.43	4.41	4.40	4.35	4.30	4.27
5	F1B	5.08	5.08	5.08	5.06	5.03	5.03
6	N	6.00	6.00	6.00	5.99	5.98	5.97
7	F2T	6.32	6.32	6.32	6.32	6.31	6.31
8	N, HB	6.65	6.66	6.66	6.63	6.57	6.55
9	W2B	7.16	7.13	7.12	7.09	7.06	7.04
10	H	8.16	8.12	8.10	8.04	7.98	7.95
11	F3T	8.95	8.95	8.94	8.94	8.94	8.93
12	V1B	10.60	10.57	10.53	10.45	10.43	10.37
13	W3B	11.03	11.03	11.02	11.02	11.02	11.01
14	F2B	11.70	11.70	11.70	11.71	11.70	11.70
15	W1T	12.83	12.83	12.83	12.83	12.95	13.02
16	F3B	15.74	15.71	15.68	15.61	15.60	15.54
17	WB, E	18.17	18.17	18.16	18.14	18.19	18.20
18	V1T	20.54	20.32	20.13	19.71	19.68	19.41
19	H2B	21.34	20.93	20.61	20.07	20.16	19.83
20	W2T	21.93	21.89	21.86	21.83	21.93	21.95
21	WB, WT	23.03	23.03	23.02	23.01	23.25	23.33
22	H1T	24.78	24.72	24.61	24.15	24.01	23.74
23	FB	25.75	25.71	25.68	25.62	25.63	25.61
24	VB, HB	30.24	30.25	30.23	30.10	30.04	29.95
25	W3T	32.34	32.35	32.36	32.36	32.83	33.08
26	VB, VT	33.95	33.90	33.86	33.76	33.72	33.67
27	FB, VT	36.10	36.08	36.06	36.00	35.99	35.95
28	H3B	49.26	49.19	49.19	49.17	49.25	49.26
29	H2T	51.84	52.29	52.36	52.13	52.99	52.67
30	WB, WT H ψ	57.50 -	- 57.42	- 56.93	- 55.86	- 55.58	- 54.90

W = WING; F = FUSELAGE; N = NACELLE; E = ENGINE; V = VERTICAL STABILIZER; H = HORIZONTAL STABILIZER;
B = BENDING; T = TORSION; ψ = YAW MOTION

Figure 8. Modes Selected for Flutter Analysis, Antisymmetric Case, Frequencies (Hz)

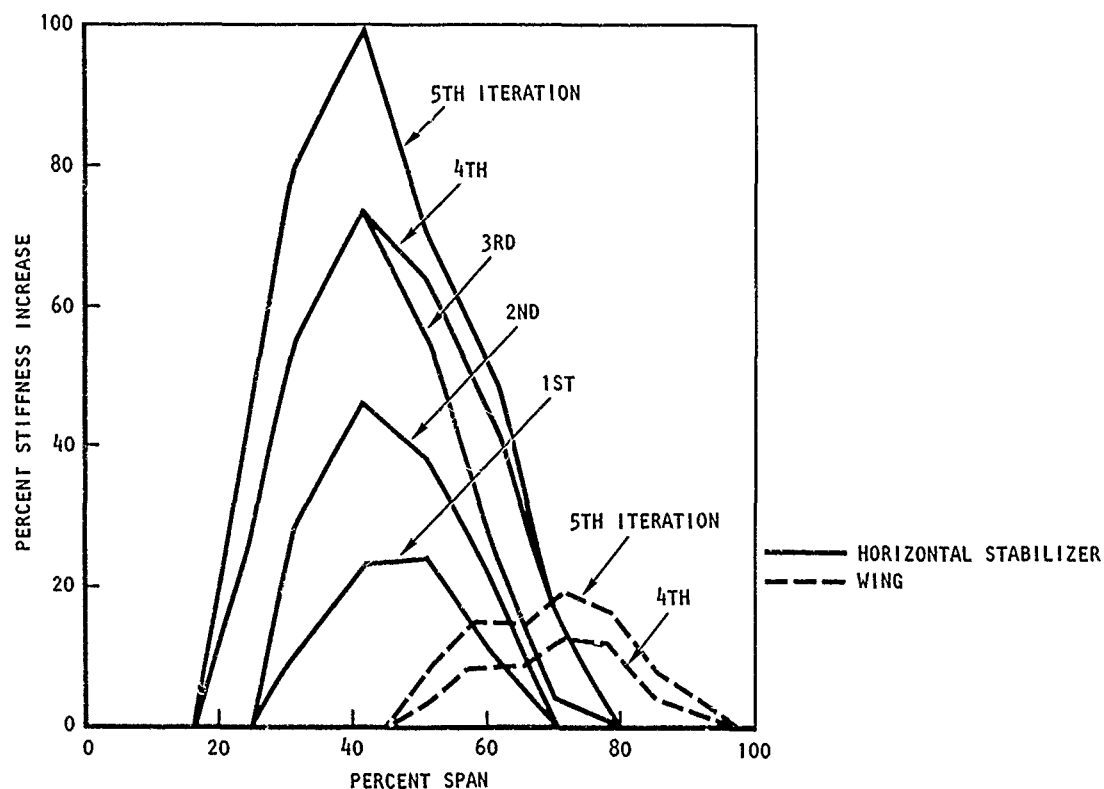


Figure 9. Optimized Stiffness Increase, Antisymmetric Case

FAST FLUTTER CLEARANCE BY PARAMETER VARIATION

by

V. Giavotto, P. Mantegazza and T. Merlini
Istituto di Ingegneria Aerospaziale del Politecnico di Milano
Via Gozli 40
20133 Milano, Italy

and

L. De Otto, M. Lucchesini and R. Mantelli
Aermacchi
Via Sanvito Silvestro 80
21100 Varese, Italy

SUMMARY

After a discussion regarding the main requirements of the study of flutter in the preliminary design, a unified computation system is proposed, which can effectively perform the various types of analysis required. This system was implemented and confirmed through the comparison with experimental results obtained with a wind tunnel model.

The computation system used for the flutter analysis of a combat aircraft with external stores proved to be effective and adequately accurate even in the hardest situations, when the gradients of the critical speed with respect to design parameters are very high.

1. INTRODUCTION

Aeroelastic considerations are so momentous in the design of modern aircrafts that their inclusion in the earliest design stages is required to prevent costly redesigns; Developing an effective methodology is not an easy problem to solve, even if relatively simplified models are to be used.

One typical example is the design of an aircraft with external wing stores, requiring the flutter clearance for hundreds of configurations.

The classic approach on the base of an aeroelastically acceptable primary structure provides that, through the proper design of pylons and the selection of store location, no flutter at all shall occur and any possible deficiency in the primary structures will be indicated, so that the several sections of the design may rapidly be iterated.

It should be noted that it could be extremely difficult to approach this problem through optimization, as such mode would require the setting of suitable flutter constraints for a large number of configurations. An optimization process having constraints on a small number of significant configurations could instead be useful, as it would supply a starting basis and/or indicate redesigns to be performed, as well as in relation to a subsequent analysis with a wide variation of parameters. Therefore in the preliminary design the operations of optimization and parameter variation turn out to be complementary to each other. Thus it is important that a unified formulation be utilized, which can supply an optimal design guideline and an effective, though not too simplified, parametric analysis for the verification of the designs worked out.

Although the above example is particularly significant, the approach described here in does not apply to it only, and it can actually be extended to any lumped parameter design, such as balancing masses, dampers, as well as mass and stiffness properties related to primary structures.

2. THEORY

The Laplace transform of the equations determining the stability conditions can be written as follows:

$$(s^2 [M(a)] + [C(a)] + [K(e)] + \frac{1}{2} \rho V^2 [A(\frac{SC}{2V}, m)]) \{q\} = 0, \quad (1)$$

where

$\{a\}$ is the vector of design parameters
 $[M], [C],$ and $[K]$ are the mass, damping and stiffness matrices respectively,
 ρ is air density
 V is flight speed
 C is a reference length
 m is Mach number
 $\{q\}$ is the vector of generalized coordinates.

19-2

The above equation (1) is related to an arbitrary flight condition. In critical flutter condition, when $s = j\omega$ - being ω a real value - equation (1) becomes as follows:

$$(-\omega^2 [M(a)] + j\omega [C(a)] + [K(a)] + \frac{1}{2} \rho V^2 [A(\frac{j\omega C, m}{2V})])\{q\} = 0. \quad (2)$$

The eigenproblems expressed by equations (1) and (2) are considerably different from the eigenproblems of linear algebra. The differences, which are well-known to flutter analysts, are connected to the presence of the aerodynamic transfer function $[A]$; particularly the eigenvalues in (2) are connected to two different variables, i.e. ω and V in equation (2).

For the solution of this problem several methodologies have been developed so far, and a push in this respect has recently been given by the need of active control design. However none of them can simplify the difficulties intrinsic in equation (2). One particular approach consists in treating equation (1) or (2) like a non-linear and non-homogeneous system of equations, thereby adding a normalization equation for $\{q\}$ so that a univocal solution can be obtained [1]. This method enables the attainment of a unified formulation as indicated below, which can be used either for the analysis or for the design:

$$\begin{cases} [F(s, V, m, \rho, a)] \{q\} = 0 \\ \{q\}^T [W] \{q\} = 1 \end{cases} \quad (3)$$

In fact, by fixing the design parameters $\{a\}$ and velocity V , from formulation (3) equation (1) is obtained, whereas, by fixing design parameters and establishing $s = j\omega$, the same formulation produces equation (2).

As far the design is concerned [2], usually s and V are fixed whereas the values of design parameters are left open, and one or several systems of equations (3) are taken on as equality constraints for the minimizing of a performance index of the following type:

$$C = \{a\}^T [z] \{a\} \quad (4)$$

With formulation (3), if we accept that by approximation the transcendental portion of $[A]$ is negligible and its rational portion is slightly affected by different flight and design conditions [3-4], we can utilize any identification of $[A]$ which can interpolate $[A]$ for any values of s by a good approximation [5-7]. The unified formulation thus attained can be an effective tool for the preliminary design.

A typical use can be the following:

- Design specifications shall be determined in which a certain number of couples of s and V values are fixed so as to obtain a certain number of equations (3). If the number of the design parameters is exactly the same as the number of equations (3), they can directly be determined by such equations. Instead if their number is higher, equations (3) will be employed as constraints for the minimizing of performance index (4).
- In the design thus generated, some sets of eigensolutions of equations (3) shall be determined for the different values of $\{a\}$ and they shall be a function of V (V - sweep mode). The results will be in the classical forms of V -g plots or root loci.
- s shall be set equal to $j\omega$ and equation (3) will be utilized for the direct search of the critical flutter conditions upon parameter variation.
- The direct search as per (c) above may generally be incapable to show up flutter mechanisms other than those determined as per stage (b). For this reason stage (b) may require to be extended by additional $\{a\}$ values so that any presence of prospective mechanisms can be ascertained.
- The results obtained shall be evaluated and, if necessary, the process shall be repeated beginning from stage (a) until an acceptable result is obtained.

It shall be noted that problem (a) can be faced properly through the use of Lagrange multipliers and algorithms that exploit Hessian sparsity. Problems (b) and (c) can instead be solved very effectively by reformulating equation (3) in a continuation form [1] with respect to V and/or $\{a\}$ variations.

Every continuation process starts from an available solution (e.g. one of the still air modes), and all the solutions of such processes can be employed as first-approximation initial solutions for further continuation processes.

It shall be pointed out that, as long as equation (3) remains a suitable model of the aeroelastic system, every solution of process (c) that satisfies equation (3) within an acceptable error is a correct solution of the flutter problem, even when great variations of $\{a\}$ occur. For this reason a high number of degrees of freedom can conveniently be maintained on account of the great effectiveness of the procedure employed. Typically, for the preliminary design of an aircraft with external stores with the physical degrees of freedom (translation and rotations), a model with $20 \div 30$ degrees of freedom will be suitable.

3. THE AEROELASTIC MODEL

The basic requirement of the model for an efficient design and/or parametric analysis of an aeroelastic system is to allow large parameter variations with no need of scheme variations. In this way both a too simple modelling and a too precise one are excluded, as the latter generally involves a specific design selection.

A reasonable compromise can be reached through a hybrid modelling, in which the main structure section is described by means of modal coordinates (vibration and static modes) and the sections subject to the largest parameter variations are described by means of physical coordinates [8 - 10]. This procedure allows a great amount of computation to be saved, since it requires one single dynamic analysis for each configuration of the clean aircraft and few aerodynamic analyses for a limited number of external stores typologies [11].

The numerous parametric design analyses required can be performed by simpler programs through the employment of smaller computers.

4. COMPUTATION SYSTEM

For the performance of the computation stages described in the previous paragraph a computation system has been developed, which provides also the integrated use of a mainframe and a minicomputer. In this specific operational environment such integrated use was the highest-effectiveness solution. In different environments however the implementation of the entire computation system on a single mainframe might prove to be more suitable, as Aermacchi actually did.

The outline of the computation system is shown in Fig. 1.

The dynamic analysis of the clean aircraft, which leads to the determination of the eigenmodes and of suitable junction modes, is performed on a mainframe by Nastran Program.

For discrete values of the reduced frequency the matrices of the coefficients of modal aerodynamic forces corresponding to different aerodynamic formulations can be computed out of the modal forms, by different programs (including Nastran).

HYDAN Program performs the assembling of the complete structure by connecting the structure of the clean aircraft represented by modal coordinates (eigenmodes and junction modes) to the variable parameter portions represented by physical coordinates (pylons and external stores). Hydan determines the free vibrating modes for the complete structure thus obtained, and these can be used by the subsequent programs as starting solutions.

FLUSW Program determines the aeroelastic eigensolutions, upon flight speed variations, through the technique mentioned above, consisting in the solution of a non-linear and non-homogeneous set of equations. The search of solutions is carried out with respect to a specific speed increment, beginning from the solution of the preceding increment, through a predictor-corrector process which is based on the computation of the derivatives of solutions with respect to speed. The starting solutions can be adequate ones, corresponding to zero speed, or to any other speed value.

FLUTT Program performs direct searches of the critical flutter speed upon variation of one of the design parameters, beginning from a critical or quasi-critical condition obtained through the same FLUTT Program for instance, in relation to the variation of another parameter.

The results of FLUSW and FLUTT Programs can be presented graphically through the use of suitable postprocessors. Such graphic presentation basically shows eigenvalues versus speed ($V - g$ plots), curve plots of the critical speed versus a design parameter, and carpet plots and/or contour plots of the critical speed versus two parameters. Graphic outputs can also be generated for the animation of structure motions corresponding to specific aeroelastic eigensolutions.

The visual presentation of the motion regarding the critical conditions has proved to be particularly useful for the purpose of a comparison with the similar films attained experimentally from the flutter model in the wind tunnel. Moreover such visual presentation can be a valid guideline in the selection of the positioning of exciters in flight flutter tests.

5. FLUTTER OF A COMBAT AIRCRAFT WITH EXTERNAL STORES

A significant example of the computation procedure is the parametric study of the flutter of a combat aircraft with external wing stores.

First the computations of the flutter of the wind tunnel model were performed for the purpose of verifying the validity of the method through a comparison with the experimental results.

5.1 Wind tunnel model

An aeroelastic half model was built: the center plane of the aircraft had a special constraint system allowing only the symmetrical motions of the fuselage, with negligible friction. The constraint was obtained by means of air cushion skids that were integral to a rigid structure simulating the inertia of the half-fuselage, working on a lapped granite surface, plane within $\pm 1 \mu$ tolerance, which was supplied by POLI S.p.A. Company, Varallo Sesia, Italy. The thrust of the air cushions was balanced by means of a bundle of rubber chords of such length, pretension, and inclination as to provide the following:

- a. a horizontal force to be such as to keep the air film thickness between the skids and the granite slab within acceptable limits (8 - 12 μ);
- b. a vertical force to be such as to balance the weight of the model;
- c. a stiffness to be in accordance with the symmetrical rigid motions of the fuselage and sufficiently low so as not to affect remarkably the structural eigenfrequencies.

Fig. 2 shows the model equipped with the suspension system as provided for still air tests, and Fig. 3 shows the same model with the suspension system faired for tunnel tests.

The model could be equipped with two pylons with different stiffness and geometry. For an experimental parametric investigation many models of the external stores were arranged, which had large variations of inertia parameters and of the center-of-gravity position. Both the model and its suspension system proved to be definitely adequate both in the still air vibration tests and in the tunnel flutter tests. Particularly the suspension system turned out to be very precise and practically devoid of frictions; clearly the latter characteristic is essential, since the presence of any friction - even a small one - might completely alter and conceal important flutter mechanisms.

Moreover the suspension allowed the easy blocking of the rigid motions of the fuselage through the more cutoff of compressed air feed to the skids. In this case, in fact, the tension of the rubber cord bundle was sufficient so as to ensure a complete restraining in the plane of symmetry.

Preliminary tests were performed with the suspension both in free and blocked states, and they clearly indicated that, by the simulation of the inertial properties of the fuselage, the freedom of its rigid motions can affect considerably the critical speed of some types of flutter. All subsequent test were performed with the suspension in a free state.

Regarding the comparison with the outcomes of the computation, tests were performed wherein stores were mounted on one pylon and on both pylons. For each pylon the mass and the radius of inertia of the store were taken on as variable parameters. The stiffnesses of the pylons and the positions of store centers-of-gravity was also varied.

5.2 Comparison of computation results with experimental results

Fig. 4 shows the finite element idealization used for the dynamic analysis of the model.

An initial comparison between the critical speeds computed and the ones measured on the wind tunnel model indicated a fair agreement regarding some configurations, whereas considerable and apparently inexplicable discrepancies were found out in relation to the other configurations.

An exhaustive examination of these cases showed two basic facts:

- a. For practical requirements the elastic properties of the pylons of the tunnel model turned out slightly different from the properties provided and employed in the computation model.
- b. In some cases the plots of the critical speeds computed versus the two inertia parameters of the store appeared like very wavy surfaces having very deep and narrow holes and very steep areas (compare figs. 7 and 14).

Regarding item a. above very accurate experimental measurements of the stiffnesses of the tunnel model pylons were performed, and on their basis the corresponding parameters of the computation model were modified. This fact led the computation values of the still-air eigenfrequencies even closer to the experimental values (Fig. 5), thus confirming that the operation was correct.

Regarding item b., the presence of deep holes in the flutter surface would indicate that the solution has areas which are very sensitive even to slight variations of the parameters. Therefore for the obtainment of a good agreement of the results a very precise correspondance of the parameters of the mathematical model to the parameters of the physical model is required. It is also necessary that the parameter variation occurring during testing be made by sufficiently small increments, so as to prevent that the presence of the holes may be completely concealed. The number of experimental measurements therefore had to be increased, in order to cover the range of parameter variations with a higher number of cases.

By this measure the agreement between the computation results and the experimental ones turned out satisfactory in all situations. For inst., Figs. 6 and 7 show the contour plots of the critical speeds obtained both from the tunnel measurements and from the computation; these plots are related to one of the most critical cases, which regards a specific stiffness value of the external pylons.

Moreover, Figs. 8, 9, and 10 show the comparison performed between the experimental results and the computed ones regarding constant mass sections of the surfaces presented in Figs. 6 and 7. A fair agreement can be seen although the configuration is a hypersensitive one (*). Based on such agreement the following conclusions could be drawn:

- the computation procedure can give acceptably accurate results;
- the deep holes in the flutter surfaces indicated by the computation were found also experimentally; thereby the good quality of the tunnel model, and particularly that of the suspension system, was confirmed;
- the presence of high gradients in the flutter surfaces can make the use of optimizing procedures very difficult - if not impossible.

It shall finally be considered that the experimental points by which the surface in fig. 6 was plotted (approx. 60) are still considerably fewer than the computed points which were used to draw the surface in Fig. 7 (approx. 800).

5.3 Flutter clearance of the actual aircraft

After being confirmed by the experimental measurements, the computation system was employed for the flutter study in the preliminary design of the actual aircraft. Thereby the analysis of a considerable amount of configurations and external stores could be carried out, and the optimal design of pylon stiffnesses and of store positions could thus be determined.

In all, the layout of 100 flutter surfaces was required and, since each of them was defined by approx. 800 computed points, approx. 80,000 flutter points had to be determined.

Fig. 11 shows the Nastran idealization of the complete aircraft. Examples of the graphic output of the computation system are given in Fig. 12, which shows the V-g plot related to a specific configuration, and in Figs. 13 and 14, which show the flutter surfaces related to two configurations, one of which (Fig. 13) is slightly sensitive to parameter variations and the other one (Fig. 14) is very sensitive to it.

(*) The discrepancies encountered are basically due to the bidimensional approximation used for the computation of aerodynamic forces. Tridimensional aerodynamics, which was used in a limited number of cases, considerably reduced such discrepancies.

The use of HP 1000 minicomputer proved to be particularly efficient: all the operations required for the layout of a surface with approx. 800 points (HYDAN, FLUSW, FLUTT Programs and postprocessors) could be completed in a mean time (flutter analyst time) of 4 hours. When the complete system was instead utilized on UNIVAC 1100/80 mainframe, the same operations required a flutter analyst time of 1 hour (CPU time 400 s.).

6. CONCLUSIONS

In conclusion the computation system developed proved to be accurate and effective, and particularly very suitable for the preliminary design. The application to the study of a flutter of an aircraft with wing stores further confirmed the complementarity of the parametric analysis to optimization methods.

It should also be remarked that the suspension made by Aermacchi to allow symmetrical rigid motions in the tunnel model is an ingenious solution to a rather difficult problem.

Finally it will be useful to point out again that, at least as far as the study of wing store flutter is concerned, the variation of parameters shall be made by very small increments; in fact the measurements performed by too large increments may totally conceal particularly critical situations.

7. REFERENCES

- [1] C. Cardani and P. Mantegazza, "Continuation and Direct Solution of the Flutter Equation", Computer and Structures, Vol. 8, 1978, pp. 185 - 192.
- [2] M. Lanz and P. Mantegazza, "An Improved Method for the Design of Flutter Suppression Systems by Eigenvalue Assignment", L'aeronautica missili e spazio, Vol. 60, N°2, June 1981, pp. 92 - 97.
- [3] R.O. Milne, "Asymptotic Solutions of Linear Integro-Differential Equations", A.R.C.R. & M. 3548, July 1966.
- [4] Z.W. Edwards, "Unsteady Aerodynamic Modeling and Active Aeroelastic Control", NASA-CR-148019, Feb. 1977.
- [5] R. Vepa, "Finite State Modeling of Aeroelastic Systems", NASA-CR-2779, Feb. 1977
- [6] M. Karpel, "Design for Active and Passive Flutter Suppression and Gust Alleviation", Ph.D. Thesis, Stanford University, NTIS N82-13147.
- [7] P. Mantegazza, "Identification of Generalized Unsteady Aerodynamic Forces From Harmonic Aerodynamic Loadings", L'aeronautica missili e spazio, Vol. 60, N° 3, Sept. 1981, pp. 154 - 160.
- [8] R.R. Craig and M.C.C. Bampton, "Coupling of Substructures for Dynamic Analyses", A.I.A.A. Journal, Vol.6, N°7, July 1968, pp. 1313 - 1319.
- [9] R.H. McNeal, "The Nastran Theoretical Manual", NASA-SP-221.
- [10] Many Authors, "Wing-With-Stores Flutter", AGARD-CP-162, 1974.
- [11] C.D. Turner, "Effect of Store Aerodynamics on Wing-Store Flutter", Journal of Aircraft, Vol. 19, N° 7, July 1982, pp. 574 - 580.

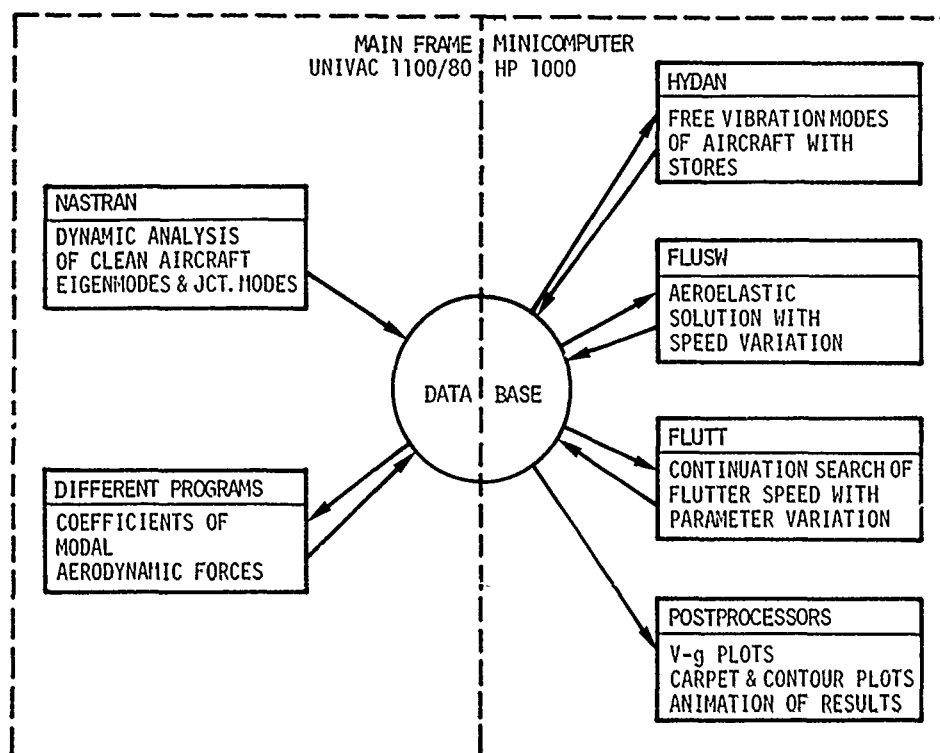


Fig. 1 - Computation System



Fig. 2 - Wind tunnel model in vibration test set-up

19-8

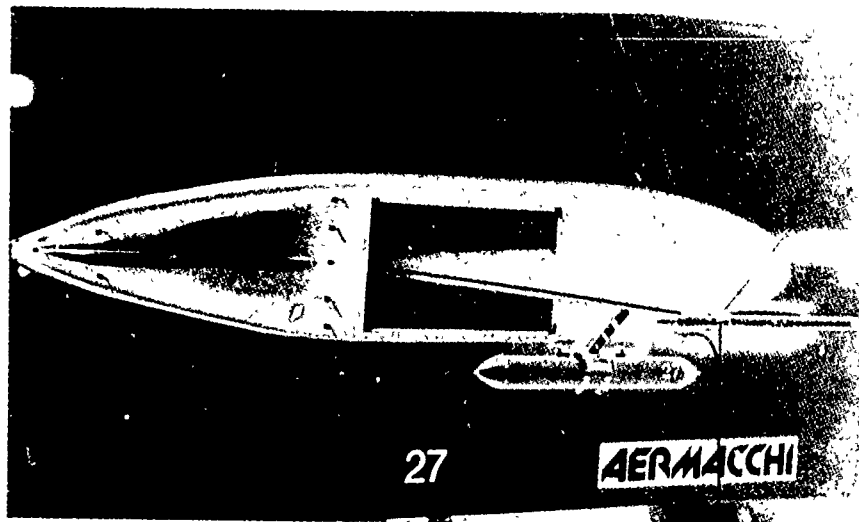


Fig. 3 - The model in AERMACCHI subsonic Wind-Tunnel

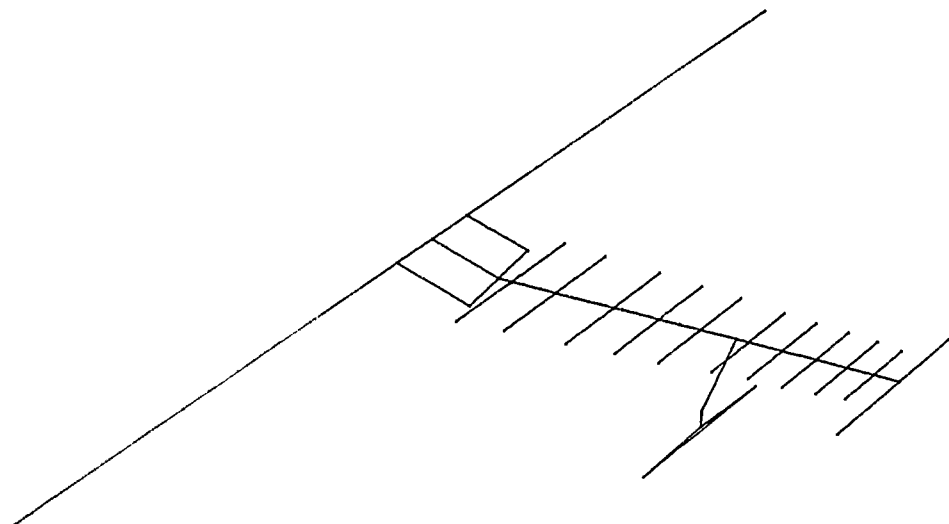


Fig. 4 - F.E. idealization of wind tunnel model

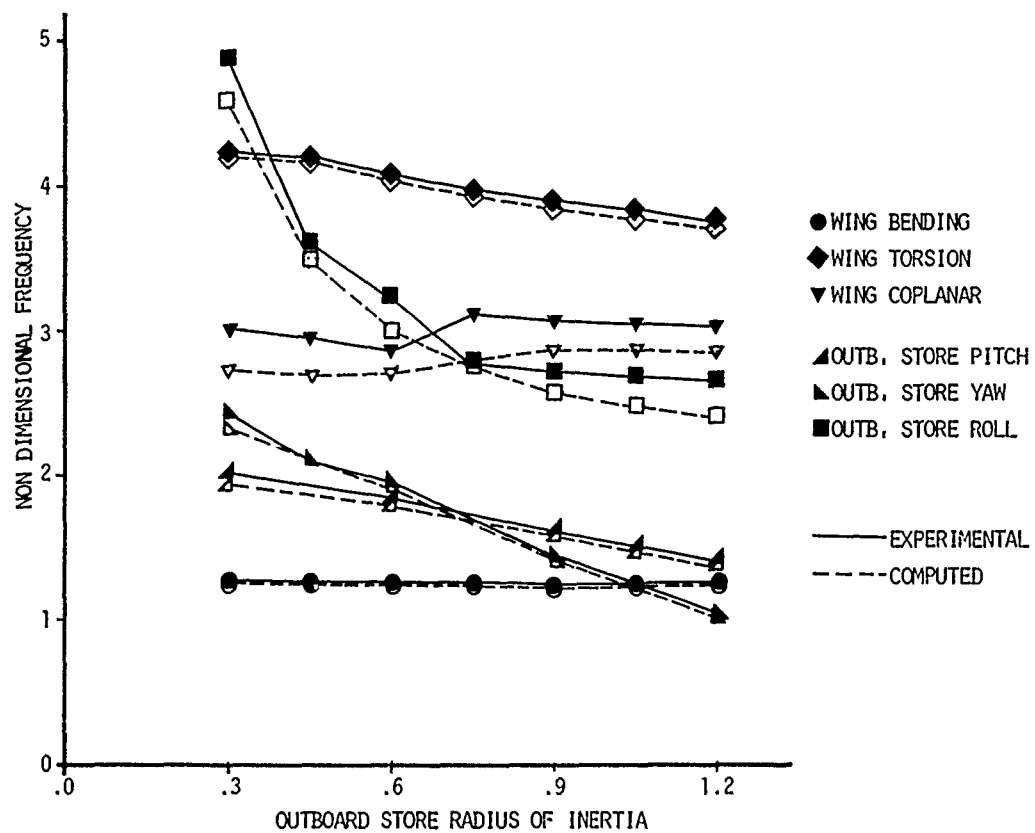


Fig. 5 - Model free vibration frequencies
(pylon stiffness K2)

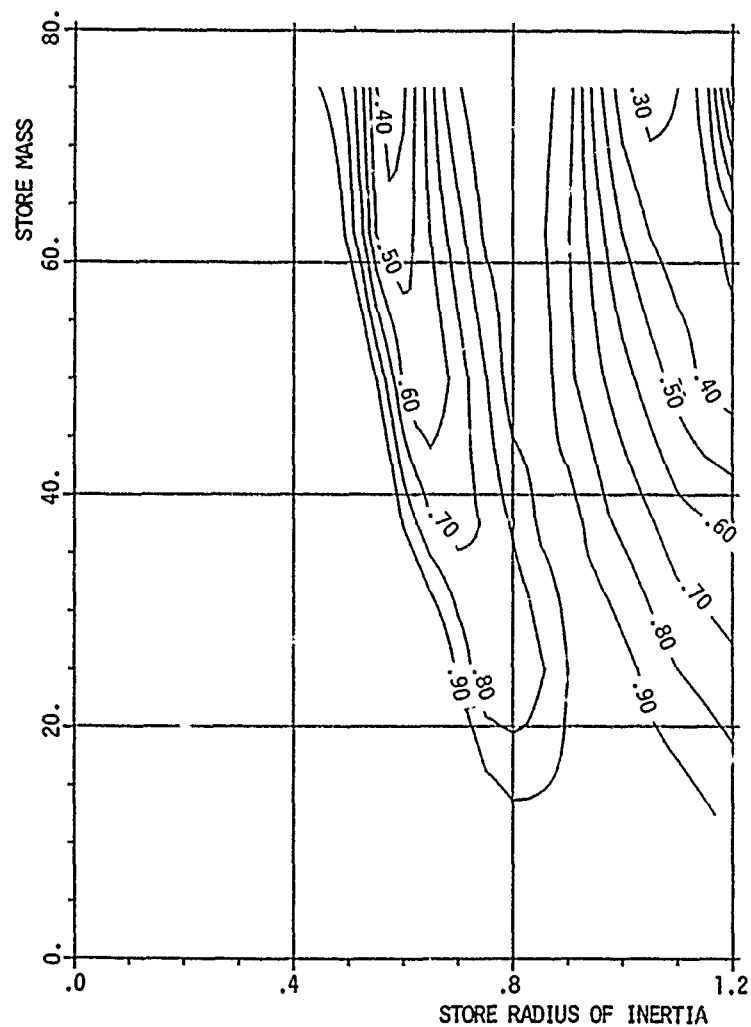


Fig. 6 - Flutter speed from wind tunnel model
(outboard pylon stiffness K2)

19-10

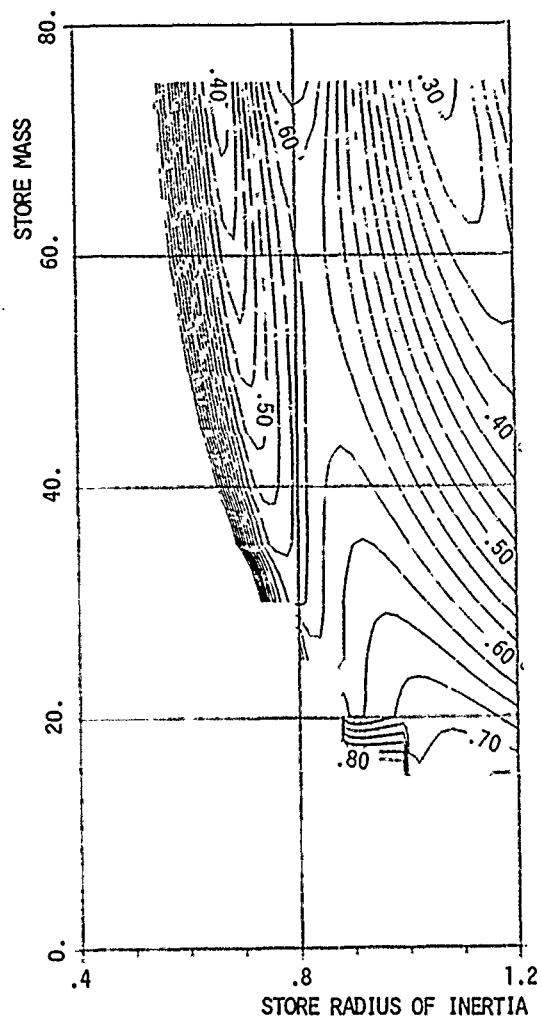


Fig. 7 - Flutter speed from computation
(outboard pylon stiffness K2)

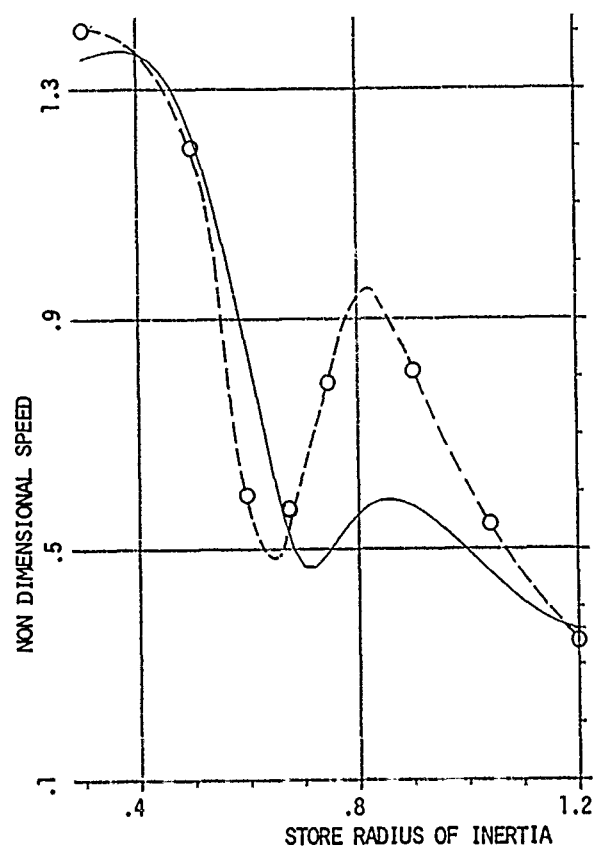


Fig. 8 - Store mass = $50 \text{ kg m}^{-1} \text{ s}^2$

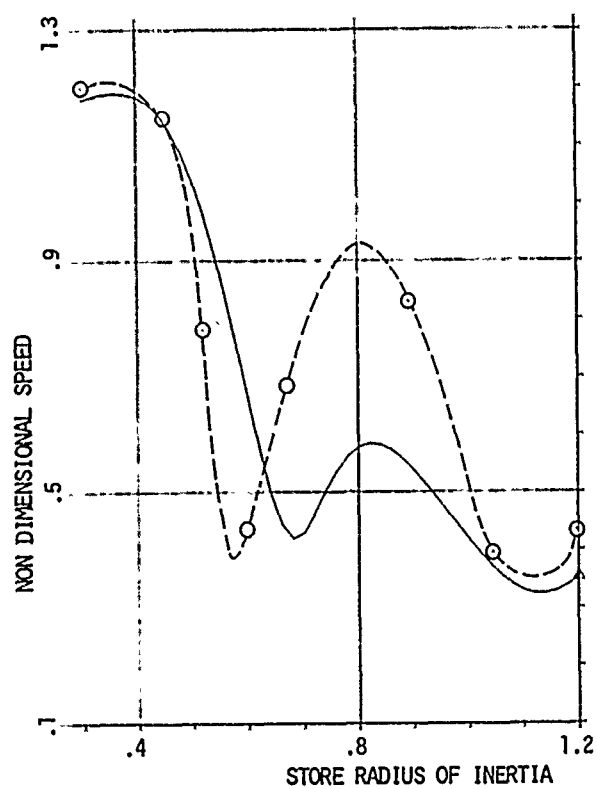


Fig. 9 - Store mass = $62.5 \text{ kg m}^{-1} \text{ s}^2$

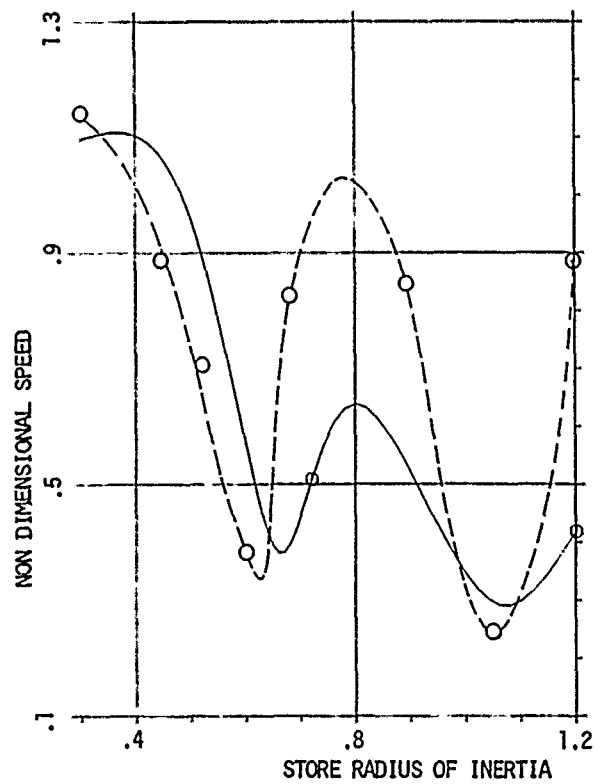


Fig. 10 - Store mass = $75 \text{ kg m}^{-1} \text{ s}^2$

Figs 8-10 - Computed and experimental flutter speed vs. radius of outb. store

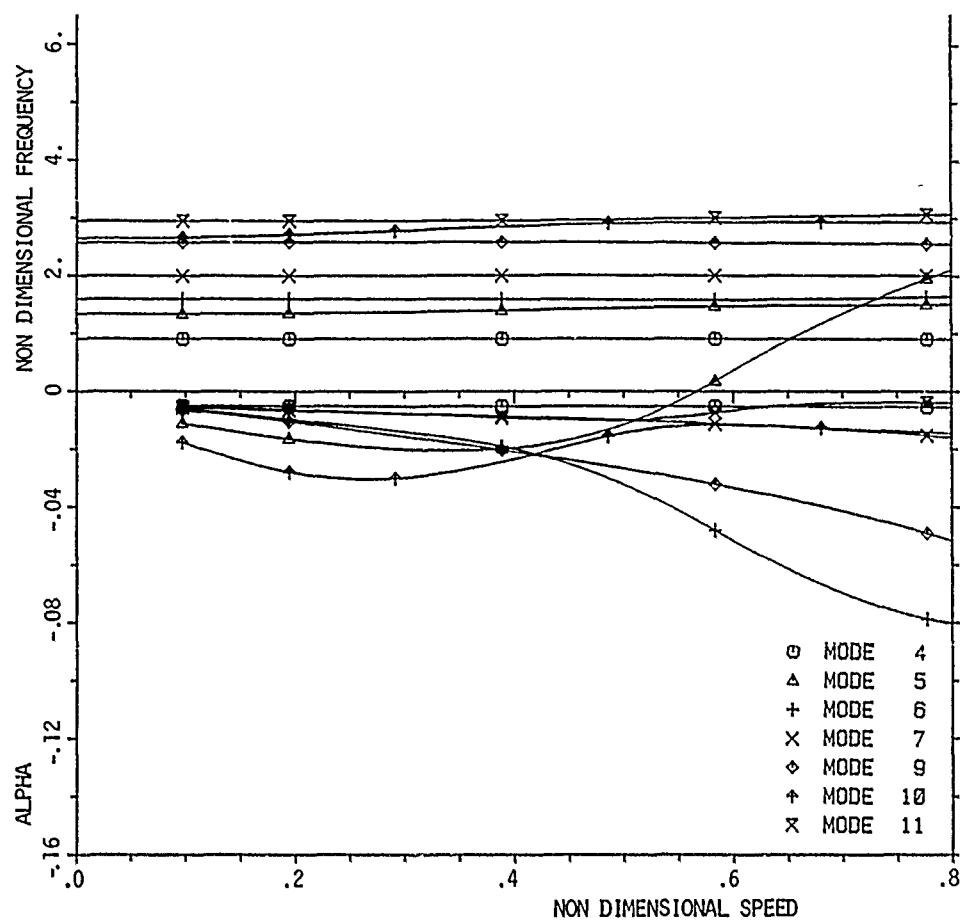


Fig.12 - V-alpha plot (stores on both pylons)

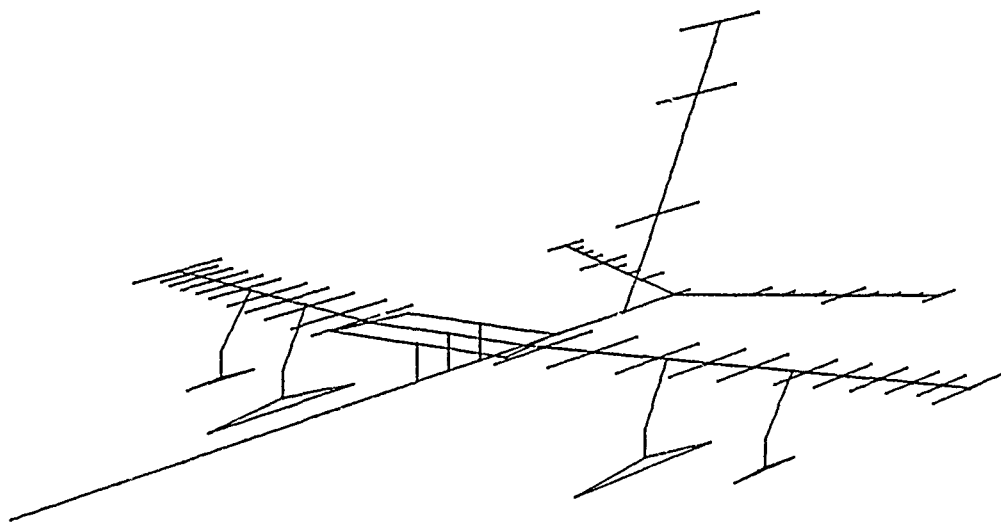


Fig.11 - F.E. idealization of the complete aircraft

19-12

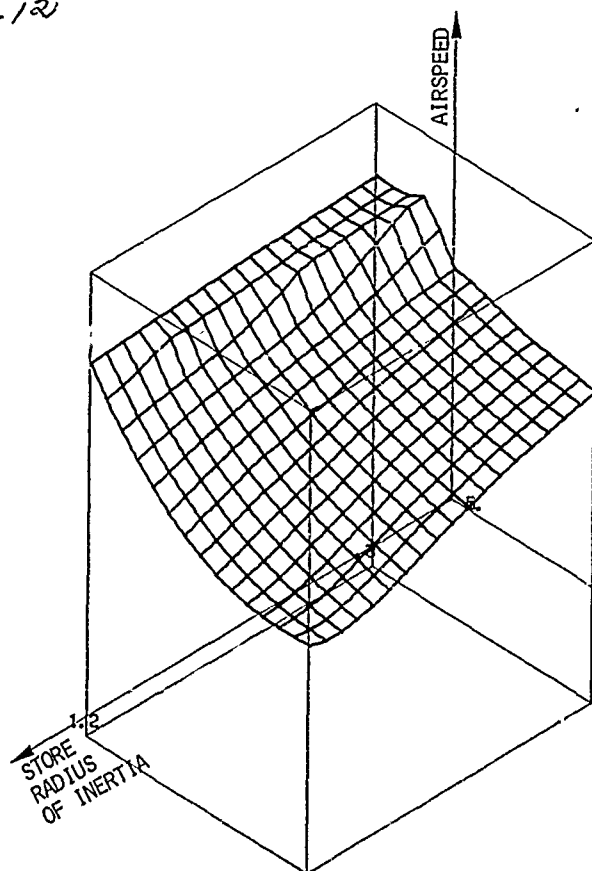


Fig. 13 - Smooth flutter surface
(H.P. 1000 MINICOMPUTER)

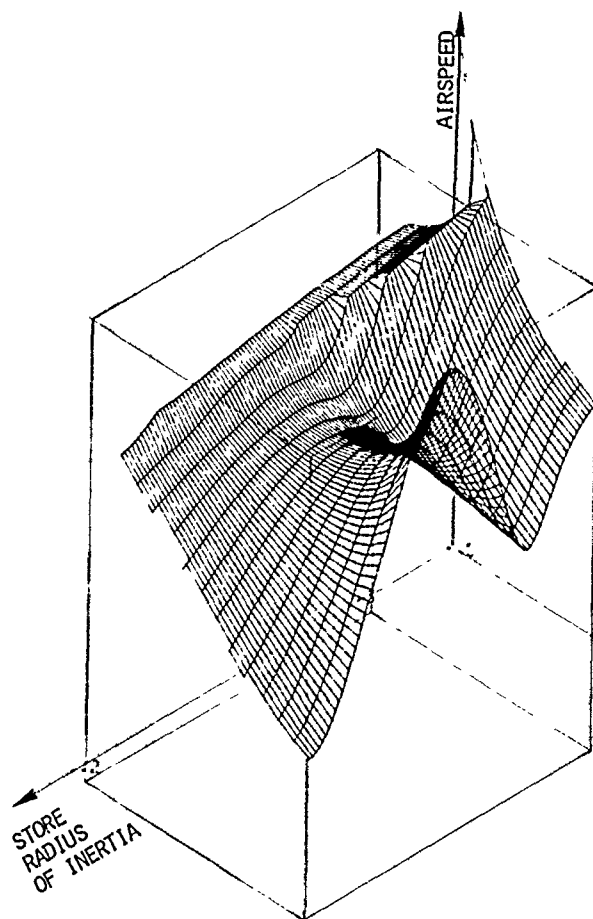
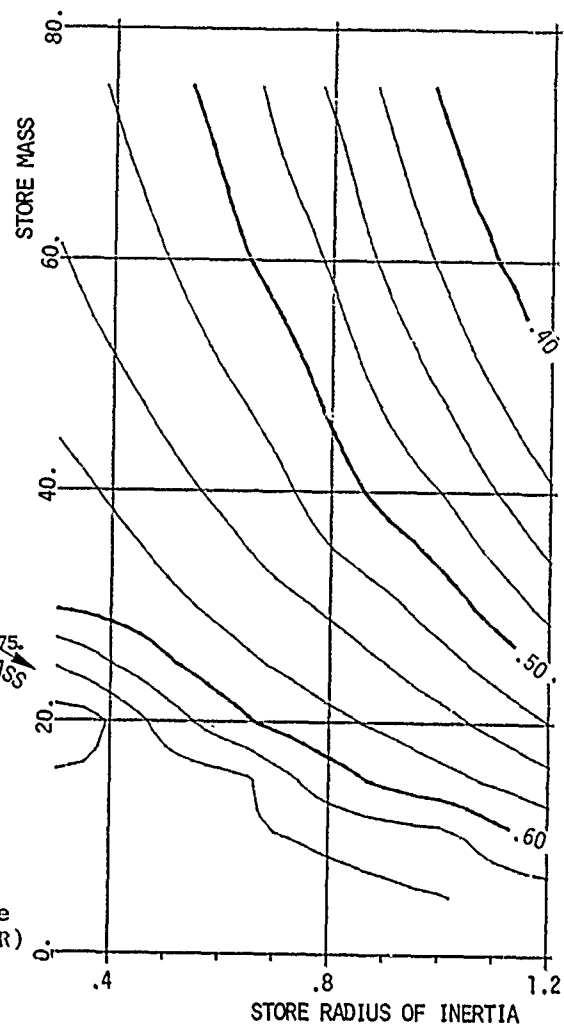
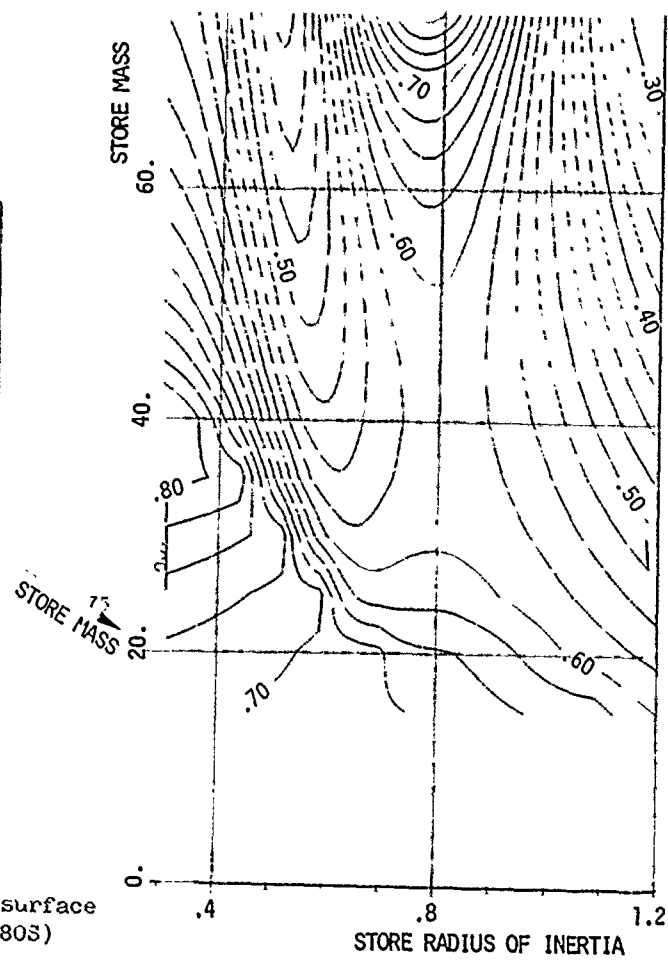


Fig. 14 - Weavy flutter surface
(UNIVAC 1100/80S)



<p>AGARD Conference Proceedings No.354 Advisory Group for Aerospace Research and Development, NATO AEROELASTIC CONSIDERATIONS IN THE PRELIMINARY DESIGN OF AIRCRAFT Published September 1983 332 pages</p> <p>This publication contains the papers presented at the SMP Spring 1983 Specialists Meeting on Aeroelastic Consideration in the Preliminary Design of Aircraft. Current aerospace design trends which involve the increasing application of composite structures have forced the use of large-scale structural analysis at an early design stage; at the same time structural optimization and aeroelastic tailoring are becoming practical tools for</p> <p>P.T.O</p>	<p>AGARD-CP-354</p> <p>Aircraft Airframes Design Aeroelasticity Flutter Dynamic structural analysis</p>	<p>AGARD Conference Proceedings No.354 Advisory Group for Aerospace Research and Development, NATO AEROELASTIC CONSIDERATIONS IN THE PRELIMINARY DESIGN OF AIRCRAFT Published September 1983 332 pages</p> <p>This publication contains the papers presented at the SMP Spring 1983 Specialists Meeting on Aeroelastic Consideration in the Preliminary Design of Aircraft. Current aerospace design trends which involve the increasing application of composite structures have forced the use of large-scale structural analysis at an early design stage; at the same time structural optimization and aeroelastic tailoring are becoming practical tools for</p> <p>P.T.O</p>	<p>AGARD-CP-354</p> <p>Aircraft Airframes Design Aeroelasticity Flutter Dynamic structural analysis</p>
<p>AGARD Conference Proceedings No.354 Advisory Group for Aerospace Research and Development, NATO AEROELASTIC CONSIDERATIONS IN THE PRELIMINARY DESIGN OF AIRCRAFT Published September 1983 332 pages</p> <p>This publication contains the papers presented at the SMP Spring 1983 Specialists Meeting on Aeroelastic Consideration in the Preliminary Design of Aircraft. Current aerospace design trends which involve the increasing application of composite structures have forced the use of large-scale structural analysis at an early design stage; at the same time structural optimization and aeroelastic tailoring are becoming practical tools for</p> <p>P.T.O</p>	<p>AGARD-CP-354</p> <p>Aircraft Airframes Design Aeroelasticity Flutter Dynamic structural analysis</p>	<p>AGARD Conference Proceedings No.354 Advisory Group for Aerospace Research and Development, NATO AEROELASTIC CONSIDERATIONS IN THE PRELIMINARY DESIGN OF AIRCRAFT Published September 1983 332 pages</p> <p>This publication contains the papers presented at the SMP Spring 1983 Specialists Meeting on Aeroelastic Consideration in the Preliminary Design of Aircraft. Current aerospace design trends which involve the increasing application of composite structures have forced the use of large-scale structural analysis at an early design stage; at the same time structural optimization and aeroelastic tailoring are becoming practical tools for</p> <p>P.T.O</p>	<p>AGARD-CP-354</p> <p>Aircraft Airframes Design Aeroelasticity Flutter Dynamic structural analysis</p>

<p>shaping the initial project. Whilst the potential for designing minimum weight structures which deform beneficially under load exists, the hazards of extracting energy from the airstream and generating unfavourable deformations and aeroelastic instabilities must also be recognized. These papers review trends in aeroelastic analysis, aeroelastic tailoring, structural optimization and flutter optimization.</p> <p>Papers presented at the 56th Meeting of the Structures and Materials Panel in London, United Kingdom, on 11-12 April 1983.</p> <p>ISBN 92-835-0338-4</p>	<p>shaping the initial project. Whilst the potential for designing minimum weight structures which deform beneficially under load exists, the hazards of extracting energy from the airstream and generating unfavourable deformations and aeroelastic instabilities must also be recognized. These papers review trends in aeroelastic analysis, aeroelastic tailoring, structural optimization and flutter optimization.</p> <p>Papers presented at the 56th Meeting of the Structures and Materials Panel in London, United Kingdom, on 11-12 April 1983.</p> <p>ISBN 92-835-0338-4</p>
<p>shaping the initial project. Whilst the potential for designing minimum weight structures which deform beneficially under load exists, the hazards of extracting energy from the airstream and generating unfavourable deformations and aeroelastic instabilities must also be recognized. These papers review trends in aeroelastic analysis, aeroelastic tailoring, structural optimization and flutter optimization.</p> <p>Papers presented at the 56th Meeting of the Structures and Materials Panel in London, United Kingdom, on 11-12 April 1983.</p> <p>ISBN 92-835-0338-4</p>	<p>shaping the initial project. Whilst the potential for designing minimum weight structures which deform beneficially under load exists, the hazards of extracting energy from the airstream and generating unfavourable deformations and aeroelastic instabilities must also be recognized. These papers review trends in aeroelastic analysis, aeroelastic tailoring, structural optimization and flutter optimization.</p> <p>Papers presented at the 56th Meeting of the Structures and Materials Panel in London, United Kingdom, on 11-12 April 1983.</p> <p>ISBN 92-835-0338-4</p>

AGARD
 NATO  OTAN
 7 RUE ANCELLE · 92200 NEUILLY-SUR-SEINE
 FRANCE
 Telephone 745.08.10 · Telex 610176

**DISTRIBUTION OF UNCLASSIFIED
 AGARD PUBLICATIONS**

AGARD does NOT hold stocks of AGARD publications at the above address for general distribution. Initial distribution of AGARD publications is made to AGARD Member Nations through the following National Distribution Centres. Further copies are sometimes available from these Centres, but if not may be purchased in Microfiche or Photocopy form from the Purchase Agencies listed below.

NATIONAL DISTRIBUTION CENTRES

BELGIUM

Coordonnateur AGARD — VSL
 Etat-Major de la Force Aérienne
 Quartier
 Rue d'I

CANADA

Defence
 Department
 Ottawa



National Aeronautics and
 Space Administration

DENMARK

Danish
 Østerb
 Copenh

Washington, D.C.
 20546

**SPECIAL FOURTH CLASS MAIL
 BOOK**

FRANCE

O.N.E.R.
 29 Avenue
 92320 G

**DEPT OF DEFENSE
 DEFENSE TECH. INFO. CENTER
 ATTN: DDC-DDA-2
 CAMERON STATION BLDG 5
 ALEXANDRIA VA 22314**

GERMANY

Fachinfo
 Physik, A
 Kernforsch
 D-7514 E

GREECE

Hellenic
 Research and Development Directorate
 Holargos, Athens

ICELAND

Director of Aviation
 c/o Flugrad
 Reykjavik

ITALY

Aeronautica Militare

ARD

Postage and Fees Paid
 National Aeronautics and
 Space Administration
 NASA-451

Official Business
 Penalty for Private Use \$300



UNITED KINGDOM

Defence Research Information Centre
 Station Square House
 St. Mary Cray
 Orpington, Kent BR5 3RE

UNITED STATES

National Aeronautics and Space Administration (NASA)
 Langley Field, Virginia 23365
 Attn: Report Distribution and Storage Unit

**THE UNITED STATES NATIONAL DISTRIBUTION CENTRE (NASA) DOES NOT HOLD
 STOCKS OF AGARD PUBLICATIONS, AND APPLICATIONS FOR COPIES SHOULD BE MADE
 DIRECT TO THE NATIONAL TECHNICAL INFORMATION SERVICE (NTIS) AT THE ADDRESS BELOW.**

PURCHASE AGENCIES

Microfiche or Photocopy

National Technical
 Information Service (NTIS)
 5285 Port Royal Road
 Springfield
 Virginia 22161, USA

Microfiche

Space Documentation Service
 European Space Agency
 10, rue Mario Nikis
 75015 Paris, France

Microfiche or Photocopy

British Library Lending
 Division
 Boston Spa, Wetherby
 West Yorkshire LS23 7BQ
 England

Requests for microfiche or photocopies of AGARD documents should include the AGARD serial number, title, author or editor, and publication date. Requests to NTIS should include the NASA accession report number. Full bibliographical references and abstracts of AGARD publications are given in the following journals:

Scientific and Technical Aerospace Reports (STAR)
 published by NASA Scientific and Technical
 Information Facility
 Post Office Box 8757
 Baltimore/Washington International Airport
 Maryland 21240, USA

Government Reports Announcements (GRA)
 published by the National Technical
 Information Services, Springfield
 Virginia 22161, USA



*Printed by Specialised Printing Services Limited
 40 Chigwell Lane, Loughton, Essex IG10 3TZ*

ISBN 92-835-0338-4